BIOTECHNOLOGY OF MICROALGAE, BASED ON MOLECULAR BIOLOGY AND BIOCHEMISTRY OF EUKARYOTIC ALGAE AND CYANOBACTERIA

EDITED BY: Takashi Osanai, Youn-Il Park and Yuki Nakamura
PUBLISHED IN: Frontiers in Microbiology

frontiers Research Topics

frontiers

ISSN 1664-8714
ISBN 978-2-88945-129-6
DOI 10.3389/978-2-88945-129-6

About Frontiers

Frontiers is more than just an open-access publisher of scholarly articles: it is a pioneering approach to the world of academia, radically improving the way scholarly research is managed. The grand vision of Frontiers is a world where all people have an equal opportunity to seek, share and generate knowledge. Frontiers provides immediate and permanent online open access to all its publications, but this alone is not enough to realize our grand goals.

Frontiers Journal Series

The Frontiers Journal Series is a multi-tier and interdisciplinary set of open-access, online journals, promising a paradigm shift from the current review, selection and dissemination processes in academic publishing. All Frontiers journals are driven by researchers for researchers; therefore, they constitute a service to the scholarly community. At the same time, the Frontiers Journal Series operates on a revolutionary invention, the tiered publishing system, initially addressing specific communities of scholars, and gradually climbing up to broader public understanding, thus serving the interests of the lay society, too.

Dedication to Quality

Each Frontiers article is a landmark of the highest quality, thanks to genuinely collaborative interactions between authors and review editors, who include some of the world's best academicians. Research must be certified by peers before entering a stream of knowledge that may eventually reach the public - and shape society; therefore, Frontiers only applies the most rigorous and unbiased reviews.
Frontiers revolutionizes research publishing by freely delivering the most outstanding research, evaluated with no bias from both the academic and social point of view.
By applying the most advanced information technologies, Frontiers is catapulting scholarly publishing into a new generation.

What are Frontiers Research Topics?

Frontiers Research Topics are very popular trademarks of the Frontiers Journals Series: they are collections of at least ten articles, all centered on a particular subject. With their unique mix of varied contributions from Original Research to Review Articles, Frontiers Research Topics unify the most influential researchers, the latest key findings and historical advances in a hot research area! Find out more on how to host your own Frontiers Research Topic or contribute to one as an author by contacting the Frontiers Editorial Office: **researchtopics@frontiersin.org**

BIOTECHNOLOGY OF MICROALGAE, BASED ON MOLECULAR BIOLOGY AND BIOCHEMISTRY OF EUKARYOTIC ALGAE AND CYANOBACTERIA

Topic Editors:
Takashi Osanai, Meiji University, Japan
Youn-Il Park, Chungnam National University, South Korea
Yuki Nakamura, Academia Sinica, Taiwan

Citation: Osanai, T., Park, Y-Il., Nakamura, Y., eds. (2017). Biotechnology of Microalgae, Based on Molecular Biology and Biochemistry of Eukaryotic Algae and Cyanobacteria. Lausanne: Frontiers Media. doi: 10.3389/978-2-88945-129-6

Table of Contents

frontiers in Microbiology

EDITORIAL
published: 01 February 2017
doi: 10.3389/fmicb.2017.00118

Editorial: Biotechnology of Microalgae, Based on Molecular Biology and Biochemistry of Eukaryotic Algae and Cyanobacteria

Takashi Osanai[1]*, *Youn-Il Park*[2]* and *Yuki Nakamura*[3]*

[1] School of Agriculture, Meiji University, Kawasaki, Japan, [2] Department of Biological Sciences, Chungnam National University, Daejeon, South Korea, [3] Institute of Plant and Microbial Biology, Academia Sinica, Taipei, Taiwan

Keywords: ***Chlamydomonas***, ***Chlorella***, **cyanobacteria, metabolic engineering, microalgae, photoreceptor,** ***Synechocystis***, **triacylglycerol**

Editorial on the Research Topic

Biotechnology of Microalgae, Based on Molecular Biology and Biochemistry of Eukaryotic Algae and Cyanobacteria

Microalgae, including eukaryotic algae and cyanobacteria, comprise a diverse group of microscopic unicellular photosynthetic organisms that inhabit almost all ecological niches. Recently, energy and resource production using microalgae have received a great deal of attention (Banerjee et al., 2016). Several species of microalgae are commercially available. They include *Arthrospira platensis*, *Chlorella* species, and *Euglena gracilis* (Koller et al., 2014; Gouveia et al., 2016; Yamada et al., 2016). Microalgae produce high-value products such as pigments, lipids, bioplastics, carbohydrates, and amino acids (Minhas et al., 2016). However, production by microalgae is generally less efficient than current industrial production. To increase productivity, a basic understanding of photosynthesis, metabolism, and the cellular structure of microalgae using molecular genetics is indispensable. Here, we introduce current researches, which cover the basic and applied science of eukaryotic algae and cyanobacteria.

The study of the primary carbon metabolism of photosynthetic organisms has a long history, and basic scientists have devoted their time to deciphering the regulatory mechanisms of primary metabolism and the biochemical properties of metabolic enzymes. Basic scientists have studied the regulator mechanisms of anabolic carbon processes such as carbon fixation, gluconeogenesis, and glycogen/starch production. However, the regulatory mechanisms of the catabolic processes of microalgae have been less well studied. The downstream metabolites of sugar catabolism are the precursors of biofuels and bulk chemicals, and an understanding of metabolic sugar regulation would therefore lead to improvements in productive capacity and chemical variety (Oliver et al., 2016). Unicellular cyanobacteria, such as *Synechocystis* and *Synechococcus* species, and filamentous cyanobacteria, such as *Nostoc* species, are the preferred microbial cell factories because they are easy to genetically manipulate (Atsumi et al., 2009; Khanna and Lindblad, 2015). Recently, there has been an increase in the number of publications dealing with the metabolic engineering of cyanobacteria. Several transcriptional regulators that activate the gene expression of sugar catabolic enzymes in cyanobacteria have been identified in *Synechocystis*; for example, an RNA polymerase sigma factor (SigE) and a response regulator (Rre37) (Osanai et al., 2011, 2014). Overexpression of these genes causes increased production of polyhydroxybutyrates, which are bioplastic polyesters (Osanai et al., 2014). Therefore, the elucidation of the regulatory mechanism of primary carbon metabolism would be important.

OPEN ACCESS

Edited by:
William James Hickey, University of Wisconsin-Madison, USA

Reviewed by:
Regina-Michaela Wittich, Spanish High Council for Scientific Research - Estación Experimental del Zaidín, Spain

***Correspondence:**
Takashi Osanai
tosanai@meiji.ac.jp
Youn-Il Park
yipark@cnu.ac.kr
Yuki Nakamura
nakamura@gate.sinica.edu.tw

Specialty section:
This article was submitted to Microbiotechnology, Ecotoxicology and Bioremediation, a section of the journal Frontiers in Microbiology

Received: *18 November 2016*
Accepted: *17 January 2017*
Published: *01 February 2017*

Citation:
Osanai T, Park Y-I and Nakamura Y (2017) Editorial: Biotechnology of Microalgae, Based on Molecular Biology and Biochemistry of Eukaryotic Algae and Cyanobacteria. Front. Microbiol. 8:118. doi: 10.3389/fmicb.2017.00118

An understanding of photosynthetic electron transport systems and light-to-chemical energy conversion is indispensable for biorefineries. Varying light conditions mean that photoautotrophs must sense light intensity, quality, and light/dark photoperiods to carry out optimal photosynthesis (Eberhard et al., 2008). Near-UV light, which causes damage to the photosynthetic apparatus, is effectively screened-out by light-blocking pigments such as anthocyanin and other near-UV absorbing pigments. The application of multiple interdisciplinary approaches has expanded our knowledge of the structure and function of traditionally well-characterized photoreceptors and their downstream signaling mechanisms. The last 10 years in particular have witnessed discoveries in the newly emerging field of plant photobiology, especially bilin photoreceptor phytochromes (Rockwell and Lagarias, 2010).

Various types of cyanobacterial phytochromes have been discovered using genomic information from *Synechocystis*, and heterocystous (*Nostoc punctiforme*) and non-heterocystous (*Microcoleus* IPPAS B353) cyanobacteria; they are distinguished by their domain structures and by the number of cysteine (Cys) amino acid residues they contain, which play a role in the attachment of tetrapyrrole chromophores. Cyanobacteria are able to sense near-UV and the entire visible light range using various bilin photoreceptors. Their biological functions are implicated in positive and negative phototaxis, state transition, and salt acclimation, and to a lesser extent in other photobiological responses such as carotenoid accumulation and filament stacking (Wiltbank and Kehoe, 2016). Moreover, photosynthesis is regulated by photoreceptors such as phototropin from the green algae *Chlamydomonas reinhardtii* (Petroutsos et al., 2016) and cyanobacterial phytochromes Cph2 from *Synechocystis* (Schwarzkopf et al., 2014); the discovery of these photoreceptors has paved the way for the study of the coevolution of light-sensing and signaling pathways. Some eukaryotic algae contain phytochromes that are responsive to the visible spectrum, rather than to canonical red/far red light (Rockwell et al., 2014), which is a fascinating aspect of phytochrome evolution. Basically, cyanobacterial bilin photoreceptors transduce signals to the immediate downstream component via phosphorylation. These phosphorylated components often act as transcriptional factors, activating the downstream cascade related to transition state and phototaxis. Using these two-component systems, optogenetic approaches can be applied to selectively regulate gene expression for nutrient uptake and augment particular metabolic pathways in the field of biotechnology (Narikawa et al., 2015).

The study of the regulatory mechanisms that maintain cellular structure is also important for both basic and applied science. Lipids are the major constituents of cellular membranes (Li-Beisson et al., 2016). More specifically, microalgae contain thylakoid membranes, which are the sites of photosynthetic reactions that require the absorption of light energy to split water, and produce oxygen, ATP, and reductants. Moreover, lipids can be converted into biofuels. Microalgae are known for their high capacity for lipid production. Triacylglycerols and other neutral lipids are the major form of storage lipids; they are often termed "oils," and represent an inert end-product of photosynthetic carbon assimilation. Compared with the higher plants in which storage lipid accumulation only occurs in limited types of tissues/cells, unicellular microalgae have a high degree of flexibility that alters cellular lipid metabolic flux (i.e., lipid biosynthesis for photosynthetic membrane constructions such as in plant leaves, or lipid accumulation for storage in plant seeds) during growth. For instance, nitrogen starvation alters the growth phase of algae and induces oil accumulation at the expense of cellular membrane lipids in many algal species. Thus, flexible lipid metabolic flux in unicellular systems, overall high lipid productivity, photosynthetic capacity that allows carbon fixation, and rapidly growing gene manipulation technologies, have promoted the use of microalgae as an emerging synthetic platform in metabolic engineering. A basic understanding of complex algal lipid metabolism will guide us to the most feasible and effective strategies for creating biofuels.

Therefore, microalgae have great potential for biofuel and biomaterial production. However, this translational research requires knowledge of molecular biology and biochemistry. Therefore, we believe that these researches contribute to crossing the "valley of death" (the gap between basic research and commercialization) in the future.

AUTHOR CONTRIBUTIONS

All the authors of this manuscript confirmed their contribution and approved it for publication.

ACKNOWLEDGMENTS

This work was supported by the Ministry of Education, Culture, Sports, Science, and Technology, Japan; by a grant to TO from ALCA (Project name "Production of cyanobacterial succinate by the genetic engineering of transcriptional regulators and circadian clocks") from the Japan Science and Technology Agency; and by the JSPS KAKENHI Grant-in-Aid for Scientific Research on Innovative Areas Grant Number 16H06559.

REFERENCES

Atsumi, S., Higashide, W., and Liao, J. C. (2009). Direct photosynthetic recycling of carbon dioxide to isobutyraldehyde. *Nat. Biotechnol.* 27, 1177–1180. doi: 10.1038/nbt.1586

Banerjee, C., Dubey, K. K., and Shukla, P. (2016). Metabolic engineering of microalgal based biofuel production: prospects and challenges. *Front. Microbiol.* 7:432. doi: 10.3389/fmicb.2016.00432

Eberhard, S., Finazzi, G., and Wollman, F. A. (2008). The dynamics of photosynthesis. *Annu. Rev. Genet.* 42, 463–515. doi: 10.1146/annurev.genet.42.110807.091452

Gouveia, L., Graça, S., Sousa, C., Ambrosano, L., Ribeiro, B., Botrel, E. P., et al. (2016). Microalgae biomass production using wastewater: treatment and costs: scale-up considerations. *Algal Res.* 16, 167–176. doi: 10.1016/j.algal.2016.03.010

Khanna, N., and Lindblad, P. (2015). Cyanobacterial hydrogenases and hydrogen metabolism revisited: recent progress and future prospects. *Int. J. Mol. Sci.* 16, 10537–10561. doi: 10.3390/ijms160510537

Koller, M., Muhr, A., and Braunegg, G. (2014). Microalgae as versatile cellular factories for valued products. *Algal Res.* 6, 52–63. doi: 10.1016/j.algal.2014.09.002

Li-Beisson, Y., Nakamura, Y., and Harwood, J. (2016). Lipids: from chemical structures, biosynthesis, and analyses to industrial applications. *Subcell. Biochem.* 86, 1–18. doi: 10.1007/978-3-319-25979-6_1

Minhas, A. K., Hodgson, P., Barrow, C. J., and Adholeya, A. (2016). A review on the assessment of stress conditions for simultaneous production of microalgal lipids and carotenoids. *Front. Microbiol.* 7:546. doi: 10.3389/fmicb.2016.00546

Narikawa, R., Nakajima, T., Aono, Y., Fushimi, K., Enomoto, G., Ni-Ni-Win, et al. (2015). A biliverdin-binding cyanobacteriochrome from the chlorophyll d-bearing cyanobacterium *Acaryochloris marina*. *Sci. Rep.* 5:7950. doi: 10.1038/srep07950

Oliver, N. J., Rabinovitch-Deere, C. A., Carroll, A. L., Nozzi, N. E., Case, A. E., and Atsumi, S. (2016). Cyanobacterial metabolic engineering for biofuel and chemical production. *Curr. Opin. Chem. Biol.* 35, 43–50. doi: 10.1016/j.cbpa.2016.08.023

Osanai, T., Oikawa, A., Azuma, M., Tanaka, K., Saito, K., Hirai, M. Y., et al. (2011). Genetic engineering of group 2 sigma factor SigE widely activates expressions of sugar catabolic genes in *Synechocystis* species PCC 6803. *J. Biol. Chem.* 286, 30962–30971. doi: 10.1074/jbc.M111.231183

Osanai, T., Oikawa, A., Numata, K., Kuwahara, A., Iijima, H., Doi, Y., et al. (2014). Pathway-level acceleration of glycogen catabolism by a response regulator in the cyanobacterium *Synechocystis* species PCC 6803. *Plant Physiol.* 164, 1831–1841. doi: 10.1104/pp.113.232025

Petroutsos, D., Tokutsu, R., Maruyama, S., Flori, S., Greiner, A., Magneschi, L., et al. (2016). A blue-light photoreceptor mediates the feedback regulation of photosynthesis. *Nature* 537, 563–566. doi: 10.1038/nature19358

Rockwell, N. C., Duanmu, D., Martin, S. S., Bachy, C., Price, D. C., Bhattacharya, D., et al. (2014). Eukaryotic algal phytochromes span the visible spectrum. *Proc. Natl. Acad. Sci. U.S.A.* 111, 3871–3876. doi: 10.1073/pnas.1401871111

Rockwell, N. C., and Lagarias, J. C. (2010). A brief history of phytochromes. *Chemphyschem* 11, 1172–1180. doi: 10.1002/cphc.200900894

Schwarzkopf, M., Yoo, Y. C., Hückelhoven, R., Park, Y. M., and Proels, R. K. (2014). Cyanobacterial phytochrome2 regulates the heterotrophic metabolism and has a function in the heat and high-light stress response. *Plant Physiol.* 164, 2157–2166. doi: 10.1104/pp.113.233270

Wiltbank, L. B., and Kehoe, D. M. (2016). Two cyanobacterial photoreceptors regulate photosynthetic light harvesting by sensing teal, green, yellow, and red light. *MBio* 7:e02130-15. doi: 10.1128/mBio.02130-15

Yamada, K., Suzuki, H., Takeuchi, T., Kazama, Y., Mitra, S., Abe, T., et al. (2016). Efficient selective breeding of live oil-rich *Euglena gracilis* with fluorescence-activated cell sorting. *Sci. Rep.* 6:26327. doi: 10.1038/srep26327

Conflict of Interest Statement: The authors declare that the research was conducted in the absence of any commercial or financial relationships that could be construed as a potential conflict of interest.

frontiers in Microbiology

PROTOCOLS
published: 21 September 2016
doi: 10.3389/fmicb.2016.01509

A Screening Method for the Isolation of Polyhydroxyalkanoate-Producing Purple Non-sulfur Photosynthetic Bacteria from Natural Seawater

*Mieko Higuchi-Takeuchi, Kumiko Morisaki and Keiji Numata**

Enzyme Research Team, Biomass Engineering Research Division, RIKEN Center for Sustainable Resource Science, Wako, Japan

Polyhydroxyalkanoates (PHAs) are a family of biopolyesters accumulated by a variety of microorganisms as carbon and energy storage under starvation conditions. We focused on marine purple non-sulfur photosynthetic bacteria as host microorganisms for PHA production and developed a method for their isolation from natural seawater. To identify novel PHA-producing marine purple non-sulfur photosynthetic bacteria, natural seawaters were cultured in nutrient-rich medium for purple non-sulfur photosynthetic bacteria, and twelve pink- or red-pigmented colonies were picked up. Gas chromatography mass spectrometry analysis revealed that four isolates synthesized PHA at levels ranging from 0.5 to 24.4 wt% of cell dry weight. The 16S ribosomal RNA sequence analysis revealed that one isolate (HM2) showed 100% identity to marine purple non-sulfur photosynthetic bacteria. In conclusion, we have demonstrated in this study that PHA-producing marine purple non-sulfur photosynthetic bacteria can be isolated from natural seawater under nutrient-rich conditions.

Keywords: polyhydroxyalkanoates, marine purple non-sulfur photosynthetic bacteria, seawater, nutrient-rich conditions, 16S rRNA

OPEN ACCESS

Edited by:
Yuki Nakamura,
Institute of Plant and Microbial Biology (Academia Sinica), Taiwan

Reviewed by:
Kesaven Bhubalan,
Universiti Malaysia Terengganu, Malaysia
Vidya De Gannes,
The University of the West Indies–St. Augustine Campus, Trinidad and Tobago

****Correspondence:***
Keiji Numata
keiji.numata@riken.jp

Specialty section:
This article was submitted to Microbiotechnology, Ecotoxicology and Bioremediation, a section of the journal Frontiers in Microbiology

Received: *27 July 2016*
Accepted: *09 September 2016*
Published: *21 September 2016*

Citation:
Higuchi-Takeuchi M, Morisaki K and Numata K (2016) A Screening Method for the Isolation of Polyhydroxyalkanoate-Producing Purple Non-sulfur Photosynthetic Bacteria from Natural Seawater. Front. Microbiol. 7:1509. doi: 10.3389/fmicb.2016.01509

INTRODUCTION

Polyhydroxyalkanoates (PHAs) are biopolyesters that many microorganisms accumulate as intracellular reservoirs of carbon and energy. PHAs have attracted increasing attention due to their biomass-based origin and biodegradability (Numata et al., 2009). However, PHA production requires a costly carbon source, such as sugars or plant oils. The use of photosynthetic organisms to produce materials is clean and eco-friendly because the energy for growth is derived from the sun, and the carbon is derived from carbon dioxide in the air. Although efforts have been made to utilize photosynthetic organisms such as cyanobacteria and higher plants for PHA production, high PHA production has not been achieved to date (Osanai et al., 2013, 2014). Anoxygenic photosynthetic bacteria are known to produce more PHA (Liebergesell et al., 1991) than cyanobacteria and higher plants. However, PHA production by photosynthetic bacteria has been studied in a small number of freshwater purple non-sulfur photosynthetic bacteria strains, such as *Rhodospirillum rubrum* (Brandl et al., 1989; Clemente et al., 2000), *Rhodopseudomonas sphaeroides* (Lorrungruang et al., 2006) and *Rhodobacter capsulatus* (Kranz et al., 1997). Purple non-sulfur photosynthetic bacteria have several advantages over other photosynthetic bacteria. One advantage is that purple non-sulfur photosynthetic bacteria can grow either aerobically in the dark or anaerobically in the

light. In addition, purple non-sulfur photosynthetic bacteria can utilize various electron acceptors, i.e., they are facultative photosynthetic bacteria (Mcewan, 1994; Basak and Das, 2007). To take advantage of these properties, purple non-sulfur photosynthetic bacteria have been tested for use in a variety of applications, including not only PHA production but also the purification of industrial wastewater (Kim et al., 2004; Wu et al., 2012) and hydrogen production (Basak and Das, 2007).

Marine microorganisms are important bioresources and expected to produce new value-added compounds, including PHA (Numata and Doi, 2012; Numata et al., 2013; Numata and Morisaki, 2015). Cultivation under marine conditions offers several advantages for the industrial production of PHA. For example, high concentrations of salts inhibit the growth of salt-sensitive bacteria species. In addition, filtered sterilized seawater can be used as a culture medium. However, PHA production under marine conditions has been reported using certain types of marine bacteria (Lopez et al., 2009; Shrivastav et al., 2010; Numata and Doi, 2012). Although PHA production by marine purple non-sulfur photosynthetic bacteria has been reported by a few groups (Chowdhury et al., 1996; Xiao and Jiao, 2011), the details of the PHA synthesis were not studied thoroughly. The small number of studies on PHA synthesis by marine purple non-sulfur photosynthetic bacteria, even though they are important host bacteria to produce PHA, is because no isolation method of PHA-producing marine purple non-sulfur photosynthetic bacteria has been established until now.

Many screening methods have been developed to detect microorganisms that accumulate PHAs. The methods most widely used for detecting PHAs are staining techniques using Nile red (Spiekermann et al., 1999), Nile blue A (Ostle and Holt, 1982) and Sudan Black (Steinbuchel et al., 1987). Using these staining techniques, a variety of PHA-producing bacteria and mutants have been isolated. However, this method is unable to discriminate PHA and lipids. Additionally, it is necessary to provide nutrient limitation conditions and suitable carbon sources to the bacterial cells to induce PHA production. Purple photosynthetic bacteria contain bacteriochlorophyll *a* or *b* and various types of carotenoids. Staining methods are not suitable for purple non-sulfur photosynthetic bacteria because these pigments interfere with staining and detection. The other method for identifying PHA-producing bacteria is the polymerase chain reaction (PCR) amplification of PHA synthesis genes using degenerate primers (Sheu et al., 2000; Shamala et al., 2003). This technique is a rapid and accurate detection system for screening large numbers of environmental isolates. However, this technique leads to detection errors because of the non-specific PCR amplification and lack of PCR products due to degenerate primer sequences. Furthermore, this method cannot detect PHA itself, and hence PHA and its induction conditions must be determined after the discovery of PHA biosynthesis genes. Therefore, it is necessary to develop a screening method for the isolation of PHA-producing marine purple non-sulfur photosynthetic bacteria.

In a previous study, we evaluated the potential use of marine purple photosynthetic bacteria for PHA production (Higuchi-Takeuchi et al., 2016). Our study demonstrated that marine purple photosynthetic bacteria were good host microorganisms for industrial PHA production using marine resources. The aim of our study is to develop an approach to isolate PHA-producing purple photosynthetic bacteria from natural marine environments. We found that purple sulfur photosynthetic bacteria did not accumulate PHA under nutrient-rich conditions, whereas some species of purple non-sulfur photosynthetic bacteria did accumulate PHA without nutrient limitation, in contrast to the well-known PHA-producing soil bacteria (Higuchi-Takeuchi et al., 2016). Purple photosynthetic bacterial cultures can be purple, red, brown or orange because of the various types of carotenoids and bacteriochlorophyll. Based on these observations, in this study, we isolated pigmented bacteria under nutrient-rich conditions as PHA-producing purple non-sulfur photosynthetic bacteria from natural seawaters.

MATERIALS AND METHODS

Culture Conditions and Seawater Sampling

Purple non-sulfur bacteria were grown in culture medium (JCM medium number 520)[1]. The composition was modified based on the medium used for isolation of purple non-sulfur bacteria (Biebl and Pfennig, 1981). Medium was composed of the following components per liter: KH_2PO_4 (0.5 g); $CaCl_2{\cdot}2H_2O$ (0.25 g); $MgSO_4{\cdot}7H_2O$ (3.0 g); NH_4Cl (0.68 g); NaCl (20 g); sodium malate (3.0 g); sodium pyruvate (3.0 g); yeast extract (0.4 g); ferric citrate (5 mg); vitamin B_{12} (2 mg); $ZnCl_2{\cdot}5H_2O$ (70 μg); $MnCl_2{\cdot}4H_2O$ (100 μg); H_3BO_3 (60 μg); $CoCl_2{\cdot}6H_2O$ (200 μg); $CuCl_2{\cdot}2H_2O$ (20 μg); $NiCl_2{\cdot}6H_2O$ (20 μg) and $Na_2MoO_4{\cdot}H_2O$ (40 μg). The pH was adjusted to 6.8. Yeast extract (Culture media grade) and ferric citrate (BioReagent grade) were purchased from Becton Dickinson (Franklin Lakes, NJ, USA) and Sigma-Aldrich (St. Louis, MO, USA), respectively. The rest chemicals (JIS Special Grade) were purchased from Wako Chemicals (Osaka, Japan).

For screening, aliquots of 100 μL of each seawater sample from all sampling points were spread in agar plates. Seawaters were cultured multiple times until pigmented-colony was obtained. Maximum number of replicates was six. Six replicates were carried out using seawaters from Naha, Tokyo-Bay and Sakata. The number of replicates was five in Omura-Bay sample, six in Tokyo-Bay, four in Aioi-Bay, two in Takamatsu and two in Yokohama. Seawaters were cultured aerobically under continuous far-red LED light conditions (730 nm, 8 Wm^{-2}) at 30°C. Addition of larger amount of seawater and concentration of seawater using filter paper might be effective for obtaining the large number of bacterial colonies. The isolated colonies were streaked onto other plates for purification. Streak plating should be done until the pure colonies from single bacteria are isolated. Transferring of small volume of cell culture (1.5 mL) into large scale culture (50 mL) is recommended for better bacterial growth. The isolates were transferred to 1.5 mL capped plastic tubes filled with liquid medium and cultured for 7–10 days under continuous

[1]http://www.jcm.riken.jp/cgi-bin/jcm/jcm_grmd?GRMD=520

far-red LED light conditions at 30°C and then transferred in 50 mL screw capped plastic tubes filled with liquid medium and cultured without stirring for 10 days. To transfer into liquid culture, transferring a small amount of bacteria cells (not a single colony) using inoculating loops under aseptic conditions is preferred for good bacterial cell growth. Bacterial cells were stored as 10% glycerol (JIS Special Grade, Wako Chemicals, Osaka, Japan) stocks at −80°C for further experiments.

About 50 mL of natural seawaters were collected from Naha (Okinawa), Omura-Bay (Nagasaki), Tokyo-Bay (Tokyo), Aioi-Bay (Hyogo), Sakata (Yamagata), Takamatsu (Kagawa) and Yokohama (Kanagawa) in Japan. Sampling points were randomly selected. One seawater sample was collected from the sea surface in each point. Sampled seawaters were stored at 4°C in the dark until use.

Analysis of PHA Content and Composition

The PHA content characterization method was modified slightly from a previous study (Chuah et al., 2013). Approximately 0.5–2 mg lyophilized cells were incubated in 1 mL of 100% ethanol at 70°C for 1 h to remove pigments. The cells were then subjected to ethanolysis in the presence of 250 μL chloroform (JIS Special Grade, Wako Chemicals, Osaka, Japan), 100 μL hydrochloric acid (JIS Special Grade, Wako Chemicals, Osaka, Japan) and 850 μL ethanol (JIS Special Grade, Wako Chemicals, Osaka, Japan) at 100°C for 4 h. After cooling, 1 mL of phosphate buffer (pH 8.1) was added to the reaction mixture and then neutralized with 0.65 N NaOH. After centrifugation at 1,500 rpm for 5 min (CF16RN, Hitachi-Koki, Tokyo, Japan), the lower chloroform layer was filtered through anhydrous sodium sulfate (JIS Special Grade, Wako Chemicals, Osaka, Japan) and incubated with molecular sieves 4A (Nacalai tesque, Kyoto, Japan) for 30 min. The PHA content and composition were determined using a gas chromatography–mass spectrometry (GC-MS) apparatus (GCMS-QP2010 Ultra, Shimadzu, Tokyo, Japan) equipped with a 30 mm × 0.25 mm DB-1 capillary gas chromatography column (Agilent Technologies, Santa Clara, CA, USA). For analysis, 1 μL of sample solution was injected with helium as a carrier gas (3.30 mL min^{-1}). The following temperature program was used to separate ethyl esters: 45°C for 1 min, temperature ramp of 7°C per min to 117°C. The interface and ion source temperatures were 250°C and 230°C, respectively. The 3HB content was determined using a calibration curve.

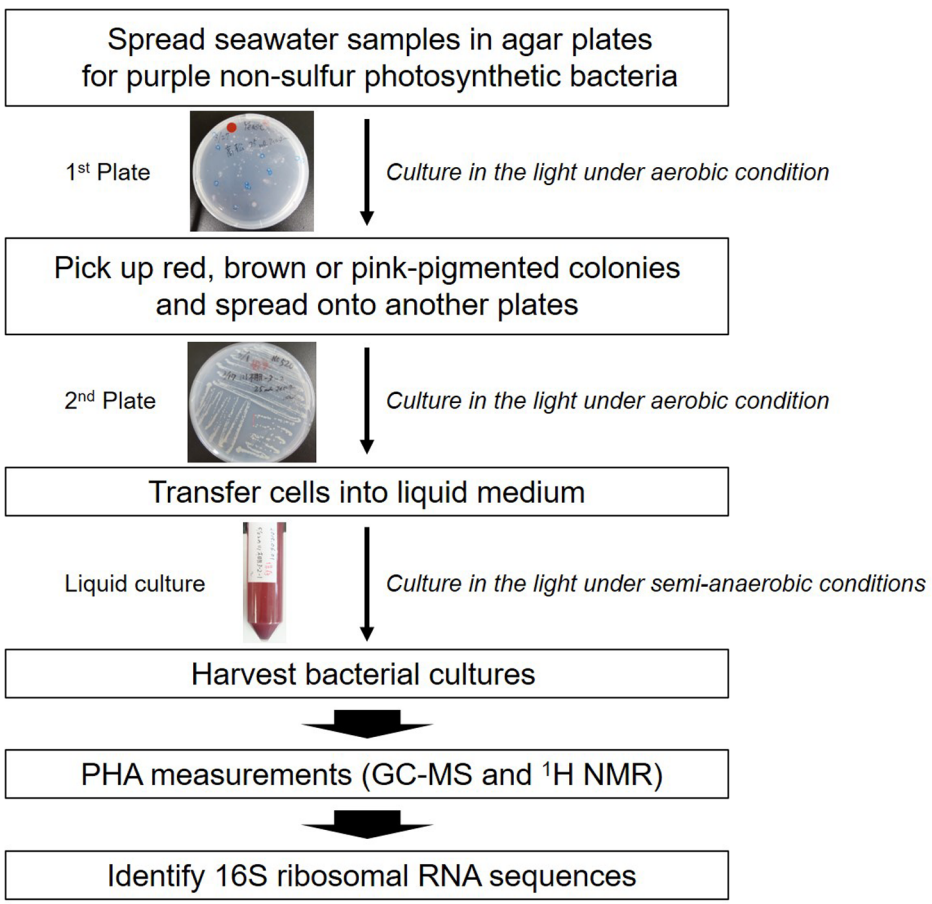

FIGURE 1 | Isolation scheme for PHA-producing purple non-sulfur photosynthetic bacteria.

Extraction of PHAs and ^{1}H NMR analysis

PHA extraction and purification was carried out according to the method reported in (Brandl et al., 1989). PHAs were extracted from 428 mg lyophilized cells using about 100 mL of chloroform (JIS Special Grade, Wako Chemicals, Osaka, Japan). The chloroform extracts were filtered and concentrated using a rotary vacuum evaporator (NA-1, AS ONE, Osaka, Japan), and the chloroform-extracted PHAs were purified by precipitation with hexane (JIS Special Grade, Wako Chemicals, Osaka, Japan) of more than 10 times the volume of the solvent. The precipitate was filtered and then air-dried without vacuum as a convenient way overnight at room temperature. The polymer solution was concentrated again using a rotary vacuum evaporator and purified by precipitation with cold methanol (JIS Special Grade, Wako Chemicals, Osaka, Japan) of more than 10 times the volume of the solvent. The purified PHA precipitate was air-dried overnight at room temperature.

The purified PHAs were analyzed by proton nuclear magnetic resonance (^{1}H NMR; JNM-Excalibur 270; JEOL, Ltd., Tokyo, Japan) to determine their chemical structures and compositions. The measuring frequency was 499.87 MHz. The sample for NMR analysis was dissolved at a concentration of 4 mg/mL in $CDCl_3$ with 0.05% (v/v) tetramethylsilane (TMS; Wako Pure Chemical Industries Ltd., Osaka, Japan).

Determination of 16S Ribosomal RNA Sequences and Phylogenetic Analysis

DNA was extracted using the DNeasy Blood & Tissue Kit (Qiagen, Hilden, Germany). The 16S ribosomal RNA sequences were determined using the Bacterial 16S rDNA PCR kit according to the manufacturer's protocol (Takara Bio, Shiga, Japan).

The phylogenetic tree was prepared based on the 16S ribosomal RNA sequences of the 13 selected purple photosynthetic bacteria and constructed using Phylogeny[2] (Castresana, 2000; Edgar, 2004; Anisimova and Gascuel, 2006; Dereeper et al., 2008; Guindon et al., 2010). NJplot was used to display the phylogenetic tree (Perriere and Gouy, 1996).

RESULTS AND DISCUSSION

The screening strategy for PHA-producing purple non-sulfur photosynthetic bacteria is shown in **Figure 1**. In the case of well-known PHA-producing bacteria, PHA production is induced under nutrient(s)-free conditions such as nitrogen, phosphorus or sulfur. We previously found that purple non-sulfur photosynthetic bacteria could accumulate PHA without nutrient deficiency (Higuchi-Takeuchi et al., 2016). Nutrient deficiency conditions are not appropriate for the isolation of PHA-producing purple non-sulfur photosynthetic bacteria from natural environments because such conditions result in poor bacterial growth. Therefore, seawaters were cultured in nutrient-rich agar plates for the growth of marine purple non-sulfur photosynthetic bacteria. To select PHA-producing purple non-sulfur photosynthetic bacteria by color, the plates were cultivated under continuous far-red light conditions. After extended cultivation, a red- or pink-pigmented colony typical of purple photosynthetic bacteria was picked up. The selected colony was cultured in liquid medium, and the harvested cells were subjected to GC-MS analysis to measure their PHA content. Lastly, the 16S rRNA sequences were determined to identify the bacterial species.

To obtain purple non-sulfur photosynthetic bacteria colonies, each seawater sample from all sampling points was spread in nutrient-rich agar plates for the growth of purple non-sulfur

[2]http://phylogeny.lirmm.fr/phylo_cgi/index.cgi

TABLE 1 | PHA content (wt%) of isolates.

Isolates	CDW (mg/L)	PHA (wt%)	Source of isolate
HM1	184	1.0	Omura-Bay (Nagasaki)
HM2	46	24.4	Omura-Bay (Nagasaki)
HM3	127	18.0	Takamatsu (Kagawa)
HM4	50	n.d.	Takamatsu (Kagawa)
HM5	49	n.d.	Aioi-Bay (Hyogo)
HM6	99	0.5	Yokohama (Kanagawa)
HM7	105	n.d.	Yokohama (Kanagawa)
HM8	64	n.d.	Yokohama (Kanagawa)
HM9	119	n.d.	Yokohama (Kanagawa)
HM10	102	n.d.	Yokohama (Kanagawa)
HM11	103	n.d.	Yokohama (Kanagawa)
HM12	95	n.d.	Yokohama (Kanagawa)

n.d., not detected.

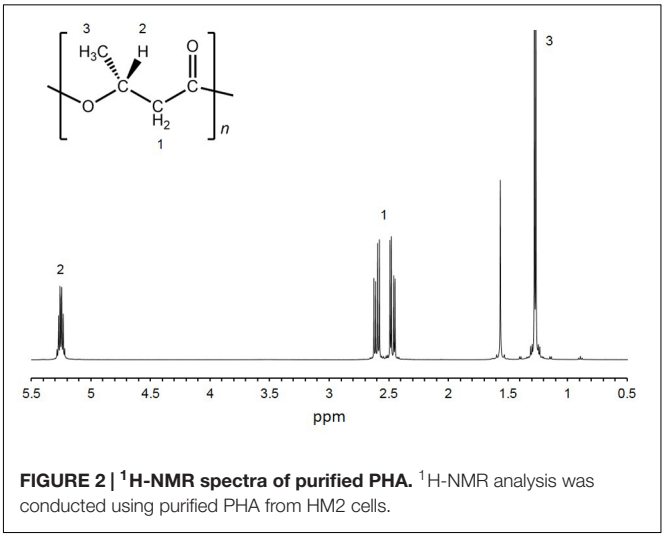

FIGURE 2 | ^{1}H-NMR spectra of purified PHA. ^{1}H-NMR analysis was conducted using purified PHA from HM2 cells.

TABLE 2 | 16S ribosomal RNA sequences of isolates.

Isolate	Closest relative	GenBank accession no.	Identity (%)	Identity (match bp/ total bp)
HM 1	*Marinobacter guineae*	KF500390	99.9	1420/1422
HM 2	*Afifella marina*	NR_117676	100.0	1336/1336
	Rhodopseudomonas julia	NR_040937		
HM 3	*Shewanella basaltis*	KC534403	99.8	1287/1290
HM 6	*Shewanella basaltis*	KC534403	99.9	1254/1255

photosynthetic bacteria and cultured aerobically in the light. Most bacterial colonies appeared white, cream or yellow in color after 1 day (Supplementary Figure 1C). Some bacteria produced pink or red colonies after 4–7 days (Supplementary Figures 1A,B). Extended incubation times may permit the appearance of more pigmented-colonies although they result in growth of bacteria other than purple non-sulfur photosynthetic bacteria. A total of twelve red or pink colonies were obtained from four seawater samples (**Table 1**). HM1 and HM2 were obtained from the seawater of Omura-Bay; HM3 and HM4 were obtained from the seawater of Takamatsu; HM5 was obtained from the seawater of Aioi-Bay; and seven isolates (HM5 to HM12) were isolated from the seawater of Yokohama. Pigmented colonies were streaked onto other plates for further isolation (Supplementary Figures 1D–G). The twelve isolates were then transferred to liquid medium and cultured in the light (Supplementary Figures 1H–K). Among the twelve isolates, HM2 exhibited a bright red color in liquid culture (Supplementay Figure 1I). The cell cultures of the other eleven isolates were red in color after centrifugation (right side of Supplementary Figures 1H,J,K), although the liquid culture appeared to exhibit a very faint pink color or no color production (left side of Supplementary Figures 1H,J,K). Based on the results of the liquid cell cultures, HM2 was the only positive strain, namely, purple photosynthetic bacteria.

Twelve isolates were cultured in growth medium and then measured the cell dry weight (CDW) and PHA content. CDW varied among the isolates, ranging from 46 to 184 mg/L culture (**Table 1**). The PHA content of the twelve isolates was measured by GC-MS. PHA was not detected in eight isolates. Four isolates (HM1, HM2, HM3 and HM6) synthesized PHA at levels ranging from 0.5 to 24.4 wt% of CDW (**Table 1**). HM2 showed the highest PHA accumulation (24.4 wt%). To verify these results, the PHA content and CDW of HM2 were measured using triplicate cultures. The CDW of HM2 was 800 ± 58 mg/L culture, and the PHA content was 24.2 ± 1.8 wt%. GC-MS analysis also revealed that four isolates synthesized a homopolymer of 3-hydroxybutyrate (3HB), namely, poly(3-hydroxybutyrate) (PHB). The chemical structure of the synthesized PHAs was determined by ^{1}H NMR with chloroform extracts from HM2 isolate. Methyl, methylene, and methine protons of 3HB units were detected by ^{1}H NMR (**Figure 2**). Thus, the ^{1}H NMR spectra confirmed the chemical structure of PHB.

The 16S ribosomal RNA sequences of four isolates were determined and compared with the databank contents using Nucleotide BLAST. Two isolates (HM3 and HM6) showed more than 99% sequence identity to *Shewanella basaltis,* and one isolate (HM1) exhibited high similarity to *Marinobacter guineae* (**Table 2**). *S. basaltis* (Chang et al., 2008) and *M. guineae* (Montes et al., 2008) are marine bacteria but not purple non-sulfur photosynthetic bacteria. The isolate HM2, which was positive by color selection in liquid culture and accumulated the largest amount of PHA, showed 100% identity to the purple non-sulfur photosynthetic bacteria *Afifella marina* (Imhoff, 1983)

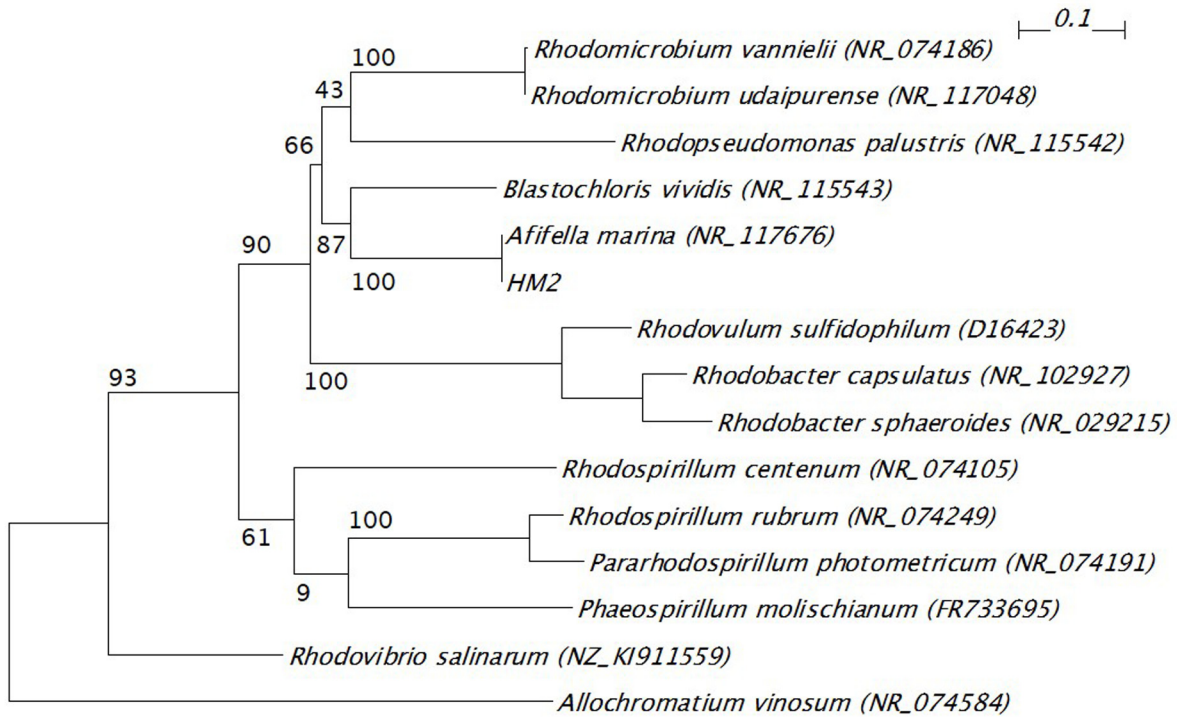

FIGURE 3 | Phylogenetic tree of 16S ribosomal RNA gene from HM2 and purple non-sulfur photosynthetic bacteria. The scale bar shows the number of nucleotide substitutions per site. GenBank accession numbers are given in parentheses. The bootstrap values are shown at branch nodes. *Allochromatium vinosum* was used as an outgroup.

and *Rhodopseudomonas julia* (Kompantseva, 1989) isolated from saline environments, indicating that bright pigmented-color in liquid culture is one of important points for isolation of purple non-sulfur bacteria. A phylogenetic tree was constructed based on the 16S rRNA sequences from HM2 and purple non-sulfur photosynthetic bacteria of the alphaproteobacteria that have been studied by whole-genome analysis (**Figure 3**). HM2 was positioned close to *Blastochloris viridis* in the phylogenetic tree. Further characterization of the isolates will be needed to determine the species.

The isolation method we described here identified the strain HM2, which showed the highest PHA production among twelve isolates, and the 16S rRNA sequences of this strain were shown to have high similarity to marine purple non-sulfur photosynthetic bacteria. Based on the data on PHA accumulation and CDW, the PHA content of HM2 was calculated to be 199 ± 16 mg/L culture. Brandl et al. (1989) reported production levels of 500 mg/L PHA in *R. sphaeroides* and 390 mg/L PHA in *R. rubrum*. HM2 showed similar levels of PHA production to these strains. Seawater sampling methods were not optimized in this study. Sampling points were randomly selected and only one seawater sample was collected from each sampling point. Further investigations for sampling methods are required to obtain a lot of marine purple non-sulfur photosynthetic bacteria from natural seawaters. Further optimization of factors such as the PHA induction conditions and screening of PHA-producing marine purple non-sulfur photosynthetic bacteria will allow the development of PHA production by photosynthetic organisms.

CONCLUSION

One isolate identified in this study accumulated 24.4 wt% PHA, and 16S rRNA gene sequence analysis revealed that this strain showed high similarity to marine purple non-sulfur photosynthetic bacteria. Thus, we successfully developed a screening method to isolate PHA-producing purple non-sulfur photosynthetic bacteria under nutrient-rich and far-red light conditions from the natural environment. With this isolation method, PHA production by marine purple non-sulfur photosynthetic bacteria will be studied widely, leading to green and eco-friendly PHA production from carbon dioxide and marine resources.

AUTHOR CONTRIBUTIONS

MH-T and KN conceived and designed the study. KM performed the experiments. MH-T analyzed the data, and MH-T and KN interpreted the data. MH-T drafted the manuscript, and KN and MK approved the manuscript.

FUNDING

This work was supported by Grants-in-Aid for Scientific Research (MH-T), the Impulsing Paradigm Change through Disruptive Technologies Program (ImPACT) (KN) and the RIKEN Biomass Engineering Program (KN).

ACKNOWLEDGMENT

We thank Mr. Ryota Sato and Miss. Nao Ifuku for the seawater sampling.

SUPPLEMENTARY MATERIAL

The Supplementary Material for this article can be found online at: http://journal.frontiersin.org/article/10.3389/fmicb.2016.01509

REFERENCES

Anisimova, M., and Gascuel, O. (2006). Approximate likelihood-ratio test for branches: a fast, accurate, and powerful alternative. *Syst. Biol.* 55, 539–552. doi: 10.1080/10635150600755453

Basak, N., and Das, D. (2007). The prospect of purple non-sulfur (PNS) photosynthetic bacteria for hydrogen production: the present state of the art. *World J. Microbiol. Biotechnol.* 23, 31–42. doi: 10.1007/s11274-006-9190-9

Biebl, H., and Pfennig, N. (1981). "Isolation of members of the family Rhodospirillaceae," in *The Prokaryotes, A Handbook on Habitats, Isolation, and Identification of Bacteria*, eds M. P. Starr, H. Stolp, H. G. Trüper, A. Balows, and H. G. Schlegel (Berlin: Springer), 267–273. doi: 10.1007/978-3-662-13187-9_14

Brandl, H., Knee, E. J. Jr., Fuller, R. C., Gross, R. A., and Lenz, R. W. (1989). Ability of the phototrophic bacterium *Rhodospirillum rubrum* to produce various poly (beta-hydroxyalkanoates): potential sources for biodegradable polyesters. *Int. J. Biol. Macromol.* 11, 49–55. doi: 10.1016/0141-8130(89)90040-8

Castresana, J. (2000). Selection of conserved blocks from multiple alignments for their use in phylogenetic analysis. *Mol. Biol. Evol.* 17, 540–552. doi: 10.1093/oxfordjournals.molbev.a026334

Chang, H. W., Roh, S. W., Kim, K. H., Nam, Y. D., Jeon, C. O., Oh, H. M., et al. (2008). *Shewanella basaltis* sp. nov., a marine bacterium isolated from black sand. *Int. J. Syst. Evol. Microbiol.* 58(Pt 8), 1907–1910. doi: 10.1099/ijs.0.65725-0

Chowdhury, W. Q., Idehara, K., Maeda, I., Umeda, F., Yagi, K., Miura, Y., et al. (1996). Factors affecting polyhydroxybutyrate biosynthesis in the marine photosynthetic bacterium Rhodo*pseudomonas* sp strain W-1S. *Appl. Biochem. Biotechnol.* 5, 361–366. doi: 10.1007/978-1-4612-0223-3_31

Chuah, J., Yamada, M., Taguchi, S., Sudesh, K., Doi, Y., and Numata, K. (2013). Biosynthesis and characterization of polyhydroxyalkanoate containing 5-hydroxyvalerate units: effects of 5HV units on biodegradability, cytotoxicity, mechanical and thermal properties. *Polym. Degrad. Stab.* 98, 331–338. doi: 10.1016/j.polymdegradstab.2012.09.008

Clemente, T., Shah, D., Tran, M., Stark, D., Padgette, S., Dennis, D., et al. (2000). Sequence of PHA synthase gene from two strains of *Rhodospirillum rubrum* and in vivo substrate specificity of four PHA synthases across two heterologous expression systems. *Appl. Microbiol. Biotechnol.* 53, 420–429. doi: 10.1007/s002530051636

Dereeper, A., Guignon, V., Blanc, G., Audic, S., Buffet, S., Chevenet, F., et al. (2008). Phylogeny.fr: robust phylogenetic analysis for the non-specialist. *Nucleic Acids Res.* 36, W465–W469. doi: 10.1093/nar/gkn180

Edgar, R. C. (2004). MUSCLE: multiple sequence alignment with high accuracy and high throughput. *Nucleic Acids Res.* 32, 1792–1797. doi: 10.1093/nar/gkh340

Guindon, S., Dufayard, J. F., Lefort, V., Anisimova, M., Hordijk, W., and Gascuel, O. (2010). New algorithms and methods to estimate maximum-likelihood phylogenies: assessing the performance of PhyML 3.0. *Syst. Biol.* 59, 307–321. doi: 10.1093/sysbio/syq010

Higuchi-Takeuchi, M., Morisaki, K., Toyooka, K., and Numata, K. (2016). Synthesis of high-molecular-weight polyhydroxyalkanoates by marine photosynthetic purple bacteria. *PLoS ONE* 11:e0160981. doi: 10.1371/journal.pone.0160981

Imhoff, J. F. (1983). *Rhodopseudomonas marina* sp. nov., a new marine phototrophic purple bacterium. *Syst. Appl. Microbiol.* 4, 512–521. doi: 10.1016/S0723-2020(83)80009-5

Kim, M. K., Choi, K. M., Yin, C. R., Lee, K. Y., Im, W. T., Lim, J. H., et al. (2004). Odorous swine wastewater treatment by purple non-sulfur bacteria, *Rhodopseudomonas palustris*, isolated from eutrophicated ponds. *Biotechnol. Lett.* 26, 819–822. doi: 10.1023/B:Bile.0000025884.50198.67

Kompantseva, E. I. (1989). A new species of budding purple bacterium: *Rhodopseudomonas julia* sp. nov. *Mikrobiologiya* 58, 319–325.

Kranz, R. G., Gabbert, K. K., Locke, T. A., and Madigan, M. T. (1997). Polyhydroxyalkanoate production in *Rhodobacter capsulatus*: genes, mutants, expression, and physiology. *Appl. Environ. Microbiol.* 63, 3003–3009.

Liebergesell, M., Hustede, E., Timm, A., Steinbuchel, A., Fuller, R. C., Lenz, R. W., et al. (1991). Formation of poly(3-hydroxyalkanoic acids) by phototrophic and chemolithotrophic bacteria. *Arch. Microbiol.* 155, 415–421. doi: 10.1007/BF00244955

Lopez, N. I., Pettinari, M. J., Stackebrandt, E., Tribelli, P. M., Potter, M., Steinbuchel, A., et al. (2009). *Pseudomonas extremaustralis* sp nov., a Poly(3-hydroxybutyrate) producer isolated from an Antarctic environment. *Curr. Microbiol.* 59, 514–519. doi: 10.1007/s00284-009-9469-9

Lorrungruang, C., Martthong, J., Sasaki, K., and Noparatnaraporn, N. (2006). Selection of photosynthetic bacterium *Rhodobacter sphaeroides* 14F for polyhydroxyalkanoate production with two-stage aerobic dark cultivation. *J. Biosci. Bioeng.* 102, 128–131. doi: 10.1263/jbb.102.128

Mcewan, A. G. (1994). Photosynthetic electron-transport and anaerobic metabolism in purple nonsulfur phototrophic bacteria. *Antonie Van Leeuwenhoek* 66, 151–164. doi: 10.1007/Bf00871637

Montes, M. J., Bozal, N., and Mercade, E. (2008). *Marinobacter guineae* sp. nov., a novel moderately halophilic bacterium from an Antarctic environment. *Int. J. Syst. Evol. Microbiol.* 58(Pt 6), 1346–1349. doi: 10.1099/ijs.0.65298-0

Numata, K., Abe, H., and Iwata, T. (2009). Biodegradability of Poly(hydroxyalkanoate) materials. *Materials* 2, 1104–1126. doi: 10.3390/ma2031104

Numata, K., and Doi, Y. (2012). Biosynthesis of polyhydroxyalkanaotes by a novel facultatively anaerobic *Vibrio* sp. under marine conditions. *Mar. Biotechnol.* 14, 323–331. doi: 10.1007/s10126-011-9416-1

Numata, K., and Morisaki, K. (2015). Screening of marine bacteria to synthesize polyhydroxyalkanoate from lignin: contribution of lignin derivatives to biosynthesis by *Oceanimonas doudoroffii*. *ACS Sustain. Chem. Eng.* 3, 569–573. doi: 10.1021/acssuschemeng.5b00031

Numata, K., Morisaki, K., Tomizawa, S., Ohtani, M., Demura, T., Miyazaki, M., et al. (2013). Synthesis of poly- and oligo(hydroxyalkanoate)s by deep-sea bacteria, *Colwellia* spp., *Moritella* spp., and *Shewanella* spp. *Polym. J.* 45, 1094–1100. doi: 10.1038/pj.2013.25

Osanai, T., Numata, K., Oikawa, A., Kuwahara, A., Iijima, H., Doi, Y., et al. (2013). Increased bioplastic production with an RNA polymerase sigma factor SigE during nitrogen starvation in *Synechocystis* sp. PCC 6803. *DNA Res.* 20, 525–535. doi: 10.1093/dnares/dst028

Osanai, T., Oikawa, A., Numata, K., Kuwahara, A., Iijima, H., Doi, Y., et al. (2014). Pathway-level acceleration of glycogen catabolism by a response regulator in the cyanobacterium *Synechocystis* species PCC 6803. *Plant Physiol.* 164, 1831–1841. doi: 10.1104/pp.113.232025

Ostle, A. G., and Holt, J. G. (1982). Nile blue-a as a fluorescent stain for poly-beta-hydroxybutyrate. *Appl. Environ. Microbiol.* 44, 238–241.

Perriere, G., and Gouy, M. (1996). WWW-Query: an on-line retrieval system for biological sequence banks. *Biochimie* 78, 364–369. doi: 10.1016/0300-9084(96)84768-7

Shamala, T. R., Chandrashekar, A., Vijayendra, S. V. N., and Kshama, L. (2003). Identification of polyhydroxyalkanoate (PHA)-producing *Bacillus* spp. using the polymerase chain reaction (PCR). *J. Appl. Microbiol.* 94, 369–374. doi: 10.1046/j.1365-2672.2003.01838.x

Sheu, D. S., Wang, Y. T., and Lee, C. Y. (2000). Rapid detection of polyhydroxyalkanoate-accumulating bacteria isolated from the environment by colony PCR. *Microbiology* 146, 2019–2025. doi: 10.1099/00221287-146-8-2019

Shrivastav, A., Mishra, S. K., Shethia, B., Pancha, I., Jain, D., and Mishra, S. (2010). Isolation of promising bacterial strains from soil and marine environment for polyhydroxyalkanoates (PHAs) production utilizing *Jatropha* biodiesel byproduct. *Int. J. Biol. Macromol.* 47, 283–287. doi: 10.1016/j.ijbiomac.2010.04.007

Spiekermann, P., Rehm, B. H. A., Kalscheuer, R., Baumeister, D., and Steinbuchel, A. (1999). A sensitive, viable-colony staining method using Nile red for direct screening of bacteria that accumulate polyhydroxyalkanoic acids and other lipid storage compounds. *Arch. Microbiol.* 171, 73–80. doi: 10.1007/s002030050681

Steinbuchel, A., Frund, C., Jendrossek, D., and Schlegel, H. G. (1987). Isolation of mutants of alcaligenes-eutrophus unable to derepress the fermentative alcohol-dehydrogenase. *Arch. Microbiol.* 148, 178–186. doi: 10.1007/Bf00414809

Wu, T. Y., Hay, J. X. W., Kong, L. B., Juan, J. C., and Jahim, J. M. (2012). Recent advances in reuse of waste material as substrate to produce biohydrogen by purple non-sulfur (PNS) bacteria. *Renew. Sustain. Energy Rev.* 16, 3117–3122. doi: 10.1016/j.rser.2012.02.002

Xiao, N., and Jiao, N. Z. (2011). Formation of polyhydroxyalkanoate in aerobic anoxygenic phototrophic bacteria and its relationship to carbon source and light availability. *Appl. Environ. Microbiol.* 77, 7445–7450. doi: 10.1128/Aem.05955-11

Conflict of Interest Statement: The authors declare that the research was conducted in the absence of any commercial or financial relationships that could be construed as a potential conflict of interest.

frontiers in Microbiology

ORIGINAL RESEARCH
published: 30 June 2016
doi: 10.3389/fmicb.2016.01047

Identification of Sporopollenin as the Outer Layer of Cell Wall in Microalga *Chlorella protothecoides*

Xi He, Junbiao Dai and Qingyu Wu**

MOE Key Laboratory of Bioinformatics, Center for Synthetic and Systems Biology, School of Life Sciences, Tsinghua University, Beijing, China

Chlorella protothecoides has been put forth as a promising candidate for commercial biodiesel production. However, the cost of biodiesel remains much higher than diesel from fossil fuel sources, partially due to the high costs of oil extraction from algae. Here, we identified the presence of a sporopollenin layer outside the polysaccharide cell wall; this was evaluated using transmission electron microscopy, 2-aminoethanol treatment, acetolysis, and Fourier Transform Infrared Spectroscopy. We also performed bioinformatics analysis of the genes of the *C. protothecoides* genome that are likely involved in sporopollenin synthesis, secretion, and translocation, and evaluated the expression of these genes via real-time PCR. We also found that that removal of this sporopollenin layer greatly improved the efficiency of oil extraction.

Keywords: biodiesel, cell wall, *Chlorophyta*, oil-extraction, sporopollenin

OPEN ACCESS

Edited by:
Youn-Il Park, Chungnam National University, South Korea

Reviewed by:
Arumugam Muthu, Council of Scientific and Industrial Research, India
Won-Joong Jeong, Korea Institute of Bioscience and Biotechnology, South Korea

****Correspondence:***
Junbiao Dai
jbdai@tsinghua.edu.cn;
Qingyu Wu
qingyu@tsinghua.edu.cn

Specialty section:
This article was submitted to Microbiotechnology, Ecotoxicology and Bioremediation, a section of the journal Frontiers in Microbiology

Received: *20 March 2016*
Accepted: *22 June 2016*
Published: *30 June 2016*

Citation:
He X, Dai J and Wu Q (2016) Identification of Sporopollenin as the Outer Layer of Cell Wall in Microalga Chlorella protothecoides. Front. Microbiol. 7:1047. doi: 10.3389/fmicb.2016.01047

INTRODUCTION

Global fossil fuel consumption has been increasing due to both population and economic growth (Lewis and Nocera, 2006), resulting in an energy shortage and a series of environmental problems such as global warming and effluent gas emissions (Chirinos et al., 2006). In response to these challenges, vigorous research programs are underway that to develop alternative biofuels, which are considered necessary for environmental and economic sustainability (Turner, 1999). Unfortunately, to date, biodiesel fuels obtained from plants and animals can't satisfy the existing demand for transport fuels. Microalgae appears to be a particularly promising candidate for use in biodiesel production because of its rapid growth rate, high oil production capacity, and lack of competition for agricultural land (Chisti, 2007). However, the price of algal biofuels remains much higher than that of conventional fossil fuel, due to the high production cost of both biomass and oil extraction (Demirbas and Fatih Demirbas, 2011). *Chlorella protothecoides*, a member of the *Chlorophyta*, can grow autotrophically when light is available. However, when *C. protothecoides* is grown in heterotrophic conditions (limited nitrogen and abundant glucose), it is able to reach very high cell densities (51.2 g L^{-1}) and accumulate large amounts of lipids within cells (55.2%; Xu et al., 2006). It is considered to be a good model for research addressing commercial biofuel production. Transition from autotrophic condition to heterotrophic condition can reduce economic costs in biomass production. Nevertheless, oil extraction from *C. protothecoides* continues to be a significant challenge; it is highly energy consuming and because the cells are hard to break without harsh conditions such as the use of a bead beater (Xiao et al., 2015). Presumably, this resistance to cell lysis may result from a special structure and/or from the composition of the cell wall. Such speculations motivated us to analyze the composition of the cell walls of *C. protothecoides*.

Microalgal cell walls are complex and poorly understood. The chlorella intraspecies variation in cell walls can be dramatic and thus it is difficult to predict which of the compounds will be present in any one strain (Gerken et al., 2013). While some chlorella have only a single layer, others have two layers with the microfibrillar layer proximal to the cytoplasmic membrane and a thin mono or trilaminar outer layer (Yamada and Sakaguchi, 1982). Previous studies about the cell walls of different algae have indicated that only a limited number of chlorella species and other green algae are capable of synthesizing recalcitrant cell walls for protection from chemical or bacterial degradation. For example, some taxa can produce sporopollenin (Geisert et al., 1987; Ueno, 2009), a major component in the cell walls of spores; it has been reported in several genera of green algae, including *Chlorella*, *Scenedesmus*, *Pediastrum*, *Chara*, *Prototheca*, and *Coelastrum* (Burczyk and Czygan, 1983; Komaristaya and Gorbulin, 2006). In addition, Pore et al. found that acid and alkaline hydrolysis of *C. protothecoides* destroyed the cells, but could not destroy the cell wall components (Pore, 1984). Furthermore, the cell wall components were found to be resistant to acetolysis, which lead them to conclude the presence of sporopollenin. However, Lu et al. reported that they could generate protoplasts of *C. protothecoides* successfully using cellulase and snailase, which suggests the absence of sporopollenin (Lu et al., 2012). Therefore, it is arguable whether sporopollenin is present in *C. protothecoides*. Due to the recalcitrant nature of sporopollenin and sporopollenin-like materials, little is known about their definite chemical structure (Brooks and Shaw, 1978; Delwiche et al., 1989). Some studies have described unique structural features (Atkinson et al., 1972), and the conserved biogenesis pathway of sporopollenin has been predicted in some detail (Ríos et al., 2013).

In this paper, we report the discovery that the cell walls of *C. protothecoides* are resistant to the cell wall degradation enzymes. This suggests the presence of a protective layer that presumably prevents enzymes from accessing the wall components. We performed transmission electron microscopy (TEM), 2-aminoethanol treatment, acetolysis, and Fourier Transform Infrared Spectroscopy and provide evidence that this presumed extra layer exists and is composed of sporopollenin. Subsequently, we performed bioinformatics analysis of the sequenced *C. protothecoides* genome to identify genes that are likely involved in sporopollenin biogenesis and analyzed the expression of these genes with real-time PCR methods. In addition, we used a microfluidic device and monitored the propagation of single algal cells in detail. We found that these cells employ the typical *Chlorella* reproduction pattern and that their cell walls contain sporopollenin throughout the entire life cycle. We conclude that this sporopollenin is likely the primary obstacle to efficient oil extraction in this important model algal species.

MATERIALS AND METHODS

Strains and Culture Conditions

C. protothecoides sp. 0710 was cultured as described previously (Yan et al., 2011). Briefly, the autotrophic algae was grown at 28°C with continuous illumination at 40 $\mu mol \cdot m^{-2} \cdot s^{-2}$. The heterotrophic algae was grown in basal medium supplemented with 30 g L^{-1} glucose and 2.5 g L^{-1} yeast extract. Cells were incubated at 28°C in flasks with shaking at 220 rpm.

Enzymatic Treatment of Cells

Enzymatic treatment was performed as to previous study (Lu et al., 2012), with slight modifications. Log-phase *Chlorella* cells were harvested by centrifugation at 3000 rpm for 5 min, then the cell pellet was suspended in 25 mM Tris buffer (pH 6.0) containing the cell wall degrading enzymes and 0.6 M D-mannitol. Besides using the same combination of cellulase and snailase as described, a list of commercially available enzymes including cellulase (Sigma Cat. No. C1184 and Newprobe R-10), snailase (Newprobe), cellulysin (Calbiochem Cat. No. 219466), hemicellulase (Sigma Cat. No. H2125), pectinase (Sigma Cat. No. P2611), pectolyase (Sigma Cat. No. P3026), lysozyme (Sigma Cat. No. L6876), and zymolase (Zymoreseach Cat. No. E1005), were applied, either individually or in combination, so as to obtain the optimal digestion condition. Each treatment was kept at 30°C for 16 h. The cells were then harvested for further analysis.

Fluorescence Microscopy

Cells, both before and after disruption, were incubated in the enzyme solution containing 2% cellulase and 1% snailase in 0.6 M sorbitol and 0.6 M mannitol at 30°C for 16 h. These cells were placed onto a clean glass slide and one drop of Calcofluor-white stain (Sigma Cat. No. P3543) and one drop of 10% potassium hydroxide were added sequentially to the slide. Following incubated for 1 min, cell wall fluorescence was examined under a confocal microscope (SP5, Leica).

Cell Wall Extraction

Cells in the logarithmic growth phase were harvested by centrifugation at 3000 rpm for 5 min. The pellet was washed three times and resuspended in deionized water. Cell wall fragments were isolated as described previously (Hills, 1973; Matias and Beveridge, 2005). The cells were then transferred into a new 2 ml microfuge tube to which 0.3 g acid-washed glass beads (Sigma Cat. No. 18406) were added and processed for 30 times, for 30 s each time, in a Mini-Beadbeater (BioSpec Cat. No. 3110BXEUR) at 5000 rpm. An equal volume of 10% SDS was added, and the samples were boiled for 5 min, followed by centrifugation at 10,000 rpm for 5 min. The supernatant was then removed and the cell wall fragments which form the white fraction on the top of pellets, were isolated and washed three times in deionized water to remove excess SDS before use in subsequent experiments.

Transmission Electron Microscopy

Transmission electron microscopic analysis was performed at the microscope facility in School of Life Sciences of Tsinghua University using a Hitachi H7650B transmission electron microscope following previously-described protocols (Burczyk and Hesse, 1981). Related measurements were taken using the metrics tool in illustrator.

Acetolysis Assay

Acetolysis was carried out for 5 min at 95–100°C in a mixture of acetic anhydride and concentrated sulfuric acid at a ratio of 9:1 (V/V). Cells were transferred to glacial acetic acid both before and after acetolysis to protect the acetic anhydride from breakdown.

Fourier Transform Infrared Spectroscopy

For infrared absorption spectroscopic analysis, the cell wall fragments were first treated with the enzyme mixture as described in the previously-detailed sample preparation protocol to remove the polysaccharide layer of the cell wall. The samples were then processed by washing at 50°C for 5 min followed by treatment with a chloroform-methanol mixture at a ratio of 2:1 (V/V) at 50°C for 5 min. The process was repeated twice. Then the residues were washed sequentially in glacial acetic acid; 0.1 M sodium acetate; 1.0 M sodium hydroxide containing 0.01% tritonX-100 in a boiling water bath for 5 min; 0.1 M sodium acetate; 0.025 M phosphate buffer (pH-7); water; absolute methanol and absolute ether. The samples were then dried overnight in air. Fourier transform infrared spectroscopy (FTIR) analysis was carried out using a Nicolet 6700 FTIR spectrometer coupled with a continuum IR microscope. Operation conditions used a KBr beam splitter and an MCT-A detector (7800–350 cm^{-1}). Spectra were obtained in the mid-infrared (4000–400 cm^{-1}) region. 32 scans were accumulated for each spectrum, with a spectral resolution of 4 cm^{-1}.

Identification of Enzymes Involved in Sporopollenin Biosynthesis

The sporopollenin-related protein sequences of *Arabidopsis* were downloaded from the Arabidopsis information resource[1] (TAIR). The protein sequences of *C. protothecoides* were then used as a database while the *Arabidopsis* proteins were used as query sequences for local BLASTP searching to identify homologous protein sequences in *C. protothecoides* (Wei et al., 2012). We also used CD-Search, a database[2] for the functional annotation of proteins (Marchler-Bauer et al., 2005), to identify conserved domains among the protein sequences of the two organisms.

The whole genome sequence has been deposited at DDBJ/EMBL/GenBank under the accession identifier APJO00000000. The sequences for sporopollenin synthesis-related genes in *C. protothecoides* have been deposited to the GenBank nucleotide database under the following accession identifiers: KF517419 (Cpr000314.3), KF517420 (Cpr001396.1), KF517421 (Cpr000450.1), KF517422 (Cpr002802.1), KF517423 (Cpr000351.1), KF517424 (Cpr004505.1), KF517425 (Cpr001179.1), KF517426 (Cpr002918.1), KF517427 (Cpr001636.6), KF517428 (Cpr004904.1), KF517429 (Cpr001668.1), KF517430 (Cpr004207.2), and KF517431 (Cpr002170.1).

Real-Time Quantitative PCR

Freshly harvested *C. protothecoides* cells were quickly frozen and grounded until the liquid nitrogen evaporated. Total RNA was then isolated using Trizol Reagent (Invitrogen, Cat. No. 15596-026) and genomic DNA was removed by treatment with RNase-free DNaseI (Takara, Cat. No. 2270A). First-strand cDNA was prepared from 4 μg of total RNA using Reverse Transcriptase XL (Takara, Cat. No. 2621) according to the product protocol. PCR amplification was performed using primers designed with Primer Premier 5.0. All primers are listed in Table S2. Actin was used as the internal control. Fluorescence-based real-time PCR reactions were performed in an optical 96-well plate with a Roche LightCycler®480 II Detection System using SYBR® Green (Invitrogen, Cat. No. 4385618). The $2^{-\Delta\Delta Ct}$ method was used to calculate the changes in relative gene expression measured from the real time quantitative PCR analyses.

Single Cell Analysis of Asexual Reproduction in *C. Protothecoides* Using a Microfluidic Device

We used a microfluidic system capable of retaining algae cells in microfluidic chambers; this system has been used successfully in yeast for related studies (Tian et al., 2013). This system enables the observation of the asexual reproduction process in single cells throughout their lifespan. The microfluidic device was kindly designed and provided by Chunxiong Luo of Peking University. Images were taken with a Nikon TE2000 time-lapse microscope; bright field images were taken once every 20 min.

Measurement of Oil Content

Lipid composition and accumulation were analyzed via GC-MS using a slightly modified version of our previously-published protocols (Lu et al., 2010). Wet algal cells treated with or without 2-aminoethanol were suspended in a mixture of 0.5 ml methanol acidified with 3% sulfuric acid and 0.5 ml chloroform containing 2.5 g L^{-1} capric acid (used as an internal standard to correct transesterification and injection volume errors). The mixture was extracted for different durations of time and then centrifuged at 6000 rpm for 5 min. The supernatant with 3 ml mixture (1.5 ml methanol acidified with 3% sulfuric acid and 1.5 ml chloroform containing 2.5 g L^{-1} capric acid) was then heated in a sealed tube at 70°C for 2 h. After cooling, 1 ml of distilled water was added and the sample was vortexed for 20 s. After separation, 1 μl of the lower phase was injected into a gas chromatograph (HP 689-, USA) using a 30 m, 0.32 mm diameter column. Nitrogen was used as the carrier gas at a flow rate of 1 ml min^{-1}. Measurements started at 80°C for 1.5 min. The temperature was increased to 140°C at a rate of 30°C min^{-1}. The next step of the method increased the temperature at a rate of 20°C min^{-1} to 300°C and held this temperature for 1 min before the analysis was terminated. The Retention times for the analytes were as follows: 4.4 min for capric acid methyl ester, 7.4 min for hexadecanoic acid, and 8.5 min for octadecanoic acid methyl ester.

RESULTS

The Cell Wall of *C. Protothecoides* Includes One Layer Resistant to Cellulose Degrading Enzymes

To study the composition of cell walls, we first stained algal cells with a commonly used cell wall dye, Calcofluor-white, which binds to cellulose and chitin (Hughes and McCully, 2009).

[1] http://www.arabidopsis.org/

[2] http://www.ncbi.nlm.nih.gov/entrez/query.fcgi?db=cdd

As shown in **Figure 1A**, whole cells stained with Calcofluor-white showed an intense, light blue fluorescence when irradiated with UV, suggesting that the cell walls of *C. protothecoides* contain cellulose or chitin, similar to other algae (Popper and Fry, 2003). The enzymatic digestion of algal cell walls has been used for a long time in algal research for the preparation of protoplasts (Aach et al., 1978). Lu et al. described a method for generating protoplasts from *C. protothecoides* using an a enzyme combination of 2% cellulase and 1% snailase (Lu et al., 2012). We therefore used the same combination of enzymes to treat the *Chlorella* cells in this study. However, this treatment failed to remove the cell wall (**Figure 1B**). Protoplasts of *Chlorella saccharophila*, *Chlorella ellipsoidea* (Braun and Aach, 1975; Yamada and Sakaguchi, 1982), and *Chlorella vulgaris* (Yang et al., 2015) were obtained using an enzyme mix containing cellulase, hemicellulose, and pectinase. We acquired a number

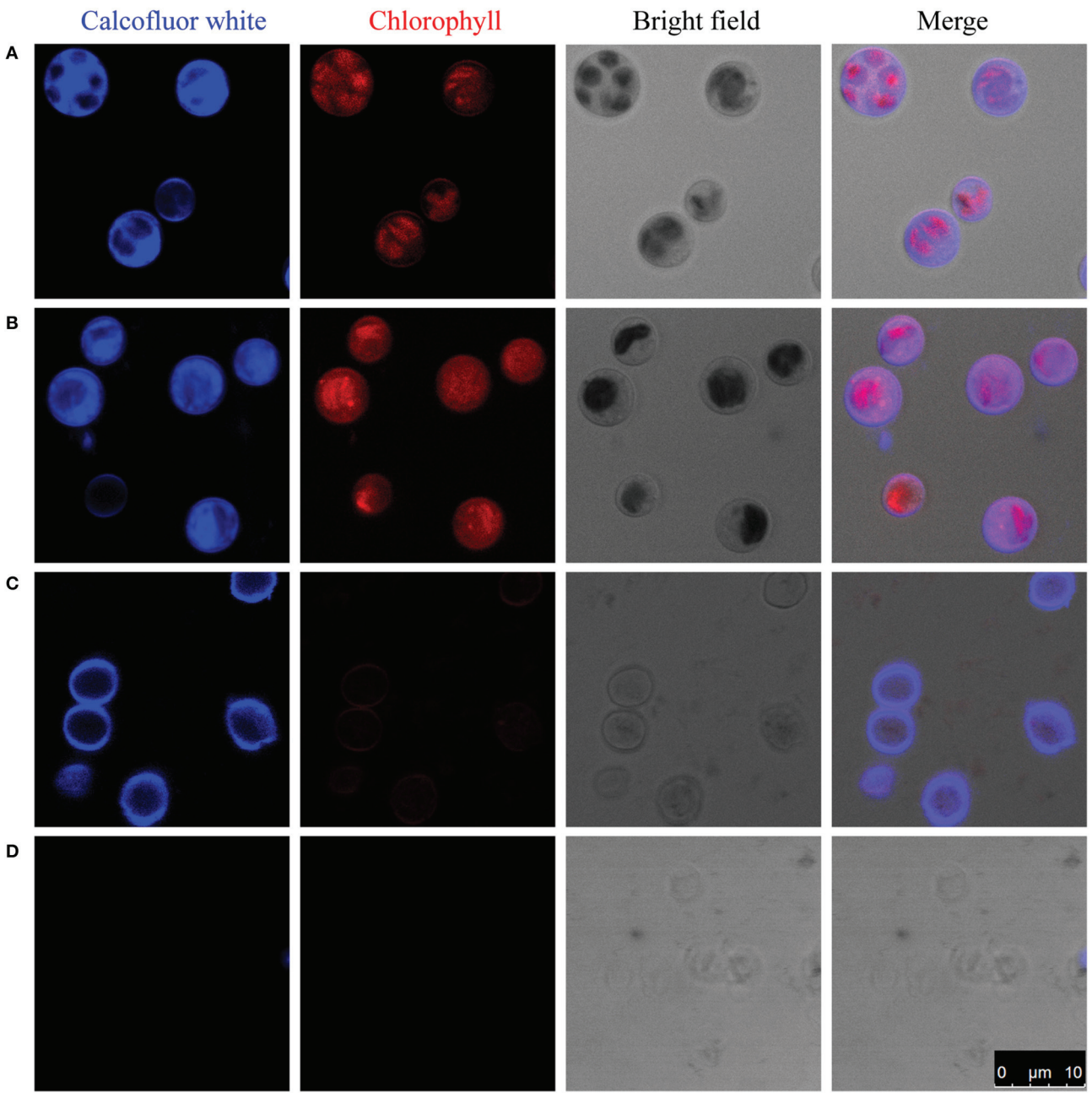

FIGURE 1 | Enzymatic digestion and Calcofluor-white staining of the cell wall of *C. protothecoides*. The blue fluorescence indicates the presence of a cell wall that contains cellulose or chitin. The red fluorescence is chloroplast autofluorescence. **(A)** Intact cells; **(B)** Intact cells after enzymatic treatment; **(C)** Disrupted cells; **(D)** Disrupted cells after enzyme treatment. Arrows show cell wall fragments after enzyme treatment.

of commercially available cell wall degrading enzymes, including cellulase, cellulysin, snailase, hemicellulase, pectinase, pectolyase, lysozyme, and zymolase, and applied these, both individually and in various combinations. None of these enzymes could generate protoplasts from *C. protothecoides* (Table S1).

One of the possibilities for the inability to get protoplasts is that these enzymes are somehow prevented from accessing the cellulose/chitin layer. To test this hypothesis, we partially disrupted the cells in mild to moderately harsh conditions and then stain the sample cells. Pre-disruption of cells with a bead beater in mild conditions retained a round globular structure and showed light blue fluorescence when stained with Calcofluor-white, indicating the presence of a cellulose/chitin layer in the cell wall around these cells (**Figure 1C**). Interestingly, following treatment with an enzyme combination of 2% cellulase and 1% snailase, most cells failed exhibit fluorescence upon Calcofluor-white staining, suggesting the loss of cellulose/chitin layer around these cells (**Figure 1D**). These results indicate that cellulose/chitin is one of the major components of the *C. protothecoides* cell wall and is protected from enzymatic degradation by a hitherto unknown mechanism.

Identification of Sporopollenin in the Cell Wall of *C. Protothecoides*

In a quest to understand what prevents the cell wall being subjected to enzymatic degradation, we examined the ultra-structure of the *C. protothecoides* cell wall using TEM. Isolated cell walls were subjected to TEM analysis, at different magnitudes, both for cells cultured heterotrophically (**Figure 2**) and for cell cultured autotrophically (Figure S1). As shown in **Figures 2A–F**, the cell wall of heterotrophic *C. protothecoides* consists of two morphologically distinct components that are referred to henceforth as the "inner" and "outer" parts of the wall. The inner part is similar to the cell wall of many plants and presumably consists of polysaccharides and proteins. The inner wall of heterotrophic algae (**Figures 2C–F**) is about 80–100 nm in thickness; wider than the inner part of the walls of autotrophic algae cells, which is about 50–60 nm (Figures S1C–F). A mixture of 2% cellulase and 1% snailase was about to completely digest the inner wall of both heterotrophic (**Figures 2G–I**) and autotrophic algae (Figures S1G–I). This observation suggested that the inner wall is probably composed of cellulose and protein, similar to the cell walls of other plants or algae (Lora et al., 2014). It is known that the polysaccharide components in the cell wall can support the structure and keep cells in a relatively constant circular state, so it was not surprising that the loss of polysaccharides following enzymatic treatment resulted in curved cell wall fragments (**Figure 2G**, Figure S1G).

The outer layer of both autotrophic and heterotrophic algae displayed a trilaminar composition and was about 10 nm in thickness (**Figure 2C**). It was sandwich-like in structure and included an electron-lucent center layer and two electron-dense zones on either side of this layer. Interestingly, the outer layer was resistant to enzymatic digestion, indicating that it was probably not made of cellulose or other polysaccharides. Previous studies have suggested that the outer layer of pollen from many plants is resistant to enzymatic digestion and is composed of sporopollenin, a material that can be dissolved in oxidizing solutions, fused potassium hydroxide, or 2-aminoethanol (Southworth, 1974; Domínguez et al., 1999). Therefore, we treated the isolated cell walls with 2-aminoethanol and found that the outer layer became smeared although the inner layer did not undergo significant changes (**Figures 3A–C**). This experiment that there is an outer layer of the *C. protothecoides* cell wall that is possibly composed of sporopollenin.

To evaluate whether or not the newly-identified layer is indeed made of sporopollenin, two additional assays were performed. First, the algal cells were subjected to acetolysis, a process to which sporopollenin is known to be resistant (Heslop-Harrison, 1969). As a control, yeast cells were treated under the same conditions. As shown in **Figure 3D**, the yeast cells were completely dissolved following acetolysis, resulting in a transparent solution. With the *C. protothecoides* samples, however, a large amount of insoluble material remained after treatment. This result is similar findings of Good and Chapman, who identified sporopollenin-containing plants (Good and Chapman, 1978). We next analyzed the composition of the outer layer directly using infrared spectroscopy. We observed two large peaks around the 3000 cm^{-1} wavelength, and noted a slight variation from 1400 to 1500 cm^{-1} (**Figure 3E**, Figure S2). This spectral data matches the previously-reported spectra of pollen as well as the outer layer of the cell walls of other sporopollenin-containing algae (Watson et al., 2007). Taken together, these results strongly support the assertion that sporopollenin is present in the outer layer of the cell walls of *C. protothecoides*.

Identification of Genes Likely Involved in Sporopollenin Biosynthesis in the Genome of *C. Protothecoides*

Genomic analysis of sporopollenin formation in higher plants has indicated that sporopollenin shares a common synthesis pathway, and a schematic model of sporopollenin formation has been proposed (Ma, 2005; Blackmore et al., 2007). We recently published a draft genome of *C. protothecoides* (Gao et al., 2014). This genome enabled us to identify genes in this alga that are homologous to enzymes known or thought to function in key roles in the sporopollenin synthesis pathway. Using *Arabidopsis* homologs as reference, we found that almost all of the genes known to be associated with sporopollenin formation could be identified in the *C. Protothecoides* genome (**Table 1**); further analysis resulted in the identification of conserved domains among these enzymes. The key genes for sporopollenin formation are visually summarized as three steps in *C. protothecoides,* as shown in **Figure 4A**. First, the formation of a callose wall that separates individual daughter cells; this is likely catalyzed by Cpr000314.3 and Cpr001396.1, which are the homologs, respectively, of CaLS5 and KNS2 in *Arabidopsis*. Pollen wall development is subsequently initiated through primexine formation around distinct daughter cells. Previous studies in plants have shown that that primexine functions as a sporopollenin receptor; four enzymes, DEX1, MS1,

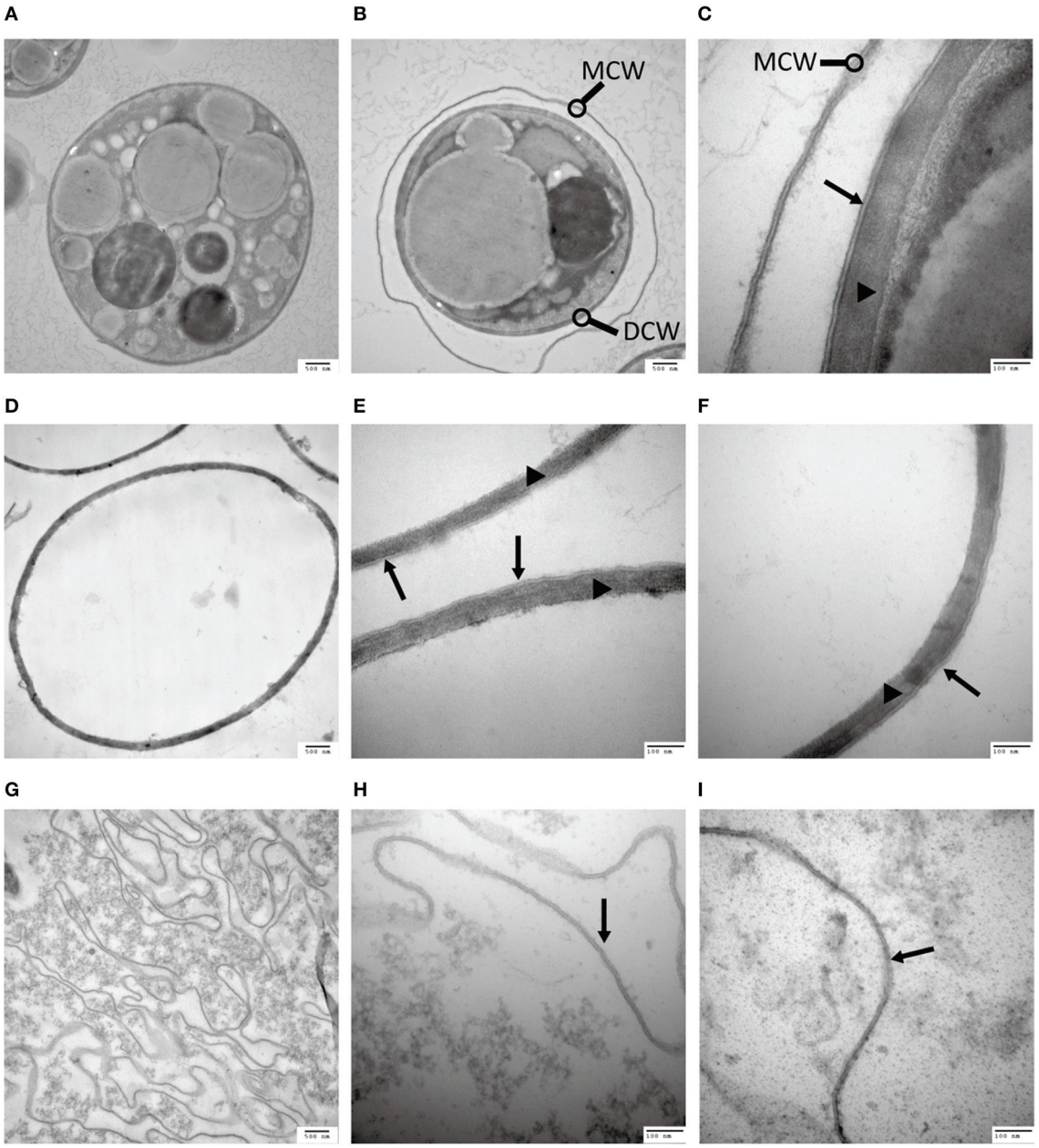

FIGURE 2 | Analysis of the *C. protothecoides* cell wall under TEM. (A) Intact heterotrophic *C. protothecoides* (×30K). **(B)** The same with **(A). (C)** Was similar with **(A,B)** but at higher magnitude (×120K). **(D)** Cell wall before enzymatic treatment (×30K). **(E)** Was similar with **(D)** but at higher magnitude (×120K). **(F)** The same with **(E). (G)** Cell wall after enzymatic treatment. (×30K). **(H)** Was similar with **(G)** but at higher magnitude (×120K). **(I)** The same with **(H)**. DCW, daughter cell wall; MCW, mother cell wall; Triangles show the inner layer of the cell wall; Arrows show the outer layer of the cell wall.

NEF1, and RPG1 are required for sporopollenin deposition and polymerization (Gabarayeva et al., 2009). Similarly, Cpr000450.1, Cpr002802.1, Cpr000351.1, and Cpr004505.1, which correspond, respectively, to the genes that encode these enzymes, were identified in the genome of *C. protothecoides*. The third step is the synthesis, secretion, and translocation of sporopollenin precursors, a process that is dependent on the synthesis of free fatty acids and their derivatives (Meuter-Gerhards et al., 1999, **Figure 4A**). Multiple enzymes are known to function in these metabolic pathways, and most of these were found in the *C. protothecoides* genome (**Table 1**). Genetic studies in *Arabidopsis* and other organisms have shown that mutations in the aforementioned genes, including, for example *CaLS5* and *KNS2,* lead to defects in primexine formation (Ariizumi et al., 2004; Dobritsa et al., 2010; Li et al., 2010). The identification of similar genes in the genome of *C. protothecoides* establishes a putative molecular basis for the existence of sporopollenin in this alga.

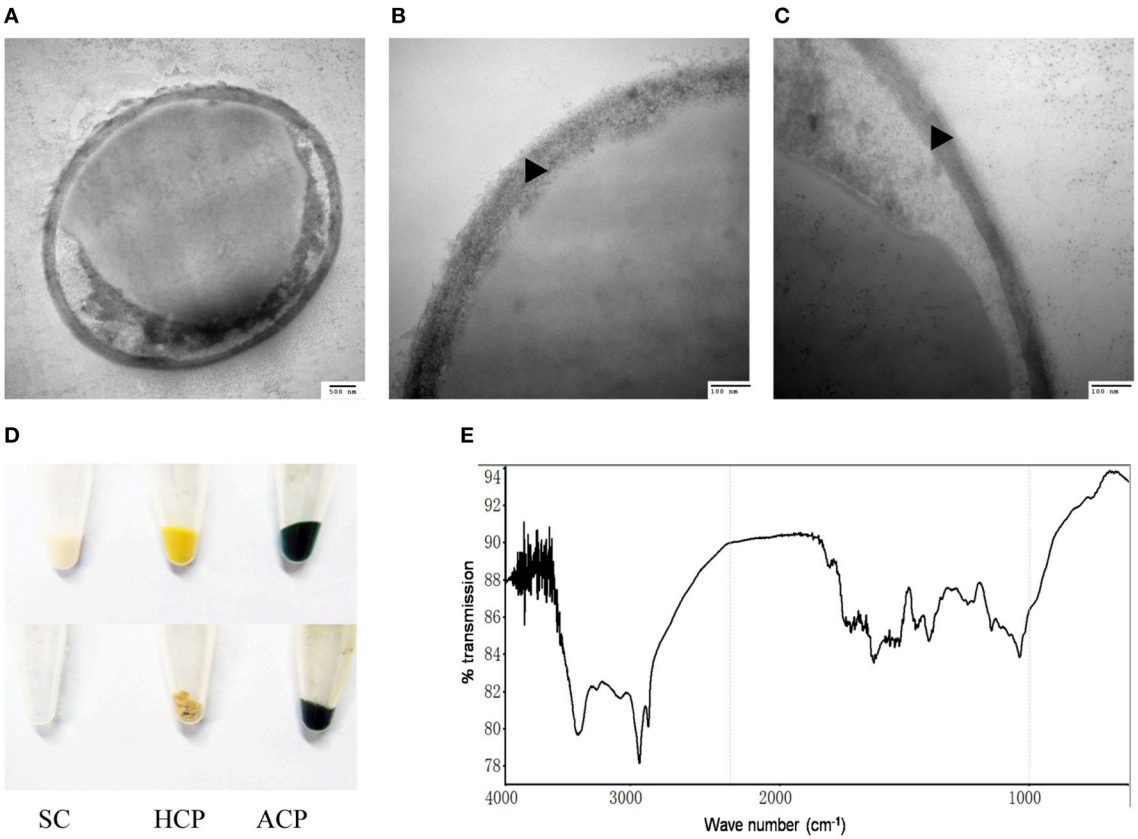

FIGURE 3 | Identification of sporopollenin in the cell wall of *C. protothecoides*. (A) Following 2-aminoethanol treatment were examined using TEM (×30K). **(B)** The same with **(A). (C)** Similar with **(A,B)** but at higher magnitude (×120K). **(D)** Acetolysis of *C. protothecoides* cells. Samples from left to right represent yeast, heterotrophic algae, and autotrophic algae. Samples before Acetolysis treatment were on the top and after treatment were at the bottom. **(E)** FTIR of the cell wall of *C. protothecoides*. SC, Saccharomyces cerevisiae; HCP, Heterotrophic *C. protothecoides*; ACP, Autotrophic *C. protothecoides*. Triangles show the inner layer of the cell wall.

To further verify the existence of above identified genes related to sporopollenin biosynthesis, primers were designed according to the sequences of the conserved domains found in *C. protothecoides* genome; PCR products of the expected sizes were amplified from *C. protothecoides* genomic DNA (Figure S3). Additionally, real time PCR was used to compare the expression of sporopollenin-synthesis genes in autotrophic and heterotrophic cells. As shown in **Figure 4B**, transcripts of all of these genes could be detected under both conditions. Of note, as compared to the cells growing in the autotrophic condition, the heterotrophic cells tended to have higher expression of these genes. It is possible that cells growing in the heterotrophic condition undergo relatively more rapid replication and that relatively higher abundances of enzymes are therefore required to satisfy growth and division demands.

The Sporopollenin Layer Exists Throughout the Entire Asexual Life Cycle and Forms an Obstacle for Oil Extraction

The continuous tracking of algal cells in a microfluidic device makes it possible to study the cell division dynamics of single cell with high temporal resolution. We monitored a time course of *C. protothecoides* cell division and observed that protoplasts divide into two, four, eight, and so on, within the mother cell wall (**Figure 4C**). When the mother cell wall ruptures, the daughter cells emerge from the autosporangium; this is a common mode of propagation for unicellular green algae. We present the entire process of the cell cycle arranged into a movie (Movie S1). Algae growing in both autotrophic and heterotrophic media showed the same division pattern (Figure S4). This propagation mechanism immediately suggests that an intact cell wall will be formed for each daughter cell within a mother cell; this was confirmed by transmission electron microscopy analysis (**Figure 4C**). This also suggests that it is not possible to obtain cells without this sporopollenin layer via targeted collection of mother cells. Therefore, an additional method to remove the sporopollenin layer might be required in order to improve the efficiency for both transformation and oil extraction.

To test this hypothesis, *C. protothecoides* cells were pre-treated with 2-aminoethanol, which was able to dissolve sporopollenin in the aforementioned experiments in our study and in previously-reported experiments (Southworth, 1974; Domínguez et al., 1999, **Figure 3A**). As expected, we found that the oil yield

TABLE 1 | Identification and analysis of likely sporopollenin synthesis-related genes in *C. protothecoides* using Arabidopsis genes as a reference.

Function In Arabidopsis	Arabidopsis gene	TAIR Reference sequence	Proposed Gene class	Sequence of best match	No. of Proposed Homologs	Bits of best match	E–scores	Protein conserved domains
CWS	CaLS5	AT2G13680.1	glucan synthase	Cpr000314.3	2	399	e^{-111}	glucan_synthase,FKS1
CWS	KNS2	AT5G11110.1	Sucrose phosphate synthase	Cpr001396.1	2	157	e^{157}	sucrose phosphate synthase
PS	DEX1	AT3G09090.1	membrane protein	Cpr000450.1	1	277	$5e^{-075}$	VCBS
PS	MS1	AT5G22260.1	Transcription factor	Cpr002802.1	2	95	$3e^{-02}0$	PHD-finger
PS	NEF1	AT5G13390.1	membrane protein	Cpr000351.1	1	69	$4e^{-012}$	/
PS	RPG1	AT5G40260.1	membrane protein	Cpr004505.1	2	54	$2e^{-008}$	MtN3_slv superfamily
SST	KAR	AT1G24470.1	glucose/ribitol dehydrogenase	Cpr001179.1	10	213	e^{-065}	17beta-HSD1_SDR_c, NADB_Rossmann superfamily
SST	ACOS5	AT1G62940.1	lipid metabolism	Cpr002918.1	11	135	e^{-168}	FACL,AFD_Class_I superfamily
SST	CYP703A2	AT1G01280.1	cytochrome P450	Cpr001636.6	7	107	5^{e-024}	p450 superfamily
SST	CYP704B1	AT1G69500.1	cytochrome P450	Cpr001636.6	10	116	8^{e-027}	p450 superfamily,CypX
SST	LAP5	AT4G34850.1	acyl groups transferase	Cpr001668.1	2	52	e^{-007}	CHS_like,cond_ enzymes superfamily, PLNO3169
SST	ABCG26	AT3G13220.1	ATP-binding transporter	Cpr004207.2	35	344	2^{e-095}	ABCG_EPDR,ABC2_ membrane superfamily
SST	GRP	AT4G38680.1	glycine rich protein	Cpr002170.1	1	80	3^{e-016}	CSP_CDS,S1_like superfamily

CWS, Callase wall Synthesis pathway; PS, Primexine Synthesis; SST, Sporopollenin synthesis secretion and translocation.

was significantly improved after 2-aminoethanol treatment as compared the no treatment control cells (**Figure 4D**). As we reported before (Xiao et al., 2015), oil extraction from *C. protothecoides* is one of the most energy-consuming steps in large scale biofuel production procedures. Our results suggest that a potential solution to help reduce the cost of this step would be the pre-treatment of cells with 2-aminoethanol.

DISCUSSION

Although, *C. protothecoides* is regarding a good candidate species for biofuel production (Heredia-Arroyo et al., 2010), its cells are notorious their hard-to-disrupt cell wall. This results in an increased cost for oil extraction from these algal cells. According to previous oil production studies, a pre-treatment process is always required to enhance the efficiency of lipid extraction (Halim et al., 2012). Currently, however, no mature pre-treatment methods can be directly applied to *C. protothecoides* to extract oil at an industrial scale. Actually, when typical methods are used, the recovery rate of lipids from *C. protothecoides* is not as high as that of other organisms (Shen et al., 2009). It has been a long-standing mystery as to why this particular alga is so resistant to mechanical stress. Several attempts to genetically transform *C. protothecoides* have been unsuccessful. Common methods such as the use of polyethylene glycerol following spheroplast generation, which are used to transform protoplasts of other yeast and fungal cells (Kindle, 1990), do not work for *C. protothecoides.* And direct enzymatic digestion using cellulase, snailase or other cell wall-degrading enzymes cannot remove the *C. protothecoides* cell wall (**Figures 1B**, **2B,D**). The identification of sporopollenin as a major component of the cell wall provides a reasonable explanation to these questions.

Knowing the composition of cell wall should greatly advance the use of *C. protothecoides* as model system for biofuel production. For example, additional pre-treatment steps can be adopted to remove sporopollenin prior to oil extraction, likely leading to increased oil yields. In addition, the identification of the sporopollenin layer promises to facilitate the development of new methods for the genetic transformation of *C. protothecoides*. A previous study suggested that microprojectile bombardment could be used to deliver DNA into *tobacco* pollen to study the expression of pollen-expressed genes (Twell et al., 1989). Given the superficially similar cell wall structure between *C. protothecoides* cells and pollen, it is conceivable that a similar method might also work to transform this alga. Furthermore, screens can be carried out to find mutants in which the synthesis of sporopollenin is blocked. Alternatively, some specific chemicals may be used to inhibit sporopollenin synthesis. These sporopollenin deficient strains may become susceptible and easy to accept foreign DNA.

Recently, an elegant study that systematically treated various *Chlorella* strains with a large number of commercially available

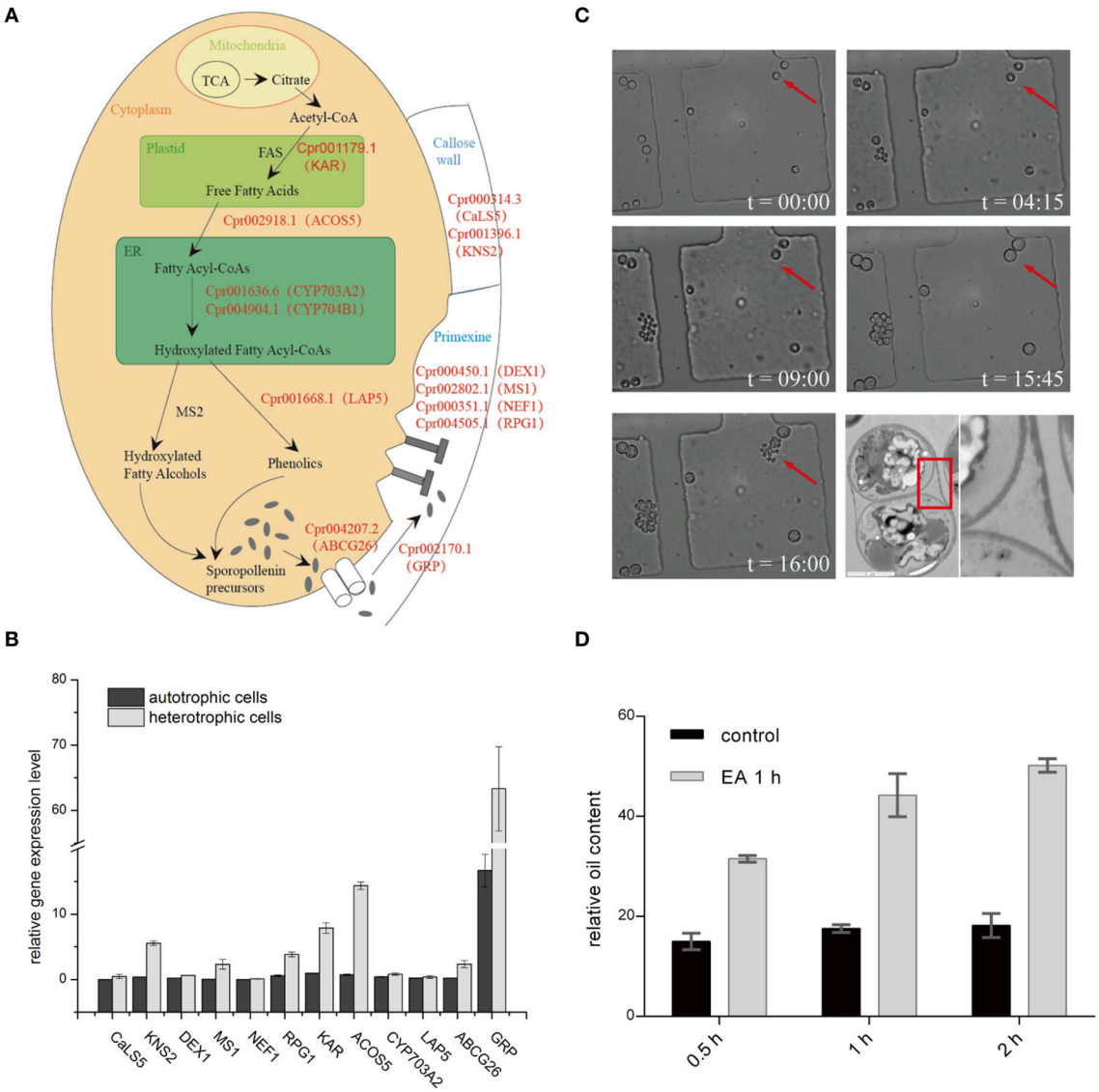

FIGURE 4 | Sporopollenin synthesis pathway in *C. protothecoides*. (A) A schematic model of sporopollenin biosynthesis in *C. protothecoides*. **(B)** Expression of genes likely required for the synthesis, secretion, and translocation of sporopollenin in autotrophic and heterotrophic cells. Selected genes from **Table 1** were tested in this assay. Error bars represents the standard error from two independent experiments. **(C)** The continuous tracking of algal cells in a microfluidic device monitored patterns and dynamic changes in cell walls during asexual reproduction in *C. protothecoides*. The time point of cell injection into the device was set as the starting point (t = 00:00). Images were taken every 15 min; only selected time points are shown. A representative TEM of a dividing cell is also shown. **(D)** Effects of 2-aminoethanol treatment on oil extraction efficiency. Wet algal cells, with or without 2-aminoethanol treatment, were suspended in the extraction mixture for 0.5, 1, or 2 h.

enzymes found that *Chlorella* is most sensitive to chitinase and lysozymes (Gerken et al., 2013). We performed a similar series of enzymatic treatments with *C. protothecoides*. Unfortunately, none of the enzymes we tested were capable of removing the cell wall of *C. protothecoides*. This frustrating result actually lead us to carefully examine its cell wall with electron microscopy, leading to our discovery of the sporopollenin layer (**Figure 2C**).

Sporopollenin is considered to be one of the toughest materials in nature and is known to be resistant to many kinds of chemical and biological attacks. It has been found in *Characium terrestre*, *Enallax coelastroides,* and *Scotiella chlorelloidea* as a high efficient barrier against physical or chemical damage and has been extremely important in the evolution of terrestrial plants (Xiong et al., 1997). However, only a few green algae species have been reported to contain sporopollenin in their cell walls (Northcote et al., 1958; Krienitz et al., 1999). The function of sporopollenin in microalgae has been proposed to be associated with resistance to environmental stress such as UV irradiation, desiccation, microbiological attack, and so on (Strohl et al., 1977).

Similarly, the presence of sporopollenin in the cell wall may help *C. protothecoides* to withstand various environmental stresses.

AUTHOR CONTRIBUTIONS

QW, JD conceived research; JD, XH designed experiments; XH performed experiments and analyzed the data; all authors wrote, commented on, and approved the contents of the manuscript.

ACKNOWLEDGMENTS

We are grateful to Dr. Vanita Uppada for critical reading of this manuscript, and grateful to Zhouqing Luo and members of the Wu lab for helpful discussions. We thank the Center of Biomedical Analysis at Tsinghua University for help with the transmission electron microscopy service. This work was supported by the National Natural Science Foundation of China (NSFC) 41030210, the Ministry of Science and Technology (MOST) projects 2011BAD14B05 and 2011CB808804 to QW, and by the Tsinghua University Initiative Scientific Research Program 20121087956 to JD.

SUPPLEMENTARY MATERIAL

The Supplementary Material for this article can be found online at: http://journal.frontiersin.org/article/10.3389/fmicb.2016.01047

REFERENCES

Aach, H. G., Bartsch, S., and Feyen, V. (1978). Studies on *Chlorella* protoplasts. *Planta* 139, 257–260. doi: 10.1007/BF00388638

Ariizumi, T., Hatakeyama, K., Hinata, K., Inatsugi, R., Nishida, I., Sato, S., et al. (2004). Disruption of the novel plant protein NEF1 affects lipid accumulation in the plastids of the tapetum and exine formation of pollen, resulting in male sterility in *Arabidopsis thaliana*. *Plant J.* 39, 170–181. doi: 10.1111/j.1365-313X.2004.02118.x

Atkinson, A. W., Gunning, B. E. S., and John, P. C. L. (1972). Sporopollenin in the cell wall of *Chlorella* and other algae: ultrastructure, chemistry, and incorporation of 14C-acetate, studied in synchronous cultures. *Planta* 107, 1–32. doi: 10.1007/BF00398011

Blackmore, S., Wortley, A. H., Skvarla, J. J., and Rowley, J. R. (2007). Pollen wall development in flowering plants. *New Phytol.* 174, 483–498. doi: 10.1111/j.1469-8137.2007.02060.x

Braun, E., and Aach, H. G. (1975). Enzymatic degradation of the cell wall of *Chlorella*. *Planta* 126, 181–185. doi: 10.1007/BF00380622

Brooks, J., and Shaw, G. (1978). Sporopollenin: a review of its chemistry, palaeochemistry and geochemistry. *Grana* 17, 91–97. doi: 10.1080/00173137809428858

Burczyk, J., and Czygan, F. C. (1983). Ocurrence of carotenoids and sporopollenin in the cell wall of *Chlorella* fusca and of Its mutants. *Z. Für Pflanzenphysiol.* 111, 169–174. doi: 10.1016/S0044-328X(83)80042-7

Burczyk, J., and Hesse, M. (1981). The ultrastructure of the outer cell wall-layer of *Chlorella* mutants with and without sporopollenin. *Plant Syst. Evol.* 138, 121–137. doi: 10.1007/BF00984613

Chirinos, L., Rose, N. L., Urrutia, R., Muñoz, P., Torrejón, F., Torres, L., et al. (2006). Environmental evidence of fossil fuel pollution in Laguna Chica de San Pedro lake sediments (Central Chile). *Environ. Pollut.* 141, 247–256. doi: 10.1016/j.envpol.2005.08.049

Chisti, Y. (2007). Biodiesel from microalgae. *Biotechnol. Adv.* 25, 294–306. doi: 10.1016/j.biotechadv.2007.02.001

Delwiche, C. F., Graham, L. E., and Thomson, N. (1989). Lignin-Like compounds and Sporopollenin *Coleochaete*, an Algal Model for Land Plant Ancestry. *Science* 245, 399–401. doi: 10.1126/science.245.4916.399

Demirbas, A., and Fatih Demirbas, M. (2011). Importance of algae oil as a source of biodiesel. *Energy Convers. Manag.* 52, 163–170. doi: 10.1016/j.enconman.2010.06.055

Dobritsa, A. A., Lei, Z., Nishikawa, S., Urbanczyk-Wochniak, E., Huhman, D. V., Preuss, D., et al. (2010). LAP5 and LAP6 encode anther-specific proteins with similarity to chalcone synthase essential for pollen exine development in Arabidopsis. *Plant Physiol.* 153, 937–955. doi: 10.1104/pp.110.157446

Domínguez, E., Mercado, J. A., Quesada, M. A., and Heredia, A. (1999). Pollen sporopollenin: degradation and structural elucidation. *Sex. Plant Reprod.* 12, 171–178. doi: 10.1007/s004970050189

Gabarayeva, N., Grigorjeva, V., Rowley, J. R., and Hemsley, A. R. (2009). Sporoderm development in *Trevesia* burckii (*Araliaceae*). I. Tetrad period: further evidence for the participation of self-assembly processes. *Rev. Palaeobot. Palynol.* 156, 211–232. doi: 10.1016/j.revpalbo.2008.12.001

Gao, C., Wang, Y., Shen, Y., Yan, D., He, X., Dai, J., et al. (2014). Oil accumulation mechanisms of the oleaginous microalga *Chlorella protothecoides* revealed through its genome, transcriptomes, and proteomes. *BMC Genomics* 15:582. doi: 10.1186/1471-2164-15-582

Geisert, M., Rose, T., Bauer, W., and Zahn, R. K. (1987). Occurrence of carotenoids and sporopollenin in nanochlorum eucaryotum, a novel marine alga with unusual characteristics. *Biosystems* 20, 133–142. doi: 10.1016/0303-2647(87)90040-2

Gerken, H. G., Donohoe, B., and Knoshaug, E. P. (2013). Enzymatic cell wall degradation of *Chlorella vulgaris* and other microalgae for biofuels production. *Planta* 237, 239–253. doi: 10.1007/s00425-012-1765-0

Good, B. H., and Chapman, R. L. (1978). The Ultrastructure of *Phycopeltis* (Chroolepidaceae: *Chlorophyta*). I. Sporopollenin in the cell walls. *Am. J. Bot.* 65, 27–33. doi: 10.2307/2442549

Halim, R., Danquah, M. K., and Webley, P. A. (2012). Extraction of oil from microalgae for biodiesel production: a review. *Biotechnol. Adv.* 30, 709–732. doi: 10.1016/j.biotechadv.2012.01.001

Heredia-Arroyo, T., Wei, W., and Hu, B. (2010). Oil Accumulation via Heterotrophic/Mixotrophic *Chlorella protothecoides*. *Appl. Biochem. Biotechnol.* 162, 1978–1995. doi: 10.1007/s12010-010-8974-4

Heslop-Harrison, J. (1969). An acetolysis-resistant membrane investing tapetum and sporogenous tissue in the anthers of certain Compositae. *Can. J. Bot.* 47, 541–542.

Hills, G. J. (1973). Cell wall assembly *in vitro* from *Chlamydomonas* reinhardi. *Planta* 115, 17–23. doi: 10.1007/BF00388601

Hughes, J., and McCully, M. E. (2009). *The Use of an Optical Brightener in the Study of Plant Structure*. Available online at: http://informahealthcare.com/doi/abs/10.3109/10520297509117082 (Accessed June 4, 2013).

Kindle, K. L. (1990). High-frequency nuclear transformation of *Chlamydomonas* reinhardtii. *Proc. Natl. Acad. Sci. U.S.A.* 87, 1228–1232.

Komaristaya, V. P., and Gorbulin, O. S. (2006). Sporopollenin in the composition of cell walls of *Dunaliella* salina Teod. *(Chlorophyta)* zygotes. *Int. J. Algae* 8, 43–52. doi: 10.1615/InterJAlgae.v8.i1.40

Krienitz, L., Takeda, H., and Hepperle, D. (1999). Ultrastructure, cell wall composition, and phylogenetic position of *Pseudodictyosphaerium jurisii* (Chlorococcales, Chlorophyta) including a comparison with other picoplanktonic green algae. *Phycologia* 38, 100–107. doi: 10.2216/i0031-8884-38-2-100.1

Lewis, N. S., and Nocera, D. G. (2006). Powering the planet: chemical challenges in solar energy utilization. *Proc. Natl. Acad. Sci. U.S.A.* 103, 15729–15735. doi: 10.1073/pnas.0603395103

Li, H., Pinot, F., Sauveplane, V., Werck-Reichhart, D., Diehl, P., Schreiber, L., et al. (2010). Cytochrome P450 family member CYP704B2 catalyzes the ω -hydroxylation of fatty acids and is required for anther cutin biosynthesis and pollen exine formation in rice. *Plant Cell Online* 22, 173–190. doi: 10.1105/tpc.109.070326

Lora, J., Herrero, M., and Hormaza, J. I. (2014). Microspore development in Annona (*Annonaceae*): differences between monad and tetrad pollen. *Am. J. Bot.* 101, 1508–1518. doi: 10.3732/ajb.1400312

Lu, Y., Ding, Y., and Wu, Q. (2010). Simultaneous saccharification of cassava starch and fermentation of algae for biodiesel production. *J. Appl. Phycol.* 23, 115–121. doi: 10.1007/s10811-010-9549-z

Lu, Y., Kong, R., and Hu, L. (2012). Preparation of protoplasts from *Chlorella protothecoides*. *World J. Microbiol. Biotechnol.* 28, 1827–1830. doi: 10.1007/s11274-011-0963-4

Ma, H. (2005). Molecular genetic analyses of microsporogenesis and microgametogenesis in flowering plants. *Annu. Rev. Plant Biol.* 56, 393–434. doi: 10.1146/annurev.arplant.55.031903.141717

Marchler-Bauer, A., Anderson, J. B., Cherukuri, P. F., DeWeese-Scott, C., Geer, L. Y., Gwadz, M., et al. (2005). CDD: a Conserved Domain Database for protein classification. *Nucleic Acids Res.* 33, D192–D196. doi: 10.1093/nar/gki069

Matias, V. R. F., and Beveridge, T. J. (2005). Cryo-electron microscopy reveals native polymeric cell wall structure in *Bacillus* subtilis 168 and the existence of a periplasmic space. *Mol. Microbiol.* 56, 240–251. doi: 10.1111/j.1365-2958.2005.04535.x

Meuter-Gerhards, A., Riegert, S., and Wiermann, R. (1999). Studies on Sporopollenin biosynthesis in *Cucurbita* maxima (DUCH.) — II. The involvement of aliphatic metabolism. *J. Plant Physiol.* 154, 431–436. doi: 10.1016/S0176-1617(99)80279-X

Northcote, D. H., Goulding, K. J., and Horne, R. W. (1958). The chemical composition and structure of the cell wall of *Chlorella pyrenoidosa*. *Biochem. J.* 70, 391–397. doi: 10.1042/bj0700391

Popper, Z. A., and Fry, S. C. (2003). Primary cell wall composition of Bryophytes and *Charophytes*. *Ann. Bot.* 91, 1–12. doi: 10.1093/aob/mcg013

Pore, R. S. (1984). Detoxification of chlordecone poisoned rats with chlorella and chlorella derived sporopollenin. *Drug Chem. Toxicol.* 7, 57–71.

Ríos, G., Tadeo, F. R., Leida, C., and Badenes, M. L. (2013). Prediction of components of the sporopollenin synthesis pathway in peach by genomic and expression analyses. *BMC Genomics* 14:40. doi: 10.1186/1471-2164-14-40

Shen, Y., Pei, Z., Yuan, W., and Mao, E. (2009). Effect of nitrogen and extraction method on algae lipid yield. *Int. J. Agric. Biol. Eng.* 2, 51–57. doi: 10.3965/ijabe.v2i1.86

Southworth, D. (1974). Solubility of pollen exines. *Am. J. Bot.* 61, 36–44. doi: 10.2307/2441242

Strohl, W. R., Larkin, J. M., Good, B. H., and Chapman, R. L. (1977). Isolation of sporopollenin from four myxobacteria. *Can. J. Microbiol.* 23, 1080–1083.

Tian, Y., Luo, C., and Ouyang, Q. (2013). A microfluidic synchronizer for fission yeast cells. *Lab. Chip* 13, 4071. doi: 10.1039/c3lc50639h

Turner, J. A. (1999). A realizable renewable energy future. *Science* 285, 687–689. doi: 10.1126/science.285.5428.687

Twell, D., Klein, T. M., Fromm, M. E., and McCormick, S. (1989). Transient expression of chimeric genes delivered into pollen by microprojectile bombardment. *Plant Physiol.* 91, 1270–1274.

Ueno, R. (2009). Visualization of sporopollenin-containing pathogenic green micro-alga *Prototheca wickerhamii* by fluorescent *in situ* hybridization (FISH). *Can. J. Microbiol.* 55, 465–472. doi: 10.1139/W08-155

Watson, J. S., Sephton, M. A., Sephton, S. V., Self, S., Fraser, W. T., Lomax, B. H., et al. (2007). Rapid determination of spore chemistry using thermochemolysis gas chromatography-mass spectrometry and micro-Fourier transform infrared spectroscopy. *Photochem. Photobiol. Sci.* 6, 689. doi: 10.1039/b617794h

Wei, K. F., Chen, J., Chen, Y. F., Wu, L. J., and Xie, D. X. (2012). Molecular phylogenetic and expression analysis of the complete WRKY transcription factor family in maize. *DNA Res.* 19, 153–164. doi: 10.1093/dnares/dsr048

Xiao, Y., Lu, Y., Dai, J., and Wu, Q. (2015). Industrial fermentation of auxenochlorella *protothecoides* for production of biodiesel and Its application in vehicle diesel engines. *Front. Bioeng. Biotechnol.* 3:164. doi: 10.3389/fbioe.2015.00164

Xiong, F., Komenda, J., Kopecký, J., and Nedbal, L. (1997). Strategies of ultraviolet-B protection in microscopic algae. *Physiol. Plant.* 100, 378–388. doi: 10.1111/j.1399-3054.1997.tb04796.x

Xu, H., Miao, X., and Wu, Q. (2006). High quality biodiesel production from a microalga *Chlorella protothecoides* by heterotrophic growth in fermenters. *J. Biotechnol.* 126, 499–507. doi: 10.1016/j.jbiotec.2006.05.002

Yamada, T., and Sakaguchi, K. (1982). Comparative studies on *Chlorella* cell walls: induction of protoplast formation. *Arch. Microbiol.* 132, 10–13. doi: 10.1007/BF00690809

Yan, D., Lu, Y., Chen, Y. F., and Wu, Q. (2011). Waste molasses alone displaces glucose-based medium for microalgal fermentation towards cost-saving biodiesel production. *Bioresour. Technol.* 102, 6487–6493. doi: 10.1016/j.biortech.2011.03.036

Yang, B., Liu, J., Liu, B., Sun, P., Ma, X., Jiang, Y., et al. (2015). Development of a stable genetic system for *Chlorella vulgaris*—A promising green alga for CO_2 biomitigation. *Algal Res.* 12, 134–141. doi: 10.1016/j.algal.2015.08.012

Conflict of Interest Statement: The authors declare that the research was conducted in the absence of any commercial or financial relationships that could be construed as a potential conflict of interest.

frontiers in Microbiology

ORIGINAL RESEARCH
published: 26 April 2016
doi: 10.3389/fmicb.2016.00588

Photoconversion and Fluorescence Properties of a Red/Green-Type Cyanobacteriochrome AM1_C0023g2 That Binds Not Only Phycocyanobilin But Also Biliverdin

*Keiji Fushimi[1], Takahiro Nakajima[2], Yuki Aono[2], Tatsuro Yamamoto[1], Ni-Ni-Win[2], Masahiko Ikeuchi[2,3], Moritoshi Sato[2] and Rei Narikawa[1]**

[1] Department of Biological Science, Faculty of Science, Shizuoka University, Shizuoka, Japan, [2] Graduate School of Arts and Sciences, University of Tokyo, Tokyo, Japan, [3] Core Research for Evolutional Science and Technology, Japan Science and Technology Agency, Saitama, Japan

OPEN ACCESS

Edited by:
Takashi Osanai, Meiji University, Japan

Reviewed by:
Youn-Il Park, Chungnam National University, South Korea
Andreas Möglich, Universität Bayreuth, Germany
Scheer Hugo, Universität München, Germany

***Correspondence:**
Rei Narikawa
narikawa.rei@shizuoka.ac.jp

Specialty section:
This article was submitted to Microbiotechnology, Ecotoxicology and Bioremediation, a section of the journal Frontiers in Microbiology

Received: *28 January 2016*
Accepted: *11 April 2016*
Published: *26 April 2016*

Citation:
Fushimi K, Nakajima T, Aono Y, Yamamoto T, Ni-Ni-Win, Ikeuchi M, Sato M and Narikawa R (2016) Photoconversion and Fluorescence Properties of a Red/Green-Type Cyanobacteriochrome AM1_C0023g2 That Binds Not Only Phycocyanobilin But Also Biliverdin. Front. Microbiol. 7:588. doi: 10.3389/fmicb.2016.00588

Cyanobacteriochromes (CBCRs) are distantly related to the red/far-red responsive phytochromes. Red/green-type CBCRs are widely distributed among various cyanobacteria. The red/green-type CBCRs covalently bind phycocyanobilin (PCB) and show red/green reversible photoconversion. Recent studies revealed that some red/green-type CBCRs from chlorophyll *d*-bearing cyanobacterium *Acaryochloris marina* covalently bind not only PCB but also biliverdin (BV). The BV-binding CBCRs show far-red/orange reversible photoconversion. Here, we identified another CBCR (AM1_C0023g2) from *A. marina* that also covalently binds not only PCB but also BV with high binding efficiencies, although BV chromophore is unstable in the presence of urea. Replacement of Ser334 with Gly resulted in significant improvement in the yield of the BV-binding holoprotein, thereby ensuring that the mutant protein is a fine platform for future development of optogenetic switches. We also succeeded in detecting near-infrared fluorescence from mammalian cells harboring PCB-binding AM1_C0023g2 whose fluorescence quantum yield is 3.0%. Here the PCB-binding holoprotein is shown as a platform for future development of fluorescent probes.

Keywords: optogenetics, linear tetrapyrrole, GFP, near-infrared fluorescence, live cell imaging

INTRODUCTION

Phytochromes and cyanobacteriochromes (CBCRs) are photoreceptors that form a large superfamily with a linear tetrapyrrole-binding GAF (cGMP-phosphodiesterase/adenylate cyclase/FhlA) domain (Ikeuchi and Ishizuka, 2008; Anders and Essen, 2015). Some CBCRs are known to be involved in regulation of light acclimation processes such as phototaxis (Yoshihara et al., 2000; Narikawa et al., 2011; Song et al., 2011; Savakis et al., 2012; Campbell et al., 2015), chromatic acclimation (Kehoe and Grossman, 1996; Hirose et al., 2010) and light-dependent cell aggregation (Enomoto et al., 2014, 2015). Only GAF domain of CBCRs is enough for chromophore ligation and photoconversion, although additional PAS (Per/Arnt/Sim) and PHY

(phytochrome-specific) domains in phytochromes are necessary. CBCRs have been roughly categorized into two types according to the chromophore they contain in the thermostable state: Phycoviolobilin (PVB) and PCB. In both cases, PCB is initially incorporated into the GAF domain and Cys residue within the GAF domain covalently ligates to $C3^1$ of the chromophore. PVB-binding CBCRs sense relatively shorter wavelength light covering ultraviolet-to-green region (Yoshihara et al., 2004; Ishizuka et al., 2006; Rockwell et al., 2008, 2012a,b; Narikawa et al., 2011; Song et al., 2011; Enomoto et al., 2012; Ma et al., 2012; Cho et al., 2015), whereas PCB-binding CBCRs sense longer wavelength light covering ultraviolet-to-red region (Hirose et al., 2008, 2013; Narikawa et al., 2008a,b, 2014; Rockwell et al., 2011, 2012c; Chen et al., 2012). These CBCRs commonly show light-induced *Z*/*E* isomerization of a double bond between rings C and D, followed by various structural changes such as reversible protochromic cycle and reversible Cys-adduct formation (Rockwell et al., 2008; Burgie et al., 2013; Hirose et al., 2013; Narikawa et al., 2013, 2014).

Among the PCB-binding CBCRs, red/green-type CBCRs are widely spread among various cyanobacteria and most extensively analyzed so far (Narikawa et al., 2008a, 2013; Fukushima et al., 2011; Chen et al., 2012; Kim et al., 2012a,b,c; Rockwell et al., 2012c, 2015a,b; Velazquez Escobar et al., 2013; Slavov et al., 2015; Song et al., 2015a,b). The red/green-type CBCRs show reversible photoconversion between a red-absorbing form (Pr) with 15*Z*-PCB and a green-absorbing form (Pg) with 15*E*-PCB. Structure of Pr form provides direct insights into chromophore–protein interaction (Narikawa et al., 2013). Detailed spectroscopic analyses based on this structure have revealed their photoconversion mechanism in which excited state destabilization and ring D distortion are suggested to occur to form blue-shifted Pg form upon red-light irradiation (Rockwell et al., 2014; Song et al., 2015a).

Recently, it has been revealed that red/green-type CBCRs (AM1_1557g2 and AM1_1870g3) derived from the chlorophyll *d*-bearing cyanobacterium *Acaryochloris marina* covalently bind not only PCB but also biliverdin (BV; Narikawa et al., 2015a,b). BV-binding ones show reversible photoconversion between far red-absorbing (Pfr) form and orange-absorbing (Po) form, whereas PCB-binding ones show normal red/green reversible photoconversion. Site-directed mutagenesis suggests that a Cys residue within the GAF domain covalently ligates not only to PCB but also to BV. BV is present in most organisms including mammals and far-red light can penetrate into deep tissues, with a potential as optogenetic and bioimaging tools (Ziegler and Möglich, 2015).

Here, we report another GAF domain (second GAF domain of AM1_C0023 called AM1_C0023g2) from *A. marina* that covalently binds not only PCB but also BV. Replacement of Ser334 with Gly resulted in significant improvement in yield of the BV-binding holoprotein. Further, we detected near-infrared fluorescence from mammalian cells harboring AM1_C0023g2-PCB whose fluorescence quantum yield is 3.0%.

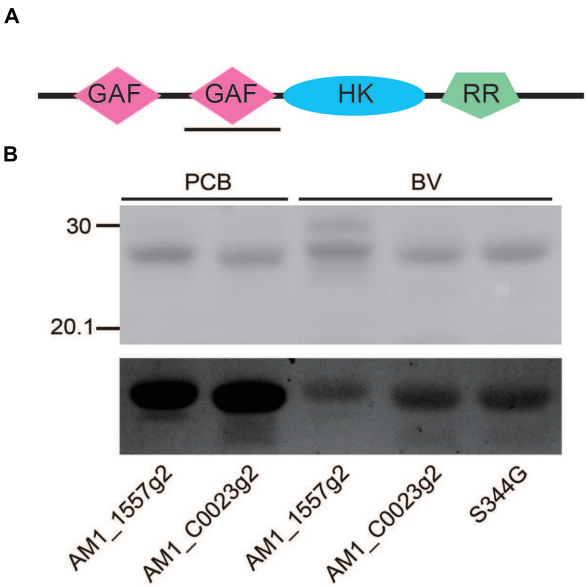

FIGURE 1 | (A) Domain structure of the full-length gene product, AM1_C0023. GAF: cGMP-phosphodiesterase/adenylate cyclase/FhlA domain, HK, Histidine kinase domain; RR, response regulator domain. Expressed second GAF domain, AM1_C0023g2, was highlighted by black solid underline. **(B)** SDS-PAGE analyses of PCB- and BV-binding AM1_1557g2 and AM1_C0023g2. Upper gel image: Coomassie Brilliant Blue stained gel. Lower gel image: Linear tetrapyrroles covalently bound to CBCR GAF domains were detected by in-gel fluorescence imaging. The Zn^{2+}-staining was performed as previously described (Berkelman and Lagarias, 1986). The gel was directly subjected to fluorescence detection. The gel image was provided with black-and-white inversion for easy detection of fluorescent bands.

MATERIALS AND METHODS

Plasmid Construction

The nucleotide sequence of AM1_C0023g2 was cloned into pET28a (Novagen) using In-fusion HD Cloning kit (TaKaRa) as described previously (Narikawa et al., 2015b). AM1_C0023g2 sequence was amplified by polymerase chain reaction (PCR) with a specific primer set (5′-CGCGGCAGCCATATGAATATTTCCGAGATTATT-3′, 5′-CTCGAATTCGGATCCTCAAGCTTCTGCTTTGTTTTT-3′) and PrimeSTAR Max DNA polymerase (TaKaRa). The inserted sequence was confirmed by sequencing with an ABI310 genetic analyzer. Replacement of AM1_C0023g2 Ser334 with Gly (denoted S334G) was performed using a specific primer set (5′-CAACAAGGATATACAGATTGTCATCTA-3′, TGTATATCCTTGTTGATAAATGTCAGC) and PrimeSTAR max DNA polymerase as described previously.

To construct GFP-fused AM1_C0023g2 and AM1_1557g2, the nucleotide sequences of GFP, AM1_C0023g2 and AM1_1557g2 were amplified by PCR with specific primer sets and Pyrobest DNA polymerase (TaKaRa). The following primer sets were used to introduce restriction enzyme sites, a flexible

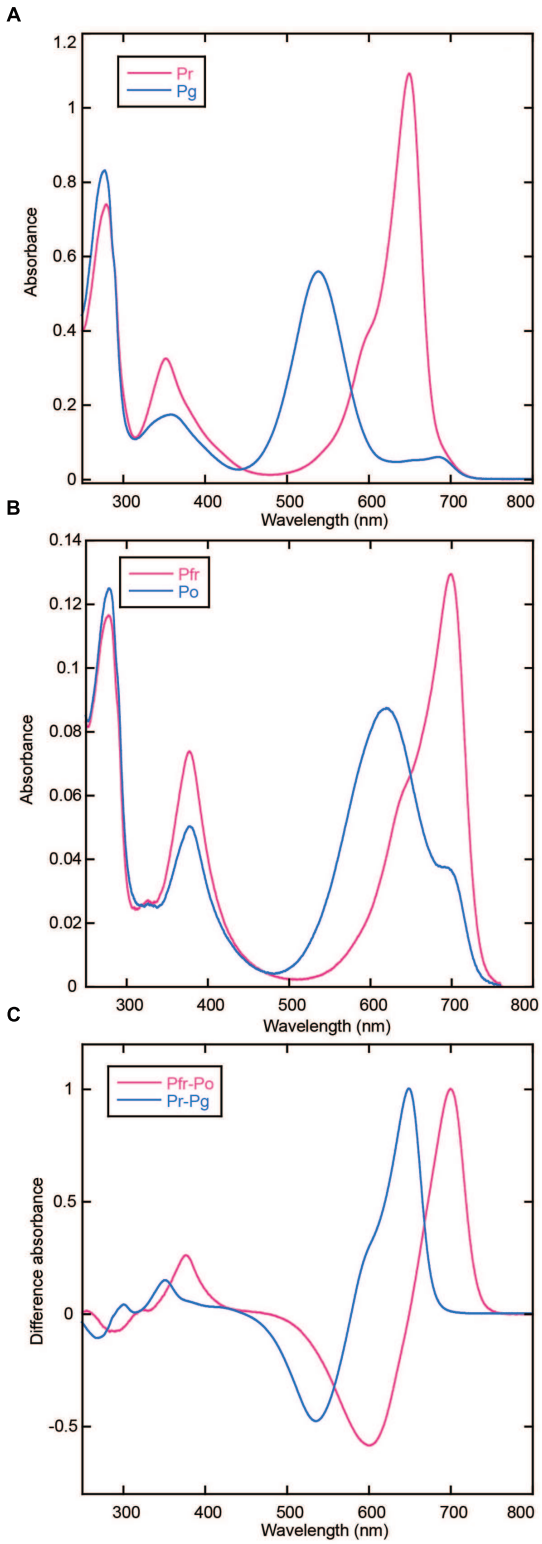

FIGURE 2 | Photoconversion of AM1_C0023g2-PCB and AM1_C0023g2-BV. (A) Absorption spectra of Pr (magenta) and Pg (blue) forms of AM1_C0023g2-PCB. **(B)** Absorption spectra of Pfr (magenta) and Po (blue) forms of AM1_C0023g2-BV. **(C)** Difference spectra of PCB- (blue) and BV-binding (magenta) AM1_C0023g2 before and after photoconversion.

peptide linker sequence, and Kozak sequence: for GFP, 5′-ATGCAAGCTTGCCACCATGGTGAGCAAGGGCGAG-3′ and 5′-GCATCTCGAGACCTCCGCTACCGCCCTTGTACAGCTCGTC-3′; for AM1_C0023g2 and AM1_1557g2, 5′-ATGCCTCGAGAGCGGCCTGGTGCCGCGC-3′ and 5′-GAGCTCGAATTCGGATCC-3′. All sequences were confirmed by sequencing with an ABI 310 genetic analyzer. These constructs were cloned into a mammalian expression vector pcDNA 3.1 (+) (Invitrogen) using the restriction enzyme sites. All the mammalian expression plasmids were purified using QIAGEN plasmid kit (Qiagen).

Expression, Purification, and SDS-PAGE

His-tagged AM1_C0023g2 was expressed in both BV- and PCB-producing *Escherichia coli* (C41 harboring pKT270 and pKT271, respectively). The His-tagged proteins were isolated by Ni-affinity chromatography as described previously (Narikawa et al., 2015b). The purified proteins were subjected to SDS-PAGE, followed by in-gel fluorescent assay and Coomassie Brilliant Blue staining as described previously (Narikawa et al., 2015b). Fluorescence was visualized through a 600 nm long path filter upon excitation with wavelength of blue (λ_{max} = 470 nm) and green light (λ_{max} = 530 nm) through a 562 nm short path filter (WSE-6100 LuminoGraph, WSE-5500 VariRays; ATTO).

Estimation of Binding Efficiencies

Protein concentration was determined by standard Bradford method (Bio-Rad). We determined extinction coefficients of free PCB (Santa Cruz Biotechnology Inc.) and free BV (Frontier Scientific) under both acidic urea and 1% SDS conditions. Extinction coefficients of the free PCB and BV under the acidic urea condition were calculated to be a little less than 30000, that is comparable to that reported previously (Glazer and Fang, 1973). On the other hand, extinction coefficients of the free PCB and BV under the 1% SDS condition were calculated to be around 17000. Although extinction coefficients of chromophores under the 1% SDS condition tend to be lower than those under the acid urea condition, PCB and BV behave similarly under both conditions. Thus, concentration of PCB bound to proteins was determined by absorbance at 666 nm when denatured with 8 M urea (pH2.0). Similarly that of BV bound to proteins was determined by absorbance at 646 nm when denatured with 1% SDS.

In Vitro Reconstitution

S334G protein that is a mutant of AM1_C0023g2 was used for *in vitro* reconstitution analysis because of its high yield of *in vivo* reconstitution system (see **Figure 4**). Free BV and the apo-S334G protein were mixed in roughly equimolar amounts and incubated for 30 min at 37°C. After removal of unbound BV by spin column, the sample was subjected to spectral analyses.

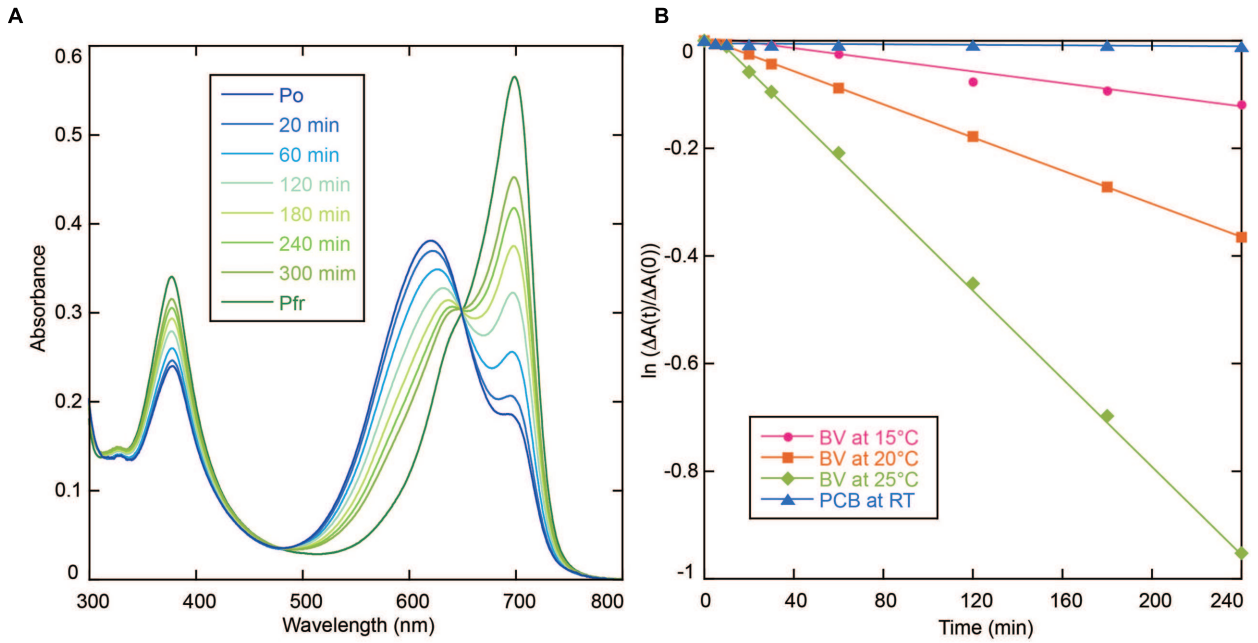

FIGURE 3 | (A) Absorption spectra of AM1_C0023g2-BV recorded during dark reversion at 25°C. **(B)** Dark reversion kinetics of PCB- (blue triangle for room temperature) and BV-binding (magenta circle for 15°C, orange square for 20°C and green diamond for 25°C) AM1_C0023g2 from metastable Pg and Po forms to thermostable Pr and Pfr forms, respectively.

Spectroscopy

Ultraviolet and visible absorption spectra were recorded with a Shimadzu UV-2600 spectrophotometer. Monochromic light of various wavelengths for photoconversion was generated using a variable wavelength light source (Opto-Spectrum Generator, Hamamatsu Photonics, Inc.). Acid denaturation of the proteins was performed with 8 M urea, pH 2.0 under the dark condition. Fluorescence spectra were recorded with a StellarNet SILVER-Nova spectrometer (StellerNet, Inc.). Fluorescence quantum yields were measured with Quantaurus-QY (Hamamatsu Photonics, Inc.).

Imaging of GFP-fused AM1_C0023g2 and AM1_1557g2 in Mammalian Cells

Human cervical carcinoma (HeLa) cells (ATCC, CCL-2) were cultured in Eagle's minimum essential medium (Sigma) supplemented with 2 mM L-glutamine (Gibco), 10% fetal bovine serum (Gibco), 100 U/mL penicillin and 100 μg/mL streptomycin (Gibco) at 37°C in 5% (v/v) CO_2. The day before transfection, HeLa cells were plated onto 35-mm glass-based dishes (Iwaki). Transfection was performed using lipofectamine 3000 (Life Technologies) according to the manufacturer's instructions. Forty-eight hours after transfection, the cells were washed with Hank's balanced salt solution (HBSS; Gibco) and replaced with HBSS containing either 20 μM PCB (Frontier Scientific) diluted from a stock solution of 20 mM in dimethyl sulfoxide (DMSO; Wako) or 0.1% (v/v) DMSO as the vehicle control. After incubation for 4 h, the cells were washed and replaced with HBSS, and imaged using a Zeiss LSM 710 confocal microscope equipped with a Plan-Apochromat 63×/1.4 oil immersion objective (Carl Zeiss), a 488 nm Ar laser, and a 633 nm He/Ne laser. Green fluorescence of GFP was detected at 493–538 nm upon excitation with the 488 nm laser (6.5 μW measured at the back aperture of the objective lens). Near-infrared fluorescence of CBCR was detected at 638–740 nm upon excitation with the 633 nm laser (67 μW measured at the back aperture of the objective lens). Data analysis was performed using ZEN 2009 (Carl Zeiss).

RESULTS AND DISCUSSION

AM1_C0023g2 Isolated from PCB-Producing and BV-Producing *E. coli*

We found that AM1_C0023 is closely related in-paralog of AM1_1557. AM1_C0023 is 71% identical to and has a domain architecture same as AM1_1557 (**Figure 1A**). Second GAF domain of AM1_C0023 (AM1_C0023g2) is 84% identical to that of AM1_1557 (AM1_1557g2). Residues highly conserved among red/green-type CBCRs and important for chromophore ligation are also conserved in AM1_C0023g2.

AM1_C0023g2 was expressed in both PCB- and BV-producing *E. coli* and purified by using nickel-affinity column chromatography. In-gel fluorescence analysis revealed that AM1_C0023g2 covalently binds not only PCB but also BV like AM1_1557g2 (**Figure 1B**). PCB-binding AM1_C0023g2 (AM1_C0023g2-PCB) showed reversible photoconversion between red-absorbing Pr form at 650 nm and green-absorbing

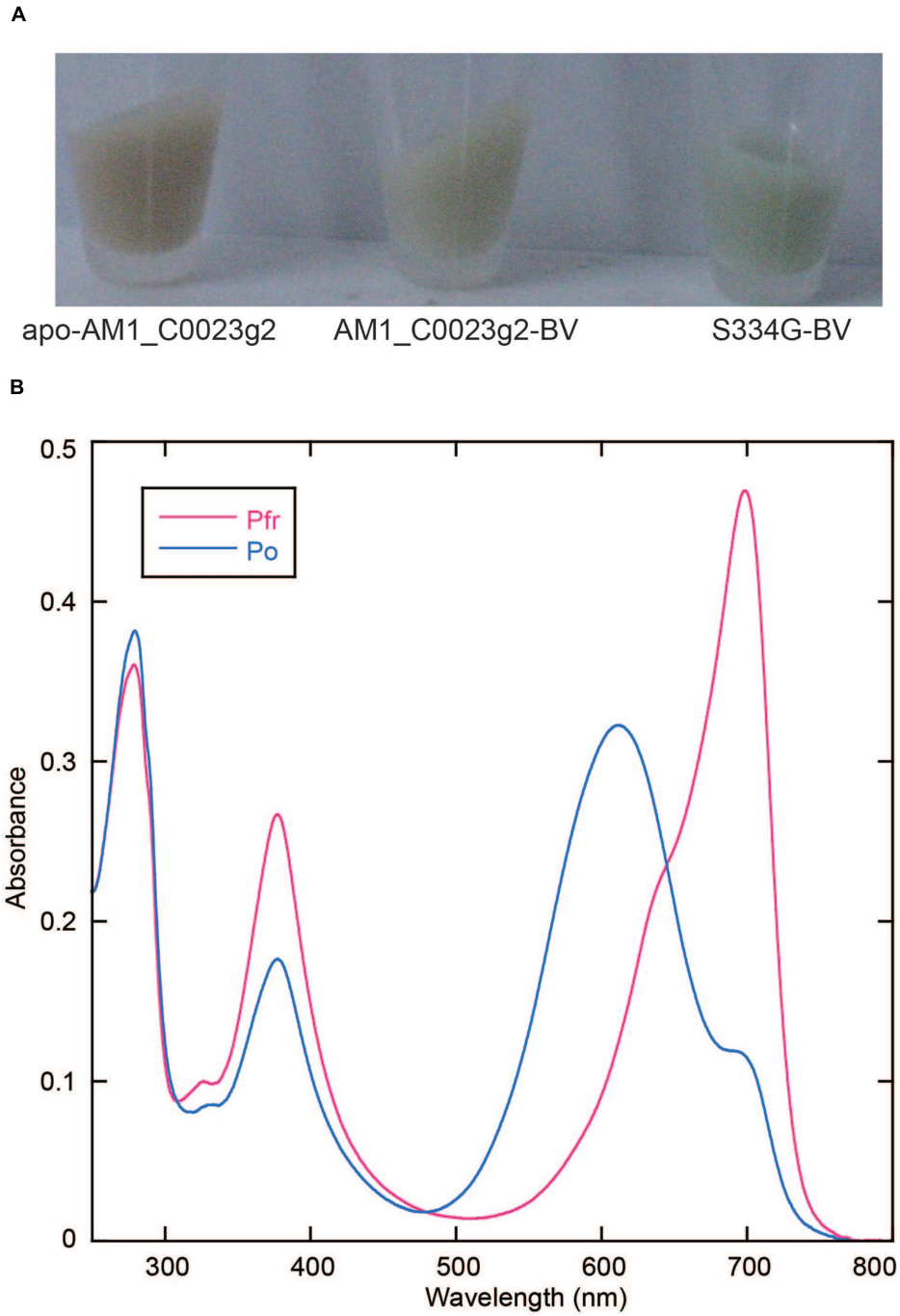

FIGURE 4 | Replacement of Ser334 of AM1_C0023g2 with Gly. (A) Photograph of cell pellets harboring apo-AM1_C0023g2, AM1_C0023g2-BV, and S334G-BV. **(B)** Absorption spectra of the Pfr and Po forms of S334G-BV.

Pg form at 539 nm (**Figure 2A**), whereas BV-binding AM1_C0023g2 (AM1_C0023g2-BV) showed reversible photoconversion between far red-absorbing Pfr form at 699 nm and orange-absorbing Po form at 618 nm (**Figure 2B**). These spectral features are almost same as those of AM1_1557g2 (Narikawa et al., 2015b). Pfr-minus-Po difference spectrum of AM1_C0023g2-BV possesses positive peaks at 700 and 377 nm and negative peaks at 601 and 284 nm, whereas Pr-minus-Pg difference spectrum of AM1_C0023g2-PCB possesses positive peaks at 650, 352, and 301 nm and negative peaks at 536 and 270 nm (**Figure 2C**).

AM1_C0023-BV Pfr showed dark reversion to Po (**Figure 3A**), whereas dark reversion of AM1_C0023-PCB Pr was hardly detected (**Figure 3B**). Half-lives for the AM1_C0023-BV during

dark reversion measured at 15, 20, and 25°C were 1356, 478, and 180 min, respectively (**Figure 3B**). Slower dark reversion was observed under lower temperature. Hardly detectable and relatively fast dark reversions of PCB- and BV-binding ones, respectively, are also consistent with those found for AM1_1557g2 and AM1_1870g3 (Narikawa et al., 2015a,b).

Site-Directed Mutagenesis of AM1_C0023g2

In the process of site-directed mutagenesis analysis to obtain proteins with higher fluorescence quantum yields, we incidentally obtained a unique mutant protein, S334G in which Ser334 was replaced with Gly. This replacement resulted in significant improvement in expression yield of BV-binding holoproteins in *E. coli* (**Figure 4A**). Colonies were picked up and grown in small-scale culture. Cell pellet of *E. coli* expressing only the wild type protein showed brown color typical of normal *E. coli*. Cell pellet of *E. coli* expressing both the wild type protein and the heme oxygenase showed pale green color. On the other hand, cell pellet of *E. coli* expressing both the S334G protein and the heme oxygenase showed deep green color. The BV-binding S334G (S334G-BV) showed reversible photoconversion between Pfr at 699 nm and Po at 611 nm (**Figure 4B**). Its Po form is about 7 nm blue-shifted than that of the wild type. Binding efficiency to BV was calculated to be 1.25-fold higher than that of the wild type protein (see Evaluation of Chromophore Binding Efficiencies). In total, judging from the Pfr absorption peak, recovery of the S334G-BV was about five-fold higher than that of the BV-binding wild type from the same culture volume. Although Gly317 of AnPixJg2 corresponding to Ser334 of AM1_C0023g2 does not directly interact with PCB, Gly317 is placed 4 residues upstream of Cys321 that covalently ligates to PCB (Narikawa et al., 2013). This replacement may indirectly affect chromophore-binding pocket to facilitate protein expression and chromophore incorporation. Apart from the underlying mechanism, we consider that S334G-BV is a good platform for further development of optogenetic switches. Slow dark recovery kinetics and almost full photoconversion (90% estimated from the absorption spectra) are favorable for long-term and acute regulation.

Chromophore Species and Configuration

Acid-denatured spectra proved that AM1_C0023g2 isolated from PCB-producing *E. coli* undoubtedly bound PCB (**Figure 5**). Absorption maximum of denatured Pr and Pg were observed at 665 and 603 nm, respectively (**Figures 5A,B**). Irradiation of denatured Pg with white light resulted in red shift of the absorbance that is almost identical to that of denatured Pr, whereas irradiation of denatured Pr with white light resulted in no significant change (**Figures 5A,B**). Pr-minus-Pg difference spectrum fits to that during photoconversion of denatured Pg (**Figure 5C**). These results clearly show that Pr and Pg bound 15*Z*- and 15*E*-PCB, respectively.

Acid-denatured spectra of AM1_C0023g2 isolated from BV-producing *E. coli* showed completely different spectra (data not shown) compared with previously reported data (Narikawa

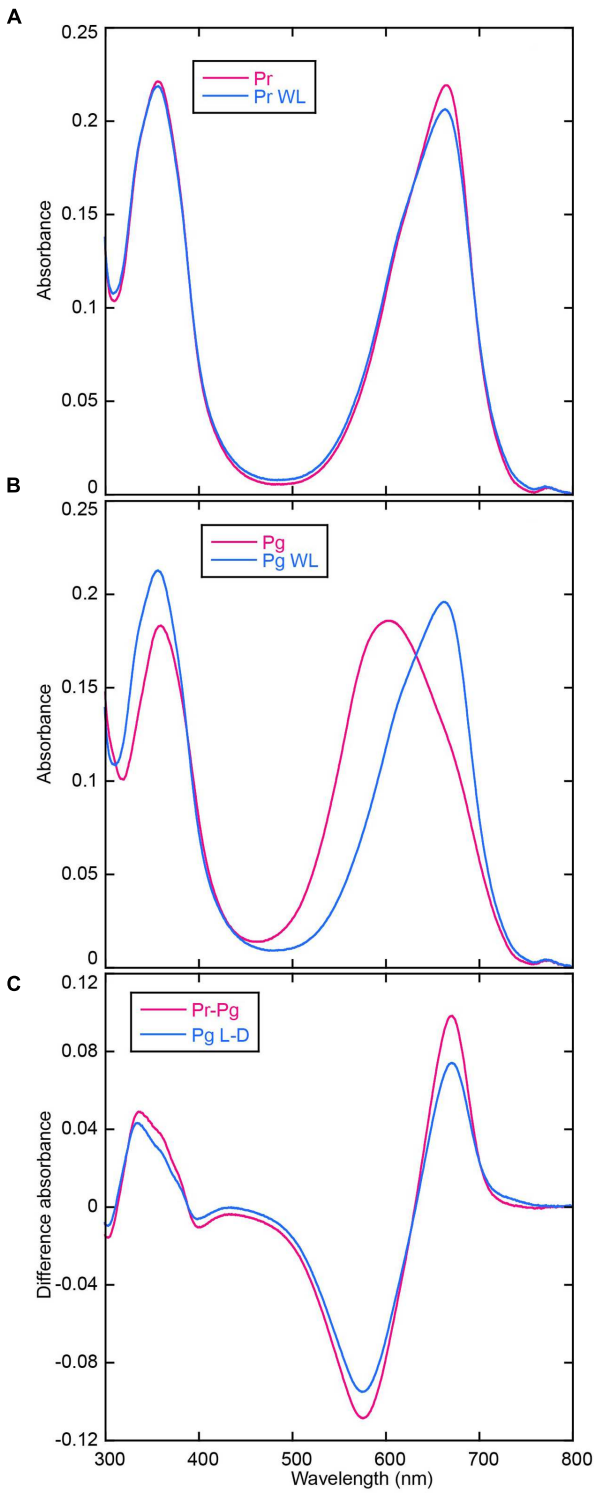

FIGURE 5 | Acid denaturation of AM1_C0023g2-PCB. (A) Absorption spectra of acid-denatured AM1_C0023g2-PCB Pr. Absorption spectra just after denaturation (Pr, magenta) and after white light illumination (Pr WL, blue). **(B)** Absorption spectra of acid-denatured AM1_C0023g2-PCB Pg. Absorption spectra just after denaturation (Pg, magenta) and after white light illumination (Pg WL, blue). **(C)** Pr-minus-Pg difference spectrum (Pr-Pg, magenta) and that during photoconversion of denatured Pg (Pg L-D, blue).

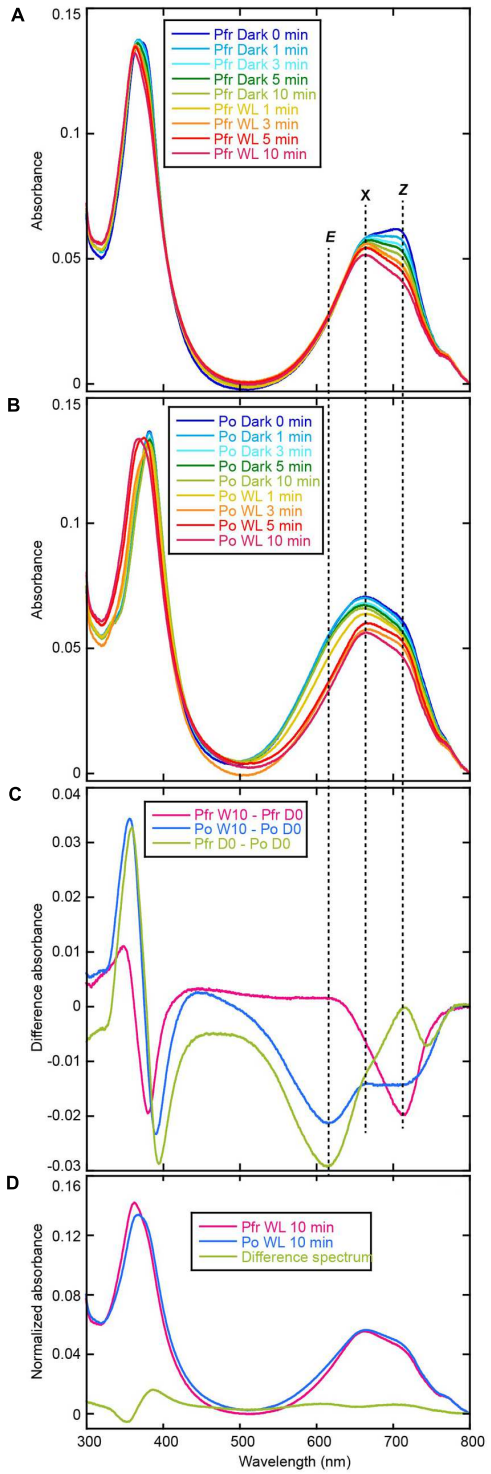

FIGURE 6 | Acid denaturation of AM1_C0023g2-BV. (A) Absorption spectra of acid-denatured AM1_C0023g2-BV Pfr during dark and light processes. **(B)** Absorption spectra of acid-denatured AM1_C0023g2-BV Po during dark and light processes. **(C)** Difference spectrum during dark and light processes of denatured Pfr (magenta), during dark and light processes of denatured Po, and of Pfr-minus-Po just after denaturation (green). **(D)** Normalized absorption spectra and difference spectrum of acid-denatured AM1_C0023g2-BV Pfr and Po after dark and light processes.

et al., 2015b). In order to monitor initial spectral change after denaturation, we denatured samples under 4°C and their absorption spectra were measured at 15°C at 0, 1, 3, 5, and 10 min. Subsequently absorption spectra during white light illumination (1, 3, 5, and 10 min) were recorded. Absorption maximum just after denaturation of Pfr form was observed at ∼700 nm (**Figure 6A**), which corresponded to 15*Z*-BV previously reported (Narikawa et al., 2015b). Absorption maximum after denaturation of Po form was observed at ∼660 nm (**Figure 6B**) with a red-shift compared with 15*E*-BV as reported earlier. Because photoconversion from Pfr to Po is incomplete (**Figure 2B**), the residual Pfr may affect the absorption peak of denatured Po resulting in red shift to ∼660 nm.

The ∼700 nm peak observed for Pfr (denatured) decreased during dark and light processes and final absorption spectrum was at ∼665 nm (**Figure 6A**). Difference spectrum during these processes showed a negative peak at ∼714 nm (**Figure 6C**, Pfr W10 – Pfr D0). From these results, we hypothesized that 15*Z*-BV just after denaturation rapidly converts to an unknown state (X) at 665 nm. On the other hand, absorption after Po denaturation slightly decreased under dark process and largely decreased under light process (**Figure 6B**). The decrease under dark process may correspond to conversion from the residual Pfr to the unknown state "X". The decrease under light process may correspond to conversion from Po to "X" via Pfr. Based on the above-mentioned hypothesis, in the case of both Pfr denaturation and Po denaturation, their final products after dark and light processes should be composed of only "X". Indeed, absorption spectra of both denatured Pfr and Po after 10 min white light illumination are at 665 nm and almost same (**Figure 6D**), which strongly supports this hypothesis.

Pfr-minus-Po difference spectrum just after denaturation showed a positive peak around ∼714 nm and a negative peak around ∼614 nm (**Figure 6C**, Pfr D0 – Po D0). These wavelengths well correspond to those obtained from the difference spectrum of denatured AM1_1557g2 (Narikawa et al., 2015b). Thus, the positive peak around 714 nm corresponds to 15*Z*-BV, whereas the negative peak around 614 nm corresponds to 15*E*-BV. However, a negative component around 745 nm was detected. Based on the above-mentioned hypothesis in which the denatured 15*Z*-BV rapidly converts into "X", 15*E*-BV from denatured Po should be more abundant than 15*Z*-BV from denatured Pfr. In such situation, absorption tail of 15*E*-BV around 745 nm should be larger than that of 15*Z*-BV, and the difference spectrum should show the minus component around 745 nm.

Difference spectrum during light and dark processes of denatured Po showed negative peaks at ∼714 and ∼614 nm (**Figure 6C**, Po W10 – Po D0). These wavelengths also correspond to 15*Z*-BV and 15*E*-BV, respectively. Major negative peak at ∼614 nm is likely to correspond to conversion from 15*E*-BV to "X" via 15*Z*-BV, whereas minor negative peak at ∼714 nm is likely to correspond to conversion from 15*Z*-BV originated in the residual Pfr to "X".

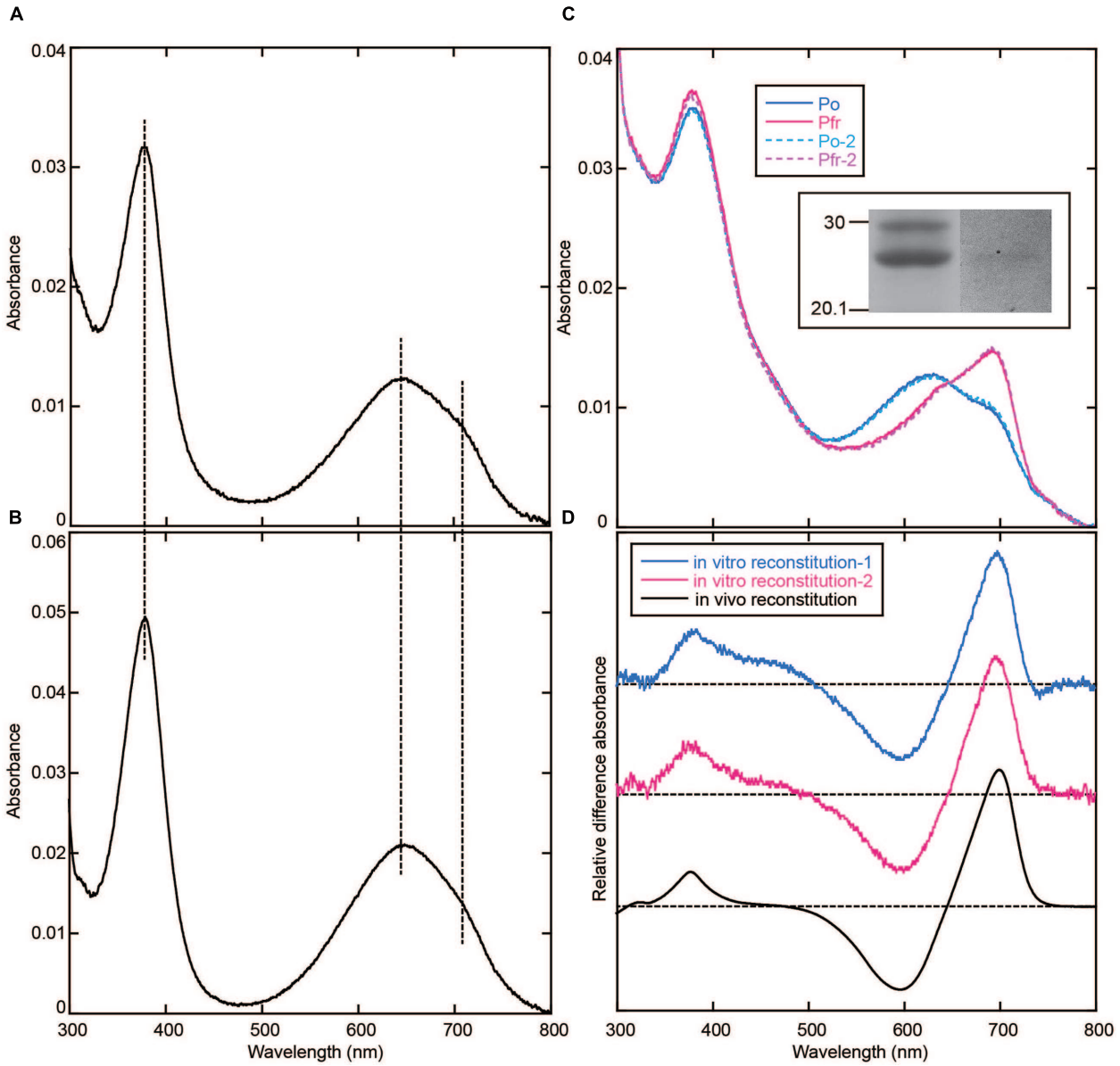

FIGURE 7 | Denaturation with 1% SDS and *in vitro* reconstitution. (A) Absorption spectrum of AM1_C0023g2-BV Pfr denatured with 1% SDS. **(B)** Absorption spectrum of AM1_1557g2-BV Pfr denatured with 1% SDS. **(C)** Absorption spectra of the Pfr and Po forms of S334G reconstituted with BV *in vitro*. Photoconversion was repeated twice. First-round Po: Solid blue line, first-round Pfr: Solid magenta line, second-round Po: Dotted cyan line, second-round Pfr: Dotted pink line. Inset: SDS-PAGE of *in vitro* reconstituted S334G. Left, CBB-stained gel. Right, in-gel fluorescence detection. **(D)** Pfr-minus-Po difference spectra of S334G reconstituted *in vitro* and *in vivo*. *In vitro* reconstitution: blue (first-round) and magenta (second-round) lines, *in vivo* reconstitution: black line.

Taking the possibility into consideration that the BV chromophore bound to AM1_C0023g2 is unstable under acidic condition, we denatured the AM1_C0023g2-BV under neutral urea condition. However, the denatured chromophore was also unstable and its absorption was rapidly bleached (data not shown). The result suggests that urea is crucial for the chromophore instability. Thus, we denatured the AM1_C0023g2-BV Pfr under 1% SDS as previously described (Ishizuka et al., 2007). As a result, its absorption maxima was observed at ∼646 nm and almost same as that of AM1_1557g2-BV Pfr (**Figures 7A,B**), indicating that their chromophores are both BV. To further confirm the result, we performed *in vitro* reconstitution analysis using S334G protein and BV chromophore. Although reconstitution efficiency was low, BV covalently bound to S334G was detected by in-gel fluorescence analysis (**Figure 7C**, inset). Far-red/orange reversible photoconversion was observed (**Figure 7C**) and is almost same as that observed for *in vivo* reconstituted one (**Figure 7D**). As a conclusion, the chromophore of AM1_C0023g2 expressed in BV-producing *E. coli* is indeed BV.

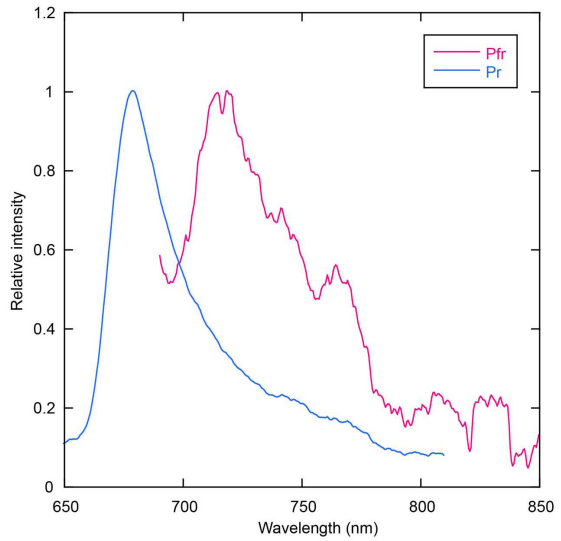

FIGURE 8 | Fluorescence spectra of AM1_C0023g2-BV Pfr (magenta) and AM1_C0023g2-PCB Pr (blue).

BV Chromophore Instability in the Presence of Urea

Although AM1_C0023g2 binds BV as well as the other BV-binding CBCRs and bacteriophytochromes, BV derived from only AM1_C0023g2 showed unstable nature in the presence of urea. Very recently, Shcherbakova et al. (2015) obtained a fluorescent protein that consists of PAS and GAF domain originally derived from a bacteriophytochrome, RpBphP1 (Shcherbakova et al., 2015). The fluorescent protein, Bph1-FP, covalently binds BV via Cys residue within the GAF domain. The crystal structure revealed that covalent-bonding site of Bph1-FP to BV is heterogeneous, namely $C3^1$ or $C3^2$. This means that a Cys residue within the GAF domain has a potential to ligate to both $C3^1$ and $C3^2$. In this context, we hypothesized that the Cys residue of AM1_C0023g2 ligates to $C3^1$ and the resultant adduct between the Cys residue and $C3^1$ of BV may affect stability of the denatured chromophore in the presence of urea, whereas Cys residues of AM1_1557g2 and AM1_1870g3 are likely to ligate to $C3^2$ of BV as well as normal bacteriophytochromes and the resultant chromophore may be stable under the same condition. Just after denaturation of Pfr form, a component

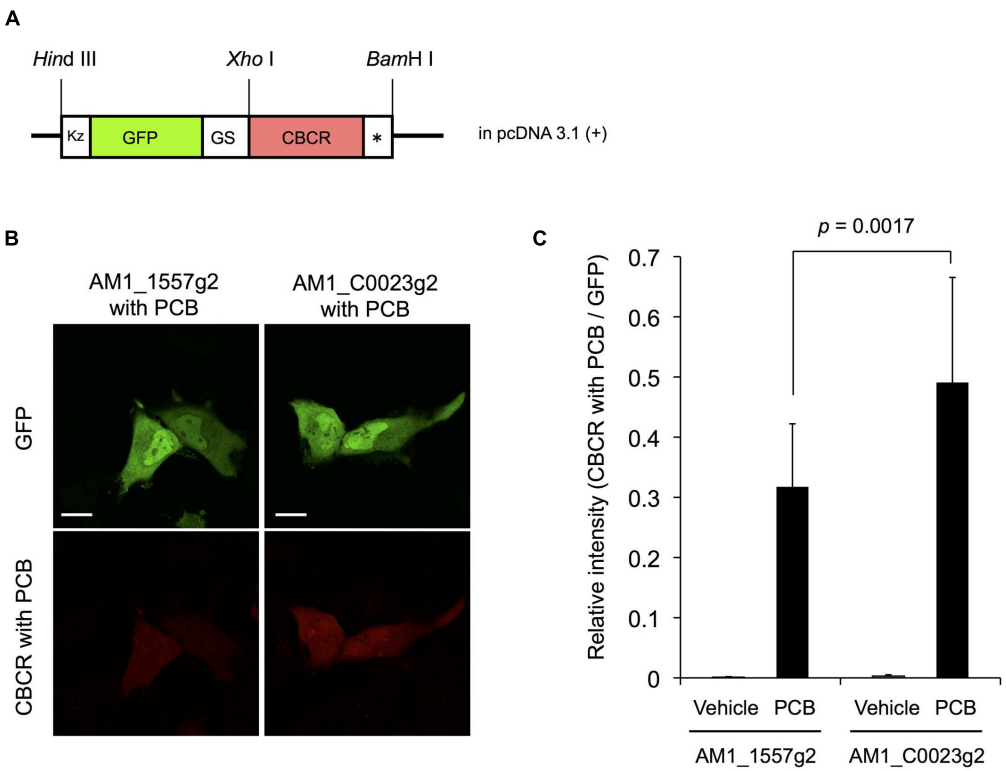

FIGURE 9 | Expression of GFP-fused AM1_1557g2 and AM1_C0023g2 in mammalian cells. (A) Schematic diagram of plasmid construct of GFP-fused AM1_1557g2 and AM1_C0023g2. Kz, Kozak sequence for efficient translation in mammalian cells; GS, a flexible peptide linker sequence (Gly-Gly-Ser-Gly-Gly); CBCR, AM1_1557g2 or AM1_C0023g2; *, stop codon. **(B)** Representative confocal fluorescence images of GFP-fused AM1_1557g2 with PCB and AM1_C0023g2 with PCB. Left column, GFP-fused AM1_1557g2 with PCB; right column, GFP-fused AM1_C0023g2 with PCB; green images, GFP fluorescence; red images, fluorescence of CBCR with PCB. Scale bars, 20 μm. **(C)** Relative intensity of fluorescence of CBCR with PCB normalized to GFP fluorescence. Error bars represent standard deviations (n = 16, 16, 16, and 17 for AM1_1557g2 with vehicle, AM1_1557g2 with PCB, AM1_C0023g2 with vehicle and AM1_C0023g2 with PCB, respectively).

corresponding to BV and at 700 nm rapidly converts into a component at 665 nm. This characteristic in absorbing around 665 nm is somehow similar to that of PCB. In this context, BV bound to AM1_C0023g2 may break down into PCB-like chromophore in the presence of urea. Urea may affect conjugated system of BV bound to AM1_C0023g2. In order to verify these hypotheses, we are now trying to crystalize both AM1_1557g2-BV and AM1_C0023g2-BV.

Evaluation of Chromophore Binding Efficiencies

We calculated binding efficiencies of AM1_C0023g2 to PCB and BV at ∼80 and ∼70%, respectively. Based on these values and in-gel fluorescence analysis (**Figure 1B**), we also estimated the binding efficiencies of AM1_1557g2 to PCB and BV at ∼50 and ∼40%, respectively. The binding efficiencies of AM1_C0023g2 to both PCB and BV are higher than those of AM1_1557g2. The binding efficiency of S334G to BV was calculated to be almost 100%, which is better than that of the wild type protein (∼70%).

Binding efficiency of AM1_C0023g2 to PCB is comparable to or slightly higher than that to BV. In this context, it is intriguing that no BV-binding holoproteins were detected from PCB-producing *E. coli* despite that BV should be present as a precursor. BV may be kept at quite low concentration in the PCB-producing *E. coli* via substrate-channeling from heme oxygenase to PcyA.

Fluorescence Spectroscopy

Room temperature fluorescence spectra of the thermostable forms of AM1_C0023g2-PCB and AM1_C0023g2-BV were measured to evaluate their potentials as fluorescent imaging probes (**Figure 8**). AM1_C0023g2-BV Pfr form fluoresces with a maximum at 718 nm, whereas AM1_C0023g2-PCB Pr form fluoresces with a maximum at 679 nm. The fluorescence maximum of AM1_C0023g2-BV Pfr is red-shifted by 39 nm compared with that of AM1_C0023g2-PCB Pr, a red shift similar to that found for their absorption spectra maxima. Fluorescence quantum yields of the Pr and Pfr forms were 3.0 and 0.2%, respectively. Fluorescence quantum yield of AM1_C0023g2-PCB Pr is about two times higher than that of AM1_1557g2-PCB Pr (Narikawa et al., 2015b).

Expression of AM1_1557g2 and AM1_C0023g2 in Mammalian Cells

We examined the fluorescence of AM1_1557g2-PCB and AM1_C0023g2-PCB in live mammalian cells. To precisely compare the fluorescence intensities of the CBCRs, we fused GFP to the CBCRs as an expression control (**Figure 9A**). HeLa cells were transfected with GFP-fused AM1_1557g2 and AM1_C0023g2 and treated with or without 20 μM PCB. Confocal fluorescence images of GFP-fused AM1_1557g2-PCB and AM1_C0023g2-PCB show bright green fluorescence of GFP, indicating that both GFP-fused AM1_1557g2 and AM1_C0023g2 were successfully expressed in the mammalian cells (**Figure 9B** upper left and right). Almost the same brightness of GFP indicates that the expression levels of GFP-fused AM1_1557g2 and AM1_C0023g2 were similar (**Figure 9B** upper left and right). No near-infrared fluorescence was detected from both cells without addition of PCB (**Figure 9C**). Low fluorescence quantum yield and/or low intrinsic BV level may be the reason for this result. On the other hand, the near-infrared fluorescence was detected from both cells after exposure to PCB. The near-infrared fluorescence of AM1_C0023g2-PCB was much higher than that of AM1_1557g2-PCB (**Figure 9B** lower right and left). Relative intensities of AM1_1557g2-PCB and AM1_C0023g2-PCB normalized to GFP intensities were 0.31 ± 0.10 and 0.49 ± 0.17, respectively (**Figure 9C**). This is the first report detecting fluorescence from PCB-binding CBCRs expressed in the mammalian cells. Their quantum yields are not so high, but comparable to those of the native phytochromes and CBCRs (Sineshchekov, 1995; Chen et al., 2012; Rockwell et al., 2012c; Pennacchietti et al., 2015). Thus, we can consider that AM1_C0023g2-PCB is appropriate for platform of fluorescent probe development as a starting material.

AUTHOR CONTRIBUTIONS

RN, MI, and MS designed the research. KF, TN, YA, TY, N-N-W, and RN performed experiments. N-N-W constructed plasmids. KF and RN performed protein purification and spectroscopic analyses. TN and YA performed fluorescence detection from mammalian cells. KF, TN, MS, and RN wrote the manuscript.

FUNDING

This work was supported by Precursory Research for Embryonic Science and Technology, Japan Science and Technology Agency, 4-1-8 Honcho Kawaguchi, Saitama 332-0012 (to RN) and Grants-in-Aid for Young Scientists (to RN, 26702036).

ACKNOWLEDGMENTS

We thank Prof. V.K. Deo (Shizuoka University) for critical reading of the manuscript. We thank Prof. K. Awai for experimental supports and helpful discussion (Shizuoka University).

REFERENCES

Anders, K., and Essen, L.-O. (2015). The family of phytochrome-like photoreceptors: diverse, complex and multi-colored, but very useful. *Curr. Opin. Struct. Biol.* 35, 7–16. doi: 10.1016/j.sbi.2015.07.005

Berkelman, T. R., and Lagarias, J. C. (1986). Visualization of bilin-linked peptides and proteins in polyacrylamide gels. *Anal. Biochem.* 156, 194–201. doi: 10.1016/0003-2697(86)90173-9

Burgie, E. S., Walker, J. M., Phillips, G. N. J., and Vierstra, R. D. (2013). A photolabile thioether linkage to phycoviolobilin provides the foundation for the

blue/green photocycles in DXCF-cyanobacteriochromes. *Structure* 21, 88–97. doi: 10.1016/j.str.2012.11.001

Campbell, E. L., Hagen, K. D., Chen, R., Risser, D. D., Ferreira, D. P., and Meeks, J. C. (2015). Genetic Analysis Reveals the Identity of the Photoreceptor for Phototaxis in Hormogonium Filaments of *Nostoc punctiforme*. *J. Bacteriol.* 197, 782–791. doi: 10.1128/JB.02374-14

Chen, Y., Zhang, J., Luo, J., Tu, J.-M., Zeng, X.-L., Xie, J., et al. (2012). Photophysical diversity of two novel cyanobacteriochromes with phycocyanobilin chromophores: photochemistry and dark reversion kinetics. *FEBS J.* 279, 40–54. doi: 10.1111/j.1742-4658.2011.08397.x

Cho, S. M., Jeoung, S. C., Song, J.-Y., Kupriyanova, E. V., Pronina, N. A., Lee, B.-W., et al. (2015). Genomic survey and biochemical analysis of recombinant candidate cyanobacteriochromes reveals enrichment for near UV/Violet sensors in the halotolerant and alkaliphilic cyanobacterium Microcoleus IPPAS B353. *J. Biol. Chem.* 290, 28502–28514. doi: 10.1074/jbc.M115.669150

Enomoto, G., Hirose, Y., Narikawa, R., and Ikeuchi, M. (2012). Thiol-based photocycle of the blue and teal light-sensing cyanobacteriochrome Tlr1999. *Biochemistry* 51, 3050–3058. doi: 10.1021/bi300020u

Enomoto, G., Ni-Ni-Win, Narikawa, R., and Ikeuchi, M. (2015). Three cyanobacteriochromes work together to form a light color-sensitive input system for c-di-GMP signaling of cell aggregation. *Proc. Natl. Acad. Sci. U.S.A.* 112, 8082–8087. doi: 10.1073/pnas.1504228112

Enomoto, G., Nomura, R., Shimada, T., Ni-Ni-Win, Narikawa, R., and Ikeuchi, M. (2014). Cyanobacteriochrome SesA is a diguanylate cyclase that induces cell aggregation in *Thermosynechococcus*. *J. Biol. Chem.* 289, 24801–24809. doi: 10.1074/jbc.M114.583674

Fukushima, Y., Iwaki, M., Narikawa, R., Ikeuchi, M., Tomita, Y., and Itoh, S. (2011). Photoconversion mechanism of a green/red photosensory cyanobacteriochrome AnPixJ: Time-resolved optical spectroscopy and FTIR analysis of the AnPixJ-GAF2 domain. *Biochemistry* 50, 6328–6339. doi: 10.1021/bi101799w

Glazer, A. N., and Fang, S. (1973). Chromophore content of blue-green algal phycobiliproteins. *J. Biol. Chem.* 248, 659–662.

Hirose, Y., Narikawa, R., Katayama, M., and Ikeuchi, M. (2010). Cyanobacteriochrome CcaS regulates phycoerythrin accumulation in *Nostoc punctiforme*, a group II chromatic adapter. *Proc. Natl. Acad. Sci. U.S.A.* 107, 8854–8859. doi: 10.1073/pnas.1000177107

Hirose, Y., Rockwell, N. C., Nishiyama, K., Narikawa, R., Ukaji, Y., Inomata, K., et al. (2013). Green/red cyanobacteriochromes regulate complementary chromatic acclimation via a protochromic photocycle. *Proc. Natl. Acad. Sci. U.S.A.* 110, 4974–4979. doi: 10.1073/pnas.1302909110

Hirose, Y., Shimada, T., Narikawa, R., Katayama, M., and Ikeuchi, M. (2008). Cyanobacteriochrome CcaS is the green light receptor that induces the expression of phycobilisome linker protein. *Proc. Natl. Acad. Sci. U.S.A.* 105, 9528–9533. doi: 10.1073/pnas.0801826105

Ikeuchi, M., and Ishizuka, T. (2008). Cyanobacteriochromes: a new superfamily of tetrapyrrole-binding photoreceptors in cyanobacteria. *Photochem. Photobiol. Sci.* 7, 1159–1167. doi: 10.1039/B802660M

Ishizuka, T., Narikawa, R., Kohchi, T., Katayama, M., and Ikeuchi, M. (2007). Cyanobacteriochrome TePixJ of *Thermosynechococcus elongatus* harbors phycoviolobilin as a chromophore. *Plant Cell Physiol.* 48, 1385–1390. doi: 10.1093/pcp/pcm106

Ishizuka, T., Shimada, T., Okajima, K., Yoshihara, S., Ochiai, Y., Katayama, M., et al. (2006). Characterization of cyanobacteriochrome TePixJ from a thermophilic cyanobacterium *Thermosynechococcus elongatus* strain BP-1. *Plant Cell Physiol.* 47, 1251–1261. doi: 10.1093/pcp/pcj095

Kehoe, D. M., and Grossman, A. R. (1996). Similarity of a chromatic adaptation sensor to phytochrome and ethylene receptors. *Science* 273, 1409–1412. doi: 10.1126/science.273.5280.1409

Kim, P. W., Freer, L. H., Rockwell, N. C., Martin, S. S., Lagarias, J. C., and Larsen, D. S. (2012a). Femtosecond photodynamics of the red/green cyanobacteriochrome NpR6012g4 from *Nostoc punctiforme*. 1, Forward dynamics. *Biochemistry* 51, 608–618. doi: 10.1021/bi201507k

Kim, P. W., Freer, L. H., Rockwell, N. C., Martin, S. S., Lagarias, J. C., and Larsen, D. S. (2012b). Femtosecond photodynamics of the red/green cyanobacteriochrome NpR6012g4 from *Nostoc punctiforme*. 2. reverse dynamics. *Biochemistry* 51, 619–630. doi: 10.1021/bi2017365

Kim, P. W., Freer, L. H., Rockwell, N. C., Martin, S. S., Lagarias, J. C., and Larsen, D. S. (2012c). Second-chance forward isomerization dynamics of the red/green cyanobacteriochrome NpR6012g4 from *Nostoc punctiforme*. *J. Am. Chem. Soc.* 134, 130–133. doi: 10.1021/ja209533x

Ma, Q., Hua, H. H., Chen, Y., Liu, B., Bin Krämer, A. L., Scheer, H., et al. (2012). A rising tide of blue-absorbing biliprotein photoreceptors - Characterization of seven such bilin-binding GAF domains in Nostoc sp, PCC7120. *FEBS J.* 279, 4095–4108. doi: 10.1111/febs.12003

Narikawa, R., Enomoto, G., Ni-Ni-Win, Fushimi, K., and Ikeuchi, M. (2014). A new type of dual-Cys cyanobacteriochrome GAF domain found in cyanobacterium *Acaryochloris marina*, which has an unusual red/blue reversible photoconversion cycle. *Biochemistry* 53, 5051–5059. doi: 10.1021/bi500376b

Narikawa, R., Fukushima, Y., Ishizuka, T., Itoh, S., and Ikeuchi, M. (2008a). A novel photoactive GAF Domain of cyanobacteriochrome AnPixJ that shows reversible green/red photoconversion. *J. Mol. Biol.* 380, 844–855. doi: 10.1016/j.jmb.2008.05.035

Narikawa, R., Fushimi, K., Ni-Ni-Win, and Ikeuchi, M. (2015a). Red-shifted red/green-type cyanobacteriochrome AM1_1870g3 from the chlorophyll d-bearing cyanobacterium *Acaryochloris marina*. *Biochem. Biophys. Res. Commun.* 461, 390–395. doi: 10.1016/j.bbrc.2015.04.045

Narikawa, R., Ishizuka, T., Muraki, N., Shiba, T., Kurisu, G., and Ikeuchi, M. (2013). Structures of cyanobacteriochromes from phototaxis regulators AnPixJ and TePixJ reveal general and specific photoconversion mechanism. *Proc. Natl. Acad. Sci. U.S.A.* 110, 918–923. doi: 10.1073/pnas.1212098110

Narikawa, R., Kohchi, T., and Ikeuchi, M. (2008b). Characterization of the photoactive GAF domain of the CikA homolog (SyCikA, Slr1969) of the cyanobacterium *Synechocystis* sp. *PCC* 6803. *Photochem. Photobiol. Sci.* 7, 1253–1259. doi: 10.1039/b811214b

Narikawa, R., Nakajima, T., Aono, Y., Fushimi, K., Enomoto, G., Ni-Ni-Win, et al. (2015b). A biliverdin-binding cyanobacteriochrome from the chlorophyll d-bearing cyanobacterium *Acaryochloris marina*. *Sci. Rep.* 5:7950. doi: 10.1038/srep07950

Narikawa, R., Suzuki, F., Yoshihara, S., Higashi, S., Watanabe, M., and Ikeuchi, M. (2011). Novel photosensory two-component system (PixA-NixB-NixC) involved in the regulation of positive and negative phototaxis of cyanobacterium *Synechocystis* sp, PCC 6803. *Plant Cell Physiol.* 52, 2214–2224. doi: 10.1093/pcp/pcr155

Pennacchietti, F., Losi, A., Xu, X., Zhao, K., Gartner, W., Viappiani, C., et al. (2015). Photochromic conversion in a red/green cyanobacteriochrome from Synechocystis PCC6803: quantum yields in solution and photoswitching dynamics in living *E. coli* cells. *Photochem. Photobiol. Sci.* 14, 229–237. doi: 10.1039/c4pp00337c

Rockwell, N. C., Martin, S. S., Feoktistova, K., and Lagarias, J. C. (2011). Diverse two-cysteine photocycles in phytochromes and cyanobacteriochromes. *Proc. Natl. Acad. Sci. U.S.A.* 108, 11854–11859. doi: 10.1073/pnas.1107844108

Rockwell, N. C., Martin, S. S., Gulevich, A. G., and Lagarias, J. C. (2012a). Phycoviolobilin formation and spectral tuning in the DXCF cyanobacteriochrome subfamily. *Biochemistry* 51, 1449–1463. doi: 10.1021/bi201783j

Rockwell, N. C., Martin, S. S., Gulevich, A. G., and Lagarias, J. C. (2014). Conserved phenylalanine residues are required for blue-shifting of cyanobacteriochrome photoproducts. *Biochemistry* 53, 3118–3130. doi: 10.1021/bi500037a

Rockwell, N. C., Martin, S. S., and Lagarias, J. C. (2012b). Mechanistic insight into the photosensory versatility of DXCF cyanobacteriochromes. *Biochemistry* 51, 3576–3585. doi: 10.1021/bi300171s

Rockwell, N. C., Martin, S. S., and Lagarias, J. C. (2012c). Red/green cyanobacteriochromes: sensors of color and power. *Biochemistry* 51, 9667–9677. doi: 10.1021/bi3013565

Rockwell, N. C., Martin, S. S., Lim, S., Lagarias, J. C., and Ames, J. B. (2015a). Characterization of red/green cyanobacteriochrome NpR6012g4 by solution nuclear magnetic resonance spectroscopy: a hydrophobic pocket for the C15-E,anti chromophore in the photoproduct. *Biochemistry* 54, 3772–3783. doi: 10.1021/acs.biochem.5b00438

Rockwell, N. C., Martin, S. S., Lim, S., Lagarias, J. C., and Ames, J. B. (2015b). Characterization of red/green cyanobacteriochrome NpR6012g4 by solution nuclear magnetic resonance spectroscopy: a protonated bilin ring system in both photostates. *Biochemistry* 54, 2581–2600. doi: 10.1021/bi501548t

Rockwell, N. C., Njuguna, S. L., Roberts, L., Castillo, E., Parson, V. L., Dwojak, S., et al. (2008). A second conserved GAF domain cysteine is required for the blue/green photoreversibility of cyanobacteriochrome Tlr0924 from *Thermosynechococcus elongatus*. *Biochemistry* 47, 7304–7316. doi: 10.1021/bi800088t

Savakis, P., De Causmaecker, S., Angerer, V., Ruppert, U., Anders, K., Essen, L.-O., et al. (2012). Light-induced alteration of c-di-GMP level controls motility of *Synechocystis* sp, PCC 6803. *Mol. Microbiol.* 85, 239–251. doi: 10.1111/j.1365-2958.2012.08106.x

Shcherbakova, D. M., Baloban, M., Pletnev, S., Malashkevich, V. N., Xiao, H., Dauter, Z., et al. (2015). Molecular basis of spectral diversity in near-infrared phytochrome-based fluorescent proteins. *Chem. Biol.* 22, 1540–1551. doi: 10.1016/j.chembiol.2015.10.007

Sineshchekov, V. A. (1995). Photobiophysics and photobiochemistry of the heterogeneous phytochrome system. *Biochim. Biophys. Acta* 1228, 125–164. doi: 10.1016/0005-2728(94)00173-3

Slavov, C., Xu, X., Zhao, K.-H., Gartner, W., and Wachtveitl, J. (2015). Detailed insight into the ultrafast photoconversion of the cyanobacteriochrome Slr1393 from *Synechocystis* sp. *Biochim. Biophys. Acta* 1847, 1335–1344. doi: 10.1016/j.bbabio.2015.07.013

Song, C., Narikawa, R., Ikeuchi, M., Gärtner, W., and Matysik, J. (2015a). Color tuning in red/green cyanobacteriochrome AnPixJ: photoisomerization at C15 causes an excited-state destabilization. *J. Phys. Chem. B* 119, 9688–9695. doi: 10.1021/acs.jpcb.5b04655

Song, C., Velazquez Escobar, F., Xu, X.-L., Narikawa, R., Ikeuchi, M., Siebert, F., et al. (2015b). A red/green cyanobacteriochrome sustains its color despite a change in the bilin chromophore's protonation state. *Biochemistry* 54, 5839–5848. doi: 10.1021/acs.biochem.5b00735

Song, J.-Y., Cho, H. S., Cho, J.-I., Jeon, J.-S., Lagarias, J. C., and Park, Y.-I. (2011). Near-UV cyanobacteriochrome signaling system elicits negative phototaxis in the cyanobacterium *Synechocystis* sp. *PCC* 6803. *Proc. Natl. Acad. Sci. U.S.A.* 108, 10780–10785. doi: 10.1073/pnas.1104242108

Velazquez Escobar, F., Utesch, T., Narikawa, R., Ikeuchi, M., Mroginski, M. A., Gärtner, W., et al. (2013). Photoconversion mechanism of the second GAF domain of cyanobacteriochrome AnPixJ and the cofactor structure of its green-absorbing state. *Biochemistry* 52, 4871–4880. doi: 10.1021/bi400506a

Yoshihara, S., Katayama, M., Geng, X., and Ikeuchi, M. (2004). Cyanobacterial phytochrome-like PixJ1 holoprotein shows novel reversible photoconversion between blue- and green-absorbing forms. *Plant Cell Physiol.* 45, 1729–1737. doi: 10.1093/pcp/pch214

Yoshihara, S., Suzuki, F., Fujita, H., Geng, X. X., and Ikeuchi, M. (2000). Novel putative photoreceptor and regulatory genes Required for the positive phototactic movement of the unicellular motile cyanobacterium *Synechocystis* sp. PCC 6803. *Plant Cell Physiol.* 41, 1299–1304. doi: 10.1093/pcp/pce010

Ziegler, T., and Möglich, A. (2015). Photoreceptor engineering. *Front. Mol. Biosci.* 2:30. doi: 10.3389/fmolb.2015.00030

Conflict of Interest Statement: The authors declare that the research was conducted in the absence of any commercial or financial relationships that could be construed as a potential conflict of interest.

The reviewer Y-IlP and handling Editor declared a current collaboration and the handling Editor states that the process nevertheless met the standards of a fair and objective review.

frontiers in Microbiology

ORIGINAL RESEARCH
published: 19 February 2016
doi: 10.3389/fmicb.2016.00193

RNA-seq Profiling Reveals Novel Target Genes of LexA in the Cyanobacterium *Synechocystis* sp. PCC 6803

Ayumi Kizawa[1], *Akihito Kawahara*[2], *Yasushi Takimura*[2], *Yoshitaka Nishiyama*[1] *and Yukako Hihara*[1,3]*

[1] Department of Biochemistry and Molecular Biology, Graduate School of Science and Engineering, Saitama University, Saitama, Japan, [2] Biological Science Laboratories, KAO Corporation, Wakayama, Japan, [3] Core Research of Evolutional Science and Technology, Japan Science and Technology Agency, Saitama, Japan

LexA is a well-established transcriptional repressor of SOS genes induced by DNA damage in *Escherichia coli* and other bacterial species. However, LexA in the cyanobacterium *Synechocystis* sp. PCC 6803 has been suggested not to be involved in SOS response. In this study, we performed RNA-seq analysis of the wild-type strain and the *lexA*-disrupted mutant to obtain the comprehensive view of LexA-regulated genes in *Synechocystis*. Disruption of *lexA* positively or negatively affected expression of genes related to various cellular functions such as phototactic motility, accumulation of the major compatible solute glucosylglycerol and subunits of bidirectional hydrogenase, photosystem I, and phycobilisome complexes. We also observed increase in the expression level of genes related to iron and manganese uptake in the mutant at the later stage of cultivation. However, none of the genes related to DNA metabolism were affected by disruption of *lexA*. DNA gel mobility shift assay using the recombinant LexA protein suggested that LexA binds to the upstream region of *pilA7*, *pilA9*, *ggpS,* and *slr1670* to directly regulate their expression, but changes in the expression level of photosystem I genes by disruption of *lexA* is likely a secondary effect.

Keywords: cyanobacteria, LexA, RNA-seq, *Synechocystis*, transcriptome

OPEN ACCESS

Edited by:
Takashi Osanai,
Meiji University, Japan

Reviewed by:
Lei Chen,
Tianjin University, China
Rei Narikawa,
Shizuoka University, Japan

***Correspondence:**
Yukako Hihara
hihara@molbiol.saitama-u.ac.jp

Specialty section:
This article was submitted to Microbiotechnology, Ecotoxicology and Bioremediation, a section of the journal Frontiers in Microbiology

Received: *07 January 2016*
Accepted: *04 February 2016*
Published: *19 February 2016*

Citation:
Kizawa A, Kawahara A, Takimura Y, Nishiyama Y and Hihara Y (2016) RNA-seq Profiling Reveals Novel Target Genes of LexA in the Cyanobacterium Synechocystis sp. PCC 6803. Front. Microbiol. 7:193. doi: 10.3389/fmicb.2016.00193

INTRODUCTION

The LexA protein in *Escherichia coli* has been well-characterized as the key regulator of the SOS response induced by DNA damage (Butala et al., 2009). Under non-stress conditions, LexA binds to the promoter regions of more than 40 genes involved in the SOS response and represses their expression. When DNA is damaged, LexA undergoes autoproteolytic cleavage upon association with RecA protein activated through binding of single-stranded DNA fragments. As a consequence of auto-cleavage of the Ala84-Gly85 peptide bond carried out by Ser119 and Lys156, LexA loses DNA binding activity, thereby inducing the SOS response.

Genes encoding LexA homologs are highly conserved in bacterial genomes and LexA-dependent transcriptional regulation of genes involved in DNA repair has been reported in various bacterial species (Erill et al., 2007; Butala et al., 2009), indicating that the regulation of SOS regulon by LexA might be a universal adaptation strategy of bacteria to DNA damage. However, LexA homologs

in several cyanobacterial species were suggested not to be involved in the typical *E. coli*-type SOS regulation. In *Anabaena* sp. PCC 7120, auto-cleavage of the Ala84-Gly85 bond of LexA does not occur at physiological pH even in the presence of activated RecA (Kumar et al., 2015). In the case of *Synechocystis* sp. PCC 6803 (S.6803), LexA lacks the conserved Ala-Gly auto-cleavage site and the serine of the Ser-Lys dyad required for auto-cleavage activity (Patterson-Fortin et al., 2006) and auto-cleavage of LexA in S.6803 has not been reported so far. DNA microarray analysis revealed that LexA depletion did not affect the expression level of genes involved in DNA metabolism (Domain et al., 2004).

The cellular processes regulated by LexA in S.6803 have been implied by studies reporting isolation of LexA as a binding factor to the promoter region of specific genes, such as the *hoxEFUYH* operon encoding bidirectional hydrogenase (Gutekunst et al., 2005; Oliveira and Lindblad, 2005), *crhR* encoding RNA helicase (Patterson-Fortin et al., 2006), and *sbtA* encoding sodium-dependent bicarbonate transporter (Lieman-Hurwitz et al., 2009). Domain et al. (2004) performed DNA microarray analysis of the LexA-depleted strain and found that most of genes affected were previously reported to be regulated by the availability of inorganic carbon (Wang et al., 2004). Kamei et al. (2001) reported that the *lexA*-disrupted mutant of the motile strain of S.6803 (denoted PCC strain) showed non-motile phenotype. DNA microarray analysis revealed that expression of the *pilA* genes encoding the subunits of the type IV pilus-like structure was lowered in the mutant. Although regulation of various cellular processes has been suggested, we currently have still a fragmentary understanding of the function of LexA in S.6803.

DNA microarray analysis has been the most popular methods of genome-wide transcriptome profiling. However, it has been supplanted by RNA-seq analysis in which isolated transcripts are converted into the complementary DNA (cDNA) followed by direct sequence in a massively parallel DNA sequencing-based approach. The advantages of RNA-seq over DNA microarray are its higher resolution and better dynamic range of detecting differential gene expression (Zhao et al., 2014). In order to obtain the comprehensive view of LexA-regulated genes in S.6803, here we performed RNA-seq analysis of the wild-type (WT) strain and the *lexA*-disrupted mutant. The results of RNA-seq analysis indicate that LexA in S.6803 regulates specific cellular functions such as phototactic motility, accumulation of the major compatible solute glucosylglycerol and subunits of bidirectional hydrogenase, and photosynthetic complexes, but not the SOS response. DNA gel mobility shift assay using the recombinant LexA protein suggested that LexA binds to the upstream region of *pilA7*, *pilA9*, *ggpS,* and *slr1670* to directly regulate their expression.

MATERIALS AND METHODS

Strains and Culture Conditions

A glucose-tolerant non-motile strain (GT strain) of *Synechocystis* sp. PCC 6803 was grown at 32°C in BG-11 medium containing 20 mM HEPES-NaOH, pH 7.0, under continuous illumination at 20 μmol photons m^{-2} s^{-1} with bubbling of air. The *lexA* (*sll1626*)-disrupted mutant (Δ*lexA*) was grown under the same conditions, except that 20 μg mL^{-1} kanamycin (Km) was added to the medium. Cell density was estimated by measuring OD_{730} using a spectrophotometer (model UV-160A, Shimadzu).

Generation of the *lexA* (*sll1626*)-Disrupted Mutant

The coding region of *lexA* (612 bp, from nucleotide 1319330 to 1318719 according to numbering in CyanoBase) was disrupted by insertion of a kanamycin resistance (Km^r) cassette. The upstream and downstream fragments including the *lexA* coding sequence were amplified by PCR from the genomic DNA of the WT strain using the primer sets lexA-F and Km-lexA-R (for amplification of 404 bp upstream fragment, from nucleotide 1319525 to 1319122) and Km-lexA-F and lexA-R (for amplification of 394 bp downstream fragment, from nucleotide 1318996 to 1318603; **Table S1**). Km^r cassette was PCR amplified from the pRL161 plasmid using the primer set Km-F and Km-R (**Table S1**). The amplified *lexA* fragments and Km^r cassette were fused together by the fusion PCR method (Wang et al., 2002) using the primer set lexA-F and lexA-R. The WT strain was transformed with the fusion PCR product and transformants (Δ*lexA* mutant) were selected in the presence of Km.

RNA Gel Blot Analysis

Isolation of total RNA by the hot phenol method and RNA gel blot analyses, using DIG RNA Labeling and Detection Kit (Roche), were performed as described previously (Muramatsu and Hihara, 2003). Template DNA fragments for *in vitro* transcription to generate RNA probes were prepared by PCR using the primers shown in **Table S1**.

Immunoblot Analysis

Total proteins were extracted from *Synechocystis* cells as described previously (Ishii and Hihara, 2008) and separated by 15% (w/v) SDS-PAGE, followed by electroblotting onto PVDF membranes (Immobilon-P; Millipore). Immunodetection was done using a rabbit polyclonal antibody raised against His-LexA recombinant protein. Goat anti-rabbit IgG conjugated to alkaline phosphatase was used as a secondary antibody.

Determination of Pigment Contents

In vivo absorption spectra of whole cells suspended in BG-11 medium were measured at room temperature using a spectrophotometer (V-650 Spectrometer, JASCO) with ISV-722 integrating sphare. Chlorophyll and phycocyanin contents were calculated from the peak heights of absorption spectra using the equations described in Arnon et al. (1974).

RNA-seq Analysis

RNA-seq analysis was carried out using cultures at $OD_{730} = 0.5$ and $OD_{730} = 1.0$ with three biological replicates. WT and Δ*lexA* were inoculated into new media at $OD_{730} = 0.1$ and incubated for 50 and 80 h, respectively, to be harvested at $OD_{730} = 0.5$. Similarly, WT and Δ*lexA* were inoculated at $OD_{730} = 0.1$ and incubated for 70 and 120 h, respectively, to be harvested at $OD_{730} = 1.0$. Isolation of total RNA by the hot phenol method

was performed as described previously (Muramatsu and Hihara, 2003). To eliminate genomic DNA from total RNA samples, each sample was added with DNase I (TaKaRa) and incubated at 37°C for 3 h. Total RNA concentration was measured with Nanodrop 2000 (Thermo Fisher Scientific). The Ribo-Zero Magnetic Kit for Bacteria (Epicentre) was used to remove ribosomal RNA from each sample. Concentration and quality of mRNA samples were examined using an Agilent 2100 Bioanalyzer. TruSeq RNA Sample Prep Kit v2 (Illumina) was used for cDNA library construction, and the libraries were sequenced using the Illumina MiSeq system. 12 samples in total were analyzed using two cartridge of MiSeq Reagent Kit v3 (Illumina).

A total of 64 million reads data was obtained from 12 samples. To quantify expression level of each gene, nucleotide sequences of obtained reads were mapped to the genomic sequence of GT-I strain of S.6803 (Kanesaki et al., 2012) (NC_017038.1; http://www.ncbi.nlm.nih.gov/nuccore/NC_017038) using CLC Genomics Workbench 7.5.1 software (Qiagen). Raw read counts were divided by length of the transcripts and total number of million mapped reads in each sample to obtain reads per kilobase per million (RPKM) values (Mortazavi et al., 2008). TCC package of R software (Sun et al., 2013) was used to detect the differentially expressed genes between WT and Δ*lexA*. A false discovery rate of <0.01 was considered to be significant.

Overexpression and Purification of His-lexA

The coding region of the *lexA* gene was amplified by PCR using the primers lexA-NdeI-F and lexA-XhoI-R (**Table S1**), containing NdeI and XhoI sites at their 5′ end, respectively. The amplified *lexA* coding fragment was cloned into the pT7Blue T-vector (Novagen), digested with NdeI and XhoI and subcloned into the same restriction sites in pET28a vector (Novagen) to express the LexA protein with an N-terminal 6 × His-tag.

E. coli BL21(DE3) harboring the His-LexA expression construct was grown to an OD_{600} = 0.6 in 250 mL of 2 × yeast extract-tryptone (YT) medium containing 20 μg mL^{-1} Km at 37°C and induced with 0.013% of isopropyl β-D-thiogalactoside for 3 h. The cells were pelleted by centrifugation at 5800 g for 2 min, resuspended in 50 mM sodium phosphate buffer, pH 7.4, containing 0.5 M NaCl and 60 mM imidazole, and disrupted by three rounds of sonication with Sonifier 450 (Branson) for 2 min with interval of 1 min on ice. After the removal of whole cells and insoluble material by centrifugation, the soluble protein fraction was filtered through a 0.2 μm filter (DISMIC-25CS; ADVANTEC). His-LexA was purified by nickel-affinity column chromatography using a HisTrap FF crude (GE Healthcare). The soluble protein fraction was applied to the column equilibrated with 20 mM phosphate buffer, pH 7.4, containing 0.5 M NaCl and 60 mM imidazole, washed with 20 mM phosphate buffer, pH 7.4, containing 0.5 M NaCl and 80 mM imidazole, and eluted with 20 mM phosphate buffer, pH 7.4, containing 0.5 M NaCl and 300 mM imidazole. Purified His-LexA was desalted by a HiTrap Desalting column (GE Healthcare). Protein composition was examined by 15% (w/v) SDS-PAGE followed by staining with Coomassie Brilliant Blue R-250.

DNA Gel Mobility Shift Assay

Probes for DNA gel mobility shift assays were obtained by PCR amplification with primers shown in **Table S1** using genomic DNA as a template. The 3′ end of the DNA fragment for each probe was labeled with digoxigenin (DIG)-ddUTP by using the terminal transferase method according to the manufacturer's instructions (DIG gel shift kit 2nd generation; Roche). Gel mobility shift assays were performed by using a DIG gel shift kit 2nd generation (Roche) according to the manufacturer's instruction except that 1 mM DTT was added to the reaction mixture.

RESULTS

Characterization of the *lexA* (*sll1626*)-Disrupted Mutant

To reveal the function of LexA in GT strain of S.6803, we disrupted the *lexA* gene by inserting a Km^r cassette within the coding region (**Figure 1A**). Although a fully segregated mutant was not obtained (**Figure 1B**), RNA gel blot and immunoblot analyses revealed that both the *lexA* transcript (**Figure 1C**) and LexA protein (**Figure 1D**) levels were below the detection limit in the partially segregated mutant (Δ*lexA*) grown under normal growth conditions. Under the same conditions, Δ*lexA* displayed several abnormal phenotypes. The doubling time of Δ*lexA* was longer (31.4 h) than that of WT (19.5 h) at log phase, whereas the difference in growth rate between strains became smaller at stationary phase (**Figure 1E**). Amounts of chlorophyll and phycocyanin in Δ*lexA* calculated from the peak heights of cellular absorption spectra were 93 and 80% of WT levels, respectively (**Figure 1F**). Microscopic observation revealed that cell size of Δ*lexA* was heterogeneous and tended to be larger than that of WT (**Figure 1G**).

RNA-seq Transcriptome Analysis

To investigate the difference in gene expression profile between WT and Δ*lexA*, total RNA was isolated from cultures incubated under normal growth conditions and RNA-seq analysis was performed. **Figure 2** shows MA plots of the gene expression data obtained from cultures at OD_{730} = 0.5 and OD_{730} = 1.0. There were 1011 genes differentially expressed between strains at OD_{730} = 0.5 as shown in magenta (**Figure 2A**). Among them, expression levels of 315 genes were more than two-fold higher and those of 28 genes were more than two-fold lower in Δ*lexA* than in WT (**Table S2**). In the case of WT and Δ*lexA* cells at OD_{730} = 1.0, there were 447 genes differentially expressed between strains (**Figure 2B**). Among them, expression levels of 360 genes were more than two-fold higher and those of 21 genes were more than two-fold lower in Δ*lexA* than in WT (**Table S3**).

Table 1 shows the list of genes whose expression was affected by disruption of *lexA*. The higher resolution and better dynamic range of RNA-seq analysis compared to DNA microarray analysis enabled listing of small ORFs such as *ssl1577*, *ggpR* (*ssl3076*), *ssr1251*, *ssr1473* and *ssr3589,* and genes with low expression level (low RPKM value) that cannot be detected by previous DNA microarray analyses. Differentially expressed genes can

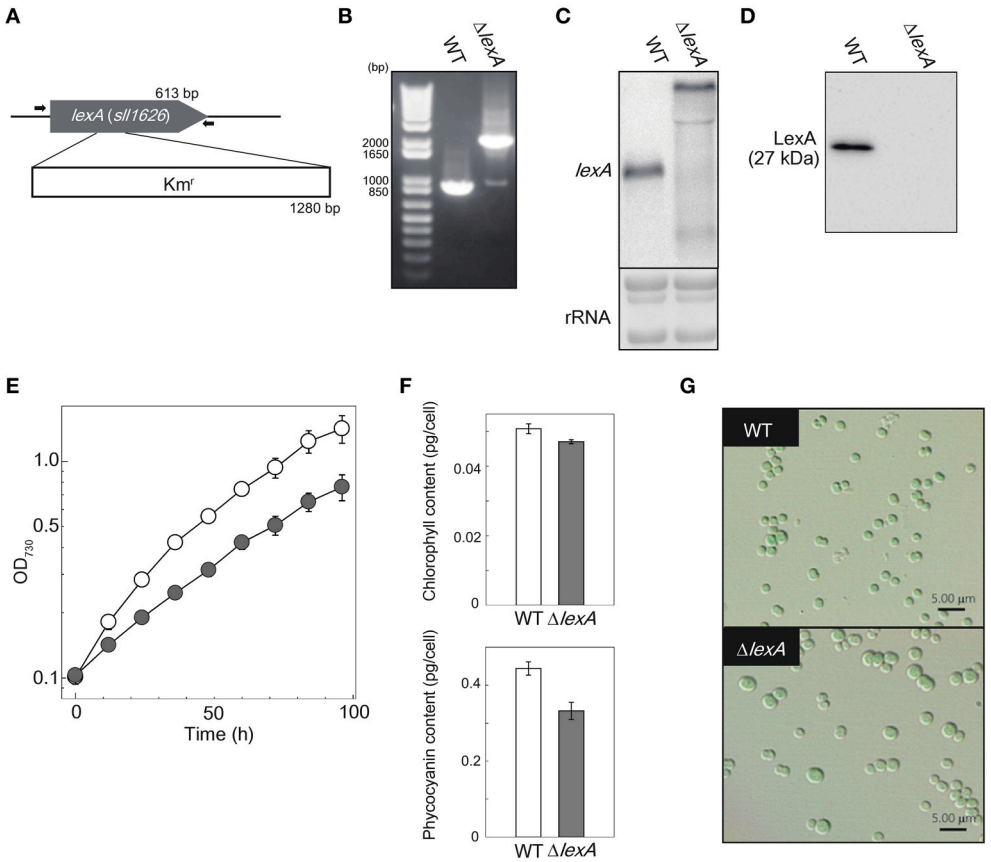

FIGURE 1 | Generation and characterization of the Δ*lexA* mutant. (A) Scheme of the construct for disruption of *lexA*. The kanamycin resistance (Km^r) cartridge was inserted into the coding region. Arrows indicate the primers used for PCR amplification shown in **(B)**. **(B)** PCR amplification of the *lexA* gene using genomic DNA from WT and the Δ*lexA* mutant as templates. **(C)** RNA gel blot analysis of the *lexA* transcripts detected by single-stranded RNA probe. 3 μg of total RNA were loaded per lane. Total RNA was stained with methylene blue to show the equal loading. **(D)** Immunoblot analysis of the LexA protein detected by anti-LexA antibody. 5 μg of total protein from cell lysate were loaded per lane. **(E)** Growth curves of WT (open circles) and the Δ*lexA* mutant (closed circles) under normal growth conditions. **(F)** Amounts of photosynthetic pigments calculated from the peak heights of cellular absorption spectra. **(G)** Observation of cell morphology by differential interference contrast microscopy.

be categorized into several groups according to related cellular functions as mentioned below.

Motility-Related Genes

The motile strain of S.6803 exhibits phototactic motility dependent on the type IV-like thick pilus structure (Brahamsha and Bhaya, 2014). In S.6803 genome, there are multiple genes homologous to the *pilA* gene encoding the subunit of the type IV pilus-like structure. Among them, *pilA1* was shown to be responsible for the thick pilus structure, motility, and transformation efficiency (Bhaya et al., 1999; Yoshihara et al., 2001), whereas functions of other *pilA*-like genes are unknown. We observed that their expression is positively or negatively affected by disruption of the *lexA* gene. Expression of *pilA7-pilA8* was largely enhanced whereas that of *pilA9-pilA10-pilA11* and *pilA1-pilA2* decreased. The observed decrease in expression level of *pilA1* and *pilA9-pilA10-pilA11* was consistent with the results of DNA microarray analysis of the Δ*lexA* mutant in the motile PCC strain (Kamei et al., 2001).

Furthermore, we observed that several genes other than *pilA* involved in motility were affected by disruption of *lexA*. Expression of *pixG-pixH-pixI-pixJ1-pixJ2-pixL* (*sll0038-0043*) encoding regulatory factors involved in positive phototaxis increased in the mutant (**Tables S2**). It has been reported that motility is controlled by cAMP level in S.6803 and inactivation of *cya1* encoding adenylate cyclase or *sycrp1* encoding cAMP receptor protein results in loss of motility (Terauchi and Ohmori, 1999; Yoshimura et al., 2002a). Although expression of *cya1* and *sycrp1* itself was not so much affected by disruption of *lexA*, decrease in expression levels of five genes, *pilA9-pilA10-pilA11-slr2018* and *cccS* (*slr1667*), out of six genes reported to be decreased by disruption of *sycrp1*(Yoshimura et al., 2002b) was observed (**Table 1**). *cccS* is also considered to be related to motility, since its disruption resulted in loss of the thick pili (Yoshimura et al., 2010). We observed expression level of *sycrp2* is lower in Δ*lexA* (**Table 1**), although involvement of SYCRP2 in regulation of motility has not been reported.

TABLE 1 | Genes with altered expression in the *lexA*-disrupted mutant.

Gene No.	Gene symbol	Definition	OD_{730} = 0.5			OD_{730} = 1.0		
			Average RPKM		Ratio	Average RPKM		Ratio
			WT	Δ*lexA*	Δ*lexA*/WT	WT	Δ*lexA*	Δ*lexA*/WT
MOTILITY								
sll1694	*pilA1*	Pilin polypeptide PilA1	7672.37	3764.79	0.49	9711.78	3875.35	0.40
sll1695	*pilA2*	Pilin polypeptide PilA2	245.64	161.17	0.66	272.03	149.86	0.55
slr1930	*pilA7*	Type 4 pilin-like protein	110.72	1163.62	10.51	148.23	1231.28	8.31
slr1931	*pilA8*	Type 4 pilin-like protein	193.59	1186.22	6.13	226.51	1250.18	5.52
slr2015	*pilA9*	Type 4 pilin-like protein	68.30	16.96	0.25	55.96	19.50	0.35
slr2016	*pilA10*	Type 4 pilin-like protein	38.83	23.24	0.60	37.41	16.90	0.45
slr2017	*pilA11*	Type 4 pilin-like protein	72.06	31.47	0.44	73.43	35.82	0.49
slr2018		Unknown protein	84.75	48.63	0.57	97.49	56.12	0.58
sll1291	*taxP2*	Two-component response regulator PatA subfamily	185.08	63.22	0.34	203.50	86.70	0.43
slr1667	*cccS*	Hypothetical protein (target gene of sycrp1)	25.66	13.57	0.53	45.84	18.36	0.40
GLUCOSYLGLYCEROL METABOLISM								
slr1670		Unknown protein	29.83	309.81	10.39	24.85	250.51	10.08
slr1672	*glpK*	Glycerol kinase	52.30	299.46	5.73	43.84	227.47	5.19
slr1673	*spoU*	Probable tRNA/rRNA methyltransferase	38.42	179.60	4.67	42.98	144.32	3.36
ssl3076	*ggpR*	Unknown protein	2.03	16.39	8.07	0.00	0.87	*N.D*
sll1566	*ggpS*	Glucosylglycerolphosphate synthase	34.65	497.47	14.36	27.78	431.85	15.54
sll1085	*glpD*	Glycerol-3-phosphate dehydrogenase	32.37	191.71	5.92	36.05	215.11	5.97
slr0529	*ggtB*	Glucosylglycerol transport system substrate-binding protein	17.28	79.09	4.58	18.76	76.80	4.09
slr0530	*ggtC*	Glucosylglycerol transport system permease protein	21.55	102.21	4.74	23.34	88.37	3.79
HYDROGENASE								
sll1220	*hoxE*	Diaphorase subunit of the bidirectional hydrogenase	100.28	48.94	0.49	62.85	32.54	0.52
sll1221	*hoxF*	Diaphorase subunit of the bidirectional hydrogenase	64.58	31.77	0.49	49.47	31.90	0.64
sll1223	*hoxU*	Diaphorase subunit of the bidirectional hydrogenase	96.63	49.39	0.51	68.18	47.23	0.69
sll1224	*hoxY*	Hydrogenase subunit of the bidirectional hydrogenase	70.59	35.93	0.51	37.57	28.59	0.76
ssl2420		Unknown protein	54.08	25.39	0.47	42.93	24.51	0.57
slr1675	*hypA1*	Putative hydrogenase expression/formation protein HypA1	31.16	266.71	8.56	33.07	195.50	5.91
PHOTOSYNTHESIS								
slr0737	*psaD*	Photosystem I subunit II	9924.04	5201.83	0.52	6914.54	4585.06	0.66
slr1835	*psaB*	P700 apoprotein subunit Ib	34540.96	22842.73	0.66	42976.65	25014.56	0.58
smr0004	*psaI*	Photosystem I subunit VIII	3093.51	2356.63	0.76	290.74	157.92	0.54
ssl0563	*psaC*	Photosystem I subunit VII	10241.74	5794.74	0.57	5317.26	3374.82	0.63
ssr0390	*psaK1*	Photosystem I subunit X	2883.40	1628.37	0.56	1635.89	1152.40	0.70
slr0012	*rbcS*	Rubisco small subunit	3477.08	1936.92	0.56	4542.25	3204.02	0.71
slr0011	*rbcX*	Possible Rubisco chaperonin	3913.65	2224.26	0.57	5157.07	3785.52	0.73
sll0247	*isiA*	Iron-stress chlorophyll-binding protein	55.34	124.36	2.25	53.76	761.15	14.16
sll0248	*isiB*	Flavodoxin	10.09	35.32	3.50	5.91	121.62	20.59
sll1577	*cpcB*	Phycocyanin beta subunit	62726.44	35125.15	0.56	54762.14	27956.67	0.51
sll1578	*cpcA*	Phycocyanin alpha subunit	79538.85	42145.92	0.53	69158.50	35179.81	0.51
sll1579	*cpcC2*	Phycobilisome rod linker polypeptide	13587.17	7921.46	0.58	12570.33	6318.76	0.50
sll1580	*cpcC1*	Phycobilisome rod linker polypeptide	14076.98	8090.37	0.57	12675.97	6193.81	0.49
ssl3093	*cpcD*	Phycobilisome small rod linker polypeptide	4048.58	2772.20	0.68	3023.79	1747.70	0.58
sll1471	*cpcG2*	Phycobilisome rod-core linker polypeptide	847.25	349.04	0.41	638.78	289.60	0.45
ssl2542	*hliA*	High light-inducible polypeptide HliA	22.74	133.52	5.87	26.31	167.07	6.35
ssr2595	*hliB*	High light-inducible polypeptide HliB	71.98	314.95	4.38	40.31	186.15	4.62

(Continued)

TABLE 1 | Continued

Gene No.	Gene symbol	Definition	OD_{730} = 0.5			OD_{730} = 1.0		
			Average RPKM		Ratio	Average RPKM		Ratio
			WT	Δ*lexA*	Δ*lexA*/WT	WT	Δ*lexA*	Δ*lexA*/WT
slr0506	*por*	Light-dependent NADPH-protochlorophyllide oxidoreductase	247.75	186.82	0.75	318.96	181.53	0.57
slr0749	*chlL*	Light-independent protochlorophyllide reductase iron protein subunit ChlL	489.76	109.67	0.22	98.28	41.69	0.42
slr0750	*chlN*	Light-independent protochlorophyllide reductase subunit ChlN	149.90	49.34	0.33	240.63	81.30	0.34
CHAPERONES								
sll0430	*htpG*	HtpG, heat shock protein 90	156.26	589.81	3.77	115.48	607.00	5.26
sll0909	*dnaJ*	DnaJ, heat shock protein 40	24.21	216.45	8.94	22.63	304.56	13.46
sll1514	*hspA*	16.6 kDa small heat shock protein	100.08	1082.85	10.82	121.59	1307.29	10.75
REGULATORY FUNCTIONS								
sll0094	*hik37*	Two-component sensor histidine kinase	52.56	33.12	0.63	74.37	39.50	0.53
sll0775		Unknown protein	29.04	391.93	13.50	40.24	339.89	8.45
sll0776	*spkD*	Serine/threonine kinase	16.14	248.58	15.40	27.99	235.49	8.41
sll0777		Putative carboxypeptidase	24.39	219.13	8.98	35.22	210.97	5.99
sll0778		ABC transporter, ATP-binding protein	14.17	72.87	5.14	17.63	71.67	4.07
sll0790	*hik31*	Two-component sensor histidine kinase	49.77	256.96	5.16	74.75	321.59	4.30
sll0797	*nrsR, rppA*	Redox-responsive and/or Ni(II)-responsive regulator, two-component response regulator OmpR subfamily	12.59	7.00	0.56	6.80	10.22	1.50
sll1003	*hik13*	Two-component sensor histidine kinase	10.65	45.77	4.30	10.70	50.35	4.71
sll1626	*lexA*	LexA repressor	1658.80	10652.12	6.42	1451.28	9173.74	6.32
sll1924	*sycrp2*	cAMP receptor protein sycrp1 homolog	23.44	13.60	0.58	11.10	13.47	1.21
slr0895	*prqR*	Transcriptional regulator	15.85	67.22	4.24	19.15	62.39	3.26
slr1564	*sigF*	Group 3 RNA polymerase sigma factor	297.21	217.21	0.73	330.72	209.54	0.63
slr1594	*patA*	Two-component response regulator PatA subfamily	40.38	195.88	4.85	49.36	265.06	5.37
slr1760	*rre8*	Two-component response regulator	15.72	104.05	6.62	26.41	88.06	3.33
slr2098	*hik21*	Two-component hybrid sensor and regulator	26.67	129.37	4.85	38.41	152.72	3.98
TRANSPORT AND BINDING PROTEINS								
sll1404	*exbB3*	Biopolymer transport ExbB protein homolog	84.83	131.51	1.55	16.17	290.69	17.98
sll1405	*exbD, sll1405*	Biopolymer transport ExbD protein homolog	28.62	59.22	2.07	13.99	118.68	8.48
sll1406	*fhuA*	Ferrichrome-iron receptor	29.10	57.61	1.98	25.09	132.90	5.30
sll1598	*mntC*	Mn transporter MntC	9.96	28.07	2.82	9.36	112.24	11.99
sll1599	*mntA*	Manganese transport system ATP-binding protein MntA	4.04	17.11	4.24	4.18	65.76	15.74
slr1295	*futA1*	Iron transport system substrate-binding protein	479.40	669.20	1.40	183.65	1131.71	6.16
slr0513	*futA2*	Iron transport system substrate-binding protein	425.93	832.10	1.95	366.04	2076.58	5.67
slr1488		Multidrug resistance family ABC transporter	15.16	46.45	3.06	17.28	130.69	7.56
OTHER CATEGORIES								
sll1358	*mncA*	Oxalate decarboxylase, periplasmic protein	248.08	94.87	0.38	133.04	73.57	0.55
sll1688	*thrC*	Threonine synthase	1010.37	704.75	0.70	1408.81	822.45	0.58
sll1709	*gdh*	3-ketoacyl-acyl carrier protein reductase	99.76	504.56	5.06	59.54	418.64	7.03
slr0518	*abfB*	Similar to alpha-L-arabinofuranosidase B	40.86	27.97	0.68	45.82	26.80	0.58
slr0786	*mapB*	Methionine aminopeptidase	6.73	20.91	3.11	6.85	35.69	5.21
slr1204	*degP*	Protease	109.11	511.99	4.69	122.90	572.69	4.66
slr1764	*capA*	Similar to tellurium resistance protein TerE	26.98	222.68	8.25	23.67	125.43	5.30
slr2097	*glbN*	Cyanoglobin	128.40	1919.90	14.95	116.38	1589.74	13.66
slr2116	*spsA*	Probable glycosyltransferase	22.84	11.76	0.51	16.60	14.06	0.85
ssr1720	*tyrS*	Similar to tyrosyl tRNA synthetase	5.26	14.68	2.79	3.77	24.90	6.61

(Continued)

TABLE 1 | Continued

Gene No.	Gene symbol	Definition	OD_{730} = 0.5			OD_{730} = 1.0		
			Average RPKM		Ratio	Average RPKM		Ratio
			WT	Δ*lexA*	Δ*lexA*/WT	WT	Δ*lexA*	Δ*lexA*/WT
UNKNOWN PROTEIN								
sll0249		Hypothetical protein	10.39	23.76	2.29	6.55	84.74	12.95
sll0327		Unknown protein	113.13	1929.23	17.05	157.08	1310.83	8.35
sll0328		Unknown protein	47.79	859.88	17.99	48.45	595.60	12.29
sll0443		Unknown protein	71.82	419.75	5.84	75.08	336.96	4.49
sll0444		Unknown protein	116.90	563.08	4.82	97.11	410.52	4.23
sll0445		Unknown protein	114.46	528.48	4.62	117.45	444.43	3.78
sll0448		Unknown protein	10.17	49.14	4.83	7.21	42.81	5.94
sll0543		Hypothetical protein	677.95	37.76	0.06	535.50	31.01	0.06
sll0783		Unknown protein	84.80	38.09	0.45	86.35	68.05	0.79
sll0846		Hypothetical protein	133.72	577.77	4.32	106.12	532.70	5.02
sll0910		Unknown protein	27.90	188.61	6.76	23.33	243.59	10.44
sll0911		Unknown protein	29.09	170.08	5.85	16.73	124.75	7.46
sll1009		Unknown protein	611.42	3545.01	5.80	926.18	3621.41	3.91
sll1119		Hypothetical protein	109.22	83.03	0.76	73.68	44.88	0.61
sll1236		Unknown protein	30.41	472.85	15.55	27.60	136.10	4.93
sll1239		Unknown protein	88.93	685.38	7.71	41.49	494.27	11.91
sll1240		Unknown protein	23.31	240.78	10.33	18.06	205.72	11.39
sll1241		Unknown protein	26.35	199.16	7.56	14.51	181.65	12.52
sll1247		Hypothetical protein	137.85	61.68	0.45	194.48	104.16	0.54
sll1359		Unknown protein	76.42	37.70	0.49	48.30	36.91	0.76
sll1396		Unknown protein	59.93	13.16	0.22	54.18	13.94	0.26
sll1472		Unknown protein	97.90	48.95	0.50	61.97	49.50	0.80
sll1483		Periplasmic protein	57.32	302.45	5.28	46.76	183.74	3.93
sll1549		Salt-enhanced periplasmic protein	232.67	121.52	0.52	18.94	215.48	11.37
sll1660		Hypothetical protein	45.49	351.04	7.72	48.25	355.40	7.37
sll1722		Hypothetical protein	18.55	130.15	7.01	13.41	45.98	3.43
sll1723		Probable glycosyltransferase	11.63	67.76	5.83	7.87	24.45	3.11
sll1851		Unknown protein	136.11	100.98	0.74	15.16	103.21	6.81
sll1913		Hypothetical protein	24.83	103.47	4.17	18.85	108.19	5.74
sll1921		Hypothetical protein	136.06	1118.71	8.22	152.96	1173.63	7.67
sll1956		Hypothetical protein	68.61	42.42	0.62	60.44	37.54	0.62
slr0105		Hypothetical protein	40.10	327.60	8.17	51.00	312.12	6.12
slr0106		Unknown protein	58.01	324.48	5.59	74.96	308.21	4.11
slr0179		Hypothetical protein	11.14	405.28	36.37	19.47	345.32	17.74
slr0196		Unknown protein	38.61	187.90	4.87	14.43	111.92	7.75
slr0317		Hypothetical protein	18.01	103.04	5.72	20.82	119.39	5.73
slr0362		Hypothetical protein	48.52	240.11	4.95	55.46	204.71	3.69
slr0364		Hypothetical protein	5.58	25.68	4.61	5.73	12.25	2.14
slr0393		Unknown protein	17.69	35.91	2.03	7.26	38.90	5.36
slr0442		Unknown protein	175.06	105.14	0.60	207.58	121.90	0.59
slr0572		Unknown protein	350.05	18.16	0.05	194.88	16.91	0.09
slr0573		Unknown protein	18.80	3.65	0.19	22.65	6.20	0.27
slr0581		Unknown protein	79.35	334.01	4.21	60.26	159.45	2.65
slr0617		Unknown protein	85.17	16.67	0.20	89.51	25.91	0.29
slr0709		Hypothetical protein	88.58	76.13	0.86	96.00	56.95	0.59
slr0868		Unknown protein	20.22	326.40	16.14	13.93	203.19	14.59

(Continued)

TABLE 1 | Continued

Gene No.	Gene symbol	Definition	OD_{730} = 0.5			OD_{730} = 1.0		
			Average RPKM		Ratio	Average RPKM		Ratio
			WT	Δ*lexA*	Δ*lexA*/WT	WT	Δ*lexA*	Δ*lexA*/WT
slr0869		Hypothetical protein	23.29	185.20	7.95	24.87	165.85	6.67
slr0870		Hypothetical protein	31.36	196.83	6.28	14.82	110.90	7.48
slr0871		Unknown protein	12.74	102.10	8.01	5.49	63.27	11.53
slr1161		Hypothetical protein	306.59	134.80	0.44	251.76	84.91	0.34
slr1162		Unknown protein	131.90	66.56	0.50	104.40	63.19	0.61
slr1278		Hypothetical protein YCF62	32.54	27.87	0.86	78.79	41.89	0.53
slr1484		Unknown protein	48.58	129.12	2.66	29.37	273.35	9.31
slr1485		Salt-induced periplasmic protein	12.48	53.60	4.29	14.24	110.54	7.76
slr1704		Hypothetical protein	162.27	1747.93	10.77	179.40	617.74	3.44
slr1767		Hypothetical protein	39.67	197.11	4.97	19.06	96.15	5.04
slr1772		Probable hydrolase, periplasmic protein	49.33	225.97	4.58	49.08	245.26	5.00
slr1788		Unknown protein	33.57	388.00	11.56	65.92	359.18	5.45
slr1789		Unknown protein	16.30	152.34	9.34	29.57	152.66	5.16
slr1798		Unknown protein	155.94	109.76	0.70	186.54	116.12	0.62
slr1920		Unknown protein	69.46	571.56	8.23	58.59	561.87	9.59
slr2119		Unknown protein	60.74	16.37	0.27	41.99	14.00	0.33
ssl1046		Hypothetical protein	573.18	21.06	0.04	291.05	10.30	0.04
ssl1378		Hypothetical protein	69.57	33.34	0.48	194.48	104.16	0.54
ssl1577		Hypothetical protein	20.16	114.07	5.66	7.78	45.35	5.83
ssr0332		Hypothetical protein	218.38	154.04	0.71	120.96	73.51	0.61
ssr1155		Hypothetical protein	670.58	374.80	0.56	164.79	140.34	0.85
ssr1251		Hypothetical protein	52.57	15.34	0.29	6.04	2.22	0.37
ssr1473		Hypothetical protein	13.23	91.14	6.89	10.36	45.68	4.41
ssr2194		Unknown protein	14.79	614.16	41.52	8.50	181.59	21.37
ssr2615		Hypothetical protein	24.65	17.45	0.71	27.18	9.41	0.35
ssr2962		Hypothetical protein	63.09	276.40	4.38	41.60	191.31	4.60
ssr3570		Unknown protein	61.19	27.67	0.45	30.69	17.30	0.56
ssr3589		Hypothetical protein	19.15	115.47	6.03	9.11	61.37	6.73

Glucosylglycerol-Related Genes

In S.6803, glucosylglycerol (GG) is a major compatible solute to adapt to high-salt or high-osmotic pressure conditions (Klähn and Hagemann, 2011). A set of genes related to GG biosynthesis (*ggp*, *glp*) and uptake (*ggt*) are organized into several gene clusters such as *ggtBCD* (*slr0529-0531*), *ggpS-glpD* (*sll1566-sll1085*), *ggpP-ggtA* (*slr0746-0747*), and *slr1670-glpK-spoU-slr1674-hypA1*(*slr1670-1675*) in S.6803 genome (Mikkat and Hagemann, 2000; Klähn et al., 2010). RNA-seq analysis revealed that expression levels of these gene clusters were significantly higher in Δ*lexA* than WT (**Table 1** and **Table S2**). Klähn et al. (2010) reported that a small ORF, *ggpR* (*ssl3076*), exists overlapping with the transcription initiation site of *ggpS* and its promoter region. Expression of *ggpR* was also induced by disruption of *lexA* (**Table 1**).

Hydogenase-Related Genes

Expression level of the *hoxE-hoxF-hoxU-hoxY-hoxH* operon encoding subunits of bidirectional NiFe-hydrogenase was lower in Δ*lexA*. This observation is consistent with the previous study reporting that LexA acts as a transcriptional activator for the *hox* operon (Gutekunst et al., 2005). On the other hand, the expression level of the *hypA1* gene involved in hydrogenase maturation increased in Δ*lexA*.

Photosynthesis-Related Genes

In S.6803, photosystem (PS) I complex is comprised of 11 subunits and genes encoding these subunits (*psa*) are dispersed throughout the genome (Kaneko et al., 1996). We found that the expression level of every PSI gene was lower in Δ*lexA* than WT. The expression level of genes encoding subunits of phycobilisome (*cpc*, *apc*) was also lower in the mutant, whereas the expression level of genes encoding PSII subunits (*psb*) was not so much affected by disruption of *lexA*. Expression levels of *chlL-chlN* encoding subunits of light-independent protochlorophyllide reductase and that of *por* encoding light-dependent protochlorophyllide reductase were lower in Δ*lexA*. Both light-dependent and -independent enzymes catalyzing the last step of chlorophyll biosynthesis are likely to be under the control of LexA. On the other hand, expression level of *hliA* and

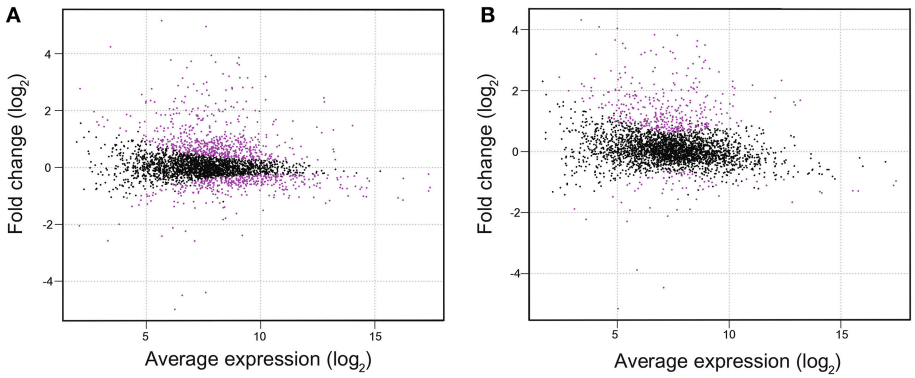

FIGURE 2 | MA plots of RNA-seq data obtained from WT and Δ*lexA* cells at OD_{730} = 0.5 (A) and OD_{730} = 1.0 (B). The MA plot, a scatterplot of log_2-fold-change (Δ*lexA* /WT) versus average expression in log_2 scale for each gene, was produced using TCC package. Dots shown in magenta indicate differentially expressed genes with a false discovery rate < 0.01.

hliB encoding high-light inducible proteins was higher in Δ*lexA* than WT.

SOS-Response Related Genes

Previous studies suggested that LexA in S.6803 is not involved in the SOS response. Neither *lexA* nor *recA* expression was induced upon UV-irradiation (Domain et al., 2004; Patterson-Fortin et al., 2006) and none of DNA metabolism-related genes was listed as genes induced or repressed by LexA depletion (Kamei et al., 2001; Domain et al., 2004). Similarly, induction or repression of DNA metabolism-related genes by disruption of *lexA* was not observed in our RNA-seq analysis.

Genes Differentially Expressed in Δ*lexA* at the Later Stage of Growth

Several genes expressed under iron-limiting conditions such as *exbB-exbD-fhuA* operon involved in inorganic iron uptake (Jiang et al., 2015), *futA1* and *futA2* encoding subunits of iron transporter (Katoh et al., 2001), and *isiA-isiB* operon encoding iron-stress inducible proteins (Vinnemeier et al., 1998) were highly induced in Δ*lexA* at OD_{730} = 1.0 but not in OD_{730} = 0.5. In the case of *mntA* and *mntC* encoding subunits of manganese transporter (Bartsevich and Pakrasi, 1995), their expression level was already higher in Δ*lexA* at OD_{730} = 0.5 and showed further increase at OD_{730} = 1.0.

DNA Gel Mobility Shift Assay

DNA gel mobility shift assay was performed to examine whether LexA directly regulates expression of putative target genes listed by RNA-seq analysis (**Figure 3**). We observed induction of the *pilA7-pilA8* operon and repression of the *pilA9-pilA10-pilA11* operon in Δ*lexA* (**Table 1**). Binding of His-LexA to the promoter regions of both operons (for the *pilA7* operon from nucleotide 2222102 to 2222304 and for the *pilA9* operon from nucleotide 755577 to 755778, according to numbering in CyanoBase) was observed, indicating that LexA directly activates or represses expression of these *pilA* operons. We also examined whether His-LexA binds to the upstream region of the two divergently transcribed operons, *ggpS-glpD* and *slr1670-glpK-spoU-slr1674-hypA1*, both of which are highly induced in Δ*lexA*. His-LexA bound to the promoter fragment of each operon (for the *ggpS* operon from nucleotide 1949371 to 1949186 and for the *slr1670* operon from nucleotide 1949332 to 1949534). It is notable that LexA-binding site for the the *ggpS* operon is within the coding region of *ggpR* (nucleotide 1949372 to 1949100). Our results suggest that LexA binds to at least two binding site located in the intergenic region of the *ggpS* and *slr1670* operons to repress their expression. Next, we examined the binding of LexA to the upstream region of PSI genes by using light-responsive promoter fragments containing the HLR1 sequence recognized by the response regulator RpaB (Seino et al., 2009). Binding of His-LexA to the promoter region of PSI genes was not observed (**Figure 3**) or much weaker than that to the *pilA7*, *pilA9*, *ggpS,* and *slr1670* promoters and not reproducible. This indicates that decrease in expression levels of PSI genes in Δ*lexA* may be a secondary effect.

DISCUSSION

Effects of Disruption of the *lexA* Gene in S.6803

In this study, we created the gene-disrupted mutant of *lexA* in GT strain of S.6803 to obtain the comprehensive view of LexA regulon by RNA-seq analysis. Although Kamei et al. (2001) successfully obtained the fully-segregated *lexA* mutant from the motile PCC strain, in most cases the Δ*lexA* mutant invariably retained the WT copy of the *lexA* gene (Domain et al., 2004; Gutekunst et al., 2005) and we also could not obtain fully-segregated mutant (**Figure 1B**). The heterogeneous appearance of the Δ*lexA* mutant cells (**Figure 1G**) may be caused by difference in the extent of segregation. However, despite the existence of the WT copy of *lexA*, immunoblot analysis revealed that LexA protein level was below the detection limit in our mutant (**Figure 1D**).

To date, LexA in S.6803 has been reported to be involved in transcriptional regulation of genes related to various cellular functions. Our RNA-seq data are consistent with some of these

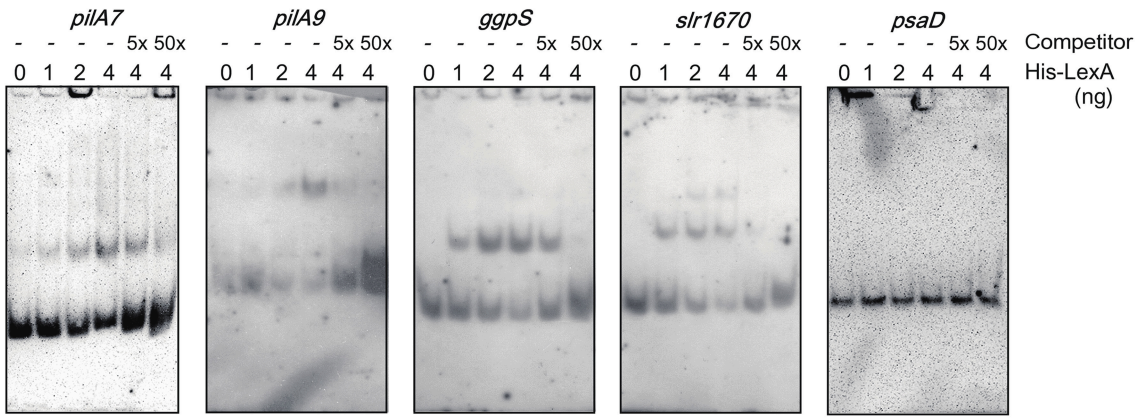

FIGURE 3 | DNA gel mobility shift assay of the promoter segments of putative target genes with His-LexA. DIG-labeled promoter segments of *pilA7*, *pilA9*, *ggpS*, *slr1670,* and *psaD* were incubated for 25 min at room temperature with His-LexA added at indicated concentrations. five-fold and 50-fold excess amounts of the non-labeled promoter segments were added as a competitor. Samples were separated on a 6% polyacrylamide gel.

reports, e.g., positive regulation of the *hox* operon reported by Gutekunst et al. (2005) and positive regulation of the *pilA* genes reported by Kamei et al. (2001). However, we could not observe the large effect of LexA depletion on carbon metabolism-related genes reported by Domain et al. (2004). Domain et al. isolated RNA for DNA microarray analysis from concentrated cultures incubated on plates for 2 h. The growth condition must be largely different from our liquid culture, which may cause the difference in gene expression profile. *in vitro* transcription/translation assay performed by Patterson-Fortin et al. (2006) showed that CrhR protein accumulation decreased in response to increasing LexA concentration. However, in our data, expression level of *crhR* was not affected by disruption of *lexA*.

RNA-seq data in this study suggested involvement of LexA in regulation of (1) phototactic motility, (2) accumulation of GG, (3) bidirectional hydrogenase, and (4) photosystem I and phycobilisome complexes. We also observed increase in expression level of genes related to iron and manganese uptake in Δ*lexA* at $OD_{730} = 1.0$. LexA may be involved in stage specific repression of these genes, but it is also possible that these genes were upregulated as a consequence of iron and manganese limitation in the mutant culture during prolonged incubation. We will discuss regulation of cellular processes (1)–(4) by LexA in the following sections.

Cellular Processes Regulated by LexA in S.6803

Phototactic Motility

Kamei et al. (2001) reported that disruption of the *lexA* gene in the motile PCC strain resulted in decrease in expression level of *pilA* genes and loss of thick pili and motility. Our RNA-seq analysis showed that expression levels of genes related to phototactic motility are largely affected by disruption of *lexA* also in the non-motile strain. In addition to the decrease in expression level of *pilA1* and *pilA9-pilA10-pilA11* reported in Kamei et al. (2001), we observed significant induction of *pilA7-pilA8*. Furthermore, expression levels of several genes related to positive phototaxis and cAMP signaling were affected. Although many non-motile mutants were so far isolated from the PCC strain, information on the mechanism of transcriptional regulation of motility-related genes is limited. Bhaya et al. (1999) reported decrease in expression level of *pilA1* and *pilA2* by disruption of the *sigF* gene encoding an alternative sigma factor. Yoshimura et al. (2002b) and Dienst et al. (2008) reported decrease in expression level of *pilA9-pilA10-pilA11-slr2018* and *cccS-cccP* by disruption of *sycrp1* encoding cAMP receptor protein and *hfq* encoding RNA chaperone homolog, respectively. Panichkin et al. (2006) reported decrease in expression level of *pilA9-pilA10-pilA11-slr2018* and increase in that of *pilA5-pilA6* and *pilA1-pilA2* by disruption of *spkA* encoding Serine/threonine protein kinase. None of these reports showed the direct interaction of these regulatory factors with *pilA* genes and LexA in this study is the first report of binding of transcriptional regulator to their upstream region (**Figure 3**). Involvement of SYCRP1 in transcriptional regulation of *pilA* genes through the direct regulation of LexA is not likely, since no SYCRP1 binding sequence has been detected in the upstream region of the *lexA* gene (Omagari et al., 2008; Xu and Su, 2009). Further examination of relationship between LexA and previously identified regulatory factors which affect motility may be a key to understanding of signal transduction mechanism regulating phototactic motility.

Accumulation of GG

In order to acclimate to high-salt or high-osmotic pressure conditions, S.6803 accumulates the compatible solute GG. Upon a salt shock, genes related to both GG biosynthesis (*ggp*, *glp*) and uptake (*ggt*) are induced (Kanesaki et al., 2002; Marin et al., 2004). GG is synthesized by a two-step reaction in S.6803. First, condensation of ADP-glucose and glycerol 3-phosphate is catalyzed by GG-phosphate synthase (GgpS) and then the intermediate is dephosphorylated by GG-phosphate phosphatase (GgpP) (Hagemann and Erdmann, 1994). Glycerol-3-phosphate

dehydrogenase (GlpD) and glycerol kinase (GlpK) are involved in the metabolism of glycerol-3-phosphate, a precursor of GG. Uptake of GG from the environment is performed by ABC transporter consisting of an ATP-binding protein (GgtA), a substrate-binding protein (GgtB) and two integral membrane proteins (GgtC and GgtD) in S.6803 (Mikkat and Hagemann, 2000). All of these genes are induced by the disruption of *lexA* (**Table 1** and **Table S2**). DNA gel mobility shift assay revealed that His-LexA protein binds to the upstream region of two divergently transcribed operons, *ggpS-glpD* and *slr1670-glpK-spoU-slr1674-hypA1* (**Figure 3**). To date, sigma factors SigF (Marin et al., 2002) and SigB (Nikkinen et al., 2012), a small protein GgpR (Klähn et al., 2010) and a response regulator Slr1588 (Chen et al., 2014) were reported to be involved in transcriptional regulation of the *ggpS-glpD* operon. Our result suggests the existence of the additional regulatory mechanism, namely, repression of the divergent *ggpS* and *slr1670* operons by LexA. Expression of *ggpR* may also be repressed by LexA, judging from the fact its expression was induced by the disruption of *lexA* (**Table 1**). Salt-stress inducible genes such as *hliA*, *hliB*, *hspA*, *prqR, degP, sll1723, sll0846, sll1483, slr1704, sll1236, slr0581,* and *ssr2194,* reported in the previous DNA microarray studies (Kanesaki et al., 2002; Marin et al., 2004), were also induced by the disruption of *lexA* (**Table 1**). There is possibility that LexA acts as a repressor for multiple salt-stress inducible genes as well as the *ggpS* and *slr1670* operons.

Bidirectional Hydogenase

Regulation of the *hox* operon by LexA has been extensively studied in S.6803 (Oliveira and Lindblad, 2009). LexA was shown to bind to two distinct regions of the *hox* promoter, −198 to −338 and −592 to −690, relative to the start codon of *hoxE* (Gutekunst et al., 2005; Oliveira and Lindblad, 2005) and work for positive regulation of hydrogenase activity (Gutekunst et al., 2005). Regulation of hydrogenase-related genes by LexA may be common among cyanobacterial species, judging from the reports on LexA homologs in *Anabaena* sp. PCC 7120 (Sjöholm et al., 2007) and *Lyngbya majuscula* CCAP 1446/4 (Ferreira et al., 2007).

Photosystem I and Phycobilisome

In the Δ*lexA* mutant, chlorophyll and phycocyanin contents were lower than those in WT (**Figure 1F**). This may be caused by decreased expression level of genes encoding subunits of PSI (*psa*), subunits of phycobilisome (*cpc*, *apc*) and both light-dependent and -independent protochlorophyllide reductase (*chlL, chlB*, *por*). It is known that these photosynthesis-related genes show the quite similar response to the changing light environment (Muramatsu and Hihara, 2012). The response regulator RpaB regulates high-light response of photosynthesis-related genes by binding to their promoter regions under low-light conditions (Wilde and Hihara, 2016). PSI genes and *hli* genes are positively- and negatively-regulated target genes of RpaB, respectively (Kappell and van Waasbergen, 2007; Seki et al., 2007; Seino et al., 2009). Repression of PSI genes and induction of *hli* genes by disruption of LexA (**Table 1**) seem to suggest overlapping roles of RpaB and LexA in regulation of photosynthetic gene expression. However, clear and reproducible band shift was not observed when binding of His-LexA to the promoter regions of PSI genes was examined (**Figure 3**). It is possible that changes in expression levels of photosynthesis-related genes in Δ*lexA* are not the consequence of loss of regulation by LexA but a secondary effect.

Search for LexA Binding Sites in the Target Promoters

Our results of DNA gel mobility shift assay suggest that LexA binds to the upstream region of *piA7*, *pilA9*, *ggpS* and *slr1670* to directly regulate their expression (**Figure 3**). To date, several nucleotide sequences for LexA binding site have been identified by DNA gel mobility shift assay, for example, 5′-TTTATTTGAACTATTTTT-3′, 5′-TTTTTCGTT GTCTAAATT-3′ (Oliveira and Lindblad, 2005), 5′-CTA-N_9(AT-rich)-CTA-3′ (Patterson-Fortin and Owttrim, 2008), and 5′-AGT AACTAGTTCG-3′ (Gutekunst et al., 2005) in S.6803 and 5′-TAGTACTAATGTTCTA-3′ in A.7120. (Mazón et al., 2004). However, these LexA binding sequences could not be found in the promoter fragments to which His-LexA bound. Instead, we found that a 5′-TTTTG(A/T)TNAC-3′ sequence commonly exists in these promoter fragments (**Figure S1**). The sequence is located around the putative transcription start site in the case of the negatively-regulated target genes, *ggpS*, *piA7,* and *slr1670*, whereas it is located further upstream region in the case of the positively-regulated *pilA9* gene. It has been reported that a certain global transcriptional regulator, such as NtcA and RpaB in S.6803, can act as both repressor and activator dependent on the location of the binding site (García-Domínguez et al., 2000; Seino et al., 2009). Binding of the transcriptional regulator causes repression when its binding site overlaps the RNA polymerase-binding site, whereas activating effect is observed when the binding site is located further upstream. The location of 5′-TTTTG(A/T)TNAC-3′ sequence in four LexA-target promoters seems consistent with the scheme.

Physiological Roles of Cyanobacterial LexA

Results of RNA-seq analysis (**Table 1**) together with DNA gel mobility shift assay (**Figure 3**) suggest LexA in S.6803 can positively or negatively regulate various cellular processes such as phototactic motility, GG accumulation and hydogenase activity. Regulation of such a wide range of cellular processes by LexA was reported in other bacterial species. For example, the *lexA* mutant of *Clostridium difficile* showed pleiotrophic phenotypes such as filamentous structure due to inhibition of cell division, decreased sporulation, decrease in swimming motility and increased biofilm formation (Walter et al., 2015). In this case, LexA acts as a regulator of DNA damage in addition to the above mentioned biological functions. In contrast, DNA microarray data from different research groups (Kamei et al., 2001; Domain et al., 2004) and our RNA-seq data suggest LexA in S.6803 is not involved in regulation of SOS genes. In S.6803, expression of *lexA* and *recA* was not induced upon UV-irradiation (Domain

et al., 2004; Patterson-Fortin et al., 2006). Similarly, in *Anabaena* sp. PCC 7120, expression of *lexA* was not induced upon UV-B exposure or treatment with a DNA damaging agent mitomycin C (Kumar et al., 2015). In these freshwater species, LexA-independent protection mechanism for DNA damage may have evolved and LexA may have become devoted to regulating other cellular processes. Then, what is the physiological meaning of the coordinated regulation of phototactic motility, GG accumulation, and hydogenase activity by LexA in S.6803? We searched for environmental conditions where LexA-target genes are coordinately regulated using CyanoEXpress gene expression database (http://cyanoexpress.sysbiolab.eu/) and found that salt stress causes induction of GG metabolism-related genes and repression of *hox* operon and *pilA* genes in WT (Shoumskaya et al., 2005; Dickson et al., 2012). The expression profile is similar to that observed by disruption of *lexA* (**Table 1**), indicating the possibility that transcriptional regulation by LexA is temporarily inactivated under salt stress conditions.

Recently, it has been suggested that the SOS response in the marine *Synechococcus* is regulated by LexA like *E. coli* (Blot et al., 2011; Tetu et al., 2013). Cyanobacterial LexA genes can be clustered into three groups, Clade A containing *Gloeobacter violaceus* PCC 7421, Clade C containing marine picocyanobacteria and Clade B containing most remaining species (Li et al., 2010). There may exist high degree of variation of LexA regulons among species belonging to these three clades. By examination of what kind of cellular processes LexA regulates, we will be able to know decision of each species about how to use the transcriptional regulator LexA for better adaptation to changing environment.

AUTHOR CONTRIBUTIONS

The study was conceived by AYK and YH, with design input from AKK. Experiments were performed by AYK and AKK. Data analysis and interpretation was done by all authors. The manuscript was prepared by AYK and YH, and reviewed by all authors.

FUNDING

This work was financially supported by the Core Research of Evolutional Science & Technology (CREST) programs from the Japan Science and Technology Agency (JST).

SUPPLEMENTARY MATERIAL

The Supplementary Material for this article can be found online at: http://journal.frontiersin.org/article/10.3389/fmicb.2016.00193

Table S1 | Oligonucleotides used in this study.

Table S2 | RNA-seq data of WT and Δ*lexA* at OD_{730} = 0.5.

Table S3 | RNA-seq data of WT and Δ*lexA* at OD_{730} = 1.0.

Figure S1 | Consensus sequences for LexA binding site in four LexA-target promoters identified with MEME.

REFERENCES

Arnon, D. I., McSwain, B. D., Tsujimoto, H. Y., and Wada, K. (1974). Photochemical activity and components of membrane preparations from blue-green algae. I. Coexistence of two photosystems in relation to chlorophyll a and removal of phycocyanin. *Biochim. Biophys. Acta* 357, 231–245. doi: 10.1016/0005-2728(74)90063-2

Bartsevich, V. V., and Pakrasi, H. B. (1995). Molecular identification of an ABC transporter complex for manganese: analysis of a cyanobacterial mutant strain impaired in the photosynthetic oxygen evolution process. *EMBO J.* 14, 1845–1853.

Bhaya, D., Watanabe, N., Ogawa, T., and Grossman, A. R. (1999). The role of an alternative sigma factor in motility and pilus formation in the cyanobacterium *Synechocystis* sp. strain PCC6803. *Proc. Natl. Acad. Sci. U.S.A.* 96, 3188–3193. doi: 10.1073/pnas.96.6.3188

Blot, N., Mella-Flores, D., Six, C., Le Corguille, G., Boutte, C., Peyrat, A., et al. (2011). Light history influences the response of the marine cyanobacterium *Synechococcus* sp. WH7803 to oxidative stress. *Plant Physiol.* 156, 1934–1954. doi: 10.1104/pp.111.174714

Brahamsha, B., and Bhaya, D. (2014). "Motility in unicellular and filamentous Cyanobacteria," in *The Cell Biology of Cyanobacteria*, eds E. Flores and A. Herrero (Dorset: Caister Academic Press), 233–262.

Butala, M., Žgur-Bertok, D., and Busby, S. J. W. (2009). The bacterial LexA transcriptional repressor. *Cell. Mol. Life Sci.* 66, 82–93. doi: 10.1007/s00018-008-8378-6

Chen, L., Wu, L., Zhu, Y., Song, Z., Wang, J., and Zhang, W. (2014). An orphan two-component response regulator Slr1588 involves salt tolerance by directly regulating synthesis of compatible solutes in photosynthetic *Synechocystis* sp. PCC 6803. *Mol. BioSyst.* 10, 1765–1774. doi: 10.1039/c4mb00095a

Dickson, D. J., Luterra, M. D., and Ely, R. L. (2012). Transcriptomic responses of *Synechocystis* sp. PCC 6803 encapsulated in silica gel. *Appl. Microbiol. Biotechnol.* 96, 183–196. doi: 10.1007/s00253-012-4307-6

Dienst, D., Duhring, U., Mollenkopf, H.-J., Vogel, J., Golecki, J., Hess, W. R., et al. (2008). The cyanobacterial homologue of the RNA chaperone Hfq is essential for motility of *Synechocystis* sp. PCC 6803. *Microbiology* 154, 3134–3143. doi: 10.1099/mic.0.2008/020222-0

Domain, F., Houot, L., Chauvat, F., and Cassier-Chauvat, C. (2004). Function and regulation of the cyanobacterial genes *lexA*, *recA* and *ruvB*: LexA is critical to the survival of cells facing inorganic carbon starvation. *Mol. Microbiol.* 53, 65–80. doi: 10.1111/j.1365-2958.2004.04100.x

Erill, I., Campoy, S., and Barbé, J. (2007). Aeons of distress: an evolutionary perspective on the bacterial SOS response. *FEMS Microbiol. Rev.* 31, 637–656. doi: 10.1111/j.1574-6976.2007.00082.x

Ferreira, D., Leitão, E., Sjöholm, J., Oliveira, P., Lindblad, P., Moradas-Ferreira, P., et al. (2007). Transcription and regulation of the hydrogenase(s) accessory genes, *hypFCDEAB*, in the cyanobacterium *Lyngbya majuscula* CCAP 1446/4. *Arch. Microbiol.* 188, 609–617. doi: 10.1007/s00203-007-0281-2

García-Domínguez, M., Reyes, J. C., and Florencio, F. J. (2000). NtcA represses transcription of *gifA* and *gifB*, genes that encode inhibitors of glutamine synthetase type I from *Synechocystis* sp. PCC 6803. *Mol. Microbiol.* 35, 1192–1201. doi: 10.1046/j.1365-2958.2000.01789.x

Gutekunst, K., Phunpruch, S., Schwarz, C., Schuchardt, S., Schulz-Friedrich, R., and Appel, J. (2005). LexA regulates the bidirectional hydrogenase in the cyanobacterium *Synechocystis* sp. PCC 6803 as a transcription activator. *Mol. Microbiol.* 58, 810–823. doi: 10.1111/j.1365-2958.2005.04867.x

Hagemann, M., and Erdmann, N. (1994). Activation and pathway of glucosylglycerol synthesis in the cyanobacterium *Synechocystis* sp. PCC 6803. *Microbiology* 140, 1427–1431. doi: 10.1099/00221287-140-6-1427

Ishii, A., and Hihara, Y. (2008). An AbrB-like transcriptional regulator, Sll0822, is essential for the activation of nitrogen-regulated genes in *Synechocystis* sp. PCC 6803. *Plant Physiol.* 148, 660–670. doi: 10.1104/pp.108.123505

Jiang, H.-B., Lou, W.-J., Ke, W.-T., Song, W.-Y., Price, N. M., and Qiu, B.-S. (2015). New insights into iron acquisition by cyanobacteria: an essential role for ExbB-ExbD complex in inorganic iron uptake. *ISME J.* 9, 297–309. doi: 10.1038/ismej.2014.123

Kamei, A., Hihara, Y., Yoshihara, S., Geng, X., Kanehisa, M., and Ikuechi, M. (2001). "Functional Analysis of *lexA*-like gene, sll1626 in *Synechocystis* sp. PCC 6803 using DNA microarray," in *PS2001 Proceedings of 12th International Congress on Photosynthesis* (Melbourne, VIC: CSIRO Publishing), S41–013.

Kaneko, T., Sato, S., Kotani, H., Tanaka, A., Asamizu, E., Nakamura, Y., et al. (1996). Sequence analysis of the genome of the unicellular cyanobacterium *Synechocystis* sp. strain PCC6803. II. Sequence determination of the entire genome and assignment of potential protein-coding regions. *DNA Res.* 3, 109–136. doi: 10.1093/dnares/3.3.109

Kanesaki, Y., Shiwa, Y., Tajima, N., Suzuki, M., Watanabe, S., Sato, N., et al. (2012). Identification of substrain-specific mutations by massively parallel whole-genome resequencing of *Synechocystis* sp. PCC 6803. *DNA Res.* 19, 67–79. doi: 10.1093/dnares/dsr042

Kanesaki, Y., Suzuki, I., Allakhverdiev, S. I., Mikami, K., and Murata, N. (2002). Salt stress and hyperosmotic stress regulate the expression of different sets of genes in *Synechocystis* sp. PCC 6803. *Biochem. Biophys. Res. Commun.* 290, 339–348. doi: 10.1006/bbrc.2001.6201

Kappell, A. D., and van Waasbergen, L. G. (2007). The response regulator RpaB binds the high light regulatory 1 sequence upstream of the high-light-inducible *hliB* gene from the cyanobacterium *Synechocystis* PCC 6803. *Arch. Microbiol.* 187, 337–342. doi: 10.1007/s00203-007-0213-1

Katoh, H., Hagino, N., and Grossman, A. R. (2001). Genes essential to iron transport in the cyanobacterium *Synechocystis* sp. strain PCC 6803. *J. Bacteriol.* 183, 2779–2784. doi: 10.1128/JB.183.9.2779-2784.2001

Klähn, S., and Hagemann, M. (2011). Compatible solute biosynthesis in cyanobacteria. *Environ. Microbiol.* 13, 551–562. doi: 10.1111/j.1462-2920.2010.02366.x

Klähn, S., Höhne, A., Simon, E., and Hagemann, M. (2010). The gene *ssl3076* encodes a protein mediating the salt-induced expression of *ggpS* for the biosynthesis of the compatible solute glucosylglycerol in *Synechocystis* sp. strain PCC 6803. *J. Bacteriol.* 192, 4403–4412. doi: 10.1128/JB.00481-10

Kumar, A., Kirti, A., and Rajaram, H. (2015). LexA protein of cyanobacterium *Anabaena* sp. strain PCC7120 exhibits in vitro pH-dependent and RecA-independent autoproteolytic activity. *Int. J. Biochem. Cell Biol.* 59, 84–93. doi: 10.1016/j.biocel.2014.12.003

Li, S., Xu, M., and Su, Z. (2010). Computational analysis of LexA regulons in cyanobacteria. *BMC Genomics* 11:527. doi: 10.1186/1471-2164-11-527

Lieman-Hurwitz, J., Haimovich, M., Shalev-Malul, G., Ishii, A., Hihara, Y., Gaathon, A., et al. (2009). A cyanobacterial AbrB-like protein affects the apparent photosynthetic affinity for CO_2 by modulating low-CO_2-induced gene expression. *Environ. Microbiol.* 11, 927–936. doi: 10.1111/j.1462-2920.2008.01818.x

Marin, K., Huckauf, J., Fulda, S., and Hagemann, M. (2002). Salt-dependent expression of glucosylglycerol-phosphate synthase, involved in osmolyte synthesis in the cyanobacterium *Synechocystis* sp. strain PCC 6803. *J. Bacteriol.* 184, 2870–2877. doi: 10.1128/JB.184.11.2870-2877.2002

Marin, K., Kanesaki, Y., Los, D. A., Murata, N., Suzuki, I., and Hagemann, M. (2004). Gene expression profiling reflects physiological processes in salt acclimation of *Synechocystis* sp. strain PCC 6803. *Plant Physiol.* 136, 300–329. doi: 10.1104/pp.104.045047

Mazón, G., Lucena, J. M., Campoy, S., Fernández de Henestrosa, A. R., Candau, P., and Barbé, J. (2004). LexA-binding sequences in Gram-positive and cyanobacteria are closely related. *Mol. Genet. Genomics* 271, 40–49. doi: 10.1007/s00438-003-0952-x

Mikkat, S., and Hagemann, M. (2000). Molecular analysis of the *ggtBCD* gene cluster of *Synechocystis* sp. strain PCC6803 encoding subunits of an ABC transporter for osmoprotective compounds. *Arch. Microbiol.* 174, 273–282. doi: 10.1007/s002030000201

Mortazavi, A., Williams, B. A., McCue, K., Schaeffer, L., and Wold, B. (2008). Mapping and quantifying mammalian transcriptomes by RNA-Seq. *Nat. Methods* 5, 621–628. doi: 10.1038/nmeth.1226

Muramatsu, M., and Hihara, Y. (2003). Transcriptional regulation of genes encoding subunits of photosystem I during acclimation to high-light conditions in *Synechocystis* sp. PCC 6803. *Planta* 216, 446–453. doi: 10.1007/s00425-002-0859-5

Muramatsu, M., and Hihara, Y. (2012). Acclimation to high-light conditions in cyanobacteria: from gene expression to physiological responses. *J. Plant Res.* 125, 11–39. doi: 10.1007/s10265-011-0454-6

Nikkinen, H.-L., Hakkila, K., Gunnelius, L., Huokko, T., Pollari, M., and Tyystjarvi, T. (2012). The SigB factor regulates multiple salt acclimation responses of the cyanobacterium *Synechocystis* sp. PCC 6803. *Plant Physiol.* 158, 514–523. doi: 10.1104/pp.111.190058

Oliveira, P., and Lindblad, P. (2005). LexA, a transcription regulator binding in the promoter region of the bidirectional hydrogenase in the cyanobacterium *Synechocystis* sp. PCC 6803. *FEMS Microbiol. Lett.* 251, 59–66. doi: 10.1016/j.femsle.2005.07.024

Oliveira, P., and Lindblad, P. (2009). Transcriptional regulation of the cyanobacterial bidirectional Hox-hydrogenase. *Dalton Trans.* 7, 9990–9996. doi: 10.1039/b908593a

Omagari, K., Yoshimura, H., Suzuki, T., Takano, M., Ohmori, M., and Sarai, A. (2008). Delta G-based prediction and experimental confirmation of SYCRP1-binding sites on the *Synechocystis* genome. *FEBS J.* 275, 4786–4795. doi: 10.1111/j.1742-4658.2008.06618.x

Panichkin, V. B., Arakawa-Kobayashi, S., Kanaseki, T., Suzuki, I., Los, D. A., Shestakov, S. V., et al. (2006). Serine/threonine protein kinase SpkA in *Synechocystis* sp. strain PCC 6803 is a regulator of expression of three putative *pilA* operons, formation of thick pili, and cell motility. *J. Bacteriol.* 188, 7696–7699. doi: 10.1128/JB.00838-06

Patterson-Fortin, L. M., Colvin, K. R., and Owttrim, G. W. (2006). A LexA-related protein regulates redox-sensitive expression of the cyanobacterial RNA helicase, *crhR*. *Nucleic Acids Res.* 34, 3446–3454. doi: 10.1093/nar/gkl426

Patterson-Fortin, L. M., and Owttrim, G. W. (2008). A *Synechocystis* LexA-orthologue binds direct repeats in target genes. *FEBS Lett.* 582, 2424–2430. doi: 10.1016/j.febslet.2008.06.009

Seino, Y., Takahashi, T., and Hihara, Y. (2009). The response regulator RpaB binds to the upstream element of photosystem I genes to work for positive regulation under low-light conditions in *Synechocystis* sp. strain PCC 6803. *J. Bacteriol.* 191, 1581–1586. doi: 10.1128/JB.01588-08

Seki, A., Hanaoka, M., Akimoto, Y., Masuda, S., Iwasaki, H., and Tanaka, K. (2007). Induction of a group 2 σ factor, RPOD3, by high light and the underlying mechanism in *Synechococcus elongatus* PCC 7942. *J. Biol. Chem.* 282, 36887–36894. doi: 10.1074/jbc.M707582200

Shoumskaya, M. A., Paithoonrangsarid, K., Kanesaki, Y., Los, D. A., Zinchenko, V. V., Tanticharoen, M., et al. (2005). Identical Hik-Rre systems are involved in perception and transduction of salt signals and hyperosmotic signals but regulate the expression of individual genes to different extents in *Synechocystis*. *J. Biol. Chem.* 280, 21531–21538. doi: 10.1074/jbc.M412174200

Sjöholm, J., Oliveira, P., and Lindblad, P. (2007). Transcription and regulation of the bidirectional hydrogenase in the cyanobacterium *Nostoc* sp. strain PCC 7120. *Appl. Environ. Microbiol.* 73, 5435–5446. doi: 10.1128/AEM.00756-07

Sun, J., Nishiyama, T., Shimizu, K., and Kadota, K. (2013). TCC: an R package for comparing tag count data with robust normalization strategies. *BMC Bioinformatics* 14:219. doi: 10.1186/1471-2105-14-219

Terauchi, K., and Ohmori, M. (1999). An adenylate cyclase, *cya1*, regulates cell motility in the cyanobacterium *Synechocystis* sp. PCC 6803. *Plant Cell Physiol.* 40, 248–251. doi: 10.1093/oxfordjournals.pcp.a029534

Tetu, S. G., Johnson, D. A., Varkey, D., Phillippy, K., Stuart, R. K., Dupont, C. L., et al. (2013). Impact of DNA damaging agents on genome-wide transcriptional profiles in two marine *Synechococcus* species. *Front. Microbiol.* 4:232. doi: 10.3389/fmicb.2013.00232

Vinnemeier, J., Kunert, A., and Hagemann, M. (1998). Transcriptional analysis of the *isiAB* operon in salt-stressed cells of the cyanobacterium *Synechocystis* sp. PCC 6803. *FEMS Microbiol. Lett.* 169, 323–330. doi: 10.1111/j.1574-6968.1998.tb13336.x

Walter, B. M., Cartman, S. T., Minton, N. P., Butala, M., and Rupnik, M. (2015). The SOS response master regulator LexA is associated with sporulation, motility and biofilm formation in *Clostridium difficile*. *PLoS ONE* 10:e0144763. doi: 10.1371/journal.pone.0144763

Wang, H.-L., Postier, B. L., and Burnap, R. L. (2002). Polymerase chain reaction-based mutagenesis identify key transporters belonging to multigene

families involved in Na^+ and pH homeostasis of *Synechocystis* sp. PCC 6803. *Mol. Microbiol.* 44, 1493–1506. doi: 10.1046/j.1365-2958.2002.02983.x

Wang, H.-L., Postier, B. L., and Burnap, R. L. (2004). Alterations in global patterns of gene expression in *Synechocystis* sp. PCC 6803 in response to inorganic carbon limitation and the inactivation of *ndhR*, a LysR family regulator. *J. Biol. Chem.* 279, 5739–5751. doi: 10.1074/jbc.M311336200

Wilde, A., and Hihara, Y. (2016). Transcriptional and posttranscriptional regulation of cyanobacterial photosynthesis. *Biochim. Biophys. Acta* 1857, 296–308. doi: 10.1016/j.bbabio.2015.11.002

Xu, M., and Su, Z. (2009). Computational prediction of cAMP receptor protein (CRP) binding sites in cyanobacterial genomes. *BMC Genomics* 10:23. doi: 10.1186/1471-2164-10-23

Yoshihara, S., Geng, X., Okamoto, S., Yura, K., Murata, T., Go, M., et al. (2001). Mutational analysis of genes involved in pilus structure, motility and transformation competency in the unicellular motile cyanobacterium *Synechocystis* sp. PCC 6803. *Plant Cell Physiol.* 42, 63–73. doi: 10.1093/pcp/pce007

Yoshimura, H., Kaneko, Y., Ehira, S., Yoshihara, S., Ikeuchi, M., and Ohmori, M. (2010). CccS and CccP are involved in construction of cell surface components in the cyanobacterium *Synechocystis* sp. strain PCC 6803. *Plant Cell Physiol.* 51, 1163–1172. doi: 10.1093/pcp/pcq081

Yoshimura, H., Yanagisawa, S., Kanehisa, M., and Ohmori, M. (2002b). Screening for the target gene of cyanobacterial cAMP receptor protein SYCRP1. *Mol. Microbiol.* 43, 843–853. doi: 10.1046/j.1365-2958.2002.02790.x

Yoshimura, H., Yoshihara, S., Okamoto, S., Ikeuchi, M., and Ohmori, M. (2002a). A cAMP receptor protein, SYCRP1, is responsible for the cell motility of *Synechocystis* sp. PCC 6803. *Plant Cell Physiol.* 43, 460–463. doi: 10.1093/pcp/pcf050

Zhao, S., Fung-Leung, W.-P., Bittner, A., Ngo, K., and Liu, X. (2014). Comparison of RNA-Seq and microarray in transcriptome profiling of activated T cells. *PLoS ONE* 9:e78644. doi: 10.1371/journal.pone.0078644

Conflict of Interest Statement: The authors declare that the research was conducted in the absence of any commercial or financial relationships that could be construed as a potential conflict of interest.

frontiers in Microbiology

ORIGINAL RESEARCH
published: 15 February 2016
doi: 10.3389/fmicb.2016.00070

In vivo Reconstitution of Algal Triacylglycerol Production in *Saccharomyces cerevisiae*

Chun-Hsien Hung[1], *Kazue Kanehara*[1] *and Yuki Nakamura*[1,2]*

[1] *Institute of Plant and Microbial Biology, Academia Sinica, Taipei, Taiwan,* [2] *Precursory Research for Embryonic Science and Technology (PRESTO), Japan Science and Technology Agency, Saitama, Japan*

The current fascination with algal biofuel production stems from a high lipid biosynthetic capacity and little conflict with land plant cultivation. However, the mechanisms which enable algae to accumulate massive oil remain elusive. An enzyme for triacylglycerol (TAG) biosynthesis in *Chlamydomonas reinhardtii*, CrDGTT2, can produce a large amount of TAG when expressed in yeast or higher plants, suggesting a unique ability of CrDGTT2 to enhance oil production in a heterologous system. Here, we performed metabolic engineering in *Saccharomyces cerevisiae* by taking advantage of CrDGTT2. We suppressed membrane phospholipid biosynthesis at the log phase by mutating *OPI3*, enhanced TAG biosynthetic pathway at the stationary phase by overexpressing *PAH1* and *CrDGTT2*, and suppressed TAG hydrolysis on growth resumption from the stationary phase by knocking out *DGK1*. The resulting engineered yeast cells accumulated about 70-fold of TAG compared with wild type cells. Moreover, TAG production was sustainable. Our results demonstrated the enhanced and sustainable TAG production in the yeast synthetic platform.

Keywords: triacylglycerol, *Chlamydomonas reinhardtii*, *Saccharomyces cerevisiae*, diacylglycerol acyltransferase type 2, metabolic engineering

OPEN ACCESS

Edited by:
Pankaj Kumar Arora,
Yeungnam University, South Korea

Reviewed by:
Shawn Chen,
Ohio University, USA
Carla C. C. R. De Carvalho,
Instituto Superior Técnico, Portugal

***Correspondence:**
Yuki Nakamura
nakamura@gate.sinica.edu.tw

Specialty section:
This article was submitted to Microbiotechnology, Ecotoxicology and Bioremediation, a section of the journal Frontiers in Microbiology

Received: *05 November 2015*
Accepted: *15 January 2016*
Published: *15 February 2016*

Citation:
Hung C-H, Kanehara K and Nakamura Y (2016) In vivo Reconstitution of Algal Triacylglycerol Production in Saccharomyces cerevisiae. Front. Microbiol. 7:70. doi: 10.3389/fmicb.2016.00070

INTRODUCTION

Biofuel production is highly demanded as an alternative to the limited fossil fuels. The current fascination with eukaryotic algae as a resource of biofuel production stems from a high lipid biosynthetic capacity and little competition for land required for plant cultivation. However, technical difficulty in gene manipulation of many eukaryotic algae species hampers potential usefulness of these organisms as a synthetic platform of metabolic engineering to produce biofuel. On the other hand, *Saccharomyces cerevisiae* is an advanced model unicellular eukaryotic microorganism for metabolic engineering as well as basic molecular biological studies on metabolism.

Triacylglycerol (TAG) is a major source of biodiesel (Durrett et al., 2008; Hu et al., 2008), which is synthesized from *sn*-1,2-diacylglycerol (DAG) by the catalysis of acyltransferase in many organisms such as *S. cerevisiae*, *Chlamydomonas reinhardtii,* and *Arabidopsis thaliana* (Sandager et al., 2002; Zhang et al., 2009; Hung et al., 2013). Because DAG is produced from phosphatidic acid (PA), which is also a substrate for the biosynthesis of major membrane phospholipids, TAG accumulation often competes with membrane lipid biosynthesis (**Figure 1**). In yeast cells, the primary metabolic flux of glycerolipids differs by the growth status. Biosynthesis of storage lipids such as TAG and membrane

lipids such as phospholipids share initial steps of the pathway up to PA production (Henry et al., 2012). In growing cells, newly synthesized glycerolipids are mostly used to produce membrane lipids required for active cell proliferation (**Figure 1**, green arrow). With entry into the stationary growth phase, the major flux switches to storage lipid biosynthesis. Here, PA is dephosphorylated to DAG by a PA phosphatase encoded by *PAH1* (Han et al., 2006), which is subsequently converted to TAG by diacylglycerol acyltransferases (DGATs; **Figure 1**, brown arrow). Stationary-phase cells can resume their growth once depleted nutrients are added, such as the dilution of cell culture with fresh medium. This growth resumption activates hydrolysis of accumulated TAG to DAG by a set of TAG lipases (Kurat et al., 2009), and DAG is further phosphorylated by DAG kinase 1 (DGK1) to PA (Han et al., 2008a,b) to provide a substrate for membrane lipid biosynthesis (**Figure 1**, orange arrow). At this phase, DGK1 encodes a key enzyme involved in phospholipid synthesis and recovery after growth resumption (Fakas et al., 2011a).

C. reinhardtii is a model organism for the study of TAG production in the eukaryotic microalgae. DGAT, which represents a major TAG biosynthetic enzyme, catalyzes the transfer of acyl moiety from acyl-CoA to DAG. In *C. reinhardtii*, DGAT is of 2 types: Type 1 with single isogene (*CrDGTT1*) and Type 2 with five isogenes (*CrDGTT1-5*) (Merchant et al., 2012). Interestingly, it was recently reported that heterologous overexpression of *CrDGTT2* in *S. cerevisiae* or *A. thaliana* increased TAG content by 9- or 25-fold, respectively (Hung et al., 2013; Sanjaya et al., 2013), suggesting highly robust enzyme function of CrDGTT2 in a heterologous system.

In this study, we aimed to perform metabolic engineering that achieves enhanced and sustainable TAG production in the synthetic platform of *S. cerevisiae* by taking advantage of *CrDGTT2* as a robust algal gene resource.

MATERIALS AND METHODS

Yeast Culture Conditions

Cells were grown in YPD media (2.0 g of Bacto peptone [Difco 211677], 1.0 g of Bacto yeast extract [Difco 212750], 2.0 g of glucose [Merck 1.08337] in 100 ml of H_2O produced by Milli-Q [Millipore]) unless otherwise stated. Cells harboring the *URA3* and *LEU2* marker plasmids were grown in synthetic complete media lacking uracil and leucine (SC -Ura, -Leu). The OD_{600} in **Figure 3A** and Supplementary Figure 1 was measured by diluting fully grown cultures to OD_{600} of 0.1 and cultured for 60 h at 30°C. In **Figures 4A–C**, yeast cells were freshly inoculated from glycerol stocks. After reaching the stationary phase, the cell culture was diluted with fresh medium to OD_{600} of 0.05 and grown for 60 h to the late stationary phase, then time-course observation was started. The dilution was conducted twice at 60 h intervals. Data are mean±SD from three biological replicates.

Cloning of Plasmid Vectors

The yeast expression vector pCH108 was created by replacing the *URA3* marker of pCH078 (Hung et al., 2013) with the *LEU2* marker derived from pRS315. First, XmaI and BclI restriction sites were created by amplifying the 4895-bp fragment of the pCH078 with the primers CH376 and CH377. Next, a 1574-bp fragment of the *LEU2* marker was amplified from pRS315 with the primers CH374 and CH375. The obtained fragments were digested with XmaI and BclI and ligated to construct pCH108. The polymerase chain reaction (PCR) was performed using Phusion polymerase (Finnzymes F-530S, ThermoFisher Scientific) under the following condition; an initial denaturing step of 5 min at 95°C followed by 35 cycles of 95°C for 30 s, 60°C for 30 s, and 72°C for 3 min and then a final extension at 72°C for 5 min. The plasmids and primers are listed in **Table 1** and Supplementary Table 1, respectively.

The 2593-bp open reading frame of *ScPAH1* (YMR165C) was amplified with the primers CH367 and CH368, cloned into pENTR/D-TOPO (Invitrogen, Carlsbad, CA), digested with AscI and NotI, and inserted into AscI/NotI sites of pCH108 to construct pCH109. This plasmid contains GPD promoter for constitutive overexpression (Blazeck et al., 2012).

Mutant Strain Construction

To produce CHY034 (*dgk1*Δ::*KANMX*, *opi3*Δ::*HIS*), a 932-bp fragment of *opi3*Δ::*HIS3* was amplified with the primers CH430 and CH431 from pRS313, and transformed into *dgk1*Δ::*KANMX*. The plasmid pCH109, which overexpresses *ScPAH1* (OE-PAH1), was transformed into CHY034 (*dgk1*Δ::*KANMX*, *opi3*Δ::*HIS*) to produce CHY138 (Δ*dgk1*Δ*opi3* OE-PAH1). Then, the plasmid pCH091, which overexpresses *CrDGTT2* (OE-CrDGTT2), was transformed into CHY138 to produce CHY101, CHY140, CHY141, and CHY142 (Δ*dgk1*Δ*opi3* OE-PAH1 OE-CrDGTT2). The transformation was performed as described previously by mixing the plasmid with the PLATE reagent, salmon sperm DNA and yeast cells (Gietz and Woods, 2002). The yeast strains are listed in **Table 2**.

Lipid Analysis

Lipid analysis was performed as follows using yeast cells obtained from 100 ml of culture by centrifugation (3000 × g for 5 min). Cells were lyophilized using freeze drier (Alpha 1-2, Martin Christ Gefriertrocknungsanlagen GmbH, Germany) and dry cell weight was measured with fine weighing scale (BEL engineering, Cat. No. M214Ai, Italy). Prior to the lipid extraction, cells were treated with pre-heated isopropanol containing 0.01% butylated hydroxytoluene at 75°C for 15 min to inactivate phospholipase activity. Total lipids were extracted essentially as described previously using chloroform-methanol solvent system (Folch et al., 1957) with the ratio of solvent (by vol): sample (by weight) as 20:1 for 100 mg of sample. Briefly, cells were suspended in chloroform:methanol (1:2, by vol) to homogenity, followed by addition of chloroform and deionized water (dH_2O). Cell suspension was vortexed

Abbreviations: CDP-DAG, cytidine diphosphate diacylglycerol; CL, cardiolipin; DAG, *sn*-1,2-diacylglycerol; G3P, glycerol 3-phosphate; LPA lysophosphatidic acid; PA, phosphatidic acid; PC, phosphatidylcholine; PE, phosphatidylethanolamine; PG, phosphatidylglycerol; PGP, phosphatidylglycerophosphate; PI, phosphatidylinositol; PS, phosphatidylserine; TAG, triacylglycerol.

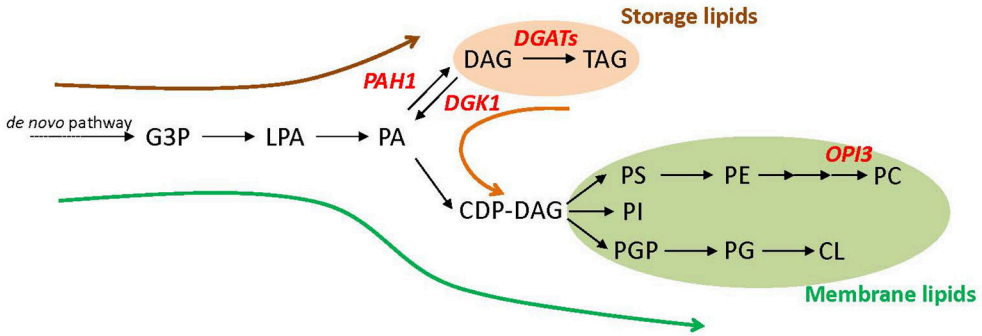

FIGURE 1 | Schematic representation of glycerolipid metabolism in *Saccharomyces cerevisiae*. Dominant metabolic flux at three different growth phases (log phase, green arrow; stationary phase, brown arrow; growth resumption from the stationary phase, orange arrow) and key metabolic genes engineered in this study (in red letters) are shown. CDP-DAG, cytidine diphosphate-diacylglycerol; CL, cardiolipin; DAG, *sn*-1,2-diacylglycerol; G3P, glycerol 3-phosphate; LPA lysophosphatidic acid; PA, phosphatidic acid; PC, phosphatidylcholine; PE, phosphatidylethanolamine; PG, phosphatidylglycerol; PGP, phosphatidylglycerophosphate; PI, phosphatidylinositol; PS, phosphatidylserine; TAG, triacylglycerol.

vigorously and left for 30 min at room temperature. Organic phase was recovered and residual lipids in cell pellet were extracted twice by vigorous vortex with chloroform. The combined organic extracts were vortexed with 1% KCl solution, and separated organic phase was washed once with dH_2O. Lipids were dried up under nitrogen stream, dissolved in chloroform:methanol (2:1, by vol) and stored at −30°C till use. Each lipid class was separated by thin layer chromatography (Silica Gel 60 F254 plate, Merck). Separation of TAG was as described previously (Hung et al., 2013) and of phospholipids involved two-dimensional separation with the solvent system of chloroform/methanol/ammonia (65:35:5, by vol) for the first dimension and chloroform/acetone/methanol/acetic acid (50:20:10:10, by vol) for the second dimension based on the previous report (Nelson, 1967). Lipid spots were identified by spraying primuline solution, scraped off and acyl moieties hydrolyzed and methylesterified to fatty acid methyl esters (FAMEs) with HCl-methanol solution by incubating the samples at 85°C for 2 h including pentadecanoic acid (15:0) as internal standard. After the incubation, the FAMEs were extracted with hexane, dried up under the nitrogen gas stream, eluted in 50 µl of hexane, and quantified with gas chromatography (GC-2010; Shimadzu, Kyoto, Japan) with FID detector (FID-2010 Plus; Shimadzu, Kyoto, Japan) equipped with a ULBON HR-SS-10 column (Shinwa Chemical Industries, Japan) (Nakamura et al., 2003). Amount of TAG was shown in % (w/w) of dry cell weight. Composition of fatty acid and phospholipid classes were shown by mol% based on the FAMEs quantified with gas chromatography. Data were averaged by three biological replicates with standard deviations as error bars.

Nile Red Staining and Microscopy of Lipid Droplets

Nile red staining and observation of lipid droplets were as described previously (Hung et al., 2013) using Nile red (Fluka, Cat. No. 72485) and DeltaVision system (Applied Precision) with a 100x objective lens (NA = 1.4) and a CoolSNAP HQ CCD camera (Photomotrics) controlled by softWoRx Suite (Applied Precision). Normarski differential interference contrast (DIC) microscopy image was taken as previously described (Fu et al., 2010).

TABLE 1 | List of plasmids used in this study.

Plasmid	Encoded gene	Promoter	Vector	Source
pRS313	–	–	pBluescript KS+	ATCC 77142
pRS315	–	–	pBluescript KS+	ATCC 77144
pCH078	–	GPD	pYES2/NTA	Hung et al., 2013
pCH091	*CrDGTT2*	GPD	pYES2/NTA	Hung et al., 2013
pCH108	–	GPD	pYES2/NTA	This work
pCH109	*ScPAH1*	GPD	pYES2/NTA	This work

Transmission Electron Microscopy

Yeast cells were grown to the stationary phase in synthetic complete medium lacking uracil and leucine (SC -Ura, -Leu) containing 8% glucose at 30°C for 48 h. Samples were frozen in a high-pressure freezer (Leica EM PACT2) at 2000–2050 bar. Freeze-substitution was performed in anhydrous ethanol (containing 0.2% glutaraldehyde and 0.1% uranyl acetate) with an automatic freeze substitution system (Leica EM AFS2). The samples were first kept at −85°C for 3 days, then switched to −60°C, −20°C, 0°C, and room temperature at 1-day intervals. After 2 times of rinse with ethanol for 12 h, the samples were embedded by infiltrating LR White resin. Ultrathin sections (70–90 nm) were prepared with use of Reichert Ultracut S or Lecia EM UC7 (Leica, Vienna, Austria) and collected on 100-mesh copper grids. The sections were stained with 5% uranyl acetate in 50% methanol for 10 min and 0.4% lead citrate for 4–6 min. Sections were observed under a transmission electron microscope (Philips CM 100) at 80 KV and images were taken with use of a Gatan Orius CCD camera.

TABLE 2 | List of *S. cerevisiae* strains used in this study.

Strain	Genotype	Source
BY4741	*MATa, his3Δ0 leu2Δ0 met15Δ0 ura3Δ0*	–
Δ*dgk1*	*dgk1*Δ::*KANMX,* BY4741	Thermo Scientific
CHY034	*dgk1*Δ::*KANMX*, *opi3*Δ::*HIS*, BY4741	This work
CHY044	pCH078, pCH108, BY4741	This work
CHY101	pCH091, pCH109, *dgk1*Δ::*KANMX*, *opi3*Δ::*HIS*, BY4741	This work
CHY138	pCH109, *dgk1*Δ::*KANMX*, *opi3*Δ::*HIS*, BY4741	This work
CHY140	pCH091, pCH109, *dgk1*Δ::*KANMX*, *opi3*Δ::*HIS*, BY4741	This work
CHY141	pCH091, pCH109, *dgk1*Δ::*KANMX*, *opi3*Δ::*HIS*, BY4741	This work
CHY142	pCH091, pCH109, *dgk1*Δ::*KANMX*, *opi3*Δ::*HIS*, BY4741	This work

RESULTS

Metabolic Engineering of *S. cerevisiae* to Enhance TAG Production

To enhance TAG levels by metabolic engineering, we genetically manipulated *S. cerevisiae* by considering the following 3 points: (1) suppressing metabolic flux to membrane lipid biosynthesis at the log phase, (2) enhancing metabolic flux to TAG biosynthesis at the stationary phase, and (3) suppressing TAG hydrolysis for membrane lipid biosynthesis on growth resumption to maintain accumulated TAG (**Figure 2A**).

For point 1, to suppress membrane lipid biosynthesis at the log phase, we blocked phosphatidylcholine (PC) biosynthesis by knocking out OPI3, which encodes an enzyme catalyzing the final step of PC biosynthesis (**Figure 1**). This is because the yeast mutant Δ*opi3* is viable with abolished PC (McGraw and Henry, 1989), whereas mutation in many other rate-limiting enzymes for phospholipid biosynthesis causes lethal effects on growth (Henry et al., 2012). For example, knocking out CDP-diacylglycerol synthase (CDS), which converts PA into CDP-DAG, causes a lethal effect (Shen et al., 1996). A significant metabolic switch is expected to be in favor of TAG production in Δ*opi3* because PC is a primary phospholipid of cellular membranes in *S. cerevisiae*. Indeed, the TAG levels in the stationary phase of Δ*opi3* cells were 4.8-fold higher than that of the wild type based on a dry cell weight (**Figure 2B**), which agrees with previous study (Fei et al., 2011). We next analyzed the fatty acid composition of TAG, which determines their quality. The Δ*opi3* cells showed an increased composition of palmitoleic acid (16:1) as compared with the wild type (**Figure 2C**). Therefore, partial blockage of primary membrane phospholipid biosynthesis by knocking out *OPI3* increases TAG with enriched mono-unsaturated fatty acid, giving better quality for biodiesel use.

For point 2, to enhance metabolic flux to TAG biosynthesis at the stationary phase, we first overexpressed *PAH1* (OE-PAH1) to stimulate PA to DAG conversion (**Figure 1**). The result showed that overexpression of *PAH1* in wild-type cells increased TAG levels by 3.9-fold as compared with the wild type (**Figure 2B**). The fatty acid composition was not altered significantly by overexpressing *PAH1* (**Figure 2C**). Since previous report showed that the Δ*pah1* mutant has reduced TAG levels (Adeyo et al., 2011; Fakas et al., 2011b), expression level of *PAH1* may have dose-dependent effect on TAG accumulation.

For point 3, to suppress TAG hydrolysis on growth resumption, we knocked out *DGK1* because previous study demonstrated that DGK1 is required for phospholipid synthesis during growth resumption from stationary phase (Fakas et al., 2011a). In agreement with this observation, TAG content in the Δ*dgk1* cells was increased 1.6-fold as compared with the wild type (**Figure 2B**), with no remarkable alteration in fatty acid composition (**Figure 2C**). Thus, suppressing membrane phospholipid biosynthesis, inducing DAG production from PA, and inhibiting TAG mobilization all increased TAG accumulation to a significant extent.

Next, we combined these three genetic manipulations to construct a strain that overexpresses *PAH1* in the Δ*dgk1*Δ*opi3* (Δ*dgk1*Δ*opi3* OE-PAH1). The TAG level was increased 9.7-fold in this strain as compared with the wild type (**Figures 2A,B**). The fatty acid composition of accumulated TAG was similar to that of Δ*opi3* (**Figure 2C**), indicating that neither overexpression of *PAH1* nor knockout of *DGK1* altered the fatty acid composition of TAG. Thus, by altering the expression of 3 genes, *OPI3*, *DGK1,* and *PAH1*, TAG production was increased by 9.7-fold as compared to the wild type in *S. cerevisiae*.

Here, to further increase TAG contents, we overexpressed *CrDGTT2* in the Δ*dgk1*Δ*opi3* OE-PAH1. The resulting TAG levels in Δ*dgk1*Δ*opi3* OE-PAH1 OE-CrDGTT2 were further increased more than 7-fold, giving 69-fold increase as compared to the wild type (**Figures 2A,B**). The fatty acid composition of accumulated TAG was not altered with overexpression of *CrDGTT2* in the Δ*dgk1*Δ*opi3* OE-PAH1 cells (**Figure 2C**). To confirm the TAG yield of the Δ*dgk1*Δ*opi3* OE-PAH1 OE-CrDGTT2 cells, we independently established three more strains with the same genotype (CHY140, CHY141, and CHY142) by transforming the plasmid to overexpress *CrDGTT2* into the Δ*dgk1*Δ*opi3* OE-PAH1. When maximal TAG level is produced at late stationary phase (60 h), these cells produced 64.8- to 73.2-fold increase (Supplementary Table 2), indicating reproducibly high yield of TAG in this engineered strain. This TAG amount was estimated to be 12.2% of total dry cell biomass (**Figure 2D**). This corresponds to 166 mg of TAG per liter of liquid broth culture, which produces about 1.35 g/L of dry cell weight. Thus, our metabolic engineering greatly increased TAG contents using a robust algal gene *CrDGTT2*.

Characterization of the Δ*dgk1*Δ*opi3* OE-PAH1 OE-CrDGTT2 Cells

We found that the Δ*dgk1*Δ*opi3* OE-PAH1 OE-CrDGTT2 cells showed reduced growth, because culture of the Δ*dgk1*Δ*opi3* OE-PAH1 OE-CrDGTT2 reached a plateau at OD_{600} of 4 while that of the wild type reached a plateau at OD_{600} of 10 in synthetic complete media lacking Ura and Leu (**Figure 3A**; see Supplementary Figure 1 for the growth curve of the strains). This growth retardation may be due to suppressed membrane lipid biosynthesis rather than massive accumulation of TAG, because the value of OD_{600} was comparable to that of the Δ*dgk1*Δ*opi3* cells (**Figure 3A**). Indeed, composition of membrane phospholipids was greatly altered as compared to the

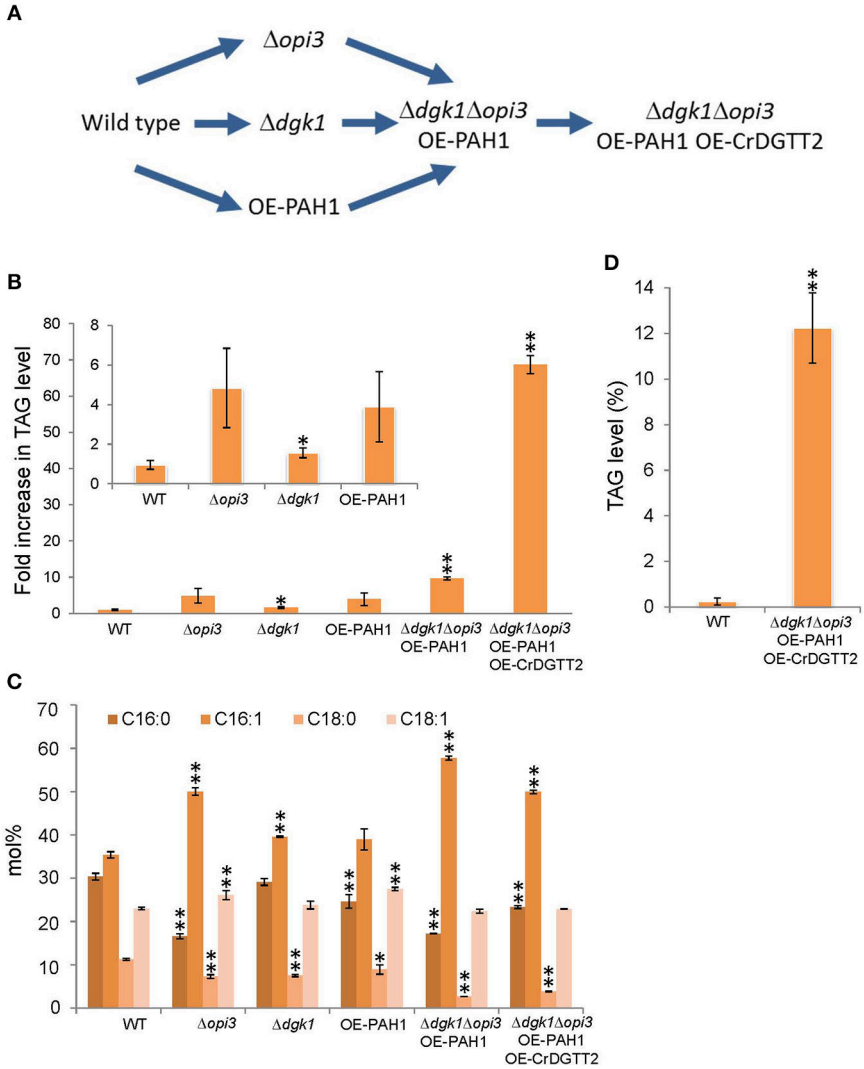

FIGURE 2 | Procedures for metabolic engineering to enhance TAG production in *S. cerevisiae*. (A) Schematic representation of the procedures. **(B)** TAG levels of early stationary phase were quantified in the strains of wild type (WT), Δ*opi3*, Δ*dgk1*, OE-PAH1, Δ*dgk1*Δ*opi3* OE-PAH1, and Δ*dgk1*Δ*opi3* OE-PAH1 OE-CrDGTT2 shown as fold increase compared to the wild type strain. **(C)** Fatty acid composition (mol%) of TAG analyzed in **(B)**. **(D)** TAG production of Δ*dgk1*Δ*opi3* OE-PAH1 OE-CrDGTT2 strain at stationary phase by dry cell weight basis. Data are mean ± SD from three biological replicates. Asterisks indicate statistical significance by Student's *t*-test (*$P < 0.05$; **$P < 0.01$). WT, wild type; OE, overexpression; 16:0, palmitic acid; 16:1, palmitoleic acid; 18:0, stearic acid; 18:1, oleic acid.

wild type (**Figure 3B**; Supplementary Table 3). We also measured level of free fatty acid; wild type cells had 5.8 ± 0.7 μg/mg dry cell weight whereas the Δ*dgk1*Δ*opi3* OE-PAH1 OE-CrDGTT2 cells had 38.2 ± 9.6 μg/mg dry cell weight. Nile red staining for lipid droplets was greater in the Δ*dgk1*Δ*opi3* OE-PAH1 OE-CrDGTT2 cells than wild type cells (**Figures 3C,E**), which supports massive production of TAG (**Figure 2**; Supplementary Table 2). The cell size of Δ*dgk1*Δ*opi3* OE-PAH1 OE-CrDGTT2 with TAG accumulation at the stationary phase was larger than wild-type cells (**Figures 3D,F**). To test whether the Δ*dgk1*Δ*opi3* OE-PAH1 OE-CrDGTT2 cells are still capable of accumulating TAG, we shifted glucose concentration of culture media from 2 to 8% at the end of log phase to trigger extra carbon uptake and fixation to carbon-containing metabolite reserves, including TAG (Kamisaka et al., 2013). As compared with the normal 2% glucose condition, this "sugar boost" further increased TAG level by 3.2-fold (**Figure 3G**; Supplementary Table 4). These data suggest that the Δ*dgk1*Δ*opi3* OE-PAH1 OE-CrDGTT2 cells have capacity to accumulate extra TAG in response to external glucose supply. We observed the ultrastructure of the Δ*dgk1*Δ*opi3* OE-PAH1 OE-CrDGTT2 cells accumulating TAG under the 8% glucose condition. Compared to the wild type (**Figure 3H**), the Δ*dgk1*Δ*opi3* OE-PAH1 OE-CrDGTT2 produced super-sized lipid droplets that occupied the primary space in the intracellular compartment (**Figure 3I**).

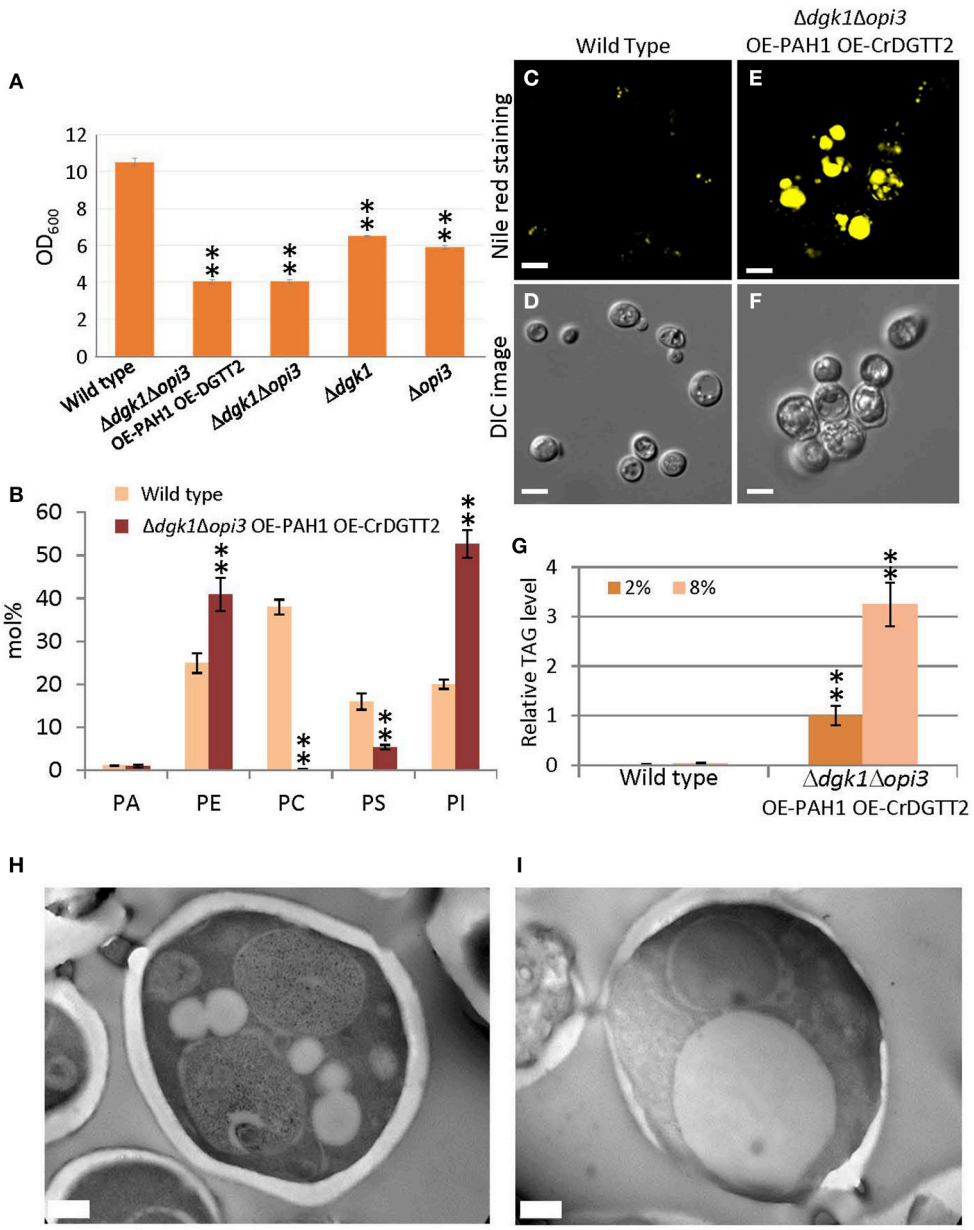

FIGURE 3 | Phenotypes of the Δ*dgk1*Δ*opi3* OE-PAH1 OE-CrDGTT2 strain. (A) The OD_{600} value of culture at stationary phase of wild type, Δ*dgk1*Δ*opi3* OE-PAH1 OE-CrDGTT2, Δ*dgk1*Δ*opi3*, Δ*dgk1,* and Δ*opi3*. Fully grown yeast cell cultures were diluted to OD_{600} of 0.1 in 10 ml synthetic complete media at 30°C, and OD_{600} was measured after 72 h of incubation, at which culture reached a plateau. Data are mean ± SD from three biological replicates. **(B)** Membrane lipid composition (mol%) of the Δ*dgk1*Δ*opi3* OE-PAH1 OE-CrDGTT2 strain. Wild type, yellow bars; the Δ*dgk1*Δ*opi3* OE-PAH1 OE-CrDGTT2 strain, brown bars. See Supplementary Table 3 for numerical values. **(C–F)** The Δ*dgk1*Δ*opi3* OE-PAH1 OE-CrDGTT2 strain at the beginning of stationary phase by Nile red staining **(E)** and Normarski differential interference contrast (DIC) microscopy image **(F)** compared with the wild type **(C,D)**. **(G)** Fold increase of TAG levels in response to glucose boost from 2 to 8% at the beginning of stationary phase. TAG level of Δ*dgk1*Δ*opi3* OE-PAH1 OE-CrDGTT2 strain under 2% glucose condition was set as 1. See Supplementary Table 4 for numerical values. **(H,I)** Transmission electron microscope images of the ultrastructure of wild type **(H)** and the Δ*dgk1*Δ*opi3* OE-PAH1 OE-CrDGTT2 **(I)** cells in response to glucose boost from 2 to 8% at the end of log phase. Data in **(A,B)** and **(G)** are mean ± SD from three biological replicates. Asterisks indicate statistical significance by Student's *t*-test (**$P < 0.01$). See **Figure 1** for abbreviations. Bars in **(C–F)** are 5 μm and **(H–I)** are 0.5 μm.

Sustainable TAG Production in the Δ*dgk1*Δ*opi3* OE-PAH1 OE-CrDGTT2 Cells

A major challenge in TAG metabolic engineering has been how to maintain accumulated TAG with continuous cell growth. This is because TAG accumulation occurs during the stationary phase in wild-type cells, when cell numbers are no longer increased. However, on growth resumption from the stationary phase, accumulated TAG is mostly hydrolyzed to DAG (TAG

mobilization) as a substrate to produce phospholipids which are required for rapid growth of cellular membranes (Athenstaedt and Daum, 2005; Kurat et al., 2009).

To demonstrate whether sustainable TAG production is possible with the Δ*dgk1*Δ*opi3* OE-PAH1 OE-CrDGTT2 cells, quantity (**Figure 4B**) and quality (**Figure 4C**) of TAG were profiled along with the cell growth (**Figure 4A**) through three consecutive repeats of growth resumption. Upon growth resumption from the stationary phase, the growth rate was slower in the Δ*dgk1*Δ*opi3* OE-PAH1 OE-CrDGTT2 than the wild type (**Figure 4A**); the Δ*dgk1*Δ*opi3* OE-PAH1 OE-CrDGTT2 cells reached stationary phase at 48 h after growth resumption with OD_{600} of 4, whereas wild type cells reached stationary phase at 36 h with OD_{600} of 10. At 60 h, these cultures were diluted again to resume the growth, which reproduced similar growth profile through the following two repeats of growth resumption. TAG level of the Δ*dgk1*Δ*opi3* OE-PAH1 OE-CrDGTT2 cells in full growth at 60 h was 13.2 to 14.5% of dry cell weight (**Figure 4B**; Supplementary Table 5). Twenty-four hours after growth resumption, TAG level was reduced transiently but was recovered to the initial levels by 60 h. Repeated dilution reproduced the same extent of TAG levels after 60 h for two more times (**Figure 4B**; Supplementary Table 5). Moreover, fatty acid composition of TAG was maintained throughout the different time points (**Figure 4C**, Supplementary Table 6), indicating stable quality of TAG. Thus, the Δ*dgk1*Δ*opi3* OE-PAH1 OE-CrDGTT2 cells could grow with reduced degradation of accumulated TAG, which favored sustainable TAG production.

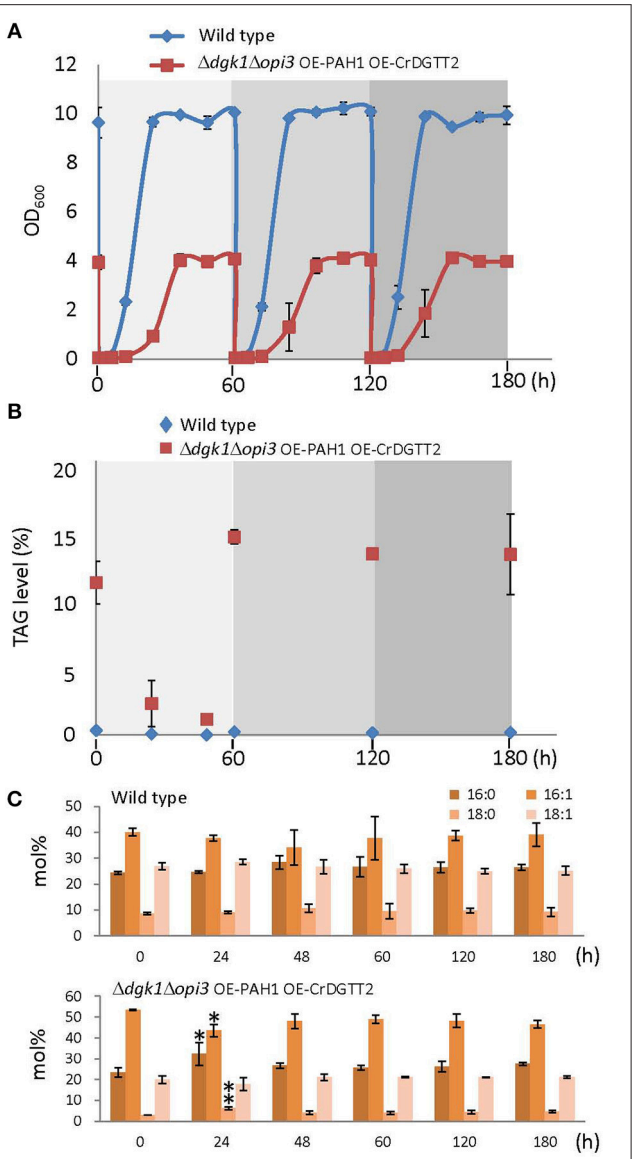

FIGURE 4 | Sustainable TAG production in the Δ*dgk1*Δ*opi3* OE-PAH1 OE-CrDGTT2 strain. (A) Growth profile of the Δ*dgk1*Δ*opi3* OE-PAH1 OE-CrDGTT2 strain with repeated resumption of growth. One hundred milliliter of cells at full growth was diluted to OD_{600} of 0.05 at 0, 60, and 120 h. **(B,C)** TAG levels **(B)** and fatty acid composition **(C)** of wild type and the Δ*dgk1*Δ*opi3* OE-PAH1 OE-CrDGTT2 strain with repeated resumption of growth. Data in **(A–C)** are mean ± SD from three biological replicates. Asterisks indicate statistical significance by Student's *t*-test (*$P < 0.05$; **$P < 0.01$). See Supplementary Tables 5, 6 for numerical values.

DISCUSSION

Our metabolic engineering to overexpress an algal gene in genetically manipulated yeast *S. cerevisiae* resulted in about 70-fold increase in TAG level, which is estimated to be 12.2% of dry cell weight (**Figure 2D**). This yield is superior to recently achieved TAG engineering in *S. cerevisiae*. For example, overexpression of a glycerol kinase and DAG acyltransferases achieved 8.2% of TAG with 2% glycerol as carbon source (Yu et al., 2013). In addition, overexpression of fatty acid biosynthesis genes produced 17% of total lipid fraction including TAG and other lipid classes (Runguphan and Keasling, 2014); because *S. cerevisiae* produces similar amounts of TAG and sterylesters as major lipid content (Beopoulos et al., 2009), our metabolic engineering may produce higher TAG contents. Moreover, our engineered *S. cerevisiae* strain diluted from full growth resumed growth with TAG accumulated (**Figure 4**). This sustainable TAG production may be an intriguing feature of this engineered strain from the viewpoint of metabolic engineering, although it may have little advantage in real industrial application since dilution requires cost of new medium. Oily yeasts such as *Lipomyces starkeyi*, *Rhodosporidium toruloides*, *Rhodotorula glutinis,* and *Yarrowia lipolytica* can produce up to 20% lipids per dry biomass (Runguphan and Keasling, 2014). For oleaginous algae, lipid levels commonly range from 20 to 50% per dry biomass, exceeding the usual yield of oleaginous yeasts (Beopoulos et al., 2009). Although levels of TAG accumulation in the Δ*dgk1*Δ*opi3* OE-PAH1 OE-CrDGTT2 cells were not superior to these oleaginous microorganisms, several advantages of using *S. cerevisiae* over other yeasts or microalgae have been pointed, such as genetic tractability, commercially available whole-genome deletion strain collection or a proven track record in different industrial applications (Tang et al., 2013). Our strategy of metabolic engineering could be applicable to these oleaginous microorganisms to further improve their lipid yields. Molecular engineering of eukaryotic algae still awaits technical developments despite that engineered algae may contribute to

the carbon neutrality owing to photosynthesis. Therefore, our TAG engineering using CrDGTT2 provides a new strategy to enhance oil production in *S. cerevisiae*. Since algal species are highly diverse, a robust enzyme similar to CrDGTT2 may be found in other oleaginous algal species. Since CrDGTT2 showed much higher expression level than any other DGTT isoforms in *S. cerevisiae* even though they were all expressed by the same promoter system, it is possible that the robustness of CrDGTT2 may be due to higher stability of mRNA in a heterologous system (Hung et al., 2013). Using algal gene resources to engineer established model microorganism can contribute to develop an innovative approach in the field of synthetic biology and has potential to produce TAG or other value-added oils for industrial demand.

In conclusion, we employed an algal gene resource, *CrDGTT2*, to reconstitute enhanced and sustainable TAG production in a yeast *S. cerevisiae* by metabolic engineering.

AUTHOR CONTRIBUTIONS

YN conceived research; KK and YN designed experiments; CH performed experiments and analyzed data; KK provided technical assistance to CH, KK, and YN wrote the manuscript; all author commented on the manuscript and approved the contents.

ACKNOWLEDGMENTS

We thank Wann-Nen Jane and Mei-Jane Fang (Institute of Plant and Microbial Biology, Academia Sinica) for technical support with microscopy. This research was supported by PRESTO, Japan Science and Technology Agency, Ministry of Science and Technology Taiwan (Grant ID: 103-2311-B-001-029-MY3), and a core operation budget from the Institute of Plant and Microbial Biology, Academia Sinica.

SUPPLEMENTARY MATERIAL

The Supplementary Material for this article can be found online at: http://journal.frontiersin.org/article/10.3389/fmicb.2016.00070

REFERENCES

Adeyo, O., Horn, P. J., Lee, S., Binns, D. D., Chandrahas, A., Chapman, K. D., et al. (2011). The yeast lipin orthologue Pah1p is important for biogenesis of lipid droplets. *J. Cell Biol.* 192, 1043–1055. doi: 10.1083/jcb.201010111

Athenstaedt, K., and Daum, G. (2005). Tgl4p and Tgl5p, two triacylglycerol lipases of the yeast *Saccharomyces cerevisiae* are localized to lipid particles. *J. Biol. Chem.* 280, 37301–37309. doi: 10.1074/jbc.M507261200

Beopoulos, A., Cescut, J., Haddouche, R., Uribelarrea, J. L., Molina-Jouve, C., and Nicaud, J. M. (2009). *Yarrowia lipolytica* as a model for bio-oil production. *Prog. Lipid Res.* 48, 375–387. doi: 10.1016/j.plipres.2009.08.005

Blazeck, J., Garg, R., Reed, B., and Alper, H. S. (2012). Controlling promoter strength and regulation in *Saccharomyces cerevisiae* using synthetic hybrid promoters. *Biotechnol. Bioeng.* 109, 2884–2895. doi: 10.1002/bit.24552

Durrett, T. P., Benning, C., and Ohlrogge, J. (2008). Plant triacylglycerols as feedstocks for the production of biofuels. *Plant J.* 54, 593–607. doi: 10.1111/j.1365-313X.2008.03442.x

Fakas, S., Konstantinou, C., and Carman, G. M. (2011a). DGK1-encoded diacylglycerol kinase activity is required for phospholipid synthesis during growth resumption from stationary phase in *Saccharomyces cerevisiae*. *J. Biol. Chem.* 286, 1464–1474. doi: 10.1074/jbc.M110.194308

Fakas, S., Qiu, Y., Dixon, J. L., Han, G. S., Ruggles, K. V., Garbarino, J., et al. (2011b). Phosphatidate phosphatase activity plays key role in protection against fatty acid-induced toxicity in yeast. *J. Biol. Chem.* 286, 29074–29085. doi: 10.1074/jbc.M111.258798

Fei, W., Shui, G., Zhang, Y., Krahmer, N., Ferguson, C., Kapterian, T. S., et al. (2011). A role for phosphatidic acid in the formation of "supersized" lipid droplets. *PLoS Genet.* 7:e1002201. doi: 10.1371/journal.pgen.1002201

Folch, J., Lees, M., and Sloane Stanley, G. H. (1957). A simple method for the isolation and purification of total lipides from animal tissues. *J. Biol. Chem.* 226, 497–509.

Fu, D., Oh, S., Choi, W., Yamauchi, T., Dorn, A., Yaqoob, Z., et al. (2010). Quantitative DIC microscopy using an off-axis self-interference approach. *Opt. Lett.* 35, 2370–2372. doi: 10.1364/OL.35.002370

Gietz, R. D., and Woods, R. A. (2002). Transformation of yeast by lithium acetate/single-stranded carrier DNA/polyethylene glycol method. *Meth. Enzymol.* 350, 87–96. doi: 10.1016/s0076-6879(02)50957-5

Han, G. S., O'Hara, L., Carman, G. M., and Siniossoglou, S. (2008a). An unconventional diacylglycerol kinase that regulates phospholipid synthesis and nuclear membrane growth. *J. Biol. Chem.* 283, 20433–20442. doi: 10.1074/jbc.M802903200

Han, G. S., O'Hara, L., Siniossoglou, S., and Carman, G. M. (2008b). Characterization of the yeast DGK1-encoded CTP-dependent diacylglycerol kinase. *J. Biol. Chem.* 283, 20443–20453. doi: 10.1074/jbc.M802866200

Han, G. S., Wu, W. I., and Carman, G. M. (2006). The *Saccharomyces cerevisiae* Lipin homolog is a Mg^{2+}-dependent phosphatidate phosphatase enzyme. *J. Biol. Chem.* 281, 9210–9218. doi: 10.1074/jbc.M600425200

Henry, S. A., Kohlwein, S. D., and Carman, G. M. (2012). Metabolism and regulation of glycerolipids in the yeast *Saccharomyces cerevisiae*. *Genetics* 190, 317–349. doi: 10.1534/genetics.111.130286

Hu, Q., Sommerfeld, M., Jarvis, E., Ghirardi, M., Posewitz, M., Seibert, M., et al. (2008). Microalgal triacylglycerols as feedstocks for biofuel production: perspectives and advances. *Plant J.* 54, 621–639. doi: 10.1111/j.1365-313X.2008.03492.x

Hung, C. H., Ho, M. Y., Kanehara, K., and Nakamura, Y. (2013). Functional study of diacylglycerol acyltransferase type 2 family in *Chlamydomonas reinhardtii*. *FEBS Lett.* 587, 2364–2370. doi: 10.1016/j.febslet.2013.06.002

Kamisaka, Y., Kimura, K., Uemura, H., and Yamaoka, M. (2013). Overexpression of the active diacylglycerol acyltransferase variant transforms *Saccharomyces cerevisiae* into an oleaginous yeast. *Appl. Microbiol. Biotechnol.* 97, 7345–7355. doi: 10.1007/s00253-013-4915-9

Kurat, C. F., Wolinski, H., Petschnigg, J., Kaluarachchi, S., Andrews, B., Natter, K., et al. (2009). Cdk1/Cdc28-dependent activation of the major triacylglycerol lipase Tgl4 in yeast links lipolysis to cell-cycle progression. *Mol. Cell* 33, 53–63. doi: 10.1016/j.molcel.2008.12.019

McGraw, P., and Henry, S. A. (1989). Mutations in the *Saccharomyces cerevisiae* opi3 gene: effects on phospholipid methylation, growth and cross-pathway regulation of inositol synthesis. *Genetics* 122, 317–330.

Merchant, S. S., Kropat, J., Liu, B., Shaw, J., and Warakanont, J. (2012). TAG, you're it! Chlamydomonas as a reference organism for understanding algal triacylglycerol accumulation. *Curr. Opin. Biotechnol.* 23, 352–363. doi: 10.1016/j.copbio.2011.12.001

Nakamura, Y., Arimitsu, H., Yamaryo, Y., Awai, K., Masuda, T., Shimada, H., et al. (2003). Digalactosyldiacylglycerol is a major glycolipid in floral organs of Petunia hybrida. *Lipids* 38, 1107–1112. doi: 10.1007/s11745-006-1166-x

Nelson, G. J. (1967). The phospholipid composition of plasma in various mammalian species. *Lipids* 2, 323–328. doi: 10.1007/BF02532119

Runguphan, W., and Keasling, J. D. (2014). Metabolic engineering of *Saccharomyces cerevisiae* for production of fatty acid-derived biofuels and chemicals. *Metab. Eng.* 21, 103–113. doi: 10.1016/j.ymben.2013.07.003

Sandager, L., Gustavsson, M. H., Ståhl, U., Dahlqvist, A., Wiberg, E., Banas, A., et al. (2002). Storage lipid synthesis is non-essential in yeast. *J. Biol. Chem.* 277, 6478–6482. doi: 10.1074/jbc.M109109200

Sanjaya, M. R., Durrett, T. P., Kosma, D. K., Lydic, T. A., Muthan, B., Koo, A. J., et al. (2013). Altered lipid composition and enhanced nutritional value of Arabidopsis leaves following introduction of an algal diacylglycerol acyltransferase 2. *Plant Cell* 25, 677–693. doi: 10.1105/tpc.112.104752

Shen, H., Heacock, P. N., Clancey, C. J., and Dowhan, W. (1996). The CDS1 gene encoding CDP-diacylglycerol synthase in *Saccharomyces cerevisiae* is essential for cell growth. *J. Biol. Chem.* 271, 789–795. doi: 10.1074/jbc.271.2.789

Tang, X., Feng, H., and Chen, W. N. (2013). Metabolic engineering for enhanced fatty acids synthesis in *Saccharomyces cerevisiae*. *Metab. Eng.* 16, 95–102. doi: 10.1016/j.ymben.2013.01.003

Yu, K. O., Jung, J., Ramzi, A. B., Choe, S. H., Kim, S. W., Park, C., et al. (2013). Development of a *Saccharomyces cerevisiae* strain for increasing the accumulation of triacylglycerol as a microbial oil feedstock for biodiesel production using glycerol as a substrate. *Biotechnol. Bioeng.* 110, 343–347. doi: 10.1002/bit.24623

Zhang, M., Fan, J., Taylor, D. C., and Ohlrogge, J. B. (2009). DGAT1 and PDAT1 acyltransferases have overlapping functions in Arabidopsis triacylglycerol biosynthesis and are essential for normal pollen and seed development. *Plant Cell* 21, 3885–3901. doi: 10.1105/tpc.109.071795

Conflict of Interest Statement: The authors declare that the research was conducted in the absence of any commercial or financial relationships that could be construed as a potential conflict of interest.

frontiers in Microbiology

ORIGINAL RESEARCH
published: 12 January 2016
doi: 10.3389/fmicb.2015.01542

Functional Specificity of Cardiolipin Synthase Revealed by the Identification of a Cardiolipin Synthase CrCLS1 in *Chlamydomonas reinhardtii*

*Chun-Hsien Hung[1], Koichi Kobayashi[2], Hajime Wada[2,3] and Yuki Nakamura[1,4]**

[1] Institute of Plant and Microbial Biology, Academia Sinica, Taipei, Taiwan, [2] Department of Life Sciences, Graduate School of Arts and Sciences, The University of Tokyo, Tokyo, Japan, [3] Japan Science and Technology Agency, CREST, Saitama, Japan, [4] Japan Science and Technology Agency, PRESTO, Saitama, Japan

OPEN ACCESS

Edited by:
Weiwen Zhang, Tianjin University, China

Reviewed by:
Alberto A. Iglesias, Instituto de Agrobiotecnología del Litoral – Consejo Nacional de Investigaciones Científicas y Tecnológicas, Argentina
Takashi Osanai, Meiji University, Japan
Song Xue, Marine Bioengineering Group Department of Biotechnology Dalian Institute of Chemical Physics Chinese Academy of Sciences, China

***Correspondence:**
Yuki Nakamura
nakamura@gate.sinica.edu.tw

Specialty section:
This article was submitted to Microbiotechnology, Ecotoxicology and Bioremediation, a section of the journal Frontiers in Microbiology

Received: *15 October 2015*
Accepted: *21 December 2015*
Published: *12 January 2016*

Citation:
Hung C-H, Kobayashi K, Wada H and Nakamura Y (2016) Functional Specificity of Cardiolipin Synthase Revealed by the Identification of a Cardiolipin Synthase CrCLS1 in Chlamydomonas reinhardtii. Front. Microbiol. 6:1542. doi: 10.3389/fmicb.2015.01542

Phosphatidylglycerol (PG) and cardiolipin (CL) are two essential classes of phospholipid in plants and algae. Phosphatidylglycerophosphate synthase (PGPS) and cardiolipin synthase (CLS) involved in the biosynthesis of PG and CL belong to CDP-alcohol phosphotransferase and share overall amino acid sequence homology. However, it remains elusive whether PGPS and CLS are functionally distinct *in vivo*. Here, we report identification of a gene encoding CLS in *Chlamydomonas reinhardtii*, *CrCLS1*, and its functional compatibility. Whereas *CrCLS1* did not complement the growth phenotype of a PGPS mutant of *Synechocystis* sp. PCC 6803, it rescued the temperature-sensitive growth phenotype, growth profile with different carbon sources, phospholipid composition and enzyme activity of Δ*crd1*, a CLS mutant of *Saccharomyces cerevisiae*. These results suggest that *CrCLS1* encodes a functional CLS of *C. reinhardtii* as the first identified algal CLS, whose enzyme function is distinct from that of PGPSs from *C. reinhardtii*. Comparison of CDP-alcohol phosphotransferase motif between PGPS and CLS among different species revealed a possible additional motif that might define the substrate specificity of these closely related enzymes.

Keywords: CDP-alcohol phosphotransferase, cardiolipin, cardiolipin synthase, phosphatidylglycerol, PGPS, *Chlamydomonas reinhardtii*, *Synechocystis* sp. PCC 6803, *Saccharomyces cerevisiae*

INTRODUCTION

Functional specificity of an enzyme is crucial in keeping metabolic reactions in order. This largely relies on the substrate specificity defined by the catalytic motif. Thus, enzymes are often categorized into groups according to the existence of common catalytic motif(s). In phospholipid metabolism, a number of important reaction steps are catalyzed by CDP-alcohol phosphotransferases (Li-Beisson et al., 2013, 2015). These include CLS, PGPS, phosphatidylinositol (PI) synthase, phosphatidylserine (PS) synthase, phosphatidylcholine (PC)

Abbreviations: CDP, cytidine 5′-diphosphate; CL, cardiolipin; CLS, cardiolipin synthase; PA, phosphatidic acid; PC, phosphatidylcholine; PE, phosphatidylethanolamine; PG, phosphatidylglycerol; PGP, phosphatidylglycerol phosphate; PGPP, phosphatidylglycerophosphate phosphatase; PGPS, phosphatidylglycerophosphate synthase; PI, phosphatidylinositol; PS, phosphatidylserine.

synthase, and aminoalcohol phosphotransferase for the biosynthesis of CL, PG, PI, PS, PC, and PE, respectively. Because these are the major phospholipid classes found in diverse organisms from bacteria to mammals and seed plants, it can be stated that CDP-alcohol phosphotransferases are crucial in the entire phospholipid metabolism.

In plants and algae, PG is an indispensable phospholipid class in photosynthetic function (Hagio et al., 2000, 2002; Sato et al., 2000; Babiychuk et al., 2003; Yu and Benning, 2003). Moreover, CL, which is an anionic phospholipid class widely distributed in different kingdom and found exclusively at the inner membrane of mitochondria (Lewis and McElhaney, 2009), has an essential role in mitochondrial function and thus plant growth (Katayama et al., 2004; Pineau et al., 2013). The biosynthesis of these lipid classes begins with the conversion of phosphatidic acid (PA) into CDP-diacylglycerol (CDP-DAG) by CDP-DAG synthase (CDS; Sato et al., 2000; Haselier et al., 2010; Zhou et al., 2013). Next, PGPS coverts CDP-DAG to phosphatidylglycerol phosphate (PGP), which is dephosphorylated by PGP phosphatase (PGPP) to produce PG (Muller and Frentzen, 2001; Hagio et al., 2000, 2002; Wu et al., 2006; Osman et al., 2010; Hung et al., 2015b). Furthermore, PG is converted to CL by CLS in mitochondria (Kadenbach et al., 1982; Jiang et al., 1997, 1999). Initially, 3 PGPSs were proposed in *Arabidopsis thaliana* (PGP1, PGP2, and PGP3) based on the amino acid sequence similarity (Xu et al., 2002). However, the third isoform (PGP3) was later shown not to be a functional PGPS but instead functions as CLS (Katayama et al., 2004). Subsequent gene knockout studies defined distinct *in vivo* function of CLS associated with mitochondrial function (Pineau et al., 2013). Thus, PGPS and CLS are functionally independent, although they are homologous and belong to the same CDP-alcohol phosphotransferase family in *A. thaliana*. Recently, we identified and characterized genes for PGPS of *Chlamydomonas reinhardtii* (Hung et al., 2015a). We demonstrated two functional PGPS isoforms; however, genome-wide search identified an additional PGPS homolog, which is more homologous with CLS. This reminded us of the case in *A. thaliana* described above. Because reciprocal genetic complementation was not performed yet in *A. thaliana* or any other model organisms, it remains elusive whether PGPS and CLS are functionally distinct *in vivo*.

In this report, we identified the additional homolog of PGPS in *C. reinhardtii*, designated *CrCLS1* (*Cre13.g604700*), and performed reciprocal functional complementation assay using *pgsA*, a PGPS mutant of *Synechocystis* sp. PCC 6803 and Δ*crd1*, a CLS mutant of *Saccharomyces cerevisiae*. The result of functional complementation in these mutants, along with phenotype observation, lipid analysis and enzyme activity assay, demonstrated that *CrCLS1* encodes a functional CLS but not PGPS. We compared sequence similarity in detail between PGPS and CLS and noted some difference adjacent to the defined CDP-OH-P motif. Our results suggest non-overlapping function of PGPS and CLS, through the identification and characterization of CLS in *C. reinhardtii* as the first report of CLS in algae.

MATERIALS AND METHODS

Strains

The strains produced in this work are listed in Supplementary Table S1.

Protein Sequence Analysis

The multiple alignment of protein sequences was performed by use of CLUSTALW[1]. The mitochondrial targeting sequence was predicted by use of the subcellular localization program MitoProtII[2] (Claros and Vincens, 1996).

Cloning of Plasmid Vectors

CrCLS1 (*Cre13.g604700*): To construct pCH069, a 1,060-bp fragment was amplified from the cDNA template of *C. reinhardtii* strain CC-503 (cw92 mt+) with the primers CH227 and CH228, and cloned into pENTR/D-TOPO. Then, to construct pCH178, the open reading frame (ORF) of *CrCLS1* was amplified from pCH069 with the primers CH831 and CH832, and inserted into *Xba*I and *Eco*RI sites of pCH078 (Hung et al., 2013). To construct pCH158, the ORF of *CrCLS1* was amplified from pCH069 with the primers CH776 and CH777 and inserted into *Nde*I and *Hpa*I sites of pTCP2031V (Satoh et al., 2001). The primers and plasmids used in this study are described in Supplementary Tables S2 and 3, respectively.

Complementation Assay of the *Synechocystis* sp. PCC 6803 *pgsA* Mutant by *CrCLS1*

Complementation assay of the *Synechocystis* sp. PCC 6803 *pgsA* mutant by *CrCLS1* (pCH158) was performed as described previously (Hung et al., 2015a).

Complementation Assay of the *S. cerevisiae* Δ*crd1* Mutant by *CrCLS1*

Complementation assay of the *S. cerevisiae* Δ*crd1* mutant by *CrCLS1* (pCH178) was performed as described previously (Hung et al., 2015a).

Lipid Extraction and Analysis

Lipid extraction and analysis were performed as previously described (Hung et al., 2013) except that 2D thin-layer chromatography (TLC) was used to separate phospholipid classes with the solvent system of chloroform/methanol/7 N ammonia 120:80:8 (by vol) for the first dimension and chloroform/methanol/acetic acid/water 170:20:15:3 (by vol) for the second dimension (Nakamura et al., 2003).

Radiolabeling Assay of CLS Activity

Logarithmically growing cells were resuspended in 5 ml SC-Ura medium at the cell density (OD_{600} of 5) with 30 μCi $KH_2{}^{32}PO_4$ (PerkinElmer). After shaking incubation for 8 h at room temperature, lipids were extracted from cells by the method

[1]http://www.genome.jp/tools/clustalw/

[2]http://ihg.gsf.de/ihg/mitoprot.html

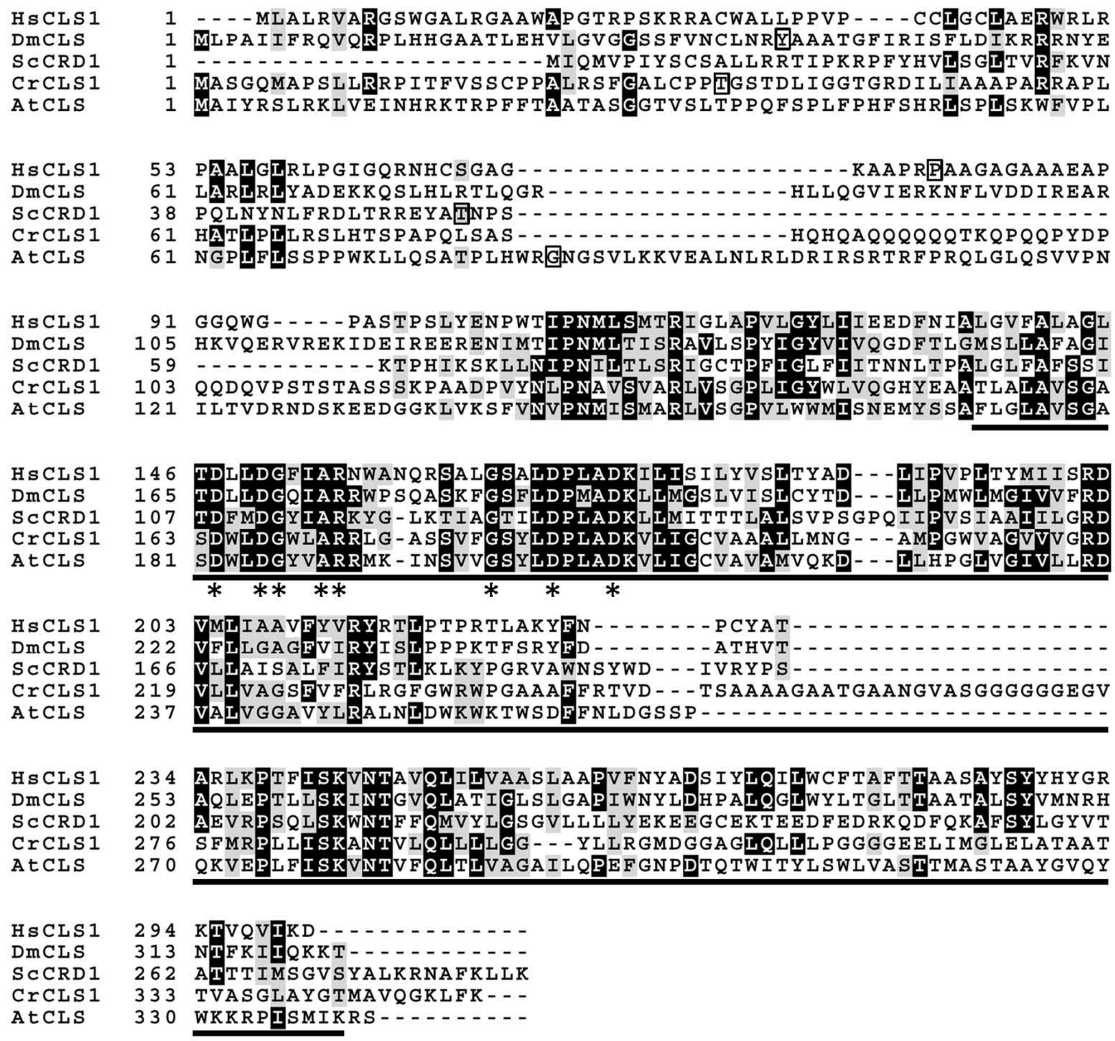

FIGURE 1 | Multiple amino acid sequence alignment of *Chlamydomonas reinhardtii* CLS1 (CrCLS1) with other known CLSs, *Saccharomyces cerevisiae* CRD1 (ScCRD1), *Homo sapiens* CLS1 (HsCLS1), *Arabidopsis thaliana* CLS (AtCLS), and *Drosophila melanogaster* CLS (DmCLS). The region conserved among proteins containing a CDP-OH-P motif (PF01066.9) is underlined. Asterisks indicate the amino acid residues conserved in all sequences of proteins with the CDP-OH-P motif. Square frames indicate the terminal amino acid residues of the predicted cleavage site of putative N-terminal mitochondrial targeting sequence.

of Bligh and Dyer (1959). Lipids spotted on a TLC plate (Silica gel 60G, Merck) were developed with chloroform/methanol/acetic acid (65:25:8, v/v/v) (Haselier et al., 2010) along with PG and CL (Sigma–Aldrich) as standards and radioactive spots were visualized by Imaging Plate (Fuji Film) and BAS-2500 (GE Healthcare). Unlabeled PG and CL were stained with 0.01% primuline in 80% (v/v) acetone and detected under UV light.

RNA Extraction and cDNA Synthesis

RNA extraction and cDNA synthesis were performed as previously described (Hung et al., 2013).

Quantitative RT-PCR

Quantitative RT-PCR analysis involved the ABI 7500 Real Time PCR System (Applied Biosystems) with the specific oligonucleotide primer sets, CH955 and CH956, CH957 and CH958, and CH531 and CH532, for *CrCLS1*, *CRD1,* and *ACT1*, respectively. Gene expression was normalized to that of *ACT1*. Data were averaged by three technical replicates in the same run and three biological replicates in separate runs. The primer sequences are described in Supplementary Table S2.

RESULTS

Sequence Analysis of CrCLS1

To compare the amino acid sequence similarity of the putative CrCLS1 with other known CLSs in different organisms, the deduced amino acid sequence of CrCLS1 was compared with those of *S. cerevisiae* CRD1, *Homo sapiens* CLS1,

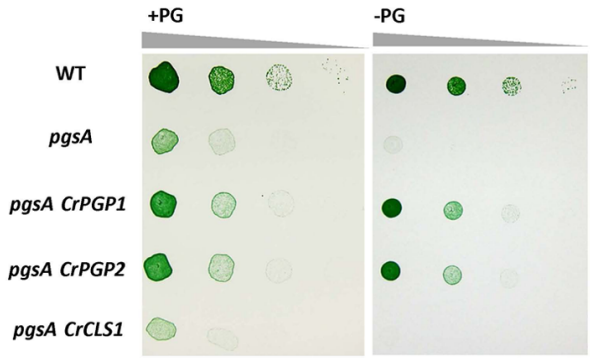

FIGURE 2 | Heterologous complementation of *Synechocystis* sp. PCC 6803 *pgsA* mutant by *CrPGP1*, *CrPGP2* and *CrCLS1*. Growth of the wild type, *pgsA*, *pgsA CrPGP1*, *pgsA CrPGP2*, and *pgsA CrCLS1* were compared on solid BG-11 media with or without PG supplementation. Spotting involved serial 10-fold dilution from left to right starting at OD_{730} of 0.05, with 5 μl each spotted onto a BG-11 agar plate with or without 20 μM PG and incubated under 50~60 μmol photons m^{-2} s^{-1} for 5 days at 30°C. Images are representative of three biological replicates.

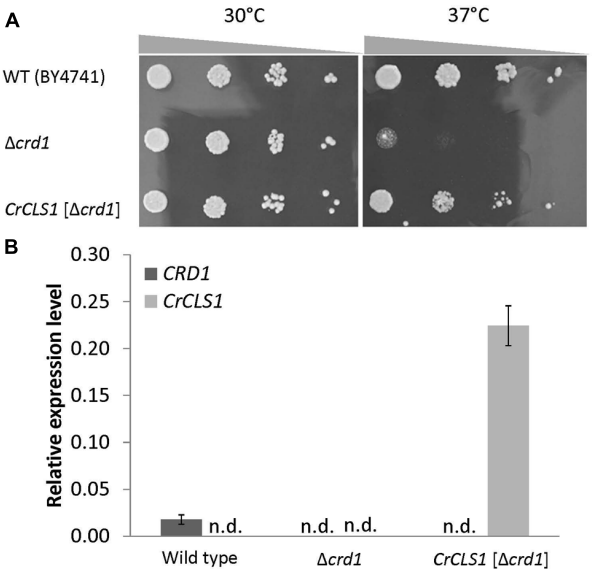

FIGURE 3 | Heterologous complementation of temperature-sensitive growth defect in the *S. cerevisiae* Δ*crd1* mutant with *C. reinhardtii CLS1*. **(A)** Culture of wild type, Δ*crd1* mutant and Δ*crd1* mutant harboring *CrCLS1* involved serial 10-fold dilution from left to right starting at OD_{600} of 0.1; 5 μL each was spotted onto YPD media and incubated for 2 days at 30°C or 37°C. Images are representative of 3 replicates. **(B)** Relative expression of *CRD1* and *CrCLS1* in wild type, Δ*crd1* and Δ*crd1 CrCLS1*. Levels are normalized to that of *ACT1*. Data are mean ± SD from three biological replicates. n.d., not detected.

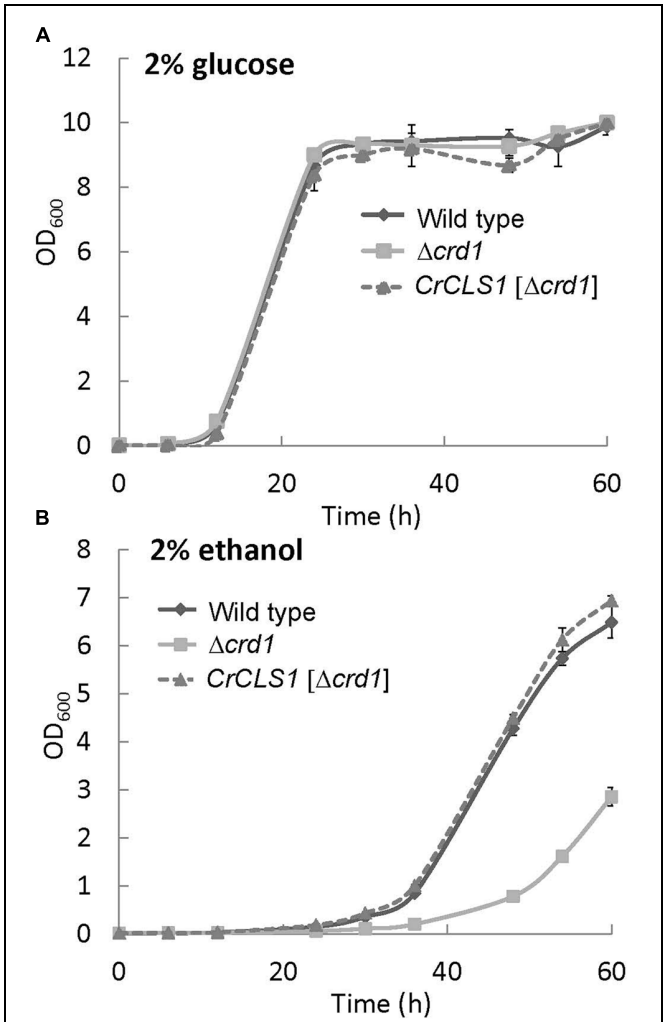

FIGURE 4 | Growth of wild type, Δ*crd1* and Δ*crd1 CrCLS1* with different carbon sources. Cells were grown in synthetic complete medium supplemented with 2% glucose **(A)** or 2% ethanol **(B)**. Cell growth was started at OD_{600} of 0.01 at 30°C. Data are mean ± SD from three biological replicates.

A. thaliana CLS, and *Drosophila melanogaster* CLS, which are functionally characterized CLS (**Figure 1**) (Tuller et al., 1998; Katayama et al., 2004; Chen et al., 2006; Acehan et al., 2011). In **Figure 1**, the region containing the CDP-OH-P motif $D(X)_2DG(X)_2AR(X)_{8-9}G(X)_3D(X)_3D$ is underlined and asterisks indicate the conserved eight amino acid residues. All eight amino acids were conserved in CrCLS1, which suggests that *CrCLS1* encodes a functional CLS. In addition, CrCLS1 contained a putative N-terminal mitochondrial targeting sequence predicted by the subcellular localization program MitoProtII, suggesting a possible localization of CrCLS1 in mitochondria, where CL is exclusively localized.

Complementation of *pgsA* by *CrCLS1*

To examine whether CrCLS1 functions as PGPS, we transformed CrCLS1 into the *pgsA* mutant of *Synechocystis* sp. PCC 6803, which abolishes PGPS activity and thus requires exogenous supplementation of PG for growth (Hagio et al., 2000). As shown in **Figure 2**, whereas the *CrPGP1* and *CrPGP2* functionally complemented the lethal phenotype of the *pgsA* mutant as reported previously (Hung et al., 2015a), *CrCLS1* failed to

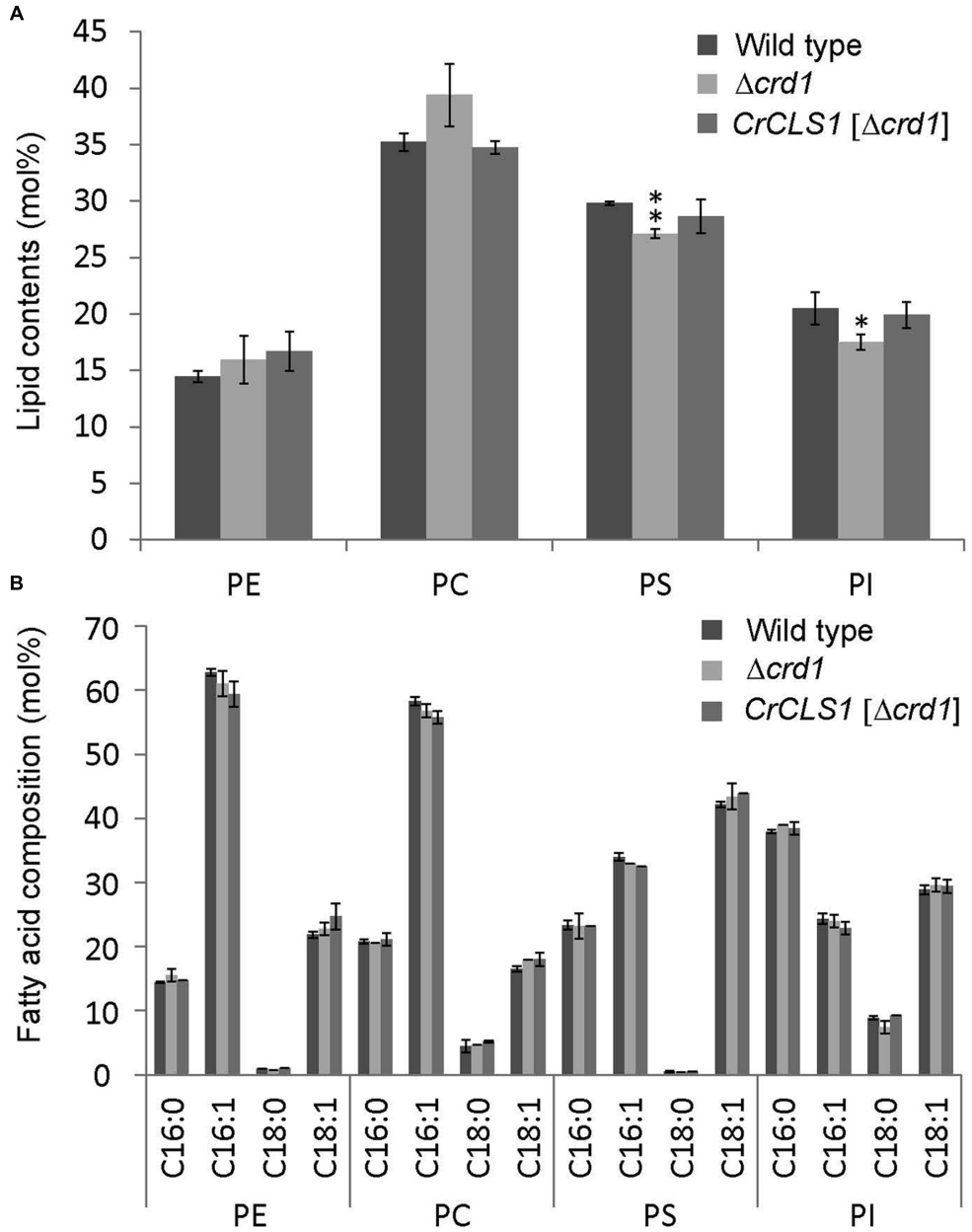

FIGURE 5 | Phospholipid content (A) and fatty acid composition (B) of wild type, Δ*crd1* and Δ*crd1 CrCLS1*. Total lipids were extracted from cells grown to stationary phase and separated by 2D thin-layer chromatography; content of phospholipids was quantified by gas chromatography. Data are mean ± SD from three biological replicates. Asterisks indicate statistical significance by Student's *t*-test (*$P < 0.05$, **$P < 0.001$). PC, phosphatidylcholine; PE, phosphatidylethanolamine; PI, phosphatidylinositol; PS, phosphatidylserine.

complement the growth phenotype, showing the rescued growth only in the presence of PG. Therefore, CrCLS1 does not function as a PGPS *in vivo* in *Synechocystis* sp. PCC 6803.

Recovery of Growth Defect in the Δ*crd1* Mutant Complemented by *CrCLS1*

To investigate whether *CrCLS1* encodes a functional CLS, we performed a heterologous complementation assay with the *S. cerevisiae* Δ*crd1* mutant, because *Synechocystis* sp. PCC 6803 does not contain CL and no other CLS mutant is known in algae. As previously reported, Crd1p has CLS activity and Δ*crd1* mutant cells show a temperature-sensitive growth defect, severe at 37°C but not at 30°C (Jiang et al., 1999). The temperature-sensitive phenotype of Δ*crd1* mutant cells was rescued by heterologous complementation of *HsCLS1* (Houtkooper et al., 2006), so we used this approach to investigate the function of CrCLS1. We cloned the ORF of *CrCLS1* into a yeast shuttle

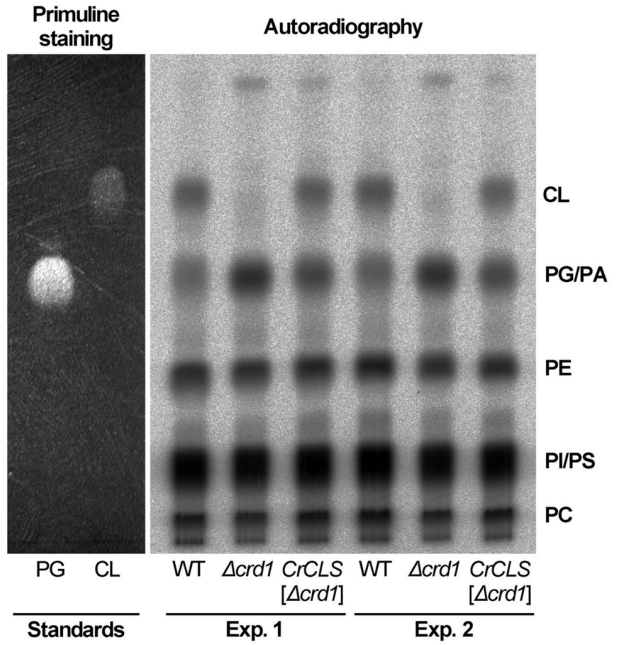

FIGURE 6 | *CrCLS* complemented cardiolipin synthesis in Δ*crd1* cells. Wild type (WT), Δ*crd1* or Δ*crd1 CrCLS* cells were grown in the presence of [^{32}P]-phosphate for 8 h at room temperature. Radioactivity incorporated into phospholipids was determined by TLC analysis and autoradiography, with unlabeled PG and CL visualized by primuline staining as standards. Two biologically independent experiments (Experiments 1 and 2) were shown. PE, phosphatidylethanolamine; PC, phosphatidylcholine; PI, phosphatidylinositol; PS, phosphatidylserine; PA, phosphatidic acid.

vector and transformed it into Δ*crd1* mutant cells. The Δ*crd1* mutant harboring *CrCLS1* fully recovered cell growth at 37°C, whereas the Δ*crd1* mutant alone showed a growth defect at this temperature (**Figure 3A**). Therefore, *CrCLS1* complemented the temperature-sensitive phenotype of Δ*crd1*, which suggests that *CrCLS1* encodes a functional CLS of *C. reinhardtii*.

Expression of *CrCLS1*

To investigate whether *CrCLS1* is appropriately expressed in the Δ*crd1* mutant, we analyzed the gene expression of *CrCLS1* in the Δ*crd1* mutant harboring *CrCLS1*. The relative gene expression of *CrCLS1* was 12.6-fold higher in the Δ*crd1* mutant harboring *CrCLS1* than *CRD1* in the wild type (**Figure 3B**). Thus, *CrCLS1* is sufficiently expressed in Δ*crd1* mutant cells, which supports the functional complementation shown in **Figure 3A**.

Effect of Different Carbon Sources on the Growth of Δ*crd1* Mutant Complemented by *CrCLS1*

A previous study showed that the growth of the Δ*crd1* mutant under aerobic conditions was affected with ethanol used as the sole carbon source (Tuller et al., 1998). To investigate whether the Δ*crd1* mutant harboring *CrCLS1* rescued the growth defect under this condition, cells were grown in synthetic complete medium supplemented with 2% glucose or 2% ethanol as the sole carbon source. The growth rates of both the Δ*crd1* mutant and Δ*crd1* harboring *CrCLS1* were indistinguishable from that of wild type in 2% glucose medium (**Figure 4A**). However, with 2% ethanol medium, the Δ*crd1* mutant harboring *CrCLS1* fully restored the growth phenotype to that of the wild type, whereas the Δ*crd1* mutant showed growth retardation, as reported (Tuller et al., 1998) (**Figure 4B**). Therefore, *CrCLS1* could complement the growth defect of the Δ*crd1* mutant with ethanol supplementation as the carbon source.

Lipid Contents of the Δ*crd1* Mutant Complemented by *CrCLS1*

The phospholipid profiles of the Δ*crd1* mutant were previously analyzed by radiolabeling (Tuller et al., 1998)

```
AtPGP1     84  HGQLDSDDNSSPPPSQSSSKVLTLPTVLTLGRVAAVPLLVATFYVDSWWGTTATTSIFIA
AtPGP2     20  SLLRNRHSSPLPSPTQLSSKVITLPTVLTLGRVAAVPILVATFYVDCWWGRTATTSIFIA
CrPGP1     91  SNGASSSGSAGSSKSNGDGVVITVPTMLTLGRVAAIPVLIAAWYWQSPHSALVTTAVFAA
CrPGP2     37  ---FYRHAALVVPHKPARQPLMTIPNVLTFFRLLLVPVLLLVWELQWHYTPTLCAVIFIA
SynPgsA     1  ----------------------MNIPNWVTVSRLLALPLLFLWLPTPEAETRWWGVGIFLL
CrCLS1    103  QQDQVPSTSTASSSKPAADPVYNLPNAVSVARLVSGPLIGYWLVQGHYEAATLALAVSGA
AtCLS     121  ILTVDRNDSKEEDGGKLVKSFVNVPNMISMARLVSGPVLWWMISNEMYSSAFLGLAVSGA
ScCRD1     47  DLTRREYATNPSKTPHIKSKLLNIPNILTLSRIGCTPFIGLFIITNNLTPALGLFAFSSI

AtPGP1    144  AAITDWLDGYLARKMRLGSAFGAFLDPVADKLMVAATLILLCTK---PIQVAELGPLP--
AtPGP2     80  AAITDWLDGYIARKMRLGSEFGAFLDPVADKLMVAATLILLCTK---PMVAVVLGPVP--
CrPGP1    151  ASLTDWLDGYLARKMNSYSAFGAFLDPVADKLMVAACLILLCTR---PLAAGPAWLAGND
CrPGP2     94  ASVTDYFDGYLARKLKIATVFGAFLDPVADKIMVATALVLLAVS---PPPPWSP------
SynPgsA    40  AASTDWLDGYLARRLNQVTELGKFLDPLVDKLLVLAPLLILLTW---QVVPPWAVG----
CrCLS1    163  S---DWLDGWLARRLGASSVFGSYLDPLADKVLIGCVAAALLMN---GAMPGWVAGVVVG
AtCLS     181  S---DWLDGYVARRMKINSVVGSYLDPLADKVLIGCVAVAMVQK---DLLHPGLVGIVLL
ScCRD1    107  T---DFMDGYIARKYGLKTIAGTILDPLADKLLMITTTLALSVPSGPQIIPVSIAAIILG
```

FIGURE 7 | Multiple amino acid sequence alignment of the core motif of CDP-OH-P between CLSs and the PGPSs. Asterisks indicate the amino acid residues conserved among proteins with the CDP-OH-P motif, and dots indicate those conserved only among PGPSs. The amino acid residues present among PGPS but not among CLS are underlined. CrCLS1, *C. reinhardtii* CLS1; ScCRD1, *S. cerevisiae* CRD1; AtCLS, *A. thaliana* CLS; CrPGP1, *C. reinhardtii* PGP1; CrPGP2, *C. reinhardtii* PGP2; AtPGP1, *A. thaliana* PGP1; AtPGP2, *A. thaliana* PGP2; SynPgsA, *Synechocystis* sp. PCC 6803 PgsA.

or mass spectrometry (Zhang et al., 2003). However, whether the Δ*crd1* mutant alters the composition of major membrane phospholipid classes remained unclear. To investigate whether the complementation of the growth defect observed in **Figures 3** and **4** is associated with lipid compositional change, we analyzed the major phospholipid composition of these strains. The Δ*crd1* mutant showed an increase in PC content and decrease in PS and PI contents as compared with the wild type (**Figure 5A**). In the Δ*crd1* mutant harboring *CrCLS1*, phospholipid composition was restored to a level similar to that of the wild type. The fatty acid composition of PE, PC, and PI was similar among the three strains (**Figure 5B**). Thus, *CrCLS1* encodes a functional CLS that complements lipid compositional changes in the Δ*crd1* mutant.

Enzyme Activity of *CrCLS1* Expressed in the Δ*crd1*

To investigate whether *CrCLS1* encodes a functional CLS to restore the CL synthesis defect in the Δ*crd1*, we performed radiolabeling assay to analyze CLS activity. As shown in **Figure 6**, the Δ*crd1* mutant harboring *CrCLS1* recovered radiolabeled spot that co-migrates with the commercial standard of CL, which is present in wild type but absent in the Δ*crd1* mutant, demonstrating that the activity of CLS was recovered in the mutant harboring *CrCLS1*. Thus, *CrCLS1* encodes a functional CLS that complements CL synthesis defect of Δ*crd1* mutant.

DISCUSSION

Present study reported identification of a *CLS* gene in *C. reinhardtii*, *CrCLS1*, and examined its *in vivo* function by heterologous complementation of *pgsA*, a PGPS mutant of *Synechocystis* sp. PCC 6803, and Δ*crd1*, a CLS mutant of *S. cerevisiae*. Whereas *CrCLS1* did not complement the growth phenotype of *pgsA*, it rescued the temperature-sensitive growth phenotype, growth profile with different carbon sources, phospholipid composition and enzyme activity of Δ*crd1* of *S. cerevisiae*. These results suggest that *CrCLS1* is a functional gene for CLS of *C. reinhardtii* as the first identified algal CLS, which is functionally incompatible with PGPS despite their sequence homology.

Physiological roles of CrCLS1 in *C. reinhardtii* are not reported yet; however, several transcriptomic studies have shown gene expression profiles in response to environmental stresses. For example, expression of *CrCLS1* is down-regulated in response to the deprivation of iron (Urzica et al., 2013) and nitrogen (Goodenough et al., 2014). Conversely, an upregulation is seen by copper deficiency (Castruita et al., 2011) and singlet oxygen stress (Wakao et al., 2014). These data suggest possible roles of CrCLS1 in adaptation to circumvent environmental stresses.

Given that both PGPS and CLS belong to the CDP-alcohol phosphotransferase family and the relevant CDP-OH-P motifs are closely related (Katayama et al., 2004), what defines substrate specificity of these enzymes?

Recently, structural basis for catalysis in a CDP-alcohol phosphotransferase was revealed by crystallographic analysis (Sciara et al., 2014). According to this structure, conserved amino acid residues in the CDP-OH-P motif are associated with CDP-DAG. Since CDP-DAG is the common substrate between CLS and PGPS, this study suggests that an additional motif recognizes the other substrate (PG for CLS; glycerol 3-phosphate for PGPS). We aligned the amino acid sequences of core CDP-OH-P motif among three CLSs (*C. reinhardtii* cardiolipin synthase 1, CrCLS1; *S. cerevisiae* CRD1, ScCRD1; *A. thaliana* CLS, AtCLS) and five PGPSs (*C. reinhardtii* PGP1, CrPGP1; *C. reinhardtii* PGP2, CrPGP2; *A. thaliana* PGP1, AtPGP1; *A. thaliana* PGP2, AtPGP2; *Synechocystis* sp. PCC 6803 PgsA, SynPgsA) (**Figure 7**). While the eight amino acid residues of the core CDP-OH-P motif $D(X)_2DG(X)_2AR(X)_{8-9}G(X)_3D(X)_3D$ indicated by asterisks in **Figure 7** were conserved between the PGPS and CLS, we noted that seven amino acids (FxxAxxT) immediately before the core CDP-OH-P motif were highly conserved among PGPSs but not CLSs (underlined in **Figure 7**). In addition, we found additional four amino acid residues that were conserved among PGPS but not in CLS (indicated by dots in **Figure 7**). It is possible that these additional residues may define the substrate specificity between PGPS and CLS. Detailed structural analysis as well as enzymatic characterization of these residues are anticipated to experimentally validate this proposal.

CONCLUSION

We suggest functional specificity of CLS by the identification and characterization of a CLS, CrCLS1, in *C. reinhardtii*.

AUTHOR CONTRIBUTIONS

KK, HW, and YN conceived research. KK and C-HH performed experiments and analyzed data. All authors wrote and commented on the manuscript and approved the contents.

ACKNOWLEDGMENTS

We thank Masahiro Ikeuchi (the University of Tokyo, Tokyo, Japan) for the supply of pTCP2031V. This research was supported by CREST (to HW) and PRESTO (to YN), Japan Science and Technology Agency, and the core budget of Institute of Plant and Microbial Biology, Academia Sinica (to YN).

SUPPLEMENTARY MATERIAL

The Supplementary Material for this article can be found online at: http://journal.frontiersin.org/article/10.3389/fmicb.2015.01542

REFERENCES

Acehan, D., Malhotra, A., Xu, Y., Ren, M., Stokes, D. L., and Schlame, M. (2011). Cardiolipin affects the supramolecular organization of ATP synthase in mitochondria. *Biophys. J.* 100, 2184–2192. doi: 10.1016/j.bpj.2011.03.031

Babiychuk, E., Muller, F., Eubel, H., Braun, H. P., Frentzen, M., and Kushnir, S. (2003). *Arabidopsis* phosphatidylglycerophosphate synthase 1 is essential for chloroplast differentiation, but is dispensable for mitochondrial function. *Plant J.* 33, 899–909. doi: 10.1046/j.1365-313X.2003.01680.x

Bligh, E. G., and Dyer, W. J. (1959). A rapid method of total lipid extraction and purification. *Can. J. Biochem. Physiol.* 37, 911–917. doi: 10.1139/o59-099

Castruita, M., Casero, D., Karpowicz, S. J., Kropat, J., Vieler, A., Hsieh, S. I., et al. (2011). Systems biology approach in *Chlamydomonas reveals* connections between copper nutrition and multiple metabolic steps. *Plant Cell* 23, 1273–1292. doi: 10.1105/tpc.111.084400

Chen, D., Zhang, X. Y., and Shi, Y. (2006). Identification and functional characterization of hCLS1, a human cardiolipin synthase localized in mitochondria. *Biochem. J.* 398, 169–176. doi: 10.1042/BJ20060303

Claros, M. G., and Vincens, P. (1996). Computational method to predict mitochondrially imported proteins and their targeting sequences. *Eur. J. Biochem.* 241, 779–786. doi: 10.1111/j.1432-1033.1996.00779.x

Goodenough, U., Blaby, I., Casero, D., Gallaher, S. D., Goodson, C., Johnson, S., et al. (2014). The path to triacylglyceride obesity in the sta6 strain of *Chlamydomonas reinhardtii*. *Eukaryot. Cell* 13, 591–613. doi: 10.1128/EC.00013-14

Hagio, M., Gombos, Z., Varkonyi, Z., Masamoto, K., Sato, N., Tsuzuki, M., et al. (2000). Direct evidence for requirement of phosphatidylglycerol in photosystem II of photosynthesis. *Plant Physiol.* 124, 795–804. doi: 10.1104/pp.124.2.795

Hagio, M., Sakurai, I., Sato, S., Kato, T., Tabata, S., and Wada, H. (2002). Phosphatidylglycerol is essential for the development of thylakoid membranes in *Arabidopsis thaliana*. *Plant Cell Physiol.* 43, 1456–1464. doi: 10.1093/pcp/pcf185

Haselier, A., Akbari, H., Weth, A., Baumgartner, W., and Frentzen, M. (2010). Two closely related genes of *Arabidopsis* encode plastidial cytidinediphosphate diacylglycerol synthases essential for photoautotrophic growth. *Plant Physiol.* 153, 1372–1384. doi: 10.1104/pp.110.156422

Houtkooper, R. H., Akbari, H., van Lenthe, H., Kulik, W., Wanders, R. J., Frentzen, M., et al. (2006). Identification and characterization of human cardiolipin synthase. *FEBS Lett.* 580, 3059–3064. doi: 10.1016/j.febslet.2006.04.054

Hung, C. H., Endo, K., Kobayashi, K., Nakamura, Y., and Wada, H. (2015a). Characterization of *Chlamydomonas reinhardtii* phosphatidylglycerophosphate synthase in *Synechocystis* sp. PCC 6803. *Front. Microbiol.* 6:842. doi: 10.3389/fmicb.2015.00842

Hung, C. H., Kobayashi, K., Wada, H., and Nakamura, Y. (2015b). Isolation and characterization of a phosphatidylglycerophosphate phosphatase1. PGPP1, in *Chlamydomonas reinhardtii*. *Plant Physiol. Biochem.* 92, 56–61. doi: 10.1016/j.plaphy.2015.04.002

Hung, C. H., Ho, M. Y., Kanehara, K., and Nakamura, Y. (2013). Functional study of diacylglycerol acyltransferase type 2 family in *Chlamydomonas reinhardtii*. *FEBS Lett.* 587, 2364–2370. doi: 10.1016/j.febslet.2013.06.002

Jiang, F., Gu, Z., Granger, J. M., and Greenberg, M. L. (1999). *Cardiolipin synthase* expression is essential for growth at elevated temperature and is regulated by factors affecting mitochondrial development. *Mol. Microbiol.* 31, 373–379. doi: 10.1046/j.1365-2958.1999.01181.x

Jiang, F., Rizavi, H. S., and Greenberg, M. L. (1997). Cardiolipin is not essential for the growth of *Saccharomyces cerevisiae* on fermentable or non-fermentable carbon sources. *Mol. Microbiol.* 26, 481–491. doi: 10.1046/j.1365-2958.1997.5841950.x

Kadenbach, B., Mende, P., Kolbe, H. V., Stipani, I., and Palmieri, F. (1982). The mitochondrial phosphate carrier has an essential requirement for cardiolipin. *FEBS Lett.* 139, 109–112. doi: 10.1016/0014-5793(82)80498-5

Katayama, K., Sakurai, I., and Wada, H. (2004). Identification of an *Arabidopsis thaliana* gene for cardiolipin synthase located in mitochondria. *FEBS Lett.* 577, 193–198. doi: 10.1016/j.febslet.2004.10.009

Lewis, R. N., and McElhaney, R. N. (2009). The physicochemical properties of cardiolipin bilayers and cardiolipin-containing lipid membranes. *Biochim. Biophys. Acta* 1788, 2069–2079. doi: 10.1016/j.bbamem.2009.03.014

Li-Beisson, Y., Beisson, F., and Riekhof, W. (2015). Metabolism of acyl-lipids in *Chlamydomonas reinhardtii*. *Plant J.* 82, 504–522. doi: 10.1111/tpj.12787

Li-Beisson, Y., Shorrosh, B., Beisson, F., Andersson, M. X., Arondel, V., Bates, P. D., et al. (2013). Acyl-lipid metabolism. *Arabidopsis Book* 11:e0161. doi: 10.1199/tab.0161

Muller, F., and Frentzen, M. (2001). Phosphatidylglycerophosphate synthases from *Arabidopsis thaliana*. *FEBS Lett.* 509, 298–302. doi: 10.1016/S0014-5793(01)03163-5

Nakamura, Y., Arimitsu, H., Yamaryo, Y., Awai, K., Masuda, T., Shimada, H., et al. (2003). Digalactosyldiacylglycerol is a major glycolipid in floral organs of *Petunia hybrida*. *Lipids* 38, 1107–1112. doi: 10.1007/s11745-006-1166-x

Osman, C., Haag, M., Wieland, F. T., Brugger, B., and Langer, T. (2010). A mitochondrial phosphatase required for cardiolipin biosynthesis: the PGP phosphatase Gep4. *EMBO J.* 29, 1976–1987. doi: 10.1038/emboj.2010.98

Pineau, B., Bourge, M., Marion, J., Mauve, C., Gilard, F., Maneta-Peyret, L., et al. (2013). The importance of cardiolipin synthase for mitochondrial ultrastructure, respiratory function, plant development, and stress responses in *Arabidopsis. Plant Cell* 25, 4195–4208. doi: 10.1105/tpc.113.118018

Sato, N., Hagio, M., Wada, H., and Tsuzuki, M. (2000). Requirement of phosphatidylglycerol for photosynthetic function in thylakoid membranes. *Proc. Natl. Acad. Sci. U.S.A.* 97, 10655–10660. doi: 10.1073/pnas.97.19.10655

Satoh, S., Ikeuchi, M., Mimuro, M., and Tanaka, A. (2001). Chlorophyll b expressed in Cyanobacteria functions as a light-harvesting antenna in photosystem I through flexibility of the proteins. *J. Biol. Chem.* 276, 4293–4297. doi: 10.1074/jbc.M008238200

Sciara, G., Clarke, O. B., Tomasek, D., Kloss, B., Tabuso, S., Byfield, R., et al. (2014). Structural basis for catalysis in a CDP-alcohol phosphotransferase. *Nat. Commun.* 5:4068. doi: 10.1038/ncomms5068

Tuller, G., Hrastnik, C., Achleitner, G., Schiefthaler, U., Klein, F., and Daum, G. (1998). YDL142c encodes cardiolipin synthase (Cls1p) and is non-essential for aerobic growth of *Saccharomyces cerevisiae*. *FEBS Lett.* 421, 15–18. doi: 10.1016/S0014-5793(97)01525-1

Urzica, E. I., Vieler, A., Hong-Hermesdorf, A., Page, M. D., Casero, D., Gallaher, S. D., et al. (2013). Remodeling of membrane lipids in iron-starved *Chlamydomonas*. *J. Biol. Chem.* 288, 30246–30258. doi: 10.1074/jbc.M113.490425

Wakao, S., Chin, B. L., Ledford, H. K., Dent, R. M., Casero, D., Pellegrini, M., et al. (2014). Phosphoprotein SAK1 is a regulator of acclimation to singlet oxygen in *Chlamydomonas reinhardtii*. *Elife* 3:e02286. doi: 10.7554/eLife.02286

Wu, F., Yang, Z., and Kuang, T. (2006). Impaired photosynthesis in phosphatidylglycerol-deficient mutant of cyanobacterium Anabaena sp. PCC7120 with a disrupted gene encoding a putative phosphatidylglyce rophosphatase. *Plant Physiol.* 141, 1274–1283. doi: 10.1104/.pp106.083451

Xu, C., Hartel, H., Wada, H., Hagio, M., Yu, B., Eakin, C., et al. (2002). The pgp1 mutant locus of *Arabidopsis* encodes a phosphatidylglycerolphosphate synthase with impaired activity. *Plant Physiol.* 129, 594–604. doi: 10.1104/pp.002725

Yu, B., and Benning, C. (2003). Anionic lipids are required for chloroplast structure and function in *Arabidopsis*. *Plant J.* 36, 762–770. doi: 10.1046/j.1365-313X.2003.01918.x

Zhang, M., Su, X., Mileykovskaya, E., Amoscato, A. A., and Dowhan, W. (2003). Cardiolipin is not required to maintain mitochondrial DNA stability or cell viability for *Saccharomyces cerevisiae* grown at elevated temperatures. *J. Biol. Chem.* 278, 35204–35210. doi: 10.1074/jbc.M306729200

Zhou, Y., Peisker, H., Weth, A., Baumgartner, W., Dormann, P., and Frentzen, M. (2013). Extraplastidial cytidinediphosphate diacylglycerol synthase activity is required for vegetative development in *Arabidopsis thaliana*. *Plant J.* 75, 867–879. doi: 10.1111/tpj.12248

Conflict of Interest Statement: The authors declare that the research was conducted in the absence of any commercial or financial relationships that could be construed as a potential conflict of interest.

frontiers in Microbiology

ORIGINAL RESEARCH
published: 24 December 2015
doi: 10.3389/fmicb.2015.01484

Metabolic Engineering and Comparative Performance Studies of *Synechocystis* sp. PCC 6803 Strains for Effective Utilization of Xylose

*Saurabh Ranade[1], Yan Zhang[2], Mecit Kaplan[1], Waqar Majeed[3] and Qingfang He[1]**

[1] Department of Biology, University of Arkansas at Little Rock, Little Rock, AR, USA, [2] Biotechnology Research Center, Shandong Academy of Agricultural Sciences, Jinan, China, [3] Center for Integrative Nanotechnology Sciences, University of Arkansas at Little Rock, Little Rock, AR, USA

Wood sugars such as xylose can be used as an inexpensive carbon source for biotechnological applications. The model cyanobacterium *Synechocystis* sp. PCC 6803 lacks the ability to catabolize wood sugars as an energy source. Here, we generated four *Synechocystis* strains that heterologously expressed XylAB enzymes, which mediate xylose catabolism, either in combination with or without one of three xylose transporters, namely XylE, GalP, or Glf. Except for *glf*, which is derived from the bacterium *Zymomonas mobilis* ZM4, the heterologous genes were sourced from *Escherichia coli* K-12. All of the recombinant strains were able to utilize xylose in the absence of catabolite repression. When xylose was the lone source of organic carbon, strains possessing the XylE and Glf transporters were most efficient in terms of dry biomass production and xylose consumption and the strain lacking a heterologous transporter was the least efficient. However, in the presence of a xylose-glucose mixed sugar source, the strains exhibited similar levels of growth and xylose consumption. This study demonstrates that various bacterial xylose transporters can boost xylose catabolism in transgenic *Synechocystis* strains, and paves the way for the sustainable production of bio-compounds and green fuels from lignocellulosic biomass.

Keywords: cyanobacteria, metabolic engineering, mixotrophy, LAHG, *Synechocystis*, xylose transporter

OPEN ACCESS

Edited by:
Takashi Osanai,
Meiji University, Japan

Reviewed by:
Weiwen Zhang,
Tianjin University, China
Wendy Schluchter,
University of New Orleans, USA

****Correspondence:***
Qingfang He
qfhe@ualr.edu

Specialty section:
This article was submitted to Microbiotechnology, Ecotoxicology and Bioremediation, a section of the journal Frontiers in Microbiology

Received: *10 November 2015*
Accepted: *09 December 2015*
Published: *24 December 2015*

Citation:
Ranade S, Zhang Y, Kaplan M, Majeed W and He Q (2015) Metabolic Engineering and Comparative Performance Studies of Synechocystis sp. PCC 6803 Strains for Effective Utilization of Xylose. Front. Microbiol. 6:1484. doi: 10.3389/fmicb.2015.01484

INTRODUCTION

Lignocellulosic material is an abundant, inexpensive, and renewable source of carbon with potential industrial applications (Ragauskas et al., 2006). Large quantities of lignocellulosic biomass are generated in agricultural, forestry, and related industries each year. This residual biomass can be used to synthesize a number of value-added products (Pothiraj et al., 2006), especially energy-rich compounds that can be used as biofuels (Ragauskas et al., 2006; Lee and Lavoie, 2013; Anwar et al., 2014). Lignocellulose is typically composed of cellulose (40–50%), hemicellulose (20–30%), and lignin (10–15%) macromolecules bound together by hydrogen and covalent bonds (Malherbe and Cloete, 2002; Kumar et al., 2009). Hydrolysis of lignocellulose yields xylose, which is the second most abundant sugar in the biosphere after glucose. Xylose accounts for up to 35% of the total dry weight (DW) of plant materials (Girio et al., 2010). Catabolism of D-xylose begins with its transport into the cell by means of specific transporter proteins. Once inside the cell, xylose is isomerized by

D-xylose isomerase (XylA) to yield D-xylulose, which in turn is irreversibly phosphorylated by the action of xylulokinase (XylB) to yield D-xylulose 5-phosphate, a pentose phosphate pathway (PPP) intermediate (**Figure 1**) (Doelle, 1975).

Few microorganisms are able to catabolize pentose sugars (Jojima et al., 2010). Even in pentose utilizing microorganisms, factors that impair pentose catabolism exist, such as catabolite repression (Vinuselvi et al., 2012), cellular redox imbalance, and insufficient transporter activities (Matsushika et al., 2009). Hence, effective utilization of pentose sugars by microorganisms requires the expression of heterologous genes (Jojima et al., 2010).

Although primarily photoautotrophic, a number of cyanobacteria can utilize organic carbon compounds (Eiler, 2006). In large-scale cyanobacterial cultures, mixotrophic growth conditions increase biomass production, whereas light and CO_2 limit cyanobacterial growth and biosynthesis (Yao et al., 2014). Their unicellular nature, ability to photosynthesize and fix carbon dioxide, and amenability to genetic modification make cyanobacteria promising host organisms for biotechnological applications (Lu, 2010).

Several groups have introduced heterologous xylose transporter and/or metabolic genes into bacterial strains either to impart or improve the ability to transport and/or catabolize xylose. In an early study, the xylose catabolic genes *xylAB* and PPP genes *talB-tktA* from *Escherichia coli* were successfully expressed with the help of the GAP and ENO promoters, respectively, in *Zymomonas mobilis* CP4 to obtain a co-fermenting strain (Zhang et al., 1995). Similarly, the *E. coli xylAB* genes were successfully expressed under the *trc* promoter in the bacterium *Corynebacterium glutamicum* R to generate a diauxically growing strain (Kawaguchi et al., 2006), and also under the *tac* promoter in *Pseudomonas putida* S12. A laboratory evolution approach was used to generate a *P. putida* S12 strain with an increased biomass yield. The strain, however, failed to overcome diauxic growth. Introduction of the transporter genes *xylFGH* under the *tac* promoter failed to improve xylose metabolism, indicating that transport was not the limiting factor (Meijnen et al., 2008). *xylAB* genes from *Streptomyces lividans* TK23, when expressed under the *tac* promoter in the actinobacteria *Rhodococcus opacus* PD630 and *Rhodococcus jostii* RHA1, yielded efficient co-fermenting strains (Xiong et al., 2012). Heterologous expression of the Glf transporter from *Z. mobilis* CP4, which had been modified by error-prone PCR and random deletion/ligation, improved xylose transport in *E. coli* BL21 (Ren et al., 2009). One of the first reported attempts to engineer a cyanobacterium that could metabolize xylose involved

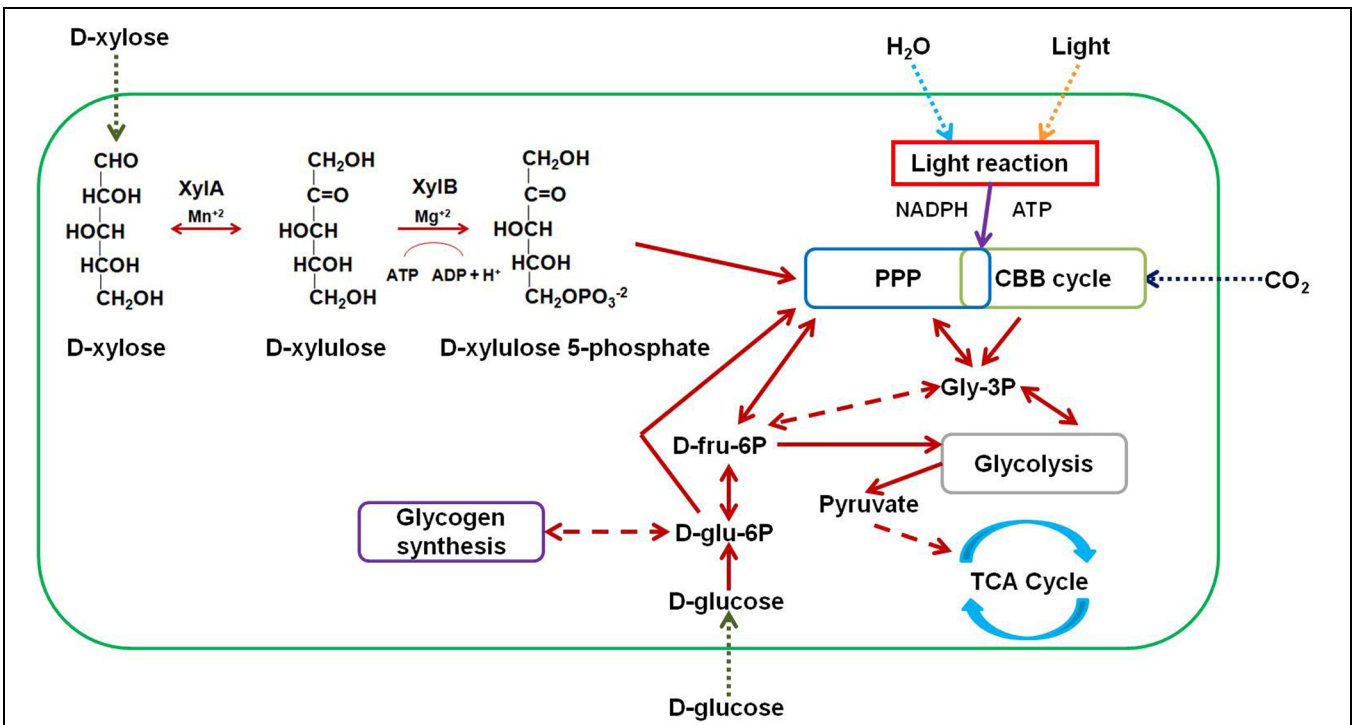

FIGURE 1 | Metabolic scheme for engineering *Synechocystis* strains. D-xylose enters the transformant strains by means of native and heterologous transporters. Direction of entry of sugars, water, inorganic carbon (CO_2), and light into the cell is shown as dotted arrows. D-xylose is converted to D-xylulose by D-xylose isomerase (XylA) in the presence of manganese ions (Mn^{+2}). D-xylulose is further converted to D-xylulose 5-phosphate by the action of D-xylulokinase (XylB) in the presence of magnesium ions (Mg^{+2}). D-xylulose 5-phosphate then enters the PPP. Bidirectional arrows indicate a reversible reaction or ability of an intermediate to enter and exit a pathway. Unidirectional arrows indicate a non-reversible reaction or the ability of an intermediate to either enter or exit a pathway. Dashed arrows indicate the involvement of one or more intermediates. Other abbreviations: CBB cycle, Calvin–Benson–Bassham cycle; ATP, adenosine triphosphate; NADPH, nicotinamide adenine dinucleotide phosphate; Gly-3P, glyceraldehyde 3-phosphate; D-fru-6P, D-fructose 6-phosphate; D-glu-6P, D-glucose 6-phosphate; TCA cycle, tricarboxylic acid cycle.

Synechococcus elongatus PCC 7942. The wild-type strain appears to catabolize xylose slowly. Expression of the *E. coli xylE* transporter gene under the control of the *trc* promoter impaired growth due to the intracellular accumulation of xylose. However, introduction of the *xylEAB* operon from the same source organism under the control of the *trc* promoter doubled growth in the presence of xylose (McEwen et al., 2013). In another study, expression of the *E. coli xylAB* genes under the *psbA* promoter increased the rate of ethylene production in the presence of xylose. Furthermore, expression of the *E. coli xylAB* genes in a glycogen synthase mutant enhanced the synthesis of keto acids. Introduction of the *E. coli* XylFGH transporter enhanced xylose utilization only at concentrations of above 10 mM (Lee et al., 2015). In addition to bacteria, several yeast strains have been engineered for effective catabolism of xylose, with strategies ranging from expression of heterologous transporter-catabolic genes from bacteria and other fungi, to random mutagenesis-evolutionary engineering of the recombinant strains (Young et al., 2010).

In this study, we compared the biomass yield and xylose uptake of four recombinant *Synechocystis* sp. PCC 6803 (hereafter *Synechocystis*) strains heterologously expressing xylose-specific catabolic genes *xylAB* without or with one of three known xylose transporters (XylE, GalP, Glf). XylE (proton symporter), GalP (proton symporter), and Glf (uniporter) are members of the Major Facilitator Superfamily (hereafter MFS) class of transporter proteins (Jojima et al., 2010). The *glf* transporter gene is native to *Z. mobilis* ZM4, whereas the other heterologous genes used in this study were sourced from *E. coli* K-12. Here we report the production of recombinant *Synechocystis* strains with various abilities to utilize xylose in the absence of catabolite repression. We show that the ability of *Synechocystis* to utilize organic carbon sources can be enhanced by the heterologous expression of efficient transporters.

MATERIALS AND METHODS

Bacterial Strains and Growth Conditions

Escherichia coli strain K-12 was used as a source organism for the amplification of xylose-specific transporter and catabolic genes. *E. coli* XL1-Blue (Stratagene) and TOP10 (Thermo Fisher Scientific) were used for DNA cloning and plasmid construction. The strains were grown at 37°C on solid LB medium or in liquid LB medium with shaking (220 rpm) in the presence of an appropriate antibiotic, if needed. Antibiotic concentrations used for selection were as follows: ampicillin (Fisher Scientific), 100 μg/ml for liquid and solid media; kanamycin (Fisher Scientific), 25 μg/ml for liquid and solid media; and spectinomycin (Fisher Scientific), 25 μg/ml for liquid medium and 50 μg/ml for solid medium.

Zymomonas mobilis ZM4 was used as a source organism for amplification of xylose transporter-specific gene. The strain was grown at 28°C on solid YP medium or in liquid YP medium (1% yeast extract, 2% Bacto-peptone) with shaking (220 rpm).

Plasmid Construction

To construct the plasmids designed to insert xylose transporter genes into *Synechocystis* sp. PCC 6803, the kanamycin resistance cassette was spliced out from plasmid pUC4K (Vieira and Messing, 1982) using *Bam*HI and inserted into pBluescript II SK+ (Stratagene) digested with *Bam*HI. The neutral site sequence (near *slr1285*; hereafter referred to as neutral site 1) (Xue et al., 2014b) was amplified from genomic DNA isolated from *Synechocystis* as upstream and downstream regions using the following primers:

5′-ACTCGGTACCGGCAATGCAATTAATTAAAAATGG-3′ (forward primer) and 5′-ACTCCTCGAGTCTATTGTTGGAAGGTTGCTG-3′ (reverse primer) for the upstream region; and 5′-ACTCACTAGTGTGAAAAAATATTGACATTAAGATATC-3′ (forward primer) and 5′-ACTCCCGCGGGGAACCAGATTTTTAGGATG-3′ (reverse primer) for the downstream region. The upstream and downstream fragments were inserted between the *Kpn*I-*Xho*I sites and *Spe*I-*Sac*II sites of the modified pBluescript SK+ plasmid, respectively. Next, a ∼0.4-kb region encompassing the *psbA2* promoter (hereafter *psbA2* promoter) was amplified from *Synechocystis* genomic DNA using the following primers:

5′-ACTCGTCGACGGTATATGGATCATAATTGTATGC-3′ (forward primer) and 5′-ACTCGAATTCTTGGTTATAATTCCTTATGTATTTGTC-3′ (reverse primer). The amplified fragment was inserted between the *Sal*I-*Eco*RI sites of the plasmid. Then, the ∼0.5-kb 5ST1T2 double terminator region was amplified from the pBTac-1 plasmid (Boehringer Mannheim) using the following primers:

5′-ACTCCTGCAGCCAAGCTTGGCTGTTTTGG-3′ (forward primer) and 5′-ACTCGGATCCATTGAAGCATTTATCAGGGTTATTG-3′ (reverse primer). The fragment was inserted between the *Pst*I-*Bam*HI sites of the modified pBluescript II SK+ plasmid. Finally, the xylose transporter genes, *xylE*, *galP,* and *glf,* were amplified from genomic DNA isolated from *E. coli* K-12 (*xylE*, *galP)* or the *Z. mobilis* ZM4 strain (*glf)*. The primers used to amplify the transporter genes were as follows:

5′-ACTCGAATTCATGAATACCCAGTATAATTC-3′ (forward primer) and 5′-ACTCCTGCAGTTACAGCGTAGCAG-3′ (reverse primer) for *xylE*; 5′-ACTCGAATTCATGCCTGACGCTAA-3′ (forward primer) and 5′-ACTCCTGCAGTTAATCGTGAGCG-3′ (reverse primer) for *galP*; and 5′-ACTCGAATTCATGAGTTCTGAAAGTAGT-3′ (forward primer) and 5′-ACTCCTGCAGCTACTTCTGGGAG-3′ (reverse primer) for *glf*.

The amplicons were inserted between the *Eco*RI-*Pst*I sites of the plasmid to generate three individual plasmids.

To construct the plasmid designed to insert xylose catabolic genes, the spectinomycin resistance cassette was spliced from plasmid pHP45Ω (Prentki and Krisch, 1984) using *Bam*HI and inserted into the pBluescript II SK+ plasmid at the *Bam*HI site. The neutral site sequence (*slr0168*; hereafter called neutral site 2) (Kunert et al., 2000) was amplified from *Synechocystis* genomic DNA as upstream and downstream regions using the following primers:

5′-ACTCGGTACCATGACTATTCAATACACCC-3′ (forward primer) and 5′-ACTCGTCGACCACCTGCACCAGACCA-3′ (reverse primer) for the upstream region; and 5′-ACTCACTAGTTTGGGGCTGGCGGATT-3′ (forward primer) and 5′-ACT

CCCGCGGCTAAGTCAGCGTAAATCTG-3′ (reverse primer) for the downstream region. The upstream and downstream fragments were inserted between the *Kpn*I-*Sal*I sites and *Spe*I-*Sac*II sites of the plasmid, respectively. The *psbA2* promoter and 5ST1T2 double terminator were amplified and cloned into the plasmid as described above. In the last step, the xylose catabolic genes *xylAB* were amplified from genomic DNA isolated from the *E. coli* K-12 strain using the following primers:

5′-ACTCGAATTCATGCAAGCCTATTTTGACCA-3′ (forward primer) and 5′-ACTCCCTGCAGGTTACGCCATTA ATGG-3′ (reverse primer). The *xylAB* amplicon was inserted between the *Eco*RI-*Pst*I sites of the plasmid.

Note that, in the case of *xylAB*, only the region from the start codon of *xylA* to the end codon of *xylB* was amplified from the source organism; no other regulatory elements from the *xylAB* operon were included.

Synechocystis Culture Conditions, Transformation, and Segregation

Synechocystis strains were grown on solid or in liquid BG-11 medium at 30°C under 50 μE $m^{-2}s^{-1}$ light intensity with shaking (200 rpm). When OD_{730} reached ∼0.8, transformations were carried out as described (Xue et al., 2014a). Once the presence of the heterologous insert was confirmed by PCR analysis, cells were streaked on BG-11 plates containing successively higher antibiotic concentrations followed by PCR tests to ensure complete segregation of the transformants.

Reverse Transcription PCR

Total RNA was isolated from 80-ml cultures of *Synechocystis* strains possessing the *xylAB* genes at OD_{730} ∼0.7, as previously described (Mohamed and Jansson, 1989). A Turbo DNA-Free Kit (Thermo Fisher Scientific) was used to remove contaminating genomic DNA. The reverse transcription reactions were carried out using Superscript III enzyme (Thermo Fisher Scientific) and random primers (New England BioLabs). The cDNA molecules thus synthesized were then used as templates for PCR, employing the same set of primers used to amplify the heterologous transporter-catabolic genes. The same primer sets were employed to check the negative controls, in which DNase-treated RNA molecules were used as templates. *petA* (*sll1317*), which was used as a positive control, was amplified using the following primers:

5′-ACTCGAATTCATGAGAAACCCTGATACTTTGGGGCT GTGGACGAAAAC-3′ (forward primer) and 5′-ACTCCTGCAG CTAGAAATTAAGTTCGGCAGCTTGAACTTTTTCAATCTG-3′ (reverse primer). For a longer template, i.e., the *xylAB* genes, the SuperScript One-Step RT-PCR system for long templates (Thermo Fisher Scientific) was used as per manufacturer's instructions. PCR products were analyzed on a 0.8% agarose gel.

Cell Extract Preparation, SDS-PAGE, and Immunoblot Analysis

Synechocystis strains (wild-type and strains possessing the *xylAB* genes) were grown under the conditions described above, until OD_{730} reached 0.6–0.8. Whole cell extracts were obtained and 20 μg protein samples were electrophoresed as described (Xue et al., 2014a). After electrophoresis, gels were blotted onto nitrocellulose membranes using the Trans-Blot System (Bio-Rad). Membranes were probed with XylA- and XylB-specific primary antibodies of rabbit origin (raised by Dr. Qiang Wang) and goat anti-rabbit alkaline phosphatase-conjugated secondary antibodies (Sigma–Aldrich). Antigen-antibody interactions were visualized using the BCIP/NBT Kit (Thermo Fisher Scientific).

Demonstration of ^{14}C-Labelled D-Xylose Uptake

Synechocystis strains (wild-type and strains harboring the *xylAB* genes) were grown as described above, until the OD_{730} reached ∼0.8. Then, 10 ml of the cells were washed thrice with BG-11 medium and OD_{730} was adjusted to 0.6. Next, 1 ml of the cultures was grown in the presence of 400 nM ^{14}C-labelled xylose [D-(1-^{14}C)] (American Radiolabeled Chemicals) in 10 ml snap-capped glass tubes under similar growth conditions for 1 h. Nine milliliters of BG-11 medium was added to the cultures and they were filtered through a 0.45 μm pore-size nitrocellulose membrane (Bio-Rad). The membranes were washed thrice with 10 ml BG-11 medium, air dried, and suspended in 10 ml scintillation fluid (PerkinElmer) for 24 h. Radioactivity was measured using an LS 6500 scintillation counter (Beckman).

Biomass Measurement

Synechocystis biomass was measured in terms of DW as previously described (Davies et al., 2014). Cultures of *Synechocystis* strains were initiated in 100 ml BG-11 liquid medium at 30°C with shaking (200 rpm) and an initial OD_{730} of 0.05. The cultures were provided with: for autotrophic growth, 50 μE m^{-2} s^{-1} light; for mixotrophic growth, 5 mM (750 mg/L) xylose and/or 5 mM glucose (900.8 mg/L) along with 50 μE m^{-2} s^{-1} light; for light-activated heterotrophic growth (hereafter LAHG) conditions (Anderson and McIntosh, 1991), 5 mM xylose (750 mg/L) and/or 5 mM glucose (900.8 mg/L) along with 50 μE m^{-2} s^{-1} light for 10 min per day; and for dark growth, neither sugar nor light. For the dark and LAHG cultures, biomass measurements were made every 24 h for 7 days, while for autotrophic and mixotrophic cultures, biomass values were estimated every 6 h for 3 days.

Enzymatic Assays for Measurement of Sugar Uptake

Enzymatic uptake assays were performed for cultures grown in the presence of 5 mM xylose and 5 mM each of xylose and glucose. One milliliter of culture, collected at the time points specified for biomass measurements, was immediately filtered using 0.45 μm pore-size nylon membrane syringe filters (Fisher Scientific) to obtain cell-free media.

The amount of xylose present in the filtered medium fractions was measured using a D-Xylose Assay Kit (Megazyme) as per manufacturer's instructions. The sequential action of xylose mutarotase and β-xylose dehydrogenase generates NADH molecules. The amount of NADH is stoichiometric with that of D-xylose and is calculated from the difference in OD_{340} values before and after β-xylose dehydrogenase action.

The amount of glucose present in the filtered medium fractions was measured using the D-Glucose Assay Kit-GOPOD Format (Megazyme) as per manufacturer's instructions. Sequential action of glucose oxidase and peroxidase generates quinoneimine. The amount of dye formed is stoichiometric with that of D-glucose and was calculated from OD_{510} values obtained for the samples relative to the OD_{510} value obtained for a standard.

Data obtained from the biomass measurements and the enzymatic assays were used to calculate the sugar uptake rates by the *Synechocystis* strains during each time interval, using a previously described mathematical formula (Munyon and Merchant, 1959).

RESULTS

Construction of *Synechocystis* Strains Possessing Heterologous Xylose-Specific Genes

Synechocystis strains possessing xylose transporter and catabolic genes were developed from a *Synechocystis* sp. PCC 6803 wild-type strain (hereafter WT). The construction process involved two rounds of transformation. In the first round, one of the three xylose transporter genes, *xylE* or *galP* from *E. coli* K-12 or *glf* from *Z. mobilis* ZM4, was introduced into neutral site 1 (Xue et al., 2014b) in WT *Synechocystis* via homologous recombination to generate three individual strains, X-Tr1, X-Tr2, and X-Tr3, respectively (**Table 1**). The plasmid constructs designed for integration of the transporter genes included the *psbA2* promoter of *Synechocystis* origin, 5ST1T2 double terminator of *E. coli* origin, kanamycin resistance cassette, neutral site 1 divided into ∼600 bp upstream and ∼600 bp downstream regions, and one of the three aforementioned transporter genes (**Figure 2A**).

In the second round of transformation, the *xylAB* genes, which are responsible for funneling xylose into the PPP, were introduced into neutral site 2 (Kunert et al., 2000) in the three *Synechocystis* strains generated in the first round of transformation as well as in the WT strain via homologous recombination to obtain four resultant strains, X-Ut1, X-Ut2, X-Ut3, and X-Ut4 (**Table 1**). The plasmid construct designed to integrate the xylose catabolic genes included the same promoter and transcriptional terminator as used in the transporter gene-specific plasmid constructs, the spectinomycin resistance cassette, neutral site 2 divided into ∼970 bp upstream and ∼970 bp downstream regions, and *xylAB* genes (**Figure 2B**). The *xylAB* genes consist of two individual genes, *xylA* (encoding D-xylose isomerase) and *xylB* (encoding D-xylulokinase), along with the ribosomal binding site (hereafter RBS) present between them.

We used the native *psbA2* promoter to drive expression of both the transporter genes and the catabolic genes. *psbA2* is a strong, light-sensitive promoter that enhances gene expression under high light conditions (Mohamed and Jansson, 1989) and regulates the expression of heterologous genes in response to variations in light intensity (Lindberg et al., 2010). This promoter has been used to express a number of heterologous genes (Zhou et al., 2014).

TABLE 1 | Synechocystis strains used in this study.

Strain	Genotype	Description
WT	Wild-type *Synechocystis* sp. 6803	Wild-type genomic sequence
X-Tr1	*xylE-ΔNeu 1*	*xylE* inserted at neutral site 1 (near *slr1285*)
X-Tr2	*galP-ΔNeu 1*	*galP* inserted at neutral site 1 (near *slr1285*)
X-Tr3	*glf-ΔNeu 1*	*glf* inserted at neutral site 1 (near *slr1285*)
X-Ut1	*xylE-ΔNeu 1::xylAB-ΔNeu 2*	*xylE* inserted at neutral site 1 (near *slr1285*), *xylAB* genes inserted at neutral site 2 (*slr0168*)
X-Ut2	*galP-ΔNeu 1::xylAB-ΔNeu 2*	*galP* inserted at neutral site 1 (near *slr1285*), *xylAB* genes inserted at neutral site 2 (*slr0168*)
X-Ut3	*glf-ΔNeu 1::xylAB-ΔNeu 2*	*glf* inserted at neutral site 1 (near *slr1285*), *xylAB* genes inserted at neutral site 2 (*slr0168*)
X-Ut4	*xylAB-ΔNeu 2*	*xylAB* genes inserted at neutral site 2 (*slr0168*)

Insertion of Heterologous Genes and Segregation of the Transformant Strains

The transporter as well as xylose utilization-specific heterologous genes were introduced into the neutral sites of the *Synechocystis* genome by homologous recombination. After each round of transformation, putative transformants were checked for the presence of heterologous gene inserts. Cells from one of the transformant colonies were cultivated successively under increasing antibiotic pressure to achieve complete segregation, in which selection of only those cells that had acquired all the genome copies carrying the insert was ensured. Only after confirmation of segregation, were strains used for the next round of transformation and further work.

For the PCR analyses represented in **Figures 3A,B**, the three strains generated after the first round of transformation, i.e., X-Tr1, X-Tr2, and X-Tr3, were used. To verify the presence of transporter-specific heterologous genes, the same sets of primers used to amplify the respective genes from genomic DNA of source organisms were employed (A1/A2 for *xylE*, B1/B2 for *galP,* and C1/C2 for *glf*, **Figure 2A**), which generated products of approximately 1.48, 1.40, and 1.42 kb in length, respectively (**Figure 3A**). To verify segregation, the forward primer used to amplify the upstream region of neutral site 1 and the reverse primer used to amplify the downstream region of neutral site 1 were employed (D1/D2, **Figure 2A**), and extension times in the PCR cycles were set specifically to amplify the wild-type (uninterrupted) neutral site 1. PCR amplifications yielded a ∼1.20-kb band representing neutral site 1 in the WT strain, but failed to generate any product for the transformants, indicating the absence of uninterrupted neutral site 1 and hence complete segregation of the strains (**Figure 3B**).

To test for the presence of the catabolic genes *xylAB* in the strains obtained after the second round of transformation, i.e., X-Ut1, X-Ut2, X-Ut3, and X-Ut4, the same set of primers used to amplify the genes from genomic DNA of the source organism was employed (E1/E2, **Figure 2B**), which generated

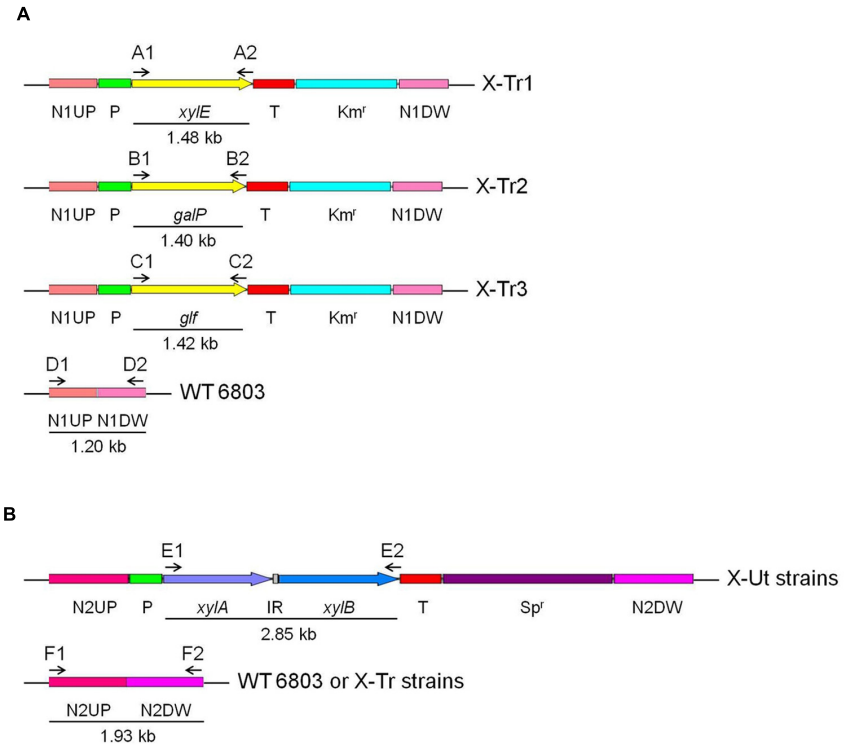

FIGURE 2 | Transformation of *Synechocystis* strains. All transgenes used in the study were expressed under the control of the *psbA2* promoter (Prm) and 5ST1T2 terminator (Trm). Intergenic region (IR), if present between individual genes, is represented as a gray box. Numbered letters and arrows represent the primer sets used to insert genes and evaluate segregation, and the direction of the amplifications, respectively. **(A)** Genes encoding the xylose transporters were inserted into neutral site 1 in the wild-type *Synechocystis* genome using upstream (N1UP) and downstream (N1DW) regions for homologous recombination. The kanamycin resistance cassette (Km^r) was used for selection and segregation of the transformants. **(B)** The *xylAB* genes, encoding enzymes that funnel xylose into the pentose phosphate pathway, were inserted into neutral site 2 in the genomes of *Synechocystis* strains carrying one of the three xylose transporter genes and the wild-type strain using upstream (N2UP) and downstream (N2DW) regions for homologous recombination. The spectinomycin resistance cassette (Sp^r) was used for selection and segregation of the transformants.

products of approximately 2.85 kb in length (**Figure 3C**). To verify the segregation with respect to neutral site 2, the forward primer used for amplification of the upstream region of neutral site 2 and the reverse primer used for amplification of the downstream region of neutral site 2 were employed (F1/F2, **Figure 2B**), and extension times in the PCR were set specifically to amplify wild-type neutral site 2. PCR amplifications yielded a ∼1.93-kb band representing neutral site 2 in the WT strain, but failed to generate any product for the transformants, indicating the absence of uninterrupted neutral site 2 and hence complete segregation of the strains (**Figure 3D**).

Expression of Heterologous Genes at the Transcriptional Level

Once the segregation of the strains obtained after the second round of transformation was confirmed, transcription of the heterologous genes for the transporters and the catabolic genes in the X-Ut1, X-Ut2, X-Ut3, and X-Ut4 strains was examined by RT-PCR. For the expression studies, both a positive and negative control were included. For the positive control, expression of *petA* (*sll1317*), which encodes apocytochrome *f*, a core subunit of the cytochrome b_6f complex, was tested. As a negative control for each strain, we examined whether the corresponding heterologous genes could be amplified from DNase-treated RNA samples obtained from each strain by PCR, to confirm the absence of any leftover DNA in the RNA samples.

When cDNA samples from the aforementioned strains were subjected to PCR using the same primer sets used to confirm gene insertion, products of the expected size were amplified. A ∼0.98-kb band was present for all positive controls and heterologous gene-specific bands were absent in the negative controls for all strains (**Figures 4A,B**). These results indicate the successful transcription of all the heterologous genes and corroborate the quality of the RNA samples.

Expression of the Catabolic Genes at the Translational Level

To study the expression of the xylose catabolic genes, *xylA* and *xylB,* at the protein level, specific polyclonal antibodies were raised by Dr. Qiang Wang (Institute of Hydrobiology, Wuhan, China) against XylA and XylB proteins overexpressed in *E. coli*. The antibodies were used to detect the presence of the proteins in the total cell extracts obtained from the X-Ut1, X-Ut2, X-Ut3, and

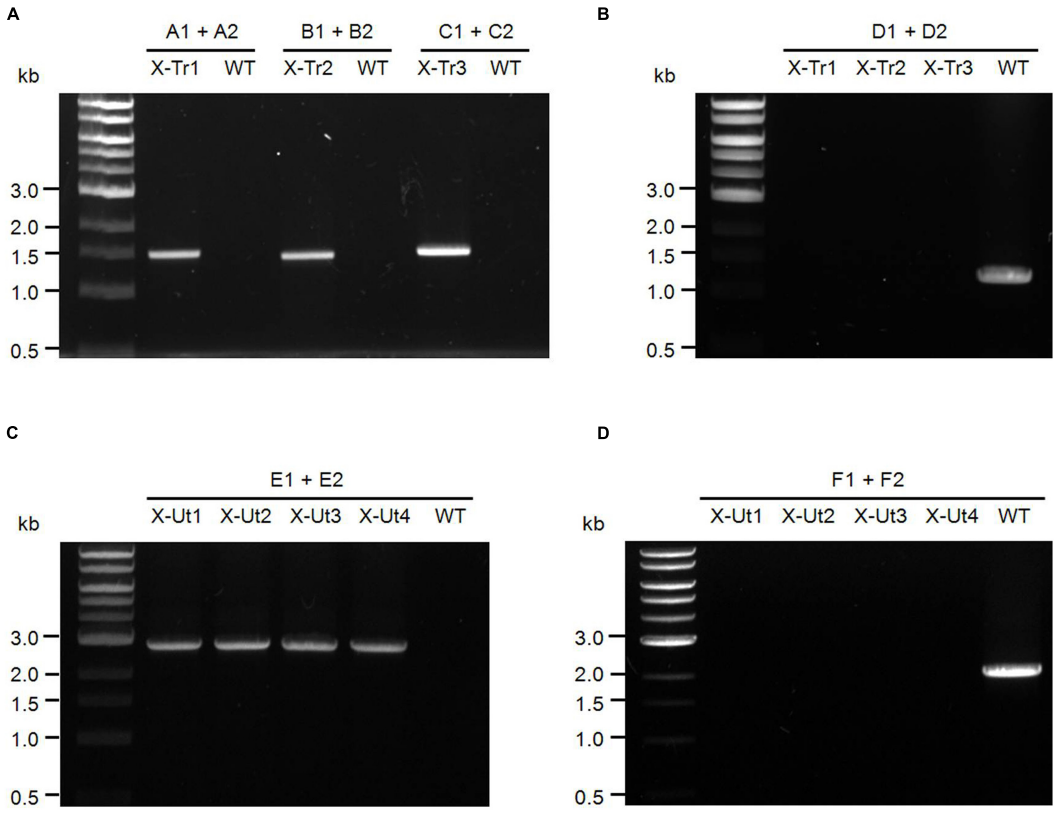

FIGURE 3 | Test of insertion of heterologous genes and chromosomal segregation for *Synechocystis* strains. (A) Primers upstream and downstream of the xylose transporter genes *xylE* (A1–A2), *galP* (B1–B2), and *glf* (C1–C2) were used to confirm the presence of the inserts in the respective transformants **(Figure 2A)** and also in the WT strain as the negative control. In the presence of the templates, primers A1–A2, B1–B2, and C1–C2 produced fragments of ∼1.48, ∼1.40, and ∼1.42 kb, respectively. **(B)** Primers upstream and downstream of intact neutral site 1 (D1–D2) were used to examine the chromosomal segregation for respective transformants **(Figure 2A)** along with the WT strain as a positive control. In the absence of uninterrupted neutral site 1, primers D1–D2 failed to produce PCR products in the transformants, whereas the WT strain yielded a ∼1.20-kb product. **(C)** Primers upstream and downstream of the xylose catabolic genes *xylAB* (E1–E2) were used to examine the insert in respective transformants **(Figure 2B)** and also in the WT strain as the negative control. In the presence of the template, primers E1–E2 produced a product of ∼2.85 kb. **(D)** Primers upstream and downstream of intact neutral site 2 (F1–F2) were used to check the chromosomal segregation for respective transformants **(Figure 2B)** along with the WT strain as the positive control. In the absence of uninterrupted neutral site 2, primers F1–F2 failed to produce PCR products in the transformants, whereas the WT strain yielded a ∼1.93-kb product.

X-Ut4 strains, and the WT strain was used as the negative control. XylA protein, with a molecular weight of ∼44 kD (Schellenberg et al., 1984), was present in the total cell extracts obtained from the transformants. Similarly, the presence of XylB protein, with an estimated molecular weight of ∼52 kD (Lawlis et al., 1984), was detected in the cell extracts isolated from the transformant strains (**Figure 5**). Expression of XylB showed that the RBS present between *xylA* and *xylB* of *E. coli* origin functioned in *Synechocystis*. Antibodies probing both of these proteins showed no cross-reaction with proteins present in the WT cell extract.

Uptake Assay of D-[^{14}C] Xylose as a Demonstration of Transporter Activity

To probe the activity of xylose transporter proteins in *Synechocystis*, we tested the ability of the X-Ut1, X-Ut2, X-Ut3, and X-Ut4 strain and also of the WT strain to take up D-[^{14}C] xylose. At the end of a 1-h incubation period, the strains showed various degrees of radioactivity. The levels of radioactivity in X-Ut1, X-Ut2, X-Ut3, and X-Ut4 were ∼653%, ∼136%, ∼77%, and ∼100% greater than those observed in the WT strain (**Figure 6**). Thus, the transformants were better able to take up and use xylose than was the WT.

Study of Biomass Accumulation Under Various Conditions

To study and compare the growth patterns exhibited by the strains generated after the first and second transformation events and the WT strain, we cultured the strains under different conditions (described in Materials and Methods). Biomass, i.e., DW, measurements were taken at 24-h intervals for 7 days in the case of dark and light-activated heterotrophic growth (LAHG) conditions and at 6-h intervals for 3 days for autotrophy and mixotrophy. In the absence of xylose, biomass yields were similar for all the strains. None of the strains were able to grow in darkness (data not shown). Under LAHG conditions in the presence of 5 mM glucose (hereafter LAHG-glucose conditions),

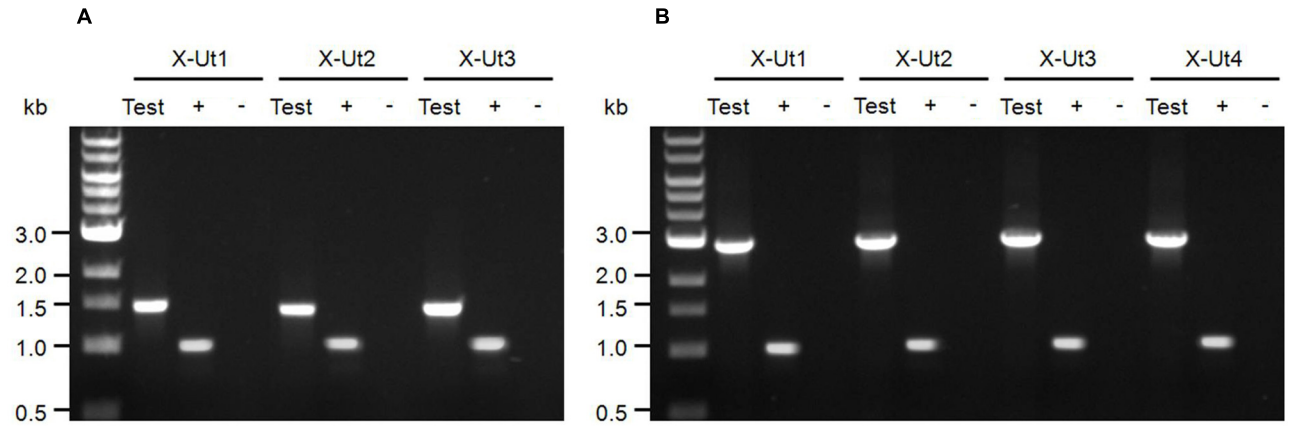

FIGURE 4 | Transcription evaluation of xylose-specific genes. (A) Primers upstream and downstream of the xylose transporter genes *xylE* (A1–A2), *galP* (B1–B2), and *glf* (C1–C2) were used **(Figure 2A)** to examine whether these genes were transcribed in the corresponding strains represented as 'Test.' In the presence of the templates, primers A1–A2, B1–B2, and C1–C2 produced products of ∼1.48, ∼1.40, and ∼1.42 kb in length, respectively. **(B)** Primers upstream and downstream of the xylose catabolic genes *xylAB* (E1–E2) were used **(Figure 2B)** to evaluate the transcription of the genes in the corresponding strains represented as 'Test.' In the presence of the templates, primers E1–E2 produced products of ∼2.85 kb. For the positive control (+), transcription of *petA* was examined using a gene-specific primer pair. The primer set produced a ∼0.99-kb product from cDNA templates of the transformants. For the negative control (–), amplification of heterologous genes from the corresponding RNA samples was evaluated using the gene-specific primer pairs. The primer pairs failed to generate any PCR product, indicating the absence of DNA contamination in the RNA samples.

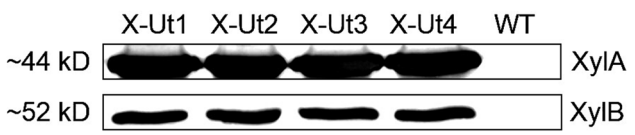

FIGURE 5 | Immunodetection of xylose catabolic proteins. Protein samples extracted from *Synechocystis* transformant strains, X-Ut1, X-Ut2, X-Ut3, and X-Ut4 and the WT strain as the negative control were probed with specific polyclonal antibodies for the XylA (D-xylose isomerase) and XylB (D-xylulokinase) enzymes. Each lane was loaded with 20 μg of total protein fraction. The expected molecular masses for XylA and XylB proteins are indicated.

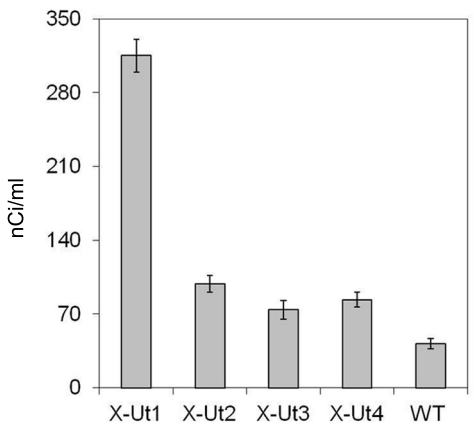

FIGURE 6 | Demonstration of D-[^{14}C] xylose uptake. To demonstrate the uptake of xylose, cultures of *Synechocystis* transformant strains, X-Ut1, X-Ut2, X-Ut3, and X-Ut4, and the WT strain at an OD_{730} of 0.6 were grown in the presence of D-[^{14}C] xylose. Radioactivity detected in the cultures is represented in nCi/ml. Data were collected from three biological replicates and presented as means ± standard deviations.

at the end of the seventh day, the strains showed biomass yields of 0.329 ± 0.010 g/L. Under autotrophy and mixotrophy in the presence of 5 mM glucose (hereafter mixotrophy-glucose conditions), at the end of third day, the biomass yields obtained for all strains were 0.244 ± 0.015 g/L and 0.993 ± 0.013 g/L, respectively.

Under LAHG conditions in the presence of 5 mM xylose (hereafter LAHG-xylose conditions), only X-Ut1, X-Ut2, X-Ut3, and X-Ut4 strains exhibited growth (data not shown for WT, X-Tr1, X-Tr2, and X-Tr3; **Figure 7A**). Under mixotrophy conditions in the presence of 5 mM xylose (hereafter mixotrophy-xylose conditions), the WT, X-Tr1, X-Tr2, and X-Tr3 strains showed biomass yields of 0.331 ± 0.014 g/L, which were similar to those obtained when grown under autotrophy, indicating the inability of the strains to utilize xylose. However, the X-Ut1, X-Ut2, X-Ut3, and X-Ut4 strains showed greater biomass yields under mixotrophy-xylose conditions than under autotrophy (**Figures 8A,B**). Biomass accumulation results demonstrate that all four of the transformants carrying the catabolic genes, namely X-Ut1, X-Ut2, X-Ut3, and X-Ut4, utilize xylose. After 7 days of culture under LAHG-xylose conditions, the X-Ut1, X-Ut2, and X-Ut3 strains showed ∼62, 28, and ∼60% greater biomass yields than did X-Ut4, respectively (**Figure 7A**). Under mixotrophy-xylose conditions, the strains carrying heterologous transporters showed higher biomass values at each time point. Notably, at the end of the second day of culture, X-Ut1, X-Ut2, and X-Ut3 strains showed ∼92, ∼34, and ∼94% greater biomass values than did the X-Ut4 strain (**Figure 8B**). For both LAHG-xylose and mixotrophy-xylose conditions, biomass

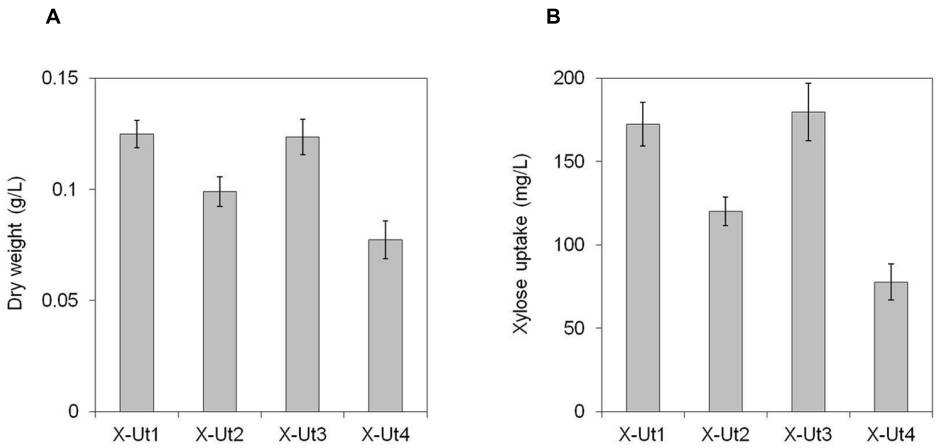

FIGURE 7 | Growth and xylose consumption under LAHG conditions in the presence of 5 mM xylose. *Synechocystis* strains X-Ut1, X-Ut2, X-Ut3, and X-Ut4 were grown in the presence of 5 mM (750 mg/L) xylose. **(A)** Dry biomass values estimated at the end of the seventh day. **(B)** Xylose consumption at the end of the seventh day exhibited by the transformant strains, determined from the measurement of residual xylose in the cell-free medium. Data were collected from three biological replicates and are presented as means ± standard deviations.

measurement data for X-Ut1, X-Ut2, X-Ut3, and X-Ut4 strains at each time point are presented in Supplementary Figures S1A and S2A.

To examine the ability of the xylose consuming strains to grow in the presence of xylose and glucose, we cultured the strains under LAHG and mixotrophic conditions in medium supplemented with 5 mM each of xylose and glucose (hereafter LAHG-mixed sugar and mixotrophy-mixed sugar conditions). The xylose consuming strains showed similar biomass yields under both conditions, in contrast to the variable yields exhibited in the presence of xylose alone (**Figures 7A**, **8A,B** and **9A**). The absence of two distinct growth phases and the simultaneous uptake of both the sugars did not indicate diauxie in these strains (data not shown).

Sugar Uptake Assays

To measure xylose uptake by the strains generated after each transformation event and by the WT strain, we first cultured the strains under LAHG-xylose and mixotrophy-xylose conditions. The WT, X-Tr1, X-Tr2, and X-Tr3 strains that lacked the catabolic genes *xylAB* showed no change in the amount of residual xylose in the medium at the tested time points, indicating their inability to utilize xylose (data not shown). On the other hand, the X-Ut1, X-Ut2, X-Ut3, and X-Ut4 strains that possessed the *xylAB* genes showed varying degrees of xylose consumption under both growth conditions (**Figures 7B** and **8C**). After 7 days of culture under LAHG-xylose conditions, xylose consumption was ∼122, 55, and ∼131% greater in the X-Ut1, X-Ut2, and X-Ut3 strains, respectively, than in X-Ut4 (**Figure 7B**). Under the same conditions, the maximum xylose uptake rates exhibited by the X-Ut1, X-Ut2, and X-Ut3 strains were ∼78, ∼45, and ∼80% higher than that exhibited by X-Ut4 (**Figure 10A**). Under mixotrophy-xylose conditions, the strains carrying heterologous transporters showed higher xylose uptake than did the strain relying only on endogenous transporter/s at each time point. Notably, at the end of the second day of culture, the X-Ut1, X-Ut2, and X-Ut3 strains showed ∼205, ∼80, and ∼209% higher levels of xylose uptake than did X-Ut4 (**Figure 8C**). Under the same conditions, the maximum xylose uptake rates exhibited by the X-Ut1, X-Ut2, and X-Ut3 strains were ∼64, ∼26, and ∼65% higher than that exhibited by X-Ut4 (**Figure 10B**). For both LAHG-xylose and mixotrophy-xylose conditions, the sugar uptake data at each time point are presented in Supplementary Figures S1B and S2B.

When grown under LAHG and mixotrophy-mixed sugar conditions, the xylose consuming strains, X-Ut1, X-Ut2, X-Ut3, and X-Ut4, consumed similar amounts of xylose (**Figure 9B**), in accordance with the biomass accumulation data. Under LAHG-mixed sugar conditions, all of the glucose was consumed by the end of the sixth day, while under mixotrophy-mixed sugar conditions, all of the glucose was consumed by the end of 48 h (data not shown). In the presence of mixed sugars, the maximum sugar uptake rates exhibited by the xylose consuming strains were very similar, in contrast to the results obtained when xylose was the only organic carbon source. Also, a sharp reduction in the maximum xylose uptake rates was observed when glucose was present along with xylose compared to when xylose was the sole sugar, with the exception of the X-Ut4 strain, which exhibited similar maximum xylose uptake rates under LAHG-xylose and LAHG-mixed sugar conditions (**Figures 10A,B**; Supplementary Table S1).

When xylose was the sole organic carbon source, the X-Ut1 and X-Ut3 strains were the most efficient in terms of biomass accumulation and xylose uptake, X-Ut2 was intermediately efficient, and X-Ut4 was the least efficient. When glucose was used in addition to xylose, no significant difference was observed in the growth and xylose consumption patterns among the xylose consuming strains, in the defined period of study. These results demonstrate that heterologous expression of

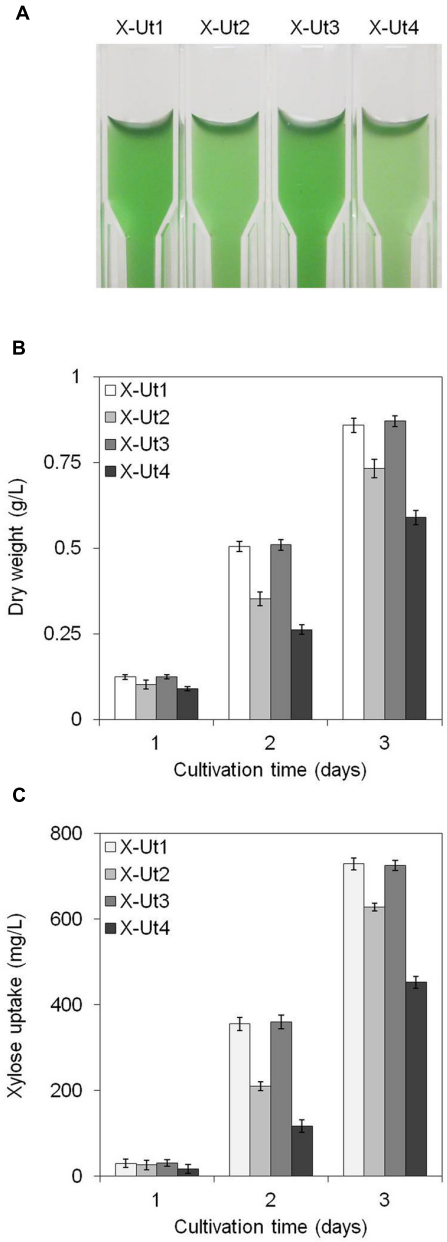

FIGURE 8 | Growth and xylose consumption under mixotrophy in the presence of 5 mM xylose. *Synechocystis* strains X-Ut1, X-Ut2, X-Ut3, and X-Ut4 were grown in the presence of 5 mM (750 mg/L) xylose. **(A)** Photograph depicting differential growth shown by the transformant strains at the end of second day of culture. **(B)** Dry biomass values estimated at the end of first, second, and third days. **(C)** Xylose consumption at the end of the first, second, and third day exhibited by the transformant strains, determined from the measurement of residual xylose in filtered cell-free medium. Data represented in graphs were collected from three biological replicates and presented as means ± standard deviations.

XylE, GalP, and Glf enhances xylose transport in *Synechocystis*, which results in more organic carbon being available for growth and metabolism via the engineered isomerase catabolic pathway.

DISCUSSION

In this study, we sought to construct and compare *Synechocystis* strains that were able to utilize xylose by the heterologous expression of genes native to *E. coli* and *Z. mobilis*. Since *Synechocystis* is a mesophilic Gram negative cyanobacterium, heterologous genes derived from other Gram-negative mesophiles, especially the ones encoding the transporters, were expected to function in the host strain. *E. coli* is naturally capable of utilization of xylose and its genes involved in the xylose metabolism have been used to engineer other bacteria and yeasts (Zhang et al., 1995; Kawaguchi et al., 2006; Meijnen et al., 2008; Young et al., 2010; Xiong et al., 2012; McEwen et al., 2013; Lee et al., 2015). Although *Z. mobilis* is not a natural xylose utilizer, its glucose transporter, Glf is able to take up xylose very efficiently and has been functionally expressed in *E. coli* in either modified or unmodified form (Weisser et al., 1995; Chen et al., 2009; Ren et al., 2009). Hence, *E. coli* and *Z. mobilis* were chosen as the source organisms for xylose specific genes in the study. Although *Synechocystis* was considered to lack xylose transporters, we independently, alongside another recent study (Lee et al., 2015), found that expression of the *xylAB* genes alone was sufficient to generate lines that could utilize xylose (**Figures 7A,B** and **8A–C**), indicating the involvement of endogenous sugar transporter/s. This also indicates that the xylose uptake observed in strains possessing non-native transporters was due to activities of both endogenous and heterologous transporters. GlcP (*sll0771*) is the only known MFS-type glucose transporter identified in *Synechocystis* (Lee et al., 2015), and this transporter shows an affinity for fructose as well (Zhang et al., 1989). Two of the heterologous MFS-type transporter proteins used in the study have also been shown to possess specificity for more than one substrate. The proton symporter GalP of *E. coli* origin, which is primarily a galactose transporter, is able to transport an array of other substrates, including xylose (Baldwin and Henderson, 1989). Similarly, the uniporter Glf of *Z. mobilis* origin, which is primarily a glucose transporter, is also able to transport fructose and xylose (Saier and Crasnier, 1996).

Our results either directly or indirectly show that we successfully expressed the xylose catabolic genes *xylAB* in *Synechocystis* (**Figures 5**, **6**, **7A,B** and **8A–C**), indicating that the *E. coli* RBS functions in *Synechocystis*. Heterologously expressed *E. coli xylAB* and *xylFGH* genes, which encode xylose catabolic enzymes and an ATP-binding cassette (ABC)-type transporter and contain unmodified RBSs, were recently shown to be involved in xylose transport and catabolism in engineered *Synechocystis* (Lee et al., 2015). In this work, we have compared the performance of *Synechocystis* strains engineered to catabolize xylose, relying on the native, non-specific xylose transporter/s with or without one of the three heterologous MFS type transporter proteins. With this strategy, we attempted to compare the performance of heterologous transporter proteins when expressed individually in *Synechocystis*, under LAHG and mixotrophic conditions. Unlike some other cyanobacterial

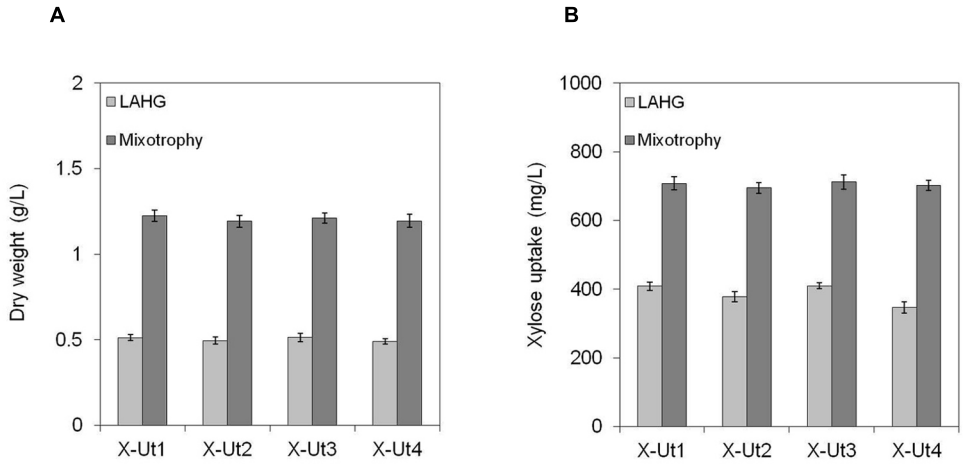

FIGURE 9 | Growth and xylose consumption in the presence of 5 mM xylose and glucose. *Synechocystis* strains X-Ut1, X-Ut2, X-Ut3, and X-Ut4 were grown in the presence of 5 mM (750 mg/L) xylose and 5 mM (900.8 mg/L) glucose. **(A)** Dry biomass values estimated at the end of the seventh day for the LAHG condition and at the end of the third day for mixotrophy. **(B)** Xylose consumption at the end of the seventh day for the LAHG condition and at the end of the third day for mixotrophy, determined by the measurement of residual xylose in the cell-free medium. Data were collected from three biological replicates and presented as means ± standard deviations.

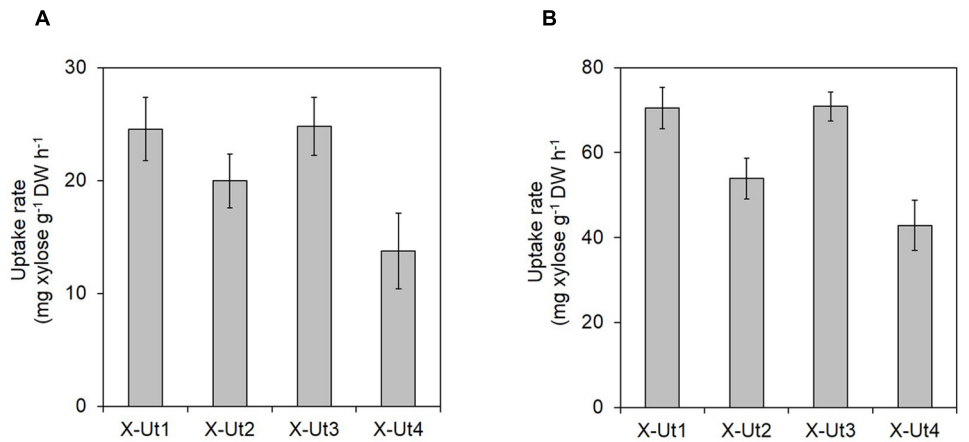

FIGURE 10 | Maximum xylose uptake rates in the presence of 5 mM xylose. *Synechocystis* strains X-Ut1, X-Ut2, X-Ut3, and X-Ut4, were grown in the presence of 5 mM (750 mg/L) xylose. Maximum xylose uptake rates [mg xylose g^{-1} dry weight (DW) h^{-1}] under **(A)** LAHG and **(B)** mixotrophy conditions were calculated using a previously described formula (Munyon and Merchant, 1959). For all the strains, maximum xylose uptake rates were observed between the sixth and seventh day under LAHG. Under mixotrophy, maximum xylose uptake rates were observed between the 42 and 48 h (for X-Ut1, X-Ut3, and X-Ut4) and the 48 and 54 h (for X-Ut2). Raw data were collected from three biological replicates. Uptake rates are presented as means ± standard deviations.

species, *Synechocystis* is unable to grow heterotrophically under complete darkness, and requires brief exposure to light for growth. This type of growth has been termed as light activated heterotrophic growth, i.e., LAHG (Anderson and McIntosh, 1991). For LAHG conditions, we illuminated *Synechocystis* cultures daily with 50 μE m^{-2} s^{-1} light for 10 min, which we consider just sufficient to support heterotrophic growth. Under LAHG-xylose conditions, *Synechocystis* strains lacking the xylose catabolic genes did not show any growth (data not shown). This indicates that, the growth exhibited by the strains expressing *xylAB* genes was the result of utilization of xylose and not due to photosynthetic electron transport. Lee et al. (2015) have compared the growth of a *Synechocystis* strain expressing *xylAB* genes with another strain expressing *xylAB* and transporter coding *xylFGH* genes in the presence of four different concentrations of xylose, under modified LAHG conditions wherein the cultures received daily illumination of 50 μE m^{-2} s^{-1} for 1 h. At the end of ninth day under modified LAHG conditions, the latter strain reached higher optical density values only at xylose concentrations of 10 and 50 mM (Lee et al., 2015). We sought to use xylose concentration as low as possible, to evaluate the xylose catabolizing strains on the basis of biomass accumulation and xylose consumption data collected

at 6-h intervals for 3 days under mixotrophy and 24-h intervals for 7 days under LAHG conditions. In contrast to the results obtained for the *Synechocystis* strain carrying the XylFGH transporter (Lee et al., 2015), we found that expression of heterologous xylose transporters was able to boost the ability of transformants to utilize xylose, even at low xylose concentrations (5 mM), when it was the sole source of organic carbon. X-Ut2, showed an intermediate ability to utilize xylose, and was more efficient than the X-Ut4 strain. The performance of X-Ut1 and X-Ut3 was the most remarkable (**Figures 7A,B**, **8A–C** and **10A,B**). Thus, among the heterologous transporters studied, GalP was the least efficient. However, we were unable to determine which of the other two transporters, XylE and Glf, was more active, since a bottleneck may exist that influences the catabolic activities of XylAB or enzymes of the PPP of *Synechocystis*. We did not find any significant difference in the biomass yields of X-Ut1 and X-Ut3 strains grown in the presence of 10 and 20 mM xylose under mixotrophic conditions at the end of third day (data not shown). During preliminary experiments performed in our laboratory, we observed that the WT, X-Tr1, X-Tr2, and X-Tr3 strains that lacked the *xylAB* genes and hence the ability to catabolize xylose showed no difference in growth under mixotrophy-xylose (up to 20 mM xylose) and autotrophy conditions (data not shown). These observations indicate the absence of osmotic stress and the presence of an efficient efflux system in *Synechocystis*.

Although X-Ut3 was one of the two most efficient strains in terms of dry biomass accumulation and xylose uptake (**Figures 7A,B**, **8A–C** and **10A,B**), it showed the lowest radioactivity among the xylose utilizing strains in the D-[^{14}C] xylose uptake study (**Figure 6**). This can be explained by the bidirectional transport ability of Glf (Marger and Saier, 1993). When heterologously expressed in the cyanobacterium *Synechococcus elongatus* PCC 7942, Glf has been shown to export monomeric sugars (Niederholtmeyer et al., 2010). On the other hand, X-Ut1 showed significantly higher levels of radioactivity. These results are not reflected in the actual growth and xylose consumption data (**Figures 6, 7A,B** and **8A–C**), indicating that a lag phase exists before xylose metabolism is fully established.

When glucose was included in the medium along with xylose, the maximum xylose uptake rates exhibited by the transformants were lower than those when xylose was the sole source of organic carbon (**Figures 10A,B**; Supplementary Table S1). This observation is in accordance with results obtained previously in which a *Synechocystis* strain carrying the *xylAB* genes showed a decrease in xylose consumption in the presence of glucose (Lee et al., 2015). Although glucose was consumed at a much faster rate than xylose (Supplementary Table S1), both sugars were utilized simultaneously with no signs of diauxy (data not shown). These results were expected, since *psbA2* is a light-dependent promoter (Mohamed and Jansson, 1989; Lindberg et al., 2010). Absence of a regulatory region linked to the promoter which can be affected by presence of a sugar and continuous exposure to light caused constant induction of the *psbA2* promoter, hence ensuring the expression of the xylose transporter and catabolic genes even in the presence of glucose. In the presence of 5 mM each of xylose and glucose, the growth and sugar consumption patterns exhibited by the *Synechocystis* strains carrying the *xylAB* genes were found to be similar to each other, which may indicate that the *Synechocystis* strains had reached their maximum capacity to process organic carbon, at least via PPP in the presence of 5 mM glucose. Although diauxy was not observed, the presence of glucose caused a decrease in the maximum xylose uptake rates, with the exception of the X-Ut4 strain under LAHG-mixed sugar conditions (**Figures 10A,B**; Supplementary Table S1). Complete consumption of glucose before that of xylose suggests that glucose was still the preferred sugar of the engineered *Synechocystis* strains.

We believe that there is scope to further improve the ability of the strains to utilize xylose. Codon optimization has been previously shown to improve the expression of heterologous genes in *Synechocystis* (Lindberg et al., 2010; Angermayr et al., 2014; Xue et al., 2014b). Another element that is correlated with the expression level of genes is RBS (Ma et al., 2002). The strength of RBSs can be predicted and improved with the aid of a predictive design tool (Salis et al., 2009). With the help of more powerful RBSs, it will be possible to truly harvest the potential of the *xylAB* and *xylFGH* genes employed in the present and in another recent study (Lee et al., 2015). Approaches such as exploration of genomes of bacteria and algae for potential sugar transporter-catabolic genes, expression of multiple heterologous transporter genes and laboratory evolution could also prove beneficial for obtaining more efficient xylose-utilizing strains.

The strains generated in this work, especially X-Ut1 and X-Ut3, can be used directly or modified further. Introducing the *xylAB* genes into a glycogen synthesis gene *glgC* (*slr1176*) knockout enhanced the production of keto acids, and half of the carbon in the keto acids could be traced to catabolized xylose (Lee et al., 2015). An excess of carbon resulting from the absence of a carbon sink and reduced nutrient availability has been demonstrated to trigger metabolic outflow (Carrieri et al., 2012; Lee et al., 2015). Efficient xylose utilization by engineered *Synechocystis* strains, in addition to the aforementioned strategies, would increase the amount of carbon available for biotechnological conversion. The work reported here represents an important step toward engineering a *Synechocystis* strain that is able to harvest carbon from the second most abundant sugar source in nature and use it to biosynthesize a range of useful compounds.

AUTHOR CONTRIBUTIONS

SR and QH conceived the research. SR, YZ, MK, and WM designed and performed the experiments. SR analysed the data. SR and QH prepared the manuscript. All the authors have read and approved of the manuscript.

FUNDING

The work was supported by National Science Foundation Grant MCB1120153 and Arkansas P3 Center Pilot Seed Grant P3-203.

ACKNOWLEDGMENTS

We thank the United States Department of Agriculture's Agricultural Research Service for *E. coli* K-12 and *Z. mobilis* ZM4 strains, Dr. Qiang Wang for anti-XylA and anti-XylB antibodies, and Dr. Nawab Ali for his help with the ^{14}C-labeled D-xylose uptake assay.

SUPPLEMENTARY MATERIAL

The Supplementary Material for this article can be found online at: http://journal.frontiersin.org/article/10.3389/fmicb.2015.01484

REFERENCES

Anderson, S., and McIntosh, L. (1991). Light-activated heterotrophic growth of the cyanobacterium *Synechocystis* sp. Strain PCC 6803: a blue-light requiring process. *J. Bacteriol.* 173, 2761–2767.

Angermayr, S. A., van der Woude, A. D., Correddu, D., Vreugdenhil, A., Verrone, V., and Hellingwerf, K. J. (2014). Exploring metabolic engineering design principles for the photosynthetic production of lactic acid by *Synechocystis* sp. *PCC* 6803. *Biotechnol. Biofuels* 7:99. doi: 10.1186/1754-6834-7-99

Anwar, Z., Gulfraz, M., and Irshad, M. (2014). Agro-industrial lignocellulosic biomass a key to unlock the future bio-energy: a brief review. *J. Radiat. Res. Appl. Sci.* 7, 163–173. doi: 10.1016/j.jrras.2014.02.003

Baldwin, S. A., and Henderson, P. J. F. (1989). Homologies between sugar transporters from eukaryotes and prokaryotes. *Annu. Rev. Physiol.* 51, 459–471. doi: 10.1146/annurev.ph.51.030189.002331

Carrieri, D., Paddock, T., Maness, P. C., Seibert, M., and Yu, J. (2012). Photocatalytic conversion of carbon dioxide to organic acids by a recombinant cyanobacterium incapable of glycogen storage. *Energy Environ. Sci.* 5, 9457–9461. doi: 10.1039/C2EE23181F

Chen, T., Zhang, J., Liang, L., Yang, R., and Lin, Z. (2009). An *in vivo*, label-free quick assay for xylose transport in *Escherichia coli*. *Anal. Biochem.* 390, 63–67. doi: 10.1016/j.ab.2009.03.048

Davies, F. K., Work, V. H., Beliaev, A. S., and Posewitz, M. C. (2014). Engineering limonene and bisabolene production in wild type and a glycogen-deficient mutant of *Synechococcus* sp. PCC 7002. *Front. Bioeng. Biotechnol.* 2:21. doi: 10.3389/fbioe.2014.00021

Doelle, H. W. (1975). "Carbohydrate metabolism," in *Bacterial Metabolism,* 2nd Edn (New York, NY: Academic Press Inc), 208–312.

Eiler, A. (2006). Evidence for the ubiquity of mixotrophic bacteria in the upper ocean: implications and consequences. *Appl. Environ. Microbiol.* 72, 7431–7437. doi: 10.1128/AEM.01559-06

Gìrio, F. M., Fonseca, C., Carvalheiro, F., Duarte, L. C., Marques, S., and Bogel-Lukasik, R. (2010). Hemicelluloses for fuel ethanol: a review. *Bioresour. Technol.* 101, 4775–4800. doi: 10.1016/j.biortech.2010.01.088

Jojima, T., Omumasaba, C. A., Inui, M., and Yukawa, H. L. (2010). Sugar transporters in efficient utilization of mixed sugar substrates: current knowledge and outlook. *Appl. Microbiol. Biotechnol.* 85, 471–480. doi: 10.1007/s00253-009-2292-1

Kawaguchi, H., Vertés, A. A., Okino, S., Inui, M., and Yukawa, H. (2006). Engineering of a xylose metabolic pathway in *Corynebacterium glutamicum*. *Appl. Environ. Microbiol.* 72, 3418–3428. doi: 10.1128/AEM.72.5.3418-3428.2006

Kumar, P., Barrett, D. M., Delwiche, M. J., and Stroeve, P. (2009). Methods for pretreatment of lignocellulosic biomass for efficient hydrolysis and biofuel production. *Ind. Eng. Chem. Res.* 48, 3713–3729. doi: 10.1021/ie801542g

Kunert, A., Hagemann, M., and Erdmann, N. (2000). Construction of promoter probe vectors for *Synechocystis* sp. PCC 6803 using the light-emitting reporter systems Gfp and LuxAB. *J. Microbiol. Methods* 41, 185–194. doi: 10.1016/S0167-7012(00)00162-7

Lawlis, V. B., Dennis, M. S., Chen, E. Y., Smith, D. H., and Henner, D. J. (1984). Cloning and sequencing of the xylose isomerase and xylulose kinase genes of *Escherichia coli*. *Appl. Environ. Microbiol.* 47, 15–21.

Lee, R. A., and Lavoie, J. M. (2013). From first to third generation biofuels: Challenges of producing a commodity from a biomass of increasing complexity. *Anim. Front.* 3, 6–11. doi: 10.2527/af.2013-0010

Lee, T. C., Xiong, W., Paddock, T., Carrieri, D., Chang, I. F., Chiu, H. F., et al. (2015). Engineered xylose utilization enhances bio-products productivity in the cyanobacterium *Synechocystis* sp. PCC 6803. *Metab. Eng.* 30, 179–189. doi: 10.1016/j.ymben.2015.06.002

Lindberg, P., Park, S., and Melis, A. (2010). Engineering a platform for photosynthetic isoprene production in cyanobacteria, using *Synechocystis* as the model organism. *Metab. Eng.* 12, 70–79. doi: 10.1016/j.ymben.2009.10.001

Lu, X. (2010). A perspective: photosynthetic production of fatty acid-based biofuels in genetically engineered cyanobacteria. *Biotechnol. Adv.* 28, 742–746. doi: 10.1016/j.biotechadv.2010.05.021

Ma, J., Campbell, A., and Karlin, S. (2002). Correlations between Shine-Dalgarno sequences and gene features such as predicted expression levels and operon structures. *J. Bacteriol.* 184, 5733–5745. doi: 10.1128/JB.184.20.5733-5745.2002

Malherbe, S., and Cloete, T. E. (2002). Lignocellulose biodegradation: fundamentals and applications. *Rev. Environ. Sci. Biotechnol.* 1, 105–114. doi: 10.1023/A:1020858910646

Marger, M. D., and Saier, Jr. M. H. (1993). A major superfamily of transmembrane facilitators that catalyse uniport, symport and antiport. *Trends Biochem. Sci.* 18, 13–20. doi: 10.1016/0968-0004(93)90081-W

Matsushika, A., Inoue, H., Kodaki, T., and Sawayama, S. (2009). Ethanol production from xylose in engineered *Saccharomyces cerevisiae* strain: current state and prospectives. *Appl. Microbiol. Biotechnol.* 84, 37–53. doi: 10.1007/s00253-009-2101-x

McEwen, J. T., Machado, I. M. P., Connor, M. R., and Atsumi, S. (2013). Engineering *Synechococcus elongates* PCC 7942 for continuous growth under diurnal conditions. *Appl. Environ. Microbiol.* 79, 1668–1675. doi: 10.1128/AEM.03326-12

Meijnen, J. P., de Winde, J. H., and Ruijssenaars, H. J. (2008). Engineering *Pseudomonas putida* S12 for efficient utilization of D-xylose and L-arabinose. *Appl. Environ. Microbiol.* 74, 5031–5037. doi: 10.1128/AEM.00924-08

Mohamed, A., and Jansson, C. (1989). Influence of light on accumulation of photosynthesis-specific transcripts in the cyanobacterium *Synechocystis* 6803. *Plant Mol. Biol.* 13, 693–700. doi: 10.1007/BF00016024

Munyon, W. H., and Merchant, D. J. (1959). The relation between glucose utilization, lactic acid production and utilization and the growth cycle of L strain fibroblasts. *Exp. Cell Res.* 17, 490–498. doi: 10.1016/0014-4827(59)90069-2

Niederholtmeyer, H., Wolfstadter, B. T., Savage, D. F., Silver, P. A., and Way, J. C. (2010). Engineering cyanobacteria to synthesize and export hydrophilic products. *Appl. Environ. Microbiol.* 76, 3462–3466. doi: 10.1128/AEM.00202-10

Pothiraj, C., Kanmani, P., and Balaji, P. (2006). Bioconversion of lignocellulose materials. *Mycobiology* 34, 159–165. doi: 10.4489/MYCO.2006.34.4.159

Prentki, P., and Krisch, H. M. (1984). In vitro insertional mutagenesis with a selectable DNA fragment. *Gene* 29, 303–313. doi: 10.1016/0378-1119(84)90059-3

Ragauskas, A. J., Williams, C. K., Davison, B. H., Britovsek, G., Cairney, J., Eckert, C. A., et al. (2006). The path forward for biofuels and biomaterials. *Science* 311, 484–489. doi: 10.1126/science.1114736

Ren, C., Chen, T., Zhang, J., Liang, L., and Lin, Z. (2009). An evolved xylose transporter from *Zymomonas mobilis* enhances sugar transport in *Escherichia coli*. *Microb. Cell Fact.* 8:66. doi: 10.1186/1475-2859-8-66

Saier, M. H. Jr., and Crasnier, M. (1996). Inducer exclusion and the regulation of sugar transport. *Res. Microbiol.* 147, 482–489. doi: 10.1016/S0923-2508(96)90150-3

Salis, H. M., Mirsky, E. A., and Voigt, C. A. (2009). Automated design of synthetic ribosome binding sites to control protein expression. *Nat. Biotechnol.* 27, 946–950. doi: 10.1038/nbt.1568

Schellenberg, G. D., Sarthy, A., Larson, A. E., Backer, M. P., Crabb, J. W., Lidstrom, M., et al. (1984). Xylose isomerase from *Escherichia coli*. Characterization of the protein and the structural gene. *J. Biol. Chem.* 259, 6826–6832.

Vieira, J., and Messing, J. (1982). The pUC plasmids, an M13mp7-derived system for insertion mutagenesis and sequencing with synthetic universal primers. *Gene* 19, 259–268. doi: 10.1016/0378-1119(82)90015-4

Vinuselvi, P., Kim, M. K., Lee, S. K., and Ghim, C. M. (2012). Rewiring carbon catabolite repression for microbial cell factory. *BMB Rep.* 45, 59–70. doi: 10.5483/BMBRep.2012.45.2.59

Weisser, P., Krämer, R., Sahm, H., and Sprenger, G. A. (1995). Functional expression of the glucose transporter of Zymomonas mobilis leads to restoration of glucose and fructose uptake in *Escherichia coli* mutants and provides evidence for its facilitator action. *J. Bacteriol.* 177, 3351–3354.

Xiong, X., Wang, X., and Chen, S. (2012). Engineering of xylose metabolic pathway in *Rhodococcus* strains. *Appl. Environ. Microbiol.* 78, 5483–5491. doi: 10.1128/AEM.08022-11

Xue, Y., Zhang, Y., Cheng, D., Daddy, S., and He, Q. (2014a). Genetically engineering *Synechocystis* sp. Pasteur Culture Collection 6803 for the sustainable production of the plant secondary metabolite p-coumaric acid. *Proc. Natl. Acad. Sci. U.S.A.* 111, 9449–9454. doi: 10.1073/pnas.13237 25111

Xue, Y., Zhang, Y., Grace, S., and He, Q. (2014b). Functional expression of an *Arabidopsis* p450 enzyme, p-coumarate-3-hydroxylase, in the cyanobacterium *Synechocystis* PCC 6803 for the biosynthesis of caffeic acid. *J. Appl. Phycol.* 26, 219–226. doi: 10.1007/s10811-013-0113-5

Yao, L., Qi, F., Tan, X., and Lu, X. (2014). Improved production of fatty alcohols in cyanobacteria by metabolic engineering. *Biotechnol. Biofuels* 7:94. doi: 10.1186/1754-6834-7–94

Young, E., Lee, S. M., and Alper, H. (2010). Optimizing pentose utilization in yeast: the need for novel tools and approaches. *Biotechnol. Biofuels* 3:24. doi: 10.1186/1754-6834-3-24

Zhang, C. C., Durand, M. C., Jeanjean, R., and Joset, F. (1989). Molecular and genetical analysis of the fructose-glucose transport sy stem in the cyanobacterium *Synechocystis* PCC 6803. *Mol. Microbiol.* 3, 1221–1229. doi: 10.1111/j.1365-2958.1989.tb00272.x

Zhang, M., Eddy, C., Deanda, K., Finkelstein, M., and Picataggio, S. (1995). Metabolic engineering of a pentose metabolism pathway in ethanologenic *Zymomonas mobilis*. *Science* 267, 240–243. doi: 10.1126/science.267.5195.240

Zhou, J., Zhang, H., Meng, H., Zhu, Y., Bao, G., Zhang, Y., et al. (2014). Discovery of a super-strong promoter enables efficient production of heterologous proteins in cyanobacteria. *Sci. Rep.* 4:4500. doi: 10.1038/srep04500

Conflict of Interest Statement: The authors declare that the research was conducted in the absence of any commercial or financial relationships that could be construed as a potential conflict of interest.

frontiers in Microbiology

ORIGINAL RESEARCH
published: 20 October 2015
doi: 10.3389/fmicb.2015.01150

Modification of photosynthetic electron transport and amino acid levels by overexpression of a circadian-related histidine kinase *hik8* in *Synechocystis* sp. PCC 6803

Ayuko Kuwahara[1†], Satomi Arisaka[2†], Masahiro Takeya[2†], Hiroko Iijima[2], Masami Yokota Hirai[1] and Takashi Osanai[1,2]*

[1] RIKEN Center for Sustainable Resource Science, Yokohama, Japan, [2] Department of Agricultural Chemistry, School of Agriculture, Meiji University, Kawasaki, Japan

OPEN ACCESS

Edited by:
Weiwen Zhang, Tianjin University, China

Reviewed by:
Jiangxin Wang, Shenzhen University, China
Lei Chen, Tianjin University, China
Josselin Noirel, Conservatoire National des Arts et Métiers, France

***Correspondence:**
Takashi Osanai
tosanai@meiji.ac.jp

[†] *These authors have contributed equally to this work.*

Specialty section:
This article was submitted to Microbiotechnology, Ecotoxicology and Bioremediation, a section of the journal Frontiers in Microbiology

Received: *19 August 2015*
Accepted: *05 October 2015*
Published: *20 October 2015*

Citation:
Kuwahara A, Arisaka S, Takeya M, Iijima H, Hirai MY and Osanai T (2015) Modification of photosynthetic electron transport and amino acid levels by overexpression of a circadian-related histidine kinase hik8 in Synechocystis sp. PCC 6803. Front. Microbiol. 6:1150. doi: 10.3389/fmicb.2015.01150

Cyanobacteria perform oxygenic photosynthesis, and the maintenance of photosynthetic electron transport chains is indispensable to their survival in various environmental conditions. Photosynthetic electron transport in cyanobacteria can be studied through genetic analysis because of the natural competence of cyanobacteria. We here show that a strain overexpressing *hik8*, a histidine kinase gene related to the circadian clock, exhibits an altered photosynthetic electron transport chain in the unicellular cyanobacterium *Synechocystis* sp. PCC 6803. Respiratory activity was down-regulated under nitrogen-replete conditions. Photosynthetic activity was slightly lower in the *hik8*-overexpressing strain than in the wild-type after nitrogen depletion, and the values of photosynthetic parameters were altered by *hik8* overexpression under nitrogen-replete and nitrogen-depleted conditions. Transcripts of genes encoding Photosystem I and II were increased by *hik8* overexpression under nitrogen-replete conditions. Nitrogen starvation triggers increase in amino acids but the magnitude of the increase in several amino acids was diminished by *hik8* overexpression. These genetic data indicate that Hik8 regulates the photosynthetic electron transport, which in turn alters primary metabolism during nitrogen starvation in this cyanobacterium.

Keywords: cyanobacteria, genetic engineering, histidine kinase, photosynthesis, *Synechocystis*

INTRODUCTION

The unicellular cyanobacterium *Synechocystis* sp. PCC 6803 (hereafter referred to as *Synechocystis* 6803) is one of the most widely studied cyanobacteria owing to its natural transformation ability and its genomic information (Ikeuchi and Tabata, 2001; Kanesaki et al., 2012). Knockout and overexpression of genes of interest in *Synechocystis* 6803 enable the researchers to investigating the molecular mechanisms of photosynthetic electron transport in this cyanobacterium (Ikeuchi and Tabata, 2001; Osanai et al., 2011).

Like other algae and plants, *Synechocystis* 6803 possesses Photosystem I and II (PSI and PSII). PSII is a multi-protein complex, localized in the thylakoid membrane, which functions as a light-driven water:plastoquinone oxidoreductase along with the Mn_4Ca cluster

(Nixon et al., 2010; Barber, 2014). The core of the PSII complex is composed of D1 and D2 proteins encoded by *psbA* and *psbD*, respectively (Mulo et al., 2009). Two chlorophyll-binding proteins CP43 and CP47, encoded by *psbC* and *psbB* respectively, are included in the reaction center of PSII (Barber, 2014). Three extrinsic proteins, PsbO, U, and V, are located on the lumenal side of cyanobacterial PSII and function as an oxygenic evolving complex (Barber, 2014). At least 20 proteins are included in PSII, and its dimeric crystal structure in thermophilic cyanobacteria has been resolved at a resolution of 1.9 Å (Umena et al., 2011). PSI is also a large membrane protein complex catalyzing light-driven electron transfer from the soluble electron carrier plastocyanin located on the lumenal side, to ferredoxin, located on the stromal side (Amunts and Nelson, 2009). The PSI complex is organized as a trimer containing 12 protein subunits (Jordan et al., 2001). The central part of the PSI core complex is formed by a heterodimer of the large transmembrane proteins PsaA and PsaB (Amunts and Nelson, 2009). The stromal loops of PsaA and PsaB are associated with the three stromal proteins PsaC, PsaD, and PsaE, which interact with ferredoxin (Amunts and Nelson, 2009). Plastocyanin is bound with PsaF at the lumenal part of PSI (Karapetyan et al., 2014). PsaI and PsaL are essential components of a trimer complex in cyanobacteria (Karapetyan et al., 2014).

The regulatory mechanisms of photosystems have been intensively studied in cyanobacteria. The D1 proteins are the main PSII subunits damaged during photoinhibition, and therefore, turnover of D1 proteins is an important photoprotective mechanism (Nixon et al., 2010). Regulation of D1 proteins at translational and post-translational levels is indispensable for the maintenance of PSII (Silva et al., 2003; Kojima et al., 2009). Down-regulation of the PSI/PSII ratio under high-light conditions is another way to acclimate to the fluctuation of light intensity (Murakami and Fujita, 1991). A response regulator, RpaB, binds the promoter regions of PSI genes and activates their gene expression under low light conditions (Seino et al., 2009). RpaB functions as a repressor of high light inducible genes in *Synechocystis* 6803 and *Synechococcus* sp. PCC 7942 (Kappell and van Waasbergen, 2007; Seki et al., 2007). Not only light conditions, but also nitrogen starvation can change the ratio of PSII and PSI activities in unicellular cyanobacteria (Görl et al., 1998). Overexpression of *sigE*, encoding an RNA polymerase sigma factor involved in sugar catabolism, modifies respiratory, and photosynthetic activities under both nitrogen-replete and nitrogen-depleted conditions (Osanai et al., 2013). Thus, light and nutrient conditions refine photosynthetic electron transport, which is altered through transcriptional cascades in *Synechocystis* 6803.

One of distinctive characteristic of cyanobacteria is their possession of circadian clocks. The central circadian oscillator consists of three proteins, KaiA, KaiB, and KaiC, and their phosphorylation cycle and transcription and translation feedback loops are essential for the generation of circadian rhythms (Ishiura et al., 1998; Nakajima et al., 2005). SasA is a histidine kinase associated with KaiC in *Synechococcus* sp. PCC 7942 (Iwasaki et al., 2000). Hik8 is an ortholog of SasA in *Synechocystis* 6803 and *hik8* knockout or overexpression alters the gene expression and metabolite levels related to primary carbon metabolism (Singh and Sherman, 2005; Osanai et al., 2015). The involvement of Hik8 in primary metabolism is thus genetically demonstrated, but its involvement in photosynthetic electron transport has not been demonstrated. The expression patterns of photosynthetic genes exhibit circadian oscillation during day/night cycle (Kucho et al., 2005), indicating that photosynthetic electron transport is under the control of circadian-related proteins.

Here we report significant changes in the expression of genes related to photosynthetic electron transport as a result of *hik8* overexpression. Analyses of respiratory and photosynthetic activities and amino acid levels, show a histidine kinase-mediated regulation of photosynthetic electron transport and primary metabolism in this cyanobacterium.

MATERIALS AND METHODS

Bacterial Growth Conditions

A glucose-tolerant (GT) strain of *Synechocystis* sp. PCC 6803, isolated by Williams (1988), and the *hik8*-overexpressing strain, designated as HOX80 (Osanai et al., 2015), were grown in modified BG-11 medium (Rippka, 1988) containing 5 mM NH_4Cl (buffered with 20 mM HEPES-KOH, pH 7.8). The GT-I strain, among GT substrains, was used in this study (Kanesaki et al., 2012). Liquid cultures were bubbled with 1% (v/v) CO_2 in air and incubated at 30°C under continuous white light (ca. 50–70 μmol photons m^{-2} s^{-1}). For nitrogen starvation, cells grown in modified BG-11 were transferred into BG-11_0 medium (BG-11 medium without NH_4Cl) by filtration. Growth and cell densities were measured at OD_{730} with a Hitachi U-3310 spectrophotometer (Hitachi High-Tech., Tokyo, Japan).

Measurement of Respiratory and Photosynthetic Activities

Chlorophyll levels of cells grown under nitrogen-replete conditions were determined by a methanol extraction method (Grimme and Boardman, 1972; Iijima et al., 2015a). Cells containing 10 μg chlorophyll were resuspended in 1 mL BG-11_0 liquid medium, supplemented with or without 5 mM NH_4Cl, and incubated at 30°C within the chamber of an Oxytherm Clark-type oxygen electrode (Hansatech Instruments, King's Lynn, UK). Cells were incubated in dark conditions with monitoring of oxygen consumption for 10 min. The rate of oxygen consumption in the final 3 min of incubation was used to calculate respiration activity. Total oxygen evolution was measured after addition of 10 μL of 1 M $NaHCO_3$ and exposure to white light of 1050 μmol photons m^{-2} s^{-1}. The rate of oxygen evolution was calculated for the final 3 min of the 7-min measurement period.

Absorption Spectra with an End-on Type Spectrophotometer

Cells were cultivated in modified BG-11 medium for 1 day (started from $OD_{730} = 0.2$), collected by filtration, and then, re-suspended in BG-11_0 medium. Absorption spectra

were measured with an end-on type spectrophotometer MPS-2450 (Shimadzu, Kyoto, Japan). The data were normalized with $OD_{730} = 1.0$.

Chlorophyll Fluorescence

Chlorophyll fluorescence was measured with an AquaPen-C AP-C 100 fluorometer (Photon Systems Instruments, Drasov, Czech Republic). Chlorophyll levels of cells grown under nitrogen-replete and nitrogen-depleted conditions were determined and cells were diluted to 0.3 μg mL^{-1} chlorophyll *a* in 2 mL $BG\text{-}11_0$ medium supplemented with or without 5 mM NH_4Cl. Chlorophyll fluorescence was measured in accordance with the manufacturer's instructions (protocol NPQ1) after dark adaptation for 5 min. The intensity of actinic light and pulse-saturated light was 300 and 1500 μmol photons m^{-2} s^{-1}, respectively. The wavelength of actinic light and pulse-saturated light was 450 nm. The F_m value was obtained after addition of 10 μM DCMU. The values of the photosynthetic parameters were calculated as described previously (Campbell et al., 1998; Sonoike et al., 2001), except that far-red light was not used in the present experiment. The values of qP, qN, NPQ, and ΦII were calculated as $(F_m' - F_s)/(F_m' - F_o')$, $1 - [(F_m' - F_o')/(F_m - F_o)]$, $(F_m' - F_s)/F_m'$, and $(F_m - F_m')/F_m'$, respectively.

RNA Isolation and Quantitative Real-time PCR

RNA isolation was performed as described previously (Osanai et al., 2014). The cDNAs were synthesized with the SuperScript III First-Strand Synthesis System (Life Technologies Japan, Tokyo, Japan) with 2 μg total RNA. Quantitative real-time PCR was performed with the StepOnePlus Real-Time PCR System (Life Technologies Japan) in accordance with the manufacturer's instructions, using the primers listed in Table S1. The expression level of *rnpB*, which encodes RNaseP subunit B, was used as an internal standard.

Amino Acid Analysis by Gas Chromatography Mass Spectrometry (GC-MS)

Cells were cultivated in modified BG-11 medium for 1 day (starting from $OD_{730} = 0.2$), and equal amounts of cells (50 mL cell culture with $OD_{730} = 1.0$) were harvested by rapid filtration. Nitrogen-starved cells were similarly collected by filtration after 4 h of cultivation in $BG\text{-}11_0$ medium. Amino acids were quantified by GC-MS as previously described (Osanai et al., 2014). All the results are listed in Table S2.

RESULTS

Alteration of Oxygen Evolution and Consumption by *Hik8* Overexpression

To study the role of Hik8 in photosynthetic electron transport, respiratory and photosynthetic activities were measured. Previous studies showed that Hik8 regulates the expression of genes related to sugar catabolism and the nitrogen-induced sigma factor *sigE* (Singh and Sherman, 2005; Osanai et al., 2015), and sugar catabolism in *Synechocystis* 6803 is particularly altered by nitrogen status (Osanai et al., 2006). Thus, we chose both nitrogen-replete and nitrogen-depleted experimental conditions. Respiratory activities of GT and HOX80 under nitrogen-replete conditions were 18.6 and 12.5 μmol O_2 mg chla^{-1} h^{-1}, respectively, and thus, the respiratory activity of HOX80 was two-thirds of that in the GT strain (**Figure 1A**). The respiratory activity in GT increased by 1.3 times after 1 day of nitrogen depletion, whereas that in HOX80 increased by 2.1 times after 1 day of nitrogen depletion (**Figures 1A,B**). Photosynthetic activity was almost the same between GT and HOX80 under nitrogen-replete and nitrogen-depleted conditions for 1 day (**Figure 1B**). After 3 days of nitrogen depletion, respiratory, and photosynthetic activities in HOX80 were slightly higher and lower, respectively, than those in GT (**Figures 1A,B**). Changes in the color of the cultures during nitrogen starvation were similar between GT and HOX80. To confirm this, the absorption spectra were measured using an end-on type spectrophotometer. The transient increase and gradual decrease after prolonged nitrogen starvation in OD_{623} (which are the peaks representing phycobilisomes) were similar between GT and HOX80 (**Figure 1C**).

Chlorophyll fluorescence was subsequently measured to determine the values of the photosynthetic parameters. The values of *Fv*/*Fm* (the maximal photochemical efficiency of PSII), *Fv*′/*Fm*′ (the photochemical efficiency of open PSII centers), qP (photochemical quenching), and ΦII (the effective quantum yield of electron transport through PSII) were decreased by *hik8* overexpression under nitrogen-replete conditions (**Figure 2**). The values of *Fv*′/*Fm*′ and ΦII in HOX80 were also lower than in GT under nitrogen-depleted conditions for 1 day (**Figure 2**).

Alteration of the Expression of Genes Related to Electron Transport

Subsequently, the transcript levels of the genes related to electron transport were measured. The transcript levels of 15 out of 22 PSII genes increased as a result of *hik8* overexpression under nitrogen-replete conditions; this increase was statistically significant (**Figures 3**, **4**). The transcript levels of genes encoding the reactive center of PSII (*psbAII*, *psbB*, *psbC*, *psbD*, and *psbD2*) increased more than 1.6 times by *hik8* overexpression under nitrogen-replete conditions (**Figure 3**). After nitrogen depletion for 1 day, the expression of all the genes except *psbAII* and *psbD2* was repressed in both GT and HOX80, and their levels were similar between the two strains (**Figures 3**, **4**).

The transcript levels of 7 out of 12 PSI genes increased as a result of *hik8* overexpression under nitrogen-replete conditions (**Figure 5**). The expression of all PSI genes was down-regulated during nitrogen starvation, and their transcript levels were similar between GT and HOX80 (**Figure 5**).

The transcript analysis of five genes encoding the terminal cytochrome *c* oxidase showed that the transcript levels of *ctaCI*, *ctaDII*, and *ctaEII* increased by *hik8* overexpression under nitrogen-replete conditions, whereas the levels of *ctaEI* decreased (**Figure 6**). The expression of five cytochrome *c* oxidase genes was induced by nitrogen depletion, and the levels were similar between GT and HOX80 (**Figure 6**).

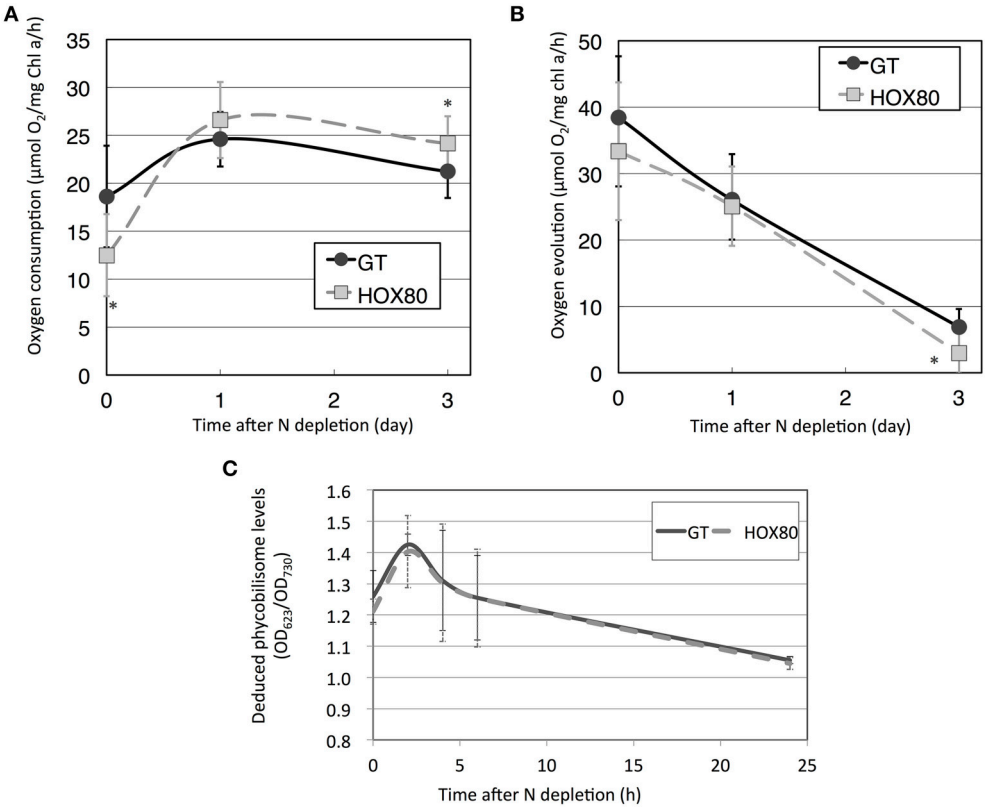

FIGURE 1 | Respiratory (A) and photosynthetic (B) activities of GT and *hik8*-overexpressing (HOX80) cells under nitrogen-replete and nitrogen-depleted conditions. Data are the mean ± SD from seven independent experiments. Differences between GT and *hik8*-overexpressing cells were analyzed with Student's *t*-test. Asterisks denote statistical significance at $^{*}P < 0.05$. **(C)** The levels of OD_{623}, representing absorption by phycobilisomes during nitrogen starvation. Data are the mean ± SD from eight independent experiments.

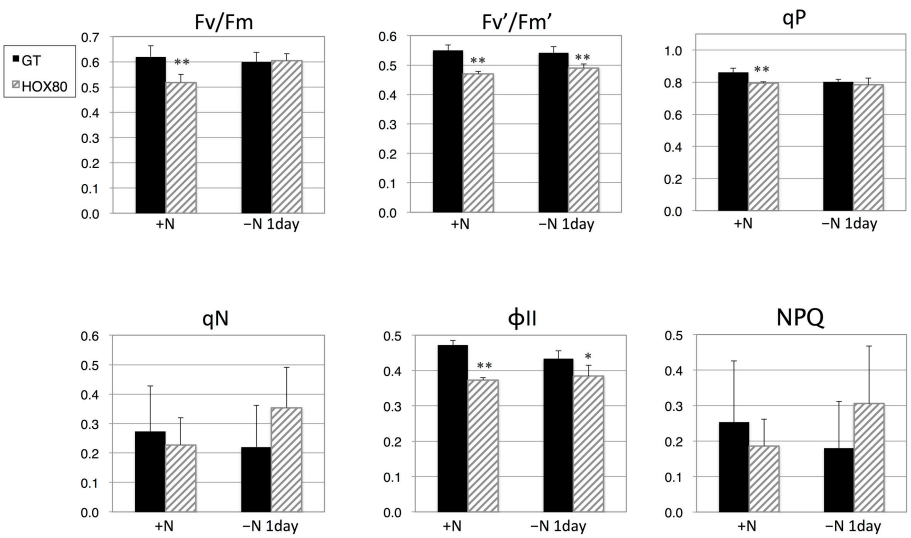

FIGURE 2 | Photosynthetic parameters for GT and *hik8*-overexpressing (HOX80) cells derived from chlorophyll fluorescence analysis. Data are the mean ± SD from five independent experiments. Differences between GT and *hik8*-overexpressing cells were analyzed with Student's *t*-test. Asterisks denote statistical significance at $^{*}P < 0.05$ and $^{**}P < 0.005$.

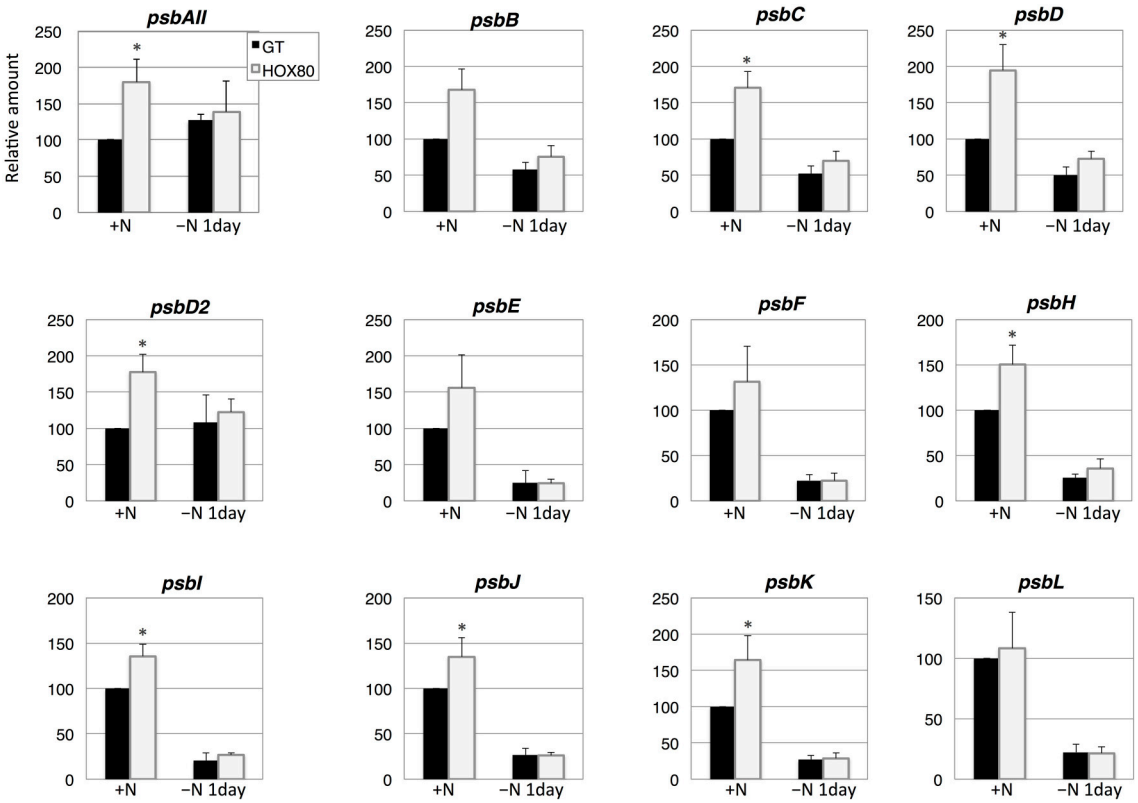

FIGURE 3 | Transcript levels of 12 genes encoding Photosystem II proteins in GT and *hik8*-overexpressing (HOX80) cells. Data are the mean ± SD from independent experiments ($n = 3$∼4). The levels were calibrated relative to the value obtained in the GT strain under nitrogen-replete conditions, which was set at 100%. Differences between GT and *hik8*-overexpressing cells were analyzed with Student's *t*-test. Asterisks denote statistical significance at $^*P < 0.05$.

Increase in Amino Acid Levels after Nitrogen Depletion was Abolished by *Hik8* Overexpression

Phycobilisome degradation during nitrogen-starved conditions is thought to provide amino acids as nitrogen sources (Richaud et al., 2001). The 18 amino acids, ornithine, and glutathione were quantified under nitrogen-replete and nitrogen-depleted conditions (**Figure 7**). The increases in valine, leucine, isoleucine, threonine, serine, phenylalanine, glutamine, and tyrosine by nitrogen depletion were abolished by *hik8* overexpression (**Figure 7**).

DISCUSSION

In this study, we examined the involvement of a histidine kinase Hik8 in photosynthetic electron transport, and our genetic analysis revealed that *hik8* overexpression modified the expression of PSII and PSI genes (**Figures 3–5**). Our analysis demonstrated that photosynthetic electron transport is regulated by a circadian-related protein in this cyanobacterium. Photosynthetic activity was partially decreased under nitrogen-depletion by *hik8* overexpression (**Figure 1B**), which is empirically consistent with a decrease in ΦII and Fv'/Fm' in HOX80 (**Figure 2**). Previous study has showed that overexpression of *sigE* accelerates sugar catabolism and decreases the values of ΦII and Fv'/Fm' (Osanai et al., 2013) and *hik8* overexpression activates sugar catabolism (Osanai et al., 2015). Thus, the degree of sugar catabolism and the values of ΦII and Fv'/Fm' may be negatively correlated in this cyanobacterium. The value of Fv/Fm also decreased by *hik8* overexpression (**Figure 2**), indicating HOX80 strain contains aberrant PSII complexes. The expression of PSII and PSI genes was up-regulated as a consequence of *hik8* overexpression (**Figures 3–5**), and thus, the proper amount of photosynthetic transcripts and/or proteins was important for the activity of oxygen evolution. RpaA is a probable cognate response regulator of Hik8 and inactivation of *rpaA* resulted in a decrease in the monomeric PSI and D1 protein levels (Majeed et al., 2012). Although the direct involvement of Hik8 in photosynthetic electron transport is unclear, RNA-seq analysis has demonstrated that RpaA does not bind with the promoters of photosynthetic genes (Markson et al., 2013), nevertheless RpaA is important in adaptation to changes in light conditions (Iijima et al., 2015b). We here genetically showed that Hik8 manipulates the expression of genes related to PSI, PSII, and cytochrome *c* oxidases.

Several groups have shown a transient increase in amino acid levels after nitrogen depletion in *Synechocystis* 6803

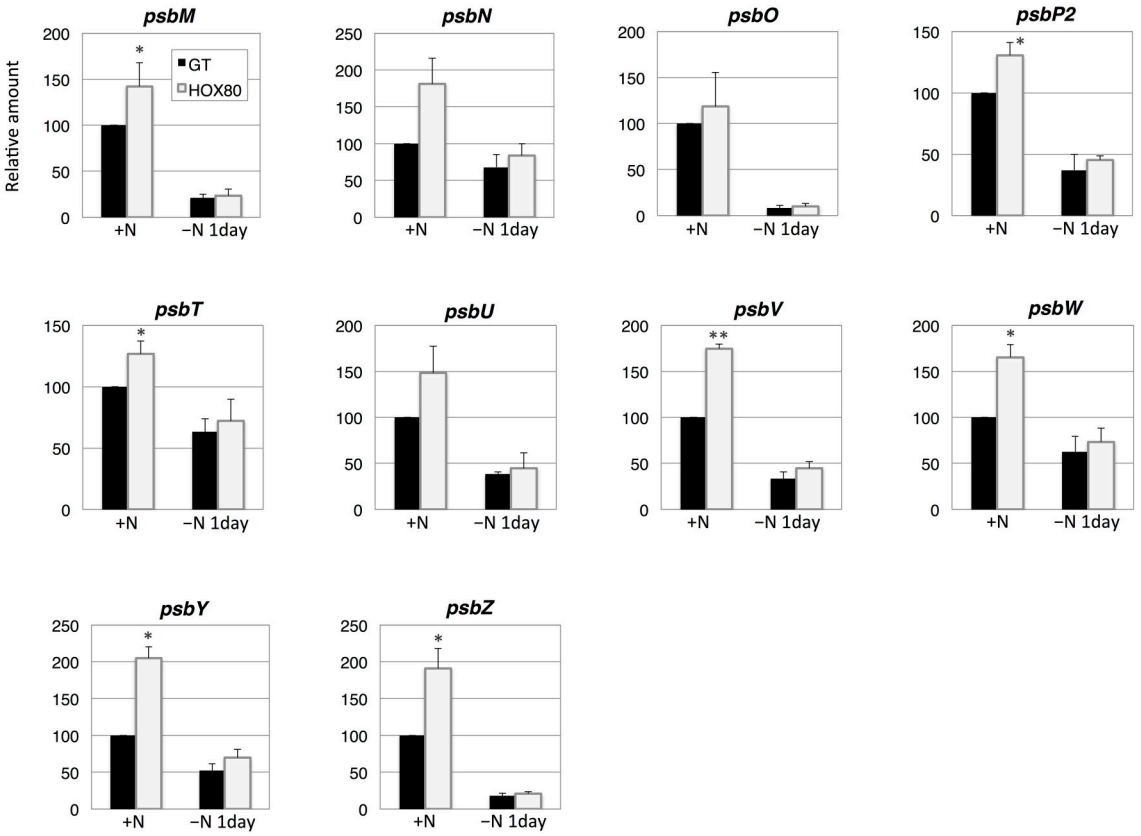

FIGURE 4 | Transcript levels of 10 genes encoding Photosystem II proteins in GT and *hik8*-overexpressing (HOX80) cells. Data are the mean ± SD from independent experiments ($n = 3$~4). The levels were calibrated relative to the value obtained in the GT strain under nitrogen-replete conditions, which was set at 100%. Differences between GT and *hik8*-overexpressing cells were analyzed with Student's *t*-test. Asterisks denote statistical significance at $^{*}P < 0.05$ and $^{**}P < 0.005$.

(Hauf et al., 2013; Kiyota et al., 2014; Osanai et al., 2014). Amino acids containing additional nitrogen molecules (glutamine, glutamate, aspartate, and asparagine) decreased after 4 h of nitrogen depletion, whereas other amino acids increased (Osanai et al., 2014). Kiyota et al. (2014) divided amino acids into two groups: NblA-dependent and NblA-independent amino acids. NblA is a protein essential for the degradation of phycobilisome in cyanobacteria (Collier and Grossman, 1994). The NblA-dependent amino acids are glutamine, glutamate, glutathione, glycine, isoleucine, leucine, methionine, phenylalanine, proline, serine, threonine, tyrosine, and valine, and the NblA-independent amino acids are alanine, asparagine, lysine, and tryptophan (Kiyota et al., 2014). All eight amino acids whose induction was modestly decreased during nitrogen starvation by *hik8* overexpression (valine, leucine, isoleucine, threonine, serine, phenylalanine, glutamine, and tyrosine) are included in the NblA-dependent group (**Figure 7**). Since the phycobilisome degradation was similar between GT and HOX80 (**Figure 1C**), the reason for the difference of the amino acid levels between GT and HOX80 after nitrogen depletion was unclear. The interaction of photosynthetic electron transport and amino acid metabolism offers intriguing insights into the mechanisms of cell maintenance in cyanobacteria, and we suggest, from this study, that a circadian-related protein is important for this integrity. In this study, we found the metabolite levels and photosynthetic electron transport concomitantly altered in HOX80.

The regulation of photosynthetic genes by a histidine kinase named CSK has been demonstrated in *Arabidopsis thaliana* (Puthiyaveetil et al., 2010). CSK regulates the activity of bacteria-type RNA polymerase through control of the phosphorylation of sigma factor Sig1 (Puthiyaveetil et al., 2010). *Synechocystis* 6803 possesses multiple sigma factors, SigA–SigI (Osanai et al., 2008), and light-induced *psbAII*/*AIII* gene expression is reduced by *sigD* knockout (Imamura et al., 2003, 2004). Microarray experiments also indicate the involvement of SigD in the expression of photosynthetic genes (Summerfield and Sherman, 2007). Photosynthetic oxygen evolution is not affected by single or double knockout of group-2 sigma factors, but the double knockout of *sigB*/*sigD* leads to sensitivity to photoinhibition because of abolished up-regulation of *psbA* expression (Pollari et al., 2008, 2009, 2011). We previously showed that Hik8 positively regulates sigma factor SigE, and genetic modification of *sigE* alters photosynthetic electron transport (Osanai et al., 2013, 2015). In this way, regulation of photosynthesis by combinations of histidine kinases and sigma factors is conserved in both

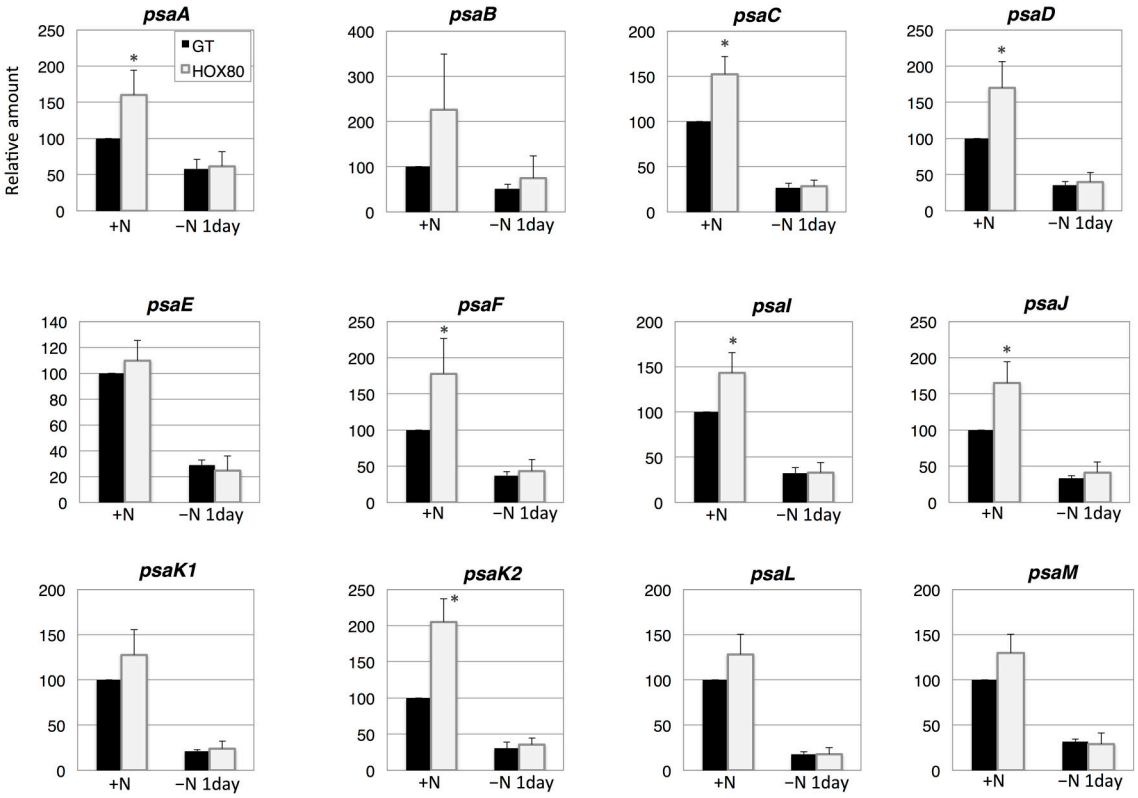

FIGURE 5 | Transcript levels of 12 genes encoding Photosystem I proteins in GT and *hik8*-overexpressing (HOX80) cells. Data are the mean ± SD from independent experiments ($n = 3$∼4). The levels were calibrated relative to the value obtained in the GT strain under nitrogen-replete conditions, which was set at 100%. Differences between GT and *hik8*-overexpressing cells were analyzed with Student's *t*-test. Asterisks denote statistical significance at $^*P < 0.05$.

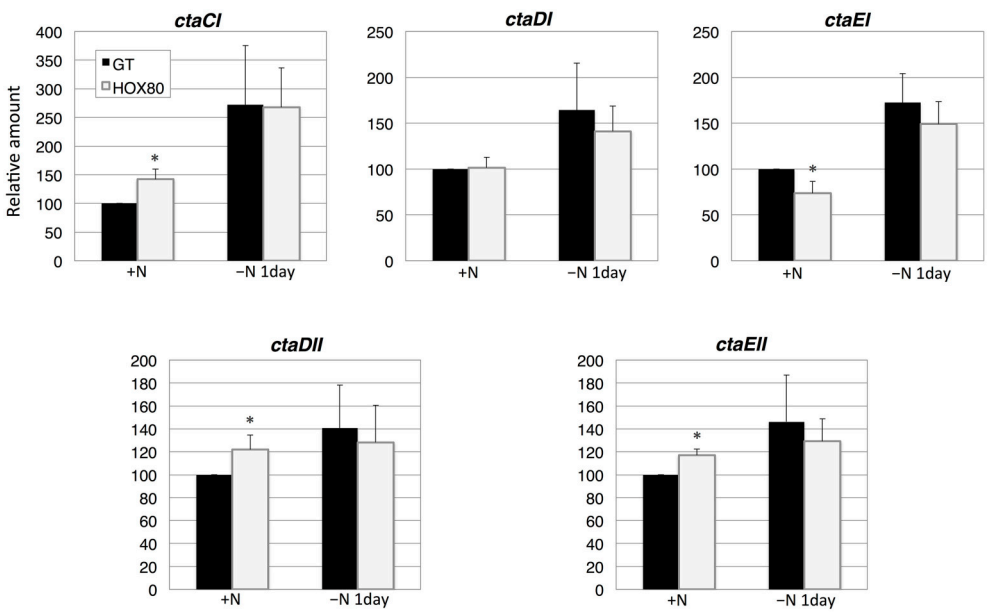

FIGURE 6 | Transcript levels of five genes encoding cytochrome *c* oxidase proteins in GT and *hik8*-overexpressing (HOX80) cells. Data are the mean ± SD from independent experiments ($n = 3$∼4). The levels were calibrated relative to the value obtained in the GT strain under nitrogen-replete conditions, which was set at 100%. Differences between GT and *hik8*-overexpressing cells were analyzed with Student's *t*-test. Asterisks denote statistical significance at $^*P < 0.05$.

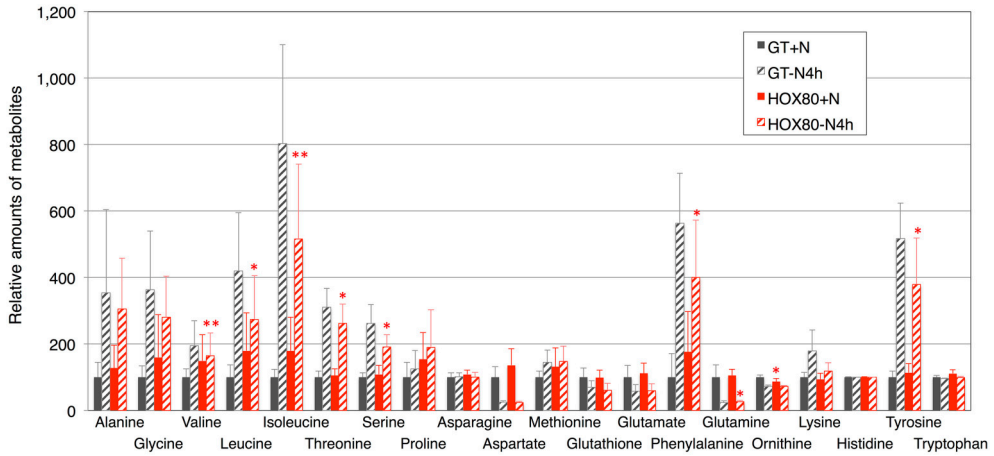

FIGURE 7 | Levels of 18 amino acids, ornithine, and glutathione. Data represent means ± SD from four independent experiments. Levels were calibrated relative to that in GT grown under nitrogen-replete conditions (set at 100%). Asterisks indicate statistically significant differences between GT and HOX80 (Student's *t*-test; $^{*}P < 0.05$, $^{**}P < 0.005$).

prokaryotic and eukaryotic photosynthetic organisms. Detailed analysis of the mechanisms controlling photosynthetic electron transport through transcriptional cascades is important, and it may also lead to an understanding of the regulatory mechanisms of primary metabolism in cyanobacteria.

ACKNOWLEDGMENTS

This work was supported by the Ministry of Education, Culture, Sports, Science, and Technology, Japan, through a grant to TO from CREST from the Japan Science and Technology Agency and ALCA from the Japan Science and Technology Agency (project name "Production of cyanobacterial succinate by the genetic engineering of transcriptional regulators and circadian clocks"). All authors contributed to the work and approved the submission of the manuscript.

SUPPLEMENTARY MATERIAL

The Supplementary Material for this article can be found online at: http://journal.frontiersin.org/article/10.3389/fmicb.2015.01150

REFERENCES

Amunts, A., and Nelson, N. (2009). Plant photosystem I design in the light of evolution. *Structure* 17, 637–650. doi: 10.1016/j.str.2009.03.006

Barber, J. (2014). Photosystem II: its function, structure, and implications for artificial photosynthesis. *Biochemistry* 79, 185–196. doi: 10.1134/s0006297914030031

Campbell, D., Hurry, V., Clarke, A. K., Gustafsson, P., and Oquist, G. (1998). Chlorophyll fluorescence analysis of cyanobacterial photosynthesis and acclimation. *Microbiol. Mol. Biol. Rev.* 62, 667–683.

Collier, J. L., and Grossman, A. R. (1994). A small polypeptide triggers complete degradation of light-harvesting phycobiliproteins in nutrient-deprived cyanobacteria. *EMBO J.* 13, 1039–1047.

Görl, M., Sauer, J., Baier, T., and Forchhammer, K. (1998). Nitrogen-starvation-induced chlorosis in *Synechococcus* PCC 7942: adaptation to long-term survival. *Microbiology* 144, 2449–2458. doi: 10.1099/00221287-144-9-2449

Grimme, L. H., and Boardman, N. K. (1972). Photochemical activities of a particle fraction P 1 obtained from the green alga *Chlorella fusca*. *Biochem. Biophys. Res. Commun.* 49, 1617–1623. doi: 10.1016/0006-291X(72)90527-X

Hauf, W., Schlebusch, M., Hüge, J., Kopka, J., Hagemann, M., and Forchhammer, K. (2013). Metabolic changes in *Synechocystis* PCC6803 upon nitrogen-starvation: excess NADPH sustains polyhydroxybutyrate accumulation. *Metabolites* 3, 101–118. doi: 10.3390/metabo3010101

Iijima, H., Nakaya, Y., Kuwahara, A., Hirai, M. Y., and Osanai, T. (2015a). Seawater cultivation of freshwater cyanobacterium *Synechocystis* sp. PCC 6803 drastically alters amino acid composition and glycogen metabolism. *Front. Microbiol.* 6:326. doi: 10.3389/fmicb.2015.00326

Iijima, H., Shirai, T., Okamoto, M., Kondo, A., Hirai, M. Y., and Osanai, T. (2015b). Changes in primary metabolism under light and dark conditions in response to overproduction of a response regulator RpaA in the unicellular cyanobacterium *Synechocystis* sp. PCC 6803. *Front. Microbiol.* 6:888. doi: 10.3389/fmicb.2015.00888

Ikeuchi, M., and Tabata, S. (2001). *Synechocystis* sp. PCC 6803—a useful tool in the study of the genetics of cyanobacteria. *Photosynth. Res.* 70, 73–83. doi: 10.1023/A:1013887908680

Imamura, S., Asayama, M., and Shirai, M. (2004). *In vitro* transcription analysis by reconstituted cyanobacterial RNA polymerase: roles of group 1 and 2 sigma factors and a core subunit, RpoC2. *Genes Cells* 9, 1175–1187. doi: 10.1111/j.1365-2443.2004.00808.x

Imamura, S., Asayama, M., Takahashi, H., Tanaka, K., Takahashi, H., and Shirai, M. (2003). Antagonistic dark/light-induced SigB/SigD, group 2 sigma factors, expression through redox potential and their roles in cyanobacteria. *FEBS Lett.* 554, 357–362. doi: 10.1016/S0014-5793(03)01188-8

Ishiura, M., Kutsuna, S., Aoki, S., Iwasaki, H., Andersson, C. R., Tanabe, A., et al. (1998). Expression of a gene cluster *kaiABC* as a circadian feedback process in cyanobacteria. *Science* 281, 1519–1523. doi: 10.1126/science.281.5382.1519

Iwasaki, H., Williams, S. B., Kitayama, Y., Ishiura, M., Golden, S. S., and Kondo, T. (2000). A *kaiC*-interacting sensory histidine kinase, SasA, necessary to sustain robust circadian oscillation in cyanobacteria. *Cell* 101, 223–233. doi: 10.1016/S0092-8674(00)80832-6

Jordan, P., Fromme, P., Witt, H. T., Klukas, O., Saenger, W., and Krauss, N. (2001). Three-dimensional structure of cyanobacterial photosystem I at 2.5 Å resolution. *Nature* 411, 909–917. doi: 10.1038/35082000

Kanesaki, Y., Shiwa, Y., Tajima, N., Suzuki, M., Watanabe, S., Sato, N., et al. (2012). Identification of substrain-specific mutations by massively parallel whole-genome resequencing of *Synechocystis* sp. PCC 6803. *DNA Res.* 19, 67–79. doi: 10.1093/dnares/dsr042

Kappell, A. D., and van Waasbergen, L. G. (2007). The response regulator RpaB binds the high light regulatory 1 sequence upstream of the high-light inducible *hliB* gene from the cyanobacterium *Synechocystis* PCC 6803. *Arch. Microbiol.* 187, 337–342. doi: 10.1007/s00203-007-0213-1

Karapetyan, N. V., Bolychevtseva, Y. V., Yurina, N. P., Terekhova, I. V., Shubin, V. V., and Brecht, M. (2014). Long-wavelength chlorophylls in Photosystem I of cyanobacteria: origin, localization, and functions. *Biochemistry* 79, 213–220. doi: 10.1134/s0006297914030067

Kiyota, H., Hirai, M. Y., and Ikeuchi, M. (2014). NblA1/A2-dependent homeostasis of amino acid pools during nitrogen starvation in *Synechocystis* sp. PCC 6803. *Metabolites* 4, 517–531. doi: 10.3390/metabo4030517

Kojima, K., Motohashi, K., Morota, T., Oshita, M., Hisabori, T., Hayashi, H., et al. (2009). Regulation of translation by the redox state of elongation factor G in the cyanobacterium *Synechocystis* sp. PCC 6803. *J. Biol. Chem.* 284, 18685–18691. doi: 10.1074/jbc.M109.015131

Kucho, K., Okamoto, K., Tsuchiya, Y., Nomura, S., Nango, M., Kanehisa, M., et al. (2005). Global analysis of circadian expression in the cyanobacterium *Synechocystis* sp. strain PCC 6803. *J. Bacteriol.* 187, 2190–2199. doi: 10.1128/JB.187.6.2190-2199.2005

Majeed, W., Zhang, Y., Xue, Y., Ranade, S., Blue, R. N., Wang, Q., et al. (2012). RpaA regulates the accumulation of monomeric photosystem I and PsbA under high light conditions in *Synechocystis* sp. PCC 6803. *PLoS ONE* 7:e45139. doi: 10.1371/journal.pone.0045139

Markson, J. S., Piechura, J. R., Puszynska, A. M., and O'Shea, E. K. (2013). Circadian control of global gene expression by the cyanobacterial master regulator RpaA. *Cell* 155, 1396–1408. doi: 10.1016/j.cell.2013.11.005

Mulo, P., Sicora, C., and Aro, E.-M. (2009). Cyanobacterial *psbA* gene family: optimization of oxygenic photosynthesis. *Cell Mol. Life Sci.* 66, 3697–3170. doi: 10.1007/s00018-009-0103-6

Murakami, A., and Fujita, Y. (1991). Regulation of photosystem stoichiometry in the photosynthetic system of the cyanophyte *Synechocystis* PCC 6714 in response to light-intensity. *Plant Cell Physiol.* 32, 223–230.

Nakajima, M., Imai, K., Ito, H., Nishiwaki, T., Murayama, Y., Iwasaki, H., et al. (2005). Reconstitution of circadian oscillation of cyanobacterial KaiC phosphorylation *in vitro*. *Science* 308, 414–415. doi: 10.1126/science.1108451

Nixon, P. J., Michoux, F., Yu, J., Boehm, M., and Komenda, J. (2010). Recent advances in understanding the assembly and repair of photosystem II. *Ann. Bot.* 106, 1–16. doi: 10.1093/aob/mcq059

Osanai, T., Ikeuchi, M., and Tanaka, K. (2008). Group 2 sigma factors in cyanobacteria. *Physiol. Plant.* 133, 490–506. doi: 10.1111/j.1399-3054.2008.01078.x

Osanai, T., Imamura, S., Asayama, M., Shirai, M., Suzuki, I., Murata, N., et al. (2006). Nitrogen induction of sugar catabolic gene expression in *Synechocystis* sp. PCC 6803. *DNA Res.* 13, 185–195. doi: 10.1093/dnares/dsl010

Osanai, T., Kuwahara, A., Iijima, H., Toyooka, K., Sato, M., Tanaka, K., et al. (2013). Pleiotropic effect of *sigE* over-expression on cell morphology, photosynthesis and hydrogen production in *Synechocystis* sp. PCC 6803. *Plant J.* 76, 456–465. doi: 10.1111/tpj.12310

Osanai, T., Oikawa, A., Azuma, M., Tanaka, K., Saito, K., Hirai, M. Y., et al. (2011). Genetic engineering of group 2 sigma factor SigE widely activates expressions of sugar catabolic genes in *Synechocystis* species PCC 6803. *J. Biol. Chem.* 286, 30962–30971. doi: 10.1074/jbc.M111.231183

Osanai, T., Oikawa, A., Shirai, T., Kuwahara, A., Iijima, H., Tanaka, K., et al. (2014). Capillary electrophoresis-mass spectrometry reveals the distribution of carbon metabolites during nitrogen starvation in *Synechocystis* sp. PCC 6803. *Environ. Microbiol.* 16, 512–524. doi: 10.1111/1462-2920.12170

Osanai, T., Shirai, T., Iijima, H., Kuwahara, A., Suzuki, I., Kondo, A., et al. (2015). Alteration of cyanobacterial sugar and amino acid metabolism by overexpression *hik8*, encoding a KaiC-associated histidine kinase. *Environ. Microbiol.* 17, 2430–2440. doi: 10.1111/1462-2920.12715

Pollari, M., Gunnelius, L., Tuominen, I., Ruotsalainen, V., Tyystjärvi, E., Salminen, T., et al. (2008). Characterization of single and double inactivation strains reveals new physiological roles for group 2 sigma factors in the cyanobacterium *Synechocystis* sp. PCC 6803. *Plant Physiol.* 147, 1994–2005. doi: 10.1104/pp.108.122713

Pollari, M., Rantamäki, S., Huokko, T., Kårlund-Marttila, A., Tyystjärvi, E., and Tyystjärvi, T. (2011). Effects of deficiency and overdose of group 2 sigma factors in triple inactivation strains of *Synechocystis* sp. strain PCC 6803. *J. Bacteriol.* 193, 265–273. doi: 10.1128/JB.01045-10

Pollari, M., Ruotsalainen, V., Rantamäki, S., Tyystjärvi, E., and Tyystjärvi, T. (2009). Simultaneous inactivation of sigma factors B and D interferes with light acclimation of the cyanobacterium *Synechocystis* sp. strain PCC 6803. *J. Bacteriol.* 191, 3992–4001. doi: 10.1128/JB.00132-09

Puthiyaveetil, S., Ibrahim, I. M., Jelicić, B., Tomasić, A., Fulgosi, H., and Allen, J. F. (2010). Transcriptional control of photosynthesis genes: the evolutionarily conserved regulatory mechanism in plastid genome function. *Genome Biol. Evol.* 2, 888–896. doi: 10.1093/gbe/evq073

Richaud, C., Zabulon, G., Joder, A., and Thomas, J.-C. (2001). Nitrogen or sulfur starvation differentially affects phycobilisome degradation and expression of the *nblA* gene in *Synechocystis* strain PCC 6803. *J. Bacteriol.* 183, 2989–2994. doi: 10.1128/JB.183.10.2989-2994.2001

Rippka, R. (1988). Isolation and purification of cyanobacteria. *Methods Enzymol.* 167, 3–27. doi: 10.1016/0076-6879(88)67004-2

Seino, Y., Takahashi, T., and Hihara, Y. (2009). The response regulator RpaB binds to the upstream element of Photosystem I genes to work positive regulation under low-light conditions in *Synechocystis* sp. strain PCC 6803. *J. Bacteriol.* 191, 1581–1586. doi: 10.1128/JB.01588-08

Seki, A., Hanaoka, M., Akimoto, Y., Masuda, S., Iwasaki, H., and Tanaka, K. (2007). Induction of a group 2 sigma factor, RPOD3, by high light and the underlying mechanism in *Synechococcus elongatus* PCC 7942. *J. Biol. Chem.* 282, 36887–36894. doi: 10.1074/jbc.M707582200

Silva, P., Thompson, E., Bailey, S., Kruse, O., Mullineaux, C. W., Robinson, C., et al. (2003). FtsH is involved in the early stages of repair of Photosystem II in *Synechocystis* sp. PCC 6803. *Plant Cell* 15, 2152–2164. doi: 10.1105/tpc.012609

Singh, A. K., and Sherman, L. A. (2005). Pleiotropic effect of a histidine kinase on carbohydrate metabolism in *Synechocystis* sp. strain PCC 6803 and its requirement for heterotrophic growth. *J. Bacteriol.* 187, 2368–2376. doi: 10.1128/JB.187.7.2368-2376.2005

Sonoike, K., Hihara, Y., and Ikeuchi, M. (2001). Physiological significance of the regulation of photosystem stoichiometry upon high light acclimation of *Synechocystis* sp. PCC 6803. *Plant Cell Physiol.* 42, 379–384. doi: 10.1093/pcp/pce046

Summerfield, T. C., and Sherman, L. A. (2007). Role of sigma factors in controlling global gene expression in light/dark transitions in the cyanobacterium *Synechocystis* sp. strain PCC 6803. *J. Bacteriol.* 189, 7829–7840. doi: 10.1128/JB.01036-07

Umena, Y., Kawakami, K., Shen, J. R., and Kamiya, N. (2011). Crystal structure of oxygen-evolving photosystem II at a resolution of 1.9 Å. *Nature* 473, 55–60. doi: 10.1038/nature09913

Williams, J. G. K. (1988). Construction of specific mutations in photosystem II photosynthetic reaction center by genetic engineering methods in *Synechocystis* 6803. *Methods Enzymol.* 167, 766–778. doi: 10.1016/0076-6879(88)67088-1

Conflict of Interest Statement: The authors declare that the research was conducted in the absence of any commercial or financial relationships that could be construed as a potential conflict of interest.

frontiers in Microbiology

ORIGINAL RESEARCH
published: 06 October 2015
doi: 10.3389/fmicb.2015.01064

Genetic manipulation of a metabolic enzyme and a transcriptional regulator increasing succinate excretion from unicellular cyanobacterium

Takashi Osanai[1,2], Tomokazu Shirai[3], Hiroko Iijima[1,2], Yuka Nakaya[1,3], Mami Okamoto[3], Akihiko Kondo[3,4] and Masami Y. Hirai[1]**

[1] RIKEN Center for Sustainable Resource Science, Yokohama, Japan, [2] Department of Agricultural Chemistry, School of Agriculture, Meiji University, Kawasaki, Japan, [3] Biomass Engineering Program, RIKEN, Yokohama, Japan, [4] Department of Chemical Science and Engineering, Graduate School of Engineering, Kobe University, Kobe, Japan

OPEN ACCESS

Edited by:
Weiwen Zhang, Tianjin University, China

Reviewed by:
Jiangxin Wang, Shenzhen University, China
Min Chen, University of Sydney, Australia

***Correspondence:**
Takashi Osanai, Department of Agricultural Chemistry, School of Agriculture, Meiji University, 1-1-1 Higashimita, Tama-ku, Kawasaki, Kanagawa 214-8571, Japan
tosanai@meiji.ac.jp
Masami Y. Hirai, RIKEN Center for Sustainable Resource Science, 1-7-22 Suehiro-cho, Tsurumi-ku, Yokohama, Kanagawa 230-0045, Japan
masami.hirai@riken.jp

Specialty section:
This article was submitted to Microbial Physiology and Metabolism, a section of the journal Frontiers in Microbiology

Received: *21 August 2015*
Accepted: *15 September 2015*
Published: *06 October 2015*

Citation:
Osanai T, Shirai T, Iijima H, Nakaya Y, Okamoto M, Kondo A and Hirai MY (2015) Genetic manipulation of a metabolic enzyme and a transcriptional regulator increasing succinate excretion from unicellular cyanobacterium. Front. Microbiol. 6:1064. doi: 10.3389/fmicb.2015.01064

Succinate is a building block compound that the U.S. Department of Energy (DOE) has declared as important in biorefineries, and it is widely used as a commodity chemical. Here, we identified the two genes increasing succinate production of the unicellular cyanobacterium *Synechocystis* sp. PCC 6803. Succinate was excreted under dark, anaerobic conditions, and its production level increased by knocking out *ackA*, which encodes an acetate kinase, and by overexpressing *sigE*, which encodes an RNA polymerase sigma factor. Glycogen catabolism and organic acid biosynthesis were enhanced in the mutant lacking *ackA* and overexpressing *sigE*, leading to an increase in succinate production reaching five times of the wild-type levels. Our genetic and metabolomic analyses thus demonstrated the effect of genetic manipulation of a metabolic enzyme and a transcriptional regulator on succinate excretion from this cyanobacterium with the data based on metabolomic technique.

Keywords: cyanobacteria, metabolism, metabolomics, sigma factor, succinate

Introduction

In 2004, the U.S. Department of Energy (DOE) selected the top 12 building block chemicals from a list of more than 300 candidates that were produced from biomass (Werpy and Petersen, 2004). Among these, four-carbon dicarboxylic acids, including succinate, were included. Succinate can be used as a precursor to numerous chemicals such as a biodegradable plastic like polybutylene succinate, fibers, and pigments (Zeikus et al., 1999; Hong and Lee, 2002; Werpy and Petersen, 2004). Succinate is currently derived from petroleum, but it could also be produced using bacteria (McKinlay et al., 2007).

Production of succinate by recombinant heterotrophic bacteria such as *Escherichia coli, Corynebacterium glutamicum, Anaerobiospirillum succiniciproducens, Actinobacillus succinogenes,* and *Mannheimia succiniciproducens* has been intensively studied (Samuelov et al., 1991; Guettler et al., 1999; Chatterjee et al., 2001; Hong and Lee, 2001; Hong et al., 2004; Lee et al., 2006). Succinate is an intermediate in the tricarboxylic acid (TCA) cycle and is excreted by succinate-producing cells during anaerobic fermentation (McKinlay et al., 2007). Succinate is produced from

phosphoenolpyruvate via the reductive branch of the TCA cycle, in which phosphoenolpyruvate is converted to oxaloacetate by phosphoenolpyruvate carboxylase (PEPC) or phosphoenolpyruvate carboxykinase (PEPCK) under anaerobic conditions (McKinlay et al., 2007). Malate is produced from oxaloacetate when catalyzed by malate dehydrogenase, and fumarate is produced from malate when catalyzed by fumarase. This is followed by the production of succinate when catalyzed by succinate dehydrogenase (SDH; McKinlay et al., 2007). The overexpression of a gene encoding PEPC in *E. coli* increases succinate production 3.8-fold (Millard et al., 1996). The introduction of PEPC, PEPCK, or malic enzyme (catalyzing a reaction from pyruvate to malate), also enhances succinate production in *E. coli* (Hong and Lee, 2001; Kim et al., 2004; Lin et al., 2005; Zhang et al., 2009). The deletion of *ldhA* (encoding L-lactate dehydrogenase), *adhE* (encoding alcohol dehydrogenase), and *ack-pta* (encoding acetate kinase and phosphotransacetylase, respectively) prevented the production of L-lactate, ethanol, and acetate, that are by-products during anaerobic fermentation, also increases the production of succinate in *E. coli* (Sánchez et al., 2005a,b; Jantama et al., 2007). In addition, the activation of the glyoxylate pathway by the deletion of iclR, which encodes the transcriptional repressor of the genes related to glyoxylate pathway, increased the succinate productivity in *E. coli* (Sánchez et al., 2005a,b). Thus, inhibition of by-product formation combined with additional genetic engineering can up-regulate succinate productivity.

Cyanobacteria are a group of bacteria that fix carbon dioxide via oxygenic photosynthesis. The potential applications of cyanobacteria in providing renewable energy and resources may reduce the environmental burden. Genome information for cyanobacteria is available (Kanesaki et al., 2012), and genetic engineering is easily performed by homologous recombination in several cyanobacterial strains, including the non-nitrogen fixing cyanobacterium *Synechocystis* sp. PCC 6803 (hereafter *Synechocystis* 6803; Ikeuchi and Tabata, 2001). The genome of *Synechocystis* 6803 was the first sequenced among the cyanobacteria (Kaneko et al., 1996), and it has been used extensively in basic and applied sciences.

There are few reports of succinate production using cyanobacteria. McNeely et al. revealed that five fermentation products, lactate, acetate, succinate, alanine, and hydrogen, were produced under dark, anaerobic conditions by the marine cyanobacterium *Synechococcus* sp. PCC 7002 (hereafter *Synechococcus* 7002; McNeely et al., 2010). A knockout of *ldhA* increased acetate and hydrogen levels, and diminished lactate production (McNeely et al., 2010). Succinate was excreted from the *ldhA* knockout cells, but it was not detected from the wild-type cells of *Synechococcus* 7002 (McNeely et al., 2010). The filamentous, non-diazotrophic cyanobacteria *Arthrospira*

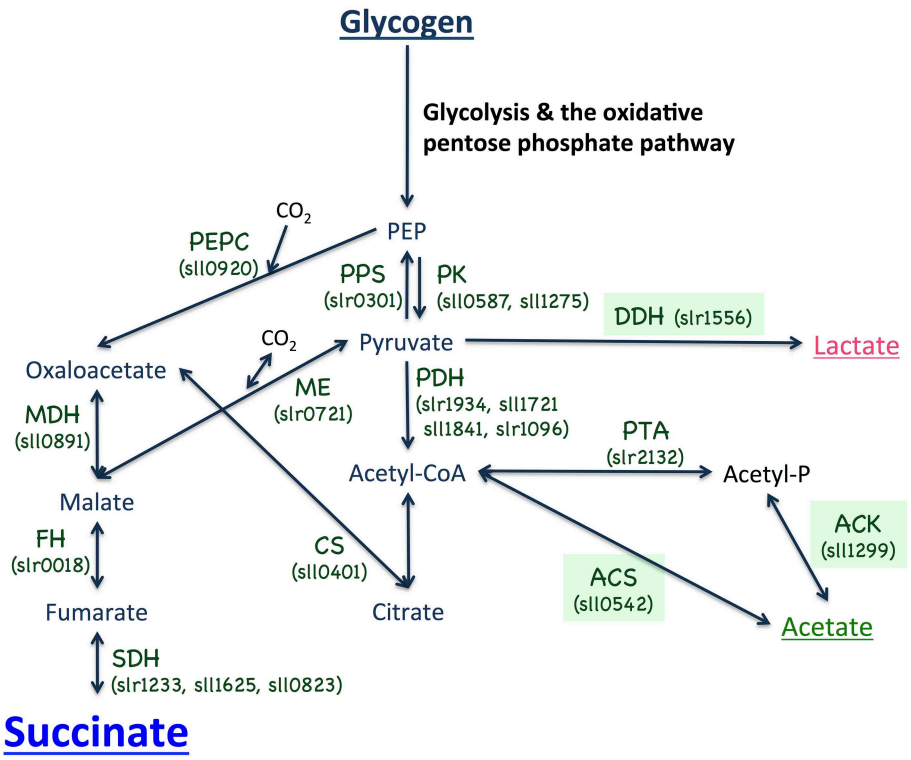

FIGURE 1 | Metabolic map surrounding succinate biosynthesis in the cyanobacterium *Synechocystis* sp. PCC 6803. PEP, phosphoenolpyruvate; PEPC, phosphoenolpyruvate carboxylase; PPS, phosphoenolpyruvate synthase; PK, pyruvate kinase; MDH, malate dehydrogenase; ME, malic enzyme; FH, fumarate hydratase; SDH, succinate dehydrogenase; PDH, pyruvate dehydrogenase; DDH, D-lactate dehydrogenase, CS, citrate synthase; PTA, phosphotransacetylase; ACK, acetate kinase; and ACS, acetyl-CoA synthetase.

maxima CS-328 cells produced lactate, acetate, ethanol, formate, and hydrogen under dark, anaerobic conditions, but succinate excretion was not detected (Carrieri et al., 2010, 2011). For *Synechocystis* 6803, hydrogen is generated under both light and dark, anaerobic conditions (Osanai et al., 2013). Organic acids, including D-lactates, were highly produced by genetically engineered *Synechocystis* 6803 cells, and succinate was also generated but its levels were only 3% of total carbon excreted, suggesting that genetic and metabolic engineering are necessary to increase succinate production (Angermayr et al., 2014; Hollinshead et al., 2014; McNeely et al., 2014). The genes encoding enzymes for organic acid production exist in the *Synechocystis* 6803 genome (**Figure 1**).

We reveal here that succinate was excreted from *Synechocystis* 6803 cells under dark, anaerobic conditions and the succinate levels were enhanced by reducing acetate biosynthesis and overexpressing *sigE* encoding a sigma factor. These results demonstrated the genetic manipulation of two types of genes increasing the succinate excretion from this cyanobacterium.

Materials and Methods

Bacterial Strains and Culture Conditions

The glucose-tolerant strain of *Synechocystis* sp. PCC 6803, isolated by Williams (Williams, 1988), was grown in modified BG-11 medium, consisting of BG-11_0 liquid medium (Rippka, 1988) supplemented with 5 mM NH_4Cl (buffered with 20 mM HEPES–KOH, pH 7.8). The GT-I strain, among GT substrains, was used in the current study (Kanesaki et al., 2012). Liquid cultures were bubbled with 1% (v/v) CO_2 in air and incubated at 30°C under continuous white light (∼50–70 μmol photons m^{-2} s^{-1}). For the mutant strains, 10, 0.3, and 10 μg/mL of kanamycin, gentamycin and chloramphenicol, respectively, were added for preculturing. Modified BG-11 medium (containing 10 mM NH_4Cl in liquid medium) was solidified with agar (1.5% w/v) for plate cultures, and similarly incubated in air at 30°C under continuous white light (∼50–70 μmol photons m^{-2} s^{-1}). Cell densities were measured at A_{730} using a Hitachi U-3310 spectrophotometer (Hitachi High-Tech., Tokyo, Japan).

For succinate production, cells grown in 70 mL modified BG-11 medium (started from A_{730} = 0.4) for 3 days were concentrated into 10 mL HEPES buffer (20 mM HEPES–KOH, pH 7.8) or modified BG-11 medium to A_{730} = 20 in a GC vial. The vial was sealed using butyl rubber, and N_2 gas was introduced using syringes for 1 h to produce anaerobic conditions. After removing the syringes, the vial was wrapped with aluminum foil and shaken at 30°C. Cell cultures were then centrifuged at 5800 × *g* for 2 min, the supernatant was filtrated, and 1 mL supernatant was freeze-dried for 1 day. The dried sample was used for high-performance liquid chromatography analysis.

Plasmid Construction of Knock-in Vectors pTCP1556, pTCP0542, and pTCP1299

The kanamycin resistance cassette of the pTKP2031V vector (Osanai et al., 2011) was removed by digestion with *Xho*I and *Aat*II (Takara Bio, Shiga, Japan). The chloramphenicol resistance cassette from pKRP10 (Reece and Phillips, 1995) was amplified by PCR with KOD polymerase (Toyobo, Osaka, Japan) and the specific primers in Table S2, digested with *Xho*I and *Aat*II, and inserted into the *Xho*I-*Aat*II sites of pTKP2031V. The resultant plasmid was named pTCP2031. Regions of *ddh* (slr1556), from −297 to +800 bp, *acs* (sll0542), from +921

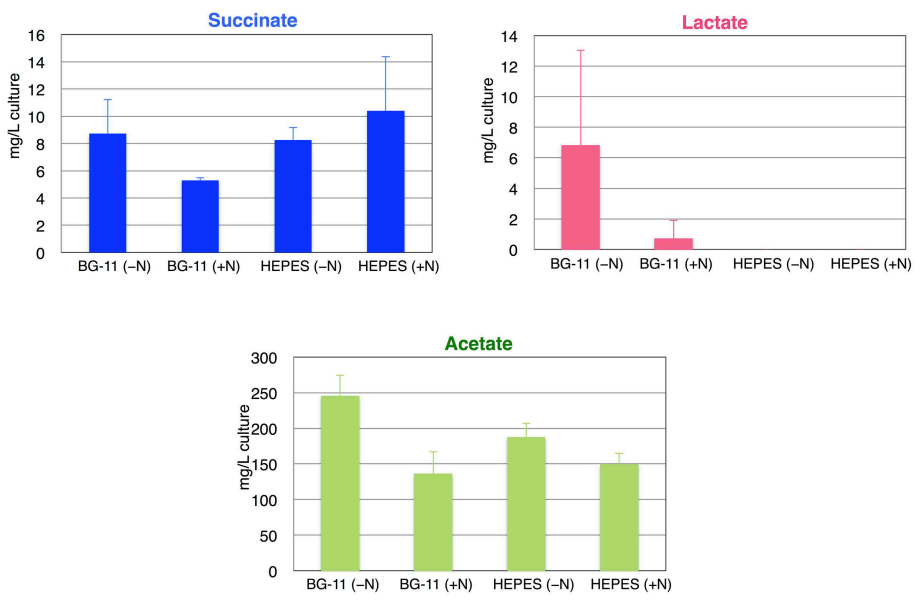

FIGURE 2 | Levels of succinate, lactate, and acetate from the wild-type cyanobacterium *Synechocystis* 6803 using different media or buffers during anaerobic conditions. Organic acids excreted from 3 days under dark, anaerobic cultivation were quantified by HPLC. Data represent means ± SD from three independent experiments. +N designates 5 mM NH_4Cl was added to the BG-11 medium or 20 mM HEPES–KOH (pH 7.8) buffer.

to +1962 bp, and *ackA* (sll1299), from +270 to +1238 bp, based on the translation initiation codons, were amplified by PCR with KOD plus neo polymerase (Toyobo) and the specific primers in Table S2. The fragments amplified by PCR were digested with *Sph*I and *Eco*RV (Takara Bio) and inserted into the *Sph*I-*Sma*I sites of the pUC119 vector (Takara Bio). The resultant plasmid was digested with *Hinc*II (for *ddh* and *ackA*) or *Apa*I (for *acs*), and the region including the chloramphenicol resistance cassette, *psbAII* promoter, and *Nde*I-*Hpa*I cloning sites of pTCP2031 was amplified with KOD plus neo polymerase and the specific primers 5′-TTTGCTTCATCGCTCGAG-3′ and 5′-ATCCAATGTGAGGTTAAC-3′, and integrated into the *Hinc*II or *Apa*I site of the plasmid. The resultant plasmids were named pTCP1556, pTCP0542, and pTCP1299 for knockouts of *ddh*, *acs*, and *ackA*, respectively. The *sigE* ORF was obtained by digestion with *Nde*I and *Hpa*I from pTGP0945-*sigE* plasmid (Osanai et al., 2014a) and cloned into the *Nde*I-*Hpa*I sites of pTCP1556, pTCP0542, and pTCP1299. The plasmids were integrated into the GT-I strain by natural transformation as described previously (Osanai et al., 2011). Knockouts and the insertion of the *sigE* ORF were confirmed by PCR using GoTaq (Promega, Fitchburg, WI, USA) with the primers in Table S2.

Immunoblotting

Cells were collected by centrifugation (5800 × *g* for 2 min), and the supernatant was removed and cells were frozen by liquid nitrogen. Then, cells were dissolved in PBS-T and disrupted by sonication as described previously (Osanai et al., 2014a). Immunoblotting was performed as described previously (Osanai et al., 2014a). Antisera against SigE were generated previously (Osanai et al., 2009).

Glycogen Measurement

Glycogen levels were measured at the Biotechnology Center of Akita Prefectural University (Akita, Japan), as described in Osanai et al. (2014a).

LC-MS/MS Analysis

Equal amounts of cells (10 mL cell culture with A_{730} = 1.0) were harvested by rapid filtration, and metabolites were extracted using a previously described method (Osanai et al., 2014b). Briefly, the cells were filtrated, and then the intermediate metabolites were quenched and extracted in 1.2 mL of solvent mixture ($CHCl_3$:CH_3OH:H_2O, 2.5:2.5:1, v/v/v) containing 10 μg/L D-(+)-camphor-10-sulfonic acid as an

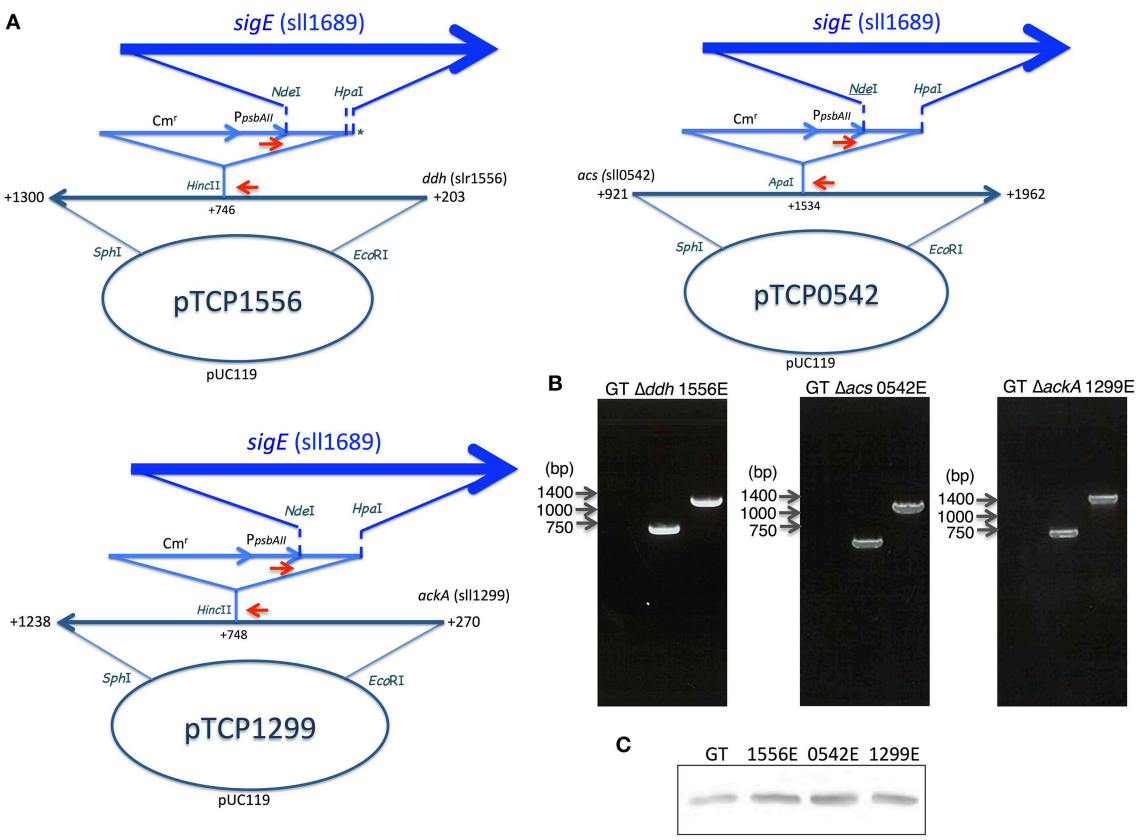

FIGURE 3 | (A) Vector maps for three vectors disrupting *ddh*, *acs*, and *ackA* with or without *sigE* overexpression. Red arrows indicate the primer sets to confirm the insertion of the vectors in the non-nitrogen fixing cyanobacterium *Synechocystis* sp. PCC 6803 genome. Asterisk (*) in pTCP1556 indicates that the *sigE* ORF was inserted into the region from *Nde*I to 55-bp downstream of the *Hpa*I site because of the star activity of *Hpa*I. **(B)** The right bottom panels show DNA fragments amplified by PCR with the primers in agarose gel electrophoresis as visualized by ethidium bromide. **(C)** Protein levels of SigE in GT, 1556E, 0542E, and 1299E strains. Immunoblotting was performed with 12 μg of total protein from cells grown under dark, anaerobic conditions for 3 days.

internal standard. After centrifugation at 15,000 × *g* at 4°C for 5 min, 400 μL of the upper phase was transferred to a new tube and vacuum-dried.

GC-MS Analysis

Equal amounts of cells (10 mL cell culture with A_{730} = 1.0) were harvested by rapid filtration as mentioned above. GC-MS was carried out using a GCMS-QP2010 Ultra, and the detailed protocol is described in Osanai et al. (2015).

Measurement of Organic Acids by High-Performance Liquid Chromatography (HPLC)

Freeze-dried supernatants were resolved in 100 μL of filtered 3 mM perchloric acid. The resolved samples were analyzed by HPLC using a LC-2000Plus Systems (JASCO, Tokyo, Japan) with a photodiode array detector and two RSpak KC-811 columns (Showa Denko, Tokyo, Japan). Organic acids were quantified with 0.2 mM bromothymol blue in 15 mM sodium phosphate buffer; peaks were detected at 445 nm. The column temperature was 60°C, and the flow rates of 3 mM perchloric acid and 0.2 mM bromothymol blue solutions were 1.0 and 1.5 mL/min, respectively.

Results

ackA Knockout and *sigE* Overexpression Enhanced Succinate Production

The identities of the excreted organic acids from the wild-type *Synechocystis* 6803 (GT) during anaerobic conditions were determined first. After cultivation for 3 days under light, aerobic conditions (1% CO_2 in the air), cells were concentrated into 10 mL BG-11_0 medium or HEPES buffer with or without nitrogen sources (5 mM NH_4Cl) in a GC-vial, subjected to anaerobic conditions by introducing N_2 gas, and incubated for 3 days under dark conditions with shaking at 30°C. Organic acids excreted into the medium or buffer were analyzed by HPLC. Succinate, lactate and acetate were detected, and the succinate levels were highest in HEPES buffer with nitrogen

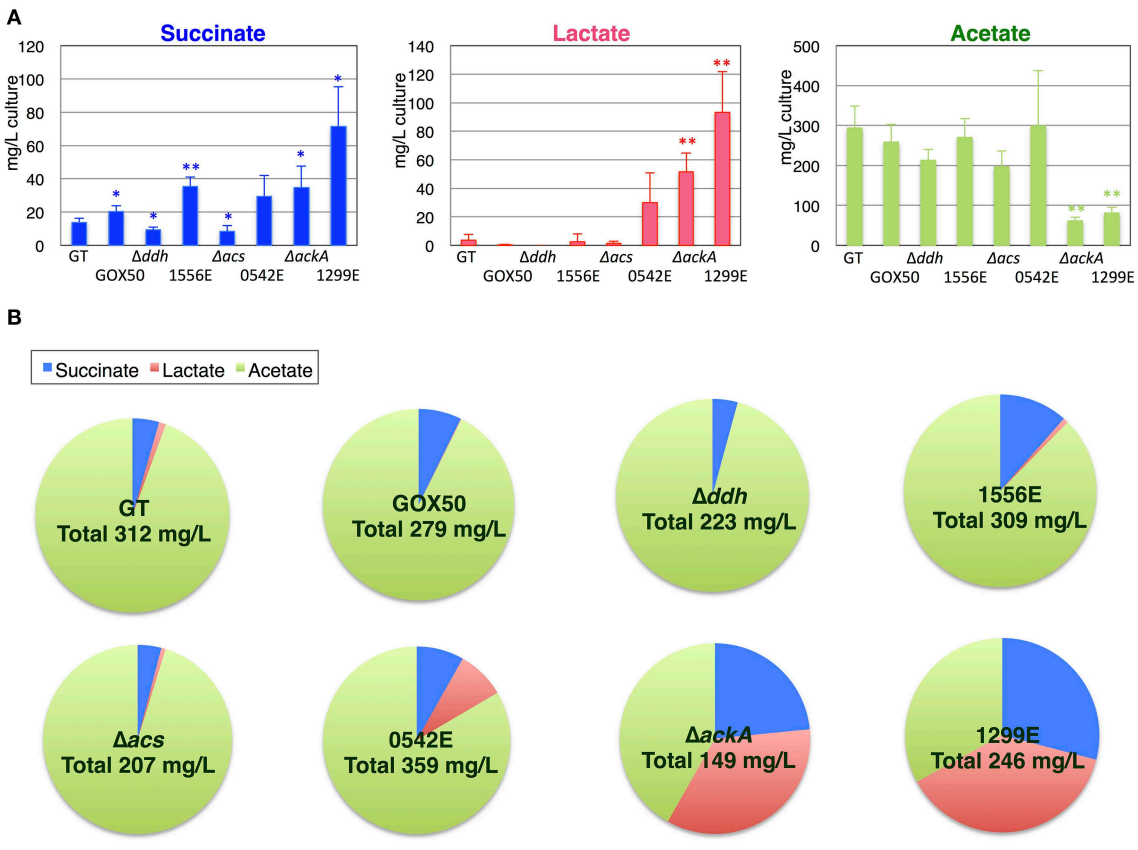

FIGURE 4 | Production of organic acids from the cyanobacterium *Synechocystis* 6803 strain overexpressing *sigE* and lacking *ddh* (slr1556), *acs* (sll0542), or *ackA* (sll1299). (A) Levels of organic acids excreted during 3 days of dark, anaerobic cultivation were quantified by HPLC. Δ*ddh*, Δ*acs*, and Δ*ddh* indicate the knockout of mutants of each gene. 1556E, 0542E, and 1299E represent the strains overexpressing *sigE* and lacking *ddh*, *acs*, or *ackA*, respectively. GOX50 designates the *sigE*-overexpressing strain. Data represent means ± SD from three or four independent experiments. Asterisks indicate statistically significant differences between GT and the mutant strains (Student's *t*-test; $^*P < 0.05$, $^{**}P < 0.005$). **(B)** The pie chart shows the ratio of succinate, lactate, and acetate excreted from the cells under anaerobic conditions. Total organic acid acids are sum of succinate, lactate, and acetate amounts excreted from the cells. Ratio is calculated by dividing the amount of each organic acid by the amounts of total organic acids.

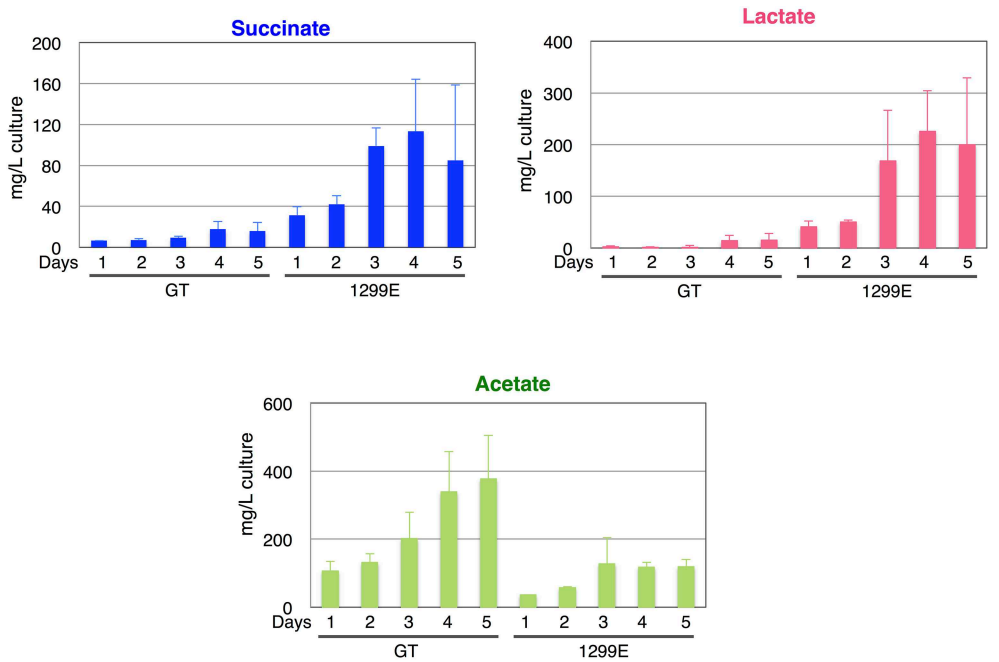

FIGURE 5 | Time-course analysis of levels of succinate, lactate, and acetate from the wild-type cyanobacterium *Synechocystis* 6803 and the 1299E strain, which overexpresses *sigE* and lacks *ackA*. Organic acids excreted from 1 to 5 days under dark, anaerobic cultivation were quantified by HPLC. Data represent means ± SD from three independent experiments.

source among the four conditions tested (**Figure 2**). Lactates were not detected in HEPES buffer (**Figure 2**). Acetate levels were higher in BG-11 or HEPES buffer without nitrogen sources than those in BG-11 or HEPES buffer with nitrogen sources (**Figure 2**). To reduce the cost of succinate production, subsequent experiments were performed using HEPES buffer without nitrogen sources.

To increase succinate production, we applied two strategies, decreasing lactate and acetate by knocking out each of the three genes (*ddh*, *acs*, or *ackA*; **Figure 1**) and promoting the sugar catabolic pathway by overexpressing *sigE,* encoding an RNA polymerase sigma factor, which activates the expression of sugar catabolic enzymes (Osanai et al., 2011). Knock-in vectors, which integrate the region containing the chloramphenicol resistance cassette, the *psbAII* promoter from the D1 protein of Photosystem II, and *Nde*I-*Hpa*I cloning sites, were constructed to generate the knockout mutants of *ddh*, *acs*, and *ackA* (**Figure 3A**). The *sigE* open reading frame (ORF) was cloned into the *Nde*I-*Hpa*I sites to generate the *sigE* overexpression strain combined with the *ddh*, *acs*, or *ackA* knockout, and the resultant strains were designated as 1556E, 0542E, and 1299E, respectively (**Figure 3A**). The insertion of these DNA fragments was confirmed by PCR (**Figure 3B**). Immunoblotting confirmed that SigE proteins in the three *sigE*-overexpressing strains were higher than in GT after 3 days of cultivation under dark, anaerobic conditions (**Figure 3C**).

Although the knockouts of *ddh* and *acs* did not increase the succinate levels, the *ackA* knockout increased the succinate level to 34.8 mg/L compared with the 13.9 mg/L produced by the parental wild-type strain under the same conditions. *sigE* overexpression (GOX50) alone increased the succinate level to 20.3 mg/L, and an additional knockout of *ddh*, *acs*, or *ackA* enhanced the levels to ∼35.6, 29.4, or 71.5 mg/L, respectively (**Figure 4A**). The wild-type cells produced less than 10 mg/L lactate, while the lactate levels increased in the *ackA* knockout to 51.7 mg/L, and *sigE* overexpression with an *acs* or *ackA* knockout enhanced the levels to 30.0 or 93.5 mg/L, respectively (**Figure 4A**). Acetate levels were decreased to 62.0 mg/L by the *ackA* knockout, compared with 294.3 mg/L acetate produced by wild-type cells, and the ratio of succinate and lactate to acetate increased in the *ackA* knockout mutant (**Figures 4A,B**). The strain lacking *ackA* and overexpressing *sigE* (1299E) had the highest succinate levels and ratios among the eight strains (**Figures 4A,B**). A time-course experiment analyzed different lengths of dark, anaerobic incubations and showed that a 3- or 4-day incubation period was long enough to produce sufficient quantities and ratios of succinate in 1299E (**Figure 5**). The succinate production rates from 1299E were 1.38 and 1.18 mg/L/h for 3- and 4-day incubation, respectively (**Figure 5**). Therefore, subsequent experiments were performed using a 3-day incubation period under dark, anaerobic conditions.

A Metabolome Analysis

A metabolome analysis using the GT and 1299E strains grown under aerobic and anaerobic conditions was then performed to clarify the metabolic profiles. After dark, aerobic cultivation, ADP-glucoses disappeared and the levels of several sugar

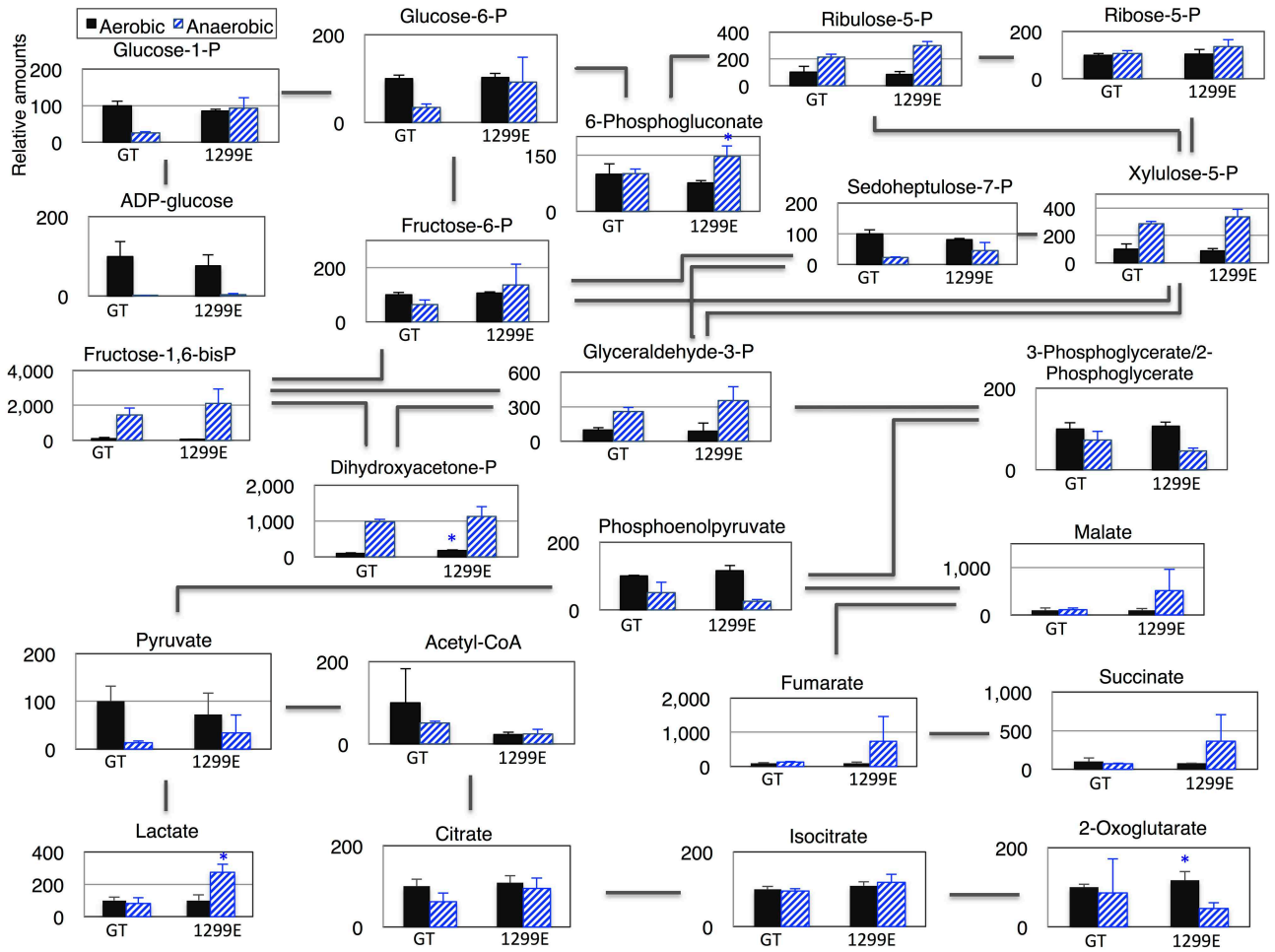

FIGURE 6 | Levels of metabolites in primary metabolism of the cyanobacterium *Synechocystis* 1299E strain, which overexpresses *sigE* and lacks *ackA*. Data represent means ± SD from three independent experiments. Metabolite levels were calibrated relative to that of corresponding metabolites in the wild-type strain (GT) under aerobic conditions (set at 100%). P designates phosphate. Asterisks indicate the statistically significant differences between GT and 1299E (Student's *t*-test; $^*P < 0.05$).

TABLE 1 | Relative glycogen levels in GT and 1299E.

Strain	Aerobic	Anaerobic
GT	100 ± 13.1	67.6 ± 10.8
1299E	104.4 ± 1.7	29.5 ± 4.8

Data represent means ± SD results from four independent experiments. Glycogen levels were calibrated relative to that in GT under light conditions (set at 100%). ND, glycogen under detectable levels.

phosphates increased (**Figure 6** and Table S1). The fructose-1, 6-bisphoshate and dihydroxyacetone phosphate levels increased more than 10 times under anaerobic conditions in the wild-type strain (**Figure 6**). Phosphoenolpyruvate, pyruvate and acetyl-CoA decreased greatly under anaerobic conditions (**Figure 6**). The levels of sugar phosphates, such as glucose-1-phosphate, glucose-6-phosphate, ribulose-5-phosphate, 6-phosphogluconate, fructose-6-phosphate, and fructose-1, 6-bisphosphate, in the 1299E strain under anaerobic conditions, were higher than those in the wild-type strain (**Figure 6**). Phosphoenolpyruvate and acetyl-CoA were lower in the 1299E strain than in the wild-type strain, and organic acids, such as succinate, lactate, malate, and fumarate, were higher in the 1299E strain than in the wild-type strain under anaerobic conditions (**Figure 6**).

The quantification of the glycogen levels before and after anaerobic cultivation for 3 days revealed that 33% of glycogen was consumed in the wild-type strain; however, 70% of glycogen were consumed in the 1299E strains (**Table 1**).

Discussion

Fermentation is closely related to sugar metabolism. In *Synechococcus* 7002, the levels of excreted fermentation products were altered by the disruption of *glgC*, which encodes ADP-glucose pyrophosphorylase (Guerra et al., 2013). Lactate

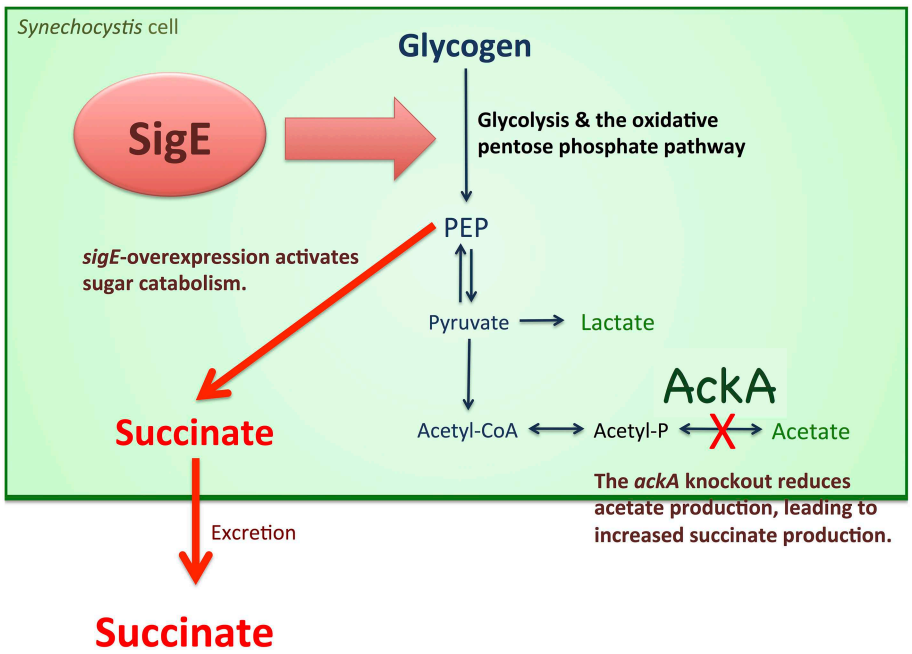

FIGURE 7 | Schematic model of succinate production from *Synechocystis* 6803. *sigE* overexpression activates sugar catabolism, possibly leading to increased succinate production. The *ackA* knockout reduces acetate biosynthesis, resulted in increased production of succinate and lactate production.

production in the *glgC* knockout strain was approximately half of that in the wild-type, while acetate and alanine production were not significantly affected (Guerra et al., 2013). The reason for the decreased lactate excretion may be the slower catabolic rate of reduced sugars in the *glgC* knockout mutant (Guerra et al., 2013). The rate of sugar catabolism, not the amount of total reduced sugars, was important for the increased lactate production (Guerra et al., 2013). This finding was consistent with our results that *sigE* overexpression, which accelerated glycogen degradation and glucose catabolism (Osanai et al., 2011), increased succinate production in *Synechocystis* 6803 (**Figures 4A**, **7**). Glycogen degradation was enhanced by *sigE* overexpression during dark, anaerobic conditions (**Table 1**), possibly leading to increases in the biosynthesis of intracellular organic acids (**Figure 6** and Table S1), which in turn led to the production of extracellular succinate at a higher level (**Figures 4A**, **7**).

A metabolome analysis revealed that the levels of fructose-1,6-bisphosphate and dihydroxyacetone phosphate increased more than 10 times after dark, anaerobic cultivation in the wild-type strain (**Figure 6**). Glyceraldehyde-3-phosphate production also increased, but 3-phosphoglycerate/2-phosphoglycerate, phosphoenolpyruvate, pyruvate, and acetyl-CoA decreased after dark, anaerobic cultivation in the wild-type strain (**Figure 6**). These results suggest that important enzymatic reactions exist downstream of glyceraldehyde-3-phosphate under dark, anaerobic conditions. Glyceraldehyde-3-phosphate dehydrogenase, which produces glycerate-1,3-bisphosphate from glyceraldehyde-3-phosphate, is encoded by *gap1* and *gap2*, and the reactions were uniquely catalyzed by the two enzymes in *Synechocystis* 6803. Gap1 catalyzes the catabolic reactions and Gap2 catalyzes the anabolic reactions (Koksharova et al., 1998). In addition, the *gap1* transcript levels are regulated by at least two transcriptional regulators, SigE and a response regulator Rre37 (Osanai et al., 2005; Azuma et al., 2011), indicating the importance of *gap1* in the sugar catabolism of *Synechocystis* 6803. The flux into the TCA cycle in *Synechocystis* is relatively low compared with other heterotrophic bacteria (You et al., 2015). Current results demonstrate that the flux into succinate can be up-regulated by our genetic modification under dark, anaerobic conditions.

A knockout of *ackA* reduced the acetate level but a knockout of *acs* did not affect the acetate level (**Figure 4A**), suggesting the major route of acetate biosynthesis under dark, anaerobic conditions is through an AckA-dependent pathway in this cyanobacterium (**Figure 1**). *Prochlorococcus* species lack *ackA* in their genomes (KEGG database URL: http://www.genome.jp/kegg-bin/show_pathway?syn00620), and thus, acetate biosynthesis pathway may be diverse among cyanobacteria. The mutant lacking *ddh* showed diminished lactate production, but lactate was produced by *sigE* overexpression even in the *ddh* knockout (**Figure 4A**). These results indicate another pathway for lactate biosynthesis exists in this cyanobacterium. Lactate can be synthesized from lactoylglutathione, which is derived from dihydroxyacetone phosphate (KEGG database URL: http://www.genome.jp/kegg-bin/show_pathway?syn00620), and the pathway may be activated by *sigE* overexpression. Our metabolome analysis revealed that NADPH disappeared, and that malate, fumarate, and succinate generally increased in the strains producing more succinate (**Figure 6** and Table S1). These

data suggest that succinate is produced through the reverse TCA cycle, as shown in **Figure 1**, as in other heterotrophic bacteria (Lee et al., 2006). Thus, the metabolic flux toward succinate production has been clarified in this cyanobacterium by the metabolome analysis. Pyruvate and phosphoenolpyruvate were severely reduced by light-to-dark transition (Iijima et al., 2015), and thus, the provision of these metabolites may be important to increase organic acid production under dark, anaerobic conditions. The current results demonstrated that a combination of the genetic manipulation of genes encoding a metabolic enzyme and a sigma factor succeeded in up-regulating the succinate levels. Future study about the detailed metabolic regulation will contribute to further understanding of the mechanistic implication of succinate excretion from this cyanobacterium.

Acknowledgments

This work was supported by the Ministry of Education, Culture, Sports, Science, and Technology, Japan, by a grant to TO from ALCA (Project name "Production of cyanobacterial succinate by the genetic engineering of transcriptional regulators and circadian clocks") from the Japan Science and Technology Agency. All authors contributed to the work and approved the submission of the manuscript.

Supplementary Material

The Supplementary Material for this article can be found online at: http://journal.frontiersin.org/article/10.3389/fmicb.2015.01064

References

Angermayr, S. A., van der Woude, A. D., Correddu, D., Vreugdenhil, A., Verrone, V., and Hellingwerf, K. J. (2014). Exploring metabolic engineering design principles for the photosynthetic production of lactic acid by *Synechocystis* sp. PCC6803. *Biotechnol. Biofuels* 7, 99. doi: 10.1186/1754-6834-7-99

Azuma, M., Osanai, T., Hirai, M. Y., and Tanaka, K. (2011). A response regulator Rre37 and an RNA polymerase sigma factor SigE represent two parallel pathways to activate sugar catabolism in a cyanobacterium *Synechocystis* sp. PCC 6803. *Plant Cell Physiol.* 52, 404–412. doi: 10.1093/pcp/pcq204

Carrieri, D., Ananyev, G., Lenz, O., Bryant, D. A., and Dismukes, G. C. (2011). Contribution of a sodium ion gradient to energy conservation during fermentation in the cyanobacterium *Arthrospira* (*Spirulina*) *maxima* CS-328. *Appl. Environ. Microbiol.* 77, 7185–7194. doi: 10.1128/AEM.00612-11

Carrieri, D., Momot, D., Brasg, I. A., Ananyev, G., Lenz, O., Bryant, D. A., et al. (2010). Boosting autofermentation rates and product yields with sodium stress cycling: application to production of renewable fuels by cyanobacteria. *Appl. Environ. Microbiol.* 76, 6455–6462. doi: 10.1128/AEM.00975-10

Chatterjee, R., Millard, C. S., Champion, K., Clark, D. P., and Donnelly, M. I. (2001). Mutation of the *ptsG* gene results in increased production of succinate in fermentation of glucose by *Escherichia coli*. *Appl. Environ. Microbiol.* 67, 148–154. doi: 10.1128/AEM.67.1.148-154.2001

Guerra, L. T., Xu, Y., Bennette, N., McNeely, K., Bryant, D. A., and Dismukes, G. C. (2013). Natural osmolytes are much less effective substrates than glycogen for catabolic energy production in the marine cyanobacterium *Synechococcus* sp. strain PCC 7002. *J. Biotechnol.* 166, 65–75. doi: 10.1016/j.jbiotec.2013.04.005

Guettler, M. V., Rumler, D., and Jain, M. K. (1999). *Actinobacillus succinogenes* sp. nov., a novel succinic-acid-producing strain from the bovine rumen. *Int. J. Syst. Bacteriol.* 49, 207–216. doi: 10.1099/00207713-49-1-207

Hollinshead, W. D., Varman, A. M., You, L., Hembree, Z., and Tan, Y. J. (2014). Boosting D-lactate production in engineered cyanobacteria using sterilized anaerobic digestion effluents. *Bioresour. Technol.* 169, 464–467. doi: 10.1016/j.biortech.2014.07.003

Hong, S. H., Kim, J. S., Lee, S. Y., In, Y. H., Choi, S. S., Rih, J. K., et al. (2004). The genome sequence of the capnophilic rumen bacterium *Mannheimia succiniciproducens*. *Nat. Biotechnol.* 22, 1275–1281. doi: 10.1038/nbt1010

Hong, S. H., and Lee, S. Y. (2001). Metabolic flux analysis for succinic acid production by recombinant *Escherichia coli* with amplified malic enzyme activity. *Biotechnol. Bioeng.* 74, 89–95. doi: 10.1002/bit.1098

Hong, S. H., and Lee, S. Y. (2002). Importance of redox balance on the production of succinic acid by metabolically engineered *Escherichia coli*. *Appl. Microbiol. Biotechnol.* 58, 286–290. doi: 10.1007/s00253-001-0899-y

Iijima, H., Shirai, T., Okamoto, M., Kondo, A., Hirai, M. Y., and Osanai, T. (2015). Changes in primary metabolism under light and dark conditions in response to overproduction of a response regulator RpaA in the unicellular cyanobacterium *Synechocystis* sp. PCC 6803. *Front. Microbiol.* 6:888. doi: 10.3389/fmicb.2015.00888

Ikeuchi, M., and Tabata, S. (2001). *Synechocystis* sp. PCC 6803 – a useful tool in the study of the genetics of cyanobacteria. *Photosynth. Res.* 70, 73–83. doi: 10.1023/A:1013887908680

Jantama, K., Haupt, M. J., Svoronos, S. A., Zhang, X., Moore, J. C., Shanmugam, K. T., et al. (2007). Combining metabolic engineering and metabolic evolution to develop nonrecombinant strains of *Escherichia coli* C that produce succinate and malate. *Biotechnol. Bioeng.* 99, 1140–1153. doi: 10.1002/bit.21694

Kaneko, T., Sato, S., Kotani, H., Tanaka, A., Asamizu, E., Nakamura, Y., et al. (1996). Sequence analysis of the genome of the unicellular cyanobacterium *Synechocystis* sp. strain PCC6803. II. Sequence determination of the entire genome and assignment of potential protein-coding regions. *DNA Res.* 3, 109–136. doi: 10.1093/dnares/3.3.109

Kanesaki, Y., Shiwa, Y., Tajima, N., Suzuki, M., Watanabe, S., Sato, N., et al. (2012). Identification of substrain-specific mutations by massively parallel whole-genome resequencing of *Synechocystis* sp. PCC 6803. *DNA Res.* 19, 67–79. doi: 10.1093/dnares/dsr042

Kim, P., Laivenieks, M., Vieille, C., and Zeikus, J. G. (2004). Effect of overexpression of *Actinobacillus succinogenes* phosphoenolpyruvate carboxykinase on succinate production in *Escherichia coli*. *Appl. Microbiol. Biotechnol.* 70, 1238–1241. doi: 10.1128/aem.70.2.1238-1241.2004

Koksharova, O., Schubert, M., Shestakov, S., and Cerff, R. (1998). Genetic and biochemical evidence for distinct key functions of two highly divergent GAPDH genes in catabolic and anabolic carbon flow of the cyanobacterium *Synechocystis* sp. PCC 6803. *Plant Mol. Biol.* 36, 183–194. doi: 10.1023/A:1005925732743

Lee, S. J., Song, H., and Lee, S. Y. (2006). Genome-based metabolic engineering of *Mannheimia succiniciproducens* for succinic acid production. *Appl. Environ. Microbiol.* 72, 1939–1948. doi: 10.1128/AEM.72.3.1939-1948.2006

Lin, H., San, K. Y., and Bennett, G. N. (2005). Effect of *Sorghum vulgare* phosphoenolpyruvate carboxylase and *Lactococcus lactis* pyruvate carboxylase coexpression on succinate production in mutant strains of *Escherichia coli*. *Appl. Microbiol. Biotechnol.* 67, 515–523. doi: 10.1007/s00253-004-1789-x

McKinlay, J. B., Vieille, C., and Zeikus, J. G. (2007). Prospects for a bio-based succinate industry. *Appl. Microbiol. Biotechnol.* 76, 727–740. doi: 10.1007/s00253-007-1057-y

McNeely, K., Kumaraswamy, G. K., Guerra, T., Bennette, N., Ananyev, G., and Dismukes, G. C. (2014). Metabolic switching of central carbon metabolism in response to nitrate: application to autofermentative hydrogen production in cyanobacteria. *J. Biotechnol.* 182–183, 83–91. doi: 10.1016/j.jbiotec.2014.04.004

McNeely, K., Xu, Y., Bennette, N., Bryand, D. A., and Dismukes, G. C. (2010). Redirecting reductant flux into hydrogen production via metabolic engineering of fermentative carbon metabolism in a cyanobacterium. *Appl. Environ. Microbiol.* 76, 5032–5038. doi: 10.1128/AEM.00862-10

Millard, C. S., Chao, Y. P., Liao, J. C., and Donnelly, M. I. (1996). Enhanced production of succinic acid by overexpression of phosphoenolpyruvate carboxylase in *Escherichia coli*. *Appl. Environ. Microbiol.* 62, 1808–1810.

Osanai, T., Imashimizu, M., Seki, A., Sato, S., Tabata, S., Imamura, S., et al. (2009). ChlH, the H subunit of the Mg-chelatase, is an anti-sigma factor for SigE in *Synechocystis* sp. PCC 6803. *Proc. Natl. Acad. Sci. U.S.A.* 106, 6860–6865. doi: 10.1073/pnas.0810040106

Osanai, T., Kanesaki, Y., Nakano, T., Takahashi, H., Asayama, M., Shirai, M., et al. (2005). Positive regulation of sugar catabolic pathways in the cyanobacterium *Synechocystis* sp. PCC 6803 by the group 2 sigma factor SigE. *J. Biol. Chem.* 280, 30653–30659. doi: 10.1074/jbc.M505043200

Osanai, T., Kuwahara, A., Iijima, H., Toyooka, K., Sato, M., Tanaka, K., et al. (2013). Pleiotropic effect of *sigE* over-expression on cell morphology, photosynthesis and hydrogen production in *Synechocystis* sp. PCC 6803. *Plant J.* 76, 456–465. doi: 10.1111/tpj.12310

Osanai, T., Oikawa, A., Azuma, M., Tanaka, K., Saito, K., Hirai, M., et al. (2011). Genetic engineering of group 2 sigma factor SigE widely activates expressions of sugar catabolic genes in *Synechocystis* species PCC 6803. *J. Biol. Chem.* 286, 30962–30971. doi: 10.1074/jbc.M111.231183

Osanai, T., Oikawa, A., Numata, K., Kuwahara, A., Iijima, H., Doi, Y., et al. (2014a). Pathway-level acceleration of glycogen catabolism by a response regulator in the cyanobacterium *Synechocystis* species PCC 6803. *Plant Physiol.* 164, 1831–1841. doi: 10.1104/pp.113.232025

Osanai, T., Oikawa, A., Shirai, T., Kuwahara, A., Iijima, H., Tanaka, K., et al. (2014b). Capillary electrophoresis-mass spectrometry reveals the distribution of carbon metabolites during nitrogen starvation in *Synechocystis* sp. PCC 6803. *Environ. Microbiol.* 16, 512–524. doi: 10.1111/1462-2920.12170

Osanai, T., Shirai, T., Iijima, H., Kuwahara, A., Suzuki, I., Kondo, A., et al. (2015). Alteration of cyanobacterial sugar and amino acid metabolism by overexpression *hik8*, encoding a KaiC-associated histidine kinase. *Environ. Microbiol.* 17, 2430–2440. doi: 10.1111/1462-2920.12715

Reece, K. S., and Phillips, G. J. (1995). New plasmids carrying antibiotic-resistance cassettes. *Gene* 165, 141–142. doi: 10.1016/0378-1119(95)00529-F

Rippka, R. (1988). Isolation and purification of cyanobacteria. *Meth. Enzymol.* 167, 3–27. doi: 10.1016/0076-6879(88)67004-2

Samuelov, N. S., Lamed, R., Lowe, S., and Zeikus, J. G. (1991). Influence of CO_2-HCO_3 levels and pH on growth, succinate production, and enzyme activities of *Anaerobiospirillum succiniciproducens*. *Appl. Environ. Microbiol.* 57, 3013–3019.

Sánchez, A. M., Bennett, G. N., and San, K. Y. (2005a). Efficient succinic acid production from glucose through overexpression of pyruvate carboxylase in an *Escherichia coli* alcohol dehydrogenase and lactate dehydrogenase mutant. *Biotechnol. Prog.* 21, 358–365. doi: 10.1021/bp049676e

Sánchez, A. M., Bennett, G. N., and San, K. Y. (2005b). Novel pathway engineering design of the anaerobic central metabolic pathway in *Escherichia coli* to increase succinate yield and productivity. *Metab. Eng.* 7, 229–239. doi: 10.1016/j.ymben.2005.03.001

Werpy, T., and Petersen, G. (2004). *Top Value Added Chemicals from Biomass, Vol. 1, Results of Screening for Potential Candidates from Sugars and Synthesis Gas*. Oak Ridge, TN: U.S. Department of Energy.

Williams, J. G. K. (1988). Construction of specific mutations in photosystem II photosynthetic reaction center by genetic engineering methods in *Synechocystis* 6803. *Meth. Enzymol.* 167, 766–778. doi: 10.1016/0076-6879(88)67088-1

You, L., He, L., and Tang, Y. J. (2015). Photoheterotrophic fluxome in *Synechocystis* sp. strain PCC 6803 and its implications for cyanobacterial bioenergetics. *J. Bacteriol.* 197, 943–950. doi: 10.1128/JB.02149-14

Zeikus, J. G., Jain, M. K., and Elankovan, P. (1999). Biotechnology of succinic acid production and markets for derived industrial products. *Appl. Microbiol. Biotechnol.* 51, 545–552. doi: 10.1007/s002530051431

Zhang, X., Jantama, K., Moore, J. C., Jarboe, L. R., Shanmugam, K. T., and Ingram, L. O. (2009). Metabolic evolution of energy-conserving pathways for succinate production in *Escherichia coli*. *Proc. Natl. Acad. Sci. U.S.A.* 106, 20180–20185. doi: 10.1073/pnas.0905396106

Conflict of Interest Statement: The authors declare that the research was conducted in the absence of any commercial or financial relationships that could be construed as a potential conflict of interest.

frontiers in Microbiology

ORIGINAL RESEARCH
published: 07 September 2015
doi: 10.3389/fmicb.2015.00912

Manipulation of oil synthesis in *Nannochloropsis* strain NIES-2145 with a phosphorus starvation–inducible promoter from *Chlamydomonas reinhardtii*

Masako Iwai[1,2], *Koichi Hori*[1,2], *Yuko Sasaki-Sekimoto*[3], *Mie Shimojima*[1] and *Hiroyuki Ohta*[1,2,3]*

[1] Graduate School of Bioscience and Biotechnology, Tokyo Institute of Technology, Yokohama, Japan, [2] JST CREST, Tokyo, Japan, [3] Earth-Life Science Institute, Tokyo Institute of Technology, Tokyo, Japan

OPEN ACCESS

Edited by:
Yuki Nakamura,
Academia Sinica, Taiwan

Reviewed by:
Mee-Len Chye,
The University of Hong Kong, Hong Kong
Norihiro Sato,
Tokyo University of Pharmacy and Life Sciences, Japan

***Correspondence:**
Hiroyuki Ohta,
Graduate School of Bioscience and Biotechnology, Tokyo Institute of Technology, 4259-B-65 Nagatsuta-cho, Midori-ku, Yokohama, Kanagawa 226-8501, Japan
ohta.h.ab@m.titech.ac.jp

Specialty section:
This article was submitted to Microbiotechnology, Ecotoxicology and Bioremediation, a section of the journal Frontiers in Microbiology

Received: 30 June 2015
Accepted: 19 August 2015
Published: 07 September 2015

Citation:
Iwai M, Hori K, Sasaki-Sekimoto Y, Shimojima M and Ohta H (2015) Manipulation of oil synthesis in Nannochloropsis strain NIES-2145 with a phosphorus starvation–inducible promoter from Chlamydomonas reinhardtii. Front. Microbiol. 6:912. doi: 10.3389/fmicb.2015.00912

Microalgae accumulate triacylglycerols (TAGs) under conditions of nutrient stress. Phosphorus (P) starvation induces the accumulation of TAGs, and the cells under P starvation maintain growth through photosynthesis. We recently reported that P starvation–dependent overexpression of type-2 diacylglycerol acyl-CoA acyltransferase (CrDGTT4) from *Chlamydomonas reinhardtii* using a sulfoquinovosyldiacylglycerol synthase 2 (SQD2) promoter, which has increased activity during P starvation, enhances TAG accumulation in *C. reinhardtii* cells. As a result, the content of C18:1 fatty acid, a preferred substrate of CrDGTT4, is increased in TAGs. Here we isolated genes encoding SQD2 from strain NIES-2145 of the eustigmatophyte *Nannochloropsis* and showed that their expression, like that in *C. reinhardtii*, was up-regulated during P starvation. To enhance oil accumulation under P starvation, we transformed pCrSQD2-CrDGTT4 into *Nannochloropsis* strain NIES-2145. The transformants had a fatty acid composition that was more similar to that of *C. reinhardtii*, which resulted in enhanced TAG accumulation and higher 18:1(9) content. The results indicated that the P starvation–inducible promoter of *C. reinhardtii* was able to drive expression of the *CrDGTT4* gene in *Nannochloropsis* strain NIES-2145 under P starvation. We conclude that the heterologous *CrSQD2* promoter is effective in manipulating TAG synthesis in *Nannochloropsis* during P starvation.

Keywords: algae, *Nannochloropsis*, phosphorus starvation, inducible promoter, triacylglycerol

Introduction

Algal biofuel technology exploits algal photosynthesis and biosynthesis processes to produce oils using only sunlight, CO_2, water and limited nutrients. Many microalgae accumulate triacylglycerols (TAGs) during nutrient stress (Giroud et al., 1988; Guschina and Harwood, 2006; Hu et al., 2008). It is estimated that the annual oil production from algae is in the range of 40,700–53,200 L ha^{-1} $year^{-1}$ (Weyer et al., 2010). Therefore, the potential use of microalgae to provide biofuel feedstock is receiving significant attention.

A eukaryotic microalga, *Chlamydomonas reinhardtii*, is a model organism for studying algal biodiesel production because of its available whole-genome sequence and the ability to manipulate gene expression within this organism (Harris, 2009). Under stress conditions, such as nitrogen (N) starvation, *Chlamydomonas* nearly stops its growth and accumulates large amounts of TAGs (Grossman, 2000; Zhang et al., 2004). We reported that *C. reinhardtii* cells in logarithmic growth phase that were diluted into fresh medium showed substantial TAG accumulation under N or P deprivation (Iwai et al., 2014). P deprivation substantially induced the accumulation of oil droplets in the cytosol but allowed the maintenance of thylakoid membranes in *C. reinhardtii* (Iwai et al., 2014).

Nannochloropsis species are unicellular photosynthetic microalgae in the class Eustigmatophyceae. Previously known as "marine Chlorella," this class was identified on the basis of its ultrastructure and named *Nannochloropsis* by Maruyama et al. (1986). Its cells are spherical to slightly ovoid, are 2–4 μm in diameter and contain ovoid or cup-shaped chloroplasts (Maruyama et al., 1986). *Nannochloropsis* are of interest because of their rapid growth and their ability to produce large quantities of TAGs and be cultured on an industrial scale (Hodgson et al., 1991; Rodolfi et al., 2009; Huerlimann et al., 2010) In recent years, *Nannochloropsis* strains have been studied for their biomass production and their lipid composition and content under different growth conditions (Hu and Gao, 2006; Converti et al., 2009; Rodolfi et al., 2009; Simionato et al., 2011; Arudchelvam and Nirmalakhandan, 2012; Vieler et al., 2012b; Wang et al., 2014). In *Nannochloropsis* strains, N deprivation induces lipid accumulation and lipid droplet formation (Rodolfi et al., 2009; Vieler et al., 2012a,b; Martin et al., 2014), and their lipid content also increases with decreasing P concentrations (Hu and Gao, 2006; Rodolfi et al., 2009; Bondioli et al., 2012).

Diacylglycerol acyltransferase (DGAT) catalyzes the last step of TAG synthesis involving *sn*-1,2 diacylglycerol and acyl-CoA (Lung and Weselake, 2006; Rajakumari et al., 2008) and includes two major types, type 1 DGAT (DGAT1) and type 2 DGAT (DGAT2) (Cases et al., 1998; Lardizabal et al., 2001; Shockey et al., 2006). There are six *DGAT* genes in *C. reinhardtii* (encoding one *DGAT1* and five *DGAT2*s) (Miller et al., 2010; Boyle et al., 2012). In contrast, 12 or 13 *DGAT* genes (encoding one or two *DGAT1*s and 11 *DGAT2*s) are present in *Nannochloropsis* strains (Radakovits et al., 2012; Vieler et al., 2012b; Wang et al., 2014). During N starvation in *Nannochloropsis oceanica* IMET1, seven DGAT transcripts are up-regulated and six other DGAT transcripts are down-regulated (Li et al., 2014).

Endogenous promoters are mainly used for the nuclear transformation of algae such as *C. reinhardtii* (Eichler-Stahlberg et al., 2009; Harris, 2009; Brueggeman et al., 2014), although stable nuclear transformation of algae is feasible with promoters from heterologous sources that are categorized in the same class (Hirata et al., 2011; Lerche and Hallmann, 2013, 2014). Transformation experiments using *Nannochloropsis* with endogenous promoters have recently been reported (Kilian et al., 2011; Vieler et al., 2012b). Additionally, a construct with the *C. reinhardtii* α-tubulin promoter was used for transforming *Nannochloropsis* (Vieler et al., 2012b). However, the stable nuclear transformation of *Nannochloropsis* using an inducible promoter from a heterologous source under specific conditions, in particular an oil-accumulating condition such as nutrient starvation, has not been reported.

In this study, we found that *Nannochloropsis* strain NIES-2145 has a homolog of the *Arabidopsis SQD2* gene. Our results suggest that there is a common expression control system in a wide range of algal species, including primary and secondary microalgae, for adaptation to low P. We used the promoter of *sulfoquinovosyldiacylglycerol (SQDG) synthase 2 (SQD2)*, which encodes the sulfoquinovosyl transferase that catalyzes the second step of sulfolipid biosynthesis (Yu et al., 2002). The transcript levels of the *SQD2* gene homologs are increased in *C. reinhardtii* and *Arabidopsis* by P starvation concomitant with increases in the SQDG content (Yu et al., 2002; Chang et al., 2005; Okazaki et al., 2009; Iwai et al., 2014). The promoter of *SQD2* induced expression of the down stream gene during P starvation, to successfully overexpress *C. reinhardtii* type-2 diacylglycerol acyl-CoA acyltransferase (CrDGTT4) in *Nannochloropsis* strain NIES-2145 under P starvation. The total lipid content, neutral lipid content and fatty acid profiles were determined. CrDGTT4 enhanced TAG accumulation under P starvation by changing the fatty acid composition to be more similar to that of *C. reinhardtii*. Therefore, the heterologous Cr*SQD2* promoter is effective in manipulating oil synthesis in *Nannochloropsis* during P starvation.

Materials and Methods

Materials and Culture Conditions

Nannochloropsis strain NIES-2145 was obtained from the Microbial Culture Collection of the National Institute for Environmental Studies, Japan. *Nannochloropsis* strain NIES-2145 was grown photoautotrophically in f/2 medium (Guillard and Ryther, 1962) or F2N50%SW medium (standard medium), which is F2N medium (Kilian et al., 2011) made with 50% artificial seawater (Wako Pure Chemical Industries, Ltd., Japan). Liquid cultures were grown in continuous white light (20–40 μmol photons m^{-2} s^{-1}) at room temperature. Nutrient deficiency was induced by centrifuging the cells for 10 min at 2000 × g, washing them twice with the respective medium and subsequently resuspending them in the standard medium without $NaNO_3$ and NH_4Cl (–N) or phosphate (–P) solutions. Agar plates were prepared using 0.8% Bacto agar (Difco, USA) in standard medium. The cells were maintained on these plates at the same light intensity at room temperature.

Analysis of Differential Gene Expression Levels

The differential expression levels of the *CrDGAT* gene and *SQD2* genes in *Nannochloropsis* strain NIES-2145 cultured in standard, -P and -N media were determined using quantitative real-time PCR (qPCR). RNA was extracted from standard, -P and -N cultures using the phenol/chloroform method. Total RNA (500 ng) was used for the synthesis of cDNA with an oligo$(dT)_{18}$ primer, random hexamers and Superscript II reverse transcriptase (Invitrogen, Carlsbad, CA). cDNA was amplified using SYBR Premix Ex Taq II (Takara, Japan). The

Thermal Cycler Dice Real Time System and Multiplate RQ software (Takara) were used for the analysis. Expression levels of the *CrDGAT* gene and *SQD2* genes were normalized to TUB mRNA expression. The *CrDGTT4* expression levels in *Nannochloropsis* cultured in -P medium were compared with those of *Nannochloropsis* cultured in the standard medium (the values of which were set to 1). Primers are listed in **Supplemental Table 1**.

Construction and Identification of *CrDGTT4*-overexpressing NIES-2145 Cell Lines

Transformation experiments were performed using a construct developed for the nuclear transformation of *Nannochloropsis*, pMD20 with a NT7 cassette (Kilian et al., 2011), except that a truncated bidirectional violaxanthin–chlorophyll a binding protein 2 promoter and the violaxanthin–chlorophyll a binding protein 1 3′ UTR from *Nannochloropsis* strain NIES-2145 were used and that the *Eco*RV restriction site was inserted between the ble gene and the violaxanthin–chlorophyll a binding protein 1 3′ UTR. To construct the expression plasmid carrying the *CrDGTT4* (XM_001693137.1) gene, pCrSQD2aDGTT4, which contains the *C. reinhardtii SQD2* promoter region and the coding sequence of the *DGTT4* gene (Iwai et al., 2014), was digested with restriction endonucleases *Eco*RV and *Spe*I and was treated using a DNA Blunting Kit (Takara). The resulting blunt-ended DNA was cloned into pMD-NT7, which was digested with restriction endonuclease *Eco*RV. Electroporation with a supplier was then used to transform the nuclear genome of *Nannochloropsis* strain NIES-2145 cells with 2–10 μg vector construct (Vieler et al., 2012b). The selection of transformants was performed on standard medium supplemented with 2 μg mL^{-1} Zeocin. Approximately 100 positive transformants were identified by growth on the selective medium, and overexpression levels in each resulting line were determined using qPCR.

Extraction and Separation of Lipids

Nannochloropsis cells were harvested by centrifugation (10 min at 3000 × g), and total lipids were extracted as described (Bligh and Dyer, 1959). The lipids were dissolved in chloroform/methanol (2:1, v/v) and stored at −20°C. Lipid classes were separated using two-dimensional thin-layer chromatography (TLC). The first dimension was developed using chloroform/methanol/7 N ammonia water (115:80:8, v/v/v). After the plates were dried for 1 h, the second dimension was developed using chloroform/methanol/acetic acid/water (170:25:15:3, v/v/v/v). TAGs were separated by TLC using the solvent system hexane/diethyl ether/acetic acid (160:40:4, v/v/v). Lipids were visualized under UV light after spraying the TLC plates with 0.001% (w/v) primuline in 80% (v/v) acetone.

Preparation of Fatty Acid Methyl Esters (FAMEs)

Each lipid was scraped off of the TLC plates. FAMEs were obtained by incubating lipids for 1 h at 85°C in the presence of 5% (v/v) hydrogen chloride–methanol solution (Wako Pure Chemical Industries) (Iwai et al., 2014). FAMEs were extracted using hexane and were determined by gas chromatography (GC). Fatty acid quantification was performed by comparing samples with the FAMEs derived from the internal standard, pentadecanoic acid (15:0).

GC Analysis

FAMEs were analyzed using a GC-2014 (Shimadzu Corporation, Kyoto, Japan) with a HR-SS-10 capillary column (length, 25 m; internal diameter, 0.25 mm; Shinwa Chemical Industries, Ltd., Japan). The fatty acid profiles were determined by comparison with a standard reference mix composed of FAMEs (Supelco 18917-1AMP, 18913-1AMP, CRM47885; Sigma-Aldrich, GLC411, GLC462; Funakoshi, Japan).

GC-mass Spectrometry (MS)

The qualitative composition of FAMEs was studied using a GS-MS (model GCMS-TQ8030; Shimadzu Corporation). High-grade pure helium was used as the carrier gas. The ionization voltage was 70 eV, and the ionization temperature was 200°C. Mass spectra were scanned every 0.2 s. For the analysis of the FAMEs, a DB-5 ms column (length, 30 m; internal diameter, 0.25 mm; Agilent Technologies, Inc., CA, USA) was used. For each sample, 1 μL was injected on the column into a helium gas flow held constant at 1.4 mL min^{-1}. The column temperature was elevated from 40°C to 320°C at a rate of 6°C min^{-1} and then kept at 320°C for 1.15 min.

SQD2 cDNA

RNA was extracted from standard and -P cultures using the phenol/chloroform method. Total RNA (500 ng) was used for the synthesis of cDNA with an oligo$(dT)_{18}$ primer, random hexamers and Superscript II reverse transcriptase (Invitrogen, Carlsbad, CA). The primers used are listed in **Supplemental Table 1**. The gene sequences were then cloned into the pMD20 vector (Takara) for DNA sequence.

Phylogenetic Analyses

Amino acid sequences were aligned using MAFFT v7.220 (Katoh and Standley, 2013). Gblocks 0.91b (Talavera and Castresana, 2007) was used to remove any poorly conserved regions. The phylogenetic analyses were performed using the maximum likelihood and the neighbor-joining methods in MEGA6 (Tamura et al., 2013), and a Bayesian analysis in MrBayes 3.2.3 (Ronquist et al., 2012). The amino acid substitution model for the maximum likelihood and Bayesian inference methods was selected using Aminosan (Tanabe, 2011). The maximum likelihood and neighbor-joining methods were performed based on the LG model + Gamma (eight categories) with 1000 bootstraps and the JTT model with 1000 bootstraps, respectively. The Bayesian analysis was performed based on the LG model + Gamma (eight categories) for 1,000,000 generations. Every 500th generation was sampled, and the first 200 trees were discarded as burn-in.

Motifs Analysis

The analysis of the motifs was performed *in silico* using New PLACE (https://sogo.dna.affrc.go.jp/cgi-bin/sogo.cgi?sid=&lang=en&pj=640&action=page&page=newplace), a database of *cis*-acting regulatory DNA elements from plants, to find the binding motifs of transcription factors.

Results

Cell Growth and Tag Accumulation in Cells under P Deprivation

Nannochloropsis strain NIES-2145 was cultured to the logarithmic phase in f/2 medium. Cultures were then centrifuged and resuspended in fresh f/2 or in N-depleted (-N) or P-depleted (-P) f/2 medium. The cultures derived from logarithmic-phase cultures were inoculated at low cell densities (1×10^6 cells mL^{-1}). Under N-deprived conditions, the *Nannochloropsis* cells were nearly white, but the cells exposed to P starvation were still green (**Figure 1**). Because *C. reinhardtii* cells diluted into P-depleted medium show substantial TAG accumulation (Iwai et al., 2014), we investigated whether TAG was accumulated in these nutrient-starved cells by quantifying lipid-derived FAMEs using GC. Cells had substantially increased TAG levels under both N and P deprivation (**Supplemental Figure 1**). Compared with cells grown in complete medium, the N-starved cells contained ∼11-fold and the P-starved cells contained ∼6-fold more TAG per cell after 13 days. The TAG accumulation in the N-starved cells is consistent with that in recent reports (Bondioli et al., 2012; Vieler et al., 2012b; Simionato et al., 2013). When the cultures were inoculated at 5×10^6 cells mL^{-1} in standard medium or –P medium, P-starved cells contained more TAG per cell than the corresponding cells maintained in the standard medium (∼7-fold more at 4 days and ∼47-fold more at 6 days; **Figure 2A**). P-starved cultures contained ∼4.6-fold more TAG per liter at 4 days and ∼4-fold more TAG per liter at 6 days than the corresponding culture maintained in the standard medium (**Figure 2B**).

Increase in SQDG and SQD2 Homolog Promoter Activity during P Starvation

Lipids extracted from *Nannochloropsis* strain NIES-2145 were separated by two-dimensional TLC, followed by GC-flame ionization detection and GC-MS. P starvation caused significant changes in lipid composition. The glycerolipid composition of *Nannochloropsis* strain NIES-2145 resembles that of the photosynthetic organism *Arabidopsis thaliana* (Li-Beisson et al., 2010), being comprised mostly of the prevalent glycoglycerolipids monogalactosyldiacylglycerol (MGDG), DGDG and SQDG, as well as the common phospholipids phosphatidylcholine (PC), phosphatidylethanolamine (PE), phosphatidylserine (PS), phosphatidylinositol (PI), and phosphatidylglycerol (PG). In addition, a betaine lipid diacylglycerol-*N*,*N*,*N*-trimethylhomoserine (DGTS) is present, as in *C. reinhardtii* (Sato and Furuya, 1985; Giroud et al., 1988). P deprivation resulted in elevated levels of SQDG and DGTS. PG, PC, and PS which contain phosphates in their head groups, decreased after P deprivation (**Figure 3**). This result corroborates previous reports on P deprivation in several species (Benning et al., 1993; Essigmann et al., 1998; Sato et al., 2000; Khozin-Goldberg and Cohen, 2006).

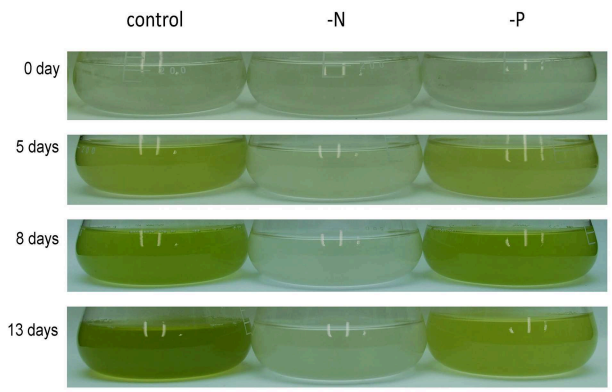

FIGURE 1 | Growth of *Nannochloropsis* NIES-2145 under standard growth conditions, N starvation and P starvation. *Nannochloropsis* cells cultured to the logarithmic phase were inoculated into standard (control), -N and -P media. Cells were cultured for the indicated times after transfer before being photographed.

Orthologs of the *SQD2* encoding the sulfoquinovosyl transferase (Yu et al., 2002) and a cyanobacterial counterpart, the *sqdX*, are highly conserved across different groups of algae and plants (**Figure 4**). We expected that the expression of homologs of the *SQD2* gene would be induced during P starvation. To determine the expression of SQD2 homologs in *Nannochloropsis* strain NIES-2145, we searched the *N. oceanica* genome (Vieler et al., 2012b) using a BLAST algorithm to identify amino acid sequences with similarity to *C. reinhardtii* and *Arabidopsis SQD2* genes. Using consensus sequences of the *SQD2* genes, we amplified the corresponding cDNA from *Nannochloropsis* strain NIES-2145. We sequenced the cDNA and found that *Nannochloropsis* strain NIES-2145 has a homolog of the *Arabidopsis SQD2* gene (**Figure 4**). **Figure 4** is based on protein comparison. Expression of the *SQD2* gene homolog, as measured by qPCR, was induced after P deprivation in *Nannochloropsis* strain NIES-2145 (**Figure 5**). The *Chlamydomonas SQD2* promoter is useful for improving transgene expression in *C. reinhardtii* when P is depleted (Iwai et al., 2014). Therefore, we expected that the *Chlamydomonas SQD2* promoter would be available for inducing transgene expression to increase TAG production in *Nannochloropsis* under P-depleted conditions.

DGAT enzymes are important for TAG accumulation. During N starvation in *N. oceanica* IMET1, seven *DGAT* transcripts are up-regulated and six other *DGAT* transcripts are down-regulated (Li et al., 2014). However, it is unclear how *DGAT* transcripts are regulated during P starvation in *Nannochloropsis* strain NIES-2145. We therefore hypothesized that the overexpression of *C. reinhardtii DGTT4* in *Nannochloropsis* would be a convenient way to increase the lipid content or alter the lipid composition of these cells.

Enhanced Tag Accumulation and Changes in Fatty Acid Profiles in *CrDGTT4*-overexpressing Lines under P Deprivation

To explore CrDGTT4 as a tool to produce TAGs in *Nannochloropsis* cells, we expressed the CrDGTT4 coding sequence in *Nannochloropsis* under the control of the *CrSQD2* promoter, which increases transcription levels during P

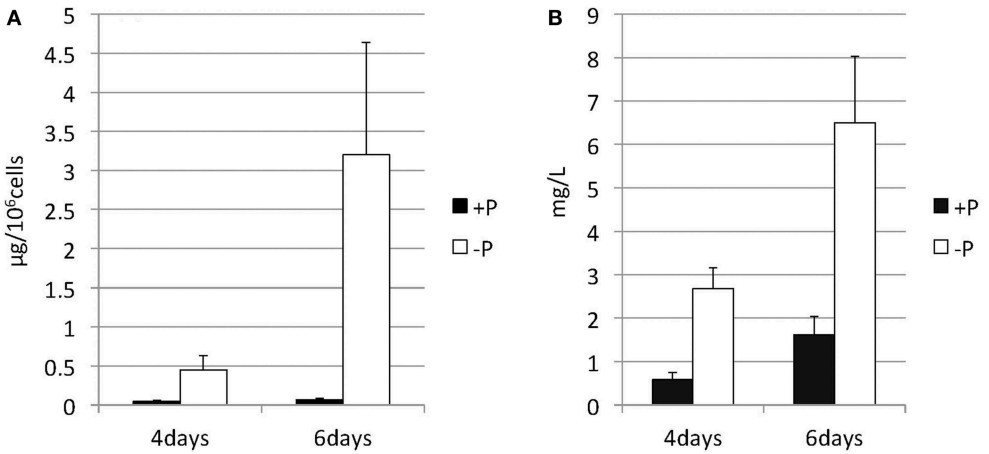

FIGURE 2 | Changes in the TAG content of *Nannochloropsis* in response to P starvation. Cells cultured to a logarithmic phase under standard conditions were then inoculated into standard (+P) or -P medium and cultured for 4 or 6 days. The y-axis is **(A)** Total TAG per 10^6 cells or **(B)** total TAG per liter of culture. Values represent the mean from three independent experiments ± SD.

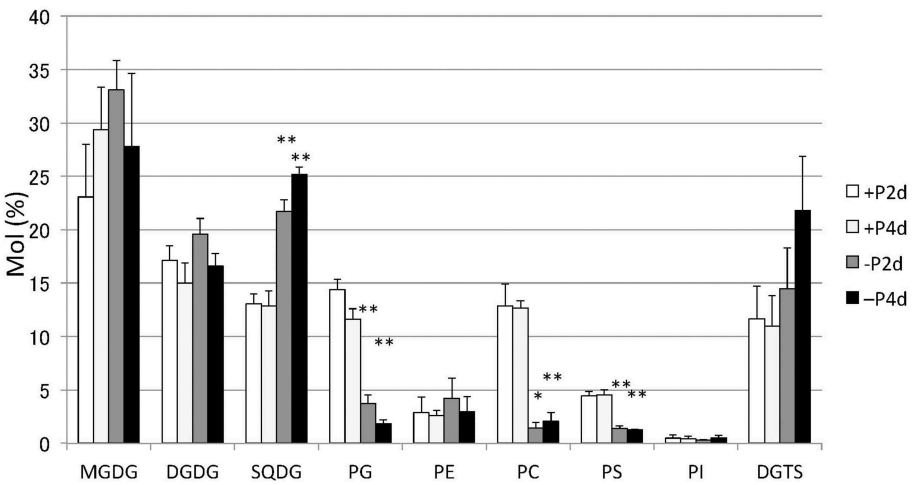

FIGURE 3 | Changes in major lipid classes in P-starved cells. Cells cultured to a logarithmic phase under standard conditions were then inoculated into standard (+P) or -P medium and cultured for 2 days (2 d) or 4 days (4 d). Lipid levels were determined by GC. Values represent the mean from three independent experiments ± SD. Asterisks indicate a statistically significant difference compared with the empty vector control based on a two-tailed Student's *t*-test (*$P < 0.05$ and **$P < 0.01$).

starvation in *C. reinhardtii* (Iwai et al., 2014). The relative level of overexpression of *CrDGTT4* was measured using qPCR. *CrDGTT4* mRNA levels in the overexpressing lines under P starvation were determined to be between 7- and 112-fold higher than in those under standard conditions (**Figure 6**), whereas no transcripts were detected in the wild-type and the empty vector controls. Thus, the *SQD2* promoter from *C. reinhardtii* is quite useful as a heterologous promoter in *Nannochloropsis* strain NIES-2145. Three overexpressing lines, #8, 9, and 21, were then selected for the subsequent experiments. To confirm the effect of *CrDGAT* gene overexpression, we compared the lipid content and fatty acid composition of the wild-type and overexpressing lines. All lines were cultured to the logarithmic phase prior to P depletion, as was done in the previous experiments.

TAG accumulation increased in *CrDGTT4*-overexpressing lines compared with the control and wild-type lines in P-depleted medium. *CrDGTT4*-overexpressing lines contained ∼1.7-fold and ∼1.3-fold more TAG per cell than the empty vector control cells at 4 and 6 days, respectively (**Figure 7**, **Supplemental Figure 2**). We next investigated if the fatty acid composition of total lipids and TAGs was altered in the

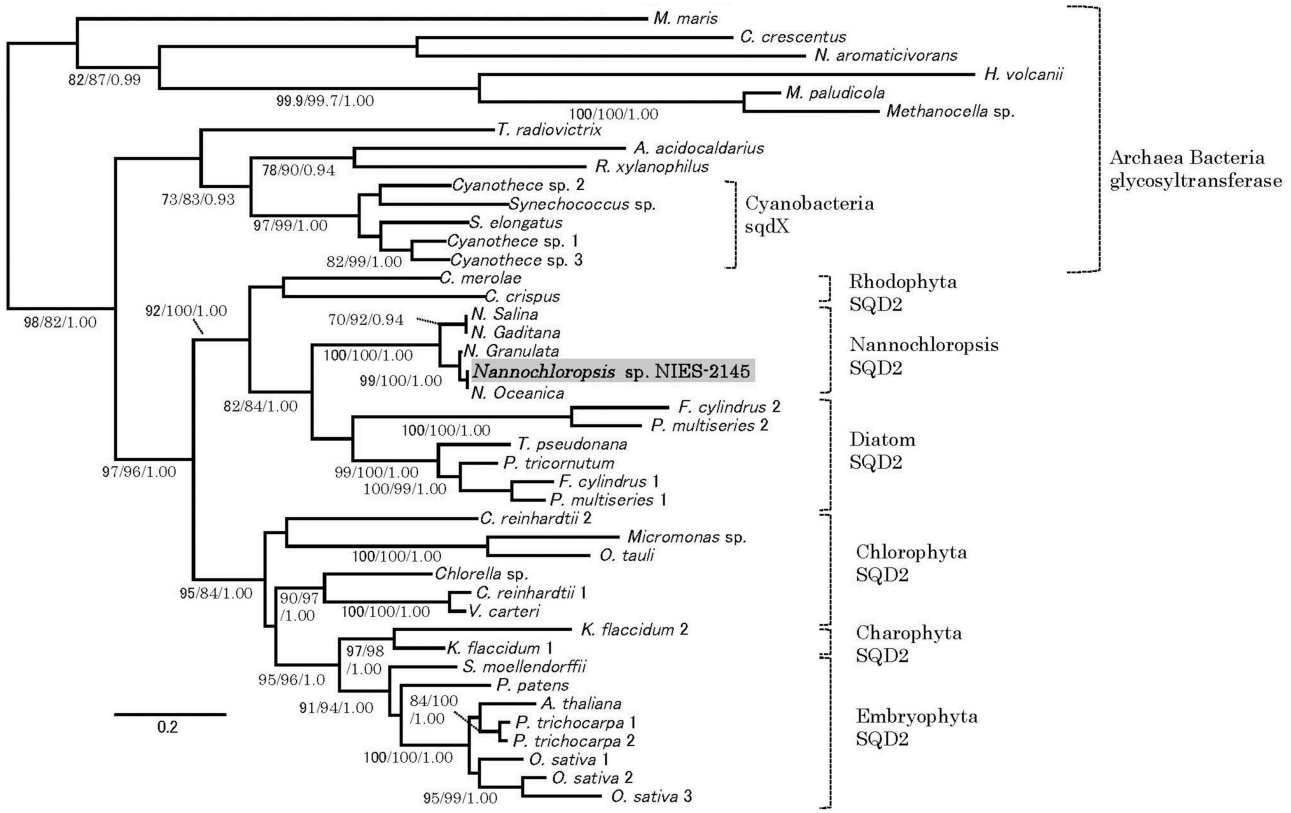

FIGURE 4 | Phylogenetic tree analysis of SQD2. A phylogeny incorporating eukaryotic SQD2, cyanobacterial sqdX and the glycosyl transferase proteins of other organisms was constructed using Bayesian inference, maximum likelihood and neighbor-joining algorithms. It is based on a protein comparison. The topologies and branch lengths were calculated using maximum likelihood. Bootstrap values (maximum likelihood and neighbor-joining) higher than 70 and Bayesian posterior probabilities (Bayesian inference) higher than 0.9 are indicated under each branch (maximum likelihood/neighbor-joining/Bayesian inference). The scale bar represents 0.2 amino acid substitutions per site. Sequence accession numbers or sequence resources for the phylogenetic tree are as follows: Archaea glycosyl transferase: *Methanocella paludicola* (YP_003355097), *Methanocella* sp. (YP_685710) and *Haloferax volcanii* (YP_003535220); Alpha-proteobacteria glycosyl transferase: *Caulobacter crescentus* (YP_002516166), *Novosphingobium aromaticivorans* (WP_011446186), and *Maricaulis maris* (WP_011642337); Cyanobacteria sqdX: *Cyanothece* sp. 1 (WP_015784192), *Cyanothece* sp. 2 (WP_012629991), *Synechococcus elongatus* (WP_011243256), *Synechococcus* sp. (WP_011429929), and *Cyanothece* sp. 3 (WP_015956855); Other bacterial glycosyl transferases: *Truepera radiovictrix* (WP_013178429), *Rubrobacter xylanophilus* (WP_011564279), and *Alicyclobacillus acidocaldarius* (WP_012810695); Rhodophyta SQD2: *Chondrus crispus* (XP_005715110), and *Cyanidioschyzon merolae* (XP_005538341); Stramenopile SQD2: *Nannochloropsis* sp. NIES-2145 (DDBJ Accession LC061442), *Nannochloropsis oceanica* IMET1 (BioProject: PRJNA202418, scaffold00247.g6721), *Nannochloropsis granulata* CCMP529 (BioProject: PRJNA65111, evm.model.NODE_3998_length_11613_cov_18.861534.4), *Nannochloropsis salina* CCMP537 (BioProject: PRJNA62503, evm.model.NODE_9973_length_179428_cov_24.782236.3), *Nannochloropsis gaditana* (EWM27152), *Phaeodactylum tricornutum* (JGI Protein ID: 50356), *Fragilariopsis cylindrus* 1 (JGI Protein ID: 207999), *Fragilariopsis cylindrus* 2 (JGI Protein ID: 158007), *Pseudo-nitzschia multiseries* 1 (JGI Protein ID: 252457), *Pseudo-nitzschia multiseries* 2 (JGI Protein ID: 145536), *Thalassiosira pseudonana* (JGI Protein ID: 38775), [Chlorophyta] *Ostreococcus tauri* (JGI Protein ID: 3203), *Micromonas* sp. (JGI Protein ID: 58169), *Chlorella* sp. (JGI Protein ID: 33086), *Volvox carteri* (Phytozome Transcript Name: Vocar20009459m), *Chlamydomonas reinhardtii* 1 (Phytozome Transcript Name: Cre01.g038550.t1.3), and *Chlamydomonas reinhardtii* 2 (Phytozome Transcript Name: Cre16.g689150.t1.2); Charophyta: *Klebsormidium flaccidum* 1 (BioProject: PRJDB718, kfl00392_0070) and *Klebsormidium flaccidum* 2 (BioProject: PRJDB718, kfl00041_0140), and Embryophyta (Phytozome Transcript Name): *Arabidopsis thaliana* (AT5G01220.1), *Populus trichocarpa* 1 (Potri.006G097600.1), *Populus trichocarpa* 2 (Potri.016G112600.1), *Oryza sativa* 1 (Os07g01030.1), *Oryza sativa* 2 (Os01g04920.1), *Oryza sativa* 3 (Os03g15840.1), *Selaginella moellendorffii* (170091), and *Physcomitrella patens* (Pp1s24_194V6.1).

CrDGTT4-overexpressing cell line. One of the overexpressing lines, line #9, was analyzed because of TAG accumulation most increased in this line. The major total fatty acids in either control or P-depleted medium were eicosapentaenoic (20:5 ω-3), palmitoleic (16:1 ω-7), and palmitic (16:0) acids (**Figure 8**). This agreed with previous analyses (Maruyama et al., 1986; Patil et al., 2007). The levels of 16:0, 16:1, oleic (18:1 ω-9), and dihomo-gamma-linolenic (20:3 ω-6) fatty acids increased, whereas 16:3, linoleic (18:2 ω-6), arachidonic (20:4 ω-6) and 20:5 fatty acids decreased under P starvation conditions (**Figure 8**). The degree of unsaturation for each fatty acid decreased as the unsaturated fatty acids were replaced with saturated fatty acids. As for the total fatty acid composition, no statistically significant differences could be observed among the wild-type,

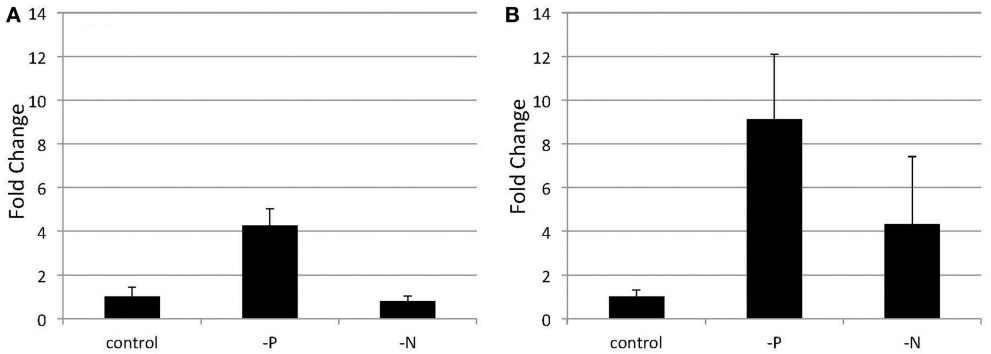

FIGURE 5 | Quantitative real-time PCR showing the induction of *SQD2* gene expression in *Nannochloropsis* after P or N starvation. Logarithmic-phase cells were transferred to standard (control), -P and -N media and cultured for 4 days **(A)** or 6 days **(B)**. The values are normalized to the expression of TUB and the SQD2/TUB ratio under standard conditions was set as 1. Values represent the mean ± SD from three independent replicates.

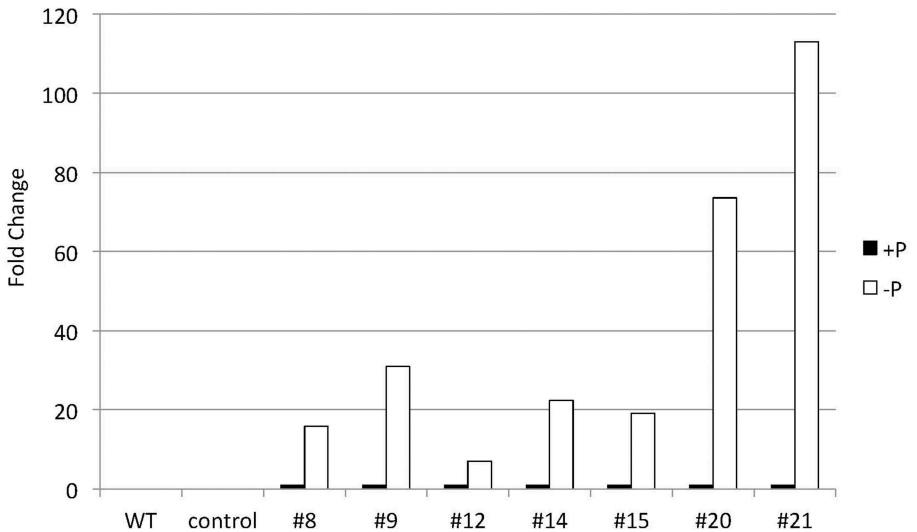

FIGURE 6 | Quantitative real-time PCR showing the induction of *CrDGTT4* gene expression in *CrDGTT4*-overexpressing cells after P deprivation. Cells were cultured for 5 days. The relative levels of *CrDGTT4* mRNA overexpression in seven cell lines were assessed under standard (+P) and -P growth conditions. The values were normalized to the expression level of TUB. The CrDGTT4/TUB ratio under standard conditions was set as 1. The levels of the wild type (WT) and empty vector control (control) are below the detection threshold.

control and overexpressing lines (**Figure 8**). In the case of TAG fatty acids in the overexpressing line, the levels of 18:1 and 20:3 fatty acids were higher, whereas 16:0, 16:1, 16:2, and 16:3 fatty acids were lower than those in the wild-type or control lines during P starvation (**Figure 9**). The levels of 20:4 and 20:5 bound to TAGs (∼0.8% and ∼2.3%, respectively) were remarkably reduced under P starvation in comparison with the levels of these fatty acids in total fatty acids (∼1–3% and ∼15%, respectively; **Figure 9**). Under P starvation, the increase in the 20:3 fatty acid in the total lipids was a reflection of its increase in TAG. It is interesting to note that the level of 18:1 fatty acids was higher in the *CrDGTT4*-overexpressing cell line than in the control line under P starvation conditions (**Figure 9**). This is consistent with our previous report on *CrDGTT4*-overexpressing *C. reinhardtii* cell lines during P starvation (Iwai et al., 2014). These results showed that the *C. reinhardtii SQD2* promoter is useful as a heterologous promoter in the secondary endosymbiotic alga *Nannochloropsis* strain NIES-2145.

P Starvation did not Cause Significant Changes in Membrane Lipid Composition between the Control Line and Overexpressing Line

The overexpressing line showed alteration in TAG, whereas no serious alterations in the major membrane lipids compared with the control line under standard growth conditions or conditions of P stress, except for PS level (**Figure 10**, **Supplemental Figure 3**). PS decreased more in the overexpressing line than in the control line under P starvation (**Supplemental Figure 3**). We investigated whether the fatty

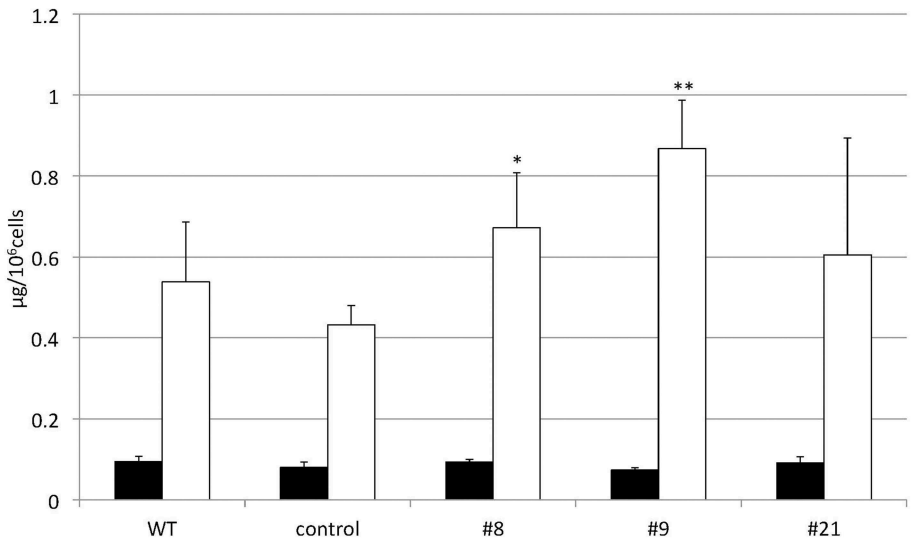

FIGURE 7 | Changes in the TAG content of *CrDGTT4*-overexpressing cells in response to P starvation. *Nannochloropsis* cells were transformed with pCrSQD2-CrDGTT4 to overexpress *CrDGTT4*. Cells cultured to a logarithmic phase under standard conditions were then inoculated into P-starved medium and cultured for 4 days. Three transformants, the empty vector control (control) and the wild type (WT) are shown. Values represent the mean ± SD from four independent replicates. Asterisks indicate a statistically significant difference compared with the empty vector control based on a two-tailed Student's *t*-test (*$P < 0.05$ and **$P < 0.01$).

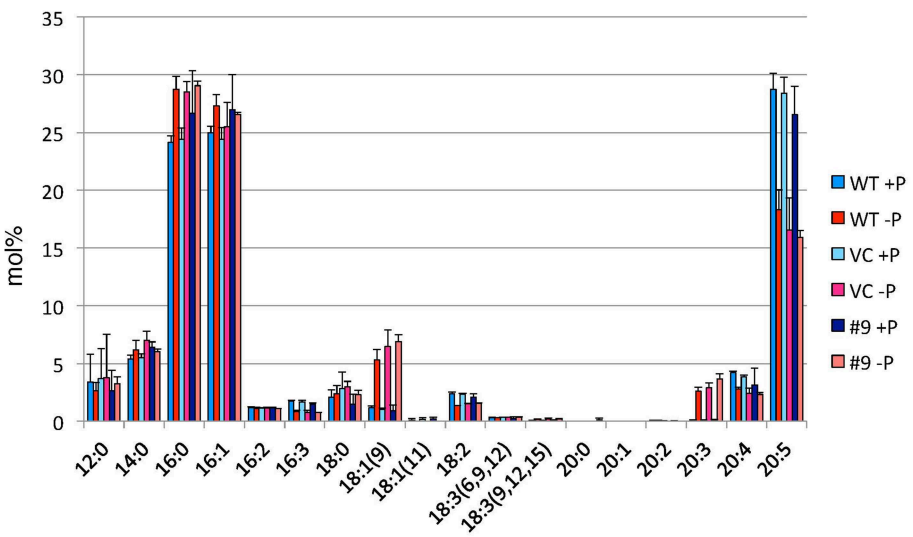

FIGURE 8 | Analysis of the fatty acid composition of total lipids in pCrSQD2-CrDGTT4 (#9), vector control (VC) and wild-type (WT) lines. Cells were cultured in control (+P) or -P medium for 4 days. Values are the mean ± SD from three independent experiments.

acid composition of the major membrane lipids was altered in the *CrDGTT4*-overexpressing cell line (**Figures 11**–**13**, **Supplemental Figures 4**–**7**). During P-depleted conditions, the enhanced incorporation of 18:1(9) fatty acid was observed in the major plastidic membrane lipids MGDG, DGDG and PG and the extra-plastidic membrane lipids PC, PS, and DGTS (**Figures 11**, **12**), whereas the enhanced incorporation of 20:3 fatty acid was observed in MGDG, DGDG, PC, and DGTS (**Figures 11**, **13**). In the contrast, there were decreases of 18:1(9) and 20:3 fatty acids in PE. There was a global decrease in the long polyunsaturated fatty acid, 20:5 (**Figure 11** and **Supplemental Figure 4**), and an increase in saturated fatty acids, for example 16:0 (**Figure 11** and **Supplemental Figure 5**), during P-depleted conditions. Although large changes occur during P depravation, no significant differences could be observed in the major membrane lipids between the control line and overexpressing line, except for the decrease of 18:1 (9) fatty acid in the major plastidic membrane lipid PG.

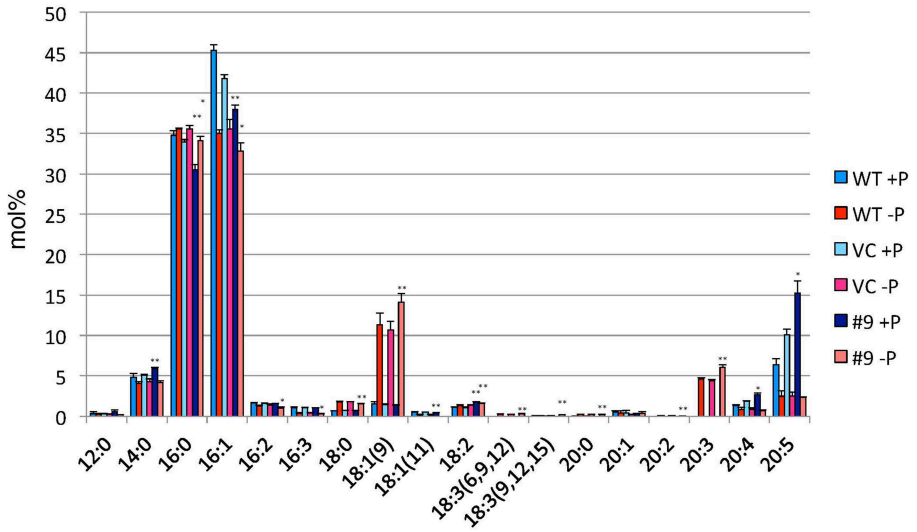

FIGURE 9 | Analysis of the fatty acid composition of the TAG fraction in pCrSQD2-CrDGTT4 (#9), the vector control (VC) and wild-type (WT) lines. Cells were cultured in control (+P) or -P medium for 4 days. Values are the mean ± SD from three independent experiments. Asterisks indicate a statistically significant difference compared with VC based on a two-tailed Student's *t*-test (*$P < 0.05$ and **$P < 0.01$).

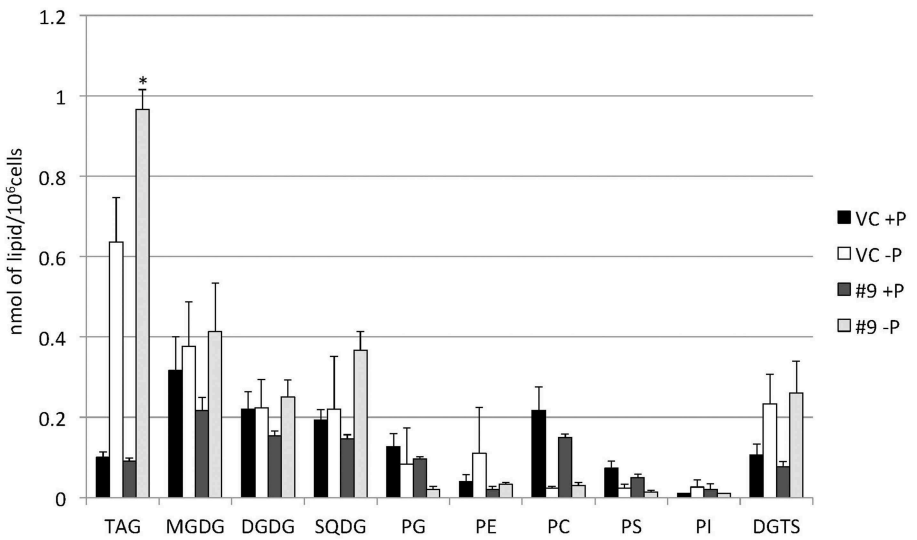

FIGURE 10 | Quantitative analysis of the various lipids. Cells were cultured in control (+P) or -P medium for 4 days. Each lipid is expressed in nmol per 10^6 cells. Values are the mean ± SD from three independent experiments. Asterisks indicate a statistically significant difference compared with VC based on a two-tailed Student's *t*-test (*$P < 0.05$).

Discussion

Whereas TAG amounts increase under N starvation, MGDG, DGDG, SQDG, PG, and PI decrease in *C. reinhardtii* cells (Siaut et al., 2011; Sakurai et al., 2014) and the polar glycerolipid contents, represented mainly by MGDG, DGDG, and SQDG and phospholipids PE and PC, are reduced in *Nannochloropsis* strains (Simionato et al., 2013; Li et al., 2014; Martin et al., 2014). However, we found that SQDG and DGTS accumulated, replacing PG and PC, respectively, in *Nannochloropsis* cells under P starvation conditions (**Figures 3**, **10**, **Supplemental Figure 3**). This result corroborates previous reports on P deprivation in several species (Benning et al., 1993, 1995; Essigmann et al., 1998; Sato et al., 2000; Khozin-Goldberg and Cohen, 2006). In *Monodus subterraneus*, which is a freshwater microalga in the class Eustigmatophyceae, DGTS and SQDG increased under P starvation conditions (Khozin-Goldberg and Cohen, 2006). In *A. thaliana,* SQDG is synthesized to replace PG in chloroplasts during P starvation so that the amount of anionic thylakoid lipid is maintained (Essigmann et al., 1998; Yu and Benning, 2003).

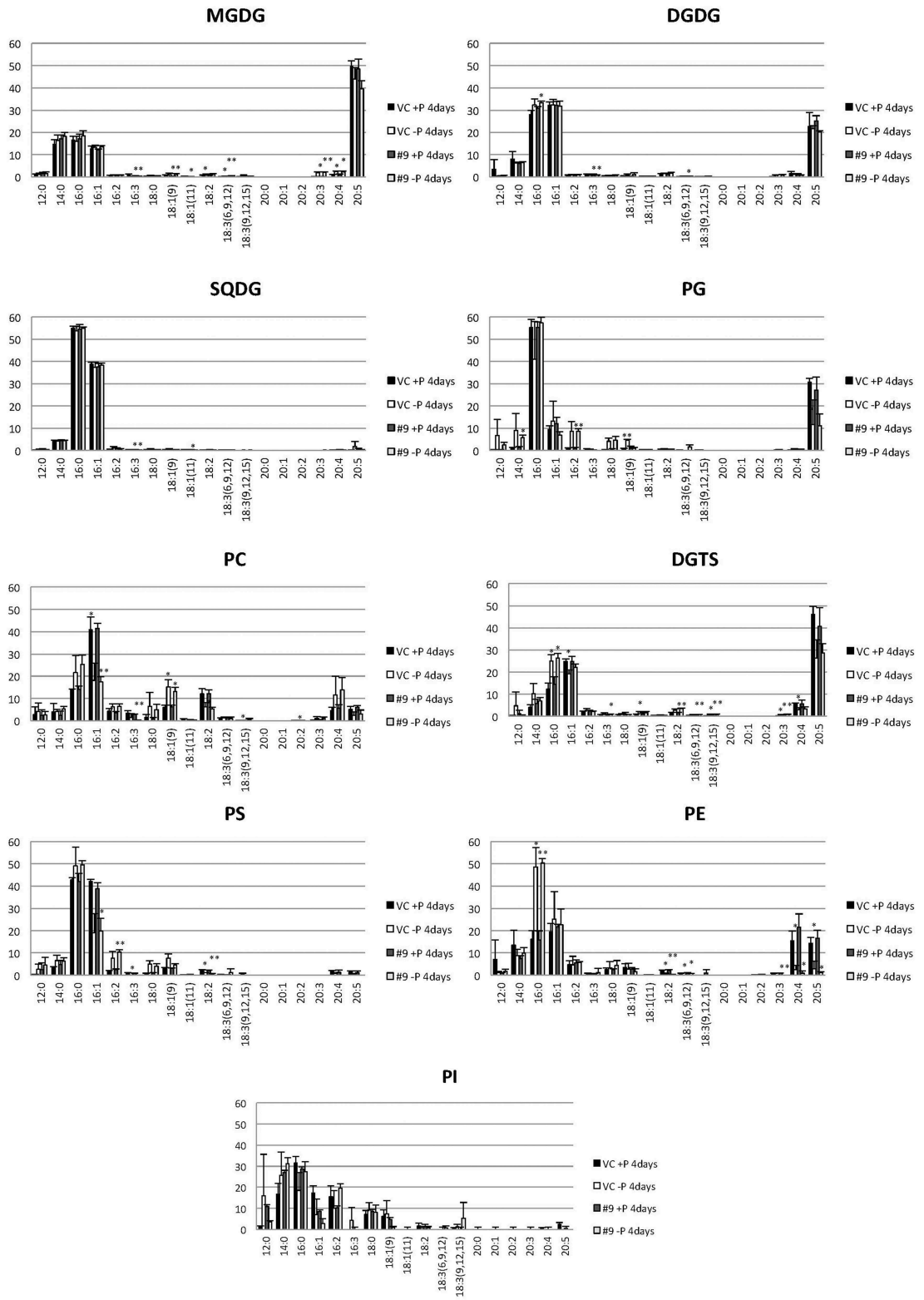

FIGURE 11 | Analysis of the fatty acid composition of the major lipids in pCrSQD2-CrDGTT4 (#9) and the vector control (VC) lines. Cells were cultured in control (+P) or -P medium for 4 days. Black bars, the vector control (VC) 4 days in control medium; white bars, VC 4 days in -P; dark gray bars, pCrSQD2-CrDGTT4 (#9) 4 days in control medium; and light gray bars, pCrSQD2-CrDGTT4 (#9) 4 days in -P. Values are the mean ± SD from three independent experiments. Asterisks indicate a statistically significant difference compared with wild-type based on a two-tailed Student's *t*-test (*$P < 0.05$ and **$P < 0.01$).

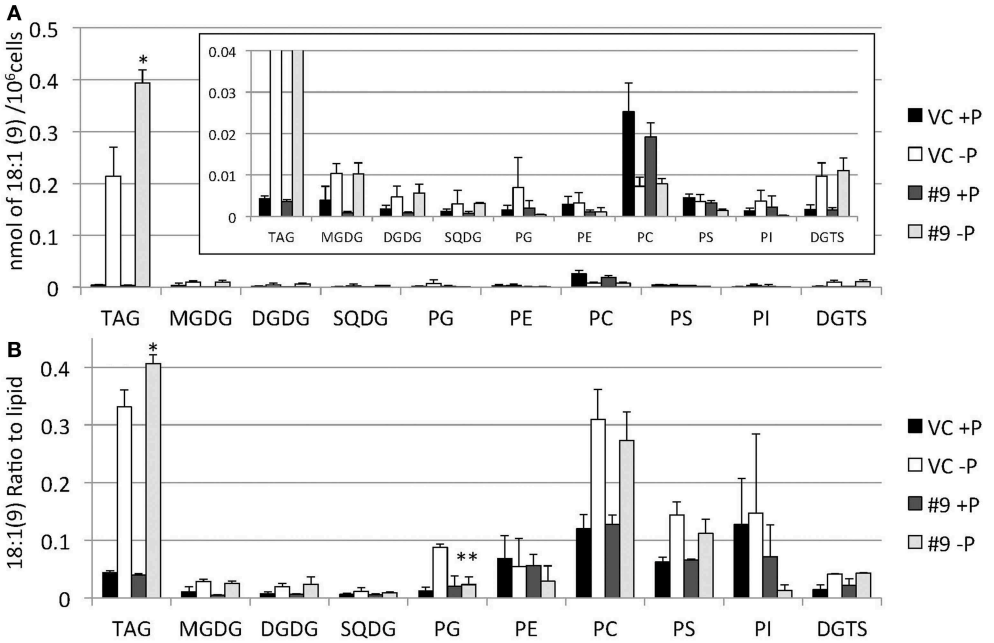

FIGURE 12 | Quantitative analysis and ratio of 18:1(9) in the various lipids. Cells were cultured in control (+P) or -P medium for 4 days. **(A)** Each 18:1(9) in the various lipids is expressed in nmol per 10^6 cells. **(B)** The y-axis is ratio of 18:1(9) in each lipid per 10^6 cells. Values are the mean ± SD from three independent experiments. Asterisks indicate a statistically significant difference compared with VC based on a two-tailed Student's *t*-test (*$P < 0.05$ and **$P < 0.01$).

In *C. reinhardtii*, mechanisms exist that maintain a constant total amount of SQDG and PG under sulfur- or P-limiting conditions (Sato et al., 2000). Therefore, our results suggest that SQDG substitutes for PG, to some extent, to sustain the functional activity of the decreased chloroplast membranes in *Nannochloropsis*, as in *C. reinhardtii*.

When the *SQD2* promoter is applied, total TAG levels per cell after 4 days of P starvation were ∼1.7-fold greater in *CrDGTT4*-overexpressing lines compared with the control line (**Figure 7**). However, the difference between *CrDGTT4*-overexpressing lines and the control line after 6 days of P starvation was less than after 4 days (**Supplemental Figure 2**). During N starvation in *N. oceanica* IMET1, seven DGAT transcripts are up-regulated and six other DGAT transcripts are down-regulated (Li et al., 2014). Our results in *Nannochloropsis* might be explained by the up-regulation of *Nannochloropsis*'s own DGATs, particularly in later stages of P depletion. The levels of 18:1(9) and 20:3 fatty acids bound to TAGs increased during P starvation in comparison with the levels of these fatty acids under standard conditions (**Figure 9**). The levels of these two fatty acids in TAG molecular species were higher in the *CrDGTT4*-overexpressing cell line than in the control line during P starvation. This may reflect the specificity of CrDGTT4. In contrast to the TAG fraction, the 18:1(9) molecular ratio of PG decreased in the *CrDGTT4*-overexpressing cell line than in the control line during P starvation (**Figures 11**, **12**). This fatty acid change may be associated with the preferential incorporation of the 18:1(9) molecular species into the TAG fraction.

It was unexpected that 20:3 fatty acid also increased in the *CrDGTT4*-overexpressing line (**Figures 11**, **13**). This may have been due to the suppression of desaturation in very long chain fatty acids, like 20:4 and 20:5 (**Figure 11** and **Supplemental Figures 6**, **7**), because of accelerated TAG accumulation. Although the exact reason is unclear, 20:3 fatty acid tends to accumulate under P starvation conditions, but not under N starvation conditions (Simionato et al., 2013; Martin et al., 2014). This fact suggests that a specific pathway for fatty acid incorporation is activated during P starvation.

The SQD2 is highly conserved from red algae to plants, as are its primary structures (**Figure 4**), and the algal SQD2 is also conserved in secondary algae, including *Nannochloropsis*. This may be due to the importance of the acidic membrane lipid SQDG, which is common to various algal species. The importance of SQDG for photosystem II was demonstrated clearly for *C. reinhardtii* and the cyanobacterium *Synechocystis* sp. PCC6803 through the characterization of mutants from each species that are deficient in the ability to synthesize SQDG (Minoda et al., 2002; Sato et al., 2003; Aoki et al., 2004; Sato, 2004). Recent work on higher plant *SQD2* genes indicated that SQD2 is also involved with another acidic lipid, glucuronosyldiacylglycerol (Okazaki et al., 2013). It is possible that algal SQD2 also produces glucuronosyldiacylglycerol, which would thus be more important under P starvation conditions.

Our results showed that the *SQD2* promoter from the green alga *C. reinhardtii* is useful as heterologous promoter in *Nannochloropsis* strain NIES-2145 cells. The results of this study suggest that there is a common expression control system in a

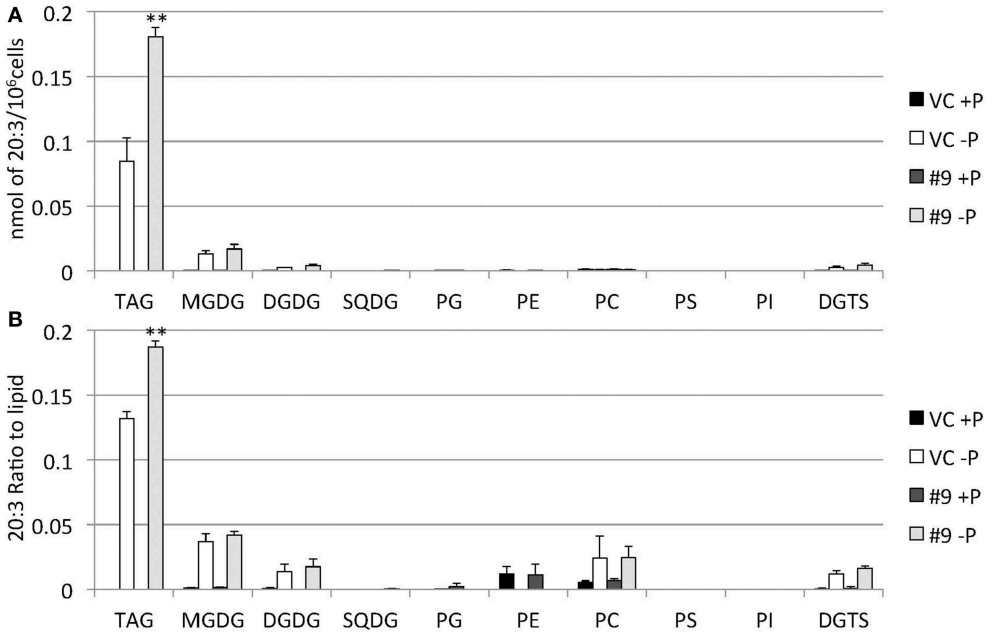

FIGURE 13 | Quantitative analysis and ratio of 20:3 in the various lipids. Cells were cultured in control (+P) or -P medium for 4 days. **(A)** Each 20:3 in the various lipids is expressed in nmol per 10^6 cells. **(B)** The y-axis is ratio of 20:3 in the various lipids per 10^6 cells. Values are the mean ± SD from three independent experiments. Asterisks indicate a statistically significant difference compared with VC based on a two-tailed Student's *t*-test (**$P < 0.01$).

wide range of algal species, including primary and secondary microalgae, for adaptation to low P. This result, together with the occurrence of SQDG synthesis genes throughout algal species, suggests that a membrane remodeling system in chloroplasts under low-P stress is itself common among various microalgae and, thus, related genes and *cis*- and *trans*-acting elements are highly conserved. This also suggests that the *SQD2* promoter from *C. reinhardtii* could be applied in various algae.

Arabidopsis SQD2 contains three PHR1-binding sequence (P1BS) motifs in its promoter. The PHR1 transcription factor binds to P1BS elements containing the consensus sequence "GNATATNC" in the promoters of a large number of P starvation–responsive genes (Franco-Zorrilla et al., 2004; Bustos et al., 2010; Pant et al., 2015). PHR1 is a well-described transcriptional regulator of P starvation in the MYB family. Most of the genes and their promoters that are involved in phospholipid degradation and glycolipid biosynthesis contain P1BS motifs in *Arabidopsis* (Pant et al., 2015). As there are no significant effects of a *PHR1* null allele on DGDG synthesis during P limitation in *Arabidopsis*, a role for PHR1 in lipid remodeling was thus excluded (Gaude et al., 2008). However, glycerolipids, including MGDG, DGDG and SQDG, their composition and the expression of most lipid-remodeling gene transcripts analyzed were all altered in the *phr1* mutant under P starvation when compared with the wild type (Pant et al., 2015). We used the *C. reinhardtii SQD2* gene (Cre01.g038550) promoter for *CrDGTT4* overexpression. Another *SQD2* gene homolog (Cre16.g689150) exists in *C. reinhardtii*. Both *C. reinhardtii SQD2* genes were up-regulated under P starvation (data not shown). We searched the promoter regions of these genes, and they do not contain P1BS motifs in their promoters but have binding motifs for many other transcription factors. *C. reinhardtii SQD2* has 14 MYB or MYC binding domains in its promoter region, whereas *Nannochloropsis oceanica SQD2* has 12 MYB or MYC binding domains in its promoter region (**Supplemental Figure 8**). There is no reliable evidence revealing which motif offers the most effective transcriptional regulation under P starvation. Further work is necessary to understand the regulation of lipid remodeling during P stress in algae.

Author Contributions

MI prepared samples of *Nannochloropsis* strain NIES-2145 for each experiment. KH performed *in silico* analysis. YS performed GC-MS analysis. MI, KH, YS and HO wrote the manuscript. MS and HO planned the project.

Acknowledgments

This work was partially supported by the KAO Corporation and JST CREST from the Ministry of Education, Sports, Science and Culture in Japan.

Supplementary Material

The Supplementary Material for this article can be found online at: http://journal.frontiersin.org/article/10.3389/fmicb.2015.00912

Supplemental Figure 1 | Changes in the TAG content of *Nannochloropsis* in response to N or P starvation. Cells cultured to the logarithmic phase under f/2 medium were then inoculated into f/2, -N or -P medium and cultured for 13 d.

Supplemental Figure 2 | Changes in the TAG content of *CrDGTT4*-overexpressing cells in response to P starvation. *Nannochloropsis* cells were transformed with pCrSQD2-CrDGTT4 to overexpress *CrDGTT4*. Cells cultured to the logarithmic phase under standard conditions were then inoculated into control (+P) or -P medium and cultured for 6 days (6 d). The transformants (#8, #9, and #21), the empty vector control (VC) and the wild type (WT) are shown. Values represent the mean ± SD from three independent replicates.

Supplemental Figure 3 | Changes in major lipid classes in P-starved cells. Black bars, the vector control (VC) 4 days in control medium (+P); white bars, VC 4 days in -P; dark gray bars, pCrSQD2-CrDGTT4 (#9) 4 days in control medium (+P); and light gray bars, pCrSQD2-CrDGTT4 (#9) 4 days in -P. Values are the mean ± SD from three independent experiments. Asterisks indicate a statistically significant difference compared with VC based on a two-tailed Student's *t*-test ($^*P < 0.05$). Small letters indicate statistically significant difference compared with the control medium based on a two-tailed Student's *t*-test ($^aP < 0.05$ and $^bP < 0.01$).

Supplemental Figure 4 | Quantitative analysis and ratio of 20:5 in the various lipids. Cells were cultured in control (+P) or -P medium for 4 days. **(A)** Each 20:5 in the various lipids is expressed in nmol per 10^6 cells. **(B)** The y-axis is ratio of 20:5 in each lipid per 10^6 cells. Values are the mean ± SD from three independent experiments. Asterisks indicate a statistically significant difference compared with VC based on a two-tailed Student's *t*-test ($^*P < 0.05$).

Supplemental Figure 5 | Quantitative analysis and ratio of 16:0 in the various lipids. Cells were cultured in control (+P) or -P medium for 4 days. **(A)** Each 16:0 in the various lipids is expressed in nmol per 10^6 cells. **(B)** The y-axis is ratio of 16:0 in each lipid per 10^6 cells. Values are the mean ± SD from three independent experiments. Asterisks indicate a statistically significant difference compared with VC based on a two-tailed Student's *t*-test ($^*P < 0.05$).

Supplemental Figure 6 | Quantitative analysis and ratio of 16:1 in the various lipids. Cells were cultured in control (+P) or –P medium for 4 days. **(A)** Each 16:1 in the various lipids is expressed in nmol per 10^6 cells. **(B)** The y-axis is ratio of 16:1 in each lipid per 10^6 cells. Values are the mean ± SD from three independent experiments. Asterisks indicate a statistically significant difference compared with VC based on a two-tailed Student's *t*-test ($^*P < 0.05$).

Supplemental Figure 7 | Quantitative analysis and ratio of 20:4 in the various lipids. Cells were cultured in control (+P) or -P medium for 4 days. **(A)** Each 20:4 in the various lipids is expressed in nmol per 10^6 cells. **(B)** The y-axis is ratio of 20:4 in each lipid per 10^6 cells. Values are the mean ± SD from three independent experiments. Asterisks indicate a statistically significant difference compared with VC based on a two-tailed Student's *t*-test ($^*P < 0.05$).

Supplemental Figure 8 | MYB/MYC binding motif in the *SQD2* promoter region of *Nannochloropsis oceanica* and *Chlamydomonas reinhardtii*. Yellow character, CTGTTA (+) strand MYB/MYC binding motif; red character, (+) and (−) strand MYB/MYC binding motif; blue character, (−) strand MYB/MYC binding motif; green character, CDS; pale green character, UTR region.

Supplemental Table 1 | Primer sequences.

References

Aoki, M., Sato, N., Meguro, A., and Tsuzuki, M. (2004). Differing involvement of sulfoquinovosyl diacylglycerol in photosystem II in two species of unicellular cyanobacteria. *Eur. J. Biochem.* 271, 685–693. doi: 10.1111/j.1432-1033.2003.03970.x

Arudchelvam, Y., and Nirmalakhandan, N. (2012). Optimizing net energy gain in algal cultivation for biodiesel production. *Bioresour. Technol.* 114, 294–302. doi: 10.1016/j.biortech.2012.02.126

Benning, C., Beatty, J. T., Prince, R. C., and Somerville, C. R. (1993). The sulfolipid sulfoquinovosyldiacylglycerol is not required for photosynthetic electron transport in *Rhodobacter sphaeroides* but enhances growth under phosphate limitation. *Proc. Natl. Acad. Sci. U.S.A.* 90, 1561–1565. doi: 10.1073/pnas.90.4.1561

Benning, C., Huang, Z. H., and Gage, D. A. (1995). Accumulation of a novel glycolipid and a betaine lipid in cells of *Rhodobacter sphaeroides* grown under phosphate limitation. *Arch. Biochem. Biophys* 317, 103–111. doi: 10.1006/abbi.1995.1141

Bligh, E. G., and Dyer, W. J. (1959). A rapid method of total lipid extraction and purification. *Can. J. Biochem. Physiol.* 37, 911–917. doi: 10.1139/o59-099

Bondioli, P., Della Bella, L., Rivolta, G., Chini Zittelli, G., Bassi, N., Rodolfi, L., et al. (2012). Oil production by the marine microalgae *Nannochloropsis* sp. F&M-M24 and *Tetraselmis suecica* F&M-M33. *Bioresour. Technol.* 114, 567–572. doi: 10.1016/j.biortech.2012.02.123

Boyle, N. R., Page, M. D., Liu, B., Blaby, I. K., Casero, D., Kropat, J., et al. (2012). Three acyltransferases and nitrogen-responsive regulator are implicated in nitrogen starvation-induced triacylglycerol accumulation in *Chlamydomonas*. *J. Biol. Chem.* 287, 15811–15825. doi: 10.1074/jbc.M111.334052

Brueggeman, A. J., Kuehler, D., and Weeks, D. P. (2014). Evaluation of three herbicide resistance genes for use in genetic transformations and for potential crop protection in algae production. *Plant Biotechnol. J.* 12, 894–902. doi: 10.1111/pbi.12192

Bustos, R., Castrillo, G., Linhares, F., Puga, M. I., Rubio, V., Pérez-Pérez, J., et al. (2010). A central regulatory system largely controls transcriptional activation and repression responses to phosphate starvation in Arabidopsis. *PLoS Genet.* 6:e1001102. doi: 10.1371/journal.pgen.1001102

Cases, S., Smith, S. J., Zheng, Y. W., Myers, H. M., Lear, S. R., Sande, E., et al. (1998). Identification of a gene encoding an acyl CoA:diacylglycerol acyltransferase, a key enzyme in triacylglycerol synthesis. *Proc. Natl. Acad. Sci. U.S.A.* 95, 13018–13023. doi: 10.1073/pnas.95.22.13018

Chang, C. W., Moseley, J. L., Wykoff, D., and Grossman, A. R. (2005). The LPB1 gene is important for acclimation of *Chlamydomonas reinhardtii* to phosphorus and sulfur deprivation. *Plant Physiol.* 138, 319–329. doi: 10.1104/pp.105.059550

Converti, A., Casazza, A. A., Ortiz, E. Y., Perego, P., and Borghi, M. D. (2009). Effect of temperature and nitrogen concentration on the growth and lipid content of *Nannochloropsis oculata* and *Chlorella vulgaris* for biodiesel production. *Chem. Eng. Process.* 48, 1146–1151. doi: 10.1016/j.cep.2009.03.006

Eichler-Stahlberg, A., Weisheit, W., Ruecker, O., and Heitzer, M. (2009). Strategies to facilitate transgene expression in *Chlamydomonas reinhardtii*. *Planta* 229, 873–883. doi: 10.1007/s00425-008-0879-x

Essigmann, B., Güler, S., Narang, R. A., Linke, D., and Benning, C. (1998). Phosphate availability affects the thylakoid lipid composition and the expression of *SQD1*, a gene required for sulfolipid biosynthesis in *Arabidopsis thaliana*. *Proc. Natl. Acad. Sci. U.S.A.* 95, 1950–1955. doi: 10.1073/pnas.95.4.1950

Franco-Zorrilla, J. M., González, E., Bustos, R., Linhares, F., Leyva, A., and Paz-Ares, J. (2004). The transcriptional control of plant responses to phosphate limitation. *J. Exp. Bot.* 55, 285–293. doi: 10.1093/jxb/erh009

Gaude, N., Nakamura, Y., Scheible, W. R., Ohta, H., and Dörmann, P. (2008). Phospholipase C5 (NPC5) is involved in galactolipid accumulation during phosphate limitation in leaves of Arabidopsis. *Plant J.* 56, 28–39. doi: 10.1111/j.1365-313X.2008.03582.x

Giroud, C., Gerber, A., and Eichenberger, W. (1988). Lipids of *Chlamydomonas reinhardtii*. Analysis of molecular species and intracellular site(s) of biosynthesis. *Plant Cell Physiol.* 29, 587–595.

Grossman, A. (2000). Acclimation of *Chlamydomonas reinhardtii* to its nutrient environment. *Protist* 151, 201–224. doi: 10.1078/1434-4610-00020

Guillard, R. R., and Ryther, J. H. (1962). Studies of marine planktonic diatoms. I. Cyclotella nana Hustedt, and Detonula confervacea (cleve) Gran. *Can. J. Microbiol.* 8, 229–239. doi: 10.1139/m62-029

Guschina, I. A., and Harwood, J. L. (2006). Lipids and lipid metabolism in eukaryotic algae. *Prog. Lipid. Res.* 45, 160–186. doi: 10.1016/j.plipres.2006.01.001

Harris, E. H. (2009). *The Chlamydomonas Sourcebook: Introduction to Chlamydomonas and its Laboratory Use, 2nd Edn*. Oxford, UK: Academic Press.

Hirata, R., Jeong, W. J., Saga, N., and Mikami, K. (2011). Heterologous activation of the *Porphyra tenera HSP70* promoter in Bangiophycean algal cells. *Bioeng. Bugs* 2, 271–274. doi: 10.4161/bbug.2.5.16938

Hodgson, P. A., Henderson, R. J., Sargent, J. R., and Leftley, J. W. (1991). Patterns of variation in the lipid class and fatty acid composition of *Nannochloropsis oculata* (Eustigmatophyceae) during batch culture. *J. Appl. Phycol.* 3, 169–181. doi: 10.1007/BF00003699

Hu, H., and Gao, K. (2006). Response of growth and fatty acid compositions of *Nannochloropsis* sp. to environmental factors under elevated CO2 concentration. *Biotechnol. Lett.* 28, 987–992. doi: 10.1007/s10529-006-9026-6

Hu, Q., Sommerfeld, M., Jarvis, E., Ghirardi, M., Posewitz, M., Seibert, M., et al. (2008). Microalgal triacylglycerols as feedstocks for biofuel production: perspectives and advances. *Plant J.* 54, 621–639. doi: 10.1111/j.1365-313X.2008.03492.x

Huerlimann, R., de Nys, R., and Heimann, K. (2010). Growth, lipid content, productivity, and fatty acid composition of tropical microalgae for scale-up production. *Biotechnol. Bioeng.* 107, 245–257. doi: 10.1002/bit.22809

Iwai, M., Ikeda, K., Shimojima, M., and Ohta, H. (2014). Enhancement of extraplastidic oil synthesis in *Chlamydomonas reinhardtii* using a type-2 diacylglycerol acyltransferase with a phosphorus starvation-inducible promoter. *Plant Biotechnol. J.* 12, 808–819. doi: 10.1111/pbi.12210

Katoh, K., and Standley, D. M. (2013). MAFFT multiple sequence alignment software version 7: improvements in performance and usability. *Mol. Biol. Evol.* 30, 772–780. doi: 10.1093/molbev/mst010

Khozin-Goldberg, I., and Cohen, Z. (2006). The effect of phosphate starvation on the lipid and fatty acid composition of the fresh water eustigmatophyte *Monodus subterraneus*. *Phytochemistry* 67, 696–701. doi: 10.1016/j.phytochem.2006.01.010

Kilian, O., Benemann, C. S., Niyogi, K. K., and Vick, B. (2011). High-efficiency homologous recombination in the oil-producing alga *Nannochloropsis* sp. *Proc. Natl. Acad. Sci. U.S.A.* 108, 21265–21269. doi: 10.1073/pnas.1105861108

Lardizabal, K. D., Mai, J. T., Wagner, N. W., Wyrick, A., Voelker, T., and Hawkins, D. J. (2001). DGAT2 is a new diacylglycerol acyltransferase gene family: purification, cloning, and expression in insect cells of two polypeptides from *Mortierella ramanniana* with diacylglycerol acyltransferase activity. *J. Biol. Chem.* 276, 38862–38869. doi: 10.1074/jbc.M106168200

Lerche, K., and Hallmann, A. (2013). Stable nuclear transformation of *Eudorina elegans*. *BMC Biotechnol.* 13:11. doi: 10.1186/1472-6750-13-11

Lerche, K., and Hallmann, A. (2014). Stable nuclear transformation of *Pandorina morum*. *BMC Biotechnol.* 14:65. doi: 10.1186/1472-6750-14-65

Li, J., Han, D., Wang, D., Ning, K., Jia, J., Wei, L., et al. (2014). Choreography of transcriptomes and lipidomes of *Nannochloropsis* reveals the mechanisms of oil synthesis in microalgae. *Plant Cell* 26, 1645–1665. doi: 10.1105/tpc.113.121418

Li-Beisson, Y., Shorrosh, B., Beisson, F., Andersson, M. X., Arondel, V., Bates, P. D., et al. (2010). Acyl-lipid metabolism. *Arabidopsis Book* 8:e0133. doi: 10.1199/tab.0133

Lung, S. C., and Weselake, R. J. (2006). Diacylglycerol acyltransferase: a key mediator of plant triacylglycerol synthesis. *Lipids* 41, 1073–1088. doi: 10.1007/s11745-006-5057-y

Martin, G. J., Hill, D. R., Olmstead, I. L., Bergamin, A., Shears, M. J., Dias, D. A., et al. (2014). Lipid profile remodeling in response to nitrogen deprivation in the microalgae *Chlorella* sp. (Trebouxiophyceae) and *Nannochloropsis* sp. (Eustigmatophyceae). *PLoS ONE* 9:e103389. doi: 10.1371/journal.pone.0103389

Maruyama, I., Nakamura, T., Matubayashi, T., Ando, Y., and Maeda, T. (1986). Identification of the alga known as "marine Chlorella" as a member of the Eustigmatophyceae. *Jpn. J. Phycol.* 34, 319–325.

Miller, R., Wu, G., Deshpande, R. R., Vieler, A., Gärtner, K., Li, X., et al. (2010). Changes in transcript abundance in *Chlamydomonas reinhardtii* following nitrogen deprivation predict diversion of metabolism. *Plant Physiol.* 154, 1737–1752. doi: 10.1104/pp.110.165159

Minoda, A., Sato, N., Nozaki, H., Okada, K., Takahashi, H., Sonoike, K., et al. (2002). Role of sulfoquinovosyl diacylglycerol for the maintenance of photosystem II in *Chlamydomonas reinhardtii*. *Eur. J. Biochem.* 269, 2353–2358. doi: 10.1046/j.1432-1033.2002.02896.x

Okazaki, Y., Otsuki, H., Narisawa, T., Kobayashi, M., Sawai, S., Kamide, Y., et al. (2013). A new class of plant lipid is essential for protection against phosphorus depletion. *Nat. Commun.* 4, 1510. doi: 10.1038/ncomms2512

Okazaki, Y., Shimojima, M., Sawada, Y., Toyooka, K., Narisawa, T., Mochida, K., et al. (2009). A chloroplastic UDP-glucose pyrophosphorylase from Arabidopsis is the committed enzyme for the first step of sulfolipid biosynthesis. *Plant Cell* 21, 892–909. doi: 10.1105/tpc.108.063925

Pant, B. D., Burgos, A., Pant, P., Cuadros-Inostroza, A., Willmitzer, L., and Scheible, W. R. (2015). The transcription factor PHR1 regulates lipid remodeling and triacylglycerol accumulation in *Arabidopsis thaliana* during phosphorus starvation. *J. Exp. Bot.* 66, 1907–1918. doi: 10.1093/jxb/eru535

Patil, V., Källqvist, T., Olsen, E., Vogt, G., and Gislerød, H. R. (2007). Fatty acid composition of 12 microalgae for possible use in aquaculture feed. *Aquacult Int.* 15, 1–9. doi: 10.1007/s10499-006-9060-3

Radakovits, R., Jinkerson, R. E., Fuerstenberg, S. I., Tae, H., Settlage, R. E., Boore, J. L., et al. (2012). Draft genome sequence and genetic transformation of the oleaginous alga *Nannochloropis gaditana*. *Nat. Commun.* 3, 686. doi: 10.1038/ncomms1688

Rajakumari, S., Grillitsch, K., and Daum, G. (2008). Synthesis and turnover of non-polar lipids in yeast. *Prog. Lipid. Res.* 47, 157–171. doi: 10.1016/j.plipres.2008.01.001

Rodolfi, L., Chini Zittelli, G., Bassi, N., Padovani, G., Biondi, N., Bonini, G., et al. (2009). Microalgae for oil: strain selection, induction of lipid synthesis and outdoor mass cultivation in a low-cost photobioreactor. *Biotechnol. Bioeng.* 102, 100–112. doi: 10.1002/bit.22033

Ronquist, F., Teslenko, M., Van der Mark, P., Ayres, D. L., Darling, A., Höhna, S., et al. (2012). MrBayes 3.2: efficient Bayesian phylogenetic inference and model choice across a large model space. *Syst. Biol.* 61, 539–542. doi: 10.1093/sysbio/sys029

Sakurai, K., Moriyama, T., and Sato, N. (2014). Detailed identification of fatty acid isomers sheds light on the probable precursors of triacylglycerol accumulation in photoautotrophically grown Chlamydomonas reinhardtii. *Eukaryot. Cell* 13, 256–266. doi: 10.1128/EC.00280-13

Sato, N. (2004). Roles of the acidic lipids sulfoquinovosyl diacylglycerol and phosphatidylglycerol in photosynthesis: their specificity and evolution. *J. Plant Res.* 117, 495–505. doi: 10.1007/s10265-004-0183-1

Sato, N., Aoki, M., Maru, Y., Sonoike, K., Minoda, A., and Tsuzuki, M. (2003). Involvement of sulfoquinovosyl diacylglycerol in the structural integrity and heat-tolerance of photosystem II. *Planta* 217, 245–251. doi: 10.1007/s00425-003-0992-9

Sato, N., and Furuya, M. (1985). Distribution of diacylglyceryltrimethylhomoserine and phosphatidylcholine in non-vascular green plants. *Plant Sci.* 38, 81–85. doi: 10.1016/0168-9452(85)90134-7

Sato, N., Hagio, M., Wada, H., and Tsuzuki, M. (2000). Environmental effects on acidic lipids of thylakoid membranes. *Biochem. Soc. Trans.* 28, 912–914. doi: 10.1042/bst0280912

Shockey, J. M., Gidda, S. K., Chapital, D. C., Kuan, J. C., Dhanoa, P. K., Bland, J. M., et al. (2006). Tung tree DGAT1 and DGAT2 have nonredundant functions in triacylglycerol biosynthesis and are localized to different subdomains of the endoplasmic reticulum. *Plant Cell* 18, 2294–2313. doi: 10.1105/tpc.106.043695

Siaut, M., Cuiné, S., Cagnon, C., Fessler, B., Nguyen, M., Carrier, P., et al. (2011). Oil accumulation in the model green alga *Chlamydomonas reinhardtii*: characterization, variability between common laboratory strains and relationship with starch reserves. *BMC Biotechnol.* 11:7. doi: 10.1186/1472-6750-11-7

Simionato, D., Block, M. A., La Rocca, N., Jouhet, J., Maréchal, E., Finazzi, G., et al. (2013). The response of *Nannochloropsis gaditana* to nitrogen starvation includes de novo biosynthesis of triacylglycerols, a decrease of chloroplast galactolipids, and reorganization of the photosynthetic apparatus. *Eukaryot. Cell* 12, 665–676. doi: 10.1128/EC.00363-12

Simionato, D., Sforza, E., Corteggiani Carpinelli, E., Bertucco, A., Giacometti, G. M., and Morosinotto, T. (2011). Acclimation of *Nannochloropsis gaditana* to different illumination regimes: effects on lipids accumulation. *Bioresour. Technol.* 102, 6026–6032. doi: 10.1016/j.biortech.2011.02.100

Talavera, G., and Castresana, J. (2007). Improvement of phylogenies after removing divergent and ambiguously aligned blocks from protein sequence alignments. *Syst. Biol.* 56, 564–577. doi: 10.1080/10635150701472164

Tamura, K., Stecher, G., Peterson, D., Filipski, A., and Kumar, S. (2013). MEGA6: Molecular Evolutionary Genetics Analysis version 6.0. *Mol. Biol. Evol.* 30, 2725–2729. doi: 10.1093/molbev/mst197

Tanabe, A. S. (2011). Kakusan4 and Aminosan: two programs for comparing nonpartitioned, proportional and separate models for combined molecular phylogenetic analyses of multilocus sequence data. *Mol. Ecol. Resour.* 11, 914–921. doi: 10.1111/j.1755-0998.2011.03021.x

Vieler, A., Brubaker, S. B., Vick, B., and Benning, C. (2012a). A lipid droplet protein of *Nannochloropsis* with functions partially analogous to plant oleosins. *Plant Physiol.* 158, 1562–1569. doi: 10.1104/pp.111.193029

Vieler, A., Wu, G., Tsai, C. H., Bullard, B., Cornish, A. J., Harvey, C., et al. (2012b). Genome, functional gene annotation, and nuclear transformation of the heterokont oleaginous alga *Nannochloropsis oceanica* CCMP1779. *PLoS Genet.* 8:e1003064. doi: 10.1371/journal.pgen.1003064

Wang, D., Ning, K., Li, J., Hu, J., Han, D., Wang, H., et al. (2014). *Nannochloropsis* genomes reveal evolution of microalgal oleaginous traits. *PLoS Genet.* 10:e1004094. doi: 10.1371/journal.pgen.1004094

Weyer, K. M., Bush, D. R., Darzins, A., and Wilso, B. D. (2010). Theoretical maximum algal oil production. *Bioenergy Res.* 3, 204–213. doi: 10.1007/s12155-009-9046-x

Yu, B., and Benning, C. (2003). Anionic lipids are required for chloroplast structure and function in *Arabidopsis*. *Plant J.* 36, 762–770. doi: 10.1046/j.1365-313X.2003.01918.x

Yu, B., Xu, C., and Benning, C. (2002). Arabidopsis disrupted in SQD2 encoding sulfolipid synthase is impaired in phosphate-limited growth. *Proc. Natl. Acad. Sci. U.S.A.* 99, 5732–5737. doi: 10.1073/pnas.082696499

Zhang, Z., Shrager, J., Jain, M., Chang, C. W., Vallon, O., and Grossman, A. R. (2004). Insights into the survival of *Chlamydomonas reinhardtii* during sulfur starvation based on microarray analysis of gene expression. *Eukaryot. Cell* 3, 1331–1348. doi: 10.1128/EC.3.5.1331-1348.2004

Conflict of Interest Statement: The authors declare that the research was conducted in the absence of any commercial or financial relationships that could be construed as a potential conflict of interest.

frontiers in Microbiology

ORIGINAL RESEARCH
published: 26 August 2015
doi: 10.3389/fmicb.2015.00888

Changes in primary metabolism under light and dark conditions in response to overproduction of a response regulator RpaA in the unicellular cyanobacterium *Synechocystis* sp. PCC 6803

Hiroko Iijima[1†], Tomokazu Shirai[2†], Mami Okamoto[2], Akihiko Kondo[2,3], Masami Yokota Hirai[2] and Takashi Osanai[1,2]*

[1] School of Agriculture, Meiji University, Kawasaki, Japan, [2] RIKEN, Center for Sustainable Resource Science, Yokohama, Japan, [3] Department of Chemical Science and Engineering, Graduate School of Engineering, Kobe University, Kobe, Japan

OPEN ACCESS

Edited by:
Weiwen Zhang, Tianjin University, China

Reviewed by:
Lei Chen, Tianjin University, China
Gopal K. Pattanayak, The University of Chicago, USA

***Correspondence:**
Takashi Osanai, School of Agriculture, Meiji University, 1-1-1, Higashimita, Tama-Ku, Kawasaki, Kanagawa 214-8571, Japan
tosanai@meiji.ac.jp

[†] *These authors have contributed equally to this work.*

Specialty section:
This article was submitted to Microbiotechnology, Ecotoxicology and Bioremediation, a section of the journal Frontiers in Microbiology

Received: *10 July 2015*
Accepted: *14 August 2015*
Published: *26 August 2015*

Citation:
Iijima H, Shirai T, Okamoto M, Kondo A, Hirai MY and Osanai T (2015) Changes in primary metabolism under light and dark conditions in response to overproduction of a response regulator RpaA in the unicellular cyanobacterium Synechocystis sp. PCC 6803. Front. Microbiol. 6:888. doi: 10.3389/fmicb.2015.00888

The study of the primary metabolism of cyanobacteria in response to light conditions is important for environmental biology because cyanobacteria are widely distributed among various ecological niches. Cyanobacteria uniquely possess circadian rhythms, with central oscillators consisting from three proteins, KaiA, KaiB, and KaiC. The two-component histidine kinase SasA/Hik8 and response regulator RpaA transduce the circadian signal from KaiABC to control gene expression. Here, we generated a strain overexpressing *rpaA* in a unicellular cyanobacterium *Synechocystis* sp. PCC 6803. The *rpaA*-overexpressing strain showed pleiotropic phenotypes, including slower growth, aberrant degradation of an RNA polymerase sigma factor SigE after the light-to-dark transition, and higher accumulation of sugar catabolic enzyme transcripts under dark conditions. Metabolome analysis revealed delayed glycogen degradation, decreased sugar phosphates and organic acids in the tricarboxylic acid cycle, and increased amino acids under dark conditions. The current results demonstrate that in this cyanobacterium, RpaA is a regulator of primary metabolism and involved in adaptation to changes in light conditions.

Keywords: amino acids, cyanobacteria, *Synechocystis*, response regulator, sugar metabolism

Introduction

Cyanobacteria are organisms performing oxygenic photosynthesis that exist in various environmental niches such as fresh water, seawater, soil, and hot springs. Studying the regulatory mechanism of cyanobacterial metabolism is important in environmental biology and biotechnology. One of the most widely studied cyanobacteria is the non-nitrogen fixing species *Synechocystis* sp. PCC 6803 (hereafter *Synechocystis* 6803). *Synechocystis* 6803 cells grow fast and are naturally transformable with homologous recombination (Berla et al., 2013).

Cyanobacteria have a circadian rhythm and their central oscillator consists of three proteins KaiABC, first found in the unicellular cyanobacterium *Synechococcus* sp. PCC 7942 (hereafter *Synechococcus* 7942; Ishiura et al., 1998). An important issue for study in the circadian system

is metabolic compensation, which is the persistence and entrainment of circadian rhythms in response to various nutrient conditions (Johnson and Egli, 2014). KaiC is an enzyme that phosphorylates and dephosphorylates its own residues in a strict order (Nishiwaki et al., 2007; Rust et al., 2007). ATP is a substrate of KaiC phosphorylation, and the ATP/ADP ratio is important for entrainment of the circadian clocks (Rust et al., 2011). KaiC phosphorylation is inhibited by ADP and integrates metabolic information into KaiC through the kinase-stimulation activity of KaiA (Rust et al., 2011). ATP is decreased under dark conditions and treatment with a dark pulse leads to a phase shift in the circadian clock (Rust et al., 2011). Oxidized quinones also input signals into the circadian clock in *Synechococcus* 7942 via the inhibition of KaiC phosphorylation (Kim et al., 2012). Thus, information on the availability of biochemical energy and light/dark conditions is transduced into circadian clocks. Glycogen metabolism entrains the circadian oscillator by providing ATP, and the mutants deficient in glycogen synthesis show the phenotype of a circadian clock that is hypersensitive to dark pulses (Pattanayak et al., 2014).

SasA is a histidine kinase interacting with KaiC in *Synechococcus* 7942 (Iwasaki et al., 2000). SasA is autophosphorylated by its histidine residue and the phosphate moiety is transferred to the cognate response regulator RpaA (Takai et al., 2006). The gene *rpaA* is the "regulator of phycobilisome association," whose protein is involved in energy transfer from phycobilisome to Photosystem I (Ashby and Mullineaux, 1999). The phosphorelay from SasA to RpaA is enhanced in the presence of KaiC (Takai et al., 2006). The knockout mutants of *sasA* or *rpaA* in *Synechococcus* 7942 grow normally under continuous light conditions, but the growth is severely retarded under light/dark cycle conditions (Takai et al., 2006). The knockout of *rpaA* alters the gene expression in *Synechococcus* 7942 widely; the genes, whose peaks of the expression are subjective dusk or dawn, are down-regulated or up-regulated, respectively, in the *rpaA* mutant (Markson et al., 2013). Chromatin-immunoprecipitation with high throughput sequencing (ChIP-Seq) analysis reveals 110 binding sites in the *Synechococcus* 7942 genome, which has A/T-rich motif included in the promoters of *kaiBC* and *rpoD6* (encoding an RNA polymerase sigma factor). *In vitro* assay demonstrates that phosphorylated RpaA binds with the promoter regions, while non-phosphorylated RpaA does not (Hanaoka et al., 2012; Markson et al., 2013).

The mechanistic implications of a circadian clock in *Synechocystis* 6803 have remained obscure due to the redundancy of *kaiABC* genes, with one *kaiA*, three *kaiB* (*kaiB1–B3*), and three *kaiC* (*kaiC1–3*; Kanesaki et al., 2012). The *kaiAB1C1* and *kaiC2B2* genes constitute an operon in the *Synechocystis* 6803 genome. KaiC1 phosphorylation is dependent on KaiA and KaiC directly interacting with KaiA (Wiegard et al., 2013). The phosphorylation of KaiC2 and KaiC3 is not dependent on KaiA, and therefore KaiAB1C1 proteins seem to be the central oscillator in *Synechocystis* 6803 (Wiegard et al., 2013). *Synechocystis* 6803 contains SasA (Hik8, sll0750) and RpaA (Rre31, slr0115) orthologs. Hik8 interacts with KaiC1, but not KaiC2 *in vivo* (Osanai et al., 2015). The knockout of *hik8* results in pleiotropic phenotypes, with the gene expression of enzymes in the glycogen catabolism, glycolysis, and the oxidative pentose phosphate (OPP) pathway altered (Singh and Sherman, 2005). The *hik8* overexpression also leads to changes in primary metabolism (Osanai et al., 2015). Glycogen and sugar phosphate levels are decreased under light conditions and amino acid levels such as glycine and lysine are increased by *hik8* overexpression (Osanai et al., 2015). The involvement of RpaA in salt and hyperosmotic stress has been shown by microarray, with the knockout of *rpaA*/*rre31* down-regulating the salt-induced gene expression (Shoumskaya et al., 2005). Nevertheless, in these studies, the involvement of RpaA in the regulation of primary metabolism and the effect of *rpaA* modification on metabolic alteration has remained unclear due to lack of metabolome data.

Here, we generated a *Synechocystis* 6803 strain overexpressing *rpaA*. The *rpaA*-overexpressing strain showed pleiotropic and similar phenotypes with the *hik8*-overexpressing strain. Genetic and metabolomic analyses indicate that RpaA plays pivotal roles in metabolic regulation under both light and dark conditions.

Materials and Methods

Bacterial Strains and Culture Conditions

The glucose-tolerant (GT) strain of *Synechocystis* sp. PCC 6803, isolated by Williams (1988), and the *rpaA*-overexpressing strain, designated as ROX310, were grown in modified BG-11 medium, which consisted of $BG\text{-}11_0$ liquid medium (Rippka, 1988) containing 5 mM NH_4Cl (buffered with 20 mM HEPES-KOH, pH 7.8). Among GT substrains, the GT-I strain was used in this study (Kanesaki et al., 2012). Liquid cultures were bubbled with 1% (v/v) CO_2 in air and incubated at 30°C under continuous white light (ca. 50–70 μmol photons $m^{-2}\,s^{-1}$). Growth and cell densities were measured at OD_{730} with a Hitachi U-3310 spectrophotometer (Hitachi High-Tech., Tokyo, Japan). Kanamycin (10 μg/mL) was added to ROX310 during pre-culture.

Construction of Plasmids for *rpaA* Overexpression

A region of the *Synechocystis* 6803 genome encoding the *rpaA* (slr0115, *rre31*) ORF was amplified by PCR using KOD Plus Neo polymerase (Toyobo, Osaka, Japan) and the specific primers 5′-GAATTATAACCATATGCCTCGAATACTGATC-3′ (forward) and 5′-ATCCAATGTGAGGTTAACCTACGTTGGACTACCG CC-3′ (reverse). The amplified PCR fragment was inserted into the *Nde*I-*Hpa*I sites of the pTKP2031V vector, using an In-Fusion HD cloning kit (Takara Bio, Shiga, Japan). The resultant plasmid was confirmed by sequencing and transformed into GT-I as described previously (Osanai et al., 2011).

Construction of Plasmids for Protease-Knockout Mutants

To construct protease-knockout mutants, the coding regions of proteases were amplified by PCR with KOD Plus Neo and the following primer sets: *clpB1*(slr1641)

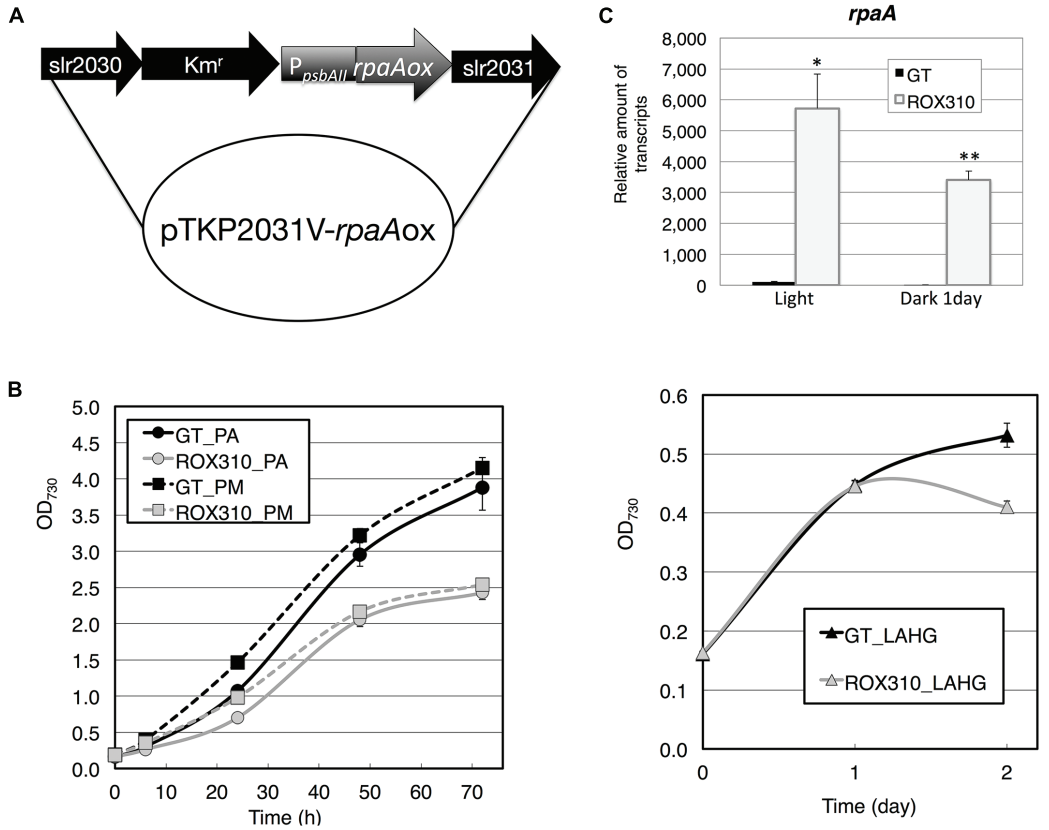

FIGURE 1 | (A) Plasmid for *rpaA* overexpression in *Synechocystis* 6803. The kanamycin resistance cassette was located upstream of the *psbAII* promoter. **(B)** Levels of *rpaA* transcripts in GT and ROX310 cells. Quantitative real-time PCR was performed with total RNA from cells grown under light and dark conditions. **(C)** Growth of GT and ROX310 cells. Left: growth of cells under photoautotrophic (PA) and photomixotrophic (PM, grown with 1 mM glucose) conditions. Right: growth of cells under light-activated heterotrophic growth conditions (LAHG, grown with 1 mM glucose under continuous dark conditions except for 15 min light per day).

5′-GGGAATTCTGCGGGATCGCAAACTA-3′ (forward) and 5′-GCGCATGCGAGCGTTGAATGGCTTCG-3′ (reverse); *clpB2* (slr0156) 5′-GGGAATTCTCCGCGCGTTTAACCTTG-3′ (forward) and 5′-GCGCATGCCCCGCTCAGCTTTTTCT-3′ (reverse); *clpC*(sll0020) 5′-GGGAATTCGCTTCCTGCCCGATAAG-3′ (forward) and 5′-GCGCATGCCACGTCTTCCAACAGGC-3′ (reverse); *clpX*(sll0535) 5′-GGGAATTCGAAGGAACGGTGGCCAA-3′ (forward) and 5′-GCGCATGCCCGTCGTTGTCCAACCA-3′ (reverse); *degP*(slr1204) 5′-GGGAATTCGTGCTGGGGGGACATTT-3′ (forward) and 5′-GCGCATGCCAGTTTGCCCACTAGGG-3′ (reverse); *degQ*(sll1679) 5′-GGGAATTCCTTGGTTACGCCGCATC-3′ (forward) and 5′-GCGCATGCACTATGCGCTGTAGGCG-3′ (reverse); and *degS*(sll1427) 5′-GGGAATTCGTGGCCGTGCTTTTACT-3′ (forward) and 5′-GCGCATGCCTTCCACCCGTTCTTGA-3′ (reverse). PCR fragments were isolated with the Wizard SV Gel and PCR Clean-up System (Promega, Madison, WI, USA) and the fragments were digested with *Eco*RI and *Sph*I. Each of the resulting fragments was cloned into pUC119 (Clontech) digested with *Eco*RI and *Sph*I. The chloramphenicol-resistant cassette obtained by digesting pKRP10 (Reece and Phillips, 1995) with *Sma*I or *Pst*I was inserted into the *Hinc*II sites of *clpB1* and *clpC*, the SmaI sites of *clpB2* and *clpX*, and the *Pst*I sites of *degP*, *degQ*, and *degS*. The resultant vectors were transformed into GT. The chloramphenicol-resistant (20 μg/mL) cells were isolated and streaked on plates several times.

Immunoblotting

Cells grown under light or dark conditions were collected by centrifugation (5,800 × *g* for 2 min), and the supernatant was removed by pipetting. The cells were frozen by liquid nitrogen. Cells were dissolved in PBS-T (137 mM NaCl, 2.7 mM KCl, 8.1 mM Na_2HPO_4, 1.5 mM KH_2PO_4, 0.1% Tween-20) and disruption by sonication and immunoblotting was performed as described previously (Osanai et al., 2014a). Antisera against SigE and GlgP(sll1356) were generated previously (Osanai et al., 2009, 2011).

RNA Isolation and Quantitative Real-Time PCR

RNA isolation and cDNA synthesis were performed as described previously (Osanai et al., 2014b). The cDNAs were synthesized with the SuperScript III First-Strand Synthesis System (Life Technologies Japan, Tokyo, Japan) with 2 μg of total RNA. Quantitative real-time PCR was performed with the

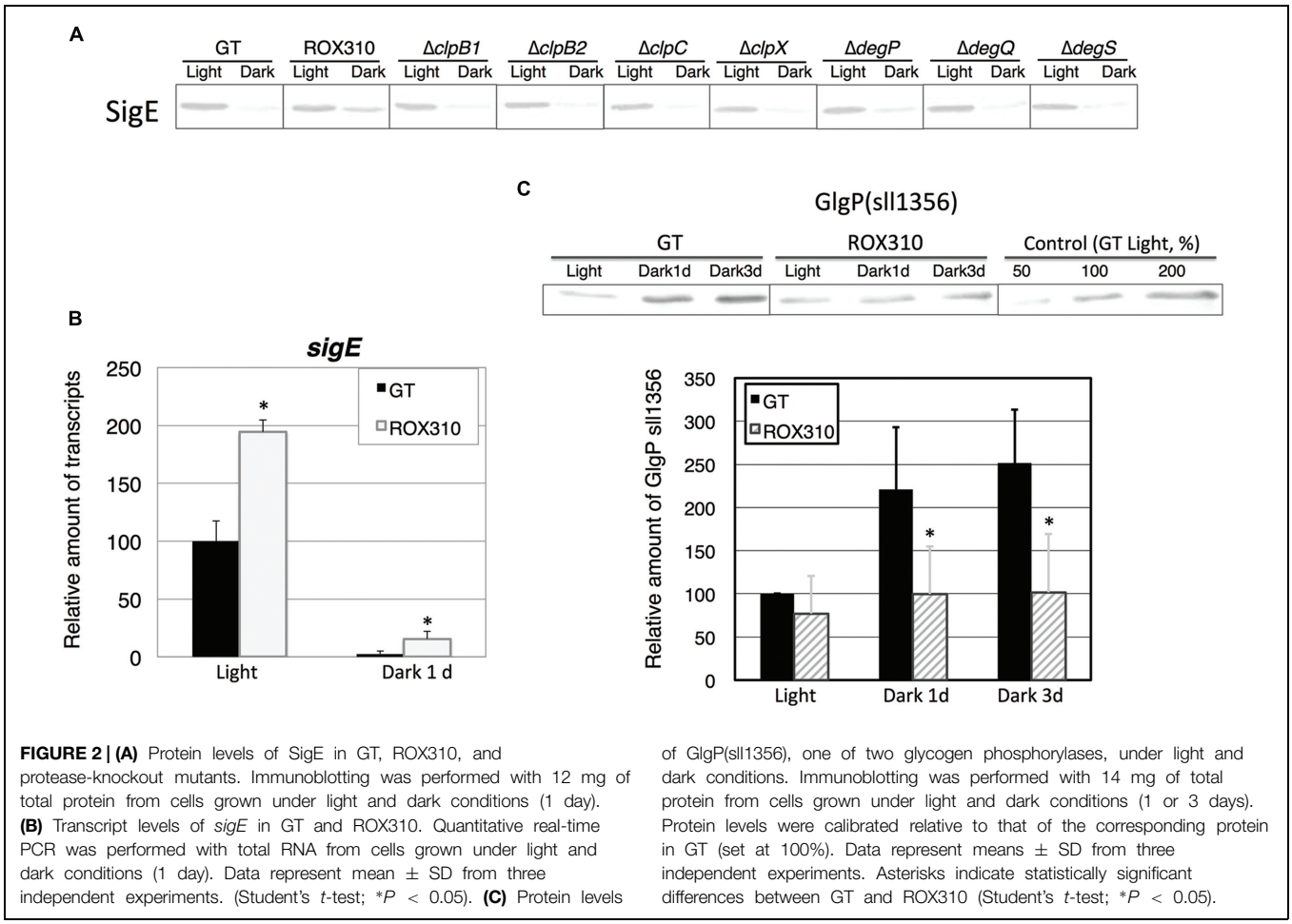

FIGURE 2 | (A) Protein levels of SigE in GT, ROX310, and protease-knockout mutants. Immunoblotting was performed with 12 mg of total protein from cells grown under light and dark conditions (1 day). **(B)** Transcript levels of *sigE* in GT and ROX310. Quantitative real-time PCR was performed with total RNA from cells grown under light and dark conditions (1 day). Data represent mean ± SD from three independent experiments. (Student's *t*-test; $^*P < 0.05$). **(C)** Protein levels of GlgP(sll1356), one of two glycogen phosphorylases, under light and dark conditions. Immunoblotting was performed with 14 mg of total protein from cells grown under light and dark conditions (1 or 3 days). Protein levels were calibrated relative to that of the corresponding protein in GT (set at 100%). Data represent means ± SD from three independent experiments. Asterisks indicate statistically significant differences between GT and ROX310 (Student's *t*-test; $^*P < 0.05$).

StepOnePlus Real-Time PCR System (Life Technologies) according to the manufacturer's instructions, using the primers listed in Supplementary Table S2. The transcript level of *rnpB*, which encodes RNaseP subunit B, was used as an internal standard as previously described (Osanai et al., 2015).

Glycogen Measurement

Glycogen levels were measured at the Biotechnology Center of Akita Prefectural University (Akita, Japan), as described previously (Osanai et al., 2014b).

LC–MS/MS Analysis

Equal amounts of cells (10 mL of cell culture with $OD_{730} = 1.0$) were harvested by rapid filtration. LC–MS/MS analysis was performed using a 100-mL aliquot of the upper phase as previously described (Osanai et al., 2014b). All metabolite analyses were performed with the cells grown without external carbon sources except CO_2.

Amino Acid Analysis by GC–MS

Equal amounts of cells (50 mL of cell culture with $OD_{730} = 1.0$) were harvested by rapid filtration. Amino acids were quantified by GC-MS as previously described (Osanai et al., 2014a).

Organic Acid Analysis by GC–MS

Equal amounts of cells (10 mL of cell culture with $OD_{730} = 1.0$) were harvested by rapid filtration using a previously described method (Osanai et al., 2014b). GC-MS was carried out using a GCMS-QP2010 Ultra equipped with a CP-Sil 8 CB-MS capillary column (30 m × 0.25 mm × 0.25 μm; Agilent, Palo Alto, CA, USA) as previously described (Osanai et al., 2014b).

Results

Slower Growth of *rpaA*-Overexpressing Strain

We generated a strain overexpressing *rpaA* by fusing the promoter of *psbAII* (encoding Photosystem II D1 protein; **Figure 1A**) and the strain was named ROX310. Quantitative real-time PCR confirmed that the expression levels of *rpaA* in ROX310 were higher than in the wild-type, glucose-tolerant (GT) strain under both light and dark conditions (**Figure 1B**). Under both photoautotrophic and photomixotrophic conditions, the *rpaA*-overexpressing strain grew more slowly than did GT (**Figure 1C**). ROX310 grew similarly to GT under light-activated heterotrophic growth (LAHG) conditions until 1 day, although it lost viability under prolonged LAHG conditions (**Figure 1C**).

Altered Protein and Transcript Levels of SigE in ROX310

Previously, the *hik8*-overexpressing strain showed aberrant protein degradation of SigE, RNA polymerase sigma factors activating sugar catabolism that is essential for dark/heterotrophic conditions, after the light-to-dark transition (Osanai et al., 2015). Immunoblotting demonstrated that *rpaA* overexpression reduced the degradation of SigE proteins under dark conditions (**Figure 2A**). To identify the proteases of SigE, we tested seven mutants lacking orthologous proteinases related to dark conditions in *Synechococcus* 7942 (Hosokawa et al., 2011), but these knockouts did not affect SigE protein levels (**Figure 2A**). The level of *sigE* transcripts was higher in ROX310 than in GT under both light and dark conditions, although the levels were similarly decreased in both strains by the light-to-dark transition (**Figure 2B**). We then quantified the levels of sugar catabolic enzymes by immunoblotting. The protein levels of GlgP(sll1356), one of two glycogen phosphorylases involved in glycogen degradation in *Synechocystis* 6803, were not induced by the *rpaA*-overexpressing strain under dark conditions (**Figure 2C**).

We measured the transcript levels of genes related to sugar catabolism in ROX310 (**Figure 3**). The transcript levels of *pfkA*(sll0765) and *fbaII* were enhanced by *rpaA* overexpression under light conditions, while that of *pfkA*(sll1196) was repressed (**Figure 3**). The transcript levels of all 12 genes were decreased at 1 day after the light-to-dark transition in both GT and ROX310; however, there were higher transcript levels of these genes in ROX310 than in GT (**Figure 3**).

Metabolome Analysis using the Cells Grown under Light and Dark Conditions

The glycogen levels were quantified under light and dark conditions. Glycogen rapidly disappeared in GT after the light-to-dark transition (**Table 1**). In ROX310, glycogen decreased after

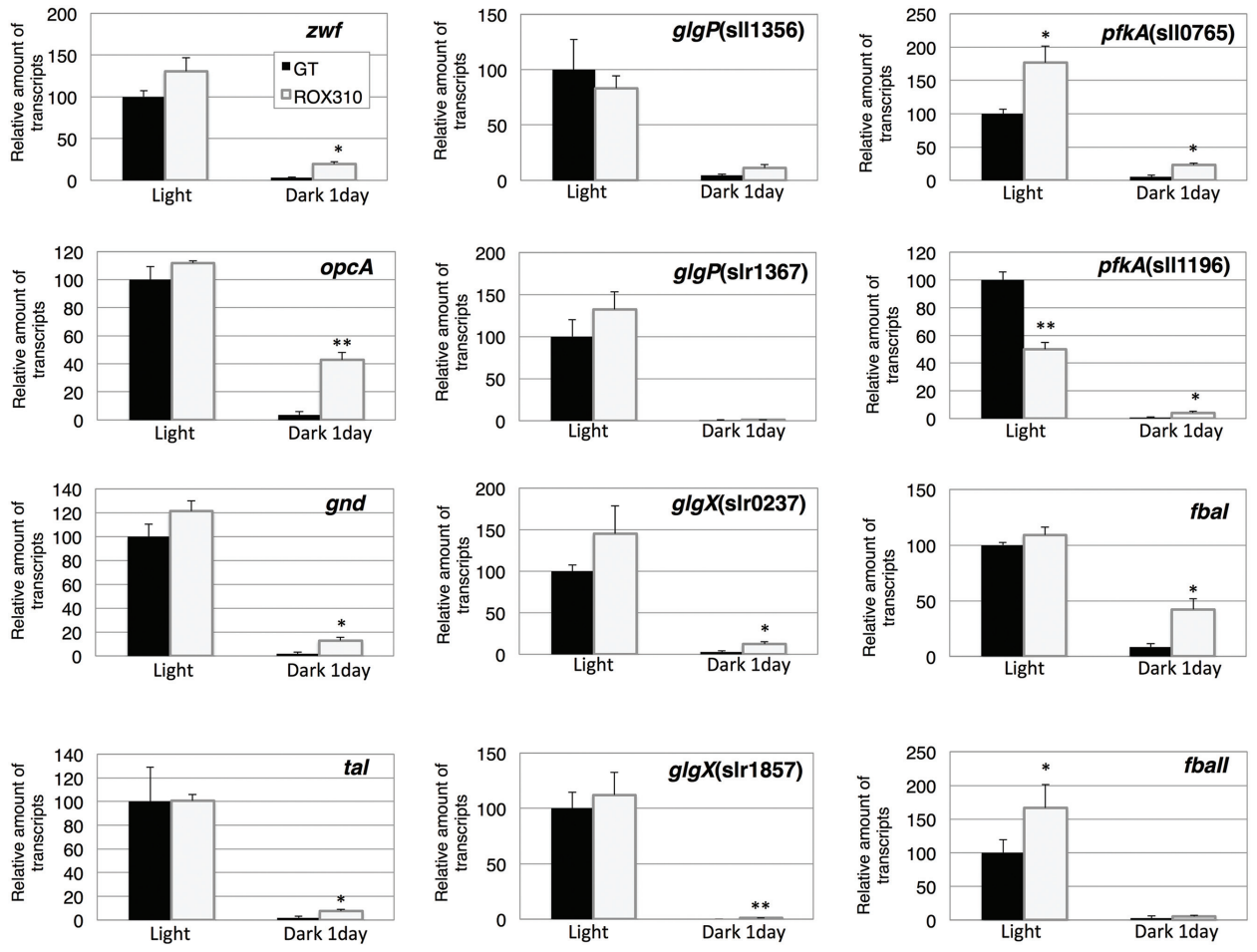

FIGURE 3 | Quantitative real-time PCR analysis of transcription in GT and ROX310. Figure shows relative transcript levels of 12 genes involved in the OPP pathway (*zwf*, *opcA*, *gnd*, *tal*), glycogen catabolism [*glgP*(sll1356), *glgP*(slr1367), *glgX*(slr0237), *glgX*(slr1857)], and glycolysis [*pfkA*(sll0745), *pfkA*(sll1196), *fbaI*, *fbaII*]. Data represent mean ± SD from three independent experiments. Transcript levels were calibrated relative to that of the corresponding transcript in GT (set at 100%). Asterisks indicate statistically significant differences between GT and ROX310 (Student's *t*-test; $^{*}P < 0.05$, $^{**}P < 0.005$).

TABLE 1 | Relative values of glycogen in GT and ROX310.

	Light	Dark 2 h	Dark 4 h	Dark 6 h
GT	100 ± 25.4	ND	ND	ND
ROX310	104 ± 32.7	21.9 ± 16.8	9.4 ± 6.4	ND

Data represent mean ± SD from four independent experiments. Glycogen levels were calibrated relative to that in the GT strain under light conditions (set at 100%). ND indicates glycogen under detectable levels.

the light-to-dark transition, but the glycogen degradation was slower than GT (**Table 1**).

LC–MS/MS analysis revealed that the levels of sugar phosphates (glucose-6-phosphate, ribose-5-phosphate, sedoheptulose-7-phosphate, fructose-6-phosphate, ribulose-5-phosphate, fructose-1,6-bisphosphate) and dihydroxyacetone phosphate were lower in ROX310 than in GT under both light and dark conditions (**Table 2**). Phosphoenolpyruvate levels were higher in ROX310 than in GT under light and dark conditions (**Table 2**). Fumarate and isocitrate levels were lower in ROX310 than in GT under light conditions (**Table 2**). Malate could not be detected in ROX310 under light conditions (**Table 2**). Organic acids in the TCA cycle were lesser in ROX310 than in GT under dark conditions (**Table 2**). NADP levels increased by *rpaA* overexpression, but other nucleotides did not (**Table 2**).

Amino acid analyses showed that the levels of glycine and proline were higher in ROX310 than in GT under light conditions (**Figure 4**). The levels of alanine, glycine, threonine, and lysine were higher in ROX310 than in GT under dark conditions (**Figure 4**). The level of ornithine was lower in ROX310 than in GT under dark conditions (**Figure 4**).

TABLE 2 | Relative levels of metabolites in primary metabolism in GT and ROX310.

Metabolites	GT_Light	GT_Dark1day	ROX310_Light	ROX310_Dark1day
Sugar phosphates and nucleotide sugars				
Glucose-6P	100 ± 20.5	10.0 ± 1.3	33.3 ± 12.4*	0.8 ± 0.2**
Ribose-5P	100 ± 11.4	18.2 ± 4.4	115.9 ± 14.3	7.3 ± 1.9*
Sedoheptulose-7P	100 ± 12.7	5.4 ± 0.6	86.0 ± 13.1	2.5 ± 0.8*
Fructose-6P	100 ± 6.7	9.2 ± 1.0	54.3 ± 4.5**	1.2 ± 0.4**
Glucose-1P	100 ± 15.7	8.1 ± 3.7	41.1 ± 19.5*	4.9 ± 0.9
Glyceraldehyde-3P	100 ± 26.2	18.6 ± 7.3	99.7 ± 25.0	6.4 ± 3.3
Xylulose-5P	100 ± 19.7	11.0 ± 2.6	131.6 ± 22.8	6.4 ± 2.0
Ribulose-5P	100 ± 24.5	10.7 ± 2.0	143.3 ± 2.0	6.0 ± 1.2*
Fructose-1,6-bisP	100 ± 29.7	38.9 ± 7.8	82.1 ± 10.2	23.7 ± 3.7*
Ribulose-1,5-bisP	100 ± 20.6	34.4 ± 10.6	74.6 ± 13.1	18.3 ± 3.6
ADP-glucose	100 ± 43.8	2.7 ± 5.4	88.1 ± 22.8	0 ± 0
Other metabolites in glycolysis and the OPP pathway				
6-Phosphogluconate	100 ± 22.1	20.8 ± 6.5	83.8 ± 3.1	18.0 ± 2.9
DHAP	100 ± 13.6	23.9 ± 3.5	101.7 ± 18.8	8.1 ± 1.3
3- or 2-Phosphoglycerate	100 ± 5.4	25.3 ± 8.1	107.1 ± 2.1*	35.7 ± 8.6
Phosphoenolpyruvate	100 ± 7.5	18.6 ± 4.2	127.7 ± 7.8**	45.5 ± 13.9
Pyruvate#	100 ± 30.6	0 ± 0	113.9 ± 12.9	0 ± 0
Lactate#	100 ± 5.4	135.1 ± 26.4	149.9 ± 51.4	92.5 ± 13.8
Metabolites in acetyl-CoA and the TCA cycle				
Acetyl-CoA	100 ± 44.1	31.7 ± 6.1	71.1 ± 3.8	42.1 ± 5.3
Citrate#	100 ± 19.0	127.2 ± 13.1	96.4 ± 5.6	161.4 ± 24.2
Isocitrate#	100 ± 3.9	110.6 ± 8.2	63.3 ± 3.9**	64.2 ± 4.1**
Succinate#	100 ± 9.5	69.5 ± 4.2	83.3 ± 16.4	53.7 ± 9.6
Malate#	100 ± 89.6	14.9 ± 29.9	0 ± 0	32.5 ± 37.5
Fumarate#	100 ± 11.8	87.1 ± 32.2	19.7 ± 25.3*	68.8 ± 20.7
Other cofactors				
AMP	100 ± 20.4	92.7 ± 17.4	92.8 ± 7.2	107.4 ± 8.8
ADP	100 ± 10.3	107.7 ± 23.9	93.6 ± 6.5	122.9 ± 6.5
ATP	100 ± 12.5	117.6 ± 7.7	90.4 ± 5.9	112.8 ± 8.0
NAD	100 ± 3.8	137.7 ± 9.5	94.1 ± 5.5	124.4 ± 13.6
NADP	100 ± 8.7	161.5 ± 17.1	131.6 ± 7.6**	215.6 ± 9.6*
NADH	100 ± 108.7	55.8 ± 17.3	18.8 ± 22.5	34.9 ± 26.5*
NADPH	100 ± 31.3	52.8 ± 12.1	61.3 ± 11.3	35.2 ± 5.7

*Data represent mean ± SD from four independent experiments. Metabolite levels were calibrated relative to that of the corresponding metabolite in GT under light conditions (set at 100%). Asterisks indicate statistically significant differences between GT and ROX310 (Student's t-test; *P < 0.05, **P < 0.005). The data from the GT strain under light and dark conditions were cited from our previous study (Osanai et al., 2015). P, phosphate; DHAP, dihydroxyacetone phosphate. Metabolites were quantified by LC–MS/MS, except for those marked by #, which were quantified by GC–MS.*

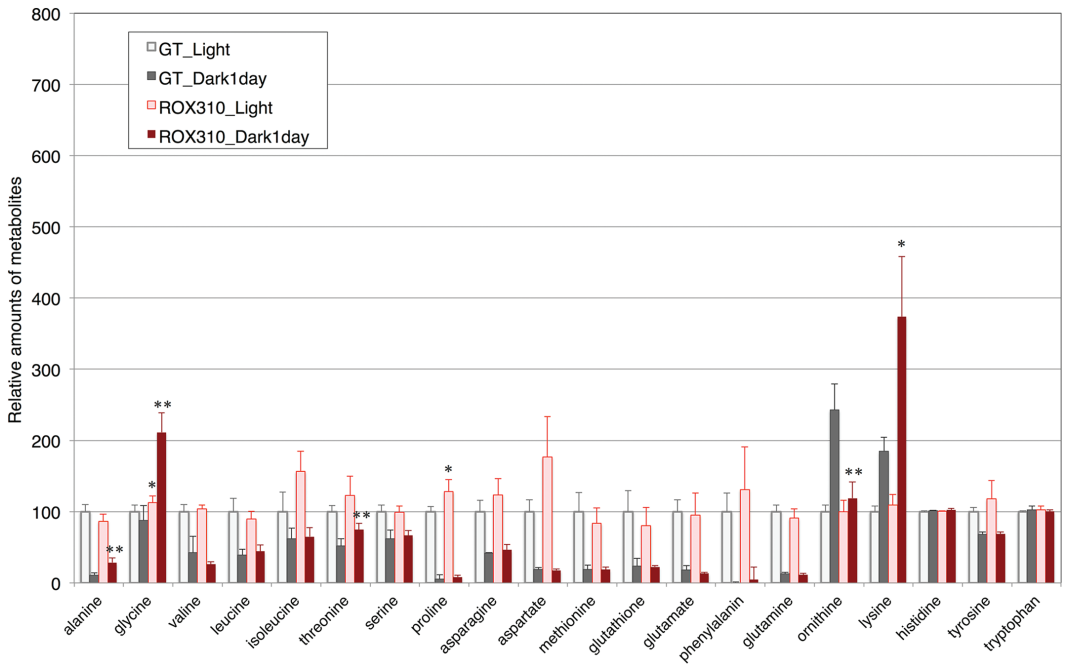

FIGURE 4 | Levels of 18 amino acids, ornithine, and glutathione in ROX310. Data represent means ± SD from four independent experiments. Levels were calibrated relative to that of GT grown under light conditions (set at 100%). Asterisks indicate statistically significant differences between GT and ROX310 (Student's *t*-test; $*P < 0.05$, $**P < 0.005$).

Alteration in Transcript Levels of Genes Encoding Circadian Clocks

Finally, expression of *kaiABC* genes was quantified. The transcript levels of *kaiA, B1*, *C1*, *B2,* and *C2* were doubled by *rpaA* overexpression under light conditions (**Figure 5**). The transcript levels of *kaiB3* and *kaiC3* were marginally increased in ROX310 under light conditions (**Figure 5**). All the transcripts of *kaiABC* were decreased after 1 day of dark cultivation, and the levels remained higher in ROX310 than those in GT (**Figure 5**).

Discussion

Here, we have performed genetic and metabolomic analyses using an *rpaA*-overexpressing strain and revealed that RpaA is involved in the regulation of primary metabolism in this unicellular cyanobacterium. The mechanism of circadian clocks in *Synechocystis* 6803, which could be different from *Synechococcus* 7942, has been less studied except Drs. Axmann's and Hellingwerf's groups (Wiegard et al., 2013; Beck et al., 2014; van Alphen and Hellingwerf, 2015), and we proceeded metabolome analyses with the circadian-related mutants of *Synechocystis* 6803. ChIP-Seq analysis in *Synechococcus* 7942 shows that RpaA binds the promoters of *kaiBC*, *sasA*, *rpaA*, and genes encoding sigma factors (*rpoD2, D5, D6*) and sugar catabolic enzymes (*glgP*, *malQ*, *zwf*, *opcA*, *gap1*, *fbaII*), activating their gene expression at night (Markson et al., 2013). These results are consistent with our analysis: the *rpaA* overexpression altered the gene expression of *sigE*, a sugar catabolic enzyme, and *kaiABC* (**Figures 2, 3,** and **5**). SigE is a sigma factor activating glycogen catabolism, glycolysis, and the OPP pathway (Osanai et al., 2005, 2011), and its expression peaks before night (Kucho et al., 2005). Combining the results of previous and current genetic analyses, the signal transduction from the circadian clock to sugar metabolism consists of the cascade of the proteins KaiABC-Hik8-RpaA-SigE in *Synechocystis* sp. PCC 6803, although further promoter analysis is required. Since RpaA altered the expression of *kaiABC* genes (**Figure 5**), feedback or feedforward regulation from RpaA to the central circadian oscillator may exist to entrain the clock by metabolic information.

The *rpaA*-overexpressing strain of *Synechocystis* 6803 exhibited several phenotypes. Results from the *rpaA*-overexpressing strain of *Synechocystis* 6803 were similar to the *rpaA*-null mutant of *Synechococcus* 7942, which showed decreased glycogen catabolism (Diamond et al., 2015). The *rpaA* knockout mutant in *Synechocystis* 6803 exhibited high light sensitive phenotype (Majeed et al., 2012), which is consistent with our results that RpaA is important in light acclimation. A previous study demonstrated that introduction of RpaA(D53E; which mimics phosphorylated RpaA) restored the RpaA function, but that the introduction of RpaA(D53A; which mimics non-phosphorylated RpaA) could not (Markson et al., 2013). Therefore, the *rpaA* overexpression in our study may have increased non-phosphorylated RpaA in the *Synechocystis* 6803 cells, leading to phenotypes that were the mixture of gain-of-function and loss-of-function of RpaA. Introduction of a phospho-mimic RpaA into *Synechocystis* 6803 may be intriguing to distinguish these phenotypes.

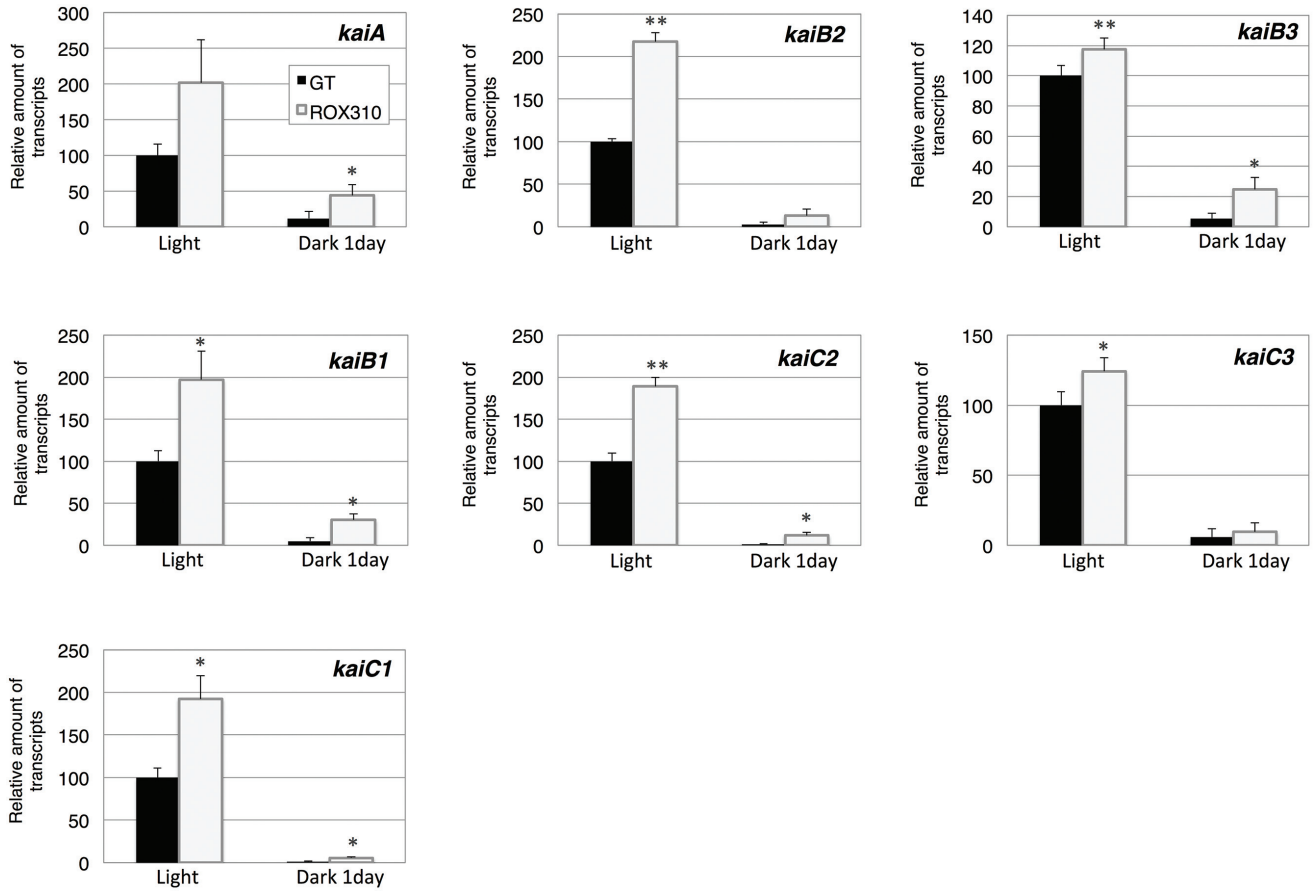

FIGURE 5 | Quantitative real-time PCR analysis of transcription in GT and ROX310. Figure shows relative transcript levels of seven genes encoding KaiABC proteins. Data represent mean ± SD from three independent experiments. Transcript levels were calibrated relative to that of the corresponding transcript in GT (set at 100%). Asterisks indicate statistically significant differences between GT and ROX310 (Student's *t*-test; $^{*}P < 0.05$, $^{**}P < 0.005$).

Overexpression of *rpaA* led to phenotypes similar to those of the *hik8* overexpressor (Osanai et al., 2015); that is, growth defects under light-activated heterotrophic conditions (**Figure 1**), aberrant degradation of SigE after the light-to-dark transition (**Figure 2A**), accumulated transcripts during darkness (**Figure 3**), decreased levels of sugar phosphates (**Table 2**), and increased levels of several amino acids under dark conditions (**Figure 4**). These similarities may be due to the overexpression of *hik8* accelerated the phosphorylation of RpaA proteins. The glycogen metabolism mutant could not grow under dark/heterotrophic conditions (Osanai et al., 2005; Singh and Sherman, 2005; Tabei et al., 2007), or treatment with high salt and oxidative stress (Suzuki et al., 2010). Thus, the growth phenotypes of ROX310 under LAHG conditions may be caused by the changes in primary metabolism (**Figure 1C**). Genetic analyses have suggested that the mutants of Clp proteases alter circadian oscillation in *Synechococcus* 7942 (Holtman et al., 2005; Imai et al., 2013). Nevertheless the aberrant degradation of SigE proteins under dark conditions in the *rpaA*-overexpressing strain (**Figure 2A**), glycogen catabolism was slowed under dark conditions (**Table 1**). These results suggest that proteins other than SigE concertedly determine the degree of glycogen degradation in *Synechocystis* 6803. Several sugar catabolic regulators, including Hik31, Rre37, and AbrB are known in *Synechocystis* 6803 (Kahlon et al., 2006; Tabei et al., 2007; Yamauchi et al., 2011). For example, Rre37 preferentially activates the gene expression of glycogen catabolic and glycolytic enzymes such as *pfkA*(sll1196; Azuma et al., 2009), and thus, further study of the relationships among several sugar catabolic regulators is necessary to elucidate the regulatory mechanism of sugar catabolism in *Synechocystis* 6803.

Control of primary carbon metabolism by a circadian clock is an important theme in cyanobacteria (Diamond et al., 2015). Decrease in glycogen and sugar phosphates was observed during dark conditions (**Tables 1** and **2**), which indicates glycogen and sugar phosphates are positively correlated in this condition. On the other hand, organic acids in the TCA cycle kept higher levels under dark conditions (**Table 2**). Thus, organic acids in the TCA cycle were not correlated with the metabolites in glycolysis and the OPP pathway. The *rpaA*-overexpressing strain showed decreased levels of sugar phosphates under both light and dark

conditions (**Table 2**), which is consistent with the fact that RpaA is important for the expression of genes related to glycogen catabolism in unicellular cyanobacteria (Diamond et al., 2015). Our immunoblotting showed that GlgP(sll1356) proteins were decreased with *rpaA* overexpression (**Figure 2C**), which may be one reason for the down-regulation of glycogen catabolism in this mutant. The metabolomic analysis also revealed that organic acids in the TCA cycle (fumarate, malate, and oxaloacetate) were lowered by *rpaA* overexpression (**Table 2**). The organic acids in the TCA cycle are an important pool of carbon sources in this cyanobacterium (Osanai et al., 2014a). Thus, the data also indicates that RpaA widely regulates primary metabolism related to the carbon sinks in this cyanobacterium. KaiC regulates the production of lysine, which has been shown to be lowered during light/dark cycles in *Synechococcus* 7942 (Diamond et al., 2015). The analysis showed lysine and glycine levels were up-regulated by *rpaA*-overexpression during the light-to-dark transition (**Figure 4**), demonstrating the involvement of RpaA in amino acid metabolism in response to light conditions. In summary, our metabolome analyses have revealed the RpaA-regulation in primary sugar and amino acid metabolism of *Synechocystis* 6803.

Acknowledgments

This work was supported by the Ministry of Education, Culture, Sports, Science, and Technology, Japan, by a grant to TO from ALCA (Project name "Production of cyanobacterial succinate by the genetic engineering of transcriptional regulators and circadian clocks") from the Japan Science and Technology Agency.

Supplementary Material

The Supplementary Material for this article can be found online at: http://journal.frontiersin.org/article/10.3389/fmicb.2015.00888

References

Ashby, M. K., and Mullineaux, C. W. (1999). Cyanobacterial ycf27 gene products regulate energy transfer from phycobilisomes to photosystems I and II. *FEMS Microbiol. Lett.* 181, 253–260. doi: 10.1111/j.1574-6968.1999.tb08852.x

Azuma, M., Osanai, T., Hirai, M. Y., and Tanaka, K. (2009). A response regulator Rre37 and an RNA polymerase sigma factor SigE represent two parallel pathways to activate sugar catabolism in a cyanobacterium *Synechocystis* sp. PCC 6803. *Plant Cell Physiol.* 52, 404–412. doi: 10.1093/pcp/pcq204

Beck, C., Hertel, S., Rediger, A., Lehmann, R., Wiegard, A., Kölsch, A., et al. (2014). Daily expression pattern of protein-encoding genes and small noncoding RNAs in *Synechocystis* sp. strain PCC 6803. *Appl. Environ. Microbiol.* 80, 5195–5206. doi: 10.1128/AEM.01086-14

Berla, B. M., Saha, R., Immethun, C. M., Maranas, C. D., Moon, T. S., and Pakrasi, H. B. (2013). Synthetic biology of cyanobacteria: unique challenges and opportunities. *Front. Microbiol.* 4:246. doi: 10.3389/fmicb.2013.00246

Diamond, S., Jun, D., Rubin, B. E., and Golden, S. S. (2015). The circadian oscillator in *Synechococcus elongatus* controls metabolite partitioning during diurnal growth. *Proc. Natl. Acad. Sci. U.S.A.* 112, E19160–E19245. doi: 10.1073/pnas.1504576112

Hanaoka, M., Takai, N., Hosokawa, N., Fujiwara, M., Akimoto, Y., Kobori, N., et al. (2012). RpaB, another response regulator operating circadian clock-dependent transcriptional regulation in *Synechococcus elongatus* PCC 7942. *J. Biol. Chem.* 287, 26321–26327. doi: 10.1074/jbc.M111.338251

Holtman, C. K., Chen, Y., Sandoval, P., Gonzales, A., Nalty, M. S., Thomas, T. L., et al. (2005). High-throughput functional analysis of the *Synechococcus elongatus* PCC 7942 genome. *DNA Res.* 12, 103–115. doi: 10.1093/dnares/12.2.103

Hosokawa, N., Hatakeyama, T. S., Kojima, T., Kikuchi, Y., Ito, H., and Iwasaki, H. (2011). Circadian transcriptional regulation by the posttranslational oscillator without de novo clock gene expression in *Synechococcus*. *Proc. Natl. Acad. Sci. U.S.A.* 108, 15396–15401. doi: 10.1073/pnas.1019612108

Imai, K., Kitayama, Y., and Kondo, T. (2013). Elucidation of the role of clp protease components in circadian rhythm by genetic deletion and overexpression in cyanobacteria. *J. Bacteriol.* 195, 4517–4526. doi: 10.1128/JB.00300-13

Ishiura, M., Kutsuna, S., Aoki, S., Iwasaki, H., Andersson, C. R., Tanabe, A., et al. (1998). Expression of a gene cluster kaiABC as a circadian feedback process in cyanobacteria. *Science* 281, 1519–1523. doi: 10.1126/science.281.5382.1519

Iwasaki, H., Williams, S. B., Kitayama, Y., Ishiura, M., Golden, S. S., and Kondo, T. (2000). A kaiC-interacting sensory histidine kinase, SasA, necessary to sustain robust circadian oscillation in cyanobacteria. *Cell* 101, 223–233. doi: 10.1016/S0092-8674(00)80832-6

Johnson, C. H., and Egli, M. (2014). Metabolic compensation and circadian resilience in prokaryotic cyanobacteria. *Annu. Rev. Biochem.* 83, 221–247. doi: 10.1146/annurev-biochem-060713-035632

Kahlon, S., Beeri, K., Ohkawa, H., Hihara, Y., Murik, O., Suzuki, I., et al. (2006). A putative sensor kinase, Hik31, is involved in the response to *Synechocystis* sp. PCC 6803 to the presence of glucose. *Microbiology* 152, 647–655. doi: 10.1099/mic.0.28510-0

Kanesaki, Y., Shiwa, Y., Tajima, N., Suzuki, M., Watanabe, S., Sato, N., et al. (2012). Identification of substrain-specific mutations by massively parallel whole-genome resequencing of *Synechocystis* sp. PCC 6803. *DNA Res.* 19, 67–79. doi: 10.1093/dnares/dsr042

Kim, Y. I., Vinyard, D. J., Ananyev, G. M., Dismukes, G. C., and Golden, S. S. (2012). Oxidized quinones signal onset of darkness directly to the cyanobacterial circadian oscillator. *Proc. Natl. Acad. Sci. U.S.A.* 109, 177651–177769. doi: 10.1073/pnas.1216401109

Kucho, K., Okamoto, K., Tsuchiya, Y., Nomura, S., Nango, M., Kanehisa, M., et al. (2005). Global analysis of circadian expression in the cyanobacterium *Synechocystis* sp. strain PCC 6803. *J. Bacteriol.* 187, 2190–2199. doi: 10.1128/JB.187.6.2190-2199.2005

Majeed, W., Zhang, Y., Xue, Y., Ranade, S., Blue, R. N., and He, Q. (2012). RpaA regulates the accumulation of monomeric photosystem I and PsbA under high light conditions in *Synechocystis* sp. PCC 6803. *PLoS ONE* 7:e45139. doi: 10.1371/journal.pone.0045139

Markson, J. S., Piechura, J. R., Puszynska, A. M., and O'Shea, E. K. (2013). Circadian control of global gene expression by the cyanobacterial master regulator RpaA. *Cell* 155, 1396–1408. doi: 10.1016/j.cell.2013.11.005

Nishiwaki, T., Satomi, Y., Kitayama, Y., Terauchi, K., Kiyohara, R., Takao, T., et al. (2007). A sequential program of dual phosphorylation of KaiC as a basis for circadian rhythm in cyanobacteria. *EMBO J.* 26, 4029–4037. doi: 10.1038/sj.emboj.7601832

Osanai, T., Imashimizu, M., Seki, A., Sato, S., Tabata, S., Imamura, S., et al. (2009). ChlH, the H subunit of the Mg-chelatase, is an anti-sigma factor for SigE in *Synechocystis* sp. PCC 6803. *Proc. Natl. Acad. Sci. U.S.A.* 106, 6860–6865. doi: 10.1073/pnas.0810040106

Osanai, T., Kanesaki, Y., Nakano, T., Takahashi, H., Asayama, M., Shirai, M., et al. (2005). Positive regulation of sugar catabolic pathways in the cyanobacterium *Synechocystis* sp. PCC 6803 by the group 2 sigma factor SigE. *J. Biol. Chem.* 280, 30653–30659. doi: 10.1074/jbc.M505043200

Osanai, T., Oikawa, A., Azuma, M., Tanaka, K., Saito, K., Hirai, M. Y., et al. (2011). Genetic engineering of group 2 sigma factor SigE widely activates expressions of sugar catabolic genes in *Synechocystis* species PCC 6803. *J. Biol. Chem.* 286, 30962–30971. doi: 10.1074/jbc.M111.231183

Osanai, T., Oikawa, A., Numata, K., Kuwahara, A., Iijima, H., Doi, Y., et al. (2014a). Pathway-level acceleration of glycogen catabolism by a response regulator in the cyanobacterium *Synechocystis* species PCC 6803. *Plant Physiol.* 164, 1831–1841. doi: 10.1104/pp.113.232025

Osanai, T., Oikawa, A., Shirai, T., Kuwahara, A., Iijima, H., Tanaka, K., et al. (2014b). Capillary electrophoresis-mass spectrometry reveals the distribution of carbon metabolites during nitrogen starvation in *Synechocystis* sp. PCC 6803. *Environ. Microbiol.* 16, 512–524. doi: 10.1111/1462-2920.12170

Osanai, T., Shirai, T., Iijima, H., Kuwahara, A., Suzuki, I., Kondo, A., et al. (2015). Alteration of cyanobacterial sugar and amino acid metabolism by overexpression hik8, encoding a KaiC-associated histidine kinase. *Environ. Microbiol.* 17, 2430–2440. doi: 10.1111/1462-2920.12715

Pattanayak, G. K., Phong, C., and Rust, M. (2014). Rhythms in energy storage control the ability of the cyanobacterial circadian clock to reset. *Curr. Biol.* 24, 1934–1938. doi: 10.1016/j.cub.2014.07.022

Reece, K. S., and Phillips, G. J. (1995). New plasmids carrying antibiotic-resistance cassettes. *Gene* 165, 141–142. doi: 10.1016/0378-1119(95)00529-F

Rippka, R. (1988). Isolation and purification of cyanobacteria. *Methods Enzymol.* 167, 3–27. doi: 10.1016/0076-6879(88)67004-2

Rust, M. J., Golden, S. S., and O'Shea, E. K. (2011). Light-driven changes in energy metabolism directly entrain the cyanobacterial circadian oscillator. *Science* 331, 220–223. doi: 10.1126/science.1197243

Rust, M. J., Markson, J. S., Lane, W. S., Fisher, D. S., and O'Shea, E. K. (2007). Ordered phosphorylation governs oscillation of a three-protein circadian clock. *Science* 318, 809–812. doi: 10.1126/science.1148596

Shoumskaya, M. A., Paithoonragsarid, K., Kanesaki, Y., Los, D. A., Zinchenko, V. V., Tanticharoen, M., et al. (2005). Identical Hik-Rre systems are involved in perception and transduction of salt signals and hyperosmotic signals but regulate the expression of individual genes to different extents in *Synechocystis*. *J. Biol. Chem.* 280, 21531–21538. doi: 10.1074/jbc.M412174200

Singh, A. K., and Sherman, L. A. (2005). Pleiotropic effect of a histidine kinase on carbohydrate metabolism in *Synechocystis* sp. strain PCC 6803 and its requirement for heterotrophic growth. *J. Bacteriol.* 187, 2368–2376. doi: 10.1128/JB.187.7.2368-2376.2005

Suzuki, E., Ohkawa, H., Moriya, K., Matsubara, T., Nagaike, Y., Iwasaki, I., et al. (2010). Carbohydrate metabolism in mutants of the cyanobacterium *Synechococcus elongatus* PCC 7942 defective in glycogen synthesis. *Appl. Environ. Microbiol.* 76, 3153–3159. doi: 10.1128/AEM.00397-08

Tabei, Y., Okada, K., and Tsuzuki, M. (2007). Sll1330 controls the expression of glycolytic genes in *Synechocystis* sp. PCC 6803. *Biochem. Biophys. Res. Commun.* 355, 1045–1050. doi: 10.1016/j.bbrc.2007.02.065

Takai, N., Nakajima, M., Oyama, T., Kito, R., Sugita, C., Sugita, M., et al. (2006). A KaiC-associating SasA-RpaA two-component regulatory system as a major circadian timing mediator in cyanobacteria. *Proc. Natl. Acad. Sci. U.S.A.* 103, 12109–12114. doi: 10.1073/pnas.0602955103

van Alphen, P., and Hellingwerf, K. J. (2015). Sustained circadian rhythms in continuous light in *Synechocystis* sp. PCC6803 growing in a well-controlled photobioreactor. *PLoS ONE* 10:e0127715. doi: 10.1371/journal.pone.0127715

Wiegard, A., Dörrich, A. K., Deinzer, H. T., Beck, C., Wilde, A., Holtzendorff, J., et al. (2013). Biochemical analysis of three putative KaiC clock proteins from *Synechocystis* sp. PCC 6803 suggests their functional divergence. *Microbiology* 159, 948–958. doi: 10.1099/mic.0.065425-0

Williams, J. G. K. (1988). Construction of specific mutations in photosystem II photosynthetic reaction center by genetic engineering methods in *Synechocystis* 6803. *Methods Enzymol.* 167, 766–778. doi: 10.1016/0076-6879(88)67088-1

Yamauchi, Y., Kaniya, Y., Kaneko, Y., and Hihara, Y. (2011). Physiological roles of the cyAbrB transcriptional regulator pair Sll0822 and Sll0359 in *Synechocystis* sp. strain PCC 6803. *J. Bacteriol.* 193, 3702–3709. doi: 10.1128/JB.00284-11

Conflict of Interest Statement: The authors declare that the research was conducted in the absence of any commercial or financial relationships that could be construed as a potential conflict of interest.

frontiers in Microbiology

ORIGINAL RESEARCH
published: 24 August 2015
doi: 10.3389/fmicb.2015.00842

Characterization of *Chlamydomonas reinhardtii* phosphatidylglycerophosphate synthase in *Synechocystis* sp. PCC 6803

Chun-Hsien Hung[1], Kaichiro Endo[2], Koichi Kobayashi[2], Yuki Nakamura[1,3] and Hajime Wada[2,4]*

[1] Institute of Plant and Microbial Biology, Academia Sinica, Taipei, Taiwan, [2] Department of Life Sciences, Graduate School of Arts and Sciences, The University of Tokyo, Tokyo, Japan, [3] PRESTO, Japan Science and Technology Agency, Saitama, Japan, [4] CREST, Japan Science and Technology Agency, Saitama, Japan

OPEN ACCESS

Edited by:
Weiwen Zhang, Tianjin University, China

Reviewed by:
Jiangxin Wang, Arizona State University, USA
Junbiao Dai, Tsinghua University, China
Norihiro Sato, Tokyo University of Pharmacy and Life Sciences, Japan

***Correspondence:**
Yuki Nakamura, Institute of Plant and Microbial Biology, Academia Sinica, 128 Section 2, Academia Road, Nankang, Taipei 11529, Taiwan
nakamura@gate.sinica.edu.tw

Specialty section:
This article was submitted to Microbiotechnology, Ecotoxicology and Bioremediation, a section of the journal Frontiers in Microbiology

Received: *02 June 2015*
Accepted: *31 July 2015*
Published: *24 August 2015*

Citation:
Hung C-H, Endo K, Kobayashi K, Nakamura Y and Wada H (2015) Characterization of Chlamydomonas reinhardtii phosphatidylglycerophosphate synthase in Synechocystis sp. PCC 6803. Front. Microbiol. 6:842. doi: 10.3389/fmicb.2015.00842

Phosphatidylglycerol (PG) is an indispensable phospholipid class with photosynthetic function in plants and cyanobacteria. However, its biosynthesis in eukaryotic green microalgae is poorly studied. Here, we report the isolation and characterization of two homologs (CrPGP1 and CrPGP2) of phosphatidylglycerophosphate synthase (PGPS), the rate-limiting enzyme in PG biosynthesis, in *Chlamydomonas reinhardtii*. Heterologous complementation of *Synechocystis* sp. PCC 6803 *pgsA* mutant by *CrPGP1* and *CrPGP2* rescued the PG-dependent growth phenotype, but the PG level and its fatty acid composition were not fully rescued in the complemented strains. As well, oxygen evolution activity was not fully recovered, although electron transport activity of photosystem II was restored to the wild-type level. Gene expression study of *CrPGP1* and *CrPGP2* in nutrient-starved *C. reinhardtii* showed differential response to phosphorus and nitrogen deficiency. Taken together, these results highlight the distinct and overlapping function of PGPS in cyanobacteria and eukaryotic algae.

Keywords: ***Chlamydomonas reinhardtii*, chloroplast, glycerolipid, phosphatidylglycerol, photosynthesis**

Introduction

Photosynthetic membranes are highly specialized biological membranes that contain distinct yet conserved classes of polar glycerolipids MGDG, DGDG, SQDG, and PG among cyanobacteria, eukaryotic microalgae, and land plants (Omata and Murata, 1983; Dorne et al., 1990; Sakurai et al., 2006). Gene knockout affecting biosynthesis of these lipids causes severe photosynthetic defects in a cyanobacterium, *Synechocystis* sp. PCC 6803 (Mendiola-Morgenthaler et al., 1985; Hagio et al., 2000; Sato et al., 2000; Aoki et al., 2004; Awai et al., 2007; Sakurai et al., 2007b), the eukaryotic green microalga *Chlamydomonas reinhardtii* (Dubertret et al., 1994; Sato et al., 1995) and the seed plant *Arabidopsis thaliana* (Dörmann et al., 1995; Hagio et al., 2002; Babiychuk et al., 2003; Kelly et al., 2003; Yu and Benning, 2003; Kobayashi et al., 2007, 2015). Biosynthesis of these lipids may be critical for photosynthesis.

Abbreviations: Chl, chlorophyll; DAG, *sn*-1,2-diacylglycerol; DCMU, 3-(3,4-dichlorophenyl)-1,1-dimethylurea; DGDG, digalactosyldiacylglycerol; MGDG, monogalactosyldiacylglycerol; MGlcDG, monoglucosyldiacylglycerol; PG, phosphatidylglycerol; PGPS, phosphatidylglycerophosphate synthase; PS, photosystem; SQDG, sulfoquinovosyldiacylglycerol.

Except for variation in fatty acid composition, the structural features of these four lipid classes are highly similar; however, the biosynthetic pathways may be diverse among cyanobacteria, eukaryotic algae and higher plants. For example, the most abundant lipid class, MGDG, is synthesized in *Synechocystis* sp. PCC 6803 by two steps (Sato and Murata, 1982): first DAG is glucosylated with UDP-glucose to form MGlcDG by MGlcDG synthase (Awai et al., 2006), which is then isomerized to MGDG by an epimerase (Awai et al., 2014). However, in *A. thaliana* and other seed plants, MGDG is synthesized by one-step galactosylation with UDP-galactose by MGDG synthases (Shimojima et al., 1997). In contrast, DGDG is produced by the further galactosylation of MGDG by DGDG synthases in both *Synechocystis* sp. PCC 6803 (Awai et al., 2007) and *A. thaliana* (Kelly and Dormann, 2002; Kelly et al., 2003).

Phosphatidylglycerol is the only major phospholipid class present in the photosynthetic membrane. It has a distinct contribution to photosynthesis. Gene knockout study revealed the crucial role of PG biosynthesis: disruption of *pgsA*, encoding PGPS in *Synechocystis* sp. PCC 6803, affects cell growth and photosynthetic activity unless PG is supplemented exogenously (Hagio et al., 2000). Arabidopsis possesses two PGPS, PGP1 and PGP2; knocking out *PGP1* severely impairs chloroplast biogenesis but not mitochondrial function (Hagio et al., 2002; Babiychuk et al., 2003), and double knockout of *PGP1* and *PGP2* further reduces PG levels to a trace amount, and causing an embryonic-lethal phenotype (Tanoue et al., 2014).

Much less is known about the biosynthesis of photosynthetic membrane lipids in *C. reinhardtii*. However, a distinct feature of chloroplast lipid metabolism has been shown: an involvement of chloroplastic galactoglycerolipid lipase in triacylglycerol production in nitrogen-starved *C. reinhardtii* (Li et al., 2012). Because the possible contribution of chloroplastic glycerolipids in triacylglycerol production is uniquely observed in *C. reinhardtii*, dissecting the similarity and distinctiveness of chloroplastic lipid biosynthesis in *C. reinhardtii* with reference to *Synechocystis* sp. PCC 6803 and *A. thaliana* is important.

In this study, we isolated two *PGPS* genes in *C. reinhardtii*, *CrPGP1* and *CrPGP2*, and assessed the molecular function by transforming them into a *pgsA* mutant of *Synechocystis* sp. PCC 6803. Moreover, gene expression profiles were examined in *C. reinhardtii* under phosphorus or nitrogen-starved conditions. The result showed distinct and overlapping functions of PGPS between cyanobacteria and eukaryotic algae.

Materials and Methods

Strains and Growth Conditions

The wild-type and *pgsA* cells of *Synechocystis* sp. PCC 6803 were grown photoautotrophically at 30°C in BG-11 medium supplemented with 20 μM PG as described previously (Sakurai et al., 2003). Growth of cultures was monitored by determining optical density at 730 nm (OD_{730}). Light was provided by fluorescent lamps with approximately 50–60 μmol photons m^{-2} s^{-1}. *C. reinhardtii* strain CC-4351 was obtained from the Chlamydomonas Resource Center and transformed with empty pChlamiRNA2 plasmid (Molnar et al., 2009). Cells were photoheterotrophically grown in TAP medium (Gorman and Levine, 1965) at 22°C. Nutrient deficiency was induced by collecting the cells by centrifugation (5 min at 3000 × *g*), washed twice with the respective media and subsequently resuspended in TAP medium, TAP medium without nitrogen (TAP-N), or phosphorus (TAP-P) by omitting NH_4Cl, or replacing potassium phosphate with 1.5 mM KCl, respectively (Quisel et al., 1996).

Molecular Cloning

CrPGP1 (Cre03.g162601)

A 937-bp fragment was amplified using cDNA synthesized from the total RNA of *C. reinhardtii* strain CC-503 (cw92 mt^+) as the template with the primers CH223 and CH224 and cloned into pENTR/D_TOPO to construct pCH067. Then, the cloned fragment was amplified with the primers CH772 and CH773 and inserted into *Nde*I and *Hpa*I sites of pTCP2031V to construct pCH167.

CrPGP2 (Cre02.g095106)

A 790-bp fragment was amplified using cDNA synthesized from the total RNA of *C. reinhardtii* strain CC-503 (cw92 mt^+) as the template with the primers CH225 and CH226 and cloned into pENTR/D_TOPO to construct pCH068. Then, the cloned fragment was amplified with the primers CH774 and CH775 and inserted into *Nde*I and *Hpa*I sites of the pTCP2031V vector which was designed to incorporate a gene of interest at a neutral site (*slr2031*) with the *psbA2* (*slr1311*) promoter and a chloramphenicol-resistance cassette (Satoh et al., 2001). The resulting plasmid pCH160 was used to transform the *pgsA* mutant of *Synechocystis* sp. PCC 6803 by homologous recombination. The strains, plasmids, and oligonucleotide primers used in this study are described in Supplementary Tables 1–3, respectively.

Complementation Assay of the *Synechocystis* sp. PCC 6803 *pgsA* Mutant by *CrPGP1* and *CrPGP2*

For culture on BG-11 agar plates, 5 μl of liquid culture was used with serial 10-fold dilution for spotting from left to right starting at OD_{730} 0.05 onto the plate with or without 20 μM PG. Plates were incubated photoautotrophically under 50∼60 μmol photons m^{-2} s^{-1} for 5 days at 30°C to observe the growth phenotype. For liquid culture, cells were photoautotrophically grown in BG-11 media. Initial growth was started at OD_{730} 0.1 by the stirring culture at 180 rpm, 50∼60 μmol photons m^{-2} s^{-1} at 30°C.

Genotype Analysis

Genomic DNA was isolated from cells of the wild type, *pgsA CrPGP1* and *pgsA CrPGP2* of *Synechocystis* sp. PCC 6803. The primers CH784 and CH785 were used for PCR analysis of genetic background; a 1,141-bp fragment could be amplified from wild-type genomic DNA, whereas a 2,341-bp fragment could be amplified from genomic DNA of *pgsA CrPGP1* or *pgsA CrPGP2*. PCR analysis of the insertion at *slr2031* involved the primers for CH982 and CH1000, for an expected 575-bp fragment from the

wild type, 2,938-bp fragment from *pgsA CrPGP1* and 2,791-bp fragment from *pgsA CrPGP2*.

Lipid Analysis

Lipids were extracted from intact cells as described in (Bligh and Dyer, 1959) and analyzed previously (Nakamura et al., 2003).

RNA Extraction and qRT-PCR Analysis

Total RNA from *Synechocystis* sp. PCC 6803 cells grown in BG-11 media by stirring culture at 180 rpm, 50∼60 μmol photons m^{-2} s^{-1} at 30°C was extracted using TRI reagent (Ambion) including DNase treatment and reverse-transcribed with SuperScript III (Invitrogen, Carlsbad, CA, USA) for cDNA synthesis. Quantitative RT-PCR involved the ABI 7500 Real Time PCR System (Applied Biosystems) with the oligonucleotide primers for *pgsA* (*slr 1522*; CH1028 and CH1029), *PGP1* (Cre03.g162601; CH919 and CH920), *PGP2* (Cre02.g095106; CH953 and CH954) and *RNase P subunit B* (*rnpB*; CH947 and CH948). Gene expression was normalized to that of *rnpB* (Yuzawa et al., 2014). Data were averaged by three technical replicates in the same run and three biological replicates in separate runs.

Total RNA extraction and cDNA synthesis from *C. reinhardtii* cells grown by stirring culture at 200 rpm, 50∼60 μmol photons m^{-2} s^{-1} at 22°C, follow the method as described above. Oligonucleotide primers used are: *Chlamydomonas G-protein beta subunit-like polypeptide* (*CBLP*; Cre06.g278222; CH1076 and CH1077), *PGP1* (Cre03.g162601; CH919 and CH920), *PGP2* (Cre02.g095106; CH953 and CH954), *monogalactosyldiacylglycerol synthase1* (*MGD1*; Cre13.g585301; CH890 and CH891), *digalactosyldiacylglycerol synthase1* (*DGD1*; Cre13.g583600; CH1060 and CH1061), *UDP-sulfoquinovose synthase* (*SQD1*; Cre16.g656400; CH1062 and CH1063), *sulfoquinovosyldiacylglycerol synthase* (*SQD2*; Cre01.g038550; CH1064 and CH1065), *nitrate reductase1* (*NIT1*; Cre09.g410950; CH1072 and CH1073) and *phosphorus starvation response protein* 1 (*PSR1*; Cre12.g495100; CH1066 and CH1067). Gene expression was normalized to that of *CBLP* (Schloss, 1990; Chang et al., 2005). Data were averaged by three technical replicates in the same run and two biological replicates in separate runs. Annotation of genes for the lipid metabolism is according to (Li-Beisson et al., 2015). The primers used are listed in Supplementary Table 3.

Assay of Photosynthetic Parameters

Photosynthetic oxygen-evolving activity from H_2O to CO_2 of intact cells was measured with a Clark-type oxygen electrode (Hansatech Instruments, Kings Lynn, UK) as described in (Gombos et al., 1991). Light from an incandescent lamp through a red optical filter was used for all oxygen evolution measurements at the light intensity 900 μmol photons m^{-2} s^{-1}. The Chl concentration of cells, determined by the method of Porra et al. (1989) with 100% methanol extraction, was adjusted to 5 μg mL^{-1}.

For measurements of 77 K fluorescence emission spectra, intact cells were suspended in BG-11 at 10 μg Chl mL^{-1}. Fluorescence emission spectra of intact cells under 435 or 600 nm excitation were recorded at 77 K with a spectrofluorometer (RF-5300PC; Shimadzu) as described (Sakurai et al., 2007a).

Measurements of relaxation of flash-induced Chl fluorescence yield were performed in intact cells (5 μg Chl mL^{-1}) by profiling the spectra following single flash excitation with or without 10 μM DCMU (Vass et al., 1999). Samples were incubated in darkness for 10 min before DCMU was added at a final concentration of 10 μM. The levels of F_o and F_m were normalized.

For measurements of absorption spectra, cells were grown by stirring culture at 180 rpm, 50∼60 μmol photons m^{-2} s^{-1} at 30°C. Absorption spectra of pigments were determined directly in intact cell suspension (OD_{730}≈0.1) by spectrophotometry (Beckman Coulter DU 800 Spectrophotometer). Spectra were normalized at 625 nm, the maximum absorption of phycobiliproteins, as described (Gombos et al., 2002).

Results

Isolation of Genes Encoding Putative PGPS from *C. reinhardtii*

To isolate genes encoding functional PGPS for the biosynthesis of PG in *C. reinhardtii*, we performed a homology search with the amino acid sequence of AtPGP1 (At2g39290), which plays a major role in biosynthesis of PG and is essential for thylakoid membrane development in *A. thaliana* (Hagio et al., 2002; Xu et al., 2002; Babiychuk et al., 2003). Two genes were found as putative genes of PGPS in *C. reinhardtii* and named *CrPGP1* (Cre03.g162601) and *CrPGP2* (Cre02.g095106), encoding 32.1 and 28.7 kDa protein, respectively. We compared the amino acid sequence of CrPGP1 and CrPGP2 with characterized PGPs in *A. thaliana* (AtPGP1 and AtPGP2) (Hagio et al., 2002; Xu et al., 2002; Babiychuk et al., 2003) and *Synechosystis* sp. PCC 6803 (PgsA) (Hagio et al., 2000) by creating multiple amino acid sequence alignment (**Figure 1A**). As can be seen, the amino acid residues conserved in all sequences of proteins with the CDP-OH-P motif (PF01066.9) indicated by asterisks were conserved in CrPGP1 and CrPGP2, suggesting that these proteins are functional PGPs. Interestingly, CrPGP1 has longer N-terminal sequence than CrPGP2, as is found between AtPGP1 and AtPGP2. Next, we compared the identity and similarity of these PGPs (**Figure 1B**). The value ranges from 31.8 to 81.1% in identity and from 62.6 to 91.0% in similarity. The identity and similarity of PGPs were higher between *C. reinhardtii* and *A. thaliana* than CrPGP1 and CrPGP2, and those with *Synechocystis* PgsA were similar between *C. reinhardtii* and *A. thaliana*.

To examine whether these two genes encode functional PGPS, we cloned *CrPGP1* and *CrPGP2* under the control of the *psbA2* promoter and stably transformed them into a neutral genomic site (*slr2031*) (Satoh et al., 2001) of the *Synechocystis* sp. PCC 6803 *pgsA* mutant, which is defective in PGPS activity (Hagio et al., 2000) (**Figure 2A**). To confirm the successful homologous recombination of *CrPGP1* and *CrPGP2* into the neutral genomic site in the *pgsA* mutant, we performed PCR-based genotyping for both *pgs*A (*slr1522*) and *slr2031* (**Figure 2B**). Compared to

A

```
CrPGP2      1 ------------------------------------------------------------MVE
SynPgsA     1 ------------------------------------------------------------
AtPGP1      1 -------MLRSGLASLIVDVNLRRTLRPSPTFSFPAHLSRCIITSRYSSRTSLRFPIQIS
AtPGP2      1 ------------------------------------------------------------
CrPGP1      1 MAMLGKVCSRLCVSTGPTQAATRALLNVHHASAGASYAHGLTASPQWQVALARRISCCSS

CrPGP2      4 ATESAEDTIPIVPLLGVTKPAESLTSPIDRRSDFYRHAALVVPHKPARQPLMTIPNVLTF
SynPgsA     1 ------------------------------------------------MNIPNWVTV
AtPGP1     54 RHQHRLSYFSSSSSSEQSRPTSSSRNSFSGHGQLDSDDNSSPPPSQSSSKVLTIPTVLTL
AtPGP2      1 -----------MGEEDTATVDQNSFGGGKDSLLRNRHSSPLPSPTQLSSKVITIPTVLTL
CrPGP1     61 SANGHASAPEPNRPSQQGETSSVTEDRASSSNGASSSGSAGSSKSNGDGVVITVPTMLTL

CrPGP2     64 FRLLLVPVLLLVWELQWHYTPTLCAVIFIAASVTDYFDGYLARKLKIATVPGAPLDPVAD
SynPgsA    10 SRLLALPLLFLWLPTPEAETRWWGVGIFLLAASTDWLDGYLARRLNQVTELGKFLDPLVD
AtPGP1    114 GRVAAVPLLVATFYVDSWWGTTATTSIFIAAAITDWLDGYLARKMRLGSAFGAFLDPVAD
AtPGP2     50 GRVAAVPILVATFYVDCWWGRTATTSIFIAAAITDWLDGYHARKMRLGSEFGAFLDPVAD
CrPGP1    121 GRVAAIPVLIAAWYWQSPHSALVTTAVFAAASLTDWLDGYLARKMNSYSAFGAFLDPVAD
                                                  *  **  **      *   *   *

CrPGP2    124 KIMVAT-ALVLLAVSPPPPWSPQWL-----TAPVVLIICREITMSALREWAAAAGGGVSK
SynPgsA    70 KLVLAPLLILLFWQVVPPWA------------VGLILAREIVIAGWEVNPQLAS--QTE
AtPGP1    174 KLMVAATLILLCTKPIQVAELGPLP--WFLTVPSIAIIGREITMSAVREWAASQNGKLLE
AtPGP2    110 KLMVAATLILLCTKPMVAVVLGPVP--WLVTVPSIAIIGREITMSAVREWAASQNGKLSE
CrPGP1    181 KLMVAACLILLCTRPLAAGPAWLAGNDWLLPVCTLAIIGREITMSALREWAATAGPEARQ

CrPGP2    178 AVKVNTLGKWKTALQMVSMSVLLVVEQPLGDLLPSYAGSPLWLHISLASYVALWGGTVLG
SynPgsA   116 IAGANLWGKWKTVTQLTAIALLLAP-------LPEIYG--------QIGTVIFWIAVVLT
AtPGP1    232 AVAVNNLGKWKTATQMIALTILLASRD----SNVGWLVA--------SCAGLLVVSAGLS
AtPGP2    168 AVAVNSLGKWKTATQMIALTILLASRD-----SSFERLLP--------SCIGLLVVSAGLS
CrPGP1    241 AVAVNAWGKWKTASQMASLTLLLVKDGGSGAAASAAAV--------ACAALLLVASWLT

CrPGP2    238 LWSLAIYFSNVWVHFVYPEAKKHH
SynPgsA   161 LISGAIYLFPPGNNKVEAG-----
AtPGP1    280 VWSLAVYMRKIWKVLMK-------
AtPGP2    216 IWSLVVYMRKIWRVLLKK------
CrPGP1    293 VQSLAIYMRGLWRFMARM------
```

B

Identity (%)

Similarity (%)

	CrPGP1	CrPGP2	AtPGP1	AtPGP2	SynPgsA
CrPGP1		45.6	50.8	49.8	31.8
CrPGP2	**68.8**		44.5	43.0	34.5
AtPGP1	**75.4**	**72.5**		81.1	35.8
AtPGP2	**74.3**	**69.7**	**91.0**		33.7
SynPgsA	**63.0**	**62.6**	**66.8**	**66.3**	

FIGURE 1 | Comparison of amino acid sequences of PGPs. **(A)** Multiple amino acid sequence alignment of two PGPs of *Chlamydomonas reinhardtii* (CrPGP1 and CrPGP2) with reference to two PGPs of *Arabidopsis thaliana* (AtPGP1 and AtPGP2) and PgsA of *Synechocystis* sp. PCC 6803 (SynPgsA). Asterisks indicate the amino acid residues conserved in all sequences of proteins with the CDP-OH-P motif (PF01066.9). **(B)** The identity and similarity of amino acid sequences among PGPs aligned in **(A)**.

the wild type, both *pgsA CrPGP1* and *pgsA CrPGP2* mutants maintained the *pgsA* background and the introduced genes were fully segregated at the *slr2031* locus by the homologous recombination. We further investigated whether *CrPGP1* and *CrPGP2* were expressed in *pgsA* by comparing mRNA levels of *CrPGP1* in *pgsA CrPGP1*, *CrPGP2* in *pgsA CrPGP2*, and *pgsA* in wild type. As shown in **Figure 2C**, both *CrPGP1* and *CrPGP2* were expressed, whose levels were fivefold and eightfold higher than that of *pgsA*. Thus, under the *psbA2* promoter control, both *CrPGP1* and *CrPGP2* were expressed in *pgsA CrPGP1* and *pgsA CrPGP2*.

Complementation of *Synechocystis* sp. PCC 6803 *pgsA* Mutant with *CrPGPs*

Previous study showed that the *pgsA* mutant of *Synechocystis* sp. PCC 6803 requires exogenous supplementation of PG for growth (Hagio et al., 2000), so we compared the growth of the wild type, *pgsA*, *pgsA CrPGP1*, and *pgsA CrPGP2* on solid BG-11 media with or without 20 μM PG. The wild-type cells grew similarly in the presence or absence of PG, whereas the *pgsA* mutant showed rescued growth only with PG (**Figure 3A**). The *pgsA CrPGP1* and *pgsA CrPGP2* showed rescued growth even in the absence of PG, which suggests that *CrPGP1* and *CrPGP2* are functional PGPS to rescue the growth defect of *pgsA*. To further investigate the growth profiles of *pgsA CrPGP1* or *pgsA CrPGP2*, we monitored the growth in liquid BG-11 media without PG. Although the growth rate was significantly restored in the transgenic strains, it was inferior to that of the wild type, with the *pgsA CrPGP1* showed slightly better growth than *pgsA CrPGP2* (**Figure 3B**). Therefore, *CrPGP1* and *CrPGP2* could functionally complement the lethal phenotype of the *pgsA* mutant, although their growth remain slightly retarded as compared with the wild type.

Lipid Composition of *pgsA CrPGP1* and *pgsA CrPGP2*

To examine whether the levels of PG and other polar glycerolipids are restored in *pgsA CrPGP1* or *pgsA CrPGP2*, we analyzed the composition of membrane lipid classes and their fatty acid composition. PG composition in the wild type was 11 mol% but was 8 and 5 mol% in *pgsA CrPGP1* and *pgsA CrPGP2*, respectively (**Figure 4A**). Moreover, composition of DGDG was

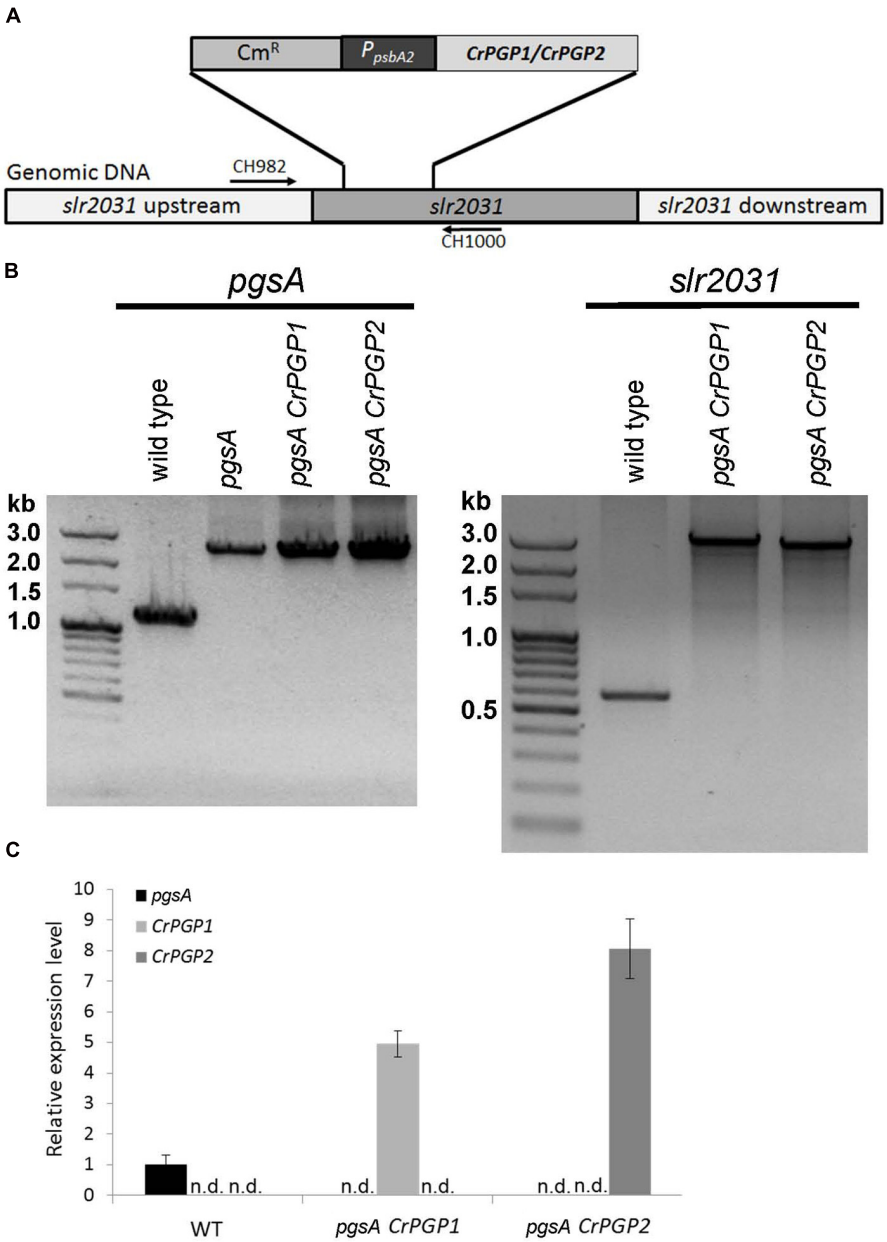

FIGURE 2 | Functional complementation of *Synechocystis sp*. PCC 6803 *pgsA* mutant with *PGP1* or *PGP2* of *Chlamydomonas reinhardtii*. **(A)** Schematic illustration of homologous recombination of *CrPGPs* at *slr2031* locus. **(B)** PCR-based genotyping analysis of the transformants for *pgsA* (left panel) and *slr2031* (right panel). **(C)** Expression level of *CrPGP1* and *CrPGP2* in the wild type, *pgsA CrPGP1* and *pgsA CrPGP2* relative to that of *pgsA* in the wild type. Levels are normalized to that of *rnpB*. Data are mean ± SD from three biological replicates. n.d., not detected.

slightly higher in the transgenic strains than the wild type. Next, we analyzed the fatty acid composition of these lipid classes (**Figures 4B–E**). The fatty acid composition of MGDG, DGDG, and SQDG was fairly similar among the three strains, but that of PG was markedly decreased in 18:3 and 18:2 composition and increased in 16:0 in *pgsA CrPGP1* and *pgsA CrPGP2* (**Figure 4E**). Hence, *CrPGP1* and *CrPGP2* produced a significant level of PG in *pgsA*, but the level was slightly lower and fatty acid composition differed from that of the wild type.

Pigment Content and Oxygen Evolution Activity of *pgsA CrPGP1* and *pgsA CrPGP2*

Previous studies have shown that PG deficiency reduces Chl content in *Synechocystis* sp. PCC 6803 and other cyanobacteria (Gombos et al., 2002; Wu et al., 2006; Bogos et al., 2010). To assess whether the expression of *CrPGPs* can restore the Chl content in *pgsA*, we examined absorption spectra of pigments in the whole cells of the wild type, *pgsA CrPGP1* and *pgsA CrPGP2* (**Figure 5**). The spectra was normalized at 625 nm, the maximum absorption

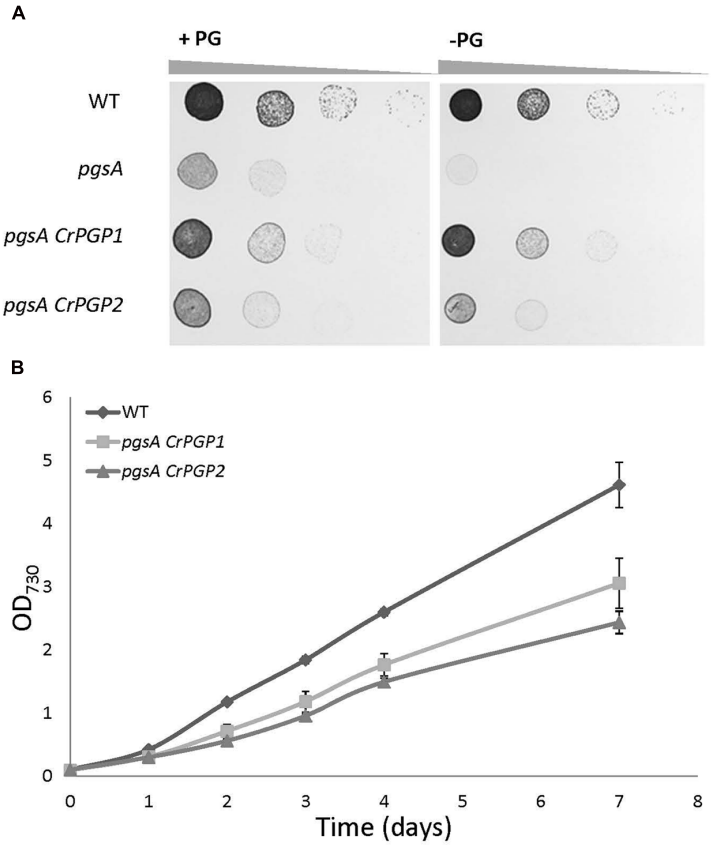

FIGURE 3 | Growth of *pgsA CrPGP1* or *pgsA CrPGP2*. (A) Growth of the wild type, *pgsA*, *pgsA CrPGP1*, or *pgsA CrPGP2* on solid BG-11 media with or without PG supplementation. Spotting involved serial 10-fold dilution from left to right starting at OD_{730} 0.05, with 5 μl each spotted onto a BG-11 agar plate with or without 20 μM PG and incubation under 50∼60 μmol photons m^{-2} s^{-1} for 5 days at 30°C. Images are representative of three biological replicates. **(B)** Growth profile of the wild type, *pgsA CrPGP1* or *pgsA CrPGP2* in liquid BG-11 media. Growth was initiated at OD_{730} 0.1 by stirring culture at 180 rpm, 50∼60 μmol photons m^{-2} s^{-1} at 30°C. Data are mean ± SD from three biological replicates.

of phycobiliproteins. Absorptions at ∼683 and ∼441 nm by Chl were lower for both *pgsA CrPGP1* and *pgsA CrPGP2* than the wild type. Indeed, the cellular Chl content in both complemented strains was decreased to 63% and 68% of the wild-type level, respectively (**Table 1**). To elucidate whether *CrPGPs* can restore the photosynthetic activity in *pgsA*, we compared the net oxygen evolution rate in complemented strains and the wild type. On a Chl content basis, oxygen evolution activities in *pgsA CrPGP1* and *pgsA CrPGP2* cells were 57 and 61% less than wild-type activities, respectively, which corresponded to 73 and 73.5% less than the wild type on a cell density basis. Therefore, the introduction of *CrPGP1* or *CrPGP2* can partially but not fully complement the loss of *pgsA* in *Synechocystis* sp. PCC 6803 in terms of photosynthetic activity as well as Chl accumulation.

Electron Transfer Kinetics in the Acceptor and Donor Side of PSII in *pgsA CrPGP1* and *pgsA CrPGP2*

The low oxygen evolution activities in the *pgsA CrPGP1* or *pgsA CrPGP2* imply impaired photosynthetic electron transport in these strains. To characterize the functionality of electron transfer within PSII in the complemented strains, we evaluated the reoxidation kinetics of Q_A, the primary electron acceptor plastoquinone (PQ) of PSII, by analyzing the decay of Chl fluorescence after a single saturating flush. The kinetics of accepter-side electron transfer from Q_A^- to the PQ pool was evaluated without DCMU (**Figure 6A**), and the kinetics from Q_A^- to the donor-side components were evaluated with DCMU, which inhibits the electron transfer from Q_A to Q_B and causes charge recombination between Q_A^- and the oxidizing-side components (**Figure 6B**). In both *pgsA CrPGP1* and *pgsA CrPGP2* cells, the fluorescence decay kinetics were almost identical to those in the wild type without or with DCMU. Thus, both complemented strains may assemble the functional PSII complex as in the wild type.

Chl Fluorescence Emission Spectra at 77 K in *pgsA CrPGP1* and *pgsA CrPGP2*

The core-antenna complexes of PSI and PSII are largely disordered in the PG-deficient *pgsA* mutant. To evaluate whether *CrPGPs* restore PS-antenna complexes in *pgsA*, we examined emission spectra of Chl fluorescence at 77 K. In both wild-type

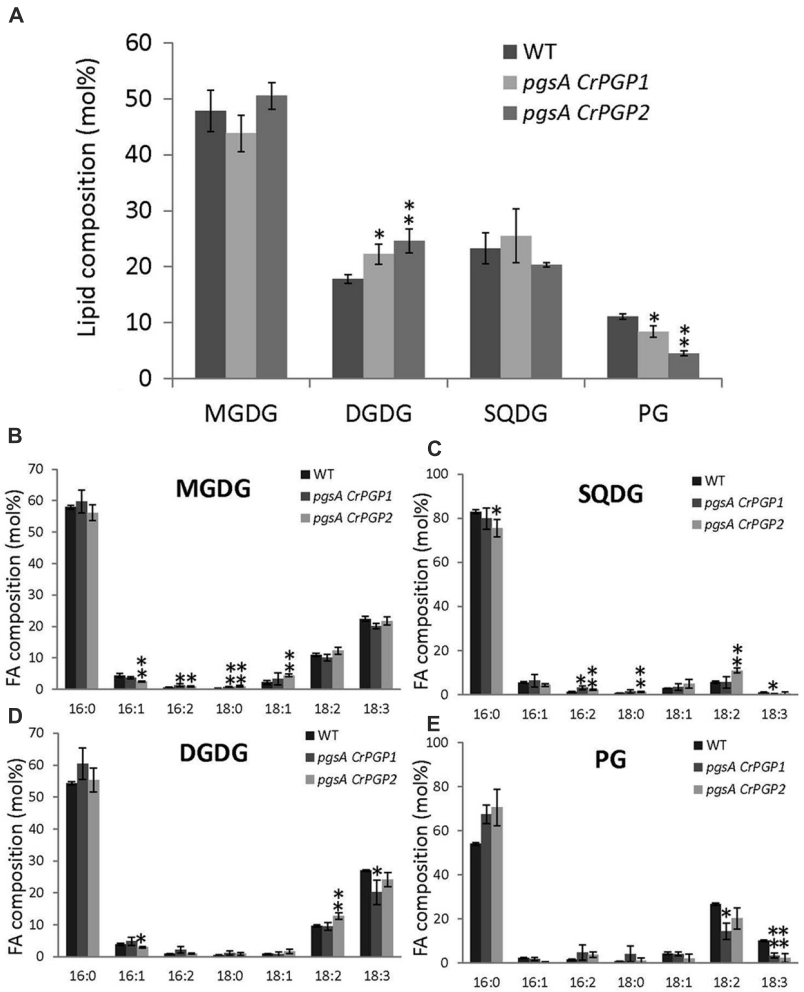

FIGURE 4 | Polar glycerolipid composition (A) and fatty acid composition of (B) MGDG; (C) SQDG; (D) DGDG; and (E) PG of the wild type, *pgsA CrPGP1* and *pgsA CrPGP2*. Data are mean ± SD from three biological replicates. Asterisks show significance (*$p < 0.05$, **$p < 0.01$) from the wild type. Unsaturated fatty acids detected in all lipid classes contain only *cis* double bonds.

and mutant cells, the preferential excitation of Chl at 435 nm resulted in four emission peaks, at ∼647, ∼681, ∼691, and ∼720 nm (**Figure 6C**). The emission peak at ∼647 nm can be attributed to phycocyanin (Rakhimberdieva et al., 2007); peaks at ∼681 nm and ∼691 nm primarily originate from CP43 and CP47, which are functionally coupled to the PSII reaction center, respectively; and the peak at ∼720 nm originates from PSI. For *pgsA CrPGP1* and *pgsA CrPGP2* cells, we found only a slight decrease in emission peak at ∼691 nm as compared with the wild type, which suggests a small change in the PSII complex in these complemented strains. By contrast, the emission from phycocyanin at 647 nm was slightly increased in the complemented strains. To examine the energy coupling between phycobilisomes and PS cores in the complemented lines, phycobilins were preferentially excited at 600 nm at 77 K (**Figure 6D**). Both *pgsA CrPGP1* and *pgsA CrPGP2* cells showed prominent emissions at ∼647 and ∼681 nm as compared with wild-type cells. The emission at ∼647 nm originates from phycocyanin, whereas that at ∼681 nm is contributed by both PSII Chl and terminal phycobilin emitters. The strong enhancement of the emission peaks at ∼647 and ∼681 nm in the complemented lines suggests that the energy transfer from phycobilisomes to the PSII reaction center is uncoupled in these cells.

Gene Expression Profiles of *CrPGP1* and *CrPGP2* under Nutrient-Limited *C. reinhardtii*

To obtain physiological insight into the role of CrPGP1 and CrPGP2, we analyzed gene expression profiles of *CrPGP1* and *CrPGP2* together with related genes for glycerolipid metabolism during phosphorus or nitrogen starvation. During phosphorus starvation, significant portion of phospholipids is replaced by non-phosphorus galactolipid DGDG, termed membrane lipid remodeling (Nakamura, 2013). Moreover, SQDG is increased and compensates for the decreased PG and maintains the total amount of anionic lipid classes (Riekhof et al., 2003).

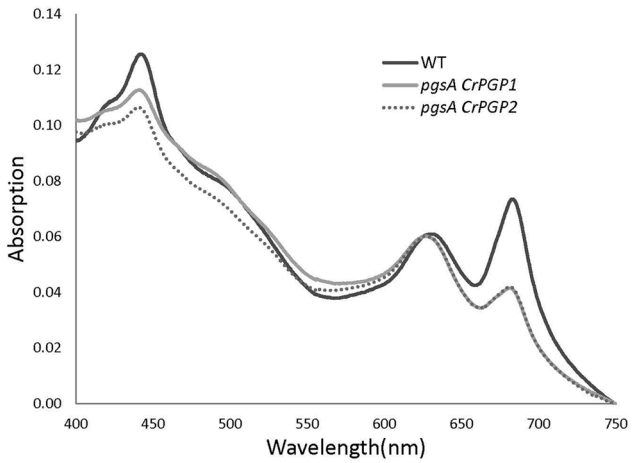

FIGURE 5 | Absorption spectra of wild type, *pgsA CrPGP1* and *pgsA CrPGP2* in BG-11 medium. The spectra were measured with whole cells ($OD_{730} \approx 0.1$) and normalized at 625 nm, the maximum absorption of phycobiliproteins.

TABLE 1 | Photosynthetic oxygen-evolving activities and Chl contents in intact cells of wild type, *pgsA CrPGP1*, and *pgsA CrPGP2* of *Synechocystis* sp. PCC 6803.

Strains	μg Chl/OD_{730}	Net electron transfer (μmol O_2 mg Chl^{-1} h^{-1})	Net electron transfer (μmol O_2 OD_{730}^{-1} h^{-1})
Wild type	0.62 ± 0.05	320 ± 20	20 ± 1.4
pgsA CrPGP1	0.39 ± 0.03	140 ± 30	5.4 ± 1.1
pgsA CrPGP2	0.42 ± 0.03	130 ± 20	5.3 ± 0.7

Intact cells were treated for 2 min in darkness, and oxygen evolution was measured at saturating light. The temperature of measurements was 30°C. Data are mean ± SD from three independent measurements.

However, gene expression profiles of enzymes related to this metabolic change were not studied previously. Here, we took two time points after switching *C. reinhardtii* to phosphorus starvation: 4 h for the early response and 5 days for the late response (**Figure 7**). *CrPSR1* is a marker gene for phosphorus starvation response (Wykoff et al., 1999). Both *CrPGP1* and *CrPGP2* showed a transient decrease at 4 h but recovered at 5 days. In contrast, the expression of *CrSQD1* and *CrSQD2*, which are required for SQDG biosynthesis, was induced at 4 h. Moreover, the gene expression of *CrDGD1* was increased but that of *CrMGD1* was not, which supports an increase in DGDG but not MGDG upon phosphorus starvation. These results showed that expression profiles of *CrPGP1* and *CrPGP2*, as well as other related genes examined in **Figure 7**, are altered under phosphorus starvation. Next, we examined nitrogen

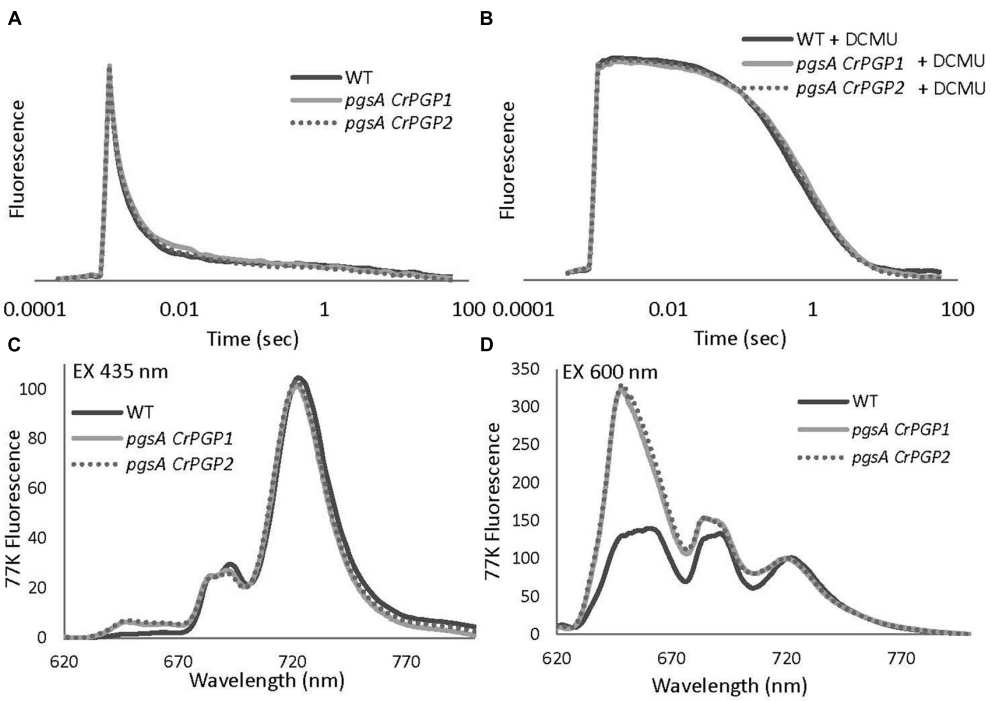

FIGURE 6 | Relaxation of flash-induced Chl fluorescence yield (A,B) and 77 K fluorescence emission spectra (C,D) of wild type, *pgsA CrPGP1* and *pgsA CrPGP2* mutant cells in BG-11 medium. The spectra resulted from a single flash excitation without **(A)** or with **(B)** 10 μM DCMU. Data are the mean from three independent experiments. In each case, Chl concentrations were adjusted to 5 μg mL^{-1}. Samples were incubated in darkness for 10 min before DCMU was added to the final concentration of 10 μM. The levels of F_o and F_m were normalized. **(C,D)** 77 K fluorescence emission spectra from the wild type, *pgsA CrPGP1* and *pgsA CrPGP2* mutant cells were measured under 435 nm **(C)** or 600 nm **(D)** excitation. Data are the mean from three independent experiments. Spectra were normalized at 720 nm to 100. In each case, Chl concentrations were adjusted to 10 μg mL^{-1}.

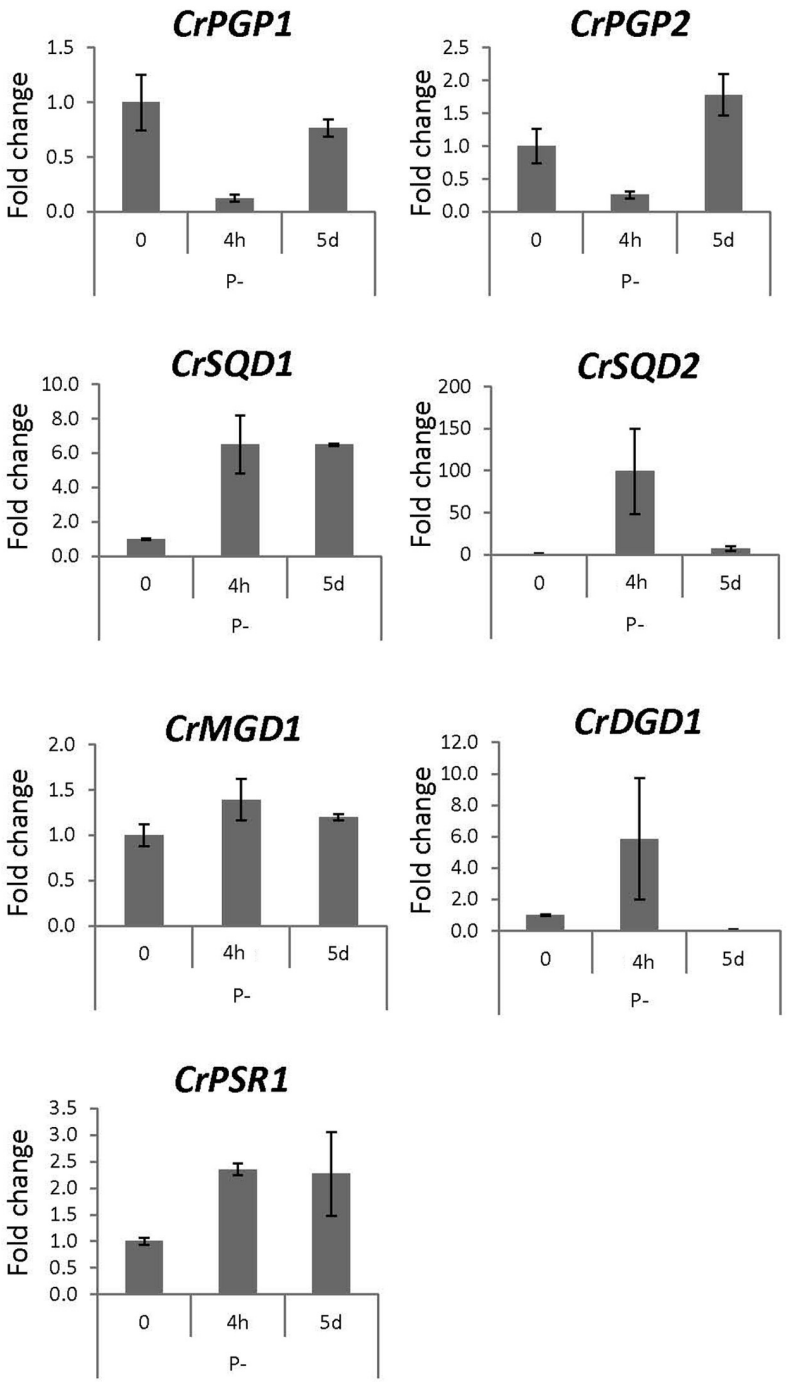

FIGURE 7 | Gene expression profile of enzymes for plastidial polar glycerolipid biosynthesis under phosphorus starvation. Wild-type *C. reinhardtii* strain CC-4351 grown in TAP media was transferred to the media devoid of phosphate and harvested at 4 h and 5 days. Total RNA was extracted to synthesize cDNA for qRT-PCR analysis. Gene expression was normalized to that of *CBLP*. Data were averaged by three technical replicates in the same run and two biological replicates in separate runs. *SQD1*, *UDP-sulfoquinovose synthase*; *SQD2*, *sulfoquinovosyldiacylglycerol synthase*; *MGD1*, *MGDG synthase1*; *DGD1*, *DGDG synthase1*; *PSR1*, *phosphorus starvation response1*.

starvation using *CrNIT1* as a marker gene (Hipkin et al., 1980). This condition severely affects photosynthesis but induces accumulation of triacylglycerol (Wang et al., 2009). As shown in **Figure 8**, *CrPGP1* but not *CrPGP2* showed decreased gene expression under nitrogen starvation. *CrSQD1* and *CrSQD2* showed transient changes in gene expression level, and *CrMGD1* and *CrDGD1* both decreased the gene expression level at different time points. Thus, *CrPGP1* and *CrPGP2* showed differential gene

expression profiles under phosphorus starvation and nitrogen starvation conditions.

Discussion

Phosphatidylglycerol synthesis is critical to maintain the stability of membrane protein complexes in photosynthesis components and in the respiratory electron transfer chain (Hagio et al., 2000; Ostrander et al., 2001; Domonkos et al., 2004; Hasan et al., 2013). This study isolated a pair of *PGPS* genes, *CrPGP1* and *CrPGP2*, in a model eukaryotic green microalga *C. reinhardtii*. The molecular function of these newly isolated PGPs was revealed by transforming them into the *pgsA* mutant of *Synechocystis* sp. PCC 6803, a representative cyanobacterium. Moreover, gene expression profiles of *CrPGP1* and *CrPGP2* were investigated in *C. reinhardtii* under phosphorus or nitrogen starvation. Strong responses of *CrPGPs*, particularly *CrPGP1*, to these conditions imply their involvements in membrane lipid remodeling in response to nutrient starvation. The results of cell growth, lipid analysis, and photosynthetic parameters in *pgsA CrPGP1* and *pgsA CrPGP2* showed distinct and overlapping function of PGPS between cyanobacteria and eukaryotic algae.

The heterologous complementation of the *pgsA* mutant phenotype by *CrPGP1* or *CrPGP2* supports that they encode a functional PGPS of *C. reinhardtii* (**Figures 3A,B**). However, the slower growth profile in *pgsA CrPGP1* or *pgsA CrPGP2* than the wild type under liquid culture suggests that *CrPGPs* cannot fully rescue the defect of *pgsA* mutant (**Figure 3B**). Our lipid analysis agrees with this idea: as compared with the wild type, *pgsA CrPGP1* and *pgsA CrPGP2* showed reduced PG contents by 73 and 45%, respectively. Although the expression level of *CrPGP2* was higher than *CrPGP1* (**Figure 2C**), expression of the CrPGP1 protein complemented the *pgsA* mutant phenotype more effectively than that of the CrPGP2. The protein sequence similarity with PgsA was slightly higher for CrPGP1 (63.0%) than CrPGP2 (62.6%). Moreover, *in silico* prediction of possible subcellular localization by ChloroP (Emanuelsson et al., 1999), TargetP (Emanuelsson et al., 2000), or PledAgro (Tardif et al., 2012) suggests that CrPGP1 may be localized at the chloroplasts or mitochondria whereas CrPGP2 may be localized somewhere other than the chloroplasts, the mitochondria or the secretory pathway. Indeed, longer N-terminal sequence was found in CrPGP1 (**Figure 1A**). Because the different subcellular localization was shown between AtPGP1 and AtPGP2 (Babiychuk et al., 2003; Tanoue et al., 2014), it is possible that CrPGP1 and CrPGP2 also have different subcellular localizations. It is possible that CrPGP1 is functionally more similar to PgsA because of the chloroplast localization. The fatty acid composition of PG showed reduced composition of 18:3 (**Figure 4E**). Because 18:3 in PG is produced by the fatty acid desaturase that desaturates acyl groups of PG, thus it is possible that PG produced by CrPGP1 and CrPGP2 may not be properly desaturated in *pgsA*, which highlights the different enzymatic features between PGP of *Synechocystis* sp. PCC 6803 and *C. reinhardtii*.

Many PG molecules are found in the PSII complex (Sakurai et al., 2006) and are present near the reaction center (Guskov et al., 2009; Umena et al., 2011). In fact, PG is indispensable for both donor- and acceptor-side activities of PSII (Hagio et al., 2000; Sato et al., 2000; Gombos et al., 2002; Sakurai et al., 2003, 2007a). Our data in **Figure 6** reveals that the expression of *CrPGPs* in *pgsA* sufficiently restored electron transfer activities of PSII to the wild-type level, although the PG levels and fatty acid composition in the complemented strains differed somewhat from those in the wild type (**Figure 4**). Thus, CrPGP activities would be enough to supply PG molecules to the PSII complex in the *pgsA* background. Meanwhile, the oxygen evolution activity in *pgsA* was not fully recovered by introducing the *CrPGPs* and remained at low levels (**Table 1**). Because phycobilisomes, which are not present in green algae including *Chlamydomonas*, may be energetically uncoupled with the PSII reaction center in the *pgsA* mutants harboring *CrPGPs* (**Figure 6D**), loss of energy transfer from phycobilisomes to the PSII reaction center in part likely reduces net photosynthesis activities in the complemented strains. The PG-deficient *pgsA* mutant showed energetic uncoupling between phycobilisomes and the PSII reaction center and not fully restored by the supplementation of PG (Sakurai et al., 2007a). Thus, *in situ* PG synthesis by native PgsA may be important for assembly of phycobilisomes with the PSII complex in *Synechocystis* sp. PCC 6803.

The expression of *CrPGP1* and *CrPGP2*, as well as the other genes showed differential profiles under two different nutrient starvation conditions (**Figures 7** and **8**). Most genes involved in glycoglycerolipid biosynthesis (*CrSQD1*, *CrSQD2*, and *CrDGD1*) showed rapid upregulation upon phosphorus starvation, whereas expression of *CrPGP1* and *CrPGP2* was decreased at 4 h after phosphorus starvation. This profile is in agreement with an increase in DGDG and SQDG levels and a decrease in PG levels under phosphorus starvation (Riekhof et al., 2003). However, the reduced expression of *CrPGP1* and *CrPGP2* was recovered at 5 days after phosphorus starvation. In addition to the membrane lipid remodeling, *C. reinhardtii* cells induce triacylglycerol biosynthesis by long-term phosphorus starvation with retaining thylakoid membrane networks (Iwai et al., 2014) and photosynthetic activity (Wykoff et al., 1998). Thus, the recovered expression of *CrPGP1* and *CrPGP2* may function to keep proper balance of lipid composition of thylakoid membranes and maintain photosynthetic activity even under long-term phosphorus starvation, at which triacylglycerol is produced possibly for an energy storage. Meanwhile, expression of most of the genes in **Figure 8** was decreased in response to nitrogen starvation. These changes agree with the actual decrease in MGDG, DGDG, SQDG, and PG, degradation of thylakoid membranes, and loss of photosynthetic activity under nitrogen starvation (Siaut et al., 2011; Iwai et al., 2014; Sakurai et al., 2014). Notably, *CrPGP1* but not *CrPGP2* showed decreased expression, whose profile was similar to that of *CrMGD1* upon nitrogen starvation. This suggests distinct roles between CrPGP1 and CrPGP2, which was also presumed by possible differences in subcellular localization and enzyme property of these isozymes. Differential expression profiles of some of lipid biosynthesis genes were previously observed. For example, the

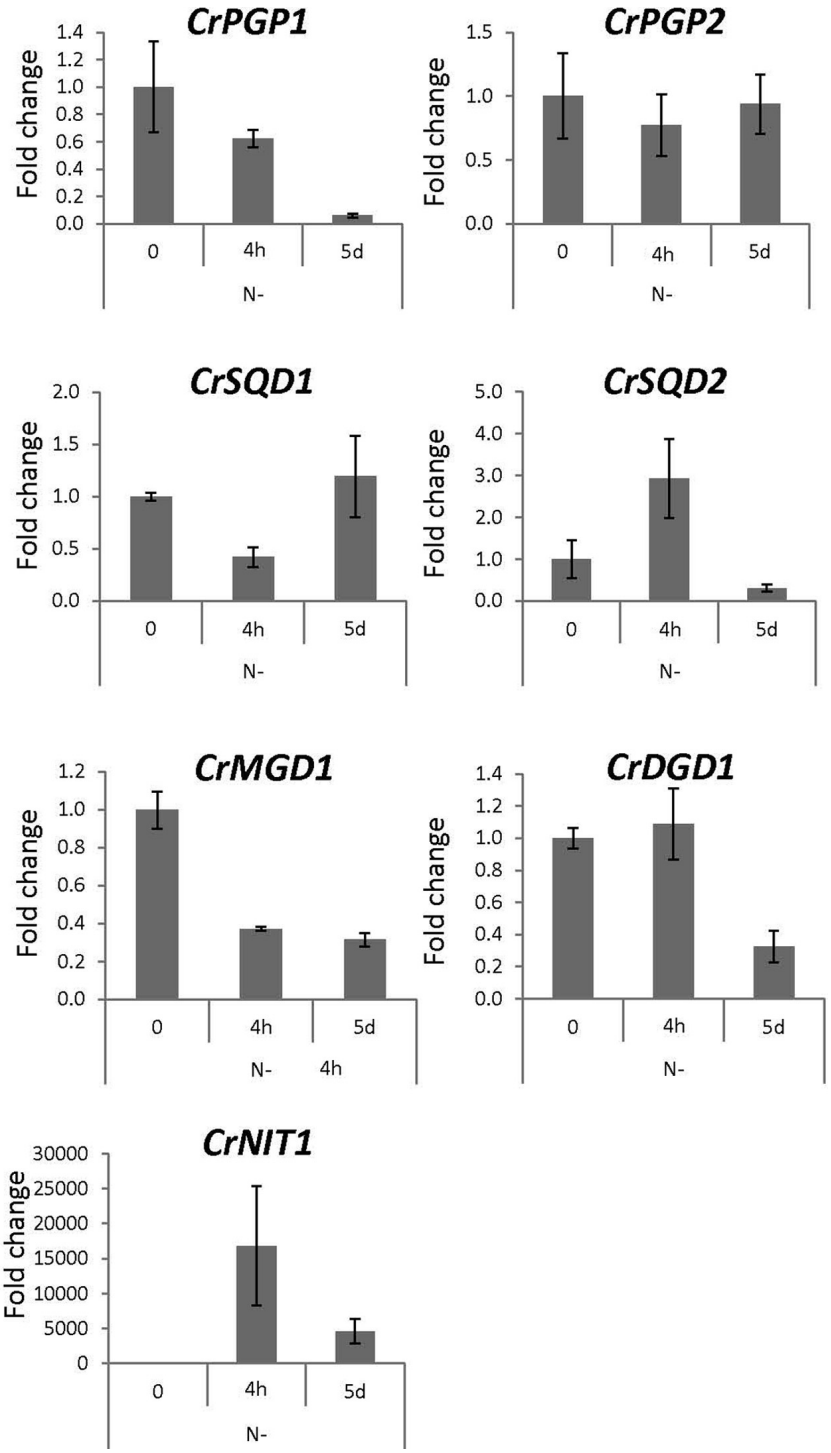

FIGURE 8 | Gene expression profile of enzymes for plastidial polar glycerolipid biosynthesis under nitrogen starvation. *NIT1, nitrate reductase 1*. See legend of **Figure 7** for sampling conditions, experimental methods, and abbreviations.

gene expression levels of *CrSQD1* showed partial recovery at later time points, *CrSQD2* expression showed fluctuation while decreasing, and *CrMGD1* expression showed faster decrease than that of *CrDGD1* upon nitrogen starvation (Boyle et al., 2012). These data are generally consistent with our results in **Figure 8**, although some differences were observed probably because of differences in growth conditions and/or time point analyzed. The distinct expression profiles among genes involved

in membrane lipid biosynthesis including *CrPGP1* and *CrPGP2* may allow *C. reinhardtii* cells to fine-tune lipid metabolism in response to various nutrient conditions.

Conclusion

Our results reveal that both *CrPGP1* and *CrPGP2* encode functional PGPS, which can contribute to PG production and the formation of photosynthetic complexes in the PG-deficient *Synechocystis pgsA* mutant. Further analyses are required to elucidate the roles of CrPGP1 and CrPGP2 in lipid metabolism and photosynthesis in *C. reinhardtii*.

Acknowledgments

This research was supported by PRESTO (to YN) and CREST (to HW), Japan Science and Technology Agency, and operation budget by Institute of Plant and Microbial Biology, Academia Sinica to YN.

Supplementary Material

The Supplementary Material for this article can be found online at: http://journal.frontiersin.org/article/10.3389/fmicb.2015.00842

References

Aoki, M., Sato, N., Meguro, A., and Tsuzuki, M. (2004). Differing involvement of sulfoquinovosyl diacylglycerol in photosystem II in two species of unicellular cyanobacteria. *Eur. J. Biochem.* 271, 685–693. doi: 10.1111/j.1432-1033.2003.03970.x

Awai, K., Kakimoto, T., Awai, C., Kaneko, T., Nakamura, Y., Takamiya, K., et al. (2006). Comparative genomic analysis revealed a gene for monoglucosyldiacylglycerol synthase, an enzyme for photosynthetic membrane lipid synthesis in cyanobacteria. *Plant Physiol.* 141, 1120–1127. doi: 10.1104/pp.106.082859

Awai, K., Ohta, H., and Sato, N. (2014). Oxygenic photosynthesis without galactolipids. *Proc. Natl. Acad. Sci. U.S.A.* 111, 13571–13575. doi: 10.1073/pnas.1403708111

Awai, K., Watanabe, H., Benning, C., and Nishida, I. (2007). Digalactosyldiacylglycerol is required for better photosynthetic growth of *Synechocystis* sp. *Plant Cell Physiol.* 48, 1517–1523. doi: 10.1093/pcp/pcm134

Babiychuk, E., Muller, F., Eubel, H., Braun, H. P., Frentzen, M., and Kushnir, S. (2003). *Arabidopsis* phosphatidylglycerophosphate synthase 1 is essential for chloroplast differentiation, but is dispensable for mitochondrial function. *Plant J.* 33, 899–909. doi: 10.1046/j.1365-313X.2003.01680.x

Bligh, E. G., and Dyer, W. J. (1959). A rapid method of total lipid extraction and purification. *Can. J. Biochem. Physiol.* 37, 911–917. doi: 10.1139/o59-099

Bogos, B., Ughy, B., Domonkos, I., Laczko-Dobos, H., Komenda, J., Abasova, L., et al. (2010). Phosphatidylglycerol depletion affects photosystem II activity in *Synechococcus* sp. PCC 7942 cells. *Photosynth. Res.* 103, 19–30. doi: 10.1007/s11120-009-9497-0

Boyle, N. R., Page, M. D., Liu, B., Blaby, I. K., Casero, D., Kropat, J., et al. (2012). Three acyltransferases and nitrogen-responsive regulator are implicated in nitrogen starvation-induced triacylglycerol accumulation in *Chlamydomonas*. *J. Biol. Chem.* 287, 15811–15825. doi: 10.1074/jbc.M111.334052

Chang, C. W., Moseley, J. L., Wykoff, D., and Grossman, A. R. (2005). The LPB1 gene is important for acclimation of *Chlamydomonas reinhardtii* to phosphorus and sulfur deprivation. *Plant Physiol.* 138, 319–329. doi: 10.1104/pp.105.059550

Domonkos, I., Malec, P., Sallai, A., Kovacs, L., Itoh, K., Shen, G., et al. (2004). Phosphatidylglycerol is essential for oligomerization of photosystem I reaction center. *Plant Physiol.* 134, 1471–1478. doi: 10.1104/pp.103.037754

Dörmann, P., Hoffmann-Benning, S., Balbo, I., and Benning, C. (1995). Isolation and characterization of an *Arabidopsis* mutant deficient in the thylakoid lipid digalactosyl diacylglycerol. *Plant Cell* 7, 1801–1810. doi: 10.1105/tpc.7.11.1801

Dorne, A. J., Joyard, J., and Douce, R. (1990). Do thylakoids really contain phosphatidylcholine? *Proc. Natl. Acad. Sci. U.S.A.* 87, 71–74. doi: 10.1073/pnas.87.1.71

Dubertret, G., Mirshahi, A., Mirshahi, M., Gerard-Hirne, C., and Tremolieres, A. (1994). Evidence from in vivo manipulations of lipid composition in mutants that the delta 3-trans-hexadecenoic acid-containing phosphatidylglycerol is involved in the biogenesis of the light-harvesting chlorophyll a/b-protein complex of *Chlamydomonas reinhardtii*. *Eur. J. Biochem.* 226, 473–482. doi: 10.1111/j.1432-1033.1994.tb20072.x

Emanuelsson, O., Nielsen, H., Brunak, S., and von Heijne, G. (2000). Predicting subcellular localization of proteins based on their N-terminal amino acid sequence. *J. Mol. Biol.* 300, 1005–1016. doi: 10.1006/jmbi.2000.3903

Emanuelsson, O., Nielsen, H., and von Heijne, G. (1999). A *Chlamydomonas* gene encodes a G protein beta subunit-like polypeptide. *Protein Sci.* 8, 978–984. doi: 10.1110/ps.8.5.978

Gombos, Z., Varkonyi, Z., Hagio, M., Iwaki, M., Kovacs, L., Masamoto, K., et al. (2002). Phosphatidylglycerol requirement for the function of electron acceptor plastoquinone Q(B) in the photosystem II reaction center. *Biochemistry* 41, 3796–3802. doi: 10.1021/bi011884h

Gombos, Z., Wada, H., and Murata, N. (1991). Direct evaluation of effects of fatty-acid unsaturation on the thermal-properties of photosynthetic activities, as studied by mutation and transformation of *Synechocystis* PCC6803. *Plant Cell Physiol.* 32, 205–211.

Gorman, D. S., and Levine, R. P. (1965). Cytochrome f and plastocyanin: their sequence in the photosynthetic electron transport chain of *Chlamydomonas reinhardii*. *Proc. Natl. Acad. Sci. U.S.A.* 54, 1665–1669. doi: 10.1073/pnas.54.6.1665

Guskov, A., Kern, J., Gabdulkhakov, A., Broser, M., Zouni, A., and Saenger, W. (2009). Cyanobacterial photosystem II at 2.9-A resolution and the role of quinones, lipids, channels and chloride. *Nat. Struct. Mol. Biol.* 16, 334–342. doi: 10.1038/nsmb.1559

Hagio, M., Gombos, Z., Varkonyi, Z., Masamoto, K., Sato, N., Tsuzuki, M., et al. (2000). Direct evidence for requirement of phosphatidylglycerol in photosystem II of photosynthesis. *Plant Physiol.* 124, 795–804. doi: 10.1104/pp.124.2.795

Hagio, M., Sakurai, I., Sato, S., Kato, T., Tabata, S., and Wada, H. (2002). Phosphatidylglycerol is essential for the development of thylakoid membranes in *Arabidopsis thaliana*. *Plant Cell Physiol.* 43, 1456–1464. doi: 10.1093/pcp/pcf185

Hasan, S. S., Stofleth, J. T., Yamashita, E., and Cramer, W. A. (2013). Lipid-induced conformational changes within the cytochrome b6f complex of oxygenic photosynthesis. *Biochemistry* 52, 2649–2654. doi: 10.1021/bi301638h

Hipkin, C. R., Al-Bassam, B. A., and Syrett, P. J. (1980). The roles of nitrate and ammonium in the regulation of the development of nitrate reductase in *Chlamydomonas reinhardii*. *Planta* 150, 13–18. doi: 10.1007/BF00385608

Iwai, M., Ikeda, K., Shimojima, M., and Ohta, H. (2014). Enhancement of extraplastidic oil synthesis in *Chlamydomonas reinhardtii* using a type-2 diacylglycerol acyltransferase with a phosphorus starvation-inducible promoter. *Plant Biotechnol. J.* 12, 808–819. doi: 10.1111/pbi.12210

Kelly, A. A., and Dormann, P. (2002). DGD2, an *Arabidopsis* gene encoding a UDP-galactose-dependent digalactosyldiacylglycerol synthase is expressed during growth under phosphate-limiting conditions. *J. Biol. Chem.* 277, 1166–1173. doi: 10.1074/jbc.M110066200

Kelly, A. A., Froehlich, J. E., and Dormann, P. (2003). Disruption of the two digalactosyldiacylglycerol synthase genes DGD1 and DGD2 in *Arabidopsis* reveals the existence of an additional enzyme of galactolipid synthesis. *Plant Cell* 15, 2694–2706. doi: 10.1105/tpc016675

Kobayashi, K., Fujii, S., Sato, M., Toyooka, K., and Wada, H. (2015). Specific role of phosphatidylglycerol and functional overlaps with other thylakoid

lipids in *Arabidopsis* chloroplast biogenesis. *Plant Cell Rep.* 34, 631–642. doi: 10.1007/s00299-014-1719-z

Kobayashi, K., Kondo, M., Fukuda, H., Nishimura, M., and Ohta, H. (2007). Galactolipid synthesis in chloroplast inner envelope is essential for proper thylakoid biogenesis, photosynthesis, and embryogenesis. *Proc. Natl. Acad. Sci. U.S.A.* 104, 17216–17221. doi: 10.1073/pnas.0704680104

Li, X., Moellering, E. R., Liu, B., Johnny, C., Fedewa, M., Sears, B. B., et al. (2012). A galactoglycerolipid lipase is required for triacylglycerol accumulation and survival following nitrogen deprivation in *Chlamydomonas reinhardtii*. *Plant Cell* 24, 4670–4686. doi: 10.1105/tpc.112.105106

Li-Beisson, Y., Beisson, F., and Riekhof, W. (2015). Metabolism of acyl-lipids in *Chlamydomonas reinhardtii*. *Plant J.* 82, 504–522. doi: 10.1111/tpj.12787

Mendiola-Morgenthaler, L., Eichenberger, W., and Boschetti, A. (1985). Isolation of chloroplast envelopes from *Chlamydomonas* - lipid and polypeptide composition. *Plant Sci.* 41, 97–104. doi: 10.1016/0168-9452(85)90109-8

Molnar, A., Bassett, A., Thuenemann, E., Schwach, F., Karkare, S., Ossowski, S., et al. (2009). Highly specific gene silencing by artificial microRNAs in the unicellular alga *Chlamydomonas reinhardtii*. *Plant J.* 58, 165–174. doi: 10.1111/j.1365-313X.2008.03767.x

Nakamura, Y. (2013). Phosphate starvation and membrane lipid remodeling in seed plants. *Prog. Lipid Res.* 52, 43–50. doi: 10.1016/j.plipres.2012.07.002

Nakamura, Y., Arimitsu, H., Yamaryo, Y., Awai, K., Masuda, T., Shimada, H., et al. (2003). Digalactosyldiacylglycerol is a major glycolipid in floral organs of *Petunia hybrida*. *Lipids* 38, 1107–1112. doi: 10.1007/s11745-006-1166-x

Omata, T., and Murata, N. (1983). Isolation and characterization of the cytoplasmic membranes from the Blue-Green Alga (*Cyanobacterium*) *Anacystis nidulans*. *Plant Cell Physiol.* 24, 1101–1112.

Ostrander, D. B., Zhang, M., Mileykovskaya, E., Rho, M., and Dowhan, W. (2001). Lack of mitochondrial anionic phospholipids causes an inhibition of translation of protein components of the electron transport chain. A yeast genetic model system for the study of anionic phospholipid function in mitochondria. *J. Biol. Chem.* 276, 25262–25272. doi: 10.1074/jbc.M103689200

Porra, R. J., Thompson, W. A., and Kriedemann, P. E. (1989). Determination of accurate extinction coefficients and simultaneous equations for assaying chlorophylls a and b extracted with four different solvents: verification of the concentration of chlorophyll standards by atomic absorption spectroscopy. *Biochim. Biophys. Acta* 975, 384–394. doi: 10.1016/S0005-2728(89)80347-0

Quisel, J. D., Wykoff, D. D., and Grossman, A. R. (1996). Biochemical characterization of the extracellular phosphatases produced by phosphorus-deprived *Chlamydomonas reinhardtii*. *Plant Physiol.* 111, 839–848. doi: 10.1104/pp.111.3.839

Rakhimberdieva, M. G., Vavilin, D. V., Vermaas, W. F., Elanskaya, I. V., and Karapetyan, N. V. (2007). Phycobilin/chlorophyll excitation equilibration upon carotenoid-induced non-photochemical fluorescence quenching in phycobilisomes of the cyanobacterium *Synechocystis* sp. PCC 6803. *Biochim. Biophys. Acta* 1767, 757–765. doi: 10.1016/j.bbabio.2006.12.007

Riekhof, W. R., Ruckle, M. E., Lydic, T. A., Sears, B. B., and Benning, C. (2003). The sulfolipids 2'-O-acyl-sulfoquinovosyldiacylglycerol and sulfoquinovosyldiacylglycerol are absent from a *Chlamydomonas reinhardtii* mutant deleted in SQD1. *Plant Physiol.* 133, 864–874. doi: 10.1104/pp.103.029249

Sakurai, I., Hagio, M., Gombos, Z., Tyystjarvi, T., Paakkarinen, V., Aro, E. M., et al. (2003). Requirement of phosphatidylglycerol for maintenance of photosynthetic machinery. *Plant Physiol.* 133, 1376–1384. doi: 10.1104/pp.103.026955

Sakurai, I., Mizusawa, N., Ohashi, S., Kobayashi, M., and Wada, H. (2007a). Effects of the lack of phosphatidylglycerol on the donor side of photosystem II. *Plant Physiol.* 144, 1336–1346. doi: 10.1104/pp.107.098731

Sakurai, I., Mizusawa, N., Wada, H., and Sato, N. (2007b). Digalactosyldiacylglycerol is required for stabilization of the oxygen-evolving complex in photosystem II. *Plant Physiol.* 145, 1361–1370. doi: 10.1104/pp.107.106781

Sakurai, I., Shen, J. R., Leng, J., Ohashi, S., Kobayashi, M., and Wada, H. (2006). Lipids in oxygen-evolving photosystem II complexes of cyanobacteria and higher plants. *J. Biochem.* 140, 201–209. doi: 10.1093/jb/mvj141

Sakurai, K., Moriyama, T., and Sato, N. (2014). Detailed identification of fatty acid isomers sheds light on the probable precursors of triacylglycerol accumulation in photoautotrophically grown *Chlamydomonas reinhardtii*. *Eukaryot. Cell* 13, 256–266. doi: 10.1128/EC.00280-13

Sato, N., Hagio, M., Wada, H., and Tsuzuki, M. (2000). Requirement of phosphatidylglycerol for photosynthetic function in thylakoid membranes. *Proc. Natl. Acad. Sci. U.S.A.* 97, 10655–10660. doi: 10.1073/pnas.97.19.10655

Sato, N., and Murata, N. (1982). Lipid biosynthesis in the blue-green alga, *Anabaena variabilis* I. *Lipid classes*. *Biochim. Biophys. Acta* 710, 271–278.

Sato, N., Tsuzuki, M., Matsuda, Y., Ehara, T., Osafune, T., and Kawaguchi, A. (1995). Isolation and characterization of mutants affected in lipid metabolism of *Chlamydomonas reinhardtii*. *Eur. J. Biochem.* 230, 987–993. doi: 10.1111/j.1432-1033.1995.0987g.x

Satoh, S., Ikeuchi, M., Mimuro, M., and Tanaka, A. (2001). Chlorophyll b expressed in Cyanobacteria functions as a light-harvesting antenna in photosystem I through flexibility of the proteins. *J. Biol. Chem.* 276, 4293–4297. doi: 10.1074/jbc.M008238200

Schloss, J. A. (1990). A *Chlamydomonas* gene encodes a G protein beta subunit-like polypeptide. *Mol. Gen. Genet.* 221, 443–452. doi: 10.1007/BF00259410

Shimojima, M., Ohta, H., Iwamatsu, A., Masuda, T., Shioi, Y., and Takamiya, K. (1997). Cloning of the gene for monogalactosyldiacylglycerol synthase and its evolutionary origin. *Proc. Natl. Acad. Sci. U.S.A.* 94, 333–337. doi: 10.1073/pnas.94.1.333

Siaut, M., Cuine, S., Cagnon, C., Fessler, B., Nguyen, M., Carrier, P., et al. (2011). Oil accumulation in the model green alga *Chlamydomonas reinhardtii*: characterization, variability between common laboratory strains and relationship with starch reserves. *BMC Biotechnol.* 11:7. doi: 10.1186/1472-6750-11-7

Tanoue, R., Kobayashi, M., Katayama, K., Nagata, N., and Wada, H. (2014). Phosphatidylglycerol biosynthesis is required for the development of embryos and normal membrane structures of chloroplasts and mitochondria in *Arabidopsis*. *FEBS Lett.* 588, 1680–1685. doi: 10.1016/j.febslet.2014.03.010

Tardif, M., Atteia, A., Specht, M., Cogne, G., Rolland, N., Brugiere, S., et al. (2012). PredAlgo: a new subcellular localization prediction tool dedicated to green algae. *Mol. Biol. Evol.* 29, 3625–3639. doi: 10.1093/molbev/mss178

Umena, Y., Kawakami, K., Shen, J. R., and Kamiya, N. (2011). Crystal structure of oxygen-evolving photosystem II at a resolution of 1.9 A. *Nature* 473, 55–60. doi: 10.1038/nature09913

Vass, I., Kirilovsky, D., and Etienne, A. L. (1999). UV-B radiation-induced donor- and acceptor-side modifications of photosystem II in the cyanobacterium *Synechocystis* sp. PCC 6803. *Biochemistry* 38, 12786–12794.

Wang, Z. T., Ullrich, N., Joo, S., Waffenschmidt, S., and Goodenough, U. (2009). Algal lipid bodies: stress induction, purification, and biochemical characterization in wild-type and starchless *Chlamydomonas reinhardtii*. *Eukaryot. Cell* 8, 1856–1868. doi: 10.1128/EC.00272-09

Wu, F., Yang, Z., and Kuang, T. (2006). Impaired photosynthesis in phosphatidylglycerol-deficient mutant of cyanobacterium *Anabaena* sp. *PCC*7120 with a disrupted gene encoding a putative phosphatidylglycerophosphatase. *Plant Physiol.* 141, 1274–1283. doi: 10.1104/pp.106.083451

Wykoff, D. D., Davies, J. P., Melis, A., and Grossman, A. R. (1998). The regulation of photosynthetic electron transport during nutrient deprivation in *Chlamydomonas reinhardtii*. *Plant Physiol.* 117, 129–139. doi: 10.1104/pp.117.1.129

Wykoff, D. D., Grossman, A. R., Weeks, D. P., Usuda, H., and Shimogawara, K. (1999). Psr1, a nuclear localized protein that regulates phosphorus metabolism in *Chlamydomonas*. *Proc. Natl. Acad. Sci. U.S.A.* 96, 15336–15341. doi: 10.1073/pnas.96.26.15336

Xu, C., Hartel, H., Wada, H., Hagio, M., Yu, B., Eakin, C., et al. (2002). The pgp1 mutant locus of *Arabidopsis* encodes a phosphatidylglycerolphosphate synthase with impaired activity. *Plant Physiol.* 129, 594–604. doi: 10.1104/pp.002725

Yu, B., and Benning, C. (2003). Anionic lipids are required for chloroplast structure and function in *Arabidopsis*. *Plant J.* 36, 762–770. doi: 10.1046/j.1365-313X.2003.01918.x

Yuzawa, Y., Shimojima, M., Sato, R., Mizusawa, N., Ikeda, K., Suzuki, M., et al. (2014). Cyanobacterial monogalactosyldiacylglycerol-synthesis pathway

is involved in normal unsaturation of galactolipids and low-temperature adaptation of *Synechocystis* sp. PCC 6803. *Biochim. Biophys. Acta* 1841, 475–483. doi: 10.1016/j.bbalip.2013.12.007

Conflict of Interest Statement: The authors declare that the research was conducted in the absence of any commercial or financial relationships that could be construed as a potential conflict of interest.

frontiers in Microbiology

ORIGINAL RESEARCH
published: 18 May 2015
doi: 10.3389/fmicb.2015.00487

Identification of a transporter Slr0982 involved in ethanol tolerance in cyanobacterium *Synechocystis* sp. PCC 6803

Yanan Zhang[1,2,3], *Xiangfeng Niu*[1,2,3], *Mengliang Shi*[1,2,3], *Guangsheng Pei*[1,2,3], *Xiaoqing Zhang*[1,2,3], *Lei Chen*[1,2,3]* and *Weiwen Zhang*[1,2,3]*

[1] Laboratory of Synthetic Microbiology, School of Chemical Engineering and Technology, Tianjin University, Tianjin, China, [2] Key Laboratory of Systems Bioengineering (Ministry of Education), Tianjin University, Tianjin, China, [3] SynBio Research Platform, Collaborative Innovation Center of Chemical Science and Engineering (Tianjin), Tianjin, China

OPEN ACCESS

Edited by:
Takashi Osanai, Meiji University, Japan

Reviewed by:
Franz Narberhaus, Ruhr University Bochum, Germany
Ethan I. Lan, National Chiao Tung University, Taiwan
Xuefeng Lu, Chinese Academy of Sciences, China

***Correspondence:**
Lei Chen and Weiwen Zhang, Laboratory of Synthetic Microbiology, School of Chemical Engineering and Technology, Tianjin University, 92 Weijin Road, Nankai District, Tianjin 300072, China
lchen@tju.edu.cn; wwzhang8@tju.edu.cn

Specialty section:
This article was submitted to Microbiotechnology, Ecotoxicology and Bioremediation, a section of the journal Frontiers in Microbiology

Received: *12 March 2015*
Accepted: *04 May 2015*
Published: *18 May 2015*

Citation:
Zhang Y, Niu X, Shi M, Pei G, Zhang X, Chen L and Zhang W (2015) Identification of a transporter Slr0982 involved in ethanol tolerance in cyanobacterium Synechocystis sp. PCC 6803. Front. Microbiol. 6:487. doi: 10.3389/fmicb.2015.00487

Cyanobacteria have been engineered to produce ethanol through recent synthetic biology efforts. However, one major challenge to the cyanobacterial systems for high-efficiency ethanol production is their low tolerance to the ethanol toxicity. With a major goal to identify novel transporters involved in ethanol tolerance, we constructed gene knockout mutants for 58 transporter-encoding genes of *Synechocystis* sp. PCC 6803 and screened their tolerance change under ethanol stress. The efforts allowed discovery of a mutant of *slr0982* gene encoding an ATP-binding cassette transporter which grew poorly in BG11 medium supplemented with 1.5% (*v/v*) ethanol when compared with the wild type, and the growth loss could be recovered by complementing *slr0982* in the Δ*slr0982* mutant, suggesting that *slr0982* is involved in ethanol tolerance in *Synechocystis*. To decipher the tolerance mechanism involved, a comparative metabolomic and network-based analysis of the wild type and the ethanol-sensitive Δ*slr0982* mutant was performed. The analysis allowed the identification of four metabolic modules related to *slr0982* deletion in the Δ*slr0982* mutant, among which metabolites like sucrose and *L*-pyroglutamic acid which might be involved in ethanol tolerance, were found important for *slr0982* deletion in the Δ*slr0982* mutant. This study reports on the first transporter related to ethanol tolerance in *Synechocystis*, which could be a useful target for further tolerance engineering. In addition, metabolomic and network analysis provides important findings for better understanding of the tolerance mechanism to ethanol stress in *Synechocystis*.

Keywords: ethanol, tolerance, transporter, metabolomics, *Synechocystis*

Introduction

Bioethanol production through microbiological processes has drawn greater attention in recent years due to increasing cost of non-renewable fossil fuels and environmental concerns related to over-utilization of fossil fuels (Hahn-Hagerdal et al., 2006). Various native or engineered microorganisms, such as *Saccharomyces cerevisiae* (Eiadpum et al., 2012; Yu et al., 2012), *Zymomonas mobiles* (Hayashi et al., 2012; Letti et al., 2012) and even *Escherichia coli*

(Zhou et al., 2008; Manow et al., 2012) have been employed for ethanol production. As an alternative, photosynthetic cyanobacteria have been recently engineered by various synthetic biology tools into an "autotrophic microbial cell factory" to produce biofuels and fine chemicals directly from CO_2 using solar energy (Angermayr et al., 2009; Ducat et al., 2011; Ruffing, 2011; Machado and Atsumi, 2012; Oliver and Atsumi, 2014), which provides a complementary approach to the above heterotrophic microorganisms. In a recent study, by systematic evaluation and selection of alcohol dehydrogenase (*adh*) genes from different cyanobacterial sources and optimization of culturing conditions, Gao et al. (2012) engineered a synthetic *Synechocystis* strain able to produce ethanol levels of 212 mg/L per day and 5.50 g/L in 26 days (Gao et al., 2012). Although significant progress has been made, current ethanol productivity in cyanobacterial systems is still largely lagging behind the yeast systems (Antoni et al., 2007). Recent studies have suggested that one of the crucial factors responsible for the low ethanol productivity of cyanobacterium cells could be their very low tolerance toward ethanol (Dunlop, 2011; Jin et al., 2014). For example, in the model cyanobacterium *Synechocystis* sp. PCC 6803 (hereafter *Synechocystis*), the cell growth was arrested by up to 50%, and started to aggregate under 1.5% (*v/v*) ethanol (Qiao et al., 2012). In another study, Kamarainen et al. (2012) also evaluated tolerance of the cyanobacterial hosts to various biofuels, and found that the *Synechocystis* growth was less than 50% of the control in BG11 medium supplemented with 2.0 g/L ethanol (Kamarainen et al., 2012). The studies suggested that it is necessary to adopt engineering strategies to ethanol tolerance in cyanobacterial systems.

Many organic solvents are toxic to microorganisms. The toxicity of organic solvents depends on its log *Pow* (the partition coefficient between n-octanol and water) and final concentration of accumulation in the cell which contribute to increase permeability of the membrane. Readily water-miscible organic solvents such as ethanol, toxicity correlates directly with hydrophobicity (Ingram, 1981). In addition, ethanol has been shown to affect the proton motive force (Cartwright et al., 1987), and to increase leakage of metabolites from cells.

A membrane transport protein (or simply transporter) is a membrane protein involved in the movement of ions, small molecules, or macromolecules, such as another protein, across a biological membrane. Protein transporters for small molecules have been suggested as an important mechanism against ethanol toxicity (Ding et al., 2009; Stanley et al., 2010; Foo et al., 2014). For example, studies showed that the FPS1 gene, encoding the plasma membrane aquaglyceroporin that can facilitate transmembrane transport of small-uncharged molecules like polyols and urea, was up-regulated in response to ethanol exposure in yeast (Aguilera et al., 2006; Teixeira et al., 2009). Similarly, a recent functional genomics study with *E. coli* under exogenous *n*-butanol stress also found that transporters were among the most regulated functional components (Rutherford et al., 2010). Another recent study, involving heterologous expressing of 43 transporters in *E. coli*, showed that selected transporter could improve cell survival under stress of biofuels such as geraniol and limonene; however, none of the transporters improved tolerance for *n*-butanol and isopentanol (Dunlop et al., 2011). Nevertheless, these early studies suggested that utilization of transporters could be one of the approaches for engineering tolerance and biofuels production strains (Ding et al., 2009; Stanley et al., 2010; Dunlop et al., 2011).

Transporters have been reported for roles against many types of environmental stresses in cyanobacteria, such as arsenate resistance in *Anabaena variabilis* (Thiel, 1988), Cu^{2+} resistance in *Nostoc calcicola* (Verma and Singh, 1991), salinity stress in *Synechococcus* sp. PCC 7942 and *Synechocystis* sp. PCC 6803 (Nomura et al., 1995; Mikkat et al., 1996), acid stress in *Synechocystis* sp. PCC 6803 (Tahara et al., 2012), and heavy metals in filamentous *Oscillatoria brevis* (Tong et al., 2002). Among all transporters in *Synechocystis*, ATP binding cassette (ABC) transporters residing in the inner membrane that are involved in the transport of a wide variety of substrates at the expense of ATP hydrolysis are the most common and well-characterized type (Davidson et al., 2008). For example, the *slr1295*, *slr0513*, *slr0327,* and *sll1878* genes encoding polypeptides of an ABC-type ferric iron transporter that played a major role in iron acquisition have been identified (Katoh et al., 2001). However, so far no transporter involved in ethanol resistance has ever been reported in any cyanobacterial species.

In this study, to discover transporters related to ethanol tolerance, we constructed a mutant library of transporter genes in *Synechocystis*, and then screened them for tolerance changes under ethanol stress. The efforts led to the discovery of the *slr0982* gene that may be involved in tolerance against ethanol stress in *Synechocystis*. In addition, to further explore the ethanol tolerance mechanism mediated by transporter Slr0982, we applied a metabolomics approach to comparatively analyze the differential cellular responses between the *Synechocystis* wild type strain and the Δ*slr0982* mutant (Wang et al., 2013). The study provides important findings for better understanding of the tolerance mechanism to ethanol stress in *Synechocystis*.

Abbreviations: AcCOA, Acetyl coenzyme A; ADP, Adenosine 5′-diphosphate; ADP-GCS, Adenosine-5′-diphosphoglucose; AKG, α-Ketoglutaric acid; AMP, Adenosine 5′-monophosphate; AMDIS, Automated Mass Spectral Deconvolution and Identification System; ATP, Adenosine 5′-triphosphate; COA, Coenzyme A hydrate; DHAP, Dihydroxyacetone phosphate; FBP, *D*-Fructose 1,6-bisphosphate; F6P, *D*-Fructose 6-phosphate; FUM, Sodium fumarate dibasic; GAP, *DL*-Glyceraldehyde 3-phosphate; GC-MS, Gas Chromatography-Mass Spectrometry; GLU, *L*-Glutamic acid; G6P, *D*-Glucose 6-phosphate; LC-MS, Liquid Chromatography–Mass Spectrometry; MSTFA, N-methyl-N-(trimethylsilyl) trifluoroacetamide; NAD, α-Nicotinamide adenine dinucleotide; NIST, National Institute of Standards and Technology; OXA, Oxaloacetic acid; PCA, Principal Component Analysis; PCR, Polymerase Chain Reaction; PEP, Phospho(enol)pyruvic acid; 3PG, *D*-(-)-3-Phosphoglyceric acid; RiBP, *D*-Ribulose 1,5-bisphosphate; R5P, *D*-Ribose 5-phosphate; RT-qPCR, Real-time Quantitative Polymerase Chain Reaction; UDP-GCS, Uridine 5′-diphosphoglucose; WGCNA, Weighted Correlation Network Analysis.

Materials and Methods

Bacterial Growth Conditions and Ethanol Treatment

Synechocystis sp. PCC 6803 and the knockout mutants constructed in this study were grown in BG11 medium

(pH 7.5) under a light intensity of approximately 50 μmol photons m^{-2} s^{-1} in an illuminating incubator of 130 rpm at 30°C (HNY-211B Illuminating Shaker, Honour, China) (Qiao et al., 2012). Cell density was measured on a UV-1750 spectrophotometer (Shimadzu, Japan) at OD_{730} or on an ELx808 Absorbance Microplate Reader (BioTek, Winooski, VT, USA) at OD_{630}. For growth and ethanol treatment, 40 μL fresh cells at OD_{630} of 0.2 collected by centrifugation and were then inoculated into 200 μL of BG11 liquid medium in 96-well cultivation plates. Ethanol at a final concentration was added at the beginning of cultivation. The 96-well cultivation plates were fixed in the shaker and measured directly on ELx808 Absorbance Microplate Reader at OD_{630} every 12 h. To ensure accuracy of finding, the mutants with differential growth patterns under ethanol stress were then confirmed by growth in 250-mL flasks, in which 10 mL fresh cells collected by centrifugation and were inoculated into 50 mL of BG11 liquid medium in a 250 mL flask. Culture samples (1 mL) were taken and measured at both OD_{730} and OD_{630} every 12 h. Growth experiments were repeated at least three times to confirm the growth patterns.

Construction and Analysis of Knockout Mutants

A fusion PCR based method was employed for the construction of gene knockout fragments (Wang et al., 2002). Briefly, for the gene target selected, three sets of primers were designed to amplify a linear DNA fragment containing the chloramphenicol resistance cassette (amplified from a plasmid pACYC184) with two flanking arms of DNA upstream and downstream of the target gene. The PCR strategy of mutant construction was shown in **Supplementary Figure S1**. The linear fused PCR amplicon was used directly for transformation into *Synechocystis* by natural transformation. The chloramphenicol-resistant transformants were obtained and passed several times on fresh BG11 plates supplemented with 10 μg/mL chloramphenicol to achieve complete chromosome segregation. The successful knockout mutants were confirmed by colony PCR and sequencing analysis. PCR primers for mutant construction and validation were listed in Supplementary Table S1. Comparative growth analysis of the wild-type *Synechocystis* and the mutants were performed in 250 mL flasks each with 50 mL BG11 medium of normal or ethanol.

Flow Cytometric Analysis

To reveal cell morphology differences, flow cytometric analysis was performed on a Calibur fluorescence-activated cell sorting (FACS) cytometer (Becton Dickinson) with the following settings: forward scatter (FCS), E00 log; side scatter, 400 V. Control and ethanol-treated cells were harvested at 24, 48, and 72 h, respectively, washed twice with phosphate buffer (pH 7.2) (Sigma-Aldrich), and then resuspended in the same phosphate buffer to a final OD_{580} of 0.3 (approximately 1.5×10^7 cells mL^{-1}). A total of 5×10^4 cells were used for each analysis according to the method by Marbouty et al. (2009). Data analysis was conducted using the CellQuest software, version 3.1 (Becton Dickinson).

Complementation of *slr0982* in the Δ*slr0982* Mutant

Gene expressing vector pXT37b was kindly provided by Dr. Xuefeng Lu of Qingdao Institute of Bioenergy and Bioprocess Technology of Chinese Academy of Sciences (Tan et al., 2011). The promoter of plastocyanin (P_{petE}) was first replaced by that of phycocyanin beta chain (P_{cpcB}) in this study. The ORF of *slr0982* was subcloned into *Nde*I/*Xho*I site of the modified pXT37b, resulting in pXT-*slr0982*. The primers sequences for *slr0982* cloning were 5′-CGCCATATGATGTCTGATACAGT CATTCGAGTGG-3′ and 5′-CCGCTCGAGTCATGCAATTTT CTCCACATTCCAG-3′. The pXT-*slr0982* was introduced back into the Δ*slr0982* mutant by natural transformation. The *slr0982*-complementation strain was named Δ*slr0982*/pXT-*slr0982*. To achieve complete chromosome segregation, Δ*slr0982*/pXT-*slr0982* was passed several times on fresh BG11 plates supplemented with 10 μg/mL spectinomycin. Homologous integration of the expressing cassette and complete segregation were confirmed by PCR analysis.

LC-MS Based Metabolomics Analysis

(i) Sample quenching, extraction, and preparation: All chemicals used for LC-MS metabolomic analyses were obtained from Sigma-Aldrich (Taufkirchen, Germany). Cells were collected by centrifugation at 8000 × *g* for 8 min at room temperature (Eppendorf 5430R, Hamburg, Germany). The cell samples were quenched and extracted rapidly with 900 μL of 80:20 methanol/H_2O (−80°C) and then frozen in liquid nitrogen. The samples were then frozen-thawed three times to release metabolites from the cells. The supernatant was collected after centrifugation at 15,000 × *g* for 5 min at −4°C and then stored at −80°C. The remaining cell pellets were re-suspended in 500 μL of 80:20 methanol/H_2O (−80°C) and the above extraction process was repeated. The supernatant from the second extraction was pooled with that from the first extraction and stored at −80°C until LC-MS analysis (Bennette et al., 2011); *(ii) LC-MS analysis*: The chromatographic separation was achieved with a SYnergi Hydro-RP (C18) 150 mm × 2.0 mm I.D., 4 μm 80 Å particles column (Phenomenex, Torrance, CA, USA) at 40°C. Mobile phase A (MPA) is an aqueous 10 mM tributylamine solution with pH 4.95 adjusted with acetic acid and Mobile phase B (MPB) is 100% methanol of HPLC grade (Darmstadt, Germany). The optimized gradient profile was determined as follows: 0 min (0% B), 8 min (35% B), 18 min (35% B), 24 min (90% B), 28 min (90% B), 30 min (50% B), 31 min (0% B). A 14-min post-time equilibration was employed, bringing total run-time to 45 min. Flow rate was set as a constant 0.2 mL/min (Park et al., 2011). LC-MS analysis was conducted on an Agilent 1260 series binary HPLC system (Agilent Technologies, Waldbronn, Germany) coupled to an Agilent 6410 triple quadrupole mass analyser equipped with an electrospray ionization (ESI) source. Injected sample volume for all cases was 10 μL; capillary voltage was 4000 V; and nebulizer gas flow rate and pressure were 10 L/min and 50 psi, respectively. Nitrogen nebulizer gas temperature was 300°C. The MS was operated in negative mode for multiple reaction monitoring (MRM) development, method optimization, and

sample analysis. Data were acquired using Agilent Mass Hunter workstation LC/QQQ acquisition software (version B.04.01) and chromatographic peaks were subsequently integrated *via* Agilent Qualitative Analysis software (version B.04.00); (*iii*) *Targeted metabolite analysis*: a total of 24 metabolites were selected for LC-MS based targeted metabolite analysis in this study as described previously (Su et al., 2014). The standard compounds for these 24 metabolites were purchased from Sigma, and their MS and MS/MS experimental parameters were optimized with the mix standard solution. All metabolomics profile data was first normalized by the internal control and the cell numbers of the samples, standardized by average, log2 transformed and then subjected to Principal Component Analysis (PCA) using software SIMCA-P 11.5 (Laiakis et al., 2010). Heatmap were created using MultiExperiment Viewer software available publically at http://www.tm4.org/.

GC-MS based Metabolomics Analysis

All chemicals used for metabolome isolation and GC/MS analyses were obtained from Sigma-Aldrich (Taufkirchen, Germany). For metabolomic analysis, cells of the wild type and the Δ*slr0982* mutant were collected from control and ethanol-stressed cultures at 24, 48, and 72 h, respectively. For each sample, cells equivalent to $\sim 10^8$ cells, were collected by centrifugation at 8000 × *g* for 10 min at 4°C (Eppendorf, Hamburg, Germany). The cell pellets were immediately frozen in liquid nitrogen and then stored at −80°C before use. The metabolomic analysis protocol included: (*i*) *Metabolome extraction*: cells were re-suspended in 1.0 mL cold 10:3:1 (*v/v/v*) methanol: chloroform: H_2O solution (MCW), and frozen in liquid nitrogen and thawed for five times. Supernatants were collected by centrifugation at 14000 × *g* for 3 min at 4°C. To normalize variation across samples, an internal standard (IS) solution (100 μg/mL U-13C-sorbitol, 10 μL) was added to 100 μL supernatant in a 1.5-mL microtube before it was dried by vacuum centrifugation for 2–3 h (4°C). (*ii*) *Sample derivatization*: derivatization was conducted according to the two-stage technique described by Roessner et al. (2001). The samples were dissolved in 10 μL methoxyamine hydrochloride (40 mg/mL in pyridine) and shaken at 30°C for 90 min, then were added with 90 μL N-methyl-N-(trimethylsilyl) trifluoroacetamide (MSTFA) and incubated at 37°C for 30 min to trimethylsilylate the polar functional groups. The derivate samples were collected by centrifugation at 14000 × *g* for 3 min before GC/MS analysis. (*iii) GC-MS analysis*: analysis was performed on a Agilent 7890A Gas Chromatograph (GC) coupled to a Agilent MSD 5975 system (Agilent Technologies, Inc., Santa Clara, CA, USA) equipped with a HP-5MS capillary column (30 m × 250 mm id). 2 μL derivatized sample was injected in splitless mode at 230°C injector temperature. The GC was operated at constant flow of 1.0 mL/min helium. The temperature program started isocratic at 45°C for 2 min, followed by temperature ramping of 5°C/min to a final temperature of 280°C, and then held constant for additional 2 min. The range of mass scan was m/z 38–650. *iv*) *Data processing and statistical analysis*: The mass fragmentation spectrum was analyzed using the Automated Mass Spectral Deconvolution and Identification System (AMDIS) (Stein, 1999) to identify the compounds by matching the data with Fiehn Library (Fiehn, 2002) and the mass spectral library of the National Institute of Standards and Technology (NIST). Peak areas of all identified metabolites were normalized against the internal standard and the acquired relative abundances for each identified metabolite were used for future data analysis. All metabolomics profile data was first normalized by the internal control and the cell numbers of the samples, log2 transformed, and then subjected to PCA using software SIMCA-P 11.5 (Laiakis et al., 2010).

Quantitative Real-time RT-PCR Analysis

The identical cultures used for metabolomics analysis were also used for RNA isolation and quantitative real-time RT-PCR (RT-qPCR) analysis of gene expression. RT-qPCR analysis was performed as described previously (Kloft et al., 2005; Wang et al., 2012). Quantification of gene expression was determined according to standard process of RT-qPCR that used serial dilutions of known concentration of chromosome DNA as template to make a standard curve. The 16s rRNA was used as an internal control. Three technical replicates were performed for each gene. Data analysis was carried out using the StepOnePlus analytical software (Applied Biosystems, Foster City, CA). Briefly, the amount of relative gene transcript was normalized by that of 16s rRNA in each sample (mutant or wild type), and the data presented were ratios of the amount of normalized transcript in the treatment between the mutant and the wild type. The gene ID and their related primer sequences used for real-time RT-qPCR analysis were also listed in Supplementary Table S1.

WGCNA Correlation Network Construction

Correlation network was created from the metabolomic data set, first by calculating weighted *Pearson* correlation matrices corresponding to metabolite abundance, and then by following the standard procedure of WGCNA to create the networks (Zhang and Horvath, 2005; Langfelder and Horvath, 2008; Wang et al., 2013). Briefly, weighted correlation matrices were transformed into matrices of connection strengths using a power function. These connection strengths were then used to calculate topological overlap (TO), a robust and biologically meaningful measurement that encapsulates the similarity of two metabolites' correlation relationships with all other metabolites in the network. Hierarchical clustering based on TO was used to group metabolites with highly similar correlation relationships into modules. Metabolite dendrograms were obtained by average linkage hierarchical clustering, while the color row underneath the dendgram showed the module assignment determined by the Dynamic Tree Cut of WGCNA. The network for each module was generated with the minimum spanning tree with dissimilarity matrix from WGCNA. The modules with correlation $r > 0.5$ or $r < -0.5$, and p-value less than 0.05 were extracted for further investigation. Hub metabolites were screened by high connectivity with other metabolites (≥ 5) in the modules strongly associated with genotypes based on correlation coefficient $r > 0.5$ or $r < -0.5$.

Pathway Enrichment Analysis

Metabolic pathway enrichment analysis of the responsive metabolites was conducted using the information from the KEGG (Kyoto Encyclopedia of Genes and Genomes) database according to the following formula (Su et al., 2014):

$$P = 1 - \sum_{i=0}^{m-1} \frac{\binom{M}{i}\binom{N-M}{n-i}}{\binom{N}{n}}$$

N is the number of all metabolites within all KEGG pathways, M is the number of metabolites within a given KEGG pathway, n is the number of the responsive metabolites within all KEGG pathways, m is the number of the responsive metabolites within a given KEGG pathway. A p-value less than 0.05 was used as a cutoff for enriched KEGG pathways.

Results and Discussion

Screening for Ethanol Sensitivity in Transporter Mutant Library

A survey showed that at least 387 putative transporter-encoding genes were present in the *Synechocystis* genome (Kaneko et al., 1996). In this study, to uncover transporter genes involved in ethanol tolerance in *Synechocystis*, we excluded all transporter genes with well-characterized functions, such as bicarbonate or phosphate transporting. To this end, a total of 58 knockout mutants of transporter genes were constructed and the gene deletion was confirmed by PCR (Supplementary Table S1). To achieve complete segregation, positive colonies were passaged through several cultivations on solid BG11 plates supplied with gradually increased chloramphenicol, and the full integration into all chromosomes was also confirmed by PCR (**Supplementary Figures S1A–M**). After 12 passages under selective pressure, full segregation was achieved for 54 transporter genes except for the Δ*slr0949*, Δ*slr1224*, Δ*slr1248*, and Δ*sll1453* genes, suggesting that these transporter genes may carry essential roles for the cellular growth under the testing conditions. The mutants, in parallel with the wild-type *Synechocystis*, were then monitored for growth under various ethanol concentrations (i.e., 1.5, 1.8, and 2.0%, *v/v*) in 96-well cultivation plates. To ensure accuracy of the growth measurement, differential growth patterns under ethanol stress were also confirmed by growth in 250-mL flasks. The screening allowed the identification of Δ*slr0982* mutant, which was more sensitive to ethanol stress than the wild type. No significant tolerance change was found for other mutants under the tested condition. The full integration of Δ*slr0982* was shown in **Supplementary Figure S1**. As shown in **Figure 1**, in the normal BG11 medium, the Δ*slr0982* mutant grew equally well as the wild-type control, suggesting the knockout of *slr0982* gene didn't affect cell growth under normal growth condition. However, in the BG11 medium supplemented with ethanol, although growth of both the wild-type strain and the Δ*slr0982* mutant was reduced, growth of the Δ*slr0982* mutant was reduced more significantly when compared with its growth in the normal BG11 medium (**Figures 1A–C**). In addition, the results showed that the ethanol sensitivity of the Δ*slr0982* mutant seemed concentration-dependent, as more growth reduction was observed in the medium supplemented with 1.8% than with 1.5% ethanol (**Figures 1A,B**). Taken together, the results showed that

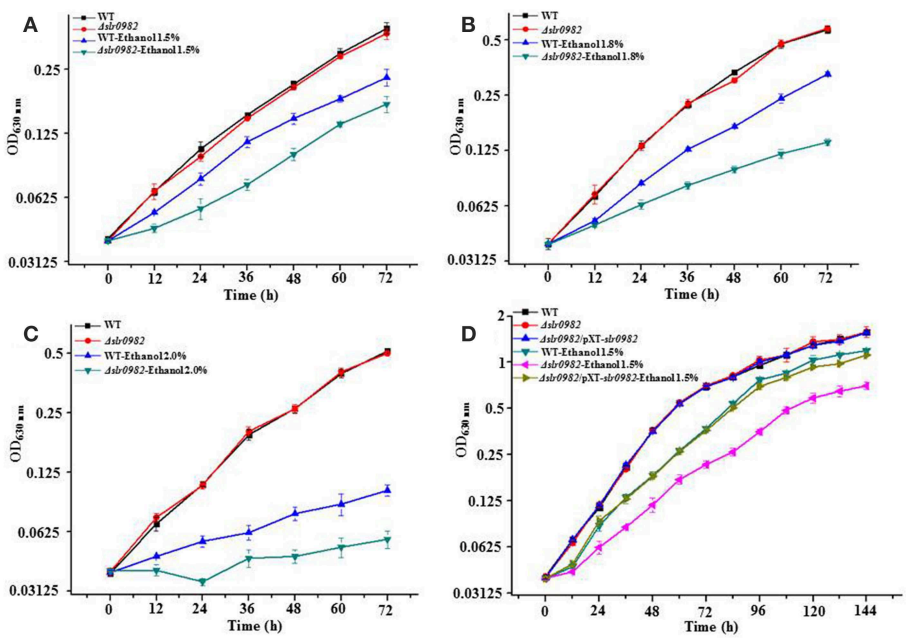

FIGURE 1 | Growth time curves of the wild type, the Δ*slr0982* mutant and Δ*slr0982*/pXT-*slr0982* in BG11 media with or without ethanol. (A) and **(D)**, 1.5% (*v/v*); **(B)** 1.8% (*v/v*); **(C)** 2.0% (*v/v*).

the Δ*slr0982* mutant was more sensitive to ethanol stress than the wild-type cells, and the *slr0982* gene may be involved in ethanol tolerance in *Synechocystis*.

To further confirm the involvement of gene *slr0982* in ethanol tolerance, we constructed a *slr0982*-complementation strain in the Δ*slr0982* mutant, and the effect of the complementation was confirmed by comparatively measuring growth time-curve of relative strains. The results showed that in the normal BG11 medium, three strains grew almost equally; while in the BG11 medium with ethanol, the growth of Δ*slr0982*/pXT-*slr0982* was almost fully recovered to that of wild type, and significantly better than the Δ*slr0982* mutant under the same ethanol stress, demonstrating that *slr0982* was involved in ethanol tolerance in *Synechocystis* (**Figure 1**).

The *slr0982* gene, also designated as *rfbB* gene, was annotated as O-antigen (OAg) transport gene in the Cyanobase genome database (Nakao et al., 2010). In a recent study, Fisher et al. (2013) studied the possible function of *slr0982* in *Synechocystis*, and the results showed no difference between OAg purified from the wild-type and the deletion mutant *slr0982*, although the bioinformatics inspection suggested the gene product *slr0982* appeared to function in OAg transport; furthermore, the results showed that exopolysaccharides (EPS) purified from the Δ*slr0982* mutant was altered in composition when compared to the wild type, suggesting that the *slr0982* gene may be involved in surface modification. In addition, analysis of the *slr0982* mutant showed that it was deficient in EPS export compared to wild-type, suggesting the Slr0982 transporter may be involved in exporting of EPS (Fisher et al., 2013). The results were consistent with early studies in yeast and *Z. mobilis* that the composition of cell membrane and cell wall can significantly influence ethanol tolerance (Hermans et al., 1991; Ding et al., 2009). Interestingly, *slr0982* seemed located within a putative operon, in which three hypothetical gene, *slr0978*, *slr0980,* and *slr0981* without any known function were located upstream, where several genes involved in polysaccharide metabolism, *slr0983* (glucose-1-phosphate cytidylyltransferase), *slr0984* (CDP-glucose 4,6-dehydratase), and *slr0985* (dTDP-4-dehydrorhamnose 3,5-epimerase) were located downstream of *slr0982*, respectively (Fisher et al., 2013). The results were also consistent with our previous RNA-seq transcriptomics analysis which showed that expression of *slr0983* was differentially regulated by ethanol exposure (Wang et al., 2012), further suggesting that the *slr0982* gene and the *slr0978-slr0985* gene cluster might be involved in ethanol tolerance.

Analysing Cell Morphology of the Wild-Type and the Δ*slr0982* Strain

Cell morphology of the wild-type *Synechocystis* and the Δ*slr0982* mutant under both control and ethanol-spiked conditions was also compared using microscopic inspection and flow cytometric analyses. Although no difference was observed with microscope, the flow cytometric analyses showed that the cell size of the Δ*slr0982* mutant was slightly increased under ethanol stress when compared with wild type. The size increase became more obvious after longer stress treatment at 48 and 72 h when compared with 24 h after ethanol stress (**Figure 2**). Many types of microbial cells are surrounded by thick exopolysaccharide chains, which are part of the network maintaining cell size, as it has been reported that altered EPS production occurred (i.e., less large EPS band while more small EPS band in the Δ*slr0982* mutant) (Fisher et al., 2013), so it is probably not surprising that the change of exopolysaccharides synthesis will affect cell size and cellular response to stress. For example, a glycogen excess *E. coli* mutant TR1-5 was found to exhibit effects on cell size and surface (adherence) properties (Romeo et al., 1993).

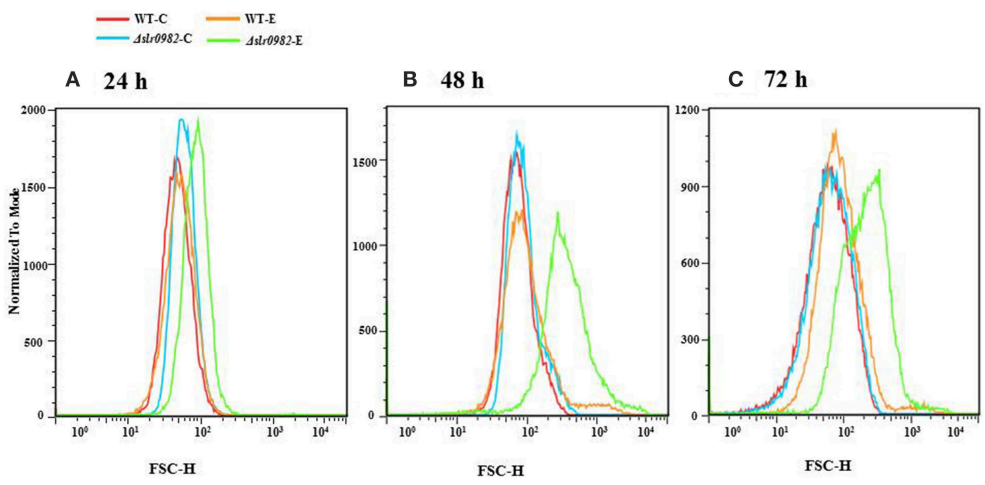

FIGURE 2 | Flow cytometric analysis of the wild type and the Δ*slr0982* mutant grown in the BG11 media with or without 1.5% (*v/v*) ethanol stress. (A) 24 h; **(B)** 48 h; **(C)** 72 h. A total of 5×10^4 cells were used for each analysis. Foward scatter (FSC) is related to cell surface area, which is directly related to cell size. And Y-axis was normalized pixel count. WT-C and WT-E: wild type grown with or without 1.5% (*v/v*) ethanol stress. Δ*slr0982*-C and Δ*slr0982*-E: the Δ*slr0982* mutant grown with or without 1.5% (*v/v*) ethanol stress.

Targeted LC-MS Metabolomic Analysis of the Wild-Type and the Δ*slr0982* Strain

LC–MS based metabolomics analysis has been recently applied to studies of cyanobacterial metabolism (Bennette et al., 2011; Schwarz et al., 2013), due to its advantages toward chemically unstable metabolites, such as the redox active nucleotides (NADPH, NADH) and the hydrolytically unstable nucleotides (ATP, GTP, cAMP, PEP) that are crucial for all major metabolic pathways. Using an optimized protocol of sampling, chromatography and mass spectral detection (Wang et al., 2014b), the LC-MS metabolomic analysis allowed successful monitoring of the intracellular levels of 24 metabolites in *Synechocystis*, including intermediates in central carbon metabolism, cellular energy charge and redox poise (Bennette et al., 2011). We eventually established reproducible analyses for 24 key metabolites in the central metabolism in *Synechocystis*, including AcCOA, ADP, ADP-GCS, AKG AMP, ATP, COA, DHAP, FBP, F6P, FUM, GAP, G6P, GLU, NAD, NADH, NADP, NADPH, UDP-GCS, OXA, PEP, 3PG, R5P, and RiBP involved in the key metabolic pathways. Using them as references, a semi-quantitative characterization of all 24 metabolites from all *Synechocystis* cell samples is achieved. With the optimized LC-MS protocol, we collected the cells of the wild type and the Δ*slr0982* mutant grown in BG11 media (control) and ethanol 1.5% (*v/v*) at three time points (i.e., 24, 48, and 72 h). Each sample consisted of three biological replicates (Supplementary Table S2). To comparatively evaluate the effects of gene knockout on *Synechocystis* metabolism, we generated PCA score plots of metabolomic profiles of the wild-type strain and the Δ*slr0982* mutant through the growth time course under ethanol stress (**Supplementary Figures S2A–C**). Analysis of the score plots revealed obvious clustering patterns of three biological replicates for each sample, suggesting good analytical quality. In addition, the metabolomic profiles of the mutant can be visibly separated from those of the wild type at both control and ethanol stress conditions, suggesting good analytical resolution which can distinguish different metabolic status in the cells. Moreover, a slightly decreasing difference between the wild type and the Δ*slr0982* mutant under ethanol stress condition was observed, probably due to the fact that the cells started aging after a longer time of ethanol-stress treatment, so that metabolomic profiles of cells were more a reflection of cell aging rather than that of ethanol stress response.

Heat maps were created for all 36 LC-MS metabolomic profiles from three time points (i.e., 24, 48, 72 h) (**Figure 3**). In the analysis, the ratio of a given metabolites was calculated between the concentration of the metabolite under a given condition and the average concentration of the metabolite in all samples at each time point. At 24 h, under control condition without ethanol stress, very similar metabolite abundance patterns were found for almost all metabolites between the wild type and the Δ*slr0982* mutant, consistent with their similar growth pattern in the normal BG11 media. However, when the wild type grown under control and ethanol stress was compared, the results showed that a majority of metabolites were found up-regulated under the ethanol stress condition, more significantly for AcCOA, NADPH, NADP, NADH, NAD, ADP-GCS, ATP, ADP, G6P, F6P, and R5P, which were key

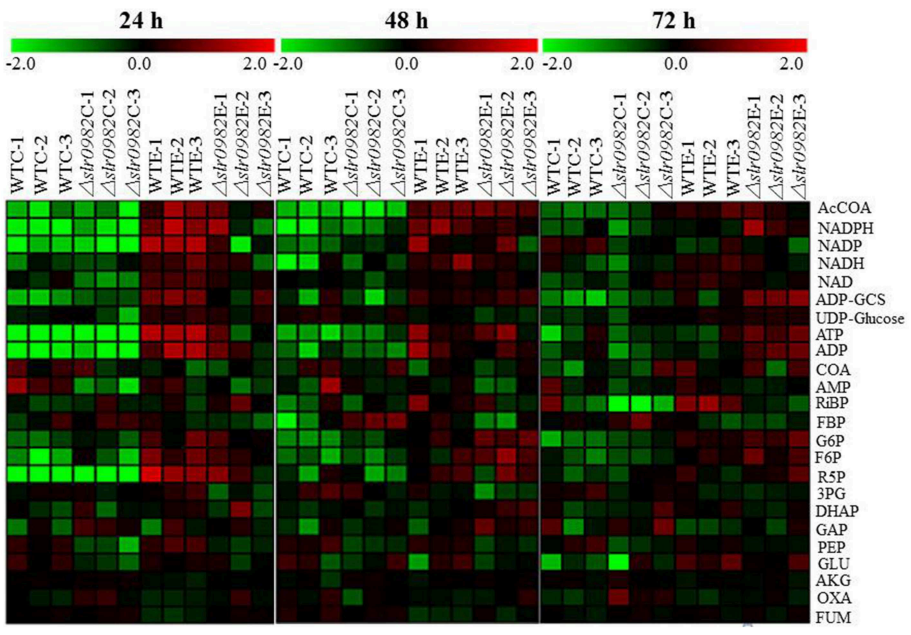

FIGURE 3 | Heat map analysis of LC-MS metabolomics. The row displays metabolite and the column represents the samples. Metabolites significantly decreased were displayed in green, while metabolites significantly increased were displayed in red. The brightness of each color corresponded to the magnitude of the difference when compared with average value. WT-C and WT-E: wild type grown with or without 1.5% (*v/v*) ethanol stress. Δ*slr0982*-C and Δ*slr0982*-E: the Δ*slr0982* mutant grown with or without 1.5% (*v/v*) ethanol stress.

co-enzyme or bioenergetics molecules participating in many important metabolic pathways, such as glycolysis, pentose phosphate pathway and TCA cycle, and well-known to have crucial roles in stress response. As an example, it has been reported that NADPH as an important coenzyme participates in ethanol tolerance in yeast, where overexpression of NADPH-dependent alcohol dehydrogenase (ADH6) significantly increased the 5-hydroxymethylfurfural tolerance (Petersson et al., 2006). Glucose-6-phosphate dehydrogenase that catalyzes the conversion from G6P and NADP to 6-phospho-*D*-glucono-1,5-lactone and NADPH was responsive to radiation stress in *Synechococcus lividus* (Conter et al., 1987). Ribose-5-phosphate isomerase that catalyzes the conversion between ribose-5-phosphate (R5P) and ribulose-5-phosphate (Ru5P) was found differentially regulated under oxidative stress conditions in photosynthetic green alga *Chlamydomonas reinhardtii* (Zaffagnini et al., 2012). Sucrose-phosphate synthase (SpsA, Sll0045) that uses F6P as substrate to form sucrose 6-phosphate is a key enzyme to synthesize one major compatible solute, sucrose, against salt stress in *Synechocystis* (Curatti et al., 1998; Desplats et al., 2005; Klahn and Hagemann, 2011).

At 48 and 72 h, under control condition without ethanol stress, differences in terms of metabolite abundance patterns were observed between the wild type and the Δ*slr0982* mutant, suggesting that after a long time of ethanol stress treatment, cellular metabolism started to diverge even though their growth patterns were similar. In addition, such a difference seemed more obvious at 72 h than 48 h (**Figure 3**). In the wild type between control and ethanol stress conditions, similar patterns of increased abundances of key molecules were found in the cells under ethanol stress condition, although the increases seemed less significantly, especially at 72 h, which was probably due to the accelerated cell aging and death after longer time of ethanol stress. However, in the Δ*slr0982* mutant cells at 48 and 72 h, the abundances of AcCOA, ADP-GCS, ATP, ADP, G6P, F6P, and R5P were enhanced when compared with 24 h (**Figure 3**). Taken together, the LC-MS targeted metabolomic analysis suggested that the *slr0982* deletion could affect or delay the up-regulation of several key metabolites responsive to ethanol stress, which may eventually contribute to the tolerance loss in the Δ*slr0982* mutant (**Figure 1**).

To validate results from LC–MS analysis, 6 genes were selected for quantitative RT-PCR analysis; they are glucose-6-phosphate isomerase (*slr1349*), 6-phosphofructokinase (*sll0745*), phosphoribulokinase (*sll1525*), phosphopyruvate hydratase (*slr0752*), citrate synthase (*sll0401*) and glutamate dehydrogenase (*slr0710*). The genes were selected because their enzymatic substrates or products were differentially regulated between the *slr0982* mutant and the control under ethanol stress condition, as revealed by the metabolomic analysis (**Figure 3**). The gene ID and their related primer sequences used for real-time RT-qPCR analysis were listed in Supplementary Table S1. Comparative RT-qPCR analysis showed these genes were down-regulated 1.5–2.6 folds under ethanol stress in the mutant when compared with the wild type (**Table 1**). In general, good agreement between the gene expression analysis and the LC–MS metabolomic analysis was observed: down-regulation of *slr1349* and *sll0745* genes was consistent with the decreased abundance of FBP, while down-regulation of *sll1525*, *slr0752*, and *slr0710* was consistent with the decreased abundances of RiBP, PEP and Glu, respectively.

TABLE 1 | RT-qPCR analysis of selected genes.

Gene ID	Gene description	Comparision	RT-qPCR ratio
slr1349	glucose-6-phosphate isomerase	Δ*slr0982*-ethanol vs. WT-ethanol	−1.771 ± 0.052
sll0745	6-phosphofructokinase	Δ*slr0982*-ethanol vs. WT-ethanol	−2.168 ± 0.229
sll1525	Phosphoribulokinase	Δ*slr0982*-ethanol vs. WT-ethanol	−1.452 ± 0.072
slr0752	phosphopyruvate hydratase	Δ*slr0982*-ethanol vs. WT-ethanol	−2.613 ± 0.282
sll0401	citrate synthase	Δ*slr0982*-ethanol vs. WT-ethanol	−2.090 ± 0.297
slr0710	glutamate dehydrogenase	Δ*slr0982*-ethanol vs. WT-ethanol	−1.773 ± 0.323

Untargeted GC-MS Metabolomic Analysis of the Wild-Type and the Δ*slr0982* Strain

Following the optimized extraction protocol established previously (Krall et al., 2009), the cells of the wild type control and the Δ*slr0982* mutant grown in BG11 media with and without 1.5% (*v/v*) ethanol stress were collected at three time points (i.e., 24, 48, and 72 h) and the further MS analysis allowed the chemical classification of a total 48 metabolites from *Synechocystis*, including various amino acids, sugars, and organic acids detected in almost all replicate samples (Supplementary Table S3). Score plots of PCA were generated to compare the mutant and the wild type in different conditions at three time points (i.e., 24, 48, and 72 h). The time-series metabolomic data showed that: (*i*) clustering of the biological replicates for each sample was clearly observed, suggesting overall good quality of the GC-MS analysis; (*ii*) interestingly, although no difference was observed for the wild type and the Δ*slr0982* mutant in terms of cell growth in the control media, clustering analysis based on their intracellular metabolites showed that they were clearly separated even at 24 h (**Figure 4**), indicating that the metabolic difference between the wild type and the Δ*slr0982* mutant, consistent with the above results from the LC-MS metabolomics (**Figure 3**); (*iii*) through the time course from 24 to 72 h under ethanol stress condition, metabolomic profiles of the Δ*slr0982* mutant were gradually moving more close to those of the wild type, probably due to the increasing cell aging and death after long ethanol stress (**Figure 4**).

WGCNA Analysis of Metabolomic Profiles Associated with the Ethanol Tolerance

To identify metabolic modules and hub metabolites related to ethanol tolerance in the Δ*slr0982* mutant, a correlation-based WGCNA analysis was applied to analysis to the GC-MS metabolomic datasets (Zhang and Horvath, 2005; Langfelder

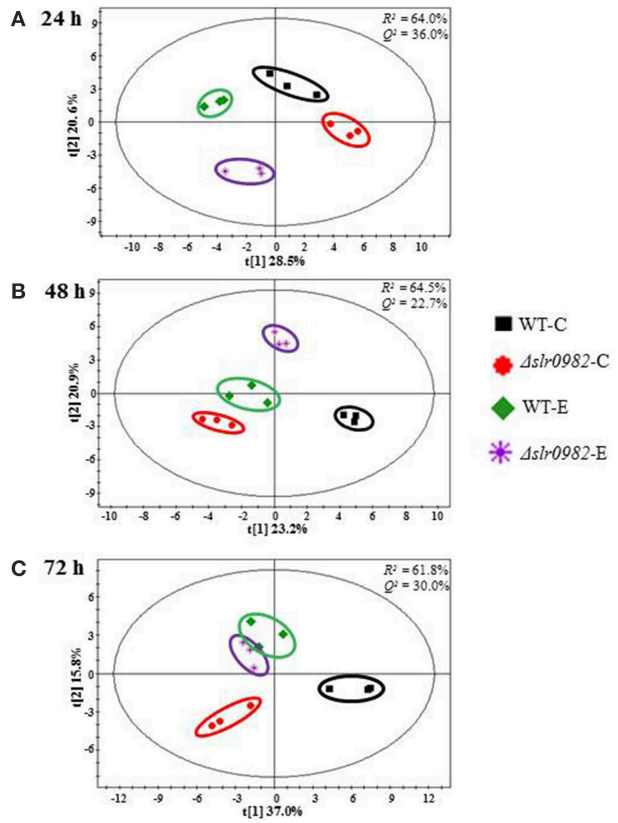

FIGURE 4 | PCA plot analysis of GC-MS metabolomic profiles. (A) 24 h; **(B)** 48 h; **(C)** 72 h. Each dot represents one biological sample, while the dots of the same color are biological replicates. Four groups of samples, the wild type and the Δ*slr0982* mutant grown in the BG11 media with or without 1.5% (*v/v*) ethanol stress are indicated by different colors, and each group is indicated by a circle. WT-C and WT-E: wild type grown with or without 1.5% (*v/v*) ethanol stress. Δ*slr0982*-C and Δ*slr0982*-E: the Δ*slr0982* mutant grown with or without 1.5% (*v/v*) ethanol stress.

and Horvath, 2008). The network analysis was not applied to LC-MS metabolomic data due to their relatively small data size. In this study, we constructed unsigned networks using a GC-MS metabolomic data set consisted of 48 metabolites, and then localized the correlated metabolites into various metabolic modules. In addition, the association of each distinguished metabolic module with mutant or ethanol stress treatment was determined. Setting a minimal number of metabolites in any module greater than 3, our WGCNA analysis showed that 6, 8, and 7 distinct metabolic modules can be detected within the metabolic networks at 24, 48, and 72 h, respectively (**Supplementary Figure S3**). Using a cutoff of correlation coefficient (r value) greater than 0.5 or less than −0.5, and their statistical confidence (p-values) less than 0.05, the analysis showed that a total of 4, 4, and 2 distinguished metabolic modules were highly associated with mutant or ethanol stress condition at 24, 48, and 72 h, respectively (**Supplementary Figures S4A–C**). At each time point, six modules (i.e., M1, M2, M3, M6, M8, and M9) were associated only with ethanol stress, three modules (i.e., M4, M5, and M7) were only associated with the knockout of the *slr0982* gene, and M10 module was associated with both the ethanol stress and the knockout of the *slr0982* gene, respectively. Metabolites included in each of the highly associated modules were presented in **Table 2**.

Using a criterion that at least two of its member metabolites identified from any given pathway, a pathway enrichment analysis was conducted and the results showed eight pathways were enriched in various distinct modules (**Table 3**). Among them, the results showed that "Tryptophan metabolism" (Map00380) was enriched with statistical significance p-values less than 0.05 in ethanol-associated module M2. Enrichment of "Tryptophan metabolism" in ethanol-associated modules was consistent with early studies in *E. coli* and *Saccharomyces cerevisiae*, in which tryptophan biosynthetic pathway was previously found up-regulated in the ethanol-tolerant *E. coli* strains by a microarray analysis, and supplementation of tryptophan to the culture medium increased the specific growth rate of *E. coli* under ethanol stress (Horinouchi et al., 2010), and overexpressing tryptophan biosynthesis genes in yeast resulted in a stress tolerance to 5% ethanol (Hirasawa et al., 2007). In addition, "Biosynthesis of unsaturated fatty acids" (Map01040) was enriched in ethanol-associated module M3, and "Fatty acid biosynthesis" (Map00061) was enriched in both ethanol-associated module M3 and M6, consistent with the well-defined roles of fatty acid, especially unsaturated fatty acids in membrane modification against ethanol stress in various microbes (Heipieper and De Bont, 1994; Chiang et al., 2008). One well-described change is the shift from *cis* to *trans* unsaturated fatty acids to decrease membrane fluidity, resulting in a corresponding increase in solvent tolerance (Dunlop, 2011). In a previous study with cyanobacteria, the acyl-lipid desaturase (*desA*) gene from *Synechocystis* was expressed in prokaryotic *E. coli* and eukaryotic *Solanum tuberosum* cells, which led to an enhanced cold tolerance due to increased unsaturated fatty acid concentration in their lipids (Amiri et al., 2010). Our previous RNA-seq transcriptomics analysis also showed that *slr1350* encoding acyl-lipid desaturase was up-regulated by ethanol exposure in *Synechocystis* (Wang et al., 2012).

Enrichment analysis showed that "Biosynthesis of secondary metabolites" (Map01110), "Chloroalkane and chloroalkene degradation" (Map00625), "Benzoate degradation" (Map00362) and "Aminobenzoate degradation"(Map00627) were enriched with statistical significance p-values less than 0.05 in module M4, M9, M10, and M10, respectively (**Table 2**). The "Biosynthesis of secondary metabolites" pathway contains many metabolites known to be related to stress conditions, such as $D(+)$ trehalose involved in salt stress in cyanobacteria (Hagemann, 2011), ethanol resistance in *E. coli* (Wang et al., 2013) and *S. cerevisiae* (Zheng et al., 2013; Wang et al., 2014a), and L-isoleucine and L-glutamic acid involved in ethanol tolerance in *E. coli* (Horinouchi et al., 2010; Wang et al., 2013). "Benzoate degradation" (Map00362) and "Aminobenzoate degradation" (Map00627) were enriched due to the same two metabolites, benzoic acid and benzene-1,2,4-triol. However, their roles in ethanol tolerance are still unclear.

TABLE 2 | Metabolites included in each of the highly associated modules*.

Modules	Conditions	Time (h)	Association (*r*)	*P*	Metabolites
M1	Ethanol	24	0.88	2.E-04	*L*-threonin, adenosine,capric acid, malonic acid, 2-amino-1-phenylethanol, 2-hydroxybutyric acid
M2	Ethanol	24	0.85	4.E-04	urea, 5-hydroxy-*L*-tryptophan, gluconic acid lactone
M3	Ethanol	24	0.69	1.E-02	*D*-allose, *DL*-isoleucine, oleic acid, heptadecanoic acid, linoleic acid, lauric acid, myristic acid, palmitic acid, stearic acid, 2-hydroxypyridine, palmitoleic acid
M4	*slr0982*	24	−0.74	6.E-03	*D*-(+)-galactose, *DL*-3,4-dihydroxyphenyl-glycol, succinic acid, *D*-glucose-6-phosphate, *L*-serine, *L*-norleucine, 3-hydroxypyridine, benzene-1,2,4-triol, phytol, *L*-(+)-lactic acid, spermidine, benzoic acid, porphine, sucrose, glycerol-1-phosphate, *L*-pyroglutamic acid, *D*-(+)-trehalose, *L*-glutamic acid
M5	*slr0982*	48	−0.88	2.E-04	malonic acid, *L*-threonine, palmitoleic acid
M6	Ethanol	48	0.65	2.E-02	urea, 2-hydroxypyridine, phytol, capric acid, succinic acid, caprylic acid, 3-hydroxypyridine, myristic acid, glycine, stearic acid
M7	*slr0982*	48	0.7	1.E-02	glycerol-1-phosphate, *D*-(+)-trehalose, 2-hydroxybutyric acid, *L*-norleucine, 2-amino-1-phenylethanol, palmitic acid, phosphoric acid
M8	Ethanol	48	−0.73	7.E-03	benzene-1,2,4-triol, *D*-allose, glycerol
M9	Ethanol	72	−0.98	9.E-09	malonic acid, glycolic acid, porphine
M10	*slr0982*	72	−0.67	2.E-02	sucrose, *D*-allose, benzene-1,2,4-triol, benzoic acid
	Ethanol	72	−0.66	2.E-02	

**GC-MS metabolomic dataset was used for this analysis. The association of each distinguished metabolic module with mutant or ethanol stress treatment was determined.*

TABLE 3 | Pathway enrichment analysis of metabolites associated with the ethanol stress condition*.

Pathways	KEGG pathway ID	Modules associated	*p*-values (over represented)	Number of associated metabolites in given KEGG pathway	Number of all metabolites in given KEGG pathway	Metabolites involved
Tryptophan metabolism	Map00380	M2	0.0400	1	1	5-hydroxy-*L*-tryptophan
Biosynthesis of unsaturated fatty acids	Map01040	M3	0.0120	4	4	palmitic acid, stearic acid, oleic acid, linoleic acid
Fatty acid biosynthesis	Map00061	M3	0.0152	5	7	palmitic acid, stearic acid, oleic acid, myristic acid, lauric acid
Biosynthesis of secondary metabolites	Map01110	M4	0.0384	10	15	benzoic acid, succinic acid, *D*(+) trehalose, *L*-glutamic acid, *D*-glucose-6-phosphate, *L*-norleucine, *D* (+) galactose, *L*-serine, spermidine, sucrose
Fatty acid biosynthesis	Map00061	M6	0.0117	4	7	capric acid,caprylic acid, myristic acid, stearic acid
Chloroalkane and chloroalkene degradation	Map00625	M9	0.0428	1	1	glycolic acid
Benzoate degradation	Map00362	M10	0.0069	2	2	benzoic acid, benzene-1,2,4-triol
Aminobenzoate degradation	Map00627	M10	0.0069	2	2	benzoic acid, benzene-1,2,4-triol

**GC-MS metabolomic dataset was used for this analysis.*

Within metabolic networks, hub metabolites that are involved in a high number of reactions are typically biologically important (Pfeiffer et al., 2005). Assuming a cutoff of connectivity greater than 5 in the networks as hub metabolites, a few hub metabolites were identified from the metabolic network constructed by the WGCNA, including sucrose and *L*-pyroglutamic acid in the module M4 at 24 h and stearic acid in the module M6 (**Figure 5**). While M6 was associated with only ethanol stress, the role of stearic acid along with several connected fatty acid may be associated with membrane modification against ethanol stress (Dunlop, 2011). M4 was associated with the *slr0982* knockout event (**Table 2**). As discussed above, sucrose was well studied as compatible solutes against salt stress in cyanobacteria (Hagemann, 2011). As osmoprotectants, pyroglutamic acid was found to accumulate in response to salt stress and function as an osmoprotectant along with sucrose, in the halotolerant methanotroph *Methylobacter alkaliphilum* (Trotsenko Iu and Khelenina, 2002). In addition, these two compouds were also

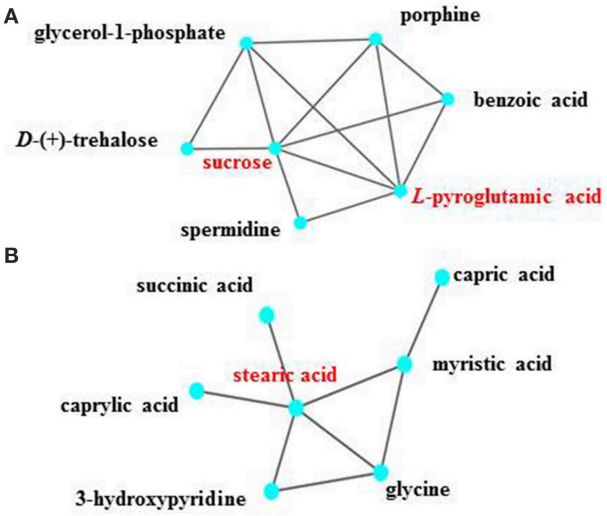

FIGURE 5 | The hub metabolites and their metabolic profiles as represented by the node and edge graph. (A) Sucrose and *L*-pyroglutamic acid in the module M4 at 24 h; **(B)** Stearic acid in the module M6 at 48 h.

found to be involved in ethanol tolerance in *Synechocystis* (Zhu et al., 2015).

Conclusions

By constructing and screening a mutant library of 58 transporter-encoding genes, a gene encoding an ABC transporter, *slr0982*, was identified to be involved in ethanol tolerance in *Synechocystis*. As the first ethanol-tolerance related transporter found in cyanobacteria, the gene could be valuable as a target of ethanol tolerance engineering for high-efficiency production in cyanobacterial systems. Although no evidence showed that Slr0982 is directly involved in the export of ethanol, the analysis suggested that it may affect transporting of other molecules important to the function and maintance of cytoplasmic membrane or extracellular structure.

To further decipher the ethanol tolerance mechanism mediated by transporter Slr0982, comparative LC-MS and GC-MS based metabolomic analyses were applied to determine the variation of intracellular intermediates in the wild type and the Δ*slr0982* mutant grown in BG 11 media with or without ethanol stress. The PCA and WGCNA analyses were used for analyzing the metabolomic data set in order to identify specific metabolites responsive to ethanol stress between mutant and wild type. The results showed that metabolites such as AcCOA, ADP-GCS, ATP, ADP, G6P, F6P, and R5P, and metabolic modules such as "Tryptophan metabolism," "Biosynthesis of unsaturated fatty acids" and "Biosynthesis of secondary metabolites" might be related to ethanol tolerance in cyanobacterium *Synechocystis*, and further analysis the mechanisms that these metabolites and modules may represent could be valuable for tolerance in *Synechocystis*. Taken together, this study provided new insights into ethanol tolerance in cyanobacterium *Synechocystis*.

Author Contributions

LC and WZ conceived of the study. YZ, LC, and WZ drafted the manuscript. YZ carried out the mutant construction, overexpression, phenotypic and RT-PCR analyses. GP carried out the metabolomic data analysis. XN and XZ carried out the LC-MS analysis. MS and XZ carried out the GC-MS analysis. All authors read and approved the final manuscript.

Acknowledgments

The research was supported by grants from National Basic Research Program of China ("973" program, project No. 2011CBA00803 and No. 2014CB745101) and National High-tech R&D Program ("863" program, project No. 2012AA02A707).

Supplementary Material

The Supplementary Material for this article can be found online at: http://journal.frontiersin.org/article/10.3389/fmicb.2015.00487/abstract

Supplementary Figure S1 | The schematic PCR strategy and valiation of the mutants. Agarose gel electrophoresis in A–M were the PCR validation data. The same row, the same group. F1, R3 and internal primers (Supplementary Table S1) were used for colony PCR validation. Lane M: 1 kb DNA markers. The other lanes: The chromosomal DNA of WT or mutant was used as PCR template.

Supplementary Figure S2 | PCA plot analysis of LC-MS metabolomic profiles. (A) 24 h; **(B)** 48 h; **(C)** 72 h. Each dot represents one biological sample, while the dots of the same color are biological replicates. Four groups of samples, the wild type and the Δ*slr0982* mutant grown in the BG11 media with or without 1.5% (*v/v*) ethanol stress are indicated by different colors, and each group is indicated by a circle. WT-C and WT-E: wild type grown with or without 1.5% (*v/v*) ethanol stress. Δ*slr0982*-C and Δ*slr0982*-E: the Δ*slr0982* mutant grown with or without 1.5% (*v/v*) ethanol stress.

Supplementary Figure S3 | Module-trait relationships of GC-MS metabolic profiles of the *Synechocystis* during ethanol-treated. (A) 24 h; **(B)** 48 h; **(C)** 72 h. Setting a minimal number of metabolites in any module greater than 3, WGCNA analysis showed that 6, 8, and 7 distinct metabolic modules with mutant or ethanol stress can be detected within the metabolic networks at 24, 48, and 72 h, respectively. Metabolites in the module significantly decreased were displayed in green, while metabolites in the module significantly increased were displayed in red.

Supplementary Figure S4 | Weighted correlation network analysis (WGCNA) of GC-MS metabolic profiles of the *Synechocystis* during ethanol-treated. (A) 24 h; **(B)** 48 h; **(C)** 72 h. The distinct modules identified at each time point were indicted by the clustering patterns of the red color squares along the diagonal inside the plots. The modules highly associated with any given ethanol stress ($r > 0.5$ or $r < -0.5$ and $p < 0.05$) were indicated with their metabolites in corresponding colors with their modules, and the correlation coefficients and *p*-values were shown in **Table 2**.

References

Aguilera, F., Peinado, R. A., Millan, C., Ortega, J. M., and Mauricio, J. C. (2006). Relationship between ethanol tolerance, H^+-ATPase activity and the lipid composition of the plasma membrane in different wine yeast strains. *Int. J. Food Microbiol.* 110, 34–42. doi: 10.1016/j.ijfoodmicro.2006.02.002

Amiri, R. M., Yur'eva, N. O., Shimshilashvili, K. R., Goldenkova-Pavlova, I. V., Pchelkin, V. P., Kuznitsova, E. I., et al. (2010). Expression of acyl-lipid △12-desaturase gene in prokaryotic and eukaryotic cells and its effect on cold stress tolerance of potato. *J. Integr. Plant Biol.* 52, 289–297. doi: 10.1111/j.1744-7909.2010.00890.x

Angermayr, S. A., Hellingwerf, K. J., Lindblad, P., and De Mattos, M. J. (2009). Energy biotechnology with cyanobacteria. *Curr. Opin. Biotechnol.* 20, 257–263. doi: 10.1016/j.copbio.2009.05.011

Antoni, D., Zverlov, V. V., and Schwarz, W. H. (2007). Biofuels from microbes. *Appl. Microbiol. Biotechnol.* 77, 23–35. doi: 10.1007/s00253-007-1163-x

Bennette, N. B., Eng, J. F., and Dismukes, G. C. (2011). An LC–MS-based chemical and analytical method for targeted metabolite quantification in the model cyanobacterium *Synechococcus* sp. PCC 7002. *Anal. Chem.* 83, 3808–3816. doi: 10.1021/ac200108a

Cartwright, C. P., Veazey, F. J., and Rose, A. H. (1987). Effect of ethanol on activity of the plasma-membrane ATPase in, and accumulation of glycine by, *Saccharomyces cerevisiae*. *J. Gen. Microbiol.* 133, 857–865. doi: 10.1099/00221287-133-4-857

Chiang, M. L., Ho, W. L., and Chou, C. C. (2008). Ethanol shock changes the fatty acid profile and survival behavior of *Vibrio parahaemolyticus* in various stress conditions. *Food Microbiol.* 25, 359–365. doi: 10.1016/j.fm.2007.10.002

Conter, A., Dupouy, D., Vincent, C., and Planel, H. (1987). Radiation stimulation during the early stationary growth phase in *Synechococcus lividus* and its correlation with photooxidative stress occurring before the stationary phase. *Health Phys.* 53, 281–286. doi: 10.1097/00004032-198709000-00007

Curatti, L., Folco, E., Desplats, P., Abratti, G., Limones, V., Herrera-Estrella, L., et al. (1998). Sucrose-phosphate synthase from *Synechocystis* sp. strain PCC 6803: identification of the spsA gene and characterization of the enzyme expressed in *Escherichia coli*. *J. Bacteriol.* 180, 6776–6779.

Davidson, A. L., Dassa, E., Orelle, C., and Chen, J. (2008). Structure, function, and evolution of bacterial ATP-binding cassette systems. *Microbiol. Mol. Biol. Rev.* 72, 317–364. doi: 10.1128/MMBR.00031-07

Desplats, P., Folco, E., and Salerno, G. L. (2005). Sucrose may play an additional role to that of an osmolyte in *Synechocystis* sp. PCC 6803 salt-shocked cells. *Plant Physiol. Biochem.* 43, 133–138. doi: 10.1016/j.plaphy.2005.01.008

Ding, J., Huang, X., Zhang, L., Zhao, N., Yang, D., and Zhang, K. (2009). Tolerance and stress response to ethanol in the yeast *Saccharomyces cerevisiae*. *Appl. Microbiol. Biotechnol.* 85, 253–263. doi: 10.1007/s00253-009-2223-1

Ducat, D. C., Way, J. C., and Silver, P. A. (2011). Engineering cyanobacteria to generate high-value products. *Trends Biotechnol.* 29, 95–103. doi: 10.1016/j.tibtech.2010.12.003

Dunlop, M. J. (2011). Engineering microbes for tolerance to next-generation biofuels. *Biotechnol. Biofuels.* 4:32. doi: 10.1186/1754-6834-4-32

Dunlop, M. J., Dossani, Z. Y., Szmidt, H. L., Chu, H. C., Lee, T. S., Keasling, J. D., et al. (2011). Engineering microbial biofuel tolerance and export using efflux pumps. *Mol. Syst. Biol.* 7, 487. doi: 10.1038/msb.2011.21

Eiadpum, A., Limtong, S., and Phisalaphong, M. (2012). High-temperature ethanol fermentation by immobilized coculture of *Kluyveromyces marxianus* and *Saccharomyces cerevisiae*. *J. Biosci. Bioeng.* 114, 325–329. doi: 10.1016/j.jbiosc.2012.04.004

Fiehn, O. (2002). Metabolomics–the link between genotypes and phenotypes. *Plant Mol. Biol.* 48, 155–171. doi: 10.1023/A:1013713905833

Fisher, M. L., Allen, R., Luo, Y., and Curtiss Iii, R. (2013). Export of extracellular polysaccharides modulates adherence of the cyanobacterium *Synechocystis*. *PLoS ONE* 8:e74514. doi: 10.1371/journal.pone.0074514

Foo, J. L., Jensen, H. M., Dahl, R. H., George, K., Keasling, J. D., Lee, T. S., et al. (2014). Improving microbial biogasoline production in *Escherichia coli* using tolerance engineering. *MBio* 5:e01932. doi: 10.1128/mBio.01932-14

Gao, Z., Zhao, H., Li, Z., Tan, X., and Lu, X. (2012). Photosynthetic production of ethanol from carbon dioxide in genetically engineered cyanobacteria. *Energ. Environ. Sci.* 5, 9857. doi: 10.1039/c2ee22675h

Hagemann, M. (2011). Molecular biology of cyanobacterial salt acclimation. *FEMS Microbiol. Rev.* 35, 87–123. doi: 10.1111/j.1574-6976.2010.00234.x

Hahn-Hagerdal, B., Galbe, M., Gorwa-Grauslund, M. F., Liden, G., and Zacchi, G. (2006). Bio-ethanol–the fuel of tomorrow from the residues of today. *Trends Biotechnol.* 24, 549–556. doi: 10.1016/j.tibtech.2006.10.004

Hayashi, T., Kato, T., and Furukawa, K. (2012). Respiratory chain analysis of *Zymomonas mobilis* mutants producing high levels of ethanol. *Appl. Environ. Microbiol.* 78, 5622–5629. doi: 10.1128/AEM.00733-12

Heipieper, H., and De Bont, J. (1994). Adaptation of *Pseudomonas putida* S12 to ethanol and toluene at the level of fatty acid composition of membranes. *Appl. Environ. Microbiol.* 60, 4440–4444.

Hermans, M. A., Neuss, B., and Sahm, H. (1991). Content and composition of hopanoids in *Zymomonas mobilis* under various growth conditions. *J. Bacteriol.* 173, 5592–5595.

Hirasawa, T., Yoshikawa, K., Nakakura, Y., Nagahisa, K., Furusawa, C., Katakura, Y., et al. (2007). Identification of target genes conferring ethanol stress tolerance to *Saccharomyces cerevisiae* based on DNA microarray data analysis. *J. Biotechnol.* 131, 34–44. doi: 10.1016/j.jbiotec.2007.05.010

Horinouchi, T., Tamaoka, K., Furusawa, C., Ono, N., Suzuki, S., Hirasawa, T., et al. (2010). Transcriptome analysis of parallel-evolved *Escherichia coli* strains under ethanol stress. *BMC Genomics* 11:579. doi: 10.1186/1471-2164-11-579

Ingram, L. O. (1981). Mechanism of lysis of *Escherichia coli* by ethanol and other chaotropic agents. *J. Bacteriol.* 146, 331–336.

Jin, H., Chen, L., Wang, J., and Zhang, W. (2014). Engineering biofuel tolerance in non-native producing microorganisms. *Biotechnol. Adv.* 32, 541–548. doi: 10.1016/j.biotechadv.2014.02.001

Kamarainen, J., Knoop, H., Stanford, N. J., Guerrero, F., Akhtar, M. K., Aro, E. M., et al. (2012). Physiological tolerance and stoichiometric potential of cyanobacteria for hydrocarbon fuel production. *J. Biotechnol.* 162, 67–74. doi: 10.1016/j.jbiotec.2012.07.193

Kaneko, T., Sato, S., Kotani, H., Tanaka, A., Asamizu, E., Nakamura, Y., et al. (1996). Sequence analysis of the genome of the unicellular cyanobacterium *Synechocystis* sp. strain PCC6803. II. Sequence determination of the entire genome and assignment of potential protein-coding regions. *DNA Res.* 3, 109–136. doi: 10.1093/dnares/3.3.109

Katoh, H., Hagino, N., Grossman, A. R., and Ogawa, T. (2001). Genes essential to iron transport in the cyanobacterium *Synechocystis* sp. strain PCC 6803. *J. Bacteriol.* 183, 2779–2784. doi: 10.1128/JB.183.9.2779-2784.2001

Klahn, S., and Hagemann, M. (2011). Compatible solute biosynthesis in cyanobacteria. *Environ. Microbiol.* 13, 551–562. doi: 10.1111/j.1462-2920.2010.02366.x

Kloft, N., Rasch, G., and Forchhammer, K. (2005). Protein phosphatase PphA from *Synechocystis* sp. PCC 6803: the physiological framework of PII-P dephosphorylation. *Microbiology* 151, 1275–1283. doi: 10.1099/mic.0.27771-0

Krall, L., Huege, J., Catchpole, G., Steinhauser, D., and Willmitzer, L. (2009). Assessment of sampling strategies for gas chromatography–mass spectrometry (GC–MS) based metabolomics of cyanobacteria. *J. Chromatogr. B.* 877, 2952–2960. doi: 10.1016/j.jchromb.2009.07.006

Laiakis, E. C., Morris, G. A., Fornace Jr, A. J., and Howie, S. R. (2010). Metabolomic analysis in severe childhood pneumonia in the Gambia, West Africa: findings from a pilot study. *PLoS ONE* 5:e12655. doi: 10.1371/journal.pone.0012655

Langfelder, P., and Horvath, S. (2008). WGCNA: an R package for weighted correlation network analysis. *BMC Bioinformatics* 9:559. doi: 10.1186/1471-2105-9-559

Letti, L. A. J., Karp, S. G., Woiciechowski, A. L., and Soccol, C.R. (2012). Ethanol production from soybean molasses by *Zymomonas mobilis*. *Biomass Bioenergy* 44, 80–86. doi: 10.1016/j.biombioe.2012.04.023

Machado, I. M., and Atsumi, S. (2012). Cyanobacterial biofuel production. *J. Biotechnol.* 162, 50–56. doi: 10.1016/j.jbiotec.2012.03.005

Manow, R., Wang, J., Wang, Y., Zhao, J., Garza, E., Iverson, A., et al. (2012). Partial deletion of rng (RNase G)-enhanced homoethanol fermentation of xylose by the non-transgenic *Escherichia coli* RM10. *J. Ind. Microbiol. Biotechnol.* 39, 977–985. doi: 10.1007/s10295-012-1100-6

Marbouty, M., Mazouni, K., Saguez, C., Cassier-Chauvat, C., and Chauvat, F. (2009). Characterization of the *Synechocystis* strain PCC 6803 penicillin-binding proteins and cytokinetic proteins FtsQ and FtsW and their network of interactions with ZipN. *J. Bacteriol.* 191, 5123–5133. doi: 10.1128/JB.00620-09

Mikkat, S., Hagemann, M., and Schoor, A. (1996). Active transport of glucosylglycerol is involved in salt adaptation of the cyanobacterium *Synechocystis* sp. strain PCC 6803. *Microbiology* 142, 1725–1732. doi: 10.1099/13500872-142-7-1725

Nakao, M., Okamoto, S., Kohara, M., Fujishiro, T., Fujisawa, T., Sato, S., et al. (2010). CyanoBase: the cyanobacteria genome database update 2010. *Nucleic Acids Res.* 38, 379–381. doi: 10.1093/nar/gkp915

Nomura, M., Ishitani, M., Takabe, T., and Rai, A. K. (1995). *Synechococcus* sp. PCC7942 transformed with *Escherichia coli* bet genes produces glycine betaine from choline and acquires resistance to salt stress. *Plant Physiol.* 107, 703–708.

Oliver, J. W., and Atsumi, S. (2014). Metabolic design for cyanobacterial chemical synthesis. *Photosynth. Res.* 120, 249–261. doi: 10.1007/s11120-014-9997-4

Park, C., Lee, Y.-J., Lee, S. Y., Oh, H. B., and Lee, J. (2011). Determination of the intracellular concentrations of metabolites in *Escherichia coli* collected during the exponential and stationary growth phases using Liquid Chromatography-Mass Spectrometry. *Bull. Korean Chem. Soc.* 32, 524–530. doi: 10.5012/bkcs.2011.32.2.524

Petersson, A., Almeida, J. R. M., Modig, T., Karhumaa, K., Hahn-Hägerdal, B., Gorwa-Grauslund, M. F., et al. (2006). A 5-hydroxymethyl furfural reducing enzyme encoded by the *Saccharomyces cerevisiae* ADH6 gene conveys HMF tolerance. *Yeast* 23, 455–464. doi: 10.1002/yea.1370

Pfeiffer, T., Soyer, O. S., and Bonhoeffer, S. (2005). The evolution of connectivity in metabolic networks. *PLoS Biol.* 3:e228. doi: 10.1371/journal.pbio.0030228

Qiao, J., Wang, J., Chen, L., Tian, X., Huang, S., Ren, X., et al. (2012). Quantitative iTRAQ LC–MS/MS proteomics reveals metabolic responses to biofuel ethanol in cyanobacterial *Synechocystis* sp. PCC 6803. *J. Proteome Res.* 11, 5286–5300. doi: 10.1021/pr300504w

Roessner, U., Luedemann, A., Brust, D., Fiehn, O., Linke, T., Willmitzer, L., et al. (2001). Metabolic profiling allows comprehensive phenotyping of genetically or environmentally modified plant systems. *Plant Cell Online* 13, 11–29. doi: 10.1105/tpc.13.1.11

Romeo, T., Gong, M., Liu, M. Y., and Brun-Zinkernagel, A. M. (1993). Identification and molecular characterization of csrA, a pleiotropic gene from *Escherichia coli* that affects glycogen biosynthesis, gluconeogenesis, cell size, and surface properties. *J. Bacteriol.* 175, 4744–4755.

Ruffing, A. M. (2011). Engineered cyanobacteria: teaching an old bug new tricks. *Bioeng. Bugs.* 2, 136–149. doi: 10.4161/bbug.2.3.15285

Rutherford, B. J., Dahl, R. H., Price, R. E., Szmidt, H. L., Benke, P. I., Mukhopadhyay, A., et al. (2010). Functional genomic study of exogenous n-butanol stress in *Escherichia coli*. *Appl. Environ. Microbiol.* 76, 1935–1945. doi: 10.1128/AEM.02323-09

Schwarz, D., Orf, I., Kopka, J., and Hagemann, M. (2013). Recent applications of metabolomics toward cyanobacteria. *Metabolites* 3, 72–100. doi: 10.3390/metabo3010072

Stanley, D., Bandara, A., Fraser, S., Chambers, P., and Stanley, G. A. (2010). The ethanol stress response and ethanol tolerance of *Saccharomyces cerevisiae*. *J. Appl. Microbiol.* 109, 13–24. doi: 10.1111/j.1365-2672.2009.04657.x

Stein, S. E. (1999). An integrated method for spectrum extraction and compound identification from gas chromatography/mass spectrometry data. *Am. Soc. Mass. Spectrom.* 10, 770–781. doi: 10.1016/S1044-0305(99)00047-1

Su, Y., Wang, J., Shi, M., Niu, X., Yu, X., Gao, L., et al. (2014). Metabolomic and network analysis of astaxanthin-producing *Haematococcus pluvialis* under various stress conditions. *Bioresour. Technol.* 170, 522–529. doi: 10.1016/j.biortech.2014.08.018

Tahara, H., Uchiyama, J., Yoshihara, T., Matsumoto, K., and Ohta, H. (2012). Role of Slr1045 in environmental stress tolerance and lipid transport in the cyanobacterium *Synechocystis* sp. PCC6803. *Biochim. Biophys. Acta Bioenerg.* 1817, 1360–1366. doi: 10.1016/j.bbabio.2012.02.035

Tan, X., Yao, L., Gao, Q., Wang, W., Qi, F., and Lu, X. (2011). Photosynthesis driven conversion of carbon dioxide to fatty alcohols and hydrocarbons in cyanobacteria. *Metab. Eng.* 13, 169–176. doi: 10.1016/j.ymben.2011.01.001

Teixeira, M. C., Raposo, L. R., Mira, N. P., Lourenço, A. B., and Sá-Correia, I. (2009). Genome-wide identification of *Saccharomyces cerevisiae* genes required for maximal tolerance to ethanol. *Appl. Environ. Microbiol.* 75, 5761–5772. doi: 10.1128/AEM.00845-09

Thiel, T. (1988). Phosphate transport and arsenate resistance in the cyanobacterium *Anabaena variabilis*. *J. Bacteriol.* 170, 1143–1147.

Tong, L., Nakashima, S., Shibasaka, M., Katsuhara, M., and Kasamo, K. (2002). A novel histidine-rich CPx-ATPase from the filamentous cyanobacterium *Oscillatoria brevis* related to multiple-heavy-metal cotolerance. *J. Bacteriol.* 184, 5027–5035. doi: 10.1128/JB.184.18.5027-5035.2002

Trotsenko, Y. A., and Khmelenina, V. N. (2002). The biology and osmoadaptation of haloalkaliphilic methanotrophs. *Microbiology* 71, 123–132. doi: 10.1023/A:1015183832622

Verma, S. K., and Singh, H. N. (1991). Evidence for energy-dependent copper efflux as a mechanism of Cu^{2+} resistance in the cyanobacterium *Nostoc calcicola*. *FEMS Microbiol. Lett.* 68, 291–294. doi: 10.1111/j.1574-6968.1991.tb04612.x

Wang, H.-L., Postier, B. L., and Burnap, R. L. (2002). Optimization of fusion PCR for *in vitro* construction of gene knockout fragments. *Biotechniques* 33, 26, 28, 30 passim.

Wang, J., Chen, L., Huang, S., Liu, J., Ren, X., Tian, X., et al. (2012). RNA-seq based identification and mutant validation of gene targets related to ethanol resistance in cyanobacterial *Synechocystis* sp. PCC 6803. *Biotechnol. Biofuels* 5:89. doi: 10.1186/1754-6834-5-89

Wang, J., Chen, L., Tian, X., Gao, L., Niu, X., Shi, M., et al. (2013). Global metabolomic and network analysis of *Escherichia coli* responses to exogenous biofuels. *J. Proteome Res.* 12, 5302–5312. doi: 10.1021/pr400640u

Wang, P. M., Zheng, D. Q., Chi, X. Q., Li, O., Qian, C. D., Liu, T. Z., et al. (2014a). Relationship of trehalose accumulation with ethanol fermentation in industrial *Saccharomyces cerevisiae* yeast strains. *Bioresour. Technol.* 152, 371–376. doi: 10.1016/j.biortech.2013.11.033

Wang, Y., Shi, M., Niu, X., Zhang, X., Gao, L., Chen, L., et al. (2014b). Metabolomic basis of laboratory evolution of butanol tolerance in photosynthetic *Synechocystis* sp. PCC 6803. *Microb. Cell Fact.* 13:151. doi: 10.1186/s12934-014-0151-y

Yu, K. O., Jung, J., Ramzi, A. B., Choe, S. H., Kim, S. W., Park, C., et al. (2012). Increased ethanol production from glycerol by *Saccharomyces cerevisiae* strains with enhanced stress tolerance from the overexpression of SAGA complex components. *Enzyme Microb. Technol.* 51, 237–243. doi: 10.1016/j.enzmictec.2012.07.003

Zaffagnini, M., Bedhomme, M., Groni, H., Marchand, C. H., Puppo, C., Gontero, B., et al. (2012). Glutathionylation in the photosynthetic model organism *Chlamydomonas reinhardtii*: a proteomic survey. *Mol. Cell. Proteomics* 11, M111.014142. doi: 10.1074/mcp.M111.014142

Zhang, B., and Horvath, S. (2005). A general framework for weighted gene co-expression network analysis. *Stat. Appl. Genet. Mol.* 4:1128. doi: 10.2202/1544-6115.1128

Zheng, D., Zhang, K., Gao, K., Liu, Z., Zhang, X., Li, O., et al. (2013). Construction of novel *Saccharomyces cerevisiae* strains for bioethanol active dry yeast (ADY) production. *PLoS ONE* 8:e85022. doi: 10.1371/journal.pone.0085022

Zhou, B., Martin, G. J., and Pamment, N. B. (2008). Increased phenotypic stability and ethanol tolerance of recombinant *Escherichia coli* KO11 when immobilized in continuous fluidized bed culture. *Biotechnol. Bioeng.* 100, 627–633. doi: 10.1002/bit.21800

Zhu, Y., Pei, G., Niu, X., Shi, M., Zhang, M., Chen, L., et al. (2015). Metabolomic analysis reveals functional overlapping of three signal transduction proteins in regulating ethanol tolerance in cyanobacterium *Synechocystis* sp. PCC 6803. *Mol. Biosyst.* 11, 770–782. doi: 10.1039/C4MB00651H

Conflict of Interest Statement: The authors declare that the research was conducted in the absence of any commercial or financial relationships that could be construed as a potential conflict of interest.

frontiers in Microbiology

ORIGINAL RESEARCH
published: 22 April 2015
doi: 10.3389/fmicb.2015.00326

Seawater cultivation of freshwater cyanobacterium *Synechocystis* sp. PCC 6803 drastically alters amino acid composition and glycogen metabolism

Hiroko Iijima[1], *Yuka Nakaya*[1], *Ayuko Kuwahara*[1], *Masami Yokota Hirai*[1] and *Takashi Osanai*[1,2,3]*

[1] RIKEN Center for Sustainable Resource Science, Yokohama, Japan, [2] Advanced Low Carbon Technology Research and Development Program (ALCA), Japan Science and Technology Agency, Kawaguchi, Japan, [3] School of Agriculture, Meiji University, Tokyo, Japan

OPEN ACCESS

Edited by:
Youn-Il Park,
Chungnam National University,
South Korea

Reviewed by:
Gopal K. Pattanayak,
The University of Chicago, USA
Reinhard Korbinian Proels,
Technische Universität München,
Germany

***Correspondence:**
Takashi Osanai,
RIKEN Center for Sustainable Resource Science, 1-7-22 Suehiro-cho, Tsurumi-ku, Yokohama, Kanagawa 230-0045, Japan
takashi.osanai.aa@riken.jp

Specialty section:
This article was submitted to Microbiotechnology, Ecotoxicology and Bioremediation, a section of the journal Frontiers in Microbiology

Received: 19 February 2015
Accepted: 01 April 2015
Published: 22 April 2015

Citation:
Iijima H, Nakaya Y, Kuwahara A, Hirai MY and Osanai T (2015) Seawater cultivation of freshwater cyanobacterium Synechocystis sp. PCC 6803 drastically alters amino acid composition and glycogen metabolism. Front. Microbiol. 6:326. doi: 10.3389/fmicb.2015.00326

Water use assessment is important for bioproduction using cyanobacteria. For eco-friendly reasons, seawater should preferably be used for cyanobacteria cultivation instead of freshwater. In this study, we demonstrated that the freshwater unicellular cyanobacterium *Synechocystis* sp. PCC 6803 could be grown in a medium based on seawater. The *Synechocystis* wild-type strain grew well in an artificial seawater (ASW) medium supplemented with nitrogen and phosphorus sources. The addition of HEPES buffer improved cell growth overall, although the growth in ASW medium was inferior to that in the synthetic BG-11 medium. The levels of proteins involved in sugar metabolism changed depending on the culture conditions. The biosynthesis of several amino acids including aspartate, glutamine, glycine, proline, ornithine, and lysine, was highly up-regulated by cultivation in ASW. Two types of natural seawater (NSW) were also made available for the cultivation of *Synechocystis* cells, with supplementation of both nitrogen and phosphorus sources. These results revealed the potential use of seawater for the cultivation of freshwater cyanobacteria, which would help to reduce freshwater consumption during biorefinery using cyanobacteria.

Keywords: amino acids, artificial seawater, cyanobacteria, natural seawater, *Synechocystis*

Introduction

The use of oxygenic photosynthetic prokaryotes as cell factories to directly convert CO_2 and water into compounds of interests by light is required for the sustainable development of the society (Branco dos Santos et al., 2014). Cyanobacteria are a group of photosynthetic bacteria that undergo oxygenic photosynthesis and fix CO_2 via the Calvin-Benson cycle. The freshwater cyanobacterium *Synechocystis* sp. PCC 6803 (hereafter *Synechocystis* 6803) is the most widely studied species among cyanobacteria, owing to their abilities of natural transformation and fast growth (Yu et al., 2013). The production of valuable products such as alcohols, alkanes, bioplastics, fatty acids, and hydrogen has been achieved by genetically engineering *Synechocystis* 6803, indicating the potential use of this bacterium as a biocatalyst (Savakis and Hellingwerf, 2014). Recent advances in the

metabolome analysis of *Synechocystis* 6803 support this idea to promote the metabolic engineering of cyanobacteria (Osanai et al., 2011, 2014b).

A life cycle assessment concluded that algal cultivation requires a much larger amount of freshwater than do conventional crops, leading to high environmental impacts with algal biorefineries (Clarens et al., 2010). The utilization of seawater and/or wastewater as alternatives would reduce the freshwater requirement of algae and cyanobacteria cultivation. Another life cycle assessment indicated, however, that wastewater-based microalgal bioproduction also has large environmental impacts, due to the need to process the wastewater for algae growth (Mu et al., 2014). Thus, growth in seawater is preferable for bioproduction using microalgae and cyanobacteria (Savakis and Hellingwerf, 2014). However, there are not many studies on the use of seawater for cultivating model cyanobacteria except marine species.

Synechocystis 6803 is known to be a freshwater cyanobacterium that is able to grow under high salt (NaCl) conditions and a near-costal area in biofilms (Reed et al., 1985; Gram et al., 2002). An increase in NaCl induces the influx of Na^+ and Cl^- into the cells. This activates the Na^+/H^+ antiporter, which decreases the intracellular Na^+ concentration, and results in an increase in the K^+ concentration to compensate (Reed et al., 1985; Hagemann, 2011). *Synechocystis* 6803 cells then accumulate compatible solutes such as glucosylglycerol and sucrose to acclimate to the high salt conditions (Reed et al., 1985; Hagemann, 2011). These compatible solutes could be imported directly from the surrounding environment into the *Synechocystis* 6803 cells (Mikkat et al., 1996, 1997). The expression of genes encoding ribosomal proteins, chaperones, and enzymes for glucosylglycerol synthesis are up-regulated by 500 mM NaCl within 30 min, while the gene expression levels related to phycobilisomes, Photosystem I subunits, and desaturases are decreased (Kanesaki et al., 2002; Marin et al., 2004). Proteomic analysis has also demonstrated increased protein levels of glucosylglycerol biosynthesis, glucosylglycerol-phosphate synthase (GgpS) and glucosylglycerol-phosphate phosphatase (GgpP or StpA), chaperones (GroEL1, DnaK2, and GrpE), elongation factors, and general stress proteins (Fulda et al., 2006). Nevertheless, the relationship between salt conditions and metabolite levels in primary metabolism has not been studied in detail. Recent metabolomic analyses have indicated that the growth of *Synechocystis* 6803 is closely associated with sugar and amino acid metabolism (Osanai et al., 2014a,d).

In this study, we revealed that *Synechocystis* 6803 cells could grow in a seawater-based medium supplemented with nitrogen and phosphorus sources, and that the addition of HEPES buffer improved cell proliferation. Several amino acids were accumulated in high amounts in the artificial seawater (ASW) medium, revealing the altered primary metabolism that occurs during seawater cultivation.

Materials and Methods

Bacterial Strains and Culture Conditions

The glucose-tolerant (GT) strain of *Synechocystis* sp. PCC 6803, isolated by Williams (1988) and the GT-I strain among GT strains was used in this study (Kanesaki et al., 2012). For preculture, the GT cells were grown in modified BG-11 medium, which is BG-11_0 liquid medium containing 5 mM NH_4Cl [buffered with 20 mM 4-(2-hydroxyethyl)piperazine-1-ethanesulfonic acid (HEPES)-KOH, pH 7.8] (Rippka, 1988). Marine Art SF-1 (Osaka Yakken, Osaka, Japan) was used as the ASW medium and contained 22.1 g/L NaCl, 9.9 g/L $MgCl_2 \bullet 6H_2O$, 1.5 g/L $CaCl_2 \bullet 2H_2O$, 3.9 g/L Na_2SO_4, 0.61 g/L KCl, 0.19 g/L $NaHCO_3$, 96 mg/L KBr, 78 mg/L $Na_2B_4O_7 \bullet 10H_2O$, 13 mg/L $SrCl_2$, 3 mg/L NaF, 1 mg/L LiCl, 81 μg/L KI, 0.6 μg/L $MnCl_2 \bullet 4H_2O$, 2 μg/L $CoCl_2 \bullet 6H_2O$, 8 μg/L $AlCl_3 \bullet 6H_2O$, 5 μg/L $FeCl_3 \bullet 6H_2O$, 2 μg/L $Na_2WO_4 \bullet 2H_2O$, and 18 μg/L $(NH_4)_6Mo_7O_{24} \bullet 4H_2O$. Two natural seawater samples were used as cultivation media, designated as NSWS (Shimano-Tennensui, seawater around Ohshima, south island of Tokyo; provided by NIHON AQUARIUM, Tokyo, Japan) and NSWN (NAGEME10, seawater around Izu Peninsula; provided by Bluelab Co. Ltd., Shizuoka, Japan). Liquid cultures were bubbled with 1% (v/v) CO_2 in air and incubated at 30°C under continuous white light (∼50–70 μmol photons $m^{-2} \cdot s^{-1}$). Cell growth and densities were measured at OD_{730} with a Hitachi U-3310 spectrophotometer (Hitachi High-Tech., Tokyo, Japan). The pH values of the media were measured with the pH meter F-52 (HORIBA, Kyoto, Japan), using the supernatant of the cultures after centrifugation (5800 × *g* for 2 min).

Glycogen Measurement

Glycogen was quantified by the Biotechnology Center of Akita Prefectural University, Japan. Cells cultivated for 3 days were concentrated to an OD_{730} value of 6.0 in 1 mL of methanol, mixed for 10 min using a vortex mixer and then pelleted by centrifugation. The supernatant was transferred to a 1.5-mL tube and dried at 65°C. Cells were resuspended in 1 mL distilled water and incubated at 100°C for 40 min. 200 μL of cell suspension was transferred to a 1.5-mL tube and the resultant monosaccharides were enzymatically degraded with 100 μL glucoamylase solution (75 U/mL), and the resultant glucose was measured by estimating the changes in OD_{340} during hexokinase and glucose-6-phosphate dehydrogenase (G6PD) reactions.

Chlorophyll Measurement

Chlorophyll contents of the cells grown for 3 days were measured using a methanol extraction method (Grimme and Boardman, 1972). 1 mL of cell culture was transferred to a 1.5-mL tube and centrifuged (20500 × *g* for 2 min) and the supernatant was removed. Cells were suspended in 1 mL methanol and vortexed for 5 min. After placing 5 min, the cell suspensions were centrifuged (20500 × *g* for 2 min) and OD_{665} of the supernatants were quantified with a Hitachi U-3310 spectrophotometer.

Quantification of Intracellular Protein Levels

5 mL of cell culture was transferred to a 15-mL tube after cultivation for 3 days. The cell cultures were centrifuged (9000 × *g* for 2 min) and the supernatant was removed. Cells were suspended in 500 μL PBS-T (3.2 mM Na_2HPO_4, 0.5 mM KH_2PO_4, 1.3 mM KCl, 135 mM NaCl, and 0.05% Tween-20, pH 7.4) supplemented with the protease inhibitor Complete Mini (Roche Diagnostics, Rotkreuz, Switzerland; one tablet/30 mL and disrupted by sonication using VC-750 instrument (EYELA, Tokyo,

Japan). After centrifugation at 9000 × *g* for 5 min at 4°C, the protein concentration in the soluble fraction was measured using BCA Protein Assay Reagent (Thermo Scientific Hudson, NH, USA) and bovine serum albumin as a standard.

Antisera Production and Immunoblotting

We previously produced antisera against isoamylases [GlgX(slr0237), GlgX(slr1857)], glycogen phosphorylases [GlgP(sll1356), GlgP(slr1367)], glyceraldehyde-3-phosphate dehydrogenase (Gap2), G6PD, 6-phosphogluconate dehydrogenase (6PGD), and an RNA polymerase sigma factor SigE (Azuma et al., 2011; Osanai et al., 2011, 2013b). Antiserum against transaldolase (Tal) was produced by Sigma-Aldrich (St. Louis, Missouri, USA) using synthetic peptide NH_2-CHAYD LDGDGFITREEWAG-COOH. Antiserum against fructose-1,6-bisphosphate aldolase (FbaI, slr0943) was commercially produced by Tampaku Seisei Kogyo (Gunma, Japan). To produce anti-FbaI, glutathione S-transferase (GST)-fused FbaI proteins were first purified. The *fbaI* DNA fragment was amplified by PCR with KOD polymerase (Toyobo, Osaka, Japan) and the specific primers; 5′-ATGGGATCCCCATGATGACTCTCGAACCA-3′ and 5′-TGAGTCGACCTACGTAATCGATGCCTG-3′. The resultant DNA fragments were digested with *Bam*HI and *Xho*I (Takara Bio, Shiga, Japan) and cloned into the *Bam*HI-*Xho*I site of pGEX5X-1 (GE Healthcare Japan, Tokyo, Japan) using DNA Ligation Mix (Takara Bio). The integrity of the sequence was confirmed by sequencing. The plasmids were introduced into *Escherichia coli* BL21 Codon Plus(DE3)-RIPL cells (Agilent Technologies, Santa Clara, CA, USA) by transformation. The transformed cells were added to 2 L of Luria-Bertani medium and the cells were cultured overnight at 30°C in the presence of 10 μM isopropyl-β-D-thiogalactopyranoside (Wako Chemicals, Osaka, Japan). Purification of the GST-fused FbaI was performed as previously described (Osanai et al., 2009). Immunoblotting was performed according to the method described by Osanai et al. (2014c).

GC-MS Analysis for Amino Acids

Equal amounts of cells (50 mL of cell culture with OD_{730} = 1.0) were harvested by rapid filtration using a previously described method (Osanai et al., 2014c). Amino acids were quantified using a GCMS-QP2010Plus apparatus (Shimadzu, Kyoto, Japan) equipped with a 10-m × 0.25-mm ZB-AAA capillary gas chromatography column. The protocol used was as described previously (Osanai et al., 2014b).

Scanning Probe Microscopy

Cells grown in liquid medium were collected by centrifugation and the supernatants were discarded. The cells were resuspended in 1 mL of sterilized water and centrifuged (20,500 × *g* for 1 min) and the supernatant was again discarded. This process was repeated two more times and the cells were then resuspended in 1 mL of sterilized water. The cell suspension was spotted onto a metal plate and dried at 96°C for 1 min. The cells were observed with a scanning probe microscope (SPM-9700; Shimadzu) according to the manufacturer's instructions.

Results

Synechocystis 6803 Cultivation with Artificial Seawater Containing Nitrogen and Phosphorus Sources

Marine Art SF-1, a widely used ASW medium for the cultivation of marine bacteria and microalgae isolated from seawater (Yamane et al., 2013), was used for *Synechocystis* 6803 cultivation. The cultivation of wild-type cells was started with a the cell concentration of OD_{730} = 0.2. Cells in ASW without a nitrogen source (5 mM NH_4Cl) hardly grew (**Figure 1**). Cells in the

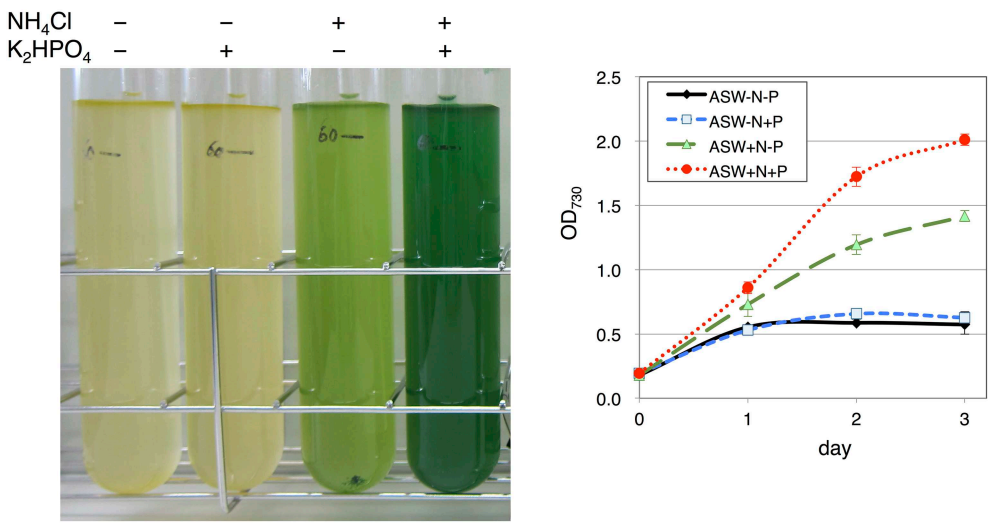

FIGURE 1 | Growth of wild-type glucose-tolerant (GT) *Synechocystis* sp. PCC 6803 cells in artificial seawater (ASW) medium. (Left) Cell cultures were photographed after cultivation for 3 days. (Right) Growth curve of the cells in ASW with/without nitrogen and phosphorus sources. N and P designate NH_4Cl and K_2HPO_4, respectively. Data represent means ± SD from three independent experiments.

presence of the nitrogen source but in the absence of a phosphorus source (0.22 mM K_2HPO_4) grew partially, reaching an OD_{730} value of 1.4 for 3 days of cultivation, showing a yellow-green color (**Figure 1**). In the presence of both nitrogen and phosphorus sources, the cell concentration reached an OD_{730} value of 2.0 by 3 days of cultivation, showing a green color (**Figure 1**).

Because 20 mM HEPES-KOH (pH 7.8) is usually added to the medium for cyanobacterial cultivation, we next tested the effect of this buffer on cell grown in the ASW medium. Unlike the cell growth in the ASW medium without HEPES buffer, which started to decrease after 2 days, the cells grew continuously in the presence of HEPES buffer (**Figure 2A**). We also compared the cell growth in ASW medium with that in a synthetic medium, BG-11. The cell density reached an OD_{730} value of 3.7 in the BG-11 medium after 3 days of cultivation, but reached only to a value of ∼2.5 in ASW containing nitrogen and phosphorus sources and HEPES buffer (**Figures 2B,C**). The pH values were around 7.0 in the BG-11 medium and in ASW with HEPES buffer, whereas the pH value was 5.0 in ASW without HEPES buffer (**Figure 2D**). Chlorophyll levels in the cells grown in ASW with HEPES buffer were higher than those in the other two conditions (**Figure 2E**). The soluble protein levels in the cells were quantified and both the protein levels of the cells grown under ASW conditions were 1.6 times of that in the cells grown in BG-11 medium (**Figure 2F**). Hereafter, cultivation in ASW medium indicates ASW medium containing both nitrogen and phosphorus sources.

Glycogen Content and Immunoblotting

Since the ASW and BG-11 media were found to produce a difference in cell growth, we estimated the difference of primary carbon metabolism according to growth conditions. Glycogen levels were first determined using the cells cultivated for 3 days in ASW with/without HEPES buffer or in BG-11 medium (**Table 1**). Glycogen levels in the cells grown in the ASW medium were similar irrespective of the presence of HEPES buffer (**Table 1**).

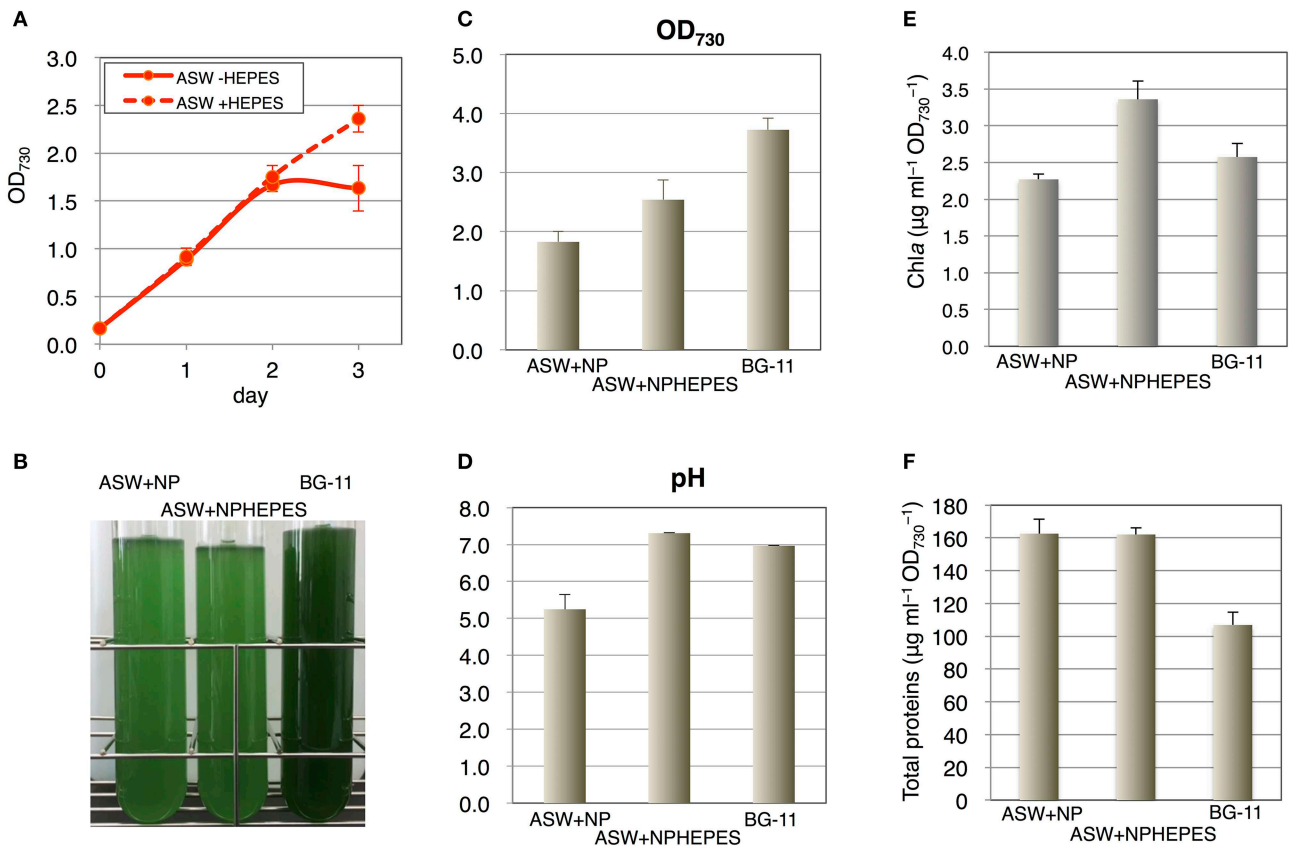

FIGURE 2 | Effect of HEPES buffer on the growth of wild-type glucose-tolerant (GT) *Synechocystis* sp. PCC 6803 cells in artificial seawater (ASW) medium. (A) Growth curve of the cells in ASW with nitrogen and phosphorus sources with/without 20 mM HEPES buffer (pH 7.8). Data represent means ± SD from three independent experiments. **(B)** Cell cultures were photographed after cultivation for 3 days. BG-11, BG-11 medium; NPHEPES, HEPES buffer with the nitrogen and phosphorous source in the form of NH_4Cl and K_2HPO_4, respectively. **(C)** OD_{730} of cell cultures after cultivation for 3 days. Data represent means ± SD from three independent experiments. **(D)** pH of cell cultures after cultivation for 3 days. Data represent means ± SD from three independent experiments. **(E)** Chlorophyll a levels of cell cultures after cultivation for 3 days. Data represent means ± SD from four independent experiments. **(F)** Intracellular soluble protein levels from the cells cultured for 3 days. Proteins were extracted by sonication and debris were removed by centrifugation. Total protein levels in the soluble fractions were quantified by BCA method. Data represent means ± SD from four independent experiments.

Glycogen levels in the cells grown in BG-11 medium was 1.7 times of that in the cells grown in ASW medium (**Table 1**).

The protein levels of glycogen catabolic enzymes, GlgP(sll1356), GlgP(slr1367), GlgX(slr0237), and GlgX(slr1857), were quantified in the cells grown for 3 days under the three medium conditions. GlgP(sll1356) protein levels in ASW with HEPES buffer and in BG-11 medium were almost 1.5–1.8 times the levels in ASW without HEPES buffer, whereas the levels of GlgP(slr1367) were similar among the three media (**Figure 3**). The levels of the GlgXs were fairly different among the three medium conditions. GlgX(slr0237) levels were higher in the ASW-based medium, particularly with HEPES buffer (**Figure 3**).

TABLE 1 | Levels of glycogen after cultivation for 3 days.

ASW + NP	ASW + NPHEPES	BG-11
100 ± 52.3	102.8 ± 55.0	166.5 ± 28.4

Data represent means ± SD from six independent experiments. Levels were calibrated relative to those from glucose-tolerant Synechocystis sp. PCC 6803 cells grown in ASW without HEPES buffer (set at 100%). ASW, artificial seawater; BG-11, BG-11 medium; NP, nitrogen and phosphorus sources in the form of NH_4Cl and K_2HPO_4, respectively; NPHEPES, HEPES buffer with nitrogen and phosphorous sources. Absolute values are listed in Table S2.

On the contrary, GlgX(slr1857) level was more abundant in BG-11 medium (**Figure 3**).

The five enzymes of glycolysis and the oxidative pentose phosphate (OPP) pathway and SigE [an RNA polymerase sigma factor activating sugar catabolism (Osanai et al., 2011)] were subsequently quantified. The protein levels of FbaI, Gap2 and 6PGD were similar among the three medium conditions tested (**Figure 4**). On the other hand, the G6PD levels was lower in ASW without HEPES buffer than under the other two conditions (**Figure 4**). The protein levels of Tal were higher in the cells grown in ASW with/without HEPES buffer than in BG-11 medium (**Figure 4**). SigE protein levels were higher in the order of BG-11 > ASW with HEPES buffer > ASW without HEPES buffer (**Figure 4**).

Amino Acid Profiles in the Different Media

To further clarify the effect of ASW on primary metabolism, the amino acid levels in the cells cultivated for 3 days under the three medium conditions were determined by GC-MS. The levels of proline, asparagine, aspartate, methionine, glutathione, glutamate, and glutamine in the cell grown in ASW with HEPES buffer were higher than those in the cells grown in BG-11 medium, whereas the levels of alanine, valine, leucine, isoleucine, threonine, serine, phenylalanine, and tyrosine were

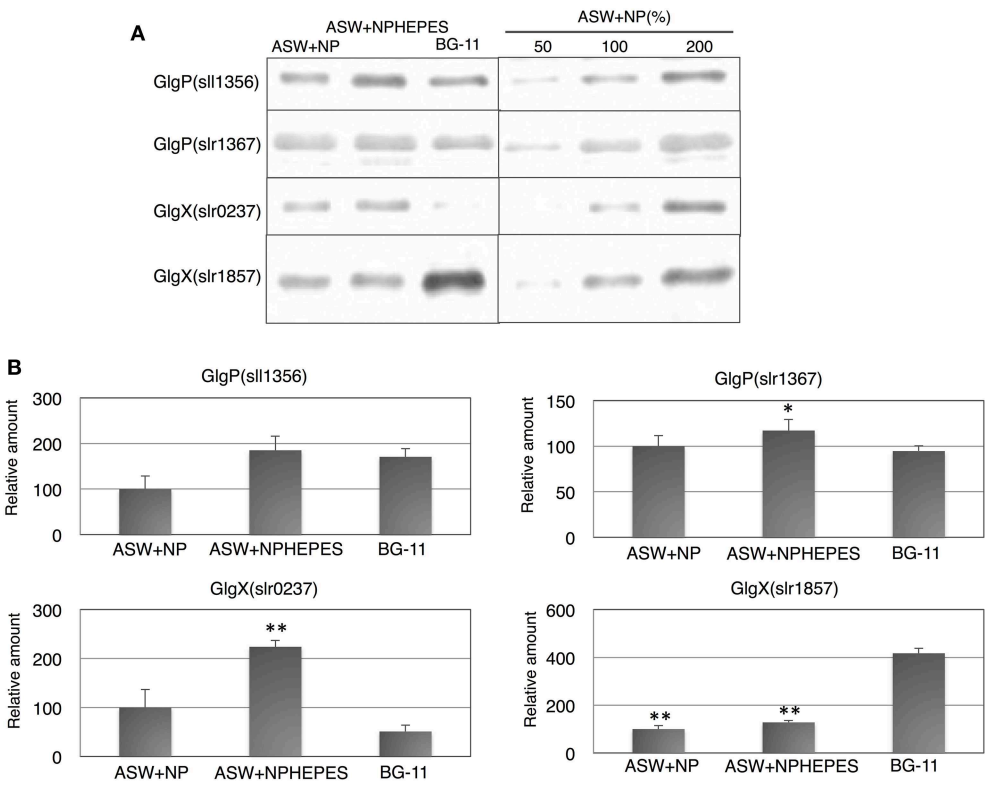

FIGURE 3 | Protein levels of four glycogen catabolic enzymes. Immunoblotting was performed with total protein from cells grown under three different medium conditions for 3 days. **(A)** One of representative data was shown. **(B)** Data represent means ± SD from three independent experiments. Levels were calibrated relative to those of the glucose-tolerant strain grown in artificial seawater (ASW) without HEPES buffer (set at 100%). N and P designate NH_4Cl and K_2HPO_4, respectively. BG-11, BG-11 medium. Asterisks (* or **) indicate that differences between proteins in the cells grown in ASW and BG-11 media using Student's *t*-test were statistically significant at $P < 0.05$ or $P < 0.005$, respectively.

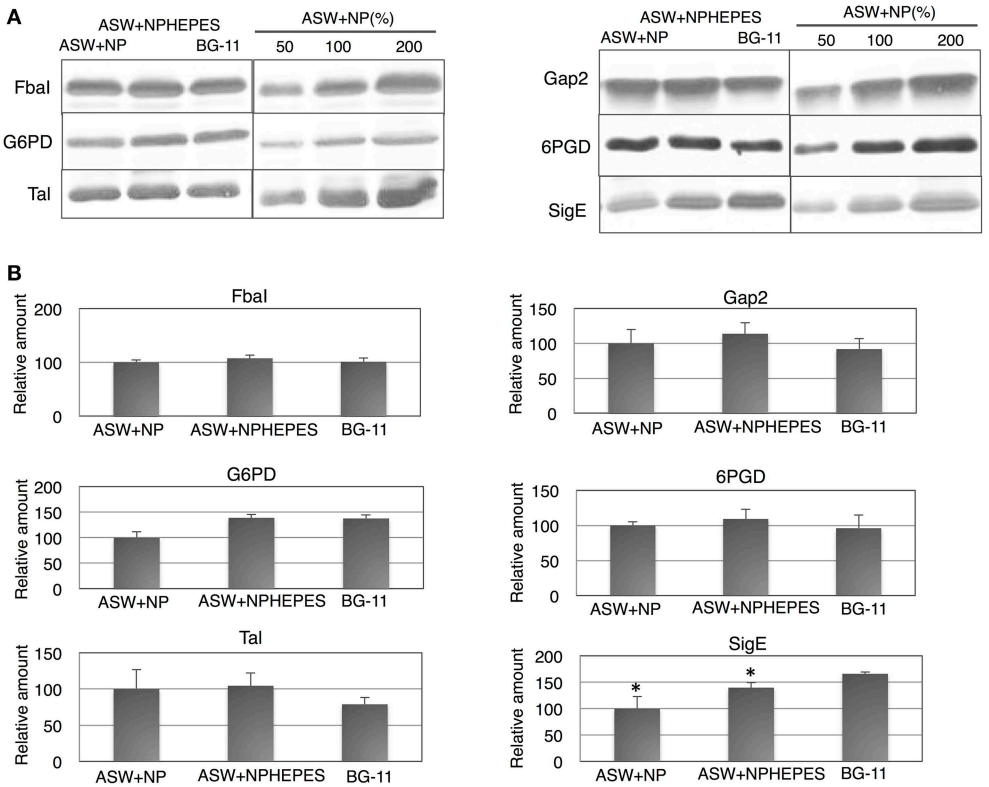

FIGURE 4 | Protein levels of for glucose catabolic enzymes and SigE. Immunoblotting was performed with total protein from cells grown under three different medium conditions for 3 days. **(A)** One of representative data was shown. **(B)** Data represent means ± SD from three independent experiments. Levels were calibrated relative to those of the glucose-tolerant strain grown in artificial seawater (ASW) without HEPES buffer (set at 100%). N and P designate NH_4Cl and K_2HPO_4, respectively. BG-11, BG-11 medium; FbaI, fructose-1,6-bisphosphate aldolase; Gap2, glyceraldehyde-3-phosphate aldolase catalyzing the anabolic reaction; G6PD, glucose-6-phosphate dehydrogenase; 6PGD, 6-phosphogluconate dehydrogenase; Tal, transaldolase; SigE, RNA polymerase group 2 sigma factor. Asterisks (*) indicate that differences between proteins in the cells grown in ASW and BG-11 media using Student's *t*-test were statistically significant at $P < 0.05$, respectively.

lower (**Figure 5** and Table S1). The levels of alanine, glycine, proline, asparagine, aspartate, methionine, glutamine, ornithine, lysine, histidine, and tryptophan in cells grown in ASW without HEPES buffer were higher than those in the cells grown in BG-11 medium, whereas the levels of valine, leucine, isoleucine, serine, glutathione, phenylalanine, and tyrosine were lower (**Figure 5**).

Morphological Changes in Artificial Seawater

Cell morphologies were observed by scanning probe microscopy to clarify the physiological phenotypes elicited by ASW cultivation. Whereas the cell structure and surface appearance were similar among the three medium conditions, the cell diameters were altered by ASW cultivation (**Figure 6**). Most of the wild-type cells in BG-11 medium were within 1.0–2.0 μm diameters (**Figure 6**). The majority of the cells grown in ASW with HEPES buffer had a diameter of 1.5–2.0 μm diameters but the distribution of cell diameters shifted to the 2.0–2.5 μm range (**Figure 6**). Many of the cells grown in ASW without HEPES buffer were also 1.5–2.0 μm in diameters, and showed a wider distribution of cell diameters from 1.0 to 3.0 μm (**Figure 6**).

Growth in Natural Seawater

Finally, the growth of the cells using natural seawater was tested. Two types of natural seawater, NSWS (from Ohshima, Japan) and NSWN (from Izu Peninsula, Japan), were purchased and tested for the effect of nitrogen and phosphorus sources. Similar to ASW, with both NSW samples, the cells grew only partially in the presence of the nitrogen sources, but they grew well when both nitrogen and phosphorus sources were present (**Figures 7A,B**). The cell density reached an OD_{730} value of ∼1.8 in NSWN, but only reached the value of 1.3 in NSWS after 3 days of cultivation (**Figures 7A,B**). The addition of HEPES buffer hardly improved the growth in NSWN medium supplemented with nitrogen and phosphorus sources (**Figure 7C**).

Discussion

The current results indicate the potential of seawater usage for cultivation of the freshwater cyanobacterium *Synechocystis* 6803. Although the cell growth in the seawater-based medium was still inferior to that in synthetic medium, the levels of several amino acids were highly up-regulated by ASW, demonstrating

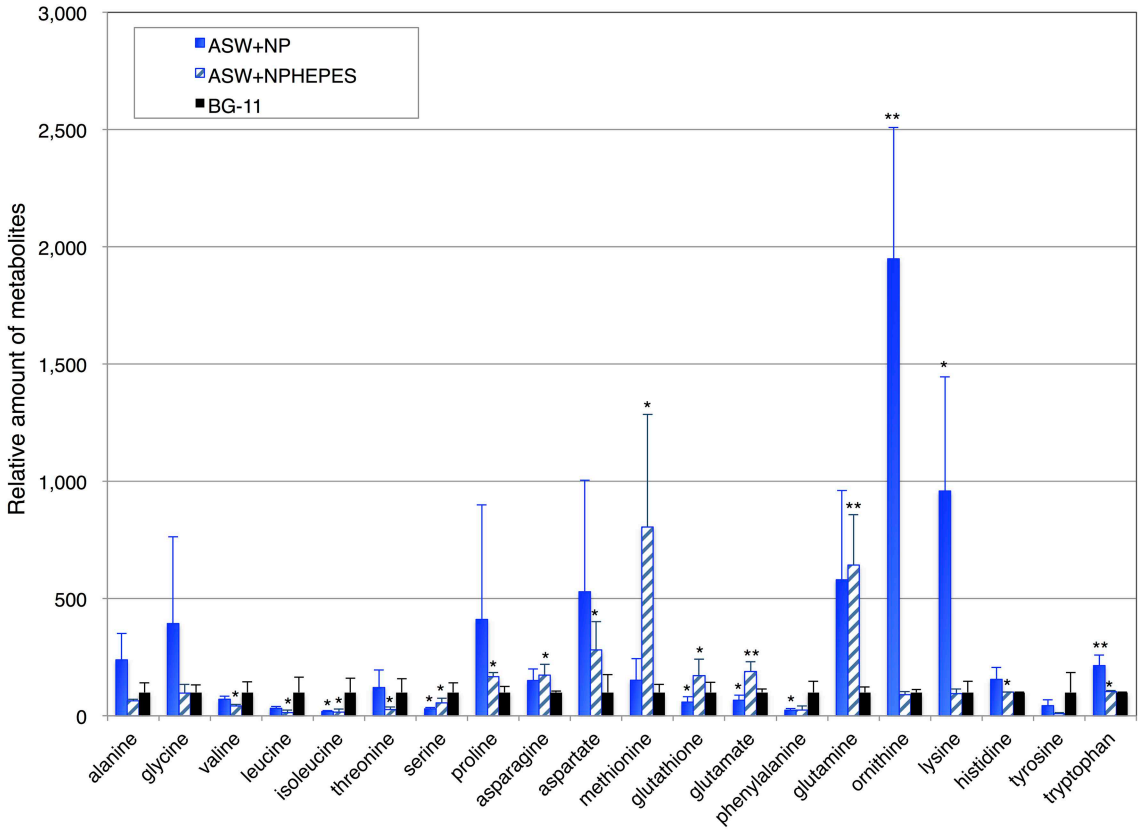

FIGURE 5 | Levels of 18 amino acids, and ornithine and glutathione. Data represent means ± SD from five independent experiments. Levels were calibrated relative to that in cells grown in BG-11 medium (set at 100%). BG-11, BG-11 medium; ASW, artificial seawater medium; NPHEPES, HEPES buffer with the nitrogen and phosphorous source in the form of NH_4Cl and K_2HPO_4, respectively. Student's *t*-test was performed and asterisks indicate statistically significant differences between BG-11 and artificial seawater with or without HEPES buffer (ASWNP or ASW NPHEPES, respectively) (*$P < 0.05$, **$P < 0.005$).

the advantage of seawater cultivation of cyanobacteria for bioproduction.

It has been revealed that *Synechocystis* 6803 cells are able to grow in an ASW medium with anaerobic digestion effluent (ADE) (Cai et al., 2013). The addition of 3% ADE to ASW gave the highest biomass productivity, but increased addition of ADE lowered the biomass and lipid productivities of *Synechocystis* 6803 (Cai et al., 2013). Other microalga such as *Nannochloropsis salina* also grew in ASW medium with ADE, but they could not grow in ASW supplemented with commercial medium containing nitrate, phosphate, and trace metals (Sheets et al., 2014). Here, we succeeded in cultivating *Synechocystis* 6803 in a seawater-based medium by adding nitrogen and phosphorus sources derived from purified chemicals (**Figures 1**, **7**). Nitrogen was particularly indispensable for *Synechocystis* 6803 culture in both ASW and NSW media (**Figures 1**, **7**). Furthermore, the addition of HEPES buffer improved the cell growth in ASW (**Figure 2**), revealing the importance of pH control for the growth of cyanobacteria in a seawater-based medium. *Synechocystis* 6803 growth in ASW was inferior to that in BG-11 medium (**Figures 2B,C**). Previous study revealed that *Synechocystis* cells can proliferate under 450 mM NaCl, but the growth retarded 60∼70% of the cells under low salt conditions (Ferjani et al., 2003). This result is consistent with the data of **Figure 2C**. Our analysis demonstrated that the protein and metabolite profiles were completely different between these two medium conditions (**Figures 3**–**5**). Chlorophyll levels in the cells grown in ASW were similar to or rather higher than those in the cells grown in BG-11 (**Figure 2E**). These results indicate that decrease in chlorophyll levels is not the cause of poor growth in ASW. Intracellular soluble protein and glycogen levels exhibited negative correlation in our experimental conditions (**Figure 2F** and **Table 1**). NSW experiment indicates not only pH but also unknown factors limited the *Synechocystis* growth in the NSW medium (**Figure 7**), and further analysis is required to reveal the physiological impacts by seawater cultivation.

Immunoblotting analysis revealed that enzymes involved in the primary metabolism switch were associated with the culture conditions (**Figures 3**, **4**), emphasizing a variety of metabolic enzymes encoded in the *Synechocystis* 6803 genome. The levels of the two GlgXs were particularly different between ASW-based and BG-11 media (**Figure 3**), indicating that GlgX(slr0237) may

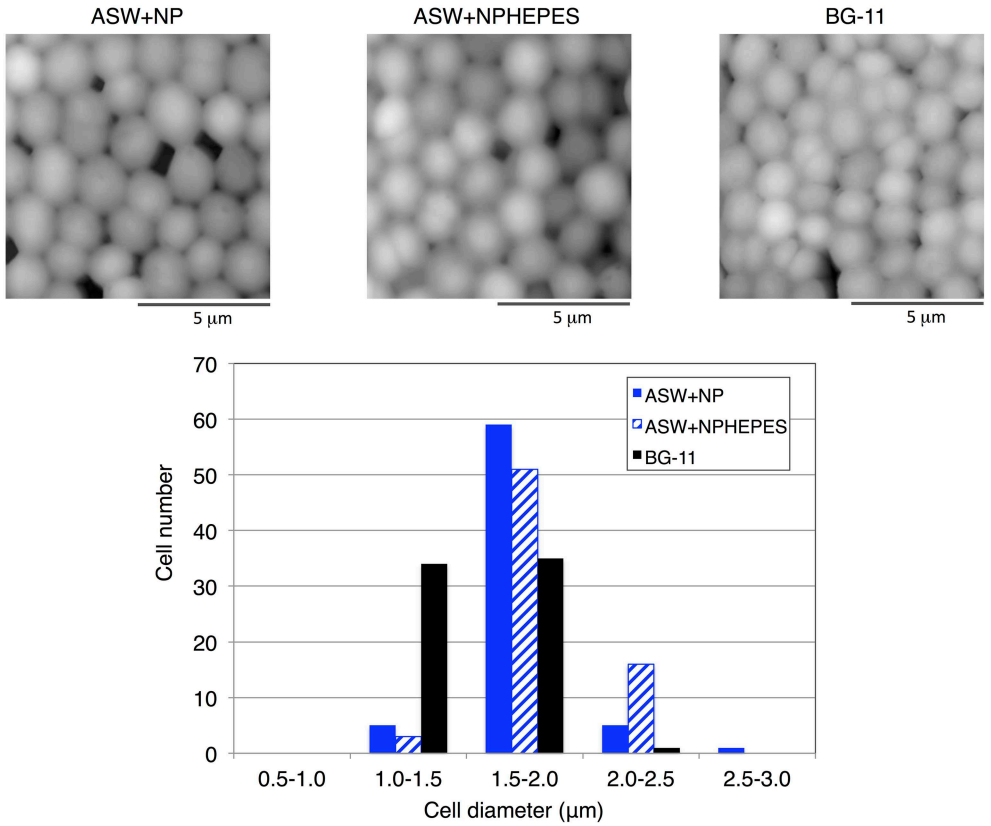

FIGURE 6 | Scanning probe micrographs of the wild-type glucose-tolerant *Synechocystis* sp. PCC 6803 cells after cultivation for 3 days under three medium conditions. The diameter of each of 70 cells was measured.

be a major isoamylase under high salt conditions. Recent omics analyses have revealed that transcript and protein levels related to primary sugar metabolism are widely altered by salt stress (Pandhal et al., 2009a; Hagemann, 2011). Transcriptome analysis has shown that the expression levels of three genes coding for proteins in sugar metabolism (viz., *pfkA*, encoding phosphofructokinase; *fbaII*, encoding fructose-1,6-bisphosphate aldolase class II; and *rpe*, encoding pentose-5-phosphate-3-epimerase) were up-regulated after salt acclimation for 24 h (Marin et al., 2004). Protein levels of glycogen phosphorylase (GlgP, slr1367), phosphoglucomutase (Pgm, sll0726), Rpe, Tal, FbaII, glucose-1-phosphate adenylyltransferase (GlgC, slr1176), and phosphoglycerate kinase (Pgk, slr0394) increased more than two-fold in cells salt-acclimated for 5 days (Fulda et al., 2006). A system biology approach based on proteomic data suggested that glycogen catabolism and glycolysis are up-regulated in salt-adapted cells, while the OPP pathway is down-regulated (Pandhal et al., 2009a,b). Thus, primary metabolism, particularly sugar metabolism, is important for salt acclimation by *Synechocystis* 6803. The protein levels of SigE, an activator of gene expression of glycogen catabolic and the OPP pathway enzymes, were higher in BG-11 than in ASW media (**Figure 4**). However, only G6PD protein levels were positively correlated with the SigE protein levels (**Figure 4**). The glycogen levels were also not correlated with SigE protein levels (**Table 1**). These results suggest the complicated regulatory mechanism determining the protein and metabolite levels under ASW conditions. Previous studies showed that mutation of sugar metabolism altered cell sizes and structures (Singh and Sherman, 2005; Osanai et al., 2013a), and therefore, the wide distribution of cell diameters under ASW cultivation (**Figure 6**) may be caused by changes in primary metabolism, aside from the salt concentration in the medium.

Amino acids are classified into six families according to their biosynthetic pathways (Umbarger, 1978). Glycine is a precursor of glycine-betaine, one of the compatible solutes accumulated under high salt conditions, and proline is a probable compatible solute in cyanobacteria (Hagemann, 2011). Proline accumulation in ASW with/without HEPES buffer may be due to the increase in salt concentration in the medium (**Figure 5**). The levels of four pyruvate family amino acids (isoleucine, valine, leucine, and alanine) were lower in cells grown in ASW with HEPES buffer than those in BG-11 medium, indicating that pyruvate biosynthesis may be altered by ASW cultivation. Previous metabolomic analysis showed that pyruvate in *Synechocystis* 6803 was exhausted under dark conditions (Osanai et al., 2014d), suggesting that the pyruvate pool size in this cyanobacterium is small and easily exhausted under stress conditions. Metabolomic analysis showed a negative correlation between salt stress and serine,

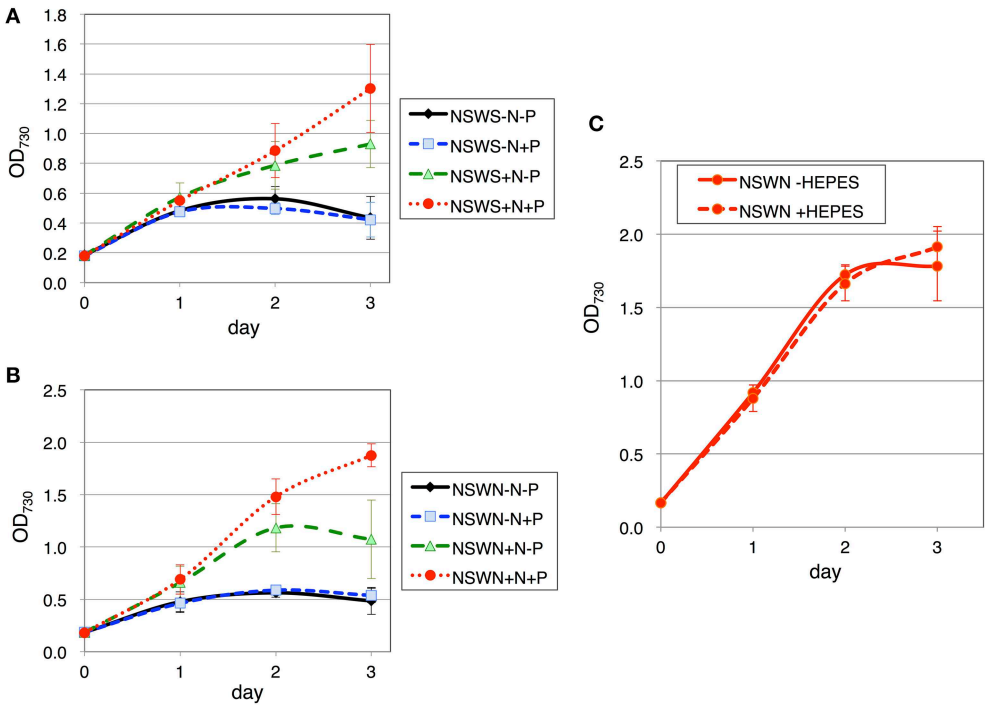

FIGURE 7 | Growth of wild-type glucose-tolerant *Synechocystis* sp. PCC 6803 cells in two natural seawater (NSW) media. Growth curve of the cells in **(A)** NSWS (Shimano-Tennensui, seawater from Oshimo, Japan) and **(B)** NSWN (NAGEME10, seawater from the Izu Peninsula, Japan) with/without nitrogen and phosphorus sources. N and P designate NH_4Cl and K_2HPO_4, respectively. Data represent means ± SD from three independent experiments. **(C)** Growth curve of the cells in NSWN supplemented with nitrogen and phosphorus sources, with/without 20 mM HEPES buffer (pH 7.8). Data represent means ± SD from three independent experiments.

valine, threonine, isoleucine, and tyrosine (Wang et al., 2014). That correlation study agreed well with our results, in that lower levels of serine, valine, threonine, isoleucine, and tyrosine were found in the cells grown in ASW with HEPES buffer than those in BG-11 medium (**Figure 5**). Alanine and glutamine were found to correlate positively with salt stress (Wang et al., 2014), a finding consistent with our results (**Figure 5**). Therefore, the differences in amino acid profiles among three medium conditions can be partly explained by the salt conditions. However, there were large differences in amino acid profiles between ASW with and ASW without HEPES buffer, suggesting that other factors, such as pH and cell growth, may affect the amino acid profiles. Poly-lysine production in *Streptomyces* sp. M-Z18 increased by acidic pH shock (Ren et al., 2015), and thus, decrease in pH may be cause of increase in lysine in the cells grown in ASW without HEPES buffer. The values of standard deviation of amino acid levels in the cells cultivated in ASW without HEPES were larger than the other two conditions (**Figure 5**), which may reflect less growth in ASW without HEPES buffer after 3-day cultivation. Future study to reveal the cause–result effect in seawater-based media will explain the changes in primary metabolism and growth of cyanobacteria.

Acknowledgments

This work was supported by the Ministry of Education, Culture, Sports, Science, and Technology, Japan; by a grant to TO by funds from ALCA (Project name "Production of cyanobacterial succinate by the genetic engineering of transcriptional regulators and circadian clocks") from the Japan Science and Technology Agency, and CREST from the Japan Science and Technology Agency.

Supplementary Material

The Supplementary Material for this article can be found online at: http://journal.frontiersin.org/article/10.3389/fmicb.2015.00326/abstract

References

Azuma, M., Osanai, T., Hirai, M. Y., and Tanaka, K. (2011). A response regulator Rre37 and an RNA polymerase sigma factor SigE represent two parallel pathways to activate sugar catabolism in a cyanobacterium *Synechocystis* sp. PCC 6803. *Plant Cell Physiol.* 52, 404–412. doi: 10.1093/pcp/pcq204

Branco dos Santos, F., Du, W., and Hellingwerf, K. J. (2014). *Synechocystis*: not just a plug-bug for CO_2, but a green *E. coli*. *Front. Bioeng. Biotecchnol.* 2:36. doi: 10.3389/fbioe.2014.00036

Cai, T., Ge, X., Park, S. Y., and Li, Y. (2013). Comparison of *Synechocystis* sp. PCC6803 and *Nannochloropsis salina* for lipid production using artificial seawater and nutrients from anaerobic digestion

effluent. *Bioresour. Technol.* 144, 255–260. doi: 10.1016/j.biortech.2013.06.101

Clarens, A. F., Resurreccion, E. P., White, M. A., and Colosi, L. M. (2010). Environmental life cycle comparison of algae to other bioenergy feedstocks. *Environ. Sci. Technol.* 44, 1813–1819. doi: 10.1021/es902838n

Ferjani, A., Mustardy, L., Sulpice, R., Marin, K., Suzuki, I., Hagemann, M., et al. (2003). Glucosylglycerol, a compatible solute, sustains cell division under salt stress. *Plant Physiol.* 131, 1628–1637. doi: 10.1104/pp.102.017277

Fulda, S., Mikkat, S., Huang, F., Huckauf, J., Marin, K., Norling, B., et al. (2006). Proteome analysis of salt stress response in the cyanobacterium *Synechocystis* sp. strain PCC 6803. *Proteomics* 6, 2733–2745. doi: 10.1002/pmic.200500538

Gram, L., Grossart, H.-P., Schlingloff, A., and Kiorboe, T. (2002). Possible quorum sensing in marine snow bacteria: production of acylated homoserine lactones by *Roseobacter* strains isolated from marine snow. *Appl. Environ. Microbiol.* 68, 4111–4116. doi: 10.1128/AEM.68.8.4111-4116.2002

Grimme, L. H., and Boardman, N. K. (1972). Photochemical activities of a particle fraction P1 obtained from the green alga *Chlorella fusca*. *Biochem. Biophys. Res. Commun.* 49, 1617–1623. doi: 10.1016/0006-291X(72)90527-X

Hagemann, M. (2011). Molecular biology of cyanobacterial salt acclimation. *FEMS Microbiol. Rev.* 35, 87–123. doi: 10.1111/j.1574-6976.2010.00234.x

Kanesaki, Y., Shiwa, Y., Tajima, N., Suzuki, M., Watanabe, S., Sato, N., et al. (2012). Identification of substrain-specific mutations by massively parallel whole-genome resequencing of *Synechocystis* sp. PCC 6803. *DNA Res.* 19, 67–79. doi: 10.1093/dnares/dsr042

Kanesaki, Y., Suzuki, I., Allakhverdiev, S. I., Mikami, K., and Murata, N. (2002). Salt stress and hyperosmotic stress regulate the expression of different sets of genes in *Synechocystis* sp. PCC 6803. *Biochem. Biophys. Res. Commun.* 290, 339–348. doi: 10.1006/bbrc.2001.6201

Marin, K., Kanesaki, Y., Los, D. A., Murata, N., Suzuki, I., and Hagemann, M. (2004). Gene expression profiling reflects physiological processes in salt acclimation of *Synechocystis* sp. strain PCC 6803. *Plant Physiol.* 136, 3290–3300. doi: 10.1104/pp.104.045047

Mikkat, S., Effmert, U., and Hagemann, M. (1997). Uptake and use of the osmoprotective compounds trehalose, glucosylglycerol, and sucrose by the cyanobacterium *Synechocystis* sp. PCC6803. *Arch. Microbiol.* 167, 112–118. doi: 10.1007/s002030050423

Mikkat, S., Hagemann, M., and Schoor, A. (1996). Active transport of glucosylglycerol is involved in salt adaptation of the cyanobacterium *Synechocystis* sp. strain PCC 6803. *Microbiology* 142, 1725–1732. doi: 10.1099/13500872-142-7-1725

Mu, D., Min, M., Krohn, B., Mullins, K. A., Ruan, R., and Hill, J. (2014). Life cycle environmental impacts of wastewater-based algal biofuels. *Environ. Sci. Technol.* 48, 11696–11704. doi: 10.1021/es5027689

Osanai, T., Imashimizu, M., Seki, A., Sato, S., Tabata, S., Imamura, S., et al. (2009). ChlH, the H subunit of the Mg-chelatase, is an anti-sigma factor for SigE in *Synechocystis* sp. PCC 6803. *Proc. Natl. Acad. Sci. USA* 106, 6860–6865. doi: 10.1073/pnas.0810040106

Osanai, T., Kuwahara, A., Iijima, H., Toyooka, K., Sato, M., Tanaka, K., et al. (2013a). Pleiotropic effect of *sigE* over-expression on cell morphology, photosynthesis and hydrogen production in *Synechocystis* sp. PCC 6803. *Plant J.* 76, 456–465. doi: 10.1111/tpj.12310

Osanai, T., Numata, K., Oikawa, A., Kuwahara, A., Iijima, H., Doi, Y., et al. (2013b). Increased bioplastic production with an RNA polymerase sigma factor SigE during nitrogen starvation in *Synechocystis* sp. PCC 6803. *DNA Res.* 20, 525–535. doi: 10.1093/dnares/dst028

Osanai, T., Oikawa, A., Azuma, M., Tanaka, K., Saito, K., Hirai, M. Y., et al. (2011). Genetic engineering of group 2 sigma factor SigE widely activates expression of sugar catabolic genes in *Synechocystis* species PCC 6803. *J. Biol. Chem.* 286, 30962–30971. doi: 10.1074/jbc.M111.231183

Osanai, T., Oikawa, A., Iijima, H., Kuwahara, A., Asayama, M., Tanaka, K., et al. (2014a). Metabolomic analysis reveals rewiring of *Synechocystis* sp. PCC 6803 primary metabolism by *ntcA* overexpression. *Environ. Microbiol.* 16, 3304–3317. doi: 10.1111/1462-2920.12554

Osanai, T., Oikawa, A., Numata, K., Kuwahara, A., Iijima, H., Doi, Y., et al. (2014b). Pathway-level acceleration of glycogen catabolism by a response regulator in the cyanobacterium *Synechocystis* species PCC 6803. *Plant Physiol.* 164, 1831–1841. doi: 10.1104/pp.113.232025

Osanai, T., Oikawa, A., Shirai, T., Kuwahara, A., Iijima, H., Tanaka, K., et al. (2014c). Capillary electrophoresis-mass spectrometry reveals the distribution of carbon metabolites during nitrogen starvation in *Synechocystis* sp. PCC 6803. *Environ. Microbiol.* 16, 512–524. doi: 10.1111/1462-2920.12170

Osanai, T., Shirai, T., Iijima, H., Kuwahara, A., Suzuki, I., Kondo, A., et al. (2014d). Alteration of cyanobacterial sugar and amino acid metabolism by overexpression hik8, encoding a KaiC-associated histidine kinase. *Environ. Microbiol.* doi: 10.1111/1462-2920.12715. [Epub ahead of print].

Pandhal, J., Noirel, J., Wright, P. C., and Biggs, C. A. (2009a). A systems biology approach to investigate the response of *Synechocystis* sp. PCC 6803 to a high salt environment. *Saline Syst.* 5:8. doi: 10.1186/1746-1448-5-8

Pandhal, J., Ow, S. Y., Wright, P. C., and Biggs, C. A. (2009b). Comparative proteomics study of salt tolerance between a nonsequenced extremely halotolerant cyanobacterium and its mildly halotolerant relative using *in vivo* metabolic labeling and *in vitro* isobaric labeling. *J. Proteome. Res.* 8, 818–828. doi: 10.1021/pr800283q

Reed, H. R., Warr, S. R. C., Richardson, D. L., Moor, D. J., and Swewart, W. D. P. (1985). Multiphasic osmotic adjustment in a euryhaline cyanobacterium. *FEMS Microbiol. Lett.* 28, 225–229. doi: 10.1111/j.1574-6968.1985.tb00796.x

Ren, X. D., Chen, X. S., Zeng, X., Wang, L., Tang, L., and Mao, Z. G. (2015). Acidic pH shock induced overproduction of ε-poly-L-lysine in fed-batch fermentation by Streptomyces sp. M-Z18 from agro-industrial by-products. *Bioprocess Biosyst. Eng.* doi: 10.1007/s00449-015-1354-2. [Epub ahead of print].

Rippka, R. (1988). Isolation and purification of cyanobacteria. *Meth. Enzymol.* 167, 3–27. doi: 10.1016/0076-6879(88)67004-2

Savakis, P., and Hellingwerf, K. J. (2014). Engineering cyanobacteria for direct biofuel production from CO_2. *Curr. Opin. Biotechnol.* 33, 8–14. doi: 10.1016/j.copbio.2014.09.007

Sheets, J. P., Ge, X., Park, S. Y., and Li, Y. (2014). Effect of outdoor conditions on *Nannochloropsis salina* cultivation in artificial seawater using nutrients from anaerobic digestion effluent. *Bioresour. Technol.* 152, 154–161. doi: 10.1016/j.biortech.2013.10.115

Singh, A. K., and Sherman, L. A. (2005). Pleiotropic effect of a histidine kinase on carbohydrate metabolism in *Synechocystis* sp. strain PCC 6803 and its requirement for heterotrophic growth. *J. Bacteriol.* 187, 2368–2376. doi: 10.1128/JB.187.7.2368-2376.2005

Umbarger, H. E. (1978). Amino acid biosynthesis and its regulation. *Ann. Rev. Biochem.* 47, 533–606. doi: 10.1146/annurev.bi.47.070178.002533

Wang, J., Zhang, X., Shi, M., Gao, L., Niu, X., Te, R., et al. (2014). Metabolomic analysis of the salt-sensitive mutants reveals changes in amino acid and fatty acid composition important to long-term salt stress in *Synechocystis* sp. PCC 6803. *Funct. Integr. Genomics* 14, 431–440. doi: 10.1007/s10142-014-0370-7

Williams, J. G. K. (1988). Construction of specific mutations in photosystem II photosynthetic reaction center by genetic engineering methods in *Synechocystis* 6803. *Methods Enzymol.* 167, 766–778.

Yamane, K., Matsuyama, S., Igarashi, K., and Kuwabara, T. (2013). Pyrolytic generation of petroleum crude oils from the marine phytomicroalgal Coccolithophore *Emiliania huxleyi* (Haptophyta) and preparation of *n*-alkane-rich biofuel. *Energy Fuels* 27, 7470–7479. doi: 10.1021/ef401618t

Yu, Y., You, L., Liu, D., Hollinshead, W., Tang, Y. J., and Zhang, F. (2013). Development of *Synechocystis* sp. PCC 6803 as a phototrophic cell factory. *Mar. Drugs* 11, 2894–2916. doi: 10.3390/md11082894

Conflict of Interest Statement: The authors declare that the research was conducted in the absence of any commercial or financial relationships that could be construed as a potential conflict of interest.

frontiers in
MICROBIOLOGY

ORIGINAL RESEARCH ARTICLE
published: 24 February 2015
doi: 10.3389/fmicb.2015.00054

The small molecule fenpropimorph rapidly converts chloroplast membrane lipids to triacylglycerols in *Chlamydomonas reinhardtii*

Hanul Kim[1], Sunghoon Jang[1], Sangwoo Kim[1], Yasuyo Yamaoka[1], Daewoong Hong[1], Won-Yong Song[1], Ikuo Nishida[2†], Yonghua Li-Beisson[3†] and Youngsook Lee[4]*†

[1] *Division of Molecular and Life Sciences, Pohang University of Science and Technology, Pohang, South Korea*
[2] *Division of Life Science, Graduate School of Science and Engineering, Saitama University, Saitama, Japan*
[3] *Department of Plant Biology and Environmental Microbiology, Commissariat à l'Énergie Atomique et aux Énergies Alternatives – Centre National de la Recherche Scientifique – Aix-Marseille University, Saint-Paul-Lez-Durance, France*
[4] *POSTECH-UZH Global Research Laboratory, Division of Integrative Biology and Biotechnology, Pohang University of Science and Technology, Pohang, South Korea*

Edited by:
Youn-Il Park, Chungnam National University, South Korea

Reviewed by:
Jae-Hyeok Lee, University of British Columbia, Canada
Byeong-Ryool Jeong, Korea Advanced Institute of Science and Technology, South Korea

****Correspondence:***
Youngsook Lee, POSTECH-UZH Global Research Laboratory, Division of Integrative Biology and Biotechnology, Pohang University of Science and Technology, 77 Cheongam-Ro, Nam-Gu, Pohang 790-784, South Korea
e-mail: ylee@postech.ac.kr

†These authors have contributed equally to this work.

Concern about global warming has prompted an intense interest in developing economical methods of producing biofuels. Microalgae provide a promising platform for biofuel production, because they accumulate high levels of lipids, and do not compete with food or feed sources. However, current methods of producing algal oil involve subjecting the microalgae to stress conditions, such as nitrogen deprivation, and are prohibitively expensive. Here, we report that the fungicide fenpropimorph rapidly causes high levels of neutral lipids to accumulate in *Chlamydomonas reinhardtii* cells. When treated with fenpropimorph (10 μg mL^{-1}) for 1 h, *Chlamydomonas* cells accumulated at least fourfold the amount of triacylglycerols (TAGs) present in the untreated control cells. Furthermore, the quantity of TAGs present after 1 h of fenpropimorph treatment was over twofold higher than that formed after 9 days of nitrogen starvation in medium with no acetate supplement. Biochemical analysis of lipids revealed that the accumulated TAGs were derived mainly from chloroplast polar membrane lipids. Such a conversion of chloroplast polar lipids to TAGs is desirable for biodiesel production, because polar lipids are usually removed during the biodiesel production process. Thus, our data exemplified that a cost and time effective method of producing TAGs is possible using fenpropimorph or similar drugs.

Keywords: membrane lipid recycling, *Chlamydomonas reinhardtii,* fenpropimorph, biofuel, triacylglycerol

INTRODUCTION

Glycerolipids are ubiquitous in all cell types. Membrane lipids consist mainly of polar glycerolipids, which assemble into a bilayer structure that delineates the boundary of cells and provides sites of interaction for many proteins. Storage lipids are mainly neutral glycerolipids, including triacylglycerols (TAGs). They are stored in lipid droplets (LDs) in the seeds of plants, adipose cells of animals, and in algal cells. Polar membrane lipids and TAGs share some common biosynthetic pathways and have a common precursor, i.e., diacylglycerols (DAGs). Under stress conditions, membrane lipids are degraded, and the released acyl chains or DAG backbones can be re-assembled into neutral lipids, and stored in LDs, which are a major energy source for re-growth when conditions turn favorable (Hu et al., 2008; Siaut et al., 2011). TAGs are highly reduced, energy-rich compounds that can provide energy for humans, livestock, and industry. The rapid conversion of membrane lipids into TAGs is industrially beneficial, because TAGs are a more efficient and cost-effective source of energy than are polar lipids and they are more readily converted into diesel.

Global warming and climate change, which are thought to result from the extensive use of fossil fuels and the consequent increase in carbon dioxide levels in the air, threaten the lives of humankind and many other organisms. Energy sources that do not increase atmospheric carbon dioxide levels, such as biodiesel, are in high demand, and photosynthetic organisms are being intensively studied as potential clean, sustainable, and renewable energy sources. Most biofuels developed to date are derived from carbohydrates from *Saccharum* (sugarcane) and *Solanum tuberosum* (potato) or from TAGs from plants such as *Elaeis guineensis* (oil palm), *Brassica napus* (canola), *Olea europaea* (olive), *Helianthus annuus* (sunflower), and *Zea mays* (maize). However, these oil-producing plants are also important sources of food and feed, thus raising an ethical argument against using such plants as energy sources (Hill et al., 2006).

During the past decade, algae have emerged as an alternative non-crop source for biofuel, because they (i) do not compete with food-providing plants for agricultural land use, (ii) some species can accumulate large amounts of lipids that can be used for biodiesel production (for example, some microalgae can accumulate up to 50% of their biomass as oils; Tornabene et al., 1983; Miao and Wu, 2006; Xu et al., 2006), and (iii) grow very fast, fixing solar energy with an efficiency that is about 10–20% higher than that of land plants (Li et al., 2008). However, despite these advantages, several technological obstacles need to be overcome

before it becomes economically feasible to culture microalgae for biofuel production. For example, microalgae accumulate massive amounts of oil when subjected to stress conditions such as nitrogen deprivation. However, it is time-consuming and costly to induce microalgal lipid accumulation through nitrogen starvation.

Chlamydomonas reinhardtii has been widely used as a model organism to investigate various microalgal processes, including lipid metabolism (Merchant et al., 2012; Liu and Benning, 2013). Furthermore, this alga displays a sexual reproduction cycle that allows genetic analysis of phenotypes. *Chlamydomonas* accumulates high levels of TAGs in LDs under stress conditions such as nutrient deficiency or exposure to high intensity light (Miller et al., 2010; Fan et al., 2011). As in terrestrial plants, two types of enzymes participate in the final step of TAG synthesis in *Chlamydomonas*, i.e., diacylglycerol acyltransferases (DGATs) and phospholipid:diacylglycerol acyltransferases (PDATs). These enzymes catalyze the formation of TAG from a DAG molecule. Genes encoding DGAT proteins in *Chlamydomonas* are strongly induced under TAG-accumulating conditions, such as nitrogen or other nutrient deprivation (Boyle et al., 2012). The PDAT in *Chlamydomonas* has been demonstrated *in vitro* to use phospholipids and galactolipids as acyl donors, and DAG as acyl acceptors (Yoon et al., 2012). Insertional mutants lacking PDAT accumulated 25% less oil than its wild-type progenitor, demonstrating the importance of the PDAT-mediated acyl-remodeling pathway in oil accumulation in *Chlamydomonas* (Boyle et al., 2012).

Altering sterol levels was reported to affect sterol and fatty acid metabolism in fungal and animal cells (Colgan et al., 2007), and to result in the cleavage of ER membrane-bound transcription factors by membrane-associated proteases, and thereby to activate transcription factors in animal cells (Sakai et al., 1998; Porter et al., 2010). The activated transcription factors move to the nucleus, where they up-regulate the expression of genes involved in the biosynthesis of sterols and fatty acids (Horton et al., 2002; Porter et al., 2010). If such a mechanism also exists in microalgae, it might represent a means of manipulating lipid accumulation. However, it is not known how changes in sterol levels affect oil metabolism in microalgae. Sterol metabolism can be altered by chemical treatment (Ryder et al., 1986; Campagnac et al., 2008). For instance, fenpropimorph is an anti-fungal chemical that inhibits Δ^{14}-reduction and/or Δ^{8}–Δ^{7} isomerization in the sterol biosynthetic pathway (Campagnac et al., 2008). This chemical effectively inhibits sterol biosynthesis and alters the composition of sterols in fungi, yeasts, and plants (Baloch et al., 1984; Ziogas et al., 1991; Debieu et al., 1992; Moebius et al., 1996; Hartmann et al., 2002; Campagnac et al., 2009). Leek seedlings grown in the presence of fenpropimorph for 7 days have decreased total sterol levels, and accumulate LDs in the roots (Hartmann et al., 2002).

Here, we report that treatment of *C. reinhardtii* with fenpropimorph very rapidly induces the formation of LDs filled with TAGs. Surprisingly, this effect is not accompanied by any changes in sterol metabolism, but appears to induce the conversion of monogalactosyldiacylglycerol (MGDG), a plastidial polar lipid, to TAGs. In addition, the drug induces cell death and cell precipitation, which might facilitate the harvesting of TAGs in an industrial setting. Thus the treatment of algae with fenpropimorph results in three favorable changes for biodiesel production: a rapid increase in cellular TAG levels; a decrease in polar lipid level *in vivo*; and the efficient precipitation of algal cells.

MATERIALS AND METHODS

CELL CULTURE AND MEASUREMENT OF CELL CONCENTRATION

The *C. reinhardtii* strain CC-125 wild type *mt*$^{+}$ (137c) was obtained from the Chlamydomonas Genetics Center (USA). *Chlamydomonas* cells were cultured in Tris-acetate phosphate (TAP) medium (Rippka et al., 1979) or in the same medium without acetate (for photoautotrophic culture) at 25°C under continuous light (25–30 μmol photons m^{-2} s^{-1}) while shaking at 160 rpm. Cell growth was monitored by measuring the optical density (OD) at 750 nm using a Safire fluorescence spectrophotometer (TECAN, Switzerland) and also by counting the cell number using a hemocytometer.

ESTIMATION OF CELL SURFACE AREA CHANGE

The areas of plastids and entire cells in the photographs of the cells were measured using ImageJ (Papadopulos et al., 2007), to estimate the changes in their surface area.

CHEMICAL TREATMENT, LD STAINING, AND QUANTIFICATION OF FLUORESCENCE INTENSITY (FI)

A stock solution of fenpropimorph (SANTA CRUZ, cat#SC-235130) was prepared in pure ethanol at a concentration of 10 mg mL^{-1} and stored at room temperature. *Chlamydomonas* cells at late mid-log phase of growth were treated by adding fenpropimorph to a final concentration of 10 μg mL^{-1} and incubated for up to 1 h under standard growth conditions in TAP medium containing acetate and nitrogen sources, except when otherwise noted. To visualize the LDs, fenpropimorph-treated cells were stained with Nile red at a final concentration of 1 μg mL^{-1} (prepared from a stock solution of 0.1 mg mL^{-1} in acetone) for 30 min in the dark at room temperature (~25°C; Kim et al., 2013). To quantify the FI of LDs, fenpropimorph-treated cells were dispensed into a 96-well plate (Tissue culture testplate, SPL) and stained with Nile red, and the fluorescence signals from LDs were measured using a Safire fluorescence spectrophotometer (TECAN, Switzerland) with a 488 nm excitation filter and a 565 nm emission filter. Stained cells were also observed under fluorescence microscopy (Ziess, Axioskop 2 MOT, Germany) using filter set 44 (excitation BP 475/40, emission BP 530/50).

LIPID EXTRACTION AND ANALYSES

Chlamydomonas CC-125 cells at late mid-log phase (approximately 6.0×10^{6} cells mL^{-1}) were treated either with 10 μg mL^{-1} of fenpropimorph for 1 h or with ethanol alone (solvent control). Cells were harvested by centrifugation at 2,000 g for 5 min. Lipid extraction and analyses were conducted following the methods described in Kim et al. (2013).

STEROL ANALYSIS

For the quantification of sterols, [25,26,26,26,27,27,27-$^{2}H_{7}$] cholesterol (AVANTI cat# 700116) was added to the total lipid extract as an internal standard. Sterol analysis was performed as previously described (Suzuki et al., 2004). Sterols were identified by comparison of their mass-spectra patterns with those of the

published mass spectra patterns on known sterols (Miller et al., 2012).

RADIOISOTOPE LABELING EXPERIMENT FOR DIACYLGLYCEROL (DAG) DETECTION

Chlamydomonas strain CC-125 cells were cultured to late mid-log phase ($\sim 6 \times 10^6$ cells mL^{-1}) in TAP medium. Cells were labeled with 0.2 μCi mL^{-1} of [^{14}C]acetate for 2 h, washed twice with acetate free TAP medium, and then treated with fenpropimorph at a concentration of 10 μg mL^{-1} for 1 h. Total lipids were extracted using chloroform/methanol/formic acid (10:10:1, by volume; Härtel et al., 2000). After centrifugation (2000 *g*; 10 min), the bottom phase was directly loaded onto a thin-layer chromatography (TLC) plate (TLC Silica gel 60, MERCK) and separated using a two-phase solvent mixture; with a first phase of [chloroform/methanol/acetic acid/water, 90/15/10/3 by volume] and a second phase of [hexane/diethyl ether/acetic acid, 80/30/1 by volume]. Neutral lipid separation was performed using the first phase solvent mixture. After completely drying the TLC plate, polar lipids were separated using the second phase solvent mixture. The plate was then exposed to an imaging plate (BAS-TR 2040S, Fujifilm) and the relative strength of the radioactivity of [^{14}C]acetate was visualized with an image analyzer (FLA-2000, Fujifilm). The neutral lipid spots containing TAG and DAG, and polar lipid spots were then scraped off the plate and recovered separately, and the radioactivity of each spot was determined by liquid scintillation counting (Tri-Carb 2910 TR, Perkin Elmer).

RESULTS

FENPROPIMORPH INDUCES TAG ACCUMULATION IN *C. reinhardtii*

Small chemical molecules are known to trigger metabolic changes, as has been demonstrated in many cell systems. In our search for an efficient and alternative method to trigger oil accumulation in microalgae, we tested the hypothesis that fenpropimorph can induce cellular changes in microalgal oil content. This hypothesis was based on the observation that fenpropimorph disturbs sterol homeostasis in other organisms, which is correlated with ER stress response, changes in fatty acid and lipid metabolism (Baloch et al., 1984; Ziogas et al., 1991; Debieu et al., 1992; Moebius et al., 1996; Hartmann et al., 2002; Campagnac et al., 2009).

Chlamydomonas cells were treated with 10 μg mL^{-1} of fenpropimorph, and the cellular oil content was tracked by monitoring the fluorescence intensity (FI) of Nile red, a lipophilic dye specific for neutral lipids (Kou et al., 2013). After just 1 h of fenpropimorph treatment, the FI increased dramatically (**Figure 1A**). Furthermore, the FI increased as the concentrations of fenpropimorph increased from 5 to 20 μg mL^{-1} (**Figure 1A**). Biochemical analyses of lipids extracted from fenpropimorph-treated cells revealed that TAGs increased 6–15-fold in fenpropimorph-treated versus control *Chlamydomonas* cells, in proportion to the increases in drug concentrations from 5 to 20 μg mL^{-1} (**Figure 1B**). The fold increase values varied between experiments, perhaps due to slight differences in culture age (within the late mid-log phase), and consequent variation in the TAG levels of the control samples which ranged between 40 and 135 nmol fatty acids in TAG per 6×10^7 cells. The effect of the drug was maximal at the late mid-log phase (at 4 days of culture under our conditions), and slightly less at the stationary phase (**Figure A1**). Microscopic observations revealed that fenpropimorph-treated cells had more LDs than did the control cells (**Figure 1C**). The effect of fenpropimorph treatment on TAG induction in *Chlamydomonas* was very rapid: TAG levels increased significantly after as little as 5 min of treatment with 10 μg mL^{-1} fenpropimorph, and became saturated at 45–85 min (i.e., longer treatment did not induce further TAG accumulation; **Figure 1D**).

FENPROPIMORPH INDUCES THE FORMATION OF MORE TAGS THAN DOES UP TO 9 DAYS OF N STARVATION IN MEDIUM WITH NO ACETATE SUPPLEMENT

Since nitrogen starvation is the most extensively studied trigger of oil accumulation in microalgae, we compared the amount of TAGs induced by fenpropimorph to that induced by N starvation. *Chlamydomonas* cells were grown in normal conditions to mid-log phase, washed to remove acetate and nitrogen from the medium, then re-suspended in TAP medium without an acetate or nitrogen source. We did not include acetate in the medium in this experiment since the biofuel industry often does not use acetate in the medium to avoid additional cost. Nile red FI value and TAG amount of cells treated with fenpropimorph for 1 h was found to be $\sim$2.5-fold higher than those cells starved of N for up to 9 days (**Figures 1E,F**).

We then tested whether the effect of fenpropimorph was dependent on the presence of acetate in the medium. Interestingly, the presence of acetate in medium did not make any significant difference in Nile red fluorescence values of *Chlamydomonas* cells treated with 10 or 15 μg mL^{-1} fenpropimorph (**Figure A2**).

FENPROPIMORPH INCREASES TAG CONTENT BY REMODELING PLASTIDIAL LIPIDS

To identify the biosynthetic origin of the fatty acids accumulated in the TAG fraction in fenpropimorph-treated cells, the fatty acid content and composition of the TAG fraction were compared between control and fenpropimorph-treated cells (**Figures 2A,B**). All fatty acid levels in TAG increased in fenpropimorph-treated cells, but the highest increases were found in 16:4(4,7,10,13) and 18:3(9,12,15) (**Figure 2A**), the two fatty acids that preferentially occur in plastidial lipids (Giroud et al., 1988; Fan et al., 2011). Fatty acid compositional analysis (mol% values) confirmed the preferential accumulation of plastidial-type fatty acids in TAGs induced by fenpropimorph (**Figure 2B**). These results suggest that the fatty acids formed in response to fenpropimorph treatment are most likely derived from recycled plastidial lipids.

To examine this possibility, we analyzed the total acyl lipid contents and individual polar membrane lipids of *Chlamydomonas*. The decrease in polar lipids mirrored the increase in TAG levels (**Figure 3A**), and the total acyl-lipid contents did not differ between the control and the chemical-treated cells (**Figure 3A**, right), suggesting that fenpropimorph most likely induced remodeling of lipids. The fatty acid composition of total lipids (**Figure 3B**) did not differ between control and fenpropimorph-treated cells, thus further supporting this possibility.

However, not all polar lipids changed to the same extent. The amounts of the most abundant plastidial galactolipids, MGDG,

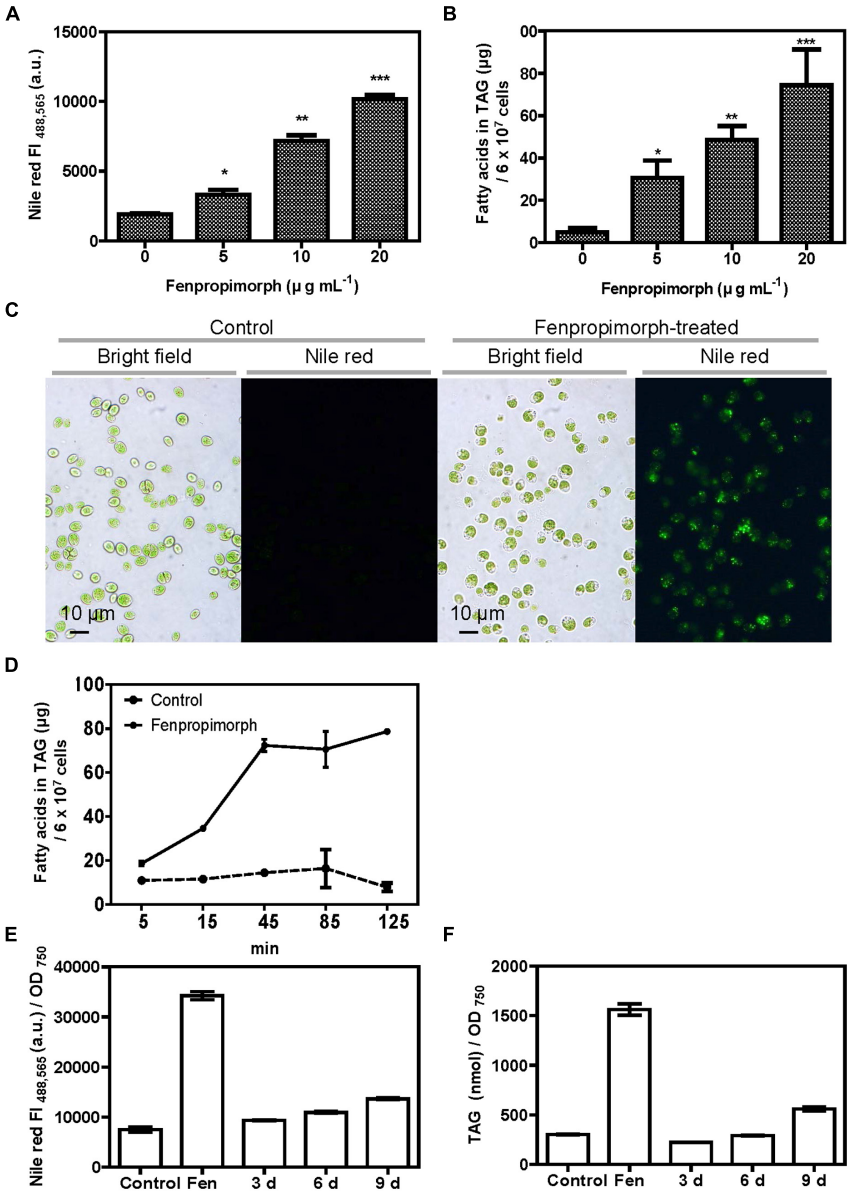

FIGURE 1 | Fenpropimorph induces neutral lipid accumulation in *Chlamydomonas reinhardtii*. **(A)** Fenpropimorph-induced LD formation occurs in a dose-dependent manner. The fluorescence intensity (FI) of a neutral lipid specific-dye, Nile red, was determined. Late mid-log phase *Chlamydomonas* cells (N+, acetate+) were treated with ethanol (solvent control) or fenpropimorph (1 h, at RT). Averages from three replicate experiments are presented. Bars represent SE. Significant differences, as determined by Student's *t*-test, are indicated by asterisks (*$p < 0.05$, **$p < 0.01$, ***$p < 0.001$). **(B)** Fenpropimorph-induced TAGs were extracted and analyzed using biochemical methods. Control cells were treated with the same volume of ethanol used to dissolve fenpropimorph. Averages from triplicate experiments are presented. Bars represent SE. Significant differences, as determined by Student's *t*-test, are indicated by asterisks (*$p < 0.05$, **$p < 0.01$, ***$p < 0.001$). **(C)** Images of Nile red-stained LD accumulation in fenpropimorph-treated cells. Cells were treated with fenpropimorph for 1 h. Images were obtained using a fluorescence microscope. **(D)** Time-dependent change in TAG concentration in fenpropimorph-treated *Chlamydomonas* cells. TAG accumulation induced by fenpropimorph (10 μg mL^{-1}) treatment was analyzed biochemically. Averages and SE from three replicate experiments are presented. TAG levels shown were converted to μg from nmol values obtained from GC experiment. The original nmol values for each time point (5, 15, 45, 85, and 125 min) were 26.8 ± 4.7, 40.9 ± 0.4, 51.2 ± 5.1, 66.1 ± 24.2, and 27.7 ± 5.7, respectively, for control samples, and 65.4 ± 3.0, 120.7 ± 1.2, 255.0 ± 8.5, 260.7 ± 21.9, and 278.0 ± 1.0, respectively, for fenpropimorph-treated samples. In experiments shown in **(A – D)**, *Chlamydomonas* cells in late mid-log phase culture in TAP medium (N+, acetate+) were used. **(E,F)** Comparison of the effect of nitrogen deprivation and fenpropimorph treatment on lipid induction efficiency in *Chlamydomonas* cells. **(E)** Nile red fluorescence intensity of control *Chlamydomonas* cells, and of cells subjected to fenpropimorph treatment (1 h, 25°C), and nitrogen deprivation (for the indicated number of days). *Chlamydomonas* cells were grown in normal conditions to mid-log phase, and washed to remove acetate and nitrogen from the medium. They were then re-suspended in TAP medium without an acetate or nitrogen source, and then either treated with ethanol (solvent control) or fenpropimorph (10 μg mL^{-1}) for 1 h, or transferred to the nitrogen-deficient conditions and incubated for 3, 6, or 9 days. The FI value was measured. Averages from three replicate experiments are presented. Bars represent SE. **(F)** Biochemical analysis of TAG content in cells treated as in **(E)**. Averages from three replicate experiments are presented. Bars represent SE.

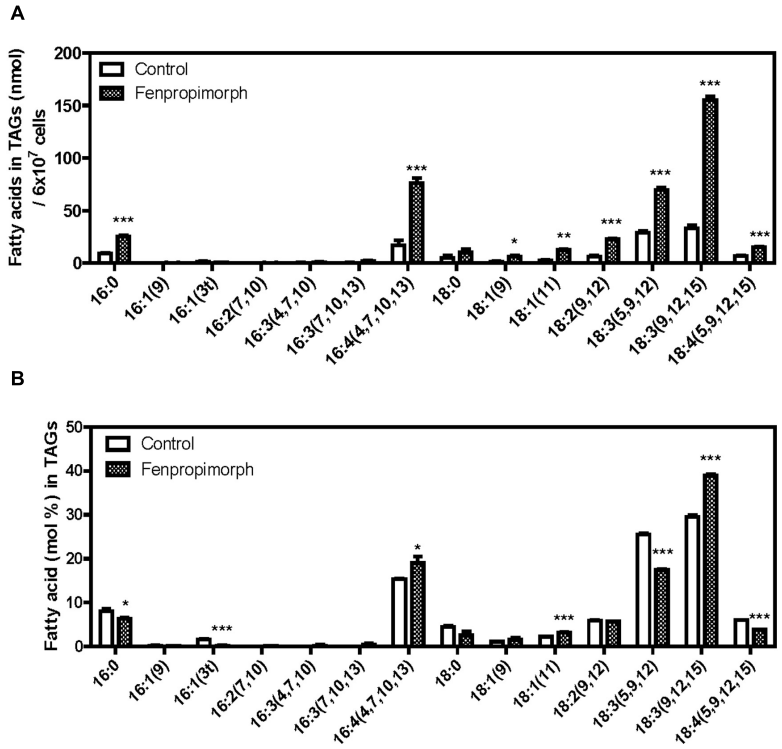

FIGURE 2 | Biochemical analysis of TAGs in fenpropimorph-treated *C. reinhardtii* in late mid-log phase culture in TAP medium (N+, acetate). (A) A comparison of the absolute amount of fatty acids in TAGs isolated from fenpropimorph-treated and control cells. Averages from three replicate experiments are presented. Bars represent SE. Significant differences, as determined by Student's *t*-test, are indicated by asterisks (*$p < 0.05$, **$p < 0.01$, ***$p < 0.001$). **(B)** Comparison of fatty acid mol% in TAGs isolated from fenpropimorph-treated cells and control cells. Averages from three replicate experiments are presented. Bars represent SE. Significant differences, as determined by Student's *t*-test, are indicated by asterisks (*$p < 0.05$, **$p < 0.01$, ***$p < 0.001$).

plastidial phospholipid phosphatidylglycerol (PG), and plastidial sulfur lipid sulfoquinovosyldiacylglycerol (SQDG) decreased to 56%, 57%, and 87% of those in untreated cells (**Figure 3C**). Compared to the above-mentioned plastidial lipids, the contribution of other membrane lipids seemed to be relatively small: the concentration of digalactosyldiacylglycerol (DGDG) changed to a much lesser extent than did that of MGDG, the diacylglyceryltrimethylhomoserine (DGTS) level did not change, and phosphatidylethanolamine (PE) and phosphatidylinositol (PI) levels were low even in the control cells (**Figure 3C**). These results are consistent with our view that the TAGs induced by fenpropimorph originate mainly from plastids, and suggest that MGDG is the major source of the fatty acids in TAGs induced by the chemical treatment. Interestingly, the levels of three pigments abundant in photosynthetic organisms were not altered (**Figure A3**), suggesting that MGDG is substantially degraded in response to the addition of fenpropimorph.

If MGDG provides the major source of fatty acids in TAGs that accumulate under fenpropimorph treatment, then the time course of the increase in the level of TAGs and the decrease in the level of MGDG should exhibit an inverse relationship. To test this possibility, we determined the content of TAG and MGDG at three time points (after 0, 10, and 60 min of chemical treatment). As shown in **Figure 4**, the level of TAGs showed a 2.8-fold change at 10 min and at the 60 min, and a 6.4-fold increase compared to the mock-treatment (**Figure 4A**). The change in MGDG level was the opposite to that of TAGs at 10 min; the level of MGDG decreased to 66% in the chemical-treated cells compared to mock-treated cells. However, it did not decrease much further, and after 60 min of the drug treatment, the level of MGDG in the drug-treated cells remained at 71% of that of the control (**Figure 4B**). The DGDG level was not affected by the drug treatment (**Figure 4C**), as found in our previous experiment (**Figure 3C**). The results shown in **Figures 3** and **4** indicate that MGDG was an important source of FAs in TAGs accumulated by fenpropimorph treatment, especially at the beginning of the response to the drug, and other polar plastidial lipids PG and SQDG, and other polar lipids PE and PI, also contributed small portions.

If MGDG is an important source of FAs in TAG induced by the drug, it might be degraded to DAG, and then used for synthesis of TAG. To test this possibility, we labeled the cells with [^{14}C]acetate, treated them with the drug, and detected radioactive TAG and DAG in control and drug-treated cells. The cells were labeled with [^{14}C]acetate for 2 h, washed twice with TAP medium without acetate, and then treated with fenpropimorph for an additional hour before lipids were extracted. Total lipids were separated twice on a TLC plate, using two different solvent mixtures (the first

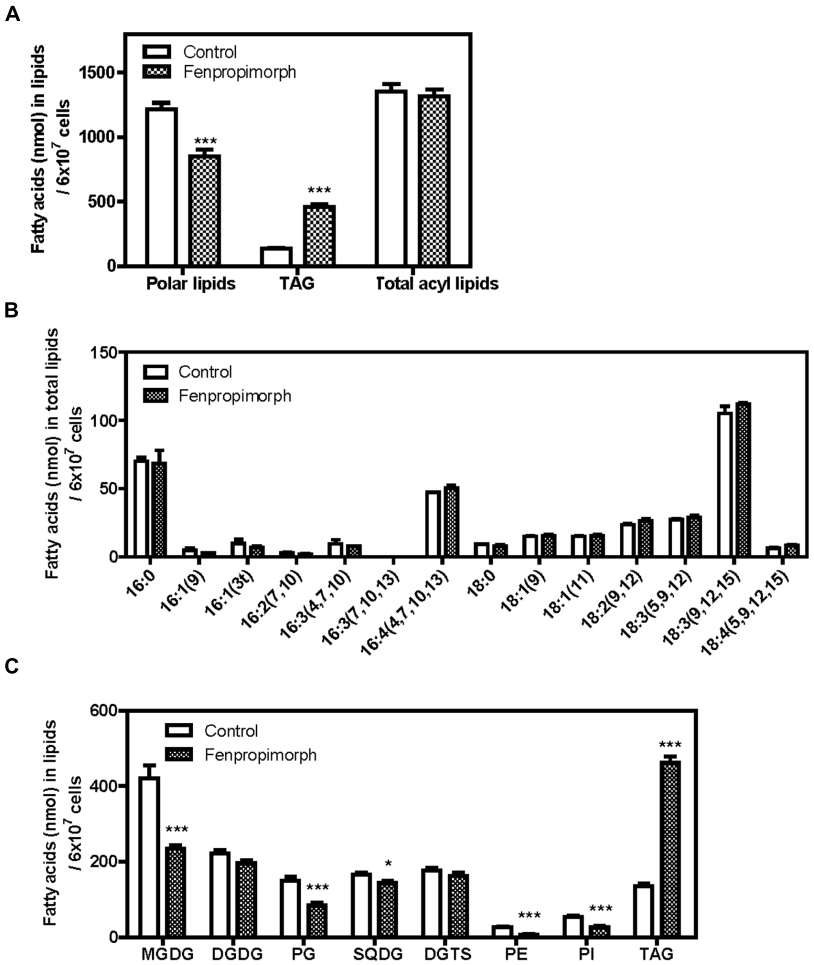

FIGURE 3 | Alterations in polar membrane lipid and TAG profiles of fenpropimorph-treated *C. reinhardtii* at late mid-log phase cultured in TAP medium (N+, acetate+). (A) Comparison of the total fatty acid amount in polar lipids, TAGs and total acyl lipids. Bars represent SE ($N = 2$, $n = 3$). Significant differences, as determined by Student's *t*-test, are indicated by asterisks (***$p < 0.001$). **(B)** Comparison of fatty acid profiles in total lipids. A representative result of 10 experiments is shown. Bars represent SE ($n = 3$). **(C)** Comparison of the concentration of major membrane lipids and TAGs between fenpropimorph-treated and control cells. Averages from three replicate experiments are presented. Bars represent SE ($N = 2$, $n = 6$). Significant differences, as determined by Student's *t*-test, are indicated by asterisks (*$p < 0.05$, ***$p < 0.001$).

for the separation of non-polar lipids, and the second for the separation of polar lipids). TAG spots were visible both under UV light (when stained with primuline; **Figure 5A**, right) and when using a radioisotope image analyzer (FLA-2000, Fujifilm; **Figure 5A**, left). DAG spots became visible only after 72 h or longer exposure of the TLC plate containing lipid extract from the fenpropimorph-treated cells, but not in that of mock-treated cells. (**Figure 5A**, left). We then compared the disintegration per minute (DPM) values of total non-polar lipids containing TAG, DAG, and free fatty acids with that of polar lipids, and found that the increase in DPM values of total non-polar lipids was equivalent to the decrease in that of the total polar lipids in cells subjected to fenpropimorph treatment (**Figure 5B**). Thus, the sum of DPM values of total lipids was similar between control and fenpropimorph-treated cells (**Figure 5B**), which again supports the notion that the fatty acids in fenpropimorph-induced TAGs originated from polar lipids.

FENPROPIMORPH-INDUCED TAG ACCUMULATION IN *Chlamydomonas* IS NOT ACCOMPANIED BY CHANGES IN STEROL CONTENT OR COMPOSITION

Fenpropimorph treatment inhibits ergosterol biosynthesis in fungi (Baloch et al., 1984; Debieu et al., 1992; Moebius et al., 1996; Hartmann et al., 2002; Campagnac et al., 2009). To uncover the mechanism underlying fenpropimorph-induced TAG accumulation in *Chlamydomonas*, we tested whether fenpropimorph treatment changed the sterol levels or composition in this organism. Interestingly, neither the level of total sterols nor its composition changed in *Chlamydomonas* cells after 60 min of fenpropimorph treatment (**Figures 6A,B**).

FENPROPIMORPH INDUCES SEVERE STRESS IN *Chlamydomonas* CELLS

To test whether fenpropimorph induces stress in the algal cells, we examined the motility of the treated cells. Immediately after treatment with fenpropimorph, most cells stopped moving, and after

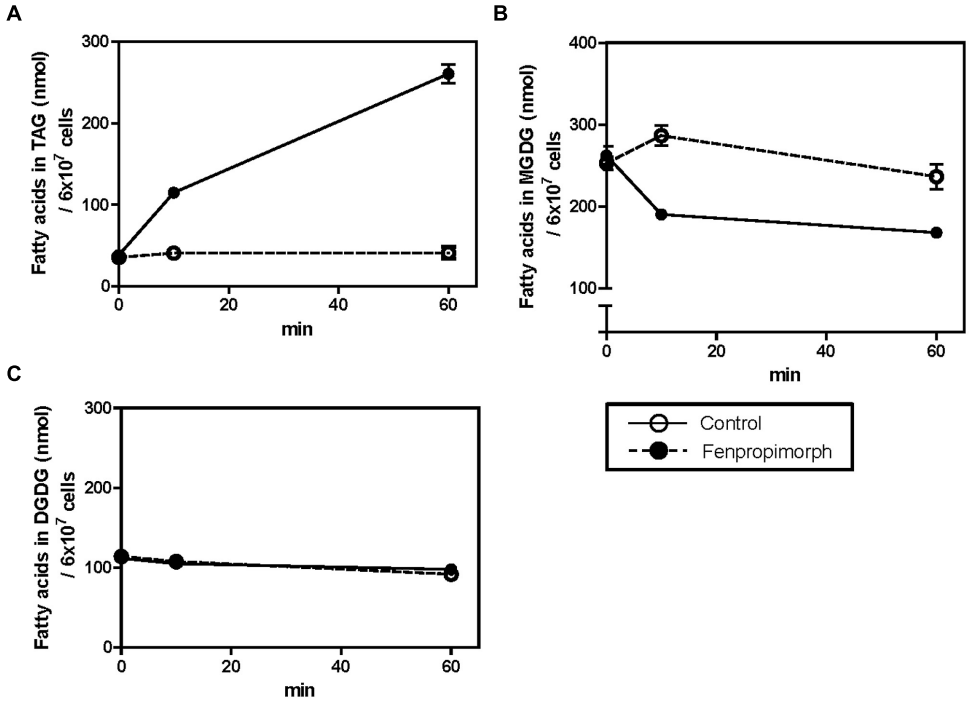

FIGURE 4 | Time-dependent changes in TAG (A), MGDG (B), and DGDG (C) contents in fenpropimorph-treated *C. reinhardtii*. The cells were treated with 10 μg mL^{-1} fenpropimorph for up to 1 h at 25°C. *Chlamydomonas* cells in late mid-log phase culture in TAP medium (N+, acetate+) were used. Averages from three replicate experiments are represented. Bars represent SE.

1 h, most sank to the bottom of the container. Forty three percent of the cells (97 out of 224 cells counted) were dead as indicated by positive staining of the nucleus with propidium iodide at 1 h after treatment with fenpropimorph (**Figure A4**). This result suggests that fenpropimorph generated severe stress in the *Chlamydomonas* cells. Microscopy observations revealed that the plastids of fenpropimorph-treated cells were shrunken (**Figures 1C** and **A5**); the area of chloroplasts in fenpropimorph-treated cells was decreased by 29.5% in the treated cells (**Figure A5B**). This drastic change in chloroplast morphology was in agreement with the results of our lipid analysis: a large proportion of plastidial lipids degraded upon treatment with fenpropimorph.

DISCUSSION

In this study, we found that fenpropimorph, a sterol biosynthesis inhibitor, rapidly (within an hour) induced at least a fourfold increase in the amount of TAGs produced by *C. reinhardtii* cells (**Figures 1** and **4**). We showed that fenpropimorph treatment induced the degradation of major chloroplastic lipids into fatty acids (**Figures 2** and **3**); recycling of the fatty acids to TAGs (**Figures 3** and **4**); and precipitation of TAG-induced cells at the end of culture. Previously reported stimuli that induce TAG, i.e., nutrient starvation, exposure to high light intensity, and salt stress, also degrade chloroplastic lipids and recycle the fatty acids to TAG (Fan et al., 2011; Siaut et al., 2011). However, striking difference exists between the previously reported stress-induced and fenpropimorph-induced TAG accumulation; it was very fast (**Figures 1** and **4**), the fastest among all triggers of algal lipid remodeling reported to date. We are not aware of any other treatment that induces such rapid remodeling of lipids as observed here with fenpropimorph treatment. Other triggers of lipid accumulation (nutrient starvation, high light intensity, and high salt) usually require several days.

The level of total sterols or its composition did not change in *Chlamydomonas* cells which accumulated TAG upon fenpropimorph treatment (**Figures 6A,B**). The very short time required for TAG accumulation may have been too short for any changes in sterol metabolism, since, in other species, the drug induced change in sterol metabolism required days (Hartmann et al., 2002; Campagnac et al., 2008, 2009). Thus the mechanism underlying the rapid accumulation of TAG in fenpropimorph-treated *Chlamydomonas* cells does not seem to involve sterol metabolism. It remains to be determined whether fenpropimorph inhibits sterol synthesis in algae to the same extent as it does in fungi, and such a test would involve the long-term treatment of *Chlamydomonas* cells with a low dosage of the drug. We did not investigate further the effect of low concentrations of fenpropimorph, since up to 24 h treatment with 1.25 or 2.5 μg mL^{-1} of fenpropimorph did not induce high accumulation of TAG (**Figure A6**), but caused almost complete suppression of the growth of *Chlamydomonas*.

The plastidial origin of most of the fatty acids assimilated into TAGs in fenpropimorph-treated cells was concluded based on results from two experiments: fatty acid methyl ester (FAME) analysis (**Figure 2**), and membrane lipids analysis (**Figure 3C**). Upon the drug treatment, the levels of chloroplastic lipids, MGDG and PG decreased to half (**Figure 3C**). The TAG induced by the

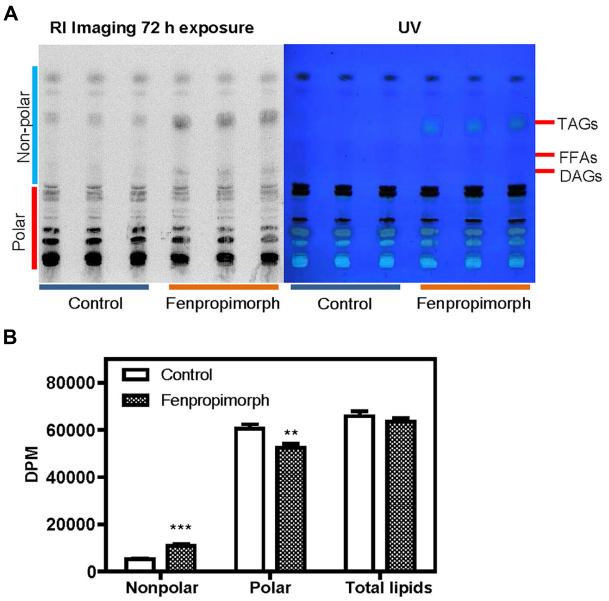

FIGURE 5 | Analysis of lipids labeled with [^{14}C]acetate in fenpropimorph-treated *C. reinhardtii*. **(A)** DAG is found to contain 14C-labeled in the fenpropimorph-treated cells. Two-phase TLC was performed as described in Materials and methods. The left image represents the radioactivity of lipids derived from [^{14}C]acetate. The right image shows primuline staining of the same TLC plate. **(B)** Disintegration per minute (DPM) values of non-polar and polar lipids of the solvent control (ethanol) and fenpropimorph-treated cells (10 μg mL^{-1}, 1 h, at 25°C) in TAP medium without acetate. Averages and SE from three replicate experiments are presented. Significant differences, as determined by Student's *t*-test, are indicated by asterisks (**$p < 0.01$, ***$p < 0.001$).

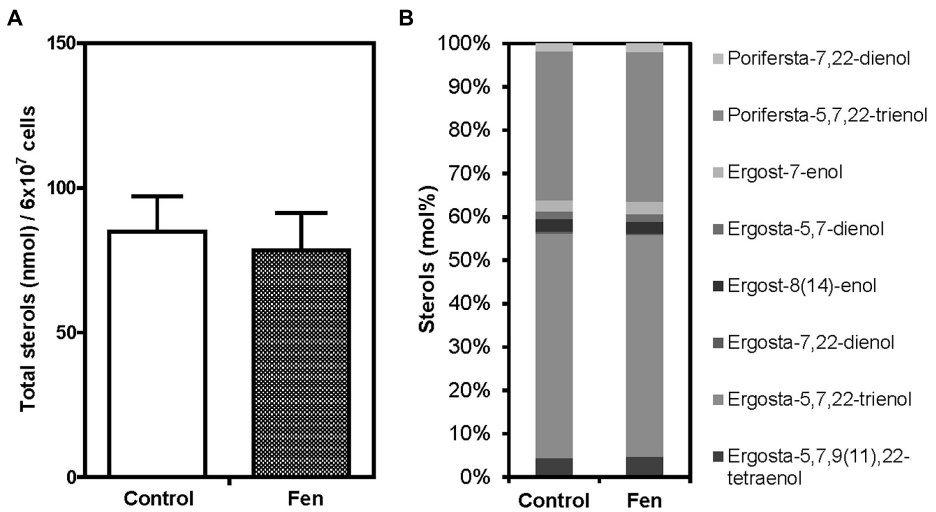

FIGURE 6 | Comparison of total sterol amount and sterol composition between control and fenpropimorph-treated *C. reinhardtii*. **(A)** Total sterol amount of control and fenpropimorph-treated (10 μg mL^{-1}, 1 h, at 25°C) cells. *Chlamydomonas* cells in late mid-log phase culture in TAP medium (N+, acetate+) were used. Averages from three replicate experiments are presented. Bars represent SE. **(B)** Sterol compositions of control and fenpropimorph-treated (10 μg mL^{-1}, 1 h, at 25°C) cells.

drug was much higher than that in control in 16:4(4,7,10,13) and 18:3(9,12,15) species of fatty acids (**Figure 2B**), which are found almost exclusively in chloroplast (Fan et al., 2011; Li et al., 2012). Chloroplast shrank upon the drug treatment (**Figure A5**), supporting the degradation of its internal lipids detected by biochemical analyses. These results and the kinetic analysis shown in **Figure 4** suggest that when the cells were exposed to fenpropimorph, MGDG was rapidly broken down within 10 min (**Figure 4B**), and the fatty acids or DAG liberated from MGDG and other plastidial lipids were used to synthesize TAG. The radioisotope analysis (**Figure 5**) indicated that the fatty acids liberated from MGDG and other plastidial lipids were transiently

incorporated into DAG, and then used to synthesize TAG, because DAG was labeled in the fenpropimorph-treated cells. While the level of MGDG, the most abundant plastidial lipid, changed much upon the drug treatment, that of DGDG, another major plastidial lipid, did not change as much, similarly as found under nitrogen deficiency condition (Li et al., 2012). The reason for the different changes of the two plastidial lipids under nitrogen deficiency was attributed to the preference of MGDG over DGDG as substrate for PGD1, an enzyme critical for TAG accumulation under nitrogen deficiency (Li et al., 2012). Thus it is tempting to speculate that PGD1 may also be involved in fenpropimorph-induced TAG accumulation.

We previously reported that Brefeldin A (BFA), a drug that inhibits the intracellular trafficking of membranes, also induced TAG accumulation (Kim et al., 2013). Both BFA and fenpropimorph inhibit basic cellular functions, and this stress may be the common cause of TAG accumulation in cells treated with these chemicals. There is a difference and similarities between fenpropimorph-induced and BFA-induced TAG accumulation. A similarity is that both drugs induced lipid remodeling regardless of the carbon or nitrogen source in the medium. The striking differences between the two drug treatments include (i) fenpropimorph induced at least fourfold higher amount of TAG, whereas BFA induced maximum 1.3-fold higher amount of TAG, than their solvent controls (compare **Figure 1** of this paper with Figures 2 and 3 of Kim et al., 2013); and (ii) the fatty acids in TAG induced by fenpropimorph were derived mostly from chloroplasts, whereas those induced by BFA treatment were from DGTS, a non-chloroplast membrane lipid (Kim et al., 2013). Thus, the two drugs function differently at the molecular level to induce TAG accumulation. Fenpropimorph might provide a useful tool in biodiesel production. Firstly, fenpropimorph treatment reduces the time for TAG induction. *Chlamydomonas* synthesizes TAGs under stress conditions, such as nutrient deficiency. Thus, a conventional method to induce TAG is to grow the cells under nutrient-rich conditions until they reach a certain density, and then to transfer the cells into nutrient-deficient medium to promote TAG accumulation. However, this process is time-consuming and expensive. In contrast to this conventional method, fenpropimorph treatment very rapidly induces TAG formation by converting polar lipids in the cell, suggesting that much time can be saved by using this drug. Moreover, the quantity of TAGs induced by 1 h treatment with fenpropimorph was much more than that produced by 9 days of nitrogen starvation in medium without acetate (**Figures 1E,F**). Under nitrogen replete condition, 10^7 cells of *Chlamydomonas* contained about 10 μg fatty acid in TAG, while treatment with fenpropimorph increased it to about 50 μg. This level of TAG induced by fenpropimorph was higher than that found in the same number of cells of *Nannochloropsis* (25 μg), Chlorella (1 μg) or *Senedesmus* (8 μg) under normal condition (Siaut et al., 2011; Vigeolas et al., 2012; Simionato et al., 2013). Moreover, the drug may be able to increase TAG levels in many species of alga. Secondly, fenpropimorph treatment can improve the efficiency of biodiesel production, as it converts polar lipids into neutral lipids. Polar lipids such as phospholipids and galactolipids are usually removed during biodiesel production, since they inhibit the purification of TAGs by forming a gum layer, reducing the final amount of TAGs that can be used in biodiesel production (Watanabe et al., 2002; Lai et al., 2005). Thus, the *in vivo* reduction of polar lipids by fenpropimorph treatment might be advantageous to the biodiesel production process. Thirdly, fenpropimorph might provide an efficient method for harvesting the algal cells, since it induces cell death, and consequently, the precipitation of cells. Thus fenpropimorph might also reduce the cost in the harvesting step.

Thus we envisage that fenpropimorph can be used to cut down the cost of biodiesel production from the algae. If applied when the culture reaches at the maximum density, this chemical can save time and simplify steps to induce TAG accumulation, harvesting the cells, and purification of TAG. Further research into the molecular mechanism underlying fenpropimorph-induced TAG accumulation in *Chlamydomonas* might reveal yet other methods to rapidly accumulate TAG in algae for biodiesel production.

ACKNOWLEDGMENTS

We thank the Chlamydomonas Genetics Center (USA) for providing the CC-125 *Chlamydomonas* line, and Dr. Kiyoshi Ohyama for identification of the sterols. This research was supported by a grant from the Global Frontier Program (2011-0031345) of the Republic of Korea awarded to Youngsook Lee, from Gyeongbuk Sea Grant Program (20090218) funded by the Ministry of Oceans and Fisheries, Korea awarded to Jae-Ung Hwang, by a Grant-in-Aid for Scientific Research (21570034) from the Ministry of Education, Culture, Sports, Science, and Technology of Japan awarded to Ikuo Nishida, and by a grant from the French ANR (DIESALG, ANR-12-BIME-0001-02) awarded to Yonghua Li-Beisson.

REFERENCES

Baloch, R. I., Mercer, E. I., Wiggins, T. E., and Baldwin, B. C. (1984). Inhibition of ergosterol biosynthesis in *Saccharomyces cerevisiae* and *Ustilago maydis* by tridemorph, fenpropimorph and fenpropidin. *Phytochemistry* 23, 2219–2226. doi: 10.1016/S0031-9422(00)80523-3

Boyle, N. R., Page, M. D., Liu, B., Blaby, I. K., Casero, D., Kropat, J., et al. (2012). Three acyltransferases and nitrogen-responsive regulator are implicated in nitrogen starvation-induced triacylglycerol accumulation in *Chlamydomonas*. *J. Biol. Chem.* 287, 15811–15825. doi: 10.1074/jbc.M111.334052

Campagnac, E., Fontaine, J., Sahraoui, A. L.-H., Laruelle, F., Durand, R., and Grandmougin-Ferjani, A. (2008). Differential effects of fenpropimorph and fenhexamid, two sterol biosynthesis inhibitor fungicides, on arbuscular mycorrhizal development and sterol metabolism in carrot roots. *Phytochemistry* 69, 2912–2919. doi: 10.1016/j.phytochem.2008.09.009

Campagnac, E., Fontaine, J., Sahraoui, A. L.-H., Laruelle, F., Durand, R., and Grandmougin-Ferjani, A. (2009). Fenpropimorph slows down the sterol pathway and the development of the arbuscular *mycorrhizal* fungus *Glomus intraradices*. *Mycorrhiza* 19, 365–374. doi: 10.1007/s00572-009-0238-1

Colgan, S. M., Tang, D., Werstuck, G. H., and Austin, R. C. (2007). Endoplasmic reticulum stress causes the activation of sterol regulatory element binding protein-2. *Int. J. Biochem. Cell Biol.* 39, 1843–1851. doi: 10.1016/j.biocel.2007.05.002

Debieu, D., Gall, C., Gredt, M., Bach, J., Malosse, C., and Leroux, P. (1992). Ergosterol biosynthesis and its inhibition by fenpropimorph in *Fusarium species*. *Phytochemistry* 31, 1223–1233. doi: 10.1016/0031-9422(92)80265-G

Fan, J., Andre, C., and Xu, C. (2011). A chloroplast pathway for the de novo biosynthesis of triacylglycerol in *Chlamydomonas reinhardtii*. *FEBS Lett.* 585, 1985–1991. doi: 10.1016/j.febslet.2011.05.018

Giroud, C., Gerber, A., and Eichenberger, W. (1988). Lipids of *Chlamydomonas reinhardtii*. Analysis of molecular species and intracellular site (s) of biosynthesis. *Plant cell physiol.* 29, 587–595.

Härtel, H., Dörmann, P., and Benning, C. (2000). DGD1-independent biosynthesis of extraplastidic galactolipids after phosphate deprivation in *Arabidopsis*. *Proc. Natl. Acad. Sci. U.S.A.* 97, 10649–10654. doi: 10.1073/pnas.180320497

Hartmann, M.-A., Perret, A.-M., Carde, J.-P., Cassagne, C., and Moreau, P. (2002). Inhibition of the sterol pathway in leek seedlings impairs phosphatidylserine and glucosylceramide synthesis but triggers an accumulation of triacylglycerols. *Biochim. Biophys. Acta* 1583, 285–296. doi: 10.1016/S1388-1981(02)00249-4

Hill, J., Nelson, E., Tilman, D., Polasky, S., and Tiffany, D. (2006). Environmental, economic, and energetic costs and benefits of biodiesel and ethanol biofuels. *Proc. Natl. Acad. Sci. U.S.A.* 103, 11206–11210. doi: 10.1073/pnas.0604600103

Horton, J. D., Goldstein, J. L., and Brown, M. S. (2002). SREBPs: activators of the complete program of cholesterol and fatty acid synthesis in the liver. *J. Clin. Invest.* 109, 1125–1131. doi: 10.1172/JCI0215593

Hu, Q., Sommerfeld, M., Jarvis, E., Ghirardi, M., Posewitz, M., Seibert, M., et al. (2008). Microalgal triacylglycerols as feedstocks for biofuel production: perspectives and advances. *Plant J.* 54, 621–639. doi: 10.1111/j.1365-313X.2008.03492.x

Kim, S., Kim, H., Ko, D., Yamaoka, Y., Otsuru, M., Kawai-Yamada, M., et al. (2013). Rapid induction of lipid droplets in *Chlamydomonas reinhardtii* and *Chlorella vulgaris* by Brefeldin A. *PLoS ONE* 8:e81978. doi: 10.1371/journal.pone.0081978

Kou, Z., Bei, S., Sun, J., and Pan, J. (2013). Fluorescent measurement of lipid content in the model organism *Chlamydomonas reinhardtii*. *J. Appl. Phycol.* 25, 1633–1641. doi: 10.1007/s10811-013-0011-x

Lai, C. C., Zullaikah, S., Vali, S. R., and Ju, Y. H. (2005). Lipase-catalyzed production of biodiesel from rice bran oil. *J. Chem. Technol. Biotechnol.* 80, 331–337. doi: 10.1002/jctb.1208

Li, X., Moellering, E. R., Liu, B., Johnny, C., Fedewa, M., Sears, B. B., et al. (2012). A galactoglycerolipid lipase is required for triacylglycerol accumulation and survival following nitrogen deprivation in *Chlamydomonas reinhardtii*. *Plant Cell* 24, 4670–4686. doi: 10.1105/tpc.112.105106

Li, Y., Horsman, M., Wu, N., Lan, C. Q., and Dubois-Calero, N. (2008). Biofuels from *microalgae*. *Biotechnol. Prog.* 24, 815–820.

Lichtenthaler, H. K., and Babani, F. (2004). "Light adaptation and senescence of the photosynthetic apparatus. Changes in pigment composition, chlorophyll fluorescence parameters and photosynthetic activity," in *Chlorophyll a Fluorescence*, eds G. C. Papageorgiou and Govindjee (Dordrecht: Springer), 713–736.

Liu, B., and Benning, C. (2013). Lipid metabolism in *microalgae* distinguishes itself. *Curr. Opin. Biotechnol.* 24, 300–309. doi: 10.1016/j.copbio.2012.08.008

Merchant, S. S., Kropat, J., Liu, B., Shaw, J., and Warakanont, J. (2012). TAG, you're it! *Chlamydomonas* as a reference organism for understanding algal triacylglycerol accumulation. *Curr. Opin. Biotechnol.* 23, 352–363. doi: 10.1016/j.copbio.2011.12.001

Miao, X., and Wu, Q. (2006). Biodiesel production from heterotrophic microalgal oil. *Bioresour. Technol.* 97, 841–846. doi: 10.1016/j.biortech.2005.04.008

Miller, M. B., Haubrich, B. A., Wang, Q., Snell, W. J., and Nes, W. D. (2012). Evolutionarily conserved Δ25 (27)-olefin ergosterol biosynthesis pathway in the alga *Chlamydomonas reinhardtii*. *J. Lipid Res.* 53, 1636–1645. doi: 10.1194/jlr.M027482

Miller, R., Wu, G., Deshpande, R. R., Vieler, A., Gärtner, K., Li, X., et al. (2010). Changes in transcript abundance in *Chlamydomonas reinhardtii* following nitrogen deprivation predict diversion of metabolism. *Plant Physiol.* 154, 1737–1752. doi: 10.1104/pp.110.165159

Moebius, F. F., Bermoser, K., Reiter, R. J., Hanner, M., and Glossmann, H. (1996). Yeast sterol C8-C7 isomerase: identification and characterization of a high-affinity binding site for enzyme inhibitors. *Biochemistry* 35, 16871–16878. doi: 10.1021/bi961996m

Papadopulos, F., Spinelli, M., Valente, S., Foroni, L., Orrico, C., Alviano, F., et al. (2007). Common tasks in microscopic and ultrastructural image analysis using image. *J. Ultrastruct. Pathol.* 31, 401–407. doi: 10.1080/01913120701719189

Porter, J. R., Burg, J. S., Espenshade, P. J., and Iglesias, P. A. (2010). Ergosterol regulates sterol regulatory element binding protein (SREBP) cleavage in fission yeast. *J. Biol. Chem.* 285, 41051–41061. doi: 10.1074/jbc.M110.144337

Rippka, R., Deruelles, J., Waterbury, J. B., Herdman, M., and Stanier, R. Y. (1979). Generic assignments, strain histories and properties of pure cultures of cyanobacteria. *J. Gen. Microbiol.* 111, 1–61. doi: 10.1099/00221287-111-1-1

Ryder, N., Frank, I., and Dupont, M. (1986). Ergosterol biosynthesis inhibition by the thiocarbamate antifungal agents tolnaftate and tolciclate. *Antimicrob. Agents Chemother.* 29, 858–860. doi: 10.1128/AAC.29.5.858

Sakai, J., Rawson, R. B., Espenshade, P. J., Cheng, D., Seegmiller, A. C., Goldstein, J. L., et al. (1998). Molecular identification of the sterol-regulated luminal protease that cleaves SREBPs and controls lipid composition of animal cells. *Mol. Cell* 2, 505–514. doi: 10.1016/S1097-2765(00)80150-1

Siaut, M., Cuiné, S., Cagnon, C., Fessler, B., Nguyen, M., Carrier, P., et al. (2011). Oil accumulation in the model green alga *Chlamydomonas reinhardtii*: characterization, variability between common laboratory strains and relationship with starch reserves. *BMC Biotechnol.* 11:7. doi: 10.1186/1472-6750-11-7

Simionato, D., Block, M. A., La Rocca, N., Jouhet, J., Maréchal, E., Finazzi, G., et al. (2013). The response of *Nannochloropsis gaditana* to nitrogen starvation includes de novo biosynthesis of triacylglycerols, a decrease of chloroplast galactolipids, and reorganization of the photosynthetic apparatus. *Eukaryot. Cell* 12, 665–676. doi: 10.1128/EC.00363-12

Suzuki, M., Kamide, Y., Nagata, N., Seki, H., Ohyama, K., Kato, H., et al. (2004). Loss of function of 3-hydroxy-3-methylglutaryl coenzyme a reductase 1 (HMG1) in *Arabidopsis* leads to dwarfing, early senescence and male sterility, and reduced sterol levels. *Plant J.* 37, 750–761. doi: 10.1111/j.1365-313X.2004.02003.x

Tornabene, T., Holzer, G., Lien, S., and Burris, N. (1983). Lipid composition of the nitrogen starved green alga *Neochloris oleoabundans*. *Enzyme Microb. Technol.* 5, 435–440. doi: 10.1016/0141-0229(83)90026-1

Vigeolas, H., Duby, F., Kaymak, E., Niessen, G., Motte, P., Franck, F., et al. (2012). Isolation and partial characterization of mutants with elevated lipid content in *Chlorella sorokiniana* and *Scenedesmus obliquus*. *J. Biotechnol.* 162, 3–12. doi: 10.1016/j.jbiotec.2012.03.017

Watanabe, Y., Shimada, Y., Sugihara, A., and Tominaga, Y. (2002). Conversion of degummed *soybean* oil to biodiesel fuel with immobilized *Candida antarctica* lipase. *J. Mol. Catal. B Enzym.* 17, 151–155. doi: 10.1016/S1381-1177(02)00022-X

Xu, H., Miao, X., and Wu, Q. (2006). High quality biodiesel production from a *microalga Chlorella* protothecoides by heterotrophic growth in fermenters. *J. Biotechnol.* 126, 499–507. doi: 10.1016/j.jbiotec.2006.05.002

Yoon, K., Han, D., Li, Y., Sommerfeld, M., and Hu, Q. (2012). Phospholipid: diacylglycerol acyltransferase is a multifunctional enzyme involved in membrane lipid turnover and degradation while synthesizing triacylglycerol in the unicellular green *microalga Chlamydomonas reinhardtii*. *Plant Cell* 24, 3708–3724. doi: 10.1105/tpc.112.100701

Ziogas, B., Oesterhelt, G., Masner, P., Steel, C., and Furter, R. (1991). Fenpropimorph: a three site inhibitor of ergosterol biosynthesis in *Nectria haematococca* var. *cucurbitae*. *Pestic. Biochem. Physiol.* 39**,** 74–83. doi: 10.1016/0048-3575(91)90215-8

Conflict of Interest Statement: The content of this paper was registered as a Korean patent 10-1428863.

Received: 16 October 2014; paper pending published: 27 October 2014; accepted: 16 January 2015; published online: 24 February 2015.

*Citation: Kim H, Jang S, Kim S, Yamaoka Y, Hong D, Song W-Y, Nishida I, Li-Beisson Y and Lee Y (2015) The small molecule fenpropimorph rapidly converts chloroplast membrane lipids to triacylglycerols in Chlamydomonas reinhardtii. Front. Microbiol. **6**:54. doi: 10.3389/fmicb.2015.00054*

This article was submitted to Microbiotechnology, Ecotoxicology and Bioremediation, a section of the journal Frontiers in Microbiology.

APPENDIX

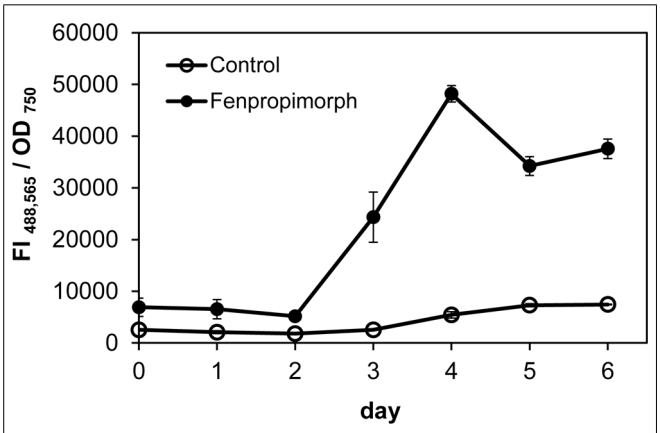

FIGURE A1 | Growth phase-dependent effect of treatment with fenpropimorph (10 μg mL^{-1}) on Nile red fluorescence of *Chlamydomonas*. The fluorescence values are normalized by optical density at 750 nm. Averages from three experimental replicates are presented. Bars represent SE.

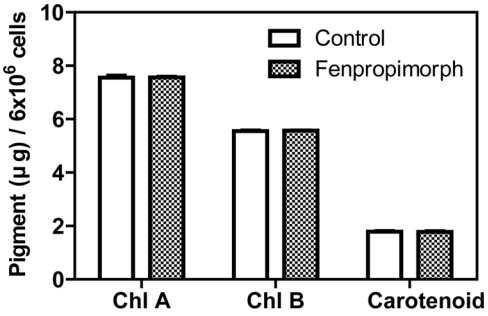

FIGURE A3 | Chlorophyll a and b and carotenoid contents of fenpropimorph-treated *Chlamydomonas* strain CC-125 cells. Cells in TAP (N+, acetate+) medium were treated with fenpropimorph (10 μg mL^{-1}) or ethanol (solvent control) for 1 h at 25°C. Chlorophyll and carotenoid contents were assayed following the method previously described (Lichtenthaler and Babani, 2004). Approximately 6.0 × 10^6 cells were collected by centrifugation (2000 *g*; 10 min), and the pellet was resuspended in 95% ethanol and mixed by vortexing. After centrifugation, the supernatant was transferred to a new 96-well plate and optical absorbance at 648 nm and 664 nm were measured using a Safire fluorescence spectrophotometer (TECAN, Switzerland). Each pigment content was calculated as described previously (Lichtenthaler and Babani, 2004). Averages and SE from three replicate experiments are presented.

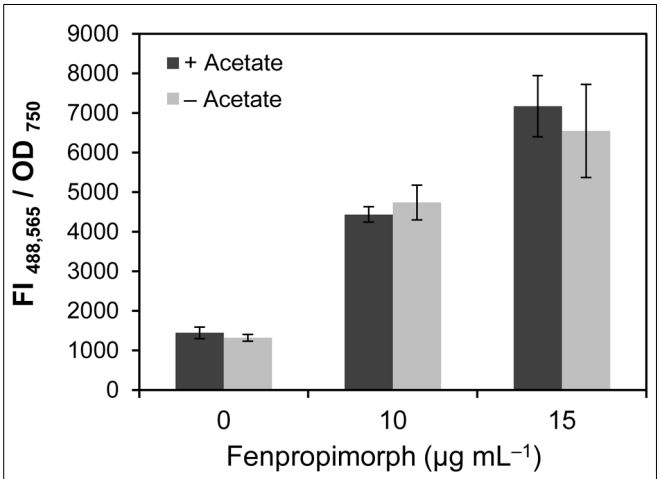

FIGURE A2 | Acetate in the medium was not necessary for the fenpropimorph effect on TAG accumulation. Note the absence of difference in Nile red fluorescence intensities of cells treated with fenpropimorph in media with or without acetate. *Chlamydomonas* cells in late mid-log phase culture in the TAP (N+, acetate+) medium were harvested, and resuspended either in the same TAP medium or in TAP medium without acetate, then treated with fenpropimorph (10 or 15 μg mL^{-1}) for 1 h at 25°C. Averages from three experimental replicates are presented. Bars represent SE.

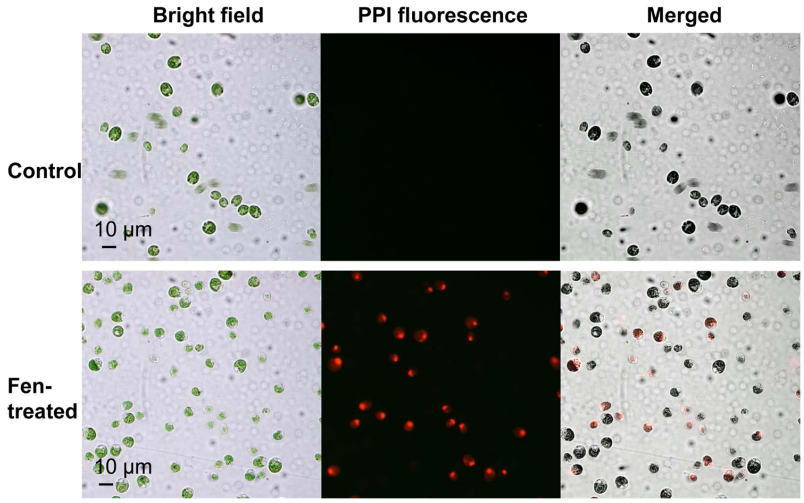

FIGURE A4 | Fenpropimorph treatment results in *Chlamydomonas* cell death. Cells in TAP (N+, acetate+) medium were treated with fenpropimorph or ethanol (solvent control) for 1 h at 25°C, then stained with propidium iodide (2 μg mL^{-1}, 15 min). Nuclear staining of cells treated with fenpropimorph suggests that the cells are dead.

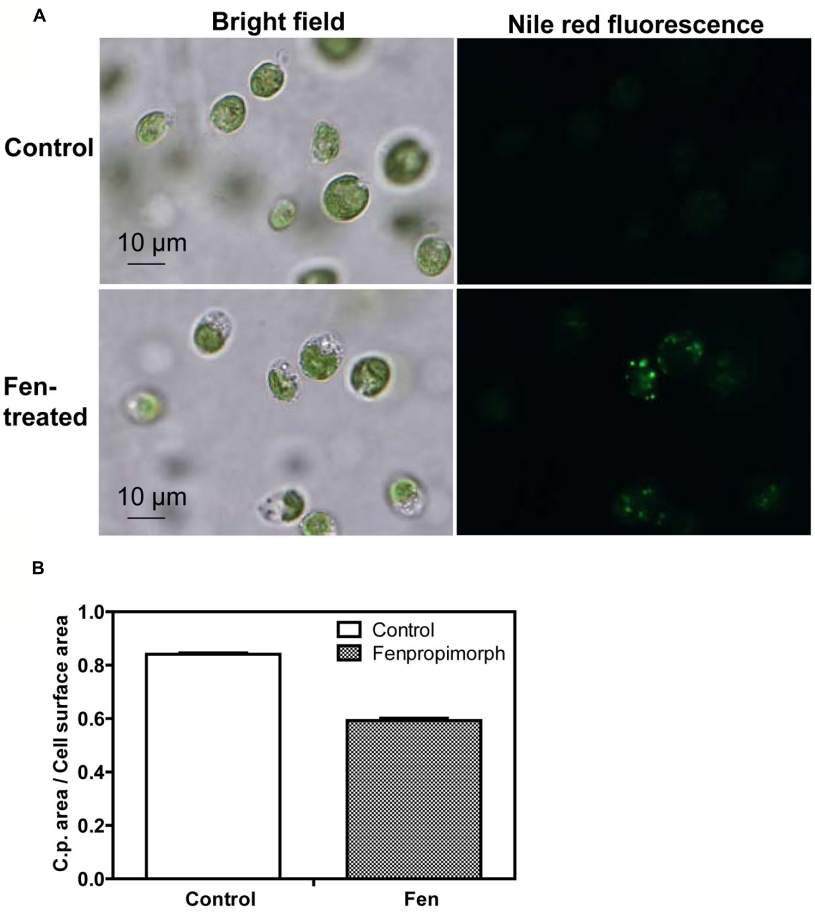

FIGURE A5 | Change in chloroplast morphology in fenpropimorph-treated *Chlamydomonas* cells. (A) Chloroplasts are shrunken in fenpropimorph-treated *Chlamydomonas* cells. **(B)** Quantification of the chloroplast area per cell surface area in microphotographs of fenpropimorph-treated *Chlamydomonas* cells. Averages from fifty experimental replicates are presented. Bars represent SE.

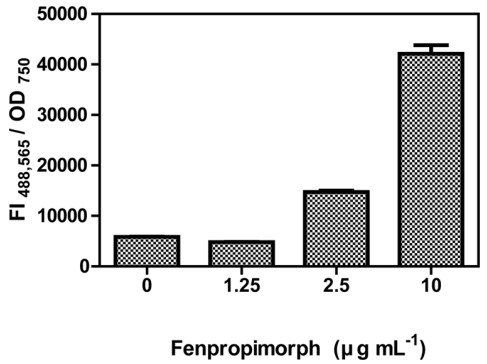

FIGURE A6 | Effect of 24-h treatment with various concentrations of fenpropimorph on Nile red fluorescence of *Chlamydomonas*. Cells were incubated till late mid-log phase in the TAP (N+, acetate+) medium, treated with fenpropimorph (1.25, 2.5, or 10 μg mL^{-1}) for 24 h at 25°C, then stained with Nile red. The fluorescence intensity (FI) was determined from three replicates and their averages are presented. Bars represent SE.

frontiers in
MICROBIOLOGY

ORIGINAL RESEARCH ARTICLE
published: 05 February 2015
doi: 10.3389/fmicb.2015.00066

Threonine 286 of fatty acid desaturase 7 is essential for ω-3 fatty acid desaturation in the green microalga *Chlamydomonas reinhardtii*

Jong-Min Lim[1†], Jayaraman Vikramathithan[1†], Kwon Hwangbo[1,2], Joon-Woo Ahn[3], Youn-Il Park[2], Dong-Woog Choi[4] and Won-Joong Jeong[1]*

[1] *Sustainable Bioresource Center, Korea Institute of Bioscience and Biotechnology, Daejeon, South Korea*
[2] *Department of Biological Science, Chungnam National University, Daejeon, South Korea*
[3] *Advanced Radiation Technology Institute – Korea Atomic Energy Research Institute, Jeonbuk, South Korea*
[4] *Department of Biology Education, Chonnam National University, South Korea*

Edited by:
Takashi Osanai, RIKEN Center for Sustainable Resource Sciences, Japan

Reviewed by:
Ji-Joon Song, Korea Advanced Institute of Science and Technology, South Korea
Daniela Morales-Sanchez, University of Nebraska-Lincoln, USA

***Correspondence:**
Won-Joong Jeong, Sustainable Bioresource Research Center, Korea Institute of Bioscience and Biotechnology, 111 Gwahangno, Yuseong-gu, Daejeon, South Korea
e-mail: wonjoong@kribb.re.kr

†These authors have contributed equally to this work.

Omega-3 fatty acid desaturases catalyze the conversion of dienoic fatty acids (C18:2 and C16:2) into trienoic fatty acids (C18:3 and C16:3), accounting for more than 50% of the total fatty acids in higher plants and the green microalga *Chlamydomonas reinhardtii*. Here, we describe a Thr residue located in the fourth transmembrane domain of fatty acid desaturase 7 (FAD7) that is essential for the biosynthesis of ω-3 fatty acids in *C. reinhardtii*. The ω-3 fatty acid deficiency in strain CC-620, which contains a putative missense mutation at Thr286 of CrFAD7, was recovered by the overexpression of CC-125 *CrFAD7*. A Ser substitution in position 286 was able to partially complement the phenotype of the ω-3 fatty acid deficiency, but other substitution variants, such as Tyr, His, Cys, and Gly, failed to do so. Prediction of the phosphorylation target site revealed that Thr286 may be phosphorylated. Analysis of the structural conformation of CC-620 CrFAD7 via topology prediction (and bends in the helix) shows that this missense mutation may collapse the catalytic structure of CrFAD7. Taken together, this study suggests that Thr286 is essential for the maintaining the catalytic structure of CrFAD7.

Keywords: CrFAD7, Thr286, fatty acid desaturase, topology, *Chlamydomonas reinhardtii*

INTRODUCTION

Fatty acids are the primary components of cell membranes. Long-chain unsaturated fatty acids are important constituents of cellular membranes and play significant roles in maintaining membrane fluidity in many organisms. Polyunsaturated fatty acids, including α-linolenic acid, are important for low-temperature responses (Gibson et al., 1994), sperm and pollen viability (Horiguchi et al., 1996; McConn and Browse, 1996; Wathes et al., 2007), and defense signaling (Kirsch et al., 1997; Wallis and Browse, 2002) in various organisms.

Membrane glycerolipid molecules comprise high levels of trienoic fatty acids, and more than 2/3 of the fatty acids available in thylakoid membranes are C18:3 or a combination of C18:3 and C16:3 (Routaboul et al., 2012). The ω-3 fatty acid desaturases (FADs) catalyze the conversion of dienoic fatty acids (C18:2 and C16:2) into trienoic fatty acids (C18:3 and C16:3). In higher plants, three ω-3 FADs—FAD3, FAD7, and FAD8—were identified and characterized (Wallis and Browse, 2002). FAD3 is specific for the endoplasmic reticulum, whereas FAD7 and its cold-inducible isozyme, FAD8, are plastid specific (Wallis and Browse, 2002). Although a large number of different FADs have been characterized from a variety of organisms, some of the more specialized enzymes are still being discovered. In the model microalga *Chlamydomonas reinhardtii*, 60% of total fatty acids are composed of ω-3 and ω-6 polyunsaturated fatty acids, of which more than 80% are ω-3 species (Giroud and Eichenberger, 1988; Siaut et al., 2011). The CrFAD7 is the only ω-3 FAD in *C. reinhardtii* and may play a similar role in low-temperature responses as in higher plants (Nguyen et al., 2013). Recently, it was reported that the CC-620 strain is a ω-3 fatty acid-deficient mutant (Pflaster et al., 2014); the segregation analysis of CC-620 × CC-125 implicated that the deficiency is attributable to a missense mutation at Thr286 in CrFAD7.

Fatty acid desaturases are grouped into soluble and integral membrane classes in higher plants (Shanklin and Somerville, 1991). The soluble acyl-carrier-protein (ACP) desaturase enzymes are found in the plastids of higher plants, whereas the more extensive group of integral membrane acyl-CoA desaturases exist in endomembrane systems in both prokaryotes and eukaryotes (Shanklin and Cahoon, 1998). Most of the membrane-bound desaturases are homodimeric proteins that contain four membrane-spanning domains and three His box motifs [HX3-4H, HX2-3HH, and (H/Q)X2-3HH] (Shanklin, 1994). The di-iron active site of these enzymes is buried within a core four-helix bundle and positioned alongside a deep, bent, narrow hydrophobic cavity in which the substrate is bound during catalysis (Shanklin, 1994). Similarly, membrane receptors and channel proteins are integral membrane proteins composed of several transmembrane (TM) α-helices that assemble through tertiary or quaternary

structures to form bundles that cross the lipid bilayer (Palczewski et al., 2000; Jiang et al., 2003). The biological function of these proteins involves conformational rearrangement of this TM bundle.

In higher plants and green algae, FAD7 also has four TM domains and His motifs. In addition, FAD7 has well-conserved Thr residues that are located distal to the active catalytic site; the roles of these Thr residues have not been studied (Shanklin, 1994; Pflaster et al., 2014). In the present study, we show that Thr286 is essential for the desaturation activity of CrFAD7 using complementation analyses with various modified FAD7s. We then discussed for the critical role of Thr286 in the maintenance of the active catalytic strucuure of CrFAD7 using prediction analysis of phosphorylation and topology. This study will help identify the physiological roles of ω-3 fatty acids in microalgae and lead to an understanding of the structure and function of membrane-bound desaturases.

MATERIALS AND METHODS

C. reinhardtii GROWTH CURVES AND CULTURE CONDITIONS

Chlamydomonas reinhardtii cultures were maintained on Tris-acetate-phosphate (TAP) agar medium at 25°C under continuous light. A single colony of *C. reinhardtii* was used to make a starter culture grown in liquid TAP medium. The starter culture was grown under 4 days of light on a rotary shaker (200 rpm). Fresh TAP liquid medium (50 ml) was prepared in 250 ml Erlenmeyer flasks. This starter culture was inoculated at an OD_{750} of 0.05. The growing cells were measured daily with an UV-visible spectrophotometer at 750 nm.

VECTOR CONSTRUCTION AND TRANSFORMATION

The coding region of *CrFAD7* (XM_001689611) cDNA was amplified by reverse transcription PCR (RT-PCR) using the primers 5′-CAT ATG CAG TGC CTG TCT CGC TCC A-3′ and 5′-GGGATATCTTAGGCCTTGCCGGCAA-3′ (restriction sites underlined). CrFAD7 genomic DNA was amplified by PCR using the following primers: 5′-ACAT ATG CAG TGC CTG TCT CGC TCC A-3′ and 5′-AGAT ATC GCC GTG CCA GAG TCT AAC T-3′ (restriction sites underlined). The *CrFAD7* cDNA and genomic DNA were cloned into expression vector pCr112 at the *Nde*I and *Eco*RV sites. This construct consists of the *psa*D promoter, *CrFAD7*, and the *psa*D terminator along with the hygromycin resistance gene for selection, which is regulated by the β-*tub* promoter and the *rbcS2* terminator. The construct was transformed into strain CC-620 using the glass bead method (Kindle, 1990). After transformation, cells were cultured in the dark without shaking for 2 days. The selection procedure was performed on agar medium containing 15 μg/ml hygromycin, and the plates were incubated under dim light for2 weeks.

RNA AND DNA ISOLATION

Total RNA was prepared from *C. reinhardtii* cells (∼ 1×10^7 cells) using the TRIzol reagent (Invitrogen, Carlsbad, CA, USA) according to the manufacturer's instructions. Five micrograms of total RNA were treated with 1 U RNase-free DNase (TaKaRa, Osaka, Japan) for 30 min, and purification was performed according to the manufacturer's instructions. For the isolation of genomic DNA, 500 μl TEN buffer (10 mM EDTA, 10 mM Tris-HCl, and 150 mM NaCl) was added to samples (∼ 1×10^7 cells). Cells were harvested and resuspended in 150 μl H_2O and 300 μl SDS-EB buffer (2% SDS, 400 mM NaCl, 100 mM Tris-HCl, pH 8.0, and 40 mM EDTA). Extraction was carried out first with 350 μl phenol:chloroform:isopropanol (24:24:1, v/v/v) and then with 300 μl chloroform:isopropanol (24:1, v/v). Genomic DNA was precipitated with two volumes of absolute ethanol and washed with 70% ethanol. The DNA pellet was resuspended in Tris-EDTA buffer.

RT-PCR ANALYSES

Reverse transcription was carried out using 2 μg total RNA, 50 μM oligo (dT), 200 U M-MLV reverse transcriptase (Promega, Madison, WI, USA), 500 μM each dNTP, and 20 U ribonuclease inhibitor. For semi-quantitative RT-PCR, cDNA was amplified with 1.5 U Ex *Taq* DNA polymerase (TaKa Ra), 100 μM each dNTP, and 10 pmol each gene-specific primer using a T1 thermal cycler (Biometra GmbH, Gottingen, Germany). Amplification was performed with 25–35 cycles of 94°C for 30 s, 56°C for 30 s, and 72°C for 30 s. To detect transcripts, the following primers were used: *CrFAD7* forward primer: 5′-TTCACCGCTGAGCGCAA-3′; reverse primer: 5′-GTGGGTGCCGATGTCGTGGT-3′; *CrFAD2* forward primer: 5′-CTTCACCAAGCGCGAGCGCA-3′; reverse primer: 5′-CTTGATGGCCTCGGTGGCCT-3′; *CrΔ4FAD* forward primer: 5′-CACCTTCGCCGTGTCGCACA-3′; reverse primer: 5′-CATCTCGCCGTCGCGCTTGA-3′; *CrFAD6* forward primer: 5′-ATGGCCAAGTGGGACTCCAC-3′; reverse primer: 5′-CCACGGTGAAGGTGCTCATC-3′; *CrFAD13* forward primer: 5′-CATGATCTCGCCCCTTAGCTACTT-3′; reverse primer: 5′-GTCCATCTGAATGTGGGACACCT-3′; α-*tubulin* forward primer: 5′-CTCGCTTCGCTTTGACGGTG–3′; reverse primer: 5′-AACGTCCTTGGGCACGACGT -3′; and *IAD5* forward primer: 5′-GCGAGGTCTCTGCTCTGGTG-3′; reverse primer: 5′-TACTCGGACTTGGCGATCCA -3′. To detect *CrFAD7* cDNA transcripts in transgenic lines, specific primers [forward 5′-TTCACCGCTGAGCGCAA-3′ located in *CrFAD7* cDNA and reverse 5′-CCTGTGGCTAATTGACCGTG-3′ located in psaD terminator] were used.

ANALYSIS OF FATTY ACID METHYL ESTERS BY GAS CHROMATOGRAPHY

Total lipids were extracted from 20 mg freeze-dried samples according to a previously described extraction method (Sasser, 1990). Saponification was performed with 2 ml saponification reagent (7.5 M NaOH:CH_3OH, 1:1, v/v) at 100°C for 30 min. For the production of fatty acid methyl esters, 4 ml methylation reagent (CH_3OH:6 N HCl, 1:1, v/v) were added to the saponified sample and incubated at 80°C for 10 min. After the reaction, 2.5 ml extraction solvent hexane:methyl tetra-butyl ether, 1:1, v/v) were added and incubated with shaking for 10 min. The upper phase was separated by centrifugation at 4,000 rpm for 10 min. A washing step was carried out with 6 ml washing solution (0.5 M NaOH). The fatty acid methyl esters were analyzed by gas chromatography (model YL-6100GC; Young Lin Science, Anyang, Korea) equipped with a flame ionization detector and an

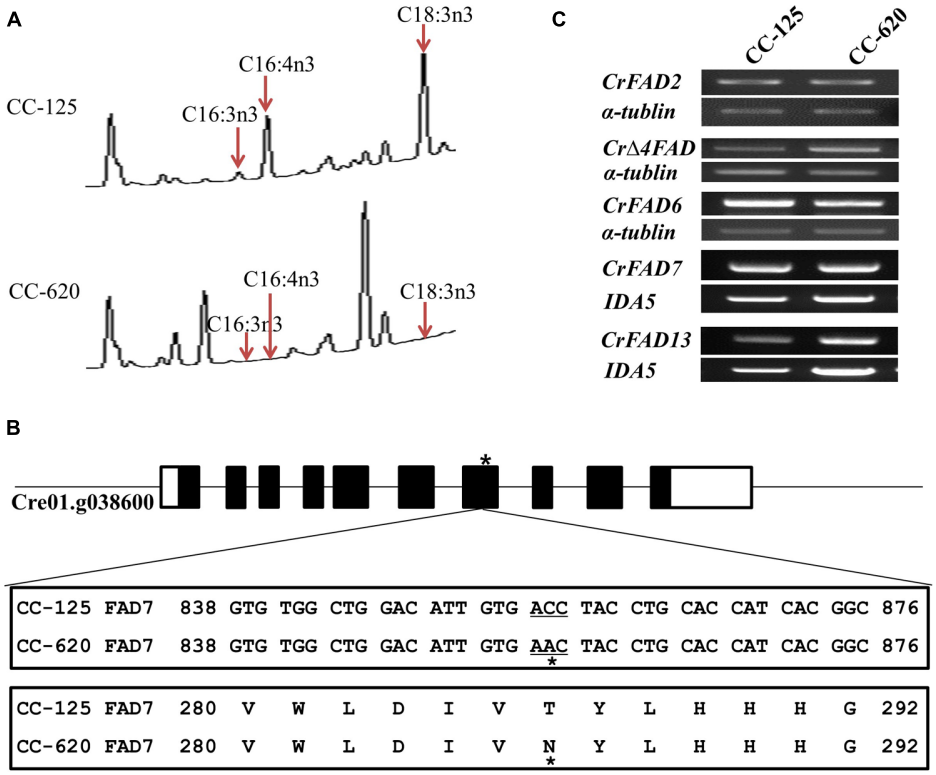

FIGURE 1 | (A) Comparison of fatty acids profiles in strains CC-125 and CC-620 from gas chromatographic analyses. Arrows indicate significant changes in specific fatty acids. **(B)** Sequence comparison (nucleotide and amino acid) of CrFAD7 in CC-620 and other wild-type strains (CC-124, CC-125, and CC-621). The black square boxes indicated the exon number or gene locus of the CrFAD7 and star indicates the missense mutation (Thr286Asn) caused by a point mutation. **(C)** RT-PCR analyses of fatty acid desaturases (FADs). *CrFAD2* (EU596472), *CrFAD7* (XM-001689611), *CrFAD6* (AB007640), *CrFAD13* (AB239770), and Δ*-4FAD* (JN089704). Genes for *IAD5* and α*-tubulin* served as internal controls.

INNOWAX capillary column (Agilent Technologies, Santa Clara, CA, USA; 30 m × 0.32 mm × 0.5 μm). Each fatty acid methyl ester component was identified and quantified using the Supelco® 37 Component Fatty Acid Methyl Ester Mix (Sigma).

SOUTHERN AND NORTHERN ANALYSES

Ten micrograms of genomic DNA were digested with *Kpn*I and separated by 0.8% agarose gel electrophoresis. The separated DNA was blotted onto a Hybond N^+ nylon membrane (Amersham Biosciences, Piscataway, NJ, USA). A 0.3-kb PCR fragment corresponding to the *C*-terminal region of *CrFAD7* was used as a probe. ^{32}P-labeled probes were produced using the Rediprime^{TM} II Random Labeling System (Amersham Biosciences), and hybridization was performed according to the manufacturer's instructions. Signals were detected using the Bio-Imaging Analyzer BAS-1800II (Fuji, Tokyo, Japan).

Total RNA was extracted from *C. reinhardtii* cells (5 ml liquid culture) using the TRIzol reagent (Invitrogen, Carlsbad, CA, USA) according to the manufacturer's instructions. Twenty micrograms of total RNA were separated by gel electrophoresis and blotted onto a Hybond-N nylon membrane (Amersham Biosciences, USA) by capillary transfer. A 0.3-kb fragment corresponding to the CrFAD7 cDNA was used as a probe. Procedures for hybridization and signal detection were as described above.

IN SILICO ANALYSES

To identity conserved Thr residues of *C. reinhardtii* FAD7, we used CrFAD7 as bait and employed the BLASTP program (BLASTP 2.2.26+) hosted at Phytozome, version 9.1 (http://www.phytozome.net). Clustal W2.1 was used for multiple sequence alignment. The accession numbers of the FAD7-homologous genes used in this study were as follows: *VcFAD7* (XP_002953984), *CnFAD7* (EF1N50714), *CosFAD7* (EIE21058), *CrFAD7* (XP_001689663), *OsFAD7* (NP_001060733), *PpFAD7* (XP_001752878), *AtFAD7* (NP-187727), *GmFAD7* (NP-001237838), *ZmFAD7* (NP-001105303), and *SspDesA* (CAA37584). Prediction analyses for phosphorylation target sites and topology were performed using the online software tools Kinase phos2 and TMHMM (Version 1), respectively. Default settings of both programs were used.

RESULTS

THE ω-3 FATTY ACID DEFICIENCY IN THE CC-620 STRAIN IS COMPLEMENTED BY CC-125 *CrFAD7* GENE EXPRESSION

We confirmed the ω-3 fatty acid deficiency in the CC-620 strain obtained from the Chlamydomonas Resource Center (**Figure 1A**). The point mutation in the seventh exon of the *CrFAD7* gene, which causes a missense mutation (Thr286Asn), was confirmed to be identical to that described in the study by

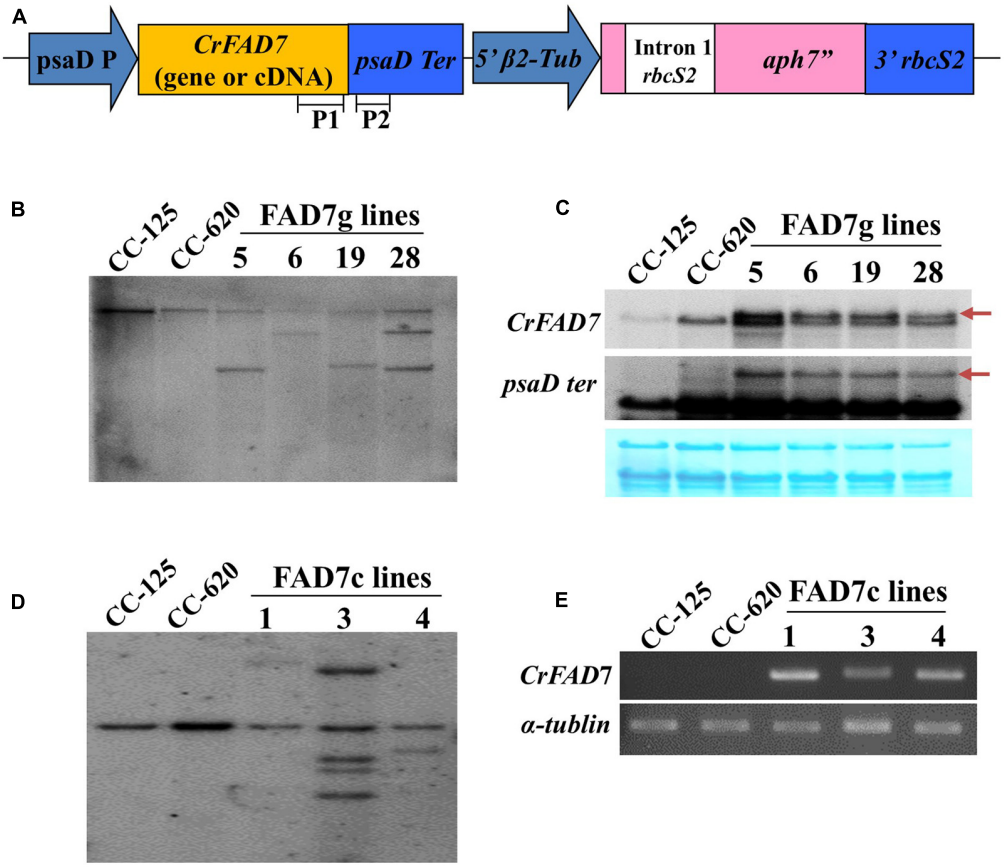

FIGURE 2 | Generation of CC-125 *CrFAD7*-expressing transgenic lines using CC-620. (A) Schematic diagram of the transformation vector. P1 and P2 indicate the regions used as probes for Southern or northern blot analysis. **(B,D)** Southern blot analysis of the *CrFAD7* gene. Genomic DNA was digested by *Xba*I and blotted against probe P1. **(C)** Northern blot analysis to identify the expression of *CrFAD7* mRNA in the *CrFAD7* genomic DNA-expressing transgenic lines; P1 probe for *CrFAD7* transcript or P2 probe for 3′ UTR (*PsaD* terminator) of *CrFAD7* transcript. Arrows indicate transcripts of transformed *CrFAD7* gene. **(E)** RT-PCR analysis to identify transcripts of transformed *CrFAD7* cDNA. α-*tubulin* served as the internal control. FAD7g lines: complementation lines with FAD7genomic DNA; FAD7c lines: complementation lines with FAD7 cDNA.

(Pflaster et al., 2014; **Figure 1B**). To identify the main cause for abnormal ω-3 fatty acid desaturation, transcript levels were investigated for *CrFAD2* (EU596472), *CrΔFAD4* (JN089704), *CrFAD6* (AB007640), *CrFAD7* (XM_001689611), and *CrFAD13* (AB239770), whose expression products are either directly or indirectly involved in ω-3 fatty acid biosynthesis. However, RT-PCR analysis detected no significant differences in the expression levels of these genes between the CC-620 and CC-125 strains (**Figure 1C**). Next, we sequenced the cDNAs of the above-mentioned genes. Except for the point mutation in the *CrFAD7* gene, no mutations were observed in the *CrFAD2*, *CrΔFAD4*, *CrFAD6*, or *CrFAD13* genes.

To reveal the phenotype of the ω-3 fatty acid deficiency in strain CC-620 by the missense mutation detected in *CrFAD7*, genetic transformation of CC-620 was carried out using genomic DNA and cDNA of CC-125 *CrFAD7*. Transgene insertion and expression were confirmed by Southern, Northern, and RT-PCR analyses (**Figures 2A–E**).

In *CrFAD7* genomic DNA-complemented strains (in transgenic lines), the normal fatty acid composition was recovered with various levels of C16:4 and C18:3n3; in comparison with CC-125, more than 80% of ω-3 fatty acids were recovered with a concomitant reduction of ω-6 fatty acids in several transgenic lines (**Figures 3A,B**). The ω-3 fatty acids hexadecatrienoic acid (C16:3n3), hexadecatetraenoic acid (C16:4), and α-linolenic acid (C18:3n3) were not detected in the CC-620 strain, whereas, the ω-3 fatty acids were found to be 1.9, 12.7, and 20.5 mol% in CC-125, and to be 1.1, 9.3, and 17.7 mol% in the complemented strain (**Figure 3**; **Table 1**). The concomitant reduction in ω-6 fatty acids was detected in the complemented transgenic lines compared to the CC-620 strain, but no significant differences in either saturated (C16:0) or monounsaturated fatty acid accumulation were observed in CC-125, CC-620, or the transgenic lines. In *CrFAD7* cDNA-complemented strains, the recovery level of ω-3 fatty acids was lower than that of *CrFAD7* genomic DNA-complemented lines (**Figures 3A,B**).

Thr286 IS CONSERVED IN HIGHER PLANTS AND GREEN ALGAE

Fatty acid desaturase 7 is a membrane-bound desaturase, but its crystal structure has not yet been solved. Analysis of conserved

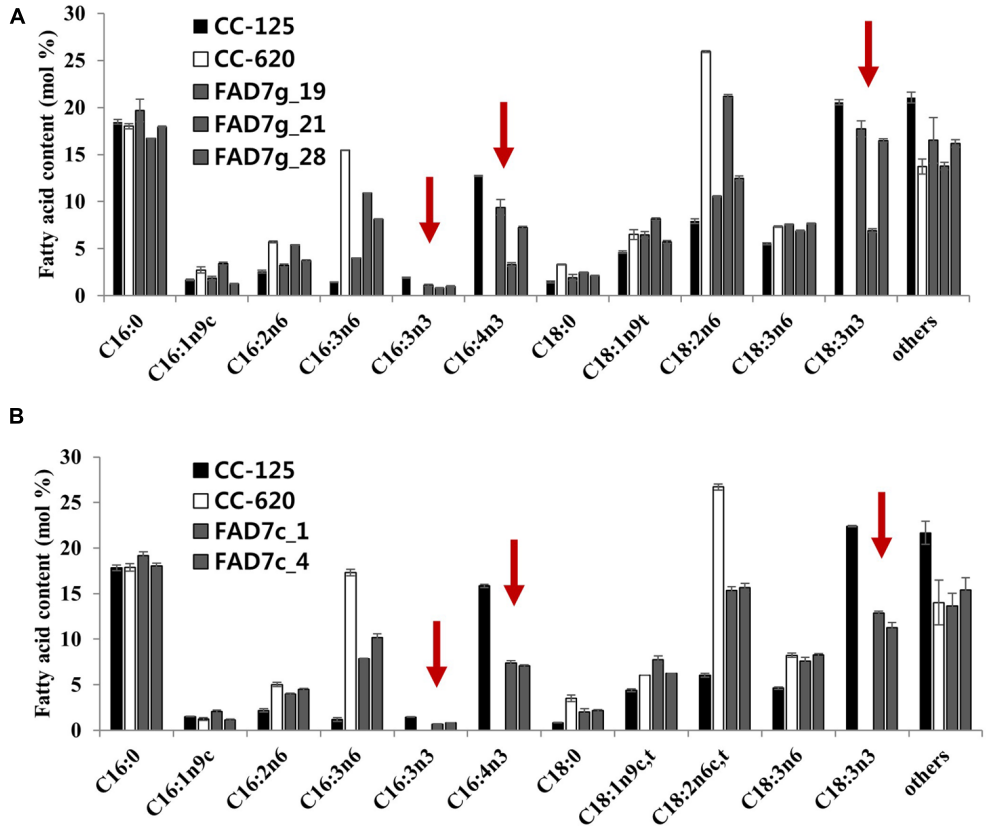

FIGURE 3 | Complementation of ω3-fatty acid deficiency in strain CC-620 by expression of the CC-125 *CrFAD7* gene. Fatty acid compositions in CC-125, CC-620, and complementary strains were compared. **(A)** Complementation using *CrFAD7* genomic DNA. FADg_19, FADg_21, and FADg_28 complementation strains expressing *CrFAD7* genomic DNA. **(B)** Complementation using *CrFAD7* cDNA. FAD7c_1 and FADc_4 complementation strains expressing *CrFAD7* cDNA. The values represent the mean ± standard error (SEM). The experiments were conducted in triplicate.

sequence motifs in FAD7 shows that the four membrane-spanning domains and three His box motifs are conserved in all FAD7 from microalgae to higher plants (Figure S1). Interestingly, the Thr residue in the fourth TM domain is specifically well conserved (Figure S1). The membrane protein topology of CrFAD7 was predicted using TMHMM. Topology prediction of CrFAD7 detected clear differences between CC-125 and CC-620 CrFAD7 (Figures S2A,B). A substitution of Ser286 for Thr286 showed a similar pattern as CC-125 CrFAD7 (Figures S2A,C). In CC-125 and Ser286-substituted CrFAD7, all four TM helices were linearly arranged, and the *C*-terminal region containing the third His box motif after the fourth TM domain was predicted to be located inside the membrane (Figures S2A,C). However, in CC-620 CrFAD7, the *C*-terminal region was predicted to be located outside of the membrane (Figure S2B), indicating that the fourth TM domain changes (or loses) its structural helix.

To test the above prediction that Thr could be replaced by Ser, we transformed the CC-620 strain with modified CrFAD7 genes that would encode Ser, Tyr, His, Cys, or Gly substitutions at position 286. Only the Ser-substituted transgenic lines recovered the missing fatty acids (**Figure 4**) but other substitution variants, such as Tyr, His, Cys, and Gly, failed to do so (Figure S3). However, the accumulation of fatty acids was partially complemented compared with CC-125. The accumulation of α-linolenic acid approached 3% in the Ser-substituted transgenic lines, whereas the accumulation approached 24% in strain CC-125. These results suggest that Thr286 is critical for proper CrFAD7 activity. To address the possible phosphorylation of Thr286 *in silico*, amino acid sequences of CC-620 and CC-125 CrFAD7 were analyzed using a phosphorylation site prediction tool, Kinase phos2. The result predicted 21 sites of phosphorylation, including Thr286, in CrFAD7 targeted by protein kinase B or G protein-coupled receptor kinase (Figure S4A). Only 20 target sites were predicted in CrFAD7 of strain CC-620 because of the absence of Thr286 in the CrFAD7 CC-620 strain (Figure S4B). Ser286 was predicted as a phosphorylation target for AKT1, a type of protein kinase B, but not for G protein-coupled receptor kinase (data not shown). In addition, the conserved Thr residues of all FAD7s (mentioned in Figure S1) were predicted to be phosphorylation targets (data not shown).

DISCUSSION

In this study, our complementation results with the modified FAD7s indicated that Thr286 is essential for CrFAD7 desaturation activity (**Figures 3** and **4**). Topology and phosphorylation prediction showed that the missense mutation may disrupt the catalytic structure of the ω-3 FAD (Figures S2 and S4).

Table 1 | Fatty acid composition of CC-125, CC-620 and one of complemented strains analyzed through GC-FID.

Fatty acid composition	CC-125	CC-620	FAD7g_19
C16:0	18.48 ± 0.251	18.01 ± 0.292	19.68 ± 1.188
C16:1n9c	1.67 ± 0.074	2.73 ± 0.336	1.86 ± 0.22
C16:2n6	2.57 ± 0.13	5.7 ± 0.098	3.21 ± 0.148
C16:3n6	1.44 ± 0.037	15.47 ± 0.018	4 ± 0.036
C16:3n3	1.93 ± 0.058	ND	1.11 ± 0.093
C16:4n3	12.73 ± 0.067	ND	9.38 ± 0.83
C18:0	1.47 ± 0.093	3.32 ± 0.061	1.93 ± 0.327
C18:1n9t	4.63 ± 0.129	6.5 ± 0.533	6.46 ± 0.357
C18:2n6	7.93 ± 0.246	25.95 ± 0.089	10.56 ± 0.083
C18:3n6	5.52 ± 0.104	7.33 ± 0.083	7.57 ± 0.039
C18:3n3	20.56 ± 0.296	ND	17.74 ± 0.852
others	21.07 ± 0.574	13.73 ± 0.794	16.51 ± 2.434
FAME	100 ± 2.059	98.74 ± 2.555	100.01 ± 6.607

ND, not detected.

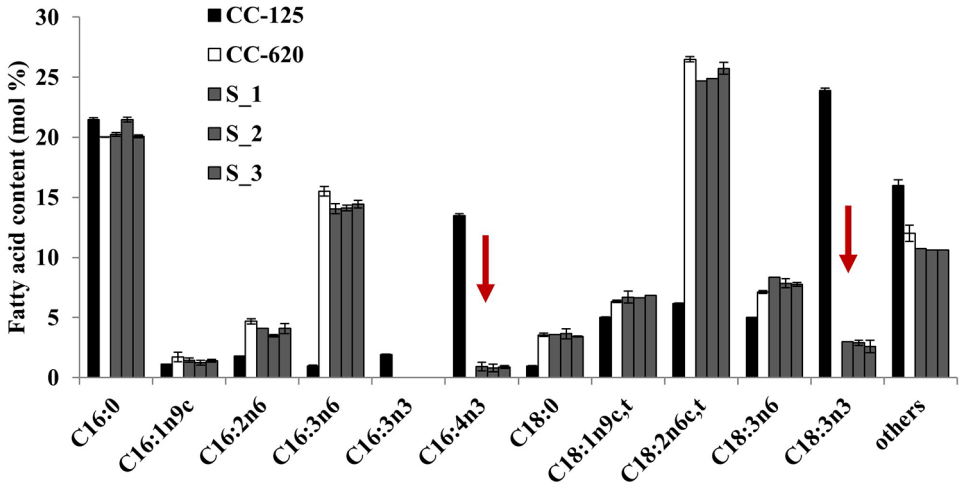

FIGURE 4 | Fatty acid composition of strain CC-620 and serine substituted lines (S_1, S_2, and S_3) expressing *CrFAD7* cDNA. The values represent the mean ± standard error (SEM). The experiments were conducted in triplicate.

Chlamydomonas reinhardtii strain CC-620 is a high-efficiency mating strain that produces autolysin and has been used previously as a common laboratory wild-type strain. Recently, Pflaster et al. (2014) reported that the ω-3 fatty acid deficiency in *C. reinhartii* strain CC-620 correlated with a single locus, possibly attributed the missense mutation (Thr286Asn) in CrFAD7. In the present study, our complementation results provide direct evidence that the missense mutation is the real cause of the ω-3 fatty acid deficiency in CC-620 (**Figures 3** and **4**). ω-3 fatty acids deficiency of CC-620 can be recovered by nuclear transformation of a wild type (CC-125) *CrFAD7* gene. Interestingly, when a cDNA encoding CC-125 *CrFAD7* was used for complementation, the transformed CC-620 produced 60% ω-3 fatty acids compared to strain CC-125, and transcription could be detected by RT-PCR. However, when genomic DNA encoding CrFAD7 was used, several transformed strains produced nearly maximal levels of ω-3 fatty acids, and transcription was clearly detected by Northern blot analyses (**Figure 2C**). These results suggest that a genomic fragment corresponding to CrFAD7 efficiently expresses the CrFAD7 transcript compared to cDNA, and that the transcript level of CrFAD7 is proportional to FAD7′s activity.

Impaired progeny production was observed when strain CC-620 was mated with its opposite mating type (Goodenough et al., 2007). Interestingly, the involvement of ω-3 fatty acids in reproduction was also reported in higher plants and animals. The *Arabidopsis* triple mutant for FAD3, 6, and 7 manifested as male sterility (McConn and Browse, 1996). The animal ω-3 fatty acid

deficiency resulted in impaired steroid hormone synthesis (Wathes et al., 2007). These findings suggest that ω-3 fatty acids may be important for reproduction in microalgae, including *C. reinhardtii*. The strain CC-620 had the additional phenotypes of slow growth and increased sensitivity at high temperature (37°C) compared to the CC-125 strain (Figure S5). However, these phenotypes were recovered in the progenies of CC-620 × CC-124, which are missing ω-3 fatty acids, indicating that the CC-620 genome contains another mutation(s) responsible for these phenotypes in addition to the FAD7 mutation.

Protein phosphorylation plays a role in various physiological responses by altering enzymatic activity, from active to inactive or vice versa (Hunter, 1995). The *in silico* prediction detected 21 and 20 Thr residues of CC-125 and CC-620 CrFAD7, respectively, as target phosphorylation sites for protein kinase B or G protein-coupled receptor kinase (Figure S4). Ser286 was predicted as a phosphorylation site. However, the replacement of Thr286 by Ser286 only partially recovered the activity of FAD7 in four transgenic lines (**Figures 4** and S3). These results suggest that Thr and Ser at position 286 can be phosphorylated by kinases and that Thr is preferred and necessary for full activity of the FAD. A significant preference for Thr or Ser as the phosphoacceptor residue has been previously reported, but this selectivity and its mechanism is unknown (Marin et al., 1986; Kuenzel et al., 1987; Litchfield et al., 1990; Kõivomägi et al., 2013).

POSSIBLE MECHANISMS OF CrFAD7 IN ω-3 FATTY ACID SYNTHESIS

In higher plants and microalgae, lipid-linked acyl desaturation is a well-known mechanism; this process is induced by FADs. All FADs have TM domains, His motif boxes, and a di-iron active site, which all play important roles in the desaturation process. Our results indicate that the conserved Thr286 in the fourth TM domain is essential for fatty acid desaturation. Thr is less polar than Ser, but both have similar structures (both contain a polar hydroxyl group), differing only in the presence of a methyl group attached to the β-carbon in Thr. A mutation of a polar amino acid in a TM helix has been reported to abolish its structure; Thr residues function cooperatively to maintain the normal structure of the TM domain through hydrogen bonding (Dawson et al., 2002). In our transgenic lines, due to the lack of this methyl group in Ser, Ser286 may not efficiently donate hydrogen molecules to maintain the correct structure of the TM domain and fails to recover the full activity of FAD7. The Thr286Asn missense mutation of the CrFAD7 protein may disrupt the structure of the TM domain, leading to a loss of CrFAD7 desaturation activity.

Mutation of Thr may directly affect the structure of the TM domain, as this single residue was able to stimulate significant helix associations in model peptides (Gratkowski et al., 2001). In the TM domain of β2-adrenergic receptors, the statistical *g*2 conformations of both Ser and Thr residues decreased their f angles and increased their c angles; a hydrogen bond was formed between the Oγ atoms of Ser and Thr, with the i-3 or i-4 carbonyl oxygen, inducing or stabilizing the angle in the helix 3–4° larger than for Ala (Ballesteros et al., 2000). This finding indicates that the local alterations in Ser and Thr in the TM domain may result in significant conformational changes across TM helices.

Based on our results, the loss of function in CC-620 CrFAD7 could be explained by a number of mechanisms. In CC-620 CrFAD7, the Thr286Asn mutation in the fourth TM domain may induce alteration of angle in the α-helix. This altered bending would induce a change in CrFAD7′s structural orientation. Structural shifts could deform the cooperative catalytic structure or cause the third *C*-terminal his motif box to be positioned too closed or too far from the catalytic active site. Alternately, the mutation may abolish the helix completely. Membrane topology prediction of the CC-620 CrFAD7 using TMHMM failed to detect a fourth helix. This would cause the third *C*-terminal his box to be located outside of membrane rather than inside (Figure S2B). In either scenario, the structural loss or alteration of the fourth TM domain would collapse the cooperative catalytic structure needed for ω-3 fatty acid desaturation. In addition, the presence or absence of position 286 phosphorylation could also induce a structural change in the fourth TM domain and alter the topology. CrFAD7 Thr286 seems to be positioned away from the catalytic site, indicating that the phosphorylation may cause a structural change in the fourth TM domain rather than directly regulating enzymatic activity. To support this, previous studies have shown that phosphorylation by kinase can alter the protein conformation and modulate its biological function (Birck et al., 1999; Groban et al., 2006; Grosely et al., 2013). Any of these three possible mechanisms would lead to TM domain structural modification and prevent CC-620 CrFAD7 from synthesizing ω-3 fatty acids.

In summary, we show that the *CrFAD7* point mutation directly causes an alteration in the fatty acid profile of the CC-620 strain using complementation analysis with a CC-125 copy of *CrFAD7*. Amino acid substitutions and predictions of phosphorylation sites revealed that Thr286 may be a target of phosphorylation by protein kinase B or G protein-coupled receptor kinase. Both TM topology prediction and the structure of the TM α-helix show that Thr286 may be essential for maintaining the correct catalytic structure of CrFAD7.

ACKNOWLEDGMENTS

This work was supported by a Grant from the Advanced Biomass R&D Center (ABC) of Korea Grant funded by the Ministry of Education, Science and Technology (ABC-2011- 0031343), a Grant from the Golden Seed Project, Ministry of Agriculture, Food, and Rural Affairs (MAFRA), the Ministry of Oceans and Fisheries (MOF), Rural Development Administration (RDA), and Korea Forest Service (KFS) and a Grant from the research program of Korea Atomic Energy Research Institute (KAERI), Republic of Korea.

SUPPLEMENTARY MATERIAL

The Supplementary Material for this article can be found online at: http://www.frontiersin.org/journal/10.3389/fmicb.2015.00066/abstract

REFERENCES

Ballesteros, J. A., Deupi, X., Olivella, M., Haaksma, E. E. J., and Pardo, L. (2000). Serine and threonine residues bend α-helices in the χ1= g- conformation. *Biophys. J.* 79, 2754–2760. doi: 10.1016/S0006-3495(00)76514-3

Birck, C., Mourey, L., Gouet, P., Fabry, B., Schumacher, J., Rousseau, P., et al. (1999). Conformational changes induced by phosphorylation of the FixJ receiver domain. *Structure* 7, 1505–1515. doi: 10.1016/S0969-2126(00)88341-0

Dawson, J. P., Weinger, J. S., and Engelman, D. M. (2002). Motifs of serine and threonine can drive association of transmembrane helices. *J. Mol. Biol.* 316, 799–805. doi: 10.1006/jmbi.2001.5353

Gibson, S., Arondel, V., Iba, K., and Somerville, C. (1994). Cloning of a temperature-regulated gene encoding a chloroplast ω-3 desaturase from *Arabidopsis thaliana* 1. *Plant Physiol.* 106, 1615–1621. doi: 10.1104/pp.106.4.1615

Giroud, C., and Eichenberger, W. (1988). Fatty acids of *Chlamydomonas reinhardtii*: structure, positional distribution and biosynthesis. *Biol. Chem. Hoppe Seyler.* 369, 18–19.

Goodenough, U., Lin, H., and Lee, J. (2007). Sex determination in *Chlamydomonas. Semin. Cell Dev. biol.* 18, 350–361. doi: 10.1016/j.semcdb.2007.02.006

Gratkowski, H., Lear, J. D., and DeGrado, W. F. (2001). Polar side chains drive the association of model transmembrane peptides. *Proc. Natl. Acad. Sci. U.S.A.* 98, 880–885. doi: 10.1073/pnas.98.3.880

Groban, E. S., Narayanan, A., and Jacobson, M. P. (2006). Conformational changes in protein loops and helices induced by post-translational phosphorylation. *PLoS. Comp. Biol.* 2:e32. doi: 10.1371/journal.pcbi.0020032

Grosely, R., Kopanic, J. L., Nabors, S., Kieken, F., Spagnol, G., Al-Mugotir, M., et al. (2013). Effects of phosphorylation on the structure and backbone dynamics of the intrinsically disordered connexin43 C-terminal domain. *J. Biol. Chem.* 288, 24857–24870. doi: 10.1074/jbc.M113.454389

Horiguchi, G., Kodama, H., Nishimura, M., and Iba, K. (1996). Role of ω-3 fatty acid desaturases in the regulation of the level of trienoic fatty acids during leaf cell maturation. *Planta* 199, 439–442. doi: 10.1007/BF00195737

Hunter, T. (1995). Protein kinases and phosphatases: the yin and yang of protein phosphorylation and signaling. *Cell* 80, 225–236. doi: 10.1016/0092-8674(95)90405-0

Jiang, Y., Lee, A., Chen, J., Ruta, V., Cadene, M., Chait, B. T., et al. (2003). X-ray structure of a voltage-dependent K+ channel. *Nature* 423, 33–41. doi: 10.1038/nature01580

Kindle, K. L. (1990). High-frequency nuclear transformation of *Chlamydomonas reinhardtii. Proc. Natl. Acad. Sci. U.S.A.* 87, 1228–1232. doi: 10.1073/pnas.87.3.1228

Kirsch, C., Takamiya-Wik, M., Reinold, S., Hahlbrock, K., and Somssich, I. E. (1997). Rapid, transient, and highly localized induction of plastidial ω-3 fatty acid desaturase mRNA at fungal infection sites in *Petroselinum crispum. Proc. Natl. Acad. Sci. U.S.A.* 94, 2079–2084. doi: 10.1073/pnas.94.5.2079

Kõivomägi, M., Örd, M., Iofik, A., Valk, E., Venta, R., Faustova, I., et al., (2013). Multisite phosphorylation networks as signal processors for Cdk1. *Nat. Struct. Mol. Biol.* 20, 1415–1424. doi: 10.1038/nsmb.2706

Kuenzel, E. A., Mulligan, J. A., Sommercorn, J., and Krebs, E. G. (1987). Substrate specificity determinants for casein kinase II as deduced from studies with synthetic peptides. *J. Biol. Chem.* 269, 9136–9140.

Litchfield, D. W., Arendt, A., Lozeman, F. J., Krebs, E. G., Hargrave, P. A., and Palczewski, K. (1990). Synthetic phosphopeptides are substrates for casein kinase II. *FEBS Lett.* 261, 117–120. doi: 10.1016/0014-5793(90)80650-8

Marin, O., Meggio, F., Marchiori, F., Borin, G., and Pinna, L. A. (1986). Site specificity of casein kinase-2 (TS) from rat liver cytosol. A study with model peptide substrates. *Eur. J. Biochem.* 160, 239–244. doi: 10.1111/j.1432-1033.1986.tb09962.x

McConn, M., and Browse, J. (1996). The critical requirement for linolenic acid is pollen development, not photosynthesis, in an *Arabidopsis* mutant. *Plant Cell* 8, 403–416. doi: 10.1105/tpc.8.3.403

Nguyen, H. M., Cuiné, S., Beyly-Adriano, A., Légeret, B., Billon, E., Auroy, P., et al. (2013). The green microalga *Chlamydomonas reinhardtii* has a single ω-3 fatty acid desaturase that localizes to the chloroplast and impacts both plastidic and extraplastidic membrane lipids. *Plant Physiol.* 163, 914–928. doi: 10.1104/pp.113.223941

Palczewski, K., Kumasaka, T., Hori, T., Behnke, C. A., Motoshima, H., Fox, B. A., et al. (2000). Crystal structure of rhodopsin: A G protein-coupled receptor. *Science* 289, 739–745. doi: 10.1126/science.289.5480.739

Pflaster, E. L., Schwabe, M. J., Becker, J., Wilkinson, M. S., Parmer, A., Clemente,T. E., et al. (2014). A high-throughput fatty acid profiling screen reveals novel variations in fatty acid biosynthesis in *Chlamydomonas reinhardtii* and related algae. *Eukaryot. Cell.* 11, 1431–1438. doi: 10.1128/EC.00128-14

Routaboul, J. M., Skidmore, C., Wallis, J. G., and Browse, J. (2012). *Arabidopsis* mutants reveal that short-and long-term thermotolerance have different requirements for trienoic fatty acids. *J. Exp. Bot.* 63, 1435–1443. doi: 10.1093/jxb/err381

Sasser, M. (1990). Identification of bacteria by gas chromatography of cellular fatty acids. *USFCC News. lett.* 20, 1–6.

Shanklin, J. (1994). Eight histidine residues are catalytically essential in a membrane-associated iron enzyme, stearoyl-CoA desaturase, and are conserved in alkane hydroxylase and xylene monooxygenase 1. *Biochemistry* 33, 12787–12794. doi: 10.1021/bi00209a009

Shanklin, J., and Cahoon, E. B. (1998). Desaturation and related modifications of fatty acids. *Annu. Rev. Plant Physiol. Plant Mol. Biol.* 49, 611–641. doi: 10.1146/annurev.arplant.49.1.611

Shanklin, J., and Somerville, C. (1991). Stearoyl-acyl-carrier-protein desaturase from higher plants is structurally unrelated to the animal and fungal homologs. *Proc. Natl. Acad. Sci. U.S.A.* 88, 2510–2514. doi: 10.1073/pnas.88.6.2510

Siaut, M., Cuiné, S., Cagnon, C., Fessler, B., Nguyen, M., Carrier, P., et al. (2011). Oil accumulation in the model green alga *Chlamydomonas reinhardtii*: Characterization, variability between common laboratory strains and relationship with starch reserves. *BMC Biotechnol.* 11:7. doi: 10.1186/1472-6750-11-7

Wallis, J. G., and Browse, J. (2002). Mutants of *Arabidopsis* reveal many roles for membrane lipids. *Prog. Lipid Res.* 41, 254–278. doi: 10.1016/S0163-7827(01)00027-3

Wathes, D. C., Abayasekara, D. R. E., and Aitken, R. J. (2007). Polyunsaturated fatty acids in male and female reproduction. *Biol. Reprod.* 77, 190–201. doi: 10.1095/biolreprod.107.060558

Conflict of Interest Statement: The authors declare that the research was conducted in the absence of any commercial or financial relationships that could be construed as a potential conflict of interest.

Received: 29 November 2014; accepted: 19 January 2015; published online: 05 February 2015.

Citation: Lim J-M, Vikramathithan J, Hwangbo K, Ahn J-W, Park Y-I, Choi D-W and Jeong W-J (2015) Threonine 286 of fatty acid desaturase 7 is essential for ω-3 fatty acid desaturation in the green microalga Chlamydomonas reinhardtii. Front. Microbiol. ***6****:66. doi: 10.3389/fmicb.2015.00066*

This article was submitted to Microbiotechnology, Ecotoxicology and Bioremediation, a section of the journal Frontiers in Microbiology.

Advantages of publishing in Frontiers

OPEN ACCESS
Articles are free to read, for greatest visibility

COLLABORATIVE PEER-REVIEW
Designed to be rigorous – yet also collaborative, fair and constructive

FAST PUBLICATION
Average 85 days from submission to publication (across all journals)

COPYRIGHT TO AUTHORS
No limit to article distribution and re-use

TRANSPARENT
Editors and reviewers acknowledged by name on published articles

SUPPORT
By our Swiss-based editorial team

IMPACT METRICS
Advanced metrics track your article's impact

GLOBAL SPREAD
5'100'000+ monthly article views and downloads

LOOP RESEARCH NETWORK
Our network increases readership for your article

Frontiers
EPFL Innovation Park, Building I • 1015 Lausanne • Switzerland
Tel +41 21 510 17 00 • Fax +41 21 510 17 01 • info@frontiersin.org
www.frontiersin.org

Find us on